CATALYSIS WITH EARLY AND LATE TRANSITION METALS: C—H ACTIVATION AT TANTALOCENE HYDRIDES AND OXIDATIVE ADDITION AT PALLADIUM SOLVATO COMPLEXES

by

Steven Mark Rehbein

A dissertation submitted in partial fulfillment
of the requirements for the degree of
of

Doctor of Philosophy

in

Chemistry

MONANA STATE UNIVERSITY
Bozeman, Montana

January 2021

©COPYRIGHT

by

Steven Mark Rehbein

2021

All Rights Reserved

DEDICATION

To all of those who have offered their love and support of me in this endeavor over the last several years.

ACKNOWLEDGEMENTS

My utmost gratitude goes to my advisor, Dr. Sharon Neufeldt, who has been nothing but supportive over the course of my graduate studies. I learned a tremendous amount in a short period of time in my first year in the when there were only a few member of the Neufeldt group, and I've enjoyed the degree of freedom I was afforded during the following years on which I continued work with the tantalocene chemistry. Sharon knows my aversion to vial-scale chemistry and endeavored to keep me away from it until the final year of my studies. Conversely, I've enjoyed the many little synthetic projects I've been assigned as much as any other part of my time spent here. Thanks go to my graduate committee members Dr. Mary Cloninger, Dr. Matthew Cook, Dr. Thomas Livinghouse, and Dr. Nick Stadie for their continued efforts and support. I also want to acknowledge the technical expertise and patience of Dr. Brian Tripet of the MSU Department of Chemistry and Biochemistry NMR Facility and the boundless patience of Doreen Brown.

I want to thank the many Neufeldt group members who I've had the pleasure of working with; those I've worked most closely with include Emily Elias, John Russell, Emily Entz, Matthew Kania, and Emma Baumgardener. All in all, it's been a great joy being a part of such a vibrant group and I've genuinely enjoyed my time therein.

I am grateful for the financial support from Montana State University, the American Chemical Society Petroleum Research Fund, and the National Science Foundation.

TABLE OF CONTENTS

List of Tables vi
List of Figures vii
List of Schemes viii
Abstract x

1. INTRODUCTION 1

Homogeneous Transition Metal Catalysis 1
C—H Activation at Early Transition Metals 2
Cross-Coupling Reactions Catalyzed by Late Transition Metals 5
References 10

2. EXPERIMENTAL AND COMPUTATIONAL EVALUATION OF TANTALOCENE HYDRIDES FOR C–H ACTIVATION OF ARENES 13

Contribution of Authors and Co-Authors 13
Manuscript Information Page 13
Abstract 14
Introduction 14
Results and Discussion 15
Density Functional Theory Calculations on the Benzene Activation Mechanism 15
Thermal H/D Exchange between Cp_2TaH_3 and C_6D_6 16
Comparison of Thermal and Photochemical Conditions for H/D Exchange 18
Activation of Toluene 18
H/D Exchange between $CpCp^*TaH_3$/$Cp^*_2TaH_3$ and C_6D_6 19
Conclusions 20
Experimental Section 21
Computational Section 22
Associated Content 22
Author Information 23
Acknowledgements 23
References 23

3. EXPERIMENTAL AND COMPUTATIONAL EVALUATION OF TANTALOCENE HYDRIDES FOR C–H ACTIVATION OF ALKANES 26

Abstract 26
Introduction 26
Results and Discussion 30
DFT Calculations of Intramolecular sp^3 C—H Activation 30
Intramolecular sp^3 C—H Activation 36
DFT Calculations of Intermolecular sp^3 C—H Activation 41
Intermolecular Aliphatic sp^3 C—H Activation 42
Conclusion 46
Experimental Section 46

TABLE OF CONTENTS – CONTINUED

Computational Section....56
References....58

4. SOLVENT COORDINATION TO PALLADIUM CAN INVERT THE SELECTIVITY OF OXIDATIVE ADDITION....63

Contribution of Authors and Co-Authors....63
Manuscript Information Page....63
Abstract....65
Introduction....65
Results and Discussion....66
Effect of Benzonitriles on Selectivity....67
Solvent Variants with Modified Coordinating Ability....67
Stochiometric Oxidative Addition Studies....68
DFT Studies....70
Stille Cross-Couplings....70
Role of Anions on Selectivity....71
Conclusions....72
Associated Content....72
Author Contributions....72
Acknowledgement....72
Notes and References....73

5. CONCLUSIONS AND PERSPECTIVE....75

C—H Activation at Early Transition Metals....75
Cross-Coupling Reactions Catalyzed by Late Transition Metals....80
References....83

REFERENCES CITED....84

APPENDICES....100

A. Appendix A: Chapter Two Supplemental....101
B. Appendix B: Chapter Four Supplemental....137

LIST OF TABLES

Table

2.1 Rate of Tantalocene Decomposition and H/D Exchange with C_6D_6 17

2.2 Calculated Geometric Parameters for LL′TaH3 and the Corresponding.....20
Benzene π-Complexes

3.1 Energetics of Aromatic C—H Activation by Tantalocene Hydrides.....35

3.2 Energetics of Intramolecular C—H Activation by Tantalocene Hydrides 36

3.3 Kinetics of Decomposition and Catalysis of Arene H/D Exchange by 37
Various Tantalocene Hydrides

3.4 Kinetics of Catalysis of Intramolecular Aliphatic H/D Exchange by.....38
Various Tantalocene Hydrides

3.5 Kinetics of Catalysis of Intramolecular Aromatic H/D Exchange by.....40
Various Tantalocene Hydrides

3.6 Energetics of Activation of Various C—H Bonds by Cp_2TaH_3 41

4.1 Effect of Benzonitriles on Selectivity 66

4.2 Modifying the Coordinating Ability of Common Solvents Leads.....67
to Changes in Selectivity

4.3 Solvent Effects on Selectivity of Stochiometric Oxidative Addition 67

4.4 Effect of Temperature on the Selectivity of the Pd/P^{t}Bu$_3$-Catalyzed 70
Suzuki Coupling of **1**

4.5 Base-Free Stille Coupling of **8** Catalyzed by Pd/P^{t}Bu$_3$ 70

4.6 Effect of Additives on the Selectivity of the Suzuki Cross-Coupling 71

LIST OF FIGURES

Figure

2.1 Hydride region of the ^{1}H NMR spectrum of Cp_2TaH_3 (A) before and (B) after heating for 1 h in the presence of C_6D_6. Acquired on a 500 MHz instrument. 17

2.2 Comparison of the hydride regions of the ^{1}H NMR spectra of $Cp^*_2TaH_3$, $CpCp^*TaH_3$, and Cp_2TaH_3 19

3.1 Homogeneous series of monosubstituted tantalocene hydrides used In these studies 34

3.2 ^{1}H NMR signals of complexes **2**-**5** at 0 h and at 6 h at 120 °C 38

3.3 σ-Complexes of hydrocarbon C—H activation by **1** 42

3.4 ^{1}H NMR evidence for H/D exchange at the hydrides of **6** 44

4.1 Hammett-type plot shows a correlation between benzonitrile donor ability and increasing reaction at triflate 67

4.2 Effect of dispersion on the stability of DMF-coordinated oxidative addition transition structures 69

5.1 Theoretical amine- and imine-based tantalum pincer complexes 77

5.2 Molecules with potentially differening coordinating ability or denticity upon photoswitching 81

LIST OF SCHEMES

Scheme

1.1 Proposed generation of tantalum alkylidene via (a) reductive elimination of dihydrogen, (b) oxidative addition of aliphatic substrate R—H, and (c) β-hydride elimination to furnish the alkylidene. 4

1.2 Methane homologation by (a) methane dehydrogenation to generate a tantalum methylidene and (b) homologation with an alkyl metal or metalloid. 5

1.3 Generalized cross-coupling reaction 6

1.4 Chemoselectivity in cross-coupling for (a) a single cross-coupling and (b) sequential cross-couplings 7

1.5 Divergent selectivity in the Suzuki cross-coupling of 4-chlorophenyl triflate 7

1.6 Solvent effect in chemodivergent Suzuki cross-coupling 8

2.1 H/D Exchange Catalyzed by Cp_2TaH_3 15

2.2 Calculated Pathways for the Reaction of Cp_2TaH_3 with Benzene via an Oxidative Addition Mechanism for C−H Activation 15

2.3 σ-Bond Metathesis Mechanisms for Benzene C− H Activation Are Predicted to be Prohibitively High Energy 16

2.4 Calculated Pathways for the Reaction of Cp2TaH3 with Toluene via an Oxidative Addition Mechanism for Aromatic or Benzylic C−H Activation 18

2.5 Comparison of Calculated Free Energy Surfaces for the Reaction of Cp_2TaH_3 and Permethylated Analogues with Benzene via an Oxidative Addition Mechanism 19

3.1 C—H Activation of Methane at Early Transition Metals 29

3.2 Reaction coordinate diagrams for the competing aromatic and Intramolecular C—H activation pathways of **1** 32

3.3 Modes of Intramolecular C—H Activation 32

LIST OF SCHEMES

Scheme

3.4 Generalized reaction coordinate diagram of intramolecular C—H activation and intermolecular aromatic C—H activation 35

3.5 Catalytic H/D exchange at several dueteroalkanes by Cp_2TaH 45

4.1 Seminal Reports on the Effects of Ligands and Solvents on the Selectivity of Cross-Coupling of a Chloroaryl Triflate 65

4.2 Expanded Solvent Effect Studies in the Pd/PtBu3-Catalyzed Suzuki Coupling 66

4.3 Base-Free Stille Coupling of 1 Catalyzed by Pd/P^{t}Bu$_3$ 70

5.1 Ziegler-Natta Polymerization Catalyst Activation 79

5.2 Photochemical Chemodivergence in Cross-Coupling 81

ABSTRACT

Herein we present our work on transition metal catalysis using metals from two sides of the periodic table: C—H activation catalyzed by early transition metals and cross-couplings catalyzed by late transition metals. In the first part, a synergistic experimental and computational approach was employed to investigate the possibility of extending the reactivity of bent tantalocene hydrides beyond aromatic C—H activation to enable activation of aliphatic substrates. *In situ* monitoring of the characteristic ^{1}H NMR metal hydride signals in the reaction of Cp_2TaH_3 and related complexes with deuterated aromatic substrates allowed for the evaluation of reaction kinetics of catalyst decomposition, H/D exchange, and off-cycle reactions. The insight gained from *in situ* reaction monitoring with aromatic substrates, combined with computational analyses, allowed for the extension of this chemistry to intra- and intermolecular aliphatic C—H activation. This work represents the first example of aliphatic C—H activation by homogeneous tantalum hydrides. In the second part, we provide compelling evidence that solvent coordination to palladium during oxidative addition of chloroaryl triflates can result in an inversion of chemoselectivity of this step. Previous investigations attributed a solvent-dependent switch in chemoselectivity to the propensity of polar solvents to stabilize anionic transition states of the type [Pd(P^tBu_3)(X)]- (X = anionic ligand). However, our detailed investigations show that solvent polarity alone is not a sufficient predictor of selectivity. Instead, solvent coordinating ability is selectivity-determining, with polar coordinating and polar noncoordinating solvents giving differing selectivity, even in the absence of anionic ligands "X". A solvent-coordinated bisligated transition state of the type Pd(P^tBu_3)(solvent) is implicated by density functional theory calculations. This work provides a new mechanistic framework for selectivity control during oxidative addition.

CHAPTER ONE

INTRODUCTION

Homogeneous Transition Metal Catalysis

While organometallic complexes are known for the large majority of the stable metallic elements—such as those of the alkali, alkaline earths, lanthanides, and actinides—the development of catalytic applications of these compounds has occurred primarily within the transition metals. Organometallic complexes of the transition metals are particularly suited to catalytic applications because of the ready availability of their *d* electrons, which behave quite differently from the *s* and *p* orbitals that dominate reactivity in organic chemistry. Complexes of the early transition metals are generally harder due to their fewer *d* electrons, and consequently are often found in a narrower range of oxidation states. Their lower electronegativity (or greater electropositivity) means they readily give up their valence electrons and thus often prefer higher oxidation states.[1] Complexes of the late transition metals are generally softer because of their greater number of *d* electrons, and in some cases may be found in a wider variety of oxidation states. The higher electronegativity of the metals late in the *d*-block means they tend to retain their valence electrons and thus prefer lower oxidation states.

Far and away the bulk of the work with transition metal catalysts has been done with the middle to late transition metals, in part due to their ease of handling given the low oxophilicity of many of the most common oxidation states for these compounds.[2] Indeed, the organometallic chemistry of the late transition metals has yielded catalytic processes that are operated at industrial scale—such as olefin metathesis[3] and carbonylation processes[4]—as well as methods for the facile creation of C—C bonds in myriad cross-coupling reactions. Widely adopted methods and

processes utilizing early transition metal organometallics are less common, although the development of early transition metal catalysts for olefin metathesis was aided in part by development of the homogeneous Ziegler-Natta-type catalysts.[5]

The unique reactivities of the transition metal catalyst are manifested in their elementary reactions, which may be grouped into seven reactions (or pairs of reactions that are the microscopic reverse of one another): (1) oxidative addition and reductive elimination, (b) transmetalation, (c) ligand substitution, (d) 1,1-addition and α-elimination, (e) 1,2-addition and β-elimination, (f) σ-bond metathesis, and (g) π-bond metathesis. Under ideal conditions, these reactions may be brought together to form a productive catalytic cycle to generate products that would either be inaccessible under noncatalytic conditions or whose preparation would otherwise be cumbersome.

Herein we present a summary of our work on transition metal catalysis using metals from two sides of the periodic table: C—H activation catalyzed by early transition metals and cross-couplings catalyzed by late transition metals.

C—H Activation at the Early Transition Metals

Carbon-hydrogen bonds are viewed as unreactive within the realm of traditional organic and organocatalytic chemistry. The inertness of the C—H bond is the result of its lack of low-energy empty orbitals or high-energy filled orbitals,[6] which is further exacerbated in the saturated hydrocarbons where the absence of functional groups means they lacks any dipole that might be exploited or functionalities that might act as directing groups. For example, methane—the simplest saturated hydrocarbon—has a C—H bond dissociation energy of 105 kcal/mol.[7] This thermodynamic stability makes it challenging to utilize light alkanes for any chemical processes other than combustion. Presently, the commercially viable processes for the conversion of light

alkanes to their heavier homologues are those of the Fischer-Tropsch-type.[8] These processes involve the high temperature cracking of hydrocarbons to a mixture of carbon monoxide and hydrogen (i.e., "syngas") and subsequent conversion by heterogeneous transition metal catalysts (often iron, cobalt, or ruthenium). Though these heterogenous catalysts have clearly demonstrated their worth, in many cases elucidation of the identity of the active catalyst species is challenging.[9] This lack of intimate knowledge about the active catalytic species hinders rational design of catalysts with higher activity.

Homogeneous transition metal catalysts offer a unique opportunity for the C—H activation of inert hydrocarbons—an ambitious goal whose investigation has been ongoing since the advent of modern organometallic chemistry.[10] Compared to their heterogeneous counterparts, homogeneous catalysts are often capable of operating at mild temperatures and pressures. In some cases, homogeneous complexes can provide easily studied analogues to heterogeneous catalysts. Furthermore, their well-defined molecular structure and well-developed methods for synthesis and characterization make their intentional and iterative design possible. Such catalysts have proven competent for the activation of a wide variety of other small molecules traditionally considered to be unreactive, such as olefins, carbon monoxide, dioxygen, and dinitrogen.[1]

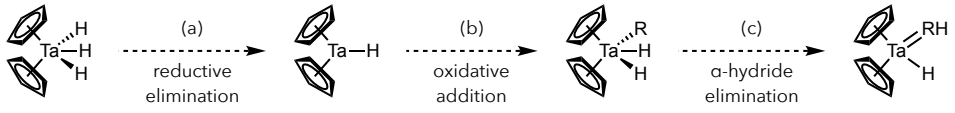
Early successes with C—H activation at transition metals exploited aromatic π-complexation between the substrate and the metal, or proceeded intramolecularly. In both cases, reactivity is facilitated by the proximity of the C—H bond to the reactive metal center. The requirement for such a pre-complexation would conspire against the activation and functionalization of aliphatic substrates. However, later work revealed examples of H/D exchange at aliphatic deuterated substrates, suggesting that perhaps such transformations may be viable. Indeed, it has long been proposed that such reactions may be more common than appreciated.[11]

Such a proposal suggests that this disparity in observation need not be indicative of the lack of such reactivity. Instead, it may result from the thermodynamic instability of the metal-alkyl complexes that would result from aliphatic C—H activation, which are therefore difficult to observe even *in situ*.

The possibility that transition metal catalyzed aliphatic C—H activation may be more common than previously appreciated may also suggest that a reexamination of catalysts known to effect intramolecular or aromatic C—H activation may be in order. The advent of modern organometallic chemistry began with the discovery of ferrocene[12] and the subsequent fervor to prepare metallocenes of the other transition metals.[10] Amongst the seminal work with these metallocenes, some were reported to effect aromatic and intramolecular C—H activation. Here we have chosen to focus on a class of metallocenes from which some of these early reports[13,14] originated—the bent metallocene hydrides of tantalum.

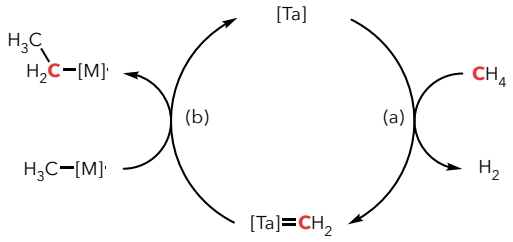
The organometallic chemistry of early *d* block metals (including tantalum) has been underexplored in large part due to the high reactivity of these complexes, especially with metals in low oxidation states. We rationalized that—if properly tempered—these reactive early transition metal complexes could provide reactive alkylidenes from aliphatic substrates resulting from C—H activation and α-elimination (Scheme 1). Such nucleophilic early transition metal alkylidenes (Schrock alkylidenes) are known catalysts, though their generation *in situ* within a catalytic cycle is less common.[15]

Scheme 1. Proposed generation of tantalum alkylidene via (a) reductive elimination of dihydrogen, (b) oxidative addition of aliphatic substrate R—H, and (c) β-hydride elimination to furnish the alkylidene.



Given the widespread underutilization of methane due to its volatility and resulting difficulties in storage and transport, we envisioned a route for the chain-growth homologation of methane originating from a tantalocene alkylidene (Scheme 2). Following generation of the tantalum methylidene from methane dehydrogenation, the methylidene could undergo homologation with an alkyl metal or metalloid (such as boron or aluminum). Similar processes have been reported for metal allene complexes with phosphorus[16a] and sulfur ylides.[Error! Bookmark not defined.b] Although we have not realized this envisioned transformation, this goal motivated the computational and experimental work with tantalocene hydrides described in Chapters 2 and 3.[17]

Scheme 2. Methane homologation by (a) methane dehydrogenation to generate a tantalum methylidene and (b) homologation with an alkyl metal or metalloid.

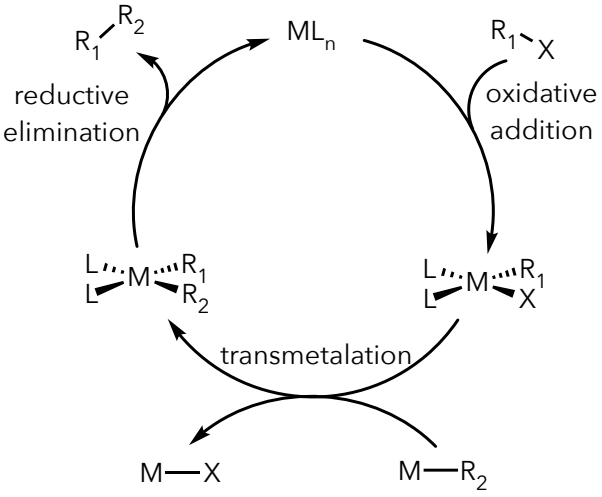


Cross-Coupling Reactions Catalyzed by Late Transition Metals

Among the success stories of late transition metal catalysis, cross-coupling reactions capable of creating new C—C or C—heteroatom bonds are a favorite among organic chemists. The principal attraction to these reactions is their flexibility and the ability to couple complex molecules that can thus be prepared separately—a feature that can save synthetic chemists significant time and effort and allow for highly modular syntheses popular in drug discovery and medicinal chemistry. The ready commercial availability of catalysts, precatalysts, and ligands, many of which can be handled on the benchtop, for myriad cross coupling reactions has dramatically increased the popularity of these reactions.

In a generalized C—C cross-coupling reaction, a low-valent transition metal catalyst (typically palladium or nickel) first undergoes oxidative addition into an organohalide or pseudohalide bond (Scheme 3). Transmetalation between this complex and an organometallic reagent (e.g., involving magnesium, zinc, tin, or copper) or organometalloid reagent (such as boronates or silanes) results in the exchange of the halide "X" for a second organic group at the metal catalyst. Reductive elimination of the two organic fragments furnishes the cross-coupled product and the regenerated catalyst.

Scheme 3. Generalized cross-coupling reaction.

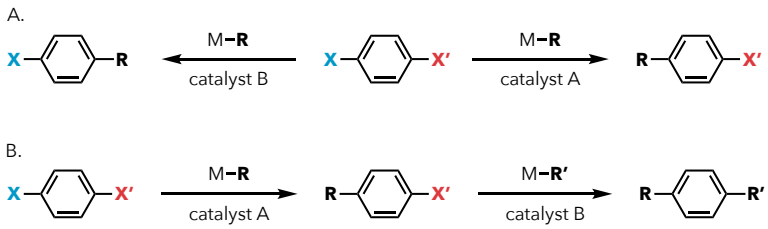


Palladium complexes are the predominant catalysts for cross coupling reactions. This preference is due to the air and water stability of many palladium complexes and their wide functional group tolerance. Palladium catalysts are thus widely employed in the Heck, Kumada, Negishi, Stille, Buchwald-Hartwig, and Suzuki cross-couplings, among others. Attempts to improve the activity of the catalysts for these reactions typically emphasize modulation of ligand environment. Through thoughtful (or serendipitous!) ligand design, chemists can control the electronic and steric parameters of the reactive metal center. Ligand denticity and bite angle can be utilized to promote certain coordination modes and their resulting geometries. Steric hindrance around a ligand can be used to make a ligand more or less labile or to influence palladium's preferred coordination number.

For aryl halide/pseudohalide substrates with more than one potentially reactive site, control over the chemo- or site-selectivity of a catalyst is desirable (Scheme 4A). In multistep syntheses,

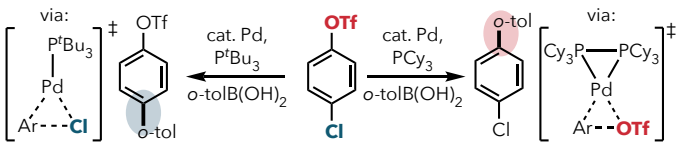
high selectivity with such substrates may allow for sequential coupling and the rapid generation of molecular complexity (Scheme 4B).

Scheme 4. Chemoselectivity in cross-coupling for (a) a single cross-coupling and (b) sequential cross-couplings



Selectivity in cross-coupling is determined by which organohalide bond undergoes oxidative addition. Several studies have examined the selectivity of oxidative addition with the substrate 4-chlorophenyl triflate (Scheme 5). In the Pd-catalyzed Suzuki cross-coupling of 4-chlorophenyl triflate with *ortho*-tolylboronic acid, Fu reported that the use of P^tBu_3 provides selectivity for the carbon-chloride bond, leaving the triflate intact.[18] Interestingly, selectivity switches and the carbon-triflate bond reacts preferentially when PCy_3 was used.[18] Schoenebeck and Houk later attributed the origin of this selectivity to the propensity of the bulky P^tBu_3 ligand to favor monoligated palladium in the oxidative addition transition state, while less bulky ligands—such as PCy_3—prefer bisligated palladium.[19]

Scheme 5. Divergent selectivity in the Suzuki cross-coupling of 4-chlorophenyl triflate.[18,19]

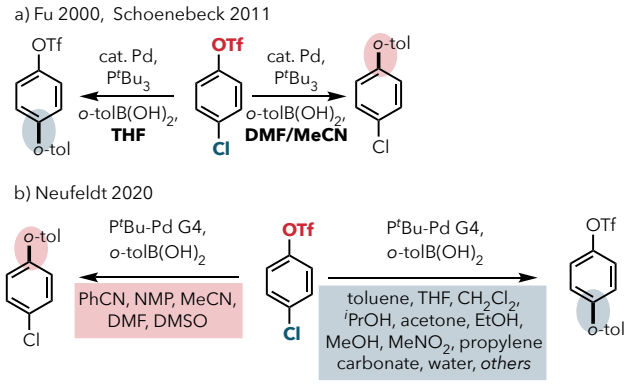


Others have provided support for the importance of the ligation state of palladium in cross coupling chemodivergence.[20] In 2011, Manabe showed that the bidentate ligand dppf could be used in a 1:1 ratio with $Pd(OAc)_2$ to achieve similar results as those obtained from PCy_2 in a 2:1 ratio to $Pd(OAc)_2$ for triflate-selectivity.[21] Work in 2016 from Sigman evaluated nearly 40

phosphine ligands for the chemoselective cross coupling of aryl chlorides and triflates.[22] Of these, only six were found to provide any preference for chloride, and all of these contained bulky *tert*-butyl or adamantyl groups. On the basis of these and related computational results, Sigman reached a similar conclusion to that of Houk and Schoenebeck:[19] the bulky ligands containing ^{t}Bu and Ad moieties favor a monoligated palladium species, while smaller ligands prefer bisligation.[22]

After her work with Houk,[19] Schoenebeck discovered an interesting solvent-controlled switch in selectivity.[23] Whereas the Pd/P^{t}Bu$_3$ system in THF showed selectivity for chloride, switching to DMF or MeCN as the reaction solvent afforded a switch in selectivity favoring triflate (Scheme 6a). In spite of this, it remains unlikely solvation would lead to sufficiently favorable relief in distortion energy such that bisligation by P^{t}Bu$_3$ woud become operative;[19] some other species must be acting as a second ligand. On the basis of their combined experimental and computational approach, Schoenebeck et al. concluded that bisligation by P^{t}Bu$_3$ and a coordinating anion originating from added base or deprotonated boronic acid was responsible for the observed selectivity. Under this regime, a more polar solvent would better stabilize an anionic palladium transition state, thus explaining why the polar solvents DMF and MeCN led to a switch in selectivity.

Scheme 6. Solvent effect in chemodivergent Suzuki cross-coupling.[18,19,24]



However, we have observed that solvent polarity alone is a poor predictor of selectivity in this system (Scheme 6b).[24] While nonpolar solvent (toluene, THF) favor reactivity at chloride, a number of polar solvents (CH_2Cl_2, ^{i}PrOH, acetone, EtOH, MeOH, $MeNO_2$, propylene carbonate, water) showed the same preference. Other polar solvents (PhCN, NMP, MeCN, DMF, DMSO) gave reactivity at triflate. Though polar solvents were previously hypothesized to give the corresponding switch to triflate selectivity by stabilizing a bisligated anionic palladium transition state ,[23] our results showing selectivity for chloride in nonpolar *and* polar solvents suggest a different mechanistic picture. In Chapter 4, we present evidence that solvent coordination to palladium induces a switch in selectivity to favor oxidative addition at triflate.

References

1. Beaumier, E.P.; Pearce, A.J.; See, X.Y.; Tonks, I.A. Modern applications of low-valent early transition metals in synthesis and catalysis. *Nat. Chem. Rev*. **2019**, *3*, 15-34.

2. Kepp, K.P. A quantitative scale of oxophilicity and thiophilicity. *Inorg. Chem*. **2016**, *55,* 9461-9470.

3. Keim, W., Oligomerization of Ethylene to α-Olefins: Discovery and Development of the Shell Higher Olefin Process (SHOP). *Angew. Chem. Int. Ed.* **2013**, *52,* 12492-12496.

4. Sunley, G.J.; Waton, D.J., High productivity methanol carbonylation catalysis using iridium: The Cativa™ process for the manufacture of acetic acid. *Catal. Today* **2000**, *58*, 293-307.

5. Collins, R.A.; Russell, A.F.; Mountford, P., Group 4 metal complexes for homogeneous olefin polymerisation: a short tutorial review. *Appl. Petrochem. Res.* **2015**, *5*, 153-171.

6. Labinger, J.A.; Bercaw, J.E. Understanding and exploiting C—H bond activation. *Nature* **2002**, *407*, 507-514.

7. Gunsalus, N.J.; Koppako, A.; Park, S.H.; Bischof, S.M.; Hashiguchi, B.G.; Periana, R.A. Homogeneous Functionalization of Methane. *Chem. Rev*. **2017**, *117*, 8521-8573.

8. Dry, M.E., The Fischer-Tropsch process: 1950-2000. *Catal. Today.* **2002**, *71*, 277-241.

9. As evidence of the great challenges associated with elucidation of the active catalytic species in heterogeneous catalysis, Gerhard Ertl was awarded the 2007 Nobel Prize in Chemistry in large part for his work on this subject with the Haber-Bosch process—89 years after Fritz Haber was awarded the same prize for developing the process.

10. (a) Cotton, F.A., Cyclopentadienyl–metal chemistry in the Wilkinson Group, Harvard, 1952–1955. *J. Organomet. Chem.* **2001**, *637-639*, 18-26; (b) Chirik, P.J. Group 4 Transition Metal

Sandwich Complexes: Still Fresh after Almost 60 Years. *Organometallics* **2010**, *29*, 1500-1517.
11. Halpern, J. Activation of Carbon-Hydrogen Bonds by Metal Complexes: Mechanism, Kinetic, and Thermodynamic Considerations. *Inorg. Chim. Acta.* **1985**, *100*, 41-48.

12. (a) Wilkinson, G.; Rosenblum, M.C.; Whiting, M.C.; Woodward, R.B., The structure of iron bis-cyclopentadienyl. *J. Am. Chem. Soc.* **1952**, *74*, 2125-2126; (b) Fischer, E. O. and Pfab, W., Cyclopentadien-Metallkomplexe, ein neuer Typ metallorganischer Verbindungen*. Zeitschrift für Naturforschung B* **1952**, 7**,** 377-379; (c) Pfab, W.; Fisher, E.O., Zur Kristallstruktur der Di-cyclopentadienyl-verbindungen des zweiwertigen Eisens, Kobalts und Nickels. *Zeitschrift für anorganische und allgemeine Chemie* **1953**, *274*, 316-322; (d) Okuda, J., Ferrocene – 65 Years After. *Eur. J. Inorg. Chem.* **2017**, *2*, 217-219.

13 (a) Barefield, E.K.; Parshall, G.W.; Tebbe, F.N. Catalysis of Aromatic Hydrogen-Deuterium Exchange by Metal Hydrides. *J. Am. Chem. Soc*. **1970**, *92*, 5234-5235; (b) Parshall, G.W. Intramolecular aromatic substitution in transition metal complexes. *Acc. Chem. Res***. 1970**, *3*, 139-144; (c) Tebbe, F.N. and Parshall, G.W. Hydride Derivatives of Niobocene and Tantalocene. *J. Am. Chem. Soc*. **1971**, *93*, 3793-3795; (d) Klabunde, U. and Parshall, G.W. Activation of Aromatic Carbon-Hydrogen Bonds by Transition Metal Complexes. II. Substituted Benzenes. *J. Am. Chem. Soc*. **1972**, *94*, 9081-9087; (e) Foust, D.F.; Rogers, R.D.; Rausch, M.D.; Atwood, J.L. Photoinduced Reactions of $(\eta^5\text{-}C_5H_5)_2M(CO)H$ (M = Nb, Ta) and the Molecular Structure of $(\eta^5\text{-}C_5H_5)_2Ta(CO)H$. *J. Am. Chem. Soc*. **1982**, *104*, 5646-5650; (f) Shilov, A.E. *Activation of Saturated Hydrocarbons by Transition Metal Complexes*; Reidel: Boston, 1984.

14. (a) Ryabov, A.D. Mechanisms of intramolecular activation of carbon-hydrogen bonds in transition-metal complexes. *Chem. Rev*. **1990**, *90*, 403-424. For intramolecular C—H activation by tantalocenes of the C—H bonds of the Cp* ligand, see: (b) Parkin, G.; Bunel, E.; Burger, B.J.; Trimmer, M.S.; Van Asselt, A.; Bercaw, J.E. Alpha- and beta-migratory insertion and elimination processes for alkyl complexes of permethyl-scandocene and permethyltantalocene. *J. Mol. Catal***. 1987**, *41*, 21-39; (c) Antonelli, D. M.; Schaefer, W. P.; Parkin, G.; Bercaw, J.E. Synthesis and characterization of $(\eta^5\text{-}C_5Me_5)_2TaCl(THF)$, a useful synthetic precursor for the preparation of oxo, imido and methylidene derivatives of permethyltantalocene. *J. Organomet. Chem*. **1993**, *462*, 213-220; (d) Riley, P.N.; Parker, J.R.; Fanwick, P.E.; Rothwell, I.P. Formation of Tantalum "Tuck-in" Complexes by Activation of Methyl C-H Bonds in Pentamethylcyclopentadiene Groups by Carbazole Ligation. *Organometallics* **1999**, *18,* 3579-3583. For other examples of intramolecular C—H activation catalyzed by organometallic tantalum complexes, see: (e) Ballard, K.R.; Gardiner, I.M.; Wigley, D.W. Evidence for intramolecular carbon-hydrogen bond activation and the formation of a tucked-in complex of hexamethylbenzene at a tantalum(III) center. *J. Am. Chem. Soc*. **1989,** *111,* 2159-2162; (f) Vilardo, J.S.; Lockwood, M.A.; Hanson, L.G.; Clark, J.R.; Parkin, B.C.; Fanwick, P.E.; Rothwell, I.P. Intramolecular activation of aromatic C–H bonds at tantalum(V) metal centers: evaluating cyclometallation 'resistant' and 'immune' aryloxide ligation. *J. Chem. Soc., Dalton Trans*. **1997**, 3353-3362; (g) Ramirez-Contreras, R.; Bhuvanesh, N.; Ozerov, O. V. Cycloaddition and C-H Activation Reactions of a Tantalum Alkylidyne. *Organometallics* **2015**, *34*, 1143-1146.

15. For an example of the difficulty is generating reactive alkylidenes *in situ*, see: Gulyás, H.; Hayano, S.; Madarász, Á.; Pápai, I.; Sxabó, M.; Bucsai, Á.; Martin, E.; Benet-Bucholz, J., Air-stable 18-electron adducts of Schrock catalysts with tuned stability constants for spontaneous release of the active species. *Commun. Chem.* **2021**, *4*, 71.

16. (a) Gibson, V. C.; Parkin, G.; Bercaw, J. E. Synthesis and Reactivity of Permethyltantalocene Derivatives Possessing η^3-Allyl, η^2-Butadiene, η^2-Methylallene,and η^1-Alkenylidene Ligands. Model Studies for the Role of Surface Vinylidenes in the Fischer−Tropsch Hydrocarbon-Chain-Lengthening Process. *Organometallics* **1991**, *10*, 220−231; (b) Ohata, J.; Teremoto, A.; Fujita, H.; Takemoto, S.; Matsuzaka, H. Linear Hydrocarbon Chain Growth from a Molecular Diruthenium Carbide Platform. *J. Am. Chem. Soc.* **2021**, *143*, 16105-16112.

17. (a) Rehbein, S.M.; Kania, M.J.; Neufeldt, S.R., Experimental and Computational Evaluation of Tantalocene Hydrides for C–H Activation of Arenes. *Organometallics* **2021**, *40*, 2666-2677; (b)) Rehbein, S.M.; Kania, M.J.; Neufeldt, S.R., Experimental and Computational Evaluation of Tantalocene Hydrides for C–H Activation of Alkanes. *Manuscript in preparation*

18. Littke, A. F.; Dai, C.; Fu, G. C. Versatile Catalysts for the Suzuki Cross-Coupling of Arylboronic Acids with Aryl and Vinyl Halides and Triflates under Mild Conditions. *J. Am. Chem. Soc*. **2000**, *122*, 4020−4028.

19. Schoenebeck, F.; Houk, K. N. Ligand-Controlled Regioselectivity in Palladium-Catalyzed Cross-coupling Reactions. *J. Am. Chem. Soc*. **2010**, *132*, 2496−2497.

20. Recent review: Reeves, E.K.; Entz, E.D.; Neufeldt, S.R., Chemodivergence between Electrophiles in Cross-Coupling Reactions. *Chem. Eur. J.* **2021**, *27*, 6161-6177.

21. Manabe, K.; Ohba, M.; Matsushima, Y., A Repetitive One-Step Method for Oligoarene Synthesis Using Catalyst Controlled Chemoselective Cross-Coupling. *Org. Lett.* **2011***, 13*, 2436-2439.

22. Niemeyer, Z.L.; Milo, A.; Hickey, D.P.; Sigman, M.S. Parameterization of phosphine ligands reveals mechanistic pathways and predicts reaction outcomes. *Nat. Chem.* **2016**, *8*, 610-617.

23. Proutiere, F.; Schoenebeck, F., Solvent Effect on Palladium-Catalyzed Cross-Coupling Reactions and Implications on the Active Catalytic Species. *Angew. Chem. Int. Ed.* **2011**, *50*, 8192-8195.

24. Reeves, E.K.; Bauman, O.R.; Mitchem, G.B.; Neufeldt, S.R., Solvent Effects on the Selectivity of Palladium-Catalyzed Suzuki-Miyaura Couplings. *Isr. J. Chem.* **2020**, *60*, 406-409.

CHAPTER TWO

EXPERIMENTAL AND COMPUTATIONAL EVALUATION OF TANTALOCENE HYDRIDES FOR C–H ACTIVATION OF ARENES

Contribution of Authors and Co-Authors

Manuscript in Chapter Two
Author: Steven M. Rehbein
Contributions: Prepared compounds of interest. Collected ^{1}H NMR data for *in situ* monitoring or catalysis kinetics. Analyzed catalysis kinetics data. Generated figures and wrote the manuscript in preparation for submission.

Co-Author: Matthew J. Kania
Contributions: Provided insight and guidance at the late stage of the project. Prepared compounds of interest. Conducted computational analysis.

Co-Author: Sharon R. Neufeldt
Contributions: Provided insight and guidance at all stages of the project. Aided in the preparation and revising of the manuscript and figures.

Manuscript Information

Steven M. Rehbein, Matthew J. Kania, Sharon R. Neufeldt
Organometallics
Status of Manuscript:
____ Prepared for submission to a peer-reviewed journal
____ Officially submitted to a peer-reviewed journal
____ Accepted by a peer-reviewed journal
__X__ Published in a peer-reviewed journal

American Chemical Society
Submitted May 23, 2021
Published online July 14, 2021
Published in issue 9 August 9, 2021
DOI: 10.1021/acs.organomet.1c0030

ORGANOMETALLICS

pubs.acs.org/Organometallics Article

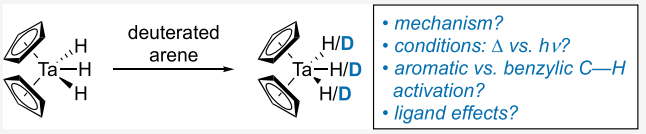
Experimental and Computational Evaluation of Tantalocene Hydrides for C−H Activation of Arenes

Steven M. Rehbein, Matthew J. Kania, and Sharon R. Neufeldt*

Cite This: *Organometallics* 2021, 40, 2666−2677 Read Online

ACCESS | Metrics & More | Article Recommendations | Supporting Information

ABSTRACT: Half a century ago, tantalocene hydrides (especially Cp_2TaH_3, where Cp = η^5-C_5H_5) were reported to catalyze H/D exchange with arenes. However, there has been very little follow-up to the seminal reports, and numerous questions about this chemistry remain unanswered. In an effort to better evaluate the potential of tantalocene hydrides for processes involving C−H activation, we have conducted a series of experimental and computational studies on these complexes. Density functional theory (DFT) calculations support a mechanism for arene C−H activation involving oxidative addition at transient Ta^{III}, rather than a σ-bond metathesis mechanism at Ta^{V}. Comparisons were made between thermal and photochemical conditions for the reaction of Cp_2TaH_3 with benzene-d_6, and H/D exchange was found to be moderately faster under thermal conditions. In a reaction with toluene, Cp_2TaH_3 activates the aromatic $C_{(sp^2)}$−H bonds but not the benzylic bonds. DFT calculations suggest that benzylic C−H activation at Ta^{III} has a barrier similar to aromatic C−H activation, but that formation of a π-complex with Cp_2TaH directs preferential aromatic C−H activation. Analogous complexes containing the less labile permethylated ligand Cp* (Cp* = η^5-C_5Me_5) were also evaluated for their ability to catalyze H/D exchange with benzene-d_6, but these complexes are less active than Cp_2TaH_3. DFT calculations indicate that the methyl groups of Cp* disfavor π-coordination of an arene to the Ta^{III} intermediate.



INTRODUCTION

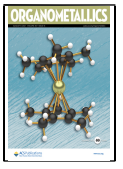
Early transition metals are underexplored as molecular catalysts for organic transformations. Compared to their later counterparts, early metals often present more significant challenges with respect to air- and functional-group sensitivity.[1] Furthermore, low-valent early transition metals are highly reducing and electropositive. As a consequence, these metals tend to be most stable in high oxidation states, and redox cycling is more difficult compared to many late transition metals.[2] Because of these characteristics, development of early transition metal catalysis lags behind the success of late metals.[3] Nevertheless, the same properties that make early metals challenging to work with also lend them unique potential as catalysts. Because they are so highly reducing, low-valent early transition metals often readily react with strong bonds such as C−H[4] or dinitrogen.[5] Furthermore, early transition metals can participate in elementary reactions that are less common with late metals (e.g., σ-bond metathesis and α-elimination).[6] As such, it is possible to imagine using early transition metals to develop novel catalytic processes that exploit unusual combinations of elementary steps.

The activation and functionalization of hydrocarbons is one area in which early transition metals show potential for unique reactivity. C−H activation is known to occur across M=X and M≡X multiple bonds (X = C or N). Examples include 1,2-addition at titanium alkylidynes[7] or at tantalum imides.[8] Alternatively, C−H activation can take place by σ-bond metathesis[6c] or by oxidative addition.[9] Basset and Copéret reported that silica-supported single-site tantalum hydrides can effect alkane coupling,[10] metathesis,[11] and hydrogenolysis[12] through mechanisms involving C−H activation at Ta^{III} by oxidative addition[13,14] or by σ-bond metathesis at Ta^{V}.[10−12] Additionally, a number of reports have described activation of hydrocarbons by tantalum ions in the gas phase.[15]

Inspired by this precedent, we have been interested in understanding how ligand environment and reaction conditions influence the reactivity of homogeneous tantalum hydrides with C−H bonds. The bent metallocene Cp_2TaH_3 (Cp = η^5-C_5H_5) was investigated in the 1970s and early 1980s for its ability to catalyze H/D exchange between arenes and D_2 (Scheme 1).[16] This reaction was proposed to proceed through oxidative addition of C−H at transient $Cp_2Ta^{III}H$, suggesting that Cp ligands are sufficiently bulky and π-accepting to stabilize electron-rich Ta^{III}. Interestingly, Cp_2TaH_3 failed to catalyze benzylic H/D exchange using toluene or *para*-xylene, even though benzylic C−H bonds are weaker and more acidic than aromatic bonds.[16d]

There has been almost no follow-up to the original publications using Cp_2TaH_3 for arene activation. As a result, the extent of this class of compound's potential for use in

Received: May 23, 2021
Published: July 14, 2021

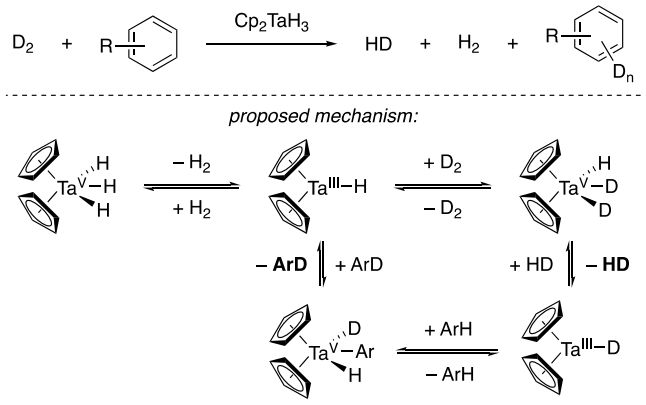


Downloaded via MONTANA STATE UNIV on December 13, 2021 at 18:52:55 (UTC).
See https://pubs.acs.org/sharingguidelines for options on how to legitimately share published articles.

ACS Publications © 2021 American Chemical Society

https://doi.org/10.1021/acs.organomet.1c00308
Organometallics 2021, 40, 2666−2677

Scheme 1. H/D Exchange Catalyzed by Cp_2TaH_3[16]



catalytic C−H activation is nebulous. In particular, several questions about the chemistry shown in Scheme 1 remain unanswered. These questions include

1. What is the mechanism of C−H activation by Cp_2TaH_3? (Hydrocarbon activation at analogous silica-supported tantalum hydrides has been proposed to occur through both oxidative addition[13,14] and σ-bond metathesis mechanisms.[10−12])
2. How do thermal[16a−d] versus photochemical[16e] conditions compare for arene C−H activation? (Both conditions have been reported in the literature.)
3. Why are benzylic $C_{(sp^3)}$−H bonds unreactive toward activation by Cp_2TaH_3?[16d]
4. How does the reactivity of tantalocene hydrides bearing less labile permethylated ligands ($CpCp^*TaH_3$ and $Cp_2^*TaH_3$, where $Cp^* = \eta^5$-C_5Me_5) compare to that of Cp_2TaH_3?

Herein, we describe a combination of computational and experimental studies that provide insights into these fundamental questions. Developing a better understanding of the chemistry between tantalocene hydrides and arenes may facilitate future exploration of these complexes' reactivity toward more challenging aliphatic hydrocarbons.

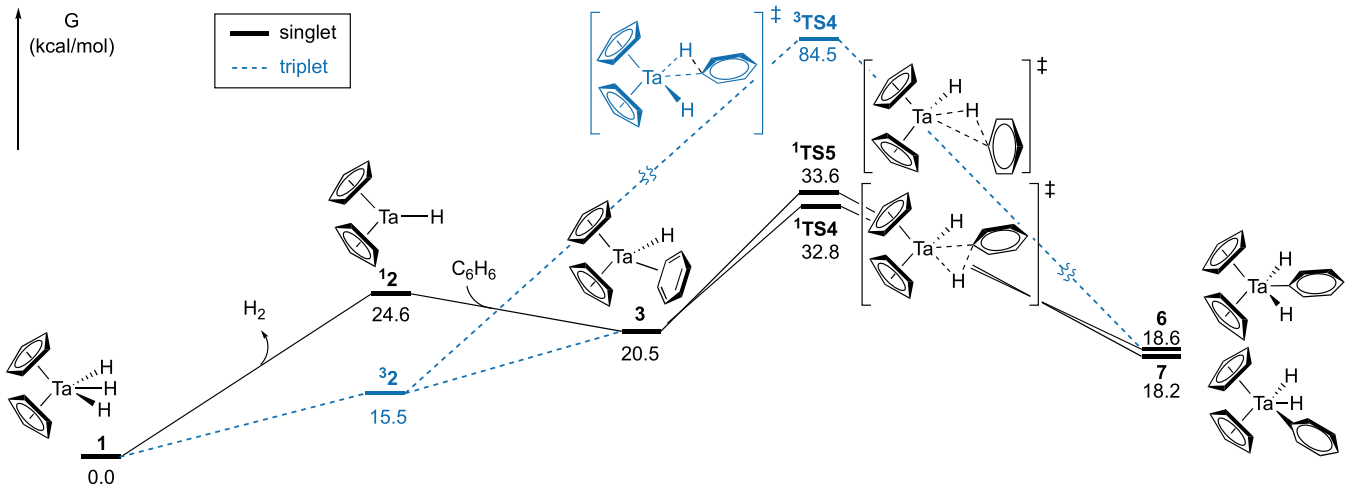
RESULTS AND DISCUSSION

In the early 1970s, Parshall and co-workers reported that both Cp_2TaH_3 and $Cp^{Me}{}_2TaH_3$ ($Cp^{Me} = \eta^5$-MeC_5H_4) catalyze H/D exchange between arenes and D_2 (or between deuterated arenes and H_2) upon heating to ~100 °C.[16a−d] This claim was based on isotope scrambling in the products observed by mass spectrometry, including HD and partially deuterated arenes (Scheme 1). The mechanism of C−H activation was proposed to proceed through a Ta^V/Ta^{III} cycle involving reductive elimination of hydrogen from Cp_2TaH_3 (or from an isotopologue) to generate Cp_2TaH followed by reversible oxidative addition of an arene C−H bond into Cp_2TaH to form Cp_2TaH_2Ar (Scheme 1). The involvement of Ta^{III} in the H/D exchange process was supported by Rausch and Atwood's 1982 report, which showed that the same process can occur under low-temperature photochemical conditions.[16e] They observed H_2, together with HD and D_2, upon photolysis of Cp_2TaH_3 in C_6D_6. The presence of H_2 in the reaction mixture is consistent with its reductive elimination from Cp_2TaH_3. Furthermore, the Ta^{III} complex $Cp_2Ta(CO)H$ was also found to catalyze photoinduced H/D exchange between arenes and hydrogen.[16e]

Density Functional Theory Calculations on the Benzene Activation Mechanism. We conducted density functional theory (DFT) calculations to investigate the mechanism of benzene activation by Cp_2TaH_3. Geometry optimizations were performed with the M06L[17] functional, the 6-31+G(d,p) basis set for carbon and hydrogen, and the LANL2DZ pseudopotential for tantalum (referred to herein as basis set 1, BS1). Energies of optimized structures were further refined at the CPCM (benzene or toluene)-M06[18]/6-311++G(2d,p)/SDD(Ta) level of theory (M06/BS2, see Computational Section for further details). The Minnesota functionals M06L and M06 were selected on the basis of prior benchmarking studies with transition metals.[17−19] We first considered the Ta^V/Ta^{III} pathway that had been proposed in the 1970s (Scheme 2).

This pathway is initiated by the endergonic reductive elimination of H_2 from Cp_2TaH_3 (**1**) to provide Cp_2TaH (**2**). At the level of theory used and with most other functionals that we evaluated (see Supporting Information), this Ta^{III} complex is predicted to be more stable in the triplet electron

Scheme 2. Calculated Pathways for the Reaction of Cp_2TaH_3 with Benzene via an Oxidative Addition Mechanism for C−H Activation



https://doi.org/10.1021/acs.organomet.1c00308
Organometallics 2021, 40, 2666−2677

configuration (S = 1, ^{3}**2**) than as a singlet (S = 0, ^{1}**2**).[12,14,20] Interestingly, some prior DFT studies on silica-supported Ta^{III} monohydrides predicted that the closed shell singlet is the more stable ground-state configuration.[12] The discrepancy between our calculations on Cp_2TaH and those on a silica-supported analogue appears to be a consequence of the supporting ligand structures used, rather than resulting from the DFT method choice (see Supporting Information).[20c] However, DFT has known limitations to making accurate predictions about electronic configurations, and different methods can be biased toward favoring either high or low spin states (see Supporting Information).[21]

On both the triplet and singlet potential energy surface, loss of H_2 is barrierless at the M06L/BS1 level of theory. Specifically, no energy maximum is detected in a relaxed scan of the potential energy along the reaction coordinate for H−H bond formation from Cp_2TaH_3 (see Supporting Information). The absence of a detectable energy maximum suggests that any activation energy associated with H_2 reductive elimination corresponds to an entropic barrier and is likely very small.[22,23]

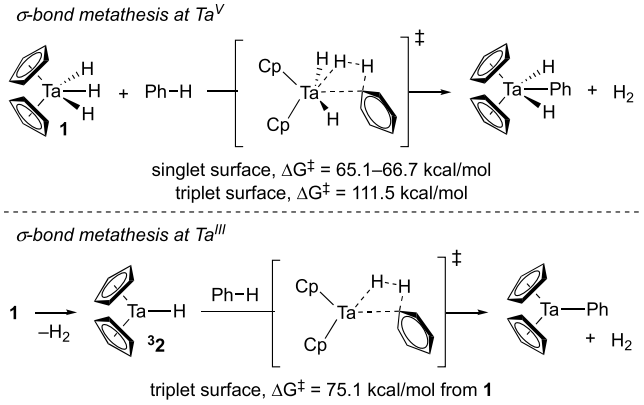
Although high spin ^{3}**2** is calculated to be more stable than low spin ^{1}**2**, the energetics of subsequent steps on the triplet energy surface are unreasonably high, suggesting that the catalytic reaction occurs on the singlet energy surface. Complex ^{1}**2** can interact with benzene to form π-complex **3**. No such π-complex can be located with spin = 1. Indeed, the Dewar−Chatt−Duncanson model for π-complexation (see Supporting Information) gives tantalum d^0 (Ta^V) character, which would preclude location of spin density on tantalum. On the singlet energy surface, π-complexation is exergonic relative to ^{1}**2**. Interestingly, the predicted favorability of π-complexation is method-dependent (see Supporting Information). Other dispersion-containing methods (e.g., B3LYP-D3) also predict that the π-complex is more stable than ^{1}**2**; however, this step is predicted to be endergonic with methods that do not include dispersion (e.g., B3LYP). The difference in predictions with and without dispersion suggests that stabilization of the π-complex can largely be attributed to attractive London dispersion interactions. Notably, even when dispersion is included, the π-complex has considerably higher energy than the starting Ta^V trihydride. However, low concentrations of H_2 and high concentrations of arenes could promote the formation of **3** under experimental conditions.

From the π-complex, oxidative addition of an aromatic C−H bond is predicted to proceed through a barrier of about 12−14 kcal/mol measured from the high-energy intermediate **3**. Two low-spin transition structures were located with nearly identical energies: one involving C−H activation to place Ph at an internal position (^{1}**TS4** resulting in **6**) and the other placing Ph at the lateral position (^{1}**TS5** resulting in **7**). Overall, the activation barrier to C−H activation through either transition structure is about 33 kcal/mol, as measured from **1**.

On the triplet energy surface, an oxidative addition transition structure placing phenyl at the internal position (^{3}**TS4**) is predicted to be prohibitively high in energy, and an oxidative addition transition structure that places phenyl at a lateral position could not be located. These results indicate that tantalum has too much Ta^V/d^0 character during reaction with benzene for triplet transition states to be energetically accessible. As such, although both ^{1}**2** and ^{3}**2** are likely formed, only ^{1}**2** lies on a productive pathway to benzene activation.

We also considered σ-bond metathesis mechanisms for C−H activation (Scheme 3). σ-Bond metathesis is a common

Scheme 3. σ-Bond Metathesis Mechanisms for Benzene C−H Activation Are Predicted to be Prohibitively High Energy



elementary reaction of d^0 metals,[6c] and this type of pathway was previously proposed for C−H activation of butane at silica-supported Ta^V trihydrides.[12,20c] Several transition structures for benzene activation by σ-bond metathesis at both Cp_2TaH_3 and Cp_2TaH were located on the singlet and triplet potential energy surfaces, respectively. However, all of the transition structures that we located are predicted to be very high energy (65−112 kcal/mol relative to **1**; see Supporting Information). As such, our calculations suggest that C−H activation is more likely to proceed through oxidative addition at Ta^{III} than by σ-bond metathesis.[24]

Thermal H/D Exchange between Cp_2TaH_3 and C_6D_6. As described above, H/D exchange between Cp_2TaH_3 and deuterated benzene has been previously reported.[16a,e] We first sought to reproduce this observation in order to establish a baseline for comparison to H/D exchange under different conditions, using other hydrocarbons, or with other tantalum hydrides.

Cp_2TaH_3 was prepared through a three-step route previously reported by Nikonov et al.[25] In our hands, this route yields Cp_2TaH_3 as a white solid that retains its color even after storage for 12 months under nitrogen. In contrast, our efforts to employ an alternative one-pot route[16d] led to a product that takes on a pink-to-red impurity within 14 days of storage. This impurity is NMR-silent[26] and can only be removed by repeated sublimations. As such, Nikonov's three-step route to Cp_2TaH_3 is preferred.

In an initial experiment, Cp_2TaH_3 (0.012 mmol) was combined with C_6D_6 (~500 equiv) and cyclohexane (NMR internal standard, 1 equiv) in a medium wall high-pressure sealed NMR tube (9″ length, 3.46 mm internal diameter) under N_2 (60 psi).[27] Consistent with previous reports,[16c,d,26b] the hydride signals of Cp_2TaH_3 display an AB_2 pattern in the upfield region of the ^{1}H NMR spectrum (Figure 1A). The protons of the Cp rings appear as a singlet at 4.76 ppm (see Supporting Information). The internal hydride appears as a triplet at −1.61 ppm, while the two lateral hydrides are represented by a doublet at −3.01 ppm. After heating at 100 °C for 1 h, new hydride signals were detected, assigned to the partially deuterated analogues of Cp_2TaH_3 (Figure 1B). The internal hydride of monodeuterated **1-d$_1$a** is shifted upfield by 51 ppb and appears as a broad doublet (the ^{1}H−D coupling

https://doi.org/10.1021/acs.organomet.1c00308
Organometallics 2021, 40, 2666−2677

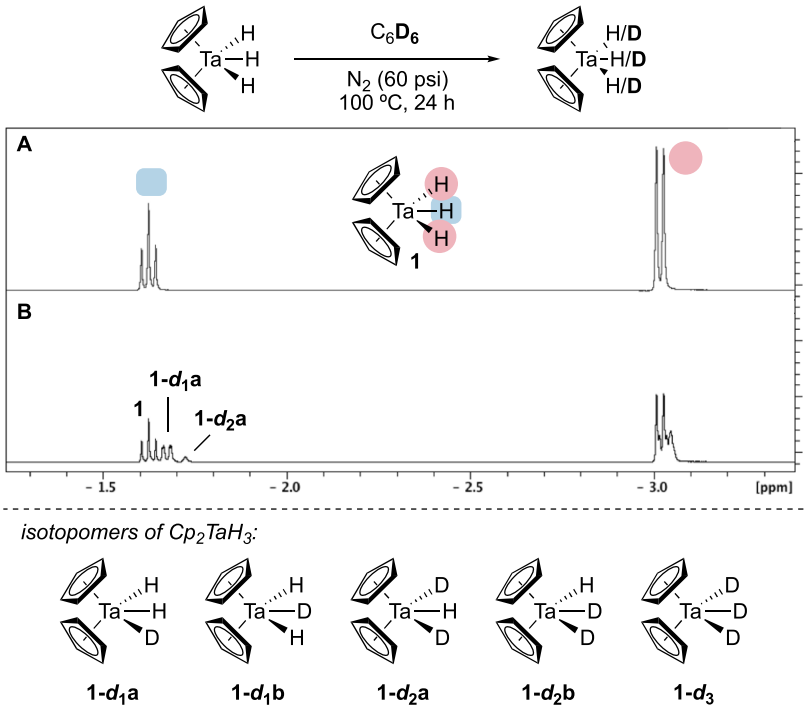


Figure 1. Hydride region of the ^{1}H NMR spectrum of Cp_2TaH_3 (A) before and (B) after heating for 1 h in the presence of C_6D_6. Acquired on a 500 MHz instrument.

constant is too small for the signal to be resolved into a doublet of 1:1:1 triplets). The internal hydride of dideuterated **1-d_2a** is shifted upfield by 99 ppb relative to Cp_2TaH_3 and appears as a broad singlet. The lateral hydride signals of the various mono- and dideuterated isotopologues overlap each other. There is no change in the appearance of the Cp signal at 4.76 ppm, suggesting that H/D exchange does not take place on this ligand.[16d] However, it is unknown whether isomers containing deuterated Cp rings would be resolved by NMR.

In subsequent experiments, the rates of H/D exchange were quantified by monitoring reactions over a period of at least 6 h. ^{1}H NMR spectra were acquired approximately once per hour. In each spectrum, the integrations of the internal and lateral hydride signals from all observed isotopologues were summed together (the regions from −1.58 to −1.75 and from −2.98 to −3.01 ppm shown in Figure 1B, represented by the term "[hydride]" below). The change in [hydride] over time is thus the negative of the uncorrected rate of H/D exchange

$$r_{\text{uncorr}} = -\frac{\text{d[hydride]}}{\text{d}t}$$

However, it is possible that some of the disappearance in hydride signals could be due to other decomposition pathways for Cp_2TaH_3. To account for this, the extent of Cp_2TaH_3 decomposition was quantified by measuring the decrease in Cp signal integration relative to the cyclohexane internal standard (this approach assumes that erosion of the Cp signal is not due to deuteration at Cp).

$$r_{\text{decomp}} = -\frac{\text{d[Cp]}}{\text{d}t}$$

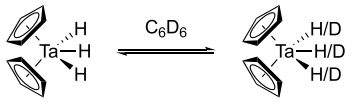
Finally, the rate of H/D exchange was corrected to account for decomposition of the tantalum complex. The corrected observed rate, denoted as r_{corr}, is thus described by the following equation

$$r_{\text{corr}} = r_{\text{uncorr}} - r_{\text{decomp}}$$

As shown in Table 1 entry 1, the rate of H/D exchange under the conditions described above is about 5× the rate of decomposition.

The extent of unproductive decomposition poses a severe barrier to the future development of Cp_2TaH_3 as a catalyst for hydrocarbon activation. However, we have found that the behavior of Cp_2TaH_3 is affected by its starting purity. In particular, although sublimation of Cp_2TaH_3 does not change

Table 1. Rate of Tantalocene Decomposition and H/D Exchange with C_6D_6[a]

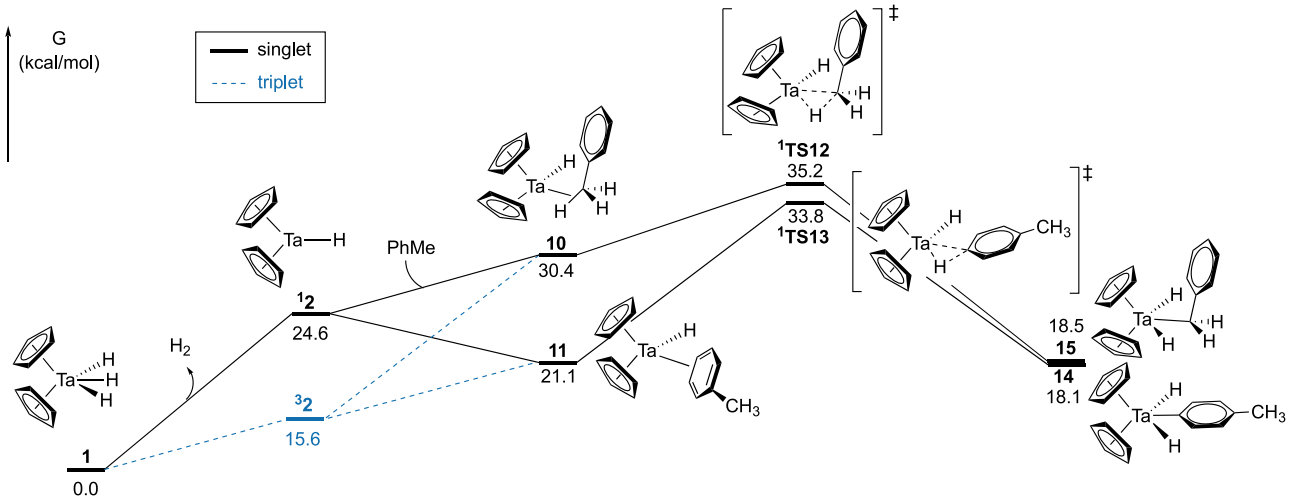


entry	complex	conditions[b]	r_{decomp}[c]	r_{corr}[d]	r_{rel}[e]
1	**1**	Δ, N_2	5.16(34)	23.95(93)	1.00
2[f]	**1**	Δ, N_2	5.57(61)	24.28(240)	1.01
3	**1**	$h\nu$, N_2	4.61(26)	16.85(59)	0.70
4	**1**	Δ, D_2	3.78(163)	1.63(30)	0.07
5	**1**	$h\nu$, D_2	2.77(18)	7.01(16)	0.29
6	**8**	Δ, N_2	1.11(22)	4.84(60)	0.20
7	**9**	Δ, N_2	0.00	0.00	0.00

[a]All experiments were performed in triplicate, and the results are an average of the collected data. Uncertainties in r_{decomp} and r_{corr} values are reported in parentheses. Reactions were followed for 6 h. [b]Δ signifies heating at 100 °C, $h\nu$ signifies irradiation at 350 nm at 35 °C; and N_2 and D_2 = atmosphere pressurized to 60 psi. [c]r_{decomp} describes the rate of catalyst decomposition, in units of $M \times h^{-1} \times 10^{-7}$. [d]$r_{\text{corr}}$ describes the rate of catalytic H/D exchange following correction accounting for decomposition, in units of $M \times h^{-1} \times 10^{-7}$. [e]$r_{\text{rel}}$ describes relative values of r_{corr} with respect to those in entry 1 [f]Tantalocene not sublimed prior to experiments.

https://doi.org/10.1021/acs.organomet.1c00308
Organometallics 2021, 40, 2666−2677

Scheme 4. Calculated Pathways for the Reaction of Cp_2TaH_3 with Toluene via an Oxidative Addition Mechanism for Aromatic or Benzylic C−H Activation



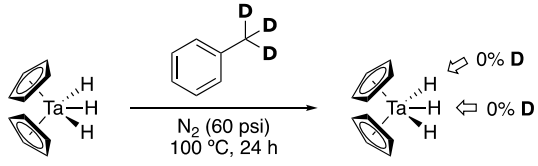
the appearance of its ^{1}H NMR spectrum, it leaves behind a quantity of off-white solids that display poor solubility in aromatic solvents. Apparently, sublimation separates Cp_2TaH_3 from NMR silent impurities (likely tantalum oxides). Although similar average rates of decomposition and H/D exchange are observed for the sublimed and unsublimed materials (Table 1 compare entries 1 and 2), variability in rate data is appreciably higher for the unsublimed complex.

Comparison of Thermal and Photochemical Conditions for H/D Exchange. H/D exchange between benzene and D_2 catalyzed by Cp_2TaH_3 has also been reported under low-temperature photochemical conditions.[16e] However, these conditions had not been directly compared to the thermal conditions. In order to evaluate the relative efficiency of thermal and photochemical conditions, we conducted photochemical H/D exchange studies analogous to those described in the section above. Cp_2TaH_3 (0.012 mmol) was combined with C_6D_6 (~500 equiv) and cyclohexane (NMR internal standard, 1 equiv) in a medium wall high-pressure sealed NMR tube (9″ length, 3.46 mm internal diameter) under N_2 (60 psi).[27] The reaction mixture was irradiated with 350 nm light at a constant temperature of 35 °C.[28,29] Under these conditions, the rate of H/D exchange is moderately slower than the thermal conditions at 100 °C (compare entries 1 and 3 of Table 1). The rate of catalyst decomposition under thermal and photochemical conditions is similar. However, whereas the reaction mixture remains colorless during thermal H/D exchange, the photochemical conditions induce a deep red color that persists for several hours upon removal from the light source.[30]

In contrast to our photochemical studies under N_2, prior literature reports described both thermal and photochemical reactions of Cp_2TaH_3 with protio-arenes under a D_2 atmosphere.[16] Furthermore, preparation of Cp_2TaD_3 has been described by an H/D exchange process involving heating Cp_2TaH_3 in C_6D_6 under D_2.[31] Interestingly, we observed that deuterium incorporation at Ta is actually *slower* under an atmosphere of D_2 compared to an equivalent initial pressure of N_2, at least in our NMR-scale experiments that allow for only a small headspace volume. This phenomenon is observed under both thermal (Table 1 entry 4) and photochemical conditions (entry 5), although it is more pronounced under the thermal conditions. This result is surprising because capture of the Ta^{III} intermediate Cp_2TaH by D_2 is expected to be fast and would lead to deuteration of tantalum. The attenuated rate of H/D exchange at Ta under D_2 may suggest that (1) reductive elimination of H_2 from Cp_2TaH_3 is kinetically inhibited under an atmosphere of D_2 or (2) dissociation of H_2 from a putative $Cp_2TaH(H_2)$ intermediate (not located computationally) is slower under D_2 pressure, thereby more strongly favoring the Cp_2TaH_3 resting state.

Overall, the results suggest that H/D exchange between Cp_2TaH_3 and C_6D_6 is moderately faster at 100 °C than under photochemical conditions at 30 °C. Furthermore, at the reaction volume investigated, deuterated isotopologues of Cp_2TaH_3 are formed faster under an atmosphere of N_2 (60 psi), where the only deuterium source is C_6D_6, than under an equivalent pressure of D_2.

Activation of Toluene. We next turned to understanding the lack of reactivity of benzylic C−H bonds toward activation by Cp_2TaH_3. In previously described studies of the reaction between Cp_2TaH_3 and toluene in the presence of D_2, H/D exchange was reported to occur only at the aromatic positions, with no deuterium incorporation at the benzylic site.[16d] We reproduced this result (see Supporting Information) and also conducted the complementary experiment shown in eq 1. In this experiment, Cp_2TaH_3 was reacted with toluene-α,α,α-d_3. No deuterium incorporation at tantalum was detected by NMR after 24 h at 100 °C.



(1)

The lack of reactivity of a weak benzylic C−H site is potentially discouraging toward the possibility of using homogeneous tantalum complexes for activating aliphatic hydrocarbons. However, we reasoned that understanding the poor reactivity of the benzylic position might provide insights into whether this limitation might be overcome.

Interestingly, DFT calculations suggest that the barrier to oxidative addition of a benzylic C−H bond of toluene at Cp_2TaH is comparable to the barrier for reaction of an

https://doi.org/10.1021/acs.organomet.1c00308
Organometallics 2021, 40, 2666−2677

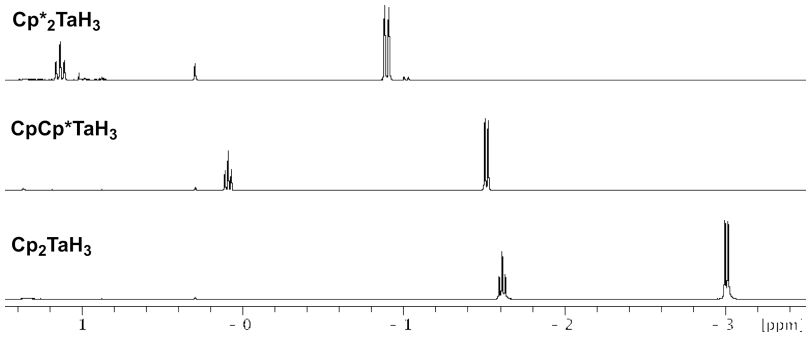
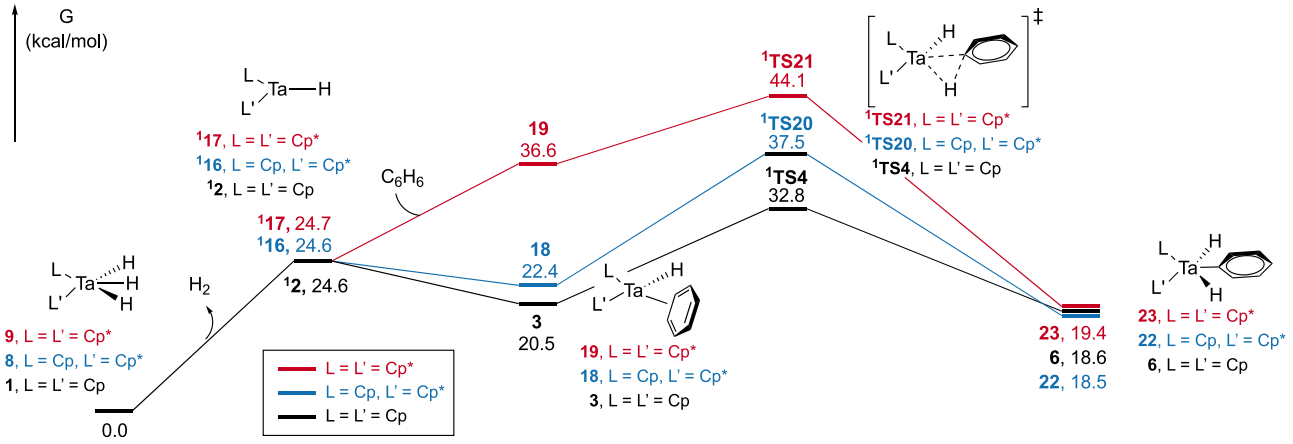


Figure 2. Comparison of the hydride regions of the ^{1}H NMR spectra of $Cp^*_2TaH_3$, $CpCp^*TaH_3$, and Cp_2TaH_3.

Scheme 5. Comparison of Calculated Free Energy Surfaces for the Reaction of Cp_2TaH_3 and Permethylated Analogues with Benzene via an Oxidative Addition Mechanism



aromatic C−H bond (compare ^{1}**TS12** and ^{1}**TS13**, Scheme 4, and see Supporting Information for other higher energy transition structures). σ-Bond metathesis transition structures for benzylic C−H activation were also located, but their energies are much higher than the oxidative addition mechanism (see Supporting Information). Despite the similarity between the predicted barriers to benzylic and aromatic C−H activation, a key difference between the reaction at the two sites is the energy of the complex immediately preceding oxidative addition. Formation of a π-complex (**11**) is exergonic from ^{1}**2** and precedes oxidative addition of an aromatic C−H bond. In contrast, the σ-complex (**10**) that precedes benzylic C−H activation is high energy. Similar to π-complexation, a σ-complex could only be located on the singlet energy surface. As such, the π-complex is expected to exist in much higher concentration than the σ-complex under the reaction conditions, which enables aromatic C−H activation to outcompete benzylic activation. Arene π-complexation to coordinatively unsaturated metal centers is typically stabilizing, and is known to often precede and direct C−H activation.[32,33]

Importantly, the similar calculated $\Delta G^{\ddagger}$ values for reaction at aromatic and benzylic C−H bonds suggest that oxidative addition of $C_{(sp^3)}$−H bonds at Ta^{III} may yet be feasible in the absence of competing aromatic bonds. Starting from a tantalocene hydride like Cp_2TaH_3, aliphatic C−H activation would be most likely to succeed under conditions where H_2 is removed from reaction to drive conversion of Cp_2TaH_3 to Cp_2TaH.

H/D Exchange between $CpCp^*TaH_3$/$Cp^*_2TaH_3$ and C_6D_6. Because the data suggest that Cp_2TaH_3 decomposes at a significant rate even under the optimal thermal conditions, we were interested in considering permethylated analogues of this compound. These analogues have been reported to be more stable and to have better solubility properties than Cp_2TaH_3.[34] However, to our knowledge, neither $Cp^*_2TaH_3$ nor Cp^*CpTaH_3 have been investigated for their ability to activate C−H bonds ($Cp^* = \eta^5$-C_5Me_5).

$Cp^*_2TaH_3$ and Cp^*CpTaH_3 were prepared through previously described divergent routes that involve common intermediates.[26c,34f] Like Cp_2TaH_3, both permethylated analogues exhibit an AB_2 splitting pattern in the hydride region of their ^{1}H NMR spectra (Figure 2). The hydride signals are shifted downfield with increasing methylation on the cyclopentadienyl rings.[35]

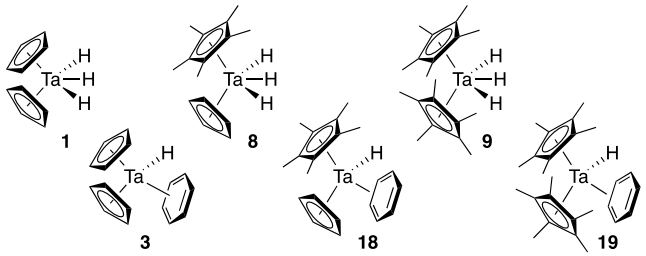
The possibility for the permethylated complexes to activate benzene was investigated. When $CpCp^*TaH_3$ was heated to 100 °C in C_6D_6 under a N_2 atmosphere, H/D exchange was observed based on the change in the hydride signals of the ^{1}H NMR spectrum. Furthermore, as expected, this complex displays greater stability toward decomposition than the parent complex Cp_2TaH_3: the decomposition rate of $CpCp^*TaH_3$ is about one-fifth of that of Cp_2TaH_3 (Table 1, entry 6). Increased catalyst stability has been noted previously upon permethylation of cyclopentadienyl ligands[34] due to preclusion of a ring α-hydrogen shift[34c] (possibly via an η^5−η^1 hapticity slip).[36] However, the pentamethyl complex is also less active toward benzene activation; the rate of deuterium incorporation at tantalum is 5× slower than that observed for Cp_2TaH_3.

https://doi.org/10.1021/acs.organomet.1c00308
Organometallics 2021, 40, 2666−2677

In keeping with a trend that permethylation increases stability while decreasing reactivity toward C−H activation, no reaction was observed with $Cp^*_2TaH_3$. Under the conditions in Table 1, this complex neither reacts with C_6D_6 nor decomposes through other routes under the applied conditions (entry 7).[37]

To better understand the decreased catalytic activity of the permethylated complexes, we conducted DFT calculations on benzene activation with $CpCp^*TaH_3$ (**8**) and $Cp^*_2TaH_3$ (**9**). Scheme 5 compares the resulting energy values to those of the corresponding reaction using Cp_2TaH_3. Although reductive elimination of H_2 remains barrierless at this level of theory for both $CpCp^*TaH_3$ and $Cp^*_2TaH_3$, the activation barriers for oxidative addition of Ph−H at Ta^{III} are higher with increased methylation of the ligands (compare structures ^{1}**TS4**, ^{1}**TS20**, and ^{1}**TS21**). These results are consistent with a steric argument for the decreased reactivity of permethylated tantalocene hydrides and qualitatively match our experimental observations. Furthermore, in contrast to the results with the unmethylated and the pentamethylated complex, formation of a π-complex between Cp^*_2TaH and benzene (**19**) is no longer stabilizing relative to low spin Cp_2TaH. The rationale for this observation appears to be sterics; π-coordination of benzene to Cp^*_2TaH leads to greater distortion of the $[Cp^*_2Ta]$ geometry than observed in the analogous reaction of Cp_2TaH or $CpCp^*TaH_3$. Table 2 compares the calculated geometries of the π-complexes to their corresponding Ta^V trihydride precursors. If the Ta^V trihydrides are assumed to have "ideal" bent sandwich geometries[38] (an assumption based on their experimental stability), increased deviation from these geometries upon formation of a π-complex is consistent with decreased stability of the π-complex. Indeed, the angle between cyclopentadienyl planes in π-complexes **3** and **18** is only ~9° larger than in the corresponding Ta^V trihydrides. However, this angle increases by almost 15° in π-complex **19** compared to $Cp^*_2TaH_3$. Additionally, the average distance between Ta and the Cp* ring centroid increases by 0.05 Å in π-complex **19**, whereas the change in this parameter is negligible in the unmethylated or pentamethylated π-complexes **3** and **18**. The increased distortion of the decamethylated π-complex **19** compared to $Cp^*_2TaH_3$ reflects the steric demand on the methyl groups in order to accommodate an incoming arene.

Table 2. Calculated Geometric Parameters for $LL'TaH_3$ and the Corresponding Benzene π-Complexes



L	L′	complex	Ta−L[a]	ΔTa−L[b]	∠L/L′[c]	Δ∠L/L′[d]
Cp	Cp	**1**	2.065	−0.005	36.2	9.7
		3	2.060		45.9	
Cp	Cp*	**8**	2.072	0.008	38.0	8.6
		18	2.080		46.6	
Cp*	Cp*	**9**	2.088	0.046	30.9	14.5
		19	2.134		45.4	

[a]Average distance (in Å) between Ta and cyclopentadienyl ligand centroids. [b]Change in the average distance between Ta and L/L′ centroids upon conversion of $LL'TaH_3$ to the corresponding π-complex. [c]Angle between cyclopentadienyl planes (in degrees). [d]Change in the angle between cyclopentadienyl planes upon conversion of $LL'TaH_3$ to the corresponding π-complex.

Taken together, the experimental and computational data suggest that the increased stability of the permethylated tantalocene hydrides is counterbalanced by lower catalytic activity. The increased steric demand of Cp* ligands, compared to Cp, raises the energy of the π-complexes and of the oxidative addition transition structures.

CONCLUSIONS

This work addressed several fundamental questions about the reaction of tantalocene hydrides with arenes. These questions were presented in the Introduction, and our findings are summarized below.

1. What is the mechanism of C−H activation by Cp_2TaH_3?

Our DFT calculations strongly support an oxidative addition mechanism for arene activation, rather than a σ-bond metathesis mechanism. The favored mechanism involves reductive elimination of H_2 to provide $Cp_2Ta^{III}H$, which is oxidized back to Ta^V upon reaction with a C−H bond. Although $Cp_2Ta^{III}H$ is predicted to be more stable in a high-spin (triplet) electron configuration, its reaction with arenes appears to take place on the singlet energy surface.

2. How do thermal versus photochemical conditions compare for arene C−H activation?

Reaction of Cp_2TaH_3 with C_6D_6 can occur under thermal conditions (100 °C) or photochemical conditions (35 °C, 350 nm). H/D exchange is moderately faster under the thermal conditions (r_{rel} = 1.0 for thermal vs 0.7 for photochemical). The difference in the rate of catalyst decomposition is approximately proportional to the difference in the H/D exchange rate. As such, the photochemical conditions do not offer any particular advantage for H/D exchange with benzene unless low temperatures are deemed desirable.

3. Why are benzylic $C_{(sp^3)}$−H bonds unreactive toward activation by Cp_2TaH_3?

DFT calculations suggest that the barrier to activation of a benzylic C−H bond is only slightly higher than the barrier for activation of an aromatic C−H bond. However, formation of a π-complex between toluene and Cp_2TaH is exergonic, whereas a σ-complex between Cp_2TaH and a benzylic C−H bond is endergonic. The stable π-complex likely directs C−H activation at an aromatic C−H bond, such that aromatic C−H activation outcompetes benzylic activation. Activation of aliphatic hydrocarbons may be feasible in the absence of π-coordinating arenes.

4. How does the reactivity of more readily handled permethylated tantalocene hydrides ($CpCp^*TaH_3$ and $Cp^*_2TaH_3$, where Cp* = η^5-C_5Me_5) compare to that of Cp_2TaH_3?

The penta- and decamethylated analogues of Cp_2TaH_3 are more stable than Cp_2TaH_3, as evidenced by a slower rate of decomposition upon heating in C_6D_6. However, their slower decomposition is counterbalanced by a correspondingly slower rate of H/D exchange with C_6D_6. In fact, $Cp^*_2TaH_3$ displays no catalytic activity (nor decomposition) at all upon heating in

https://doi.org/10.1021/acs.organomet.1c00308
Organometallics 2021, 40, 2666−2677

C_6D_6 at 100 °C for several hours. The results of DFT calculations are consistent with a steric explanation for the lack of reactivity of $Cp^*_2TaH_3$. In particular, the [Cp^*_2Ta] framework undergoes more extensive unfavorable distortion upon π-coordination compared to the corresponding [Cp_2Ta] or [CpCp*Ta] scaffolds.

The use of early transition metals for hydrocarbon activation is attractive because of their high reactivity toward inert bonds. Although homogeneous tantalum hydrides are potential candidates for catalytic hydrocarbon upgrading, strategies to enhance the stability of such complexes without detracting from their activity will be necessary in order to realize their potential as C−H activation catalysts. Furthermore, activation of $C_{(sp^3)}$−H bonds by homogeneous tantalocene hydrides remains elusive.

EXPERIMENTAL SECTION

General Materials and Methods. Sodium bis(trimethylsilyl)-amide and *tert*-butylamine were obtained from Acros Organics and used as received. Methyl iodide and pyridine were obtained from Acros Organics in ACROSeal bottles and used as received. Dicyclopentadiene was obtained from Acros Organics and passed across a short silica plug to remove water and stabilizer prior to use. Sodium metal (foil-wrapped sticks in mineral oil) was obtained from Acros Organics and washed with copious hexanes prior to use. $TaCl_5$ was obtained from Acros Organics and purified by sublimation prior to use. Di-*n*-butyl ether, sodium metasilicate, and triphenyl phosphite were obtained from Alfa Aesar and used as received. Potassium hydride (30% w/w in mineral oil) was obtained from Alfa Aesar, washed with copious hexanes, and then dried under high vacuum before use. Isotopically labeled compounds (C_6D_6, $CDCl_3$, D_2, DMSO-d_6, and toluene-α,α,α-d_3) were obtained from Cambridge Isotopes. Dichloromethane, diethyl ether (Et_2O), pentane, tetrahydrofuran (THF), and toluene were obtained from Fisher Chemical, degassed, and dried on a JC Meyer solvent system prior to use. Magnesium turnings and tri-*n*-butyltin chloride were obtained from Oakwood Chemical and used as received. Trimethylphosphine was either prepared according to a procedure adapted from the literature (*vide infra*)[39] or purchased from Strem and used as received. 1,2,3,4,5-Pentamethylcyclopentadiene and lithium aluminum hydride were obtained from TCI America and used as received. Unless otherwise noted, all operations were performed in a nitrogen-filled glovebox or using air-free techniques in oven-dried glassware. NMR spectra were recorded at 298 K on a Bruker DRX 500 MHz (500.233 MHz for ^{1}H) spectrometer. Elevated-pressure ^{1}H NMR experiments were performed in 9 in. Wilmad Glass medium-wall high-pressure precision NMR tubes. ^{1}H NMR chemical shifts are reported in parts per million (ppm) relative to TMS, with the residual solvent peak used as an internal reference [$CHCl_3$ (7.26 ppm), C_6D_5H (7.16 ppm), and DMSO-d_5 (2.50 ppm)].

General Procedure for Measuring H/D Exchange Rates by ^{1}H NMR. In a 4 mL vial within a glovebox, tantalocene trihydride (0.2 mol % relative to arene) was fully dissolved in a solution of deuterated arene (1.80 mL) containing cyclohexane (0.2 mol % relative to arene). The resulting solution was divided equally (0.60 mL each) into three medium-wall high-pressure precision NMR tubes (Wilmad, 9″ length, 3.46 mm internal diameter), and the tubes were sealed with Teflon stopcocks and removed from the glovebox. One at a time, the tubes were connected to a Schlenk line and pressurized to 60 psi (4.14 bar) with the desired gas. In experiments using H_2 or D_2, the tube was immersed in liquid nitrogen until the contents were frozen (about 1 min) and then evacuated and refilled three times with the desired gas, sealed, and warmed to room temperature in a water bath (about 2 min). In experiments using a nitrogen atmosphere, low-temperature evacuation−refill cycles were unnecessary as the headspace of the tube was already filled with nitrogen from the glovebox.[40] Initial ^{1}H NMR spectra (500 MHz, 32 scans, D1 relaxation delay = 10 s) were obtained of each sample (time = 0 h), and the samples were heated in a Chemglass NMR tube reaction heating block or irradiated at 350 nm in a Rayonet RPR-1000 photochemical reactor for a total of 6 h (not including breaks for acquiring NMR spectra). NMR spectra were acquired approximately every hour (exact times were recorded and used during analysis of the results). During processing, the integration values of all signals were standardized relative to the cyclohexane signal (the cyclohexane signal integration was set to 10). Integration values were then normalized by multiplying the integral by a scalar value to correct for the actual initial concentrations at t = 0.

*Synthesis of NaCp·1/3 THF (**24**).* The title compound was prepared according to a procedure adapted from the literature.[41] Sodium (2.00 g, 87.0 mmol) was added to dicyclopentadiene (160 mL), and the mixture was heated at 160 °C for 24 h until hydrogen evolution ceased and no sodium remained. The copious white solid was collected by vacuum filtration. This solid was heated in toluene (60 mL) and THF (6 mL) at reflux for 1 h, after which it was collected by vacuum filtration, washed with copious pentane, and dried *in vacuo* to give a free-flowing off-white solid (6.78 g, 60.5 mmol, 69% yield). Spectral data are consistent with those previously reported.[41]

*Synthesis of Ta(=NCMe$_3$)Cl$_3$(py)$_2$ (**25**).* The title compound was prepared according to a procedure adapted from the literature.[25c] *tert*-Butylamine (5.9 mL, 56 mmol) and pyridine (20.0 mL, 250 mmol) were added sequentially to a stirred heterogeneous mixture of freshly sublimed $TaCl_5$ (10.00 g, 27.9 mmol) and Na_2SiO_3 (6.84 g, 56.0 mmol) in toluene (80 mL) and Et_2O (20 mL). The mixture was stirred for 18 h, after which it was filtered over Celite. The Celite plug was washed with toluene, and the combined filtrates were concentrated *in vacuo* to give an opaque yellow solid. Recrystallization from dichloromethane/pentane at −25 °C gave large yellow crystals after 5 d (8.04 g, 56% yield). An additional product can be obtained from the same recrystallization liquor with additional time and pentane additions. Spectral data are consistent with those previously reported.[25c]

*Synthesis of Cp$_2$Ta(=NCMe$_3$)Cl (**26**).* The title compound was prepared according to a procedure adapted from the literature.[25b] While cooling to −84 °C,[42] a solution of NaCp·1/3 THF (1.88 g, 16.88 mmol, 2.1 equiv) in Et_2O (60 mL) and THF (15 mL) was added to a heterogeneous solution of Ta(=NCMe$_3$)Cl$_3$(py)$_2$ (4.13 g, 8.00 mmol, 1.0 equiv) in Et_2O (270 mL). The mixture was allowed to slowly warm to room temperature and stirred for 18 h, after which solvent removal *in vacuo* gave an opaque red solid. Extraction into pentane (3 × 50 mL) and concentration of the combined extracts gave a deep red oily-to-waxy product (2.79 g, 83% yield). Spectral data are consistent with those previously reported.[25b]

*Synthesis of Cp$_2$TaH$_3$ (**1**).* The title compound was prepared according to a procedure adapted from the literature.[25a] While cooling to −84 °C, a solution of $Cp_2Ta(=NCMe_3)Cl$ (2.79 g, 6.68 mmol, 1.0 equiv) in Et_2O (65 mL) was added to a suspension of $LiAlH_4$ (1.02 g, 26.8 mmol, 4.0 equiv) in Et_2O (65 mL). The mixture was allowed to slowly warm to room temperature and stirred for 18 h, after which it was cooled to 0 °C and degassed deionized water was added dropwise (1.96 mL, 108 mmol, 16 equiv). Extraction of the mixture into Et_2O (3 × 50 mL) and concentration of the combined extracts gave an off-white solid (0.90 g, 43% yield). Spectral data are consistent with those previously reported.[25a]

Synthesis of NaCp (**27**).* The title compound was prepared according to a procedure adapted from the literature.[43] 1,2,3,4,5-Pentamethylcyclopentadiene (7.43 g, 54.6 mmol, 1.0 equiv) was added dropwise to a stirred solution of sodium bis(trimethylsilyl)-amide (9.17 g, 50.0 mmol, 0.92 equiv) in Et_2O (45 mL), and the opaque suspension was allowed to stir for 18 h. After this time, the solid product was collected by vacuum filtration, washed with Et_2O (2 × 5 mL) and pentane (2 × 10 mL), and dried *in vacuo* to give a white solid (5.69 g, 40.0 mmol, 72% yield). Spectral data are consistent with those previously reported.[43]

Synthesis of (n-Bu)$_3$SnCp (**28**).* The title compound was prepared according to a procedure adapted from the literature.[44] (n-Bu_3)SnCl (9.0 mL, 33.2 mmol, 1.0 equiv) was added dropwise to a stirred suspension of NaCp* (5.25 g, 33.2 mmol, 1.0 equiv) in toluene (200

https://doi.org/10.1021/acs.organomet.1c00308
Organometallics 2021, 40, 2666−2677

mL), rapidly yielding a change from a colorless opaque suspension to a pale yellow translucent solution. The mixture was stirred for 2 days at room temperature, after which it was filtered across Celite and washed with copious toluene, and the combined filtrates concentrated *in vacuo* to give a pale yellow oil (13.24 g, 31.1 mmol, 94% yield). Spectral data are consistent with those previously reported.[44]

*Synthesis of Cp*TaCl$_4$.* The title compound was prepared according to a procedure adapted from the literature.[44] (*n*-Bu)$_3$SnCp* (13.24 g, 31.14 mmol, 1.2 equiv) was added to a suspension of freshly sublimed $TaCl_5$ (9.40 g, 26.25 mmol, 1.0 equiv) in toluene (110 mL), resulting in the immediate formation of a fine yellow solid. The suspension was allowed to stir for 24 h, after which the solid was collected by vacuum filtration, washed with pentane (3 × 10 mL), and dried under vacuum to give a free-flowing yellow powder (11.32 g, 24.6 mmol, 94% yield) that was used without further purification.

*Synthesis of PMe$_3$ (**29**).* The title compound was prepared according to a procedure adapted from the literature.[39] Dibutyl ether (200 mL) was added to iodine-activated Mg turnings (11.68 g, 480.5 mmol), and methyl iodide (23.5 mL, 377.5 mmol, 1 equiv) was then added slowly, taking care to avoid an excessively exothermic reaction upon initiation of the Grignard formation. After the addition of methyl iodide, the mixture was cautiously brought to reflux for 24 h and then allowed to cool to room temperature. The solution was decanted from the remaining magnesium by cannula transfer, and a solution of triphenyl phosphite (27.0 mL, 310.3 mmol, 0.8 equiv) in dibutyl ether (40 mL) was added slowly with cooling to 0 °C. The mixture was then heated to 40 °C for 3 h, after which the product was obtained as a pure, colorless liquid by distillation (6.0 mL, 58.2 mmol, 57% yield). Spectral data are consistent with those previously reported.[39]

*Synthesis of Cp*TaCl$_3$(PMe$_3$).* The title compound was prepared according to a procedure adapted from the literature.[26c] While cooling to −84 °C, THF (50 mL) was transferred to a flask containing Cp*TaCl$_4$ (7.27 g, 15.9 mmol, 1.0 equiv) and magnesium turnings (0.19 g, 7.9 mmol, 0.5 equiv), followed by the addition of a solution of PMe$_3$ (1.72 mL, 16.9 mmol, 1.1 equiv) in THF (5 mL). The reaction mixture was allowed to slowly warm to room temperature, during which the mixture changed from a yellow suspension to a deep-red solution. After stirring for 24 h, the solvent was removed *in vacuo* and the resulting brown solid (8.97 g) was used without further purification or characterization.

*Synthesis of CpCp*TaCl$_2$.* The title compound was prepared according to a procedure adapted from the literature.[26c] While cooling to −84 °C, a solution of PMe$_3$ (0.24 mL, 2.3 mmol, 0.4 equiv) in toluene (40 mL) was added to a mixture of crude Cp*TaCl$_3$(PMe$_3$) (4.00 g, ∼6.3 mmol, ∼1.0 equiv) and NaCp·1/3 THF (0.76 g, 6.8 mmol, 1.1 equiv) and the mixture was warmed to room temperature and then heated at 100 °C for 18 h. Solvent removal *in vacuo* gave a green-brown solid that was purified by Soxhlet extraction into toluene (20 mL, 24 h). Concentration of the extract gave a brown solid (1.12 g) that was used without further purification.

Synthesis of KCp (**30**).* The title compound was prepared according to a procedure adapted from the literature.[45] 1,2,3,4,5-pentamethylcyclopentadiene (6.00 g, 43.5 mmol, 1.2 equiv) was added slowly to a suspension of potassium hydride (1.50 g, 37.5 mmol, 1.0 equiv) in THF (60 mL), and the mixture was stirred for 18 h, during which a white solid formed. This solid was collected by vacuum filtration, washed with THF (30 mL), and dried *in vacuo* to give a fine white solid (4.50 g, 25.8 mmol, 69% yield). Spectral data are consistent with those previously reported.[45]

*Synthesis of CpCp*TaH$_3$ (**2**).* The title compound was prepared according to a procedure adapted from the literature.[26c] While cooling to −84 °C, Et$_2$O (65 mL) was added to a mixture of CpCp*TaCl$_2$ (1.10 g, ∼2.40 mmol, ∼1.0 equiv) and LiAlH$_4$ (0.54 g, 14.3 mmol, 6.0 equiv) and the mixture was allowed to slowly warm to room temperature and stirred for 24 h. The mixture was cooled to 0 °C and then degassed. Deionized water (0.72 mL, 40.0 mmol, 17 equiv) was added dropwise. The mixture was allowed to slowly warm to room temperature, after which it was extracted into pentane (2 × 30 mL). The solvent was removed from the combined extracts under vacuum to give an off-white solid (0.59 g, 65% yield). Spectral data are consistent with those previously reported.[26c]

Synthesis of Cp$_2^*$TaCl$_2$. The title compound was prepared according to a procedure adapted from the literature.[26c] While cooling to −84 °C, a solution of PMe$_3$ (0.05 mL, 0.50 mmol) in toluene (25 mL) was added to a mixture of crude Cp*TaCl$_3$(PMe$_3$) (4.00 g) and KCp* (1.30 g, 7.46 mmol) and the mixture was warmed to room temperature and then heated at 100 °C for 18 h. Solvent removal *in vacuo* gave a brown solid that was purified via Soxhlet extraction into toluene (25 mL, 24 h). Concentration of the extract gave a brown solid (2.27 g) that was used without further purification or characterization.

*Synthesis of Cp$_2^*$TaH$_3$ (**3**).* The title compound was prepared according to a procedure adapted from the literature.[25a] While cooling to −84 °C, Et$_2$O (30 mL) was added to a mixture of Cp$_2^*$TaCl$_2$ (0.50 g, 0.96 mmol, 1.0 equiv) and LiAlH$_4$ (0.25 g, 6.6 mmol, 6.9 equiv) and the mixture was allowed to slowly warm to room temperature and stirred for 18 h. The mixture was cooled to 0 °C and then degassed. Deionized water (1.0 mL, 55.5 mmol, 57.9 equiv) was added dropwise. The mixture was allowed to slowly warm to room temperature, after which it was extracted into pentane (2 × 25 mL), and the solvent was removed from the combined extracts *in vacuo* to give an off-white solid (0.36 g, 0.79 mmol, 84% yield). Spectral data are consistent with those previously reported.[26c]

COMPUTATIONAL SECTION

Calculations were performed with Gaussian 16.[46] An ultrafine integration grid and the keyword 5d were used for all calculations. Except when evaluating other methods as specified in the Supporting Information, geometry optimizations of the stationary points were carried out in the gas phase with the M06L[17] functional with BS1 (BS1 = the LANL2DZ pseudopotential for Ta and the 6-31+G(d,p) basis for all other atoms). Frequency analyses were carried out at the same level to evaluate the zero-point vibrational energy and thermal corrections at 298 K. The nature of the stationary points was determined in each case according to the appropriate number of negative eigenvalues of the Hessian matrix. Forward and reverse intrinsic reaction coordinate calculations were carried out on the optimized transition structures to ensure that they indeed connect the appropriate reactants and products.[47] Multiple conformations and configurations were considered for all structures, and the lowest energy structures are reported. Unless otherwise specified in the Supporting Information, single-point energy calculations were performed with the M06[18] functional with BS2 (BS2 = the SDD pseudopotential for Ta and the 6-311++G(2d,p) basis set for all other atoms). Bulk solvent effects in benzene for computations in Schemes 2 and 5, and toluene for computations in Scheme 4, were considered implicitly in the single-point energy calculations through the CPCM solvation model.[48] Bond lengths were measured using Gaussview 5.0,[49] and cyclopentadienyl plane angles were measured using Mercury 3.0.[50]

ASSOCIATED CONTENT

Supporting Information

The Supporting Information is available free of charge at https://pubs.acs.org/doi/10.1021/acs.organomet.1c00308.

NMR spectra, rate data, computational details, and energies of calculated structures (PDF)

Cartesian coordinates of calculated structures (XYZ)

https://doi.org/10.1021/acs.organomet.1c00308
Organometallics 2021, 40, 2666−2677

AUTHOR INFORMATION

Corresponding Author

Sharon R. Neufeldt − *Department of Chemistry and Biochemistry, Montana State University, Bozeman, Montana 59717, United States;* orcid.org/0000-0001-7995-3995; Email: sharon.neufeldt@montana.edu

Authors

Steven M. Rehbein − *Department of Chemistry and Biochemistry, Montana State University, Bozeman, Montana 59717, United States;* orcid.org/0000-0002-9240-1260

Matthew J. Kania − *Department of Chemistry and Biochemistry, Montana State University, Bozeman, Montana 59717, United States;* orcid.org/0000-0003-4445-9780

Complete contact information is available at: https://pubs.acs.org/10.1021/acs.organomet.1c00308

Notes

The authors declare no competing financial interest.

ACKNOWLEDGMENTS

Acknowledgement is made to the donors of The American Chemical Society Petroleum Research Fund (57849-DNI3) and to Montana State University for support of this research. Calculations were performed on Comet at SDSC and Bridges-2 at the Pittsburgh Supercomputing Center through XSEDE (CHE170089), which is supported by NSF (ACI-1548562), and on the Hyalite High-Performance Computing System at MSU. NMR spectra were recorded on an instrument funded by NSF (NSF-MRI:DBI-1532078) and the Murdock Charitable Trust Foundation (2015066:MNL). The authors thank Brian Tripet, Thomas Livinghouse, Michael Mock, and Nicholas Stadie for helpful discussions and the MSU NMR Core Facility for their expertise. Emily K. Reeves is gratefully acknowledged for early work on this project.

REFERENCES

(1) Kepp, K. P. A quantitative scale of oxophilicity and thiophilicity. *Inorg. Chem.* **2016**, *55*, 9461−9470.

(2) Beaumier, E. P.; Pearce, A. J.; See, X. Y.; Tonks, I. A. Modern applications of low-valent early transition metals in synthesis and catalysis. *Nat. Rev. Chem.* **2019**, *3*, 15−34.

(3) (a) Hartwig, J. *Organotransition Metal Chemistry: From Bonding to Catalysis*, 1st ed; University Science Books: Melville, New York, 2010. (b) Crabtree, R. H. *The Organometallic Chemistry of the Transition Metals*, 7th ed; John Wiley & Sons Inc.: Hoboken, New Jersey, 2019.

(4) Selected reviews: (a) Shilov, A. E.; Shul'pin, G. B. Activation of C—H bonds by metal complexes. *Chem. Rev.* **1997**, *97*, 2879−2932. (b) Labinger, J. A.; Bercaw, J. E. Understanding and exploiting C−H bond activation. *Nature* **2002**, *417*, 507−514. (c) Chirik, P. J. Group 4 Transition Metal Sandwich Complexes: Still Fresh after Almost 60 Years. *Organometallics* **2010**, *29*, 1500−1517. (d) Kuhl, N.; Hopkinson, M. N.; Wencel-Delord, J.; Glorius, F. Beyond Directing Groups: Transition-Metal-Catalyzed C—H Activation of Simple Arenes. *Angew. Chem., Int. Ed.* **2012**, *51*, 10236−10254. (e) Xue, X.-S.; Ji, P.; Zhou, B.; Cheng, J.-P. The Essential Role of Bond Energetics in C—H Activation/Functionalization. *Chem. Rev.* **2017**, *117*, 8622−8648.

(5) Selected reviews: (a) Fryzuk, M. D.; Johnson, S. A. The continuing story of dinitrogen activation. *Coord. Chem. Rev.* **2000**, *200−202*, 379−409. (b) Ohki, Y.; Fryzuk, M. D. Dinitrogen Activation by Group 4 Metal Complexes. *Angew. Chem., Int. Ed.* **2007**, *46*, 3180−3183. (c) Tanaka, H.; Nishibayashi, Y.; Yoshizawa, K. Interplay between Theory and Experiment for Ammonia Synthesis Catalyzed by Transition Metal Complexes. *Acc. Chem. Res.* **2016**, *49*, 987−995. (d) Burford, R. J.; Yeo, A.; Fryzuk, M. D. Dinitrogen activation by group 4 and group 5 metal complexes supported by phosphine-amido containing ligand manifolds. *Coord. Chem. Rev.* **2017**, *334*, 84−99.

(6) Representative examples: (a) Mindiola, D. J. Oxidatively Induced Abstraction Reactions. A Synthetic Approach to Low-Coordinate and Reactive Early Transition Metal Complexes Containing Metal—Ligand Multiple Bonds. *Acc. Chem. Res.* **2006**, *39*, 813−821. (b) Nomura, K.; Zhang, S. Design of Vanadium Complex Catalysts for Precise Olefin Polymerization. *Chem. Rev.* **2011**, *111*, 2342−2362. (c) Waterman, R. σ-Bond Metathesis: A 30-Year Restrospective. *Organometallics* **2013**, *32*, 7249−7263.

(7) (a) Bailey, B. C.; Fan, H.; Baum, E. W.; Huffman, J. C.; Baik, M.-H.; Mindiola, D. J. Intermolecular C-H Bond Activation Promoted by a Titanium Alkylidyne. *J. Am. Chem. Soc.* **2005**, *127*, 16016−16017. (b) Flores, J. A.; Cavaliere, V. N.; Buck, D.; Pintér, B.; Chen, G.; Crestani, M. G.; Baik, M.-H.; Mindiola, D. J. Methane activation and exchange by titanium-carbon multiple bonds. *Chem. Sci.* **2011**, *2*, 1457−1462.

(8) Schaller, C. P.; Wolczanski, P. T. Methane vs Benzene Activation via Transient $^{t}Bu_3SiNHTa(=NSi^{t}Bu_3)_2$: Structure of $(py)_2MeTa(=NSi^{t}Bu_3)_2$. *Inorg. Chem.* **1993**, *32*, 131−144.

(9) Examples: (a) Curtis, M. D.; Bell, L. G.; Butler, W. M. C—H Activation. Synthesis of Silyl Derivatives of Niobocene and Tantalocene Hydrides, Their H/D Exchange Reactions with C_6D_6, and the Structure of $Cp_2Ta(H)_2SiMe_2Ph$. *Organometallics* **1985**, *4*, 701−707. (b) Jiang, Q.; Pestana, D. C.; Carroll, P. J.; Berry, D. H. Thermochemical Aspects of Arene C-H Activation by Tantalum Silyl Complexes: Relative Ta-Si and Ta-C Bond Enthalpies. *Organometallics* **1994**, *13*, 3679−3691. (c) Li, C.; Dinoi, C.; Coppel, Y.; Etienne, M. CH Bond Activation of Methane by a Transient η^2-Cyclopropene/Metallabicyclobutane Complex of Niobium. *J. Am. Chem. Soc.* **2015**, *137*, 12450−12453.

(10) Soulivong, D.; Norsic, S.; Taoufik, M.; Copéret, C.; Thivolle-Cazat, J.; Chakka, S.; Basset, J.-M. Non-Oxidative Coupling Reaction of Methane to Ethane and Hydrogen Catalyzed by the Silica-Supported Tantalum Hydride: $(SiO)_2Ta$-H. *J. Am. Chem. Soc.* **2008**, *130*, 5044−5045.

(11) (a) Vidal, V.; Théolier, A.; Thivolle-Cazat, J.; Basset, J.-M. Metathesis of Alkanes Catalyzed by Silica-Supported Transition Metal Hydrides. *Science* **1997**, *276*, 99−102. (b) Thieuleux, C.; Copéret, C.; Dufaud, V.; Marangelli, C.; Kuntz, E.; Basset, J.-M. Heterogeneous well-defined catalysts for metathesis of inert and not so inert bonds. *J. Mol. Catal. A: Chem.* **2004**, *213*, 47−57. (c) Basset, J. M.; Copéret, C.; Lefort, L.; Maunders, B. M.; Maury, O.; Le Roux, E.; Saggio, G.; Soignier, S.; Soulivong, D.; Sunley, G. J.; Taoufik, M.; Thivolle-Cazat, J. Primary Products and Mechanistic Considerations in Alkane Metathesis. *J. Am. Chem. Soc.* **2005**, *127*, 8604−8605. (d) Le Roux, E.; Taoufik, M.; Copéret, C.; de Mallmann, A.; Thivolle-Cazat, J.; Basset, J.-M.; Maunders, B. M.; Sunley, G. J. Development of Tungsten-Based Heterogeneous Alkane Metathesis Catalysts Through a Structure−Activity Relationship. *Angew. Chem., Int. Ed.* **2005**, *44*, 6755−6758. (e) Chen, Y.; Edy, A.; Ali, H.; Bilel, H.; Lyndon, E.; Basset, J. M. Alkane Metathesis with the Tantalum Methylidene $[(\equiv SiO)Ta(:CH_2)Me_2]/[(\equiv SiO)_2Ta(:CH_2)Me]$ Generated from Well-Defined Surface Organometallic Complex $[(\equiv SiO)Ta^{V}Me_4]$. *J. Am. Chem. Soc.* **2015**, *137*, 588−591.

(12) Pasha, F. A.; Cavallo, L.; Basset, J. M. Mechanism of n-Butane Hydrogenolysis Promoted by Ta-Hydrides Supported on Silica. *ACS Catal.* **2014**, *4*, 1868−1874.

(13) Vidal, V.; Théolier, A.; Thivolle-Cazat, J.; Basset, J.-M. Activation and Functionalisation of the C-H Bonds of Methane and Higher Alkanes by a Silica-supported Tantalum Hydride Complex. *J. Chem. Soc., Chem. Commun.* **1995**, 991−992.

(14) Based on computations, Lin and coworkers favor an alternative pathway involving oxidative addition at low-valent d^2 Ta(III) that stands in contrast to work by Cavallo and Basset (ref 12) Lin, X.; Xi, Y.; Zhang, G.; Phillips, D. L.; Guo, W. A Reaction Mechanism of

Methane Coupling on a Silica-Supported Single-Site Tantalum Catalyst. *Organometallics* **2014**, *33*, 2172−2181.

(15) Selected examples: (a) Buckner, S. W.; MacMahon, T. J.; Byrd, G. D.; Freiser, B. S. Gas-phase reactions of niobium(1+) and tantalum(1+) with alkanes and alkenes. Carbon-hydrogen bond activation and ligand-coupling mechanisms. *Inorg. Chem.* **1989**, *28*, 3511−3518. (b) Wesendrup, R.; Schwarz, H. Tantalum-Mediated Coupling of Methane and Carbon Dioxide in the Gas Phase. *Angew. Chem., Int. Ed.* **1995**, *34*, 2033−2035. (c) Parke, L. G.; Hinton, C. S.; Armentrout, P. B. Experimental and Theoretical Studies of the Activation of Methane by Ta+. *J. Phys. Chem. C* **2007**, *111*, 17773−17787. (d) Lapoutre, V. J. F.; Redlich, B.; van der Meer, A. F. G.; Oomens, J.; Bakker, J. M.; Sweeney, A.; Mookherjee, A.; Armentrout, P. B. Structures of the Dehydrogenation Products of Methane Activation by 5d Transition Metal Cations. *J. Phys. Chem. A* **2013**, *117*, 4115−4126. (e) Eckhard, J. F.; Masubuchi, T.; Tschurl, M.; Barnett, R. N.; Landman, U.; Heiz, U. Thermal Dehydrogenation of Methane Enhanced by μ^2-Oxo Ligands in Tantalum Cluster Cations [TaxO]+, x = 4, 5. *J. Phys. Chem. C* **2018**, *122*, 25628−25637.

(16) (a) Barefield, E. K.; Parshall, G. W.; Tebbe, F. N. Catalysis of Aromatic Hydrogen-Deuterium Exchange by Metal Hydrides. *J. Am. Chem. Soc.* **1970**, *92*, 5234−5235. (b) Parshall, G. W. Intramolecular aromatic substitution in transition metal complexes. *Acc. Chem. Res.* **1970**, *3*, 139−144. (c) Parshall, G. W.; Tebbe, F. N. Hydride Derivatives of Niobocene and Tantalocene. *J. Am. Chem. Soc.* **1971**, *93*, 3793−3795. (d) Klabunde, U.; Parshall, G. W. Activation of Aromatic Carbon-Hydrogen Bonds by Transition Metal Complexes. II. Substituted Benzenes. *J. Am. Chem. Soc.* **1972**, *94*, 9081−9087. (e) Foust, D. F.; Rogers, R. D.; Rausch, M. D.; Atwood, J. L. Photoinduced Reactions of $(\eta^5\text{-}C_5H_5)_2M(CO)H$ (M = Nb, Ta) and the Molecular Structure of $(\eta^5\text{-}C_5H_5)_2Ta(CO)H$. *J. Am. Chem. Soc.* **1982**, *104*, 5646−5650.

(17) Zhao, Y.; Truhlar, D. G. A New Local Density Functional for Main-Group Thermochemistry, Transition Metal Bonding, Thermochemical Kinetics, and Noncovalent Interactions. *J. Chem. Phys.* **2006**, *125*, 194101.

(18) Zhao, Y.; Truhlar, D. G. The M06 suite of density functionals for main group thermochemistry, thermochemical kinetics, noncovalent interactions, excited states, and transition elements: two new functionals and systematic testing of four M06-class functionals and 12 other functionals. *Theor. Chem. Acc.* **2008**, *120*, 215−241.

(19) Moltved, K. A.; Kepp, K. P. Chemical Bond Energies of 3d Transition Metals Studied by Density Functional Theory. *J. Chem. Theory Comput.* **2018**, *14*, 3479−3492.

(20) (a) Brookes, N. J.; Ariafard, A.; Stranger, R.; Yates, B. F. Scission of Carbon Monoxide Using TaR_3, R = (N(tBu)Ph) or $OSi(tBu)_3$): A DFT Investigation. *Chem.—Eur. J.* **2010**, *16*, 8117−8132. (b) Solans-Monfort, X.; Chow, C.; Gouré, E.; Kaya, Y.; Basset, J.-M.; Taoufik, M.; Quadrelli, E. A.; Eisenstein, O. Successive Heterolytic Cleavages of H_2 Achieve N_2 Splitting on Silica-Supported Tantalum Hydrides: A DFT Proposed Mechanism. *Inorg. Chem.* **2012**, *51*, 7237−7249. (c) Núñez-Zarur, F.; Solans-Monfort, X.; Restrepo, A. Mechanistic Insights into Alkane Metathesis Catalyzed by Silica-Supported Tantalum Hydrides: A DFT Study. *Inorg. Chem.* **2017**, *56*, 10458−10473.

(21) (a) Cramer, C. J.; Truhlar, D. G. Density functional theory for transition metals and transition metal chemistry. *Phys. Chem. Chem. Phys.* **2009**, *11*, 10757−10816. (b) Neese, F. A critical evaluation of DFT, including time-dependent DFT, applied to bioinorganic chemistry. *J. Biol. Inorg Chem.* **2006**, *11*, 702−711.

(22) Reductive elimination of H_2 from silica-supported tantalum hydrides has also been found to be barrierless based on DFT calculations; see ref 12.

(23) Woo, T. K.; Blöchl, P. E.; Ziegler, T. Monomer Capture in Brookhart's Ni(II) Diimine Olefin Polymerization Catalyst: Static and Dynamic Quantum Mechanics/Molecular Mechanics Study. *J. Phys. Chem. A* **2000**, *104*, 121−129.

(24) H−H activation via a σ-bond metathesis pathway was ruled out on the basis of parahydrogen induced polarization experiments: (a) Millar, S. P.; Zubris, D. L.; Bercaw, J. E.; Eisenberg, R. On the Mechanism of Dihydrogen Addition to Tantalocene Complexes. *J. Am. Chem. Soc.* **1998**, *120*, 5329−5330. (b) Bregel, D. C.; Oldham, S. M.; Eisenberg, R. Mechanistic Studies on the Addition of Dihydrogen to Tantalocene Complexes. *J. Am. Chem. Soc.* **2002**, *124*, 13827−13832.

(25) (a) Findlay, A. E.; Leelasubcharoen, S.; Kuzmina, L. G.; Howard, J. A. K.; Nikonov, G. I. Phosphido-bridged Ta/Rh bimetallic complex: synthesis, structure, and catalytic hydrosilylation of acetophenone. *Dalton Trans.* **2010**, *39*, 9264−9269. (b) Schmidt, S.; Sundermeyer, J. Höhervalente derivate der d-metall-säuren X. Imidokomplexe des fünf- und vierwertigen niobs und tantals mit halbsandwich- und metallocen- struktur. *J. Organomet. Chem.* **1994**, *472*, 127−138. (c) Korolev, A. V.; Rheingold, A. L.; Williams, D. S. A General Route to Labile Niobium and Tantalum d^0 Monoimides. Discussion of Metal-Nitrogen Vibrational Modes. *Inorg. Chem.* **1997**, *36*, 2647−2655.

(26) Various highly colored group 5 M(III)-aluminate species intermediate in the preparation of the M(V) metallocene trihydrides are known, from red (a) to orange (b) to yellow (c). However, we have observed none of the characteristic high-upfield ^{1}H NMR signals corresponding to the bridging hydrides in these and similar aluminates in our samples: (a) Fryzuk, M. D.; Clentsmith, G. K. B.; Rettig, S. J. Coordination behavior of $LiBEt_4$ towards $(\eta^5\text{-}C_5H_5)_2ReH$, $(\eta^5\text{-}C_5H_5)_2WH_2$ and $(\eta^5\text{-}C_5H_5)_2TaH_3$. Solid state structure of $[(\eta^5\text{-}C_5H_5)_2TaH \cdot AlH_2(OCH_2CH_2CH_2CH_3)]_2$. *Inorg. Chim. Acta* **1997**, *259*, 51−59. (b) Labinger, J. A.; Wong, K. S. Mechanism of Formation of $(\eta^5\text{-}C_5H_5)_2NbH_3$ from the Reaction of $(\eta^5\text{-}C_5H_5)_2NbCl_2$ with Hydroaluminate Reducing Agents. *J. Organomet. Chem.* **1979**, *170*, 373−384. (c) Gibson, V. C.; Bercaw, J. E.; Bruton, W. J.; Sanner, R. D. "Bent-Sandwich" Derivatives of Tantalum Bearing One or Two Pentamethylcyclopentadienyl Ligands. *Organometallics* **1986**, *5*, 976−979.

(27) Elevated pressures were utilized in these experiments to increase the solvent boiling point above the temperature of the heating block in order to avoid ambiguity about the actual reaction temperature.

(28) The absorbance maximum of Cp_2TaH_3 is at 235 nm (see Supporting Information). However, irradiation of Cp_2TaH_3 at 254 nm (the closest available wavelength match for our Rayonet photochemical reactor) results in rapid catalyst decomposition. We have found the use of 350 nm lamps to be the best compromise between promoting catalysis while limiting decomposition. This result is in agreement with previous observations Margulieux, G. W.; Semproni, S. P.; Chirik, P. J. Photochemically Induced Reductive Elimination as a Route to a Zirconocene Complex with a Strongly Activated N_2 Ligand. *Angew. Chem., Int. Ed.* **2014**, *53*, 9189−9192.

(29) An additional potentially complicating factor with irradiating near the absorbance maximum of Cp_2TaH_3 is the isomerization of benzene to fulvene and benzvalene that could complicate analysis and likely provide species that are more reactive than benzene itself. For examples, see: (a) Wilzbach, K. E.; Ritscher, J. S.; Kaplan, L. Benzvalene, the tricyclic valance isomer of benzene. *J. Am. Chem. Soc.* **1967**, *89*, 1031−1032. (b) Kaplan, L.; Wilzbach, K. E. Photolysis of benzene vapor. Benzvalene formation at wavelengths 2537-2370 Å. *J. Am. Chem. Soc.* **1968**, *90*, 3291−3292.

(30) Though the exact species responsible for the red coloration of these samples remains elusive, a strong candidate is that of the paramagnetic (^{1}H NMR silent) $17e^-$ species $(\eta_5\text{-}C_5H_5)_2TaH_2$, resulting from photochemically-induced radical abstraction of a single hydrogen from **1**. For literature support, see (a) which includes EPR spectroscopy (but not isolation) of $(\eta_5\text{-}C_5H_5)_2TaH_2$ and EPR spectroscopy and isolation of the deep-red isoelectronic paramagnetic complex $(\eta_5\text{-}CH_3C_5H_5)_2Ta(CH_3)_2$ and (b) which includes isolation of a photochemically generated $17e^-$ species in a low-temperature matrix: (a) Elson, I. H.; Kochi, J. K.; Klabunde, U.; Manzer, L. E.; Parshall, G. W.; Tebbe, F. N. Paramagentic hydride and alkyl complexes of niobium(IV) and tantalum(IV). *J. Am. Chem. Soc.* **1974**, *96*, 7374−7376. (b) Baynham, R. F. G.; Chetwynd-Talbot, J.;

https://doi.org/10.1021/acs.organomet.1c00308
Organometallics 2021, 40, 2666−2677

Grebenik, P.; Perutz, R. N.; Powell, M. H. A. Photochemistry of $M(\eta^5\text{-}C_5H_5)_2(H)CO$ and $M(\eta^5\text{-}C_5H_5)_2H_3$ (M = Nb, Ta) in low temperature matrices. *J. Organomet. Chem.* **1985**, *284*, 229−242.

(31) Deutsch, P. P.; Maguire, J. A.; Jones, W. D.; Eisenberg, R. Hydride abstraction. The reaction of [bis(diphenylphosphino)-ethane]carbonylhaloiridium with bis(cyclopentadienyl)-trihydridotantalum. *Inorg. Chem.* **1990**, *29*, 686−690.

(32) (a) Jia, C.; Kitamura, T.; Fujiwara, Y. Catalytic Functionalization of Arenes and Alkanes via C-H Bond Activation. *Acc. Chem. Res.* **2001**, *34*, 633−639. (b) Walton, J. W.; Wilkinson, L. A.; Paymore, N. J.; Elliot, P. P. π-Coordinated arene metal complexes and catalysis. *Organometallic Chemistry: Volume 42*; Royal Society of Chemistry: Cambridge, U.K., 2019; pp 125−171. (c) Rej, S.; Das, A.; Chatani, N. Strategic evolution in transition metal-catalyzed directed C−H bond activation and future directions. *Coord. Chem. Rev.* **2021**, *431*, 213683. (d) Williams, L. J.; Bhonoah, Y.; Wilkinson, L. A.; Walton, J. W. As Nice as π: Aromatic Reactions Activated by π -Coordination to Transition Metals. *Chem.—Eur. J.* **2021**, *27*, 3650−3660.

(33) For a closely related insertion into a C−F bond, see Gianetti, T. L.; Bergman, R. G.; Arnold, J. Carbon−fluorine bond cleavage in fluoroarenes via a niobium(III) imido complex: from stoichiometric to catalytic hydrodefluorination. *Chem. Sci.* **2014**, *5*, 2517−2524.

(34) (a) Brintzinger, H.; Bercaw, J. E. Bis(pentamethylcyclopentadienyl)titanium(II). Isolation and Reactions with Hydrogen, Nitrogen, and Carbon Monoxide. *J. Am. Chem. Soc.* **1971**, *93*, 2045−2046. (b) McLain, S. J.; Wood, C. D.; Schrock, R. R. Preparation and Characterization of Tantalum(III) Olefin Complexes and Tantalum-(V) Metallacyclopentane Complexes Made from Acyclic α Olefins. *J. Am. Chem. Soc.* **1979**, *101*, 4558−4570. (c) McLain, S. J.; Sancho, J.; Schrock, R. R. Metallacyclopentane to Metallacyclobutane Ring Contraction. *J. Am. Chem. Soc.* **1979**, *101*, 5451−5453. (d) McLain, S. J.; Sancho, J.; Schrock, R. R. Selective Dimerization of Monosubstituted α-Olefins by Tantalacyclopentane Catalysts. *J. Am. Chem. Soc.* **1980**, *102*, 5610−5618. (e) Van Asselt, A.; Burger, B. J.; Gibson, V. C.; Bercaw, J. E. Hydrido methylidene, hydrido vinylidene, hydrido oxo, and hydrido formaldehyde derivatives of bis-(pentamethylcyclopentadienyl)tantalum. *J. Am. Chem. Soc.* **1986**, *108*, 5347−5349. (f) Antonelli, D. M.; Schaefer, W. P.; Parkin, G.; Bercaw, J. E. Synthesis and characterization of $(\eta^5\text{-}C_5Me_5)_2TaCl$-(THF), a useful synthetic precursor for the preparation of oxo, imido and methylidene derivatives of permethyltantalocene. *J. Organomet. Chem.* **1993**, *462*, 213−220.

(35) The downfield trend of the hydride signals with increasing methylation of the Cp rings is perhaps counterintuitive, since the permethylated ligands are more electron-rich than the unmethylated Cp rings. However, this trend is consistent with a slight elongation of the Ta···ligand distance with permethylation. With increasing methylation, the average distance between Ta and the centroid of the Cp (or Cp*) ligands increases, presumably due to sterics, suggesting less electron donation from Cp (Cp*) to tantalum (see Table 2, complexes **1**, **8**, and **9**).

(36) Gibson, V. C.; Parkin, G.; Bercaw, J. E. Synthesis and reactivity of permethyltantalocene derivatives processing η^3-allyl, η^2-butadiene, η^2-methylallene, and η^1-alkenylidene ligands. Model studies for the role of surface vinylidenes in the Fischer-Tropsch hydrocarbon-chain-lengthening process. *Organometallics* **1991**, *10*, 220−231.

(37) Although we have not observed H/D exchange between $Cp^*_2TaH_3$ and C_6D_6 under N_2, a modest amount of H/D exchange between $Cp^*_2TaH_3$ and D_2 can be observed at extended reaction times.

(38) Green, J. C. Bent metallocenes revisited. *Chem. Soc. Rev.* **1998**, *27*, 263−271.

(39) Wolfsberger, W.; Schmidbaur, H. Eine befriendegende darstellungsmethode für trimethylphosphin. *Synth. React. Inorg. Met.-Org. Chem.* **1974**, *4*, 149−156.

(40) Performing evacuation-refill cycles with N_2 (analogous to those performed with H_2 or D_2) was found to not affect reaction rate. As such, the rate depression observed in experiments under pressures of H_2 or D_2 is not related to the multiple evacuation-refill cycles.

(41) Tay, B.-Y.; Wang, C.; Stubbs, L. P.; Jacob, C.; van Meurs, M. Deuterated dimethyl sulfoxide as a good NMR solvent for the characterization of alkali metal cyclopentadienides, amides, alkoxides and phenoxides. *J. Organomet. Chem.* **2011**, *696*, 3431−3435.

(42) This and all other −84 °C cold baths were prepared from ethyl acetate and liquid nitrogen.

(43) Thomson, R. K.; Monreal, M. J.; Masuda, J. D.; Scott, B. L.; Kiplinger, J. L. Lutetium gets a crown: Synthesis, structure and reaction chemistry of the separated ion pair complex, $[Li(12\text{-crown-}4)_2][(C_5Me_5)_2LuMe_2]$. *J. Organomet. Chem.* **2011**, *696*, 3966−3973.

(44) Sanner, R. D.; Carter, S. T.; Bruton, W. J., Jr. The preparation of mono(η^5-pentamethylcyclopentadienyl) compounds of tantalum-(V). *J. Organomet. Chem.* **1982**, *240*, 157−162.

(45) Rabe, G.; Roesky, H. W.; Stalke, D.; Pauer, F.; Sheldrick, G. M. The preparation and crystal structures of sodium and potassium pentamethylcyclopentadienyl pyridine solvates. *J. Organomet. Chem.* **1991**, *403*, 11−19.

(46) Frisch, M. J.; Trucks, G. W.; Schlegel, H. B.; Scuseria, G. E.; Robb, M. A.; Cheeseman, J. R.; Scalmani, G.; Barone, V.; Petersson, G. A.; Nakatsuji, H.; Li, X.; Caricato, M.; Marenich, A. V.; Bloino, J.; Janesko, B. G.; Gomperts, R.; Mennucci, B.; Hratchian, H. P.; Ortiz, J. V.; Izmaylov, A. F.; Sonnenberg, J. L.; Williams-Young, D.; Ding, F.; Lipparini, F.; Egidi, F.; Goings, J.; Peng, B.; Petrone, A.; Henderson, T.; Ranasinghe, D.; Zakrzewski, V. G.; Gao, J.; Rega, N.; Zheng, G.; Liang, W.; Hada, M.; Ehara, M.; Toyota, K.; Fukuda, R.; Hasegawa, J.; Ishida, M.; Nakajima, T.; Honda, Y.; Kitao, O.; Nakai, H.; Vreven, T.; Throssell, K.; Montgomery, J. A., Jr.; Peralta, J. E.; Ogliaro, F.; Bearpark, M. J.; Heyd, J. J.; Brothers, E. N.; Kudin, K. N.; Staroverov, V. N.; Keith, T. A.; Kobayashi, R.; Normand, J.; Raghavachari, K.; Rendell, A. P.; Burant, J. C.; Iyengar, S. S.; Tomasi, J.; Cossi, M.; Millam, J. M.; Klene, M.; Adamo, C.; Cammi, R.; Ochterski, J. W.; Martin, R. L.; Morokuma, K.; Farkas, O.; Foresman, J. B.; Fox, D. J. *Gaussian 16*; Gaussian Inc.: Wallingford CT, 2016.

(47) (a) Gonzalez, C.; Schlegel, H. B. An Improved Algorithm for Reaction Path Following. *J. Chem. Phys.* **1989**, *90*, 2154−2161. (b) Gonzalez, C.; Schlegel, H. B. Reaction Path Following in Mass-Weighted Internal Coordinates. *J. Phys. Chem.* **1990**, *94*, 5523−5527. (c) Fukui, K. The Path of Chemical Reactions - the IRC Approach. *Acc. Chem. Res.* **1981**, *14*, 363−368.

(48) Cossi, M.; Rega, N.; Scalmani, G.; Barone, V. Energies, structures, and electronic properties of molecules in solution with the C-PCM solvation model. *J. Comput. Chem.* **2003**, *24*, 669−681.

(49) Dennington, R.; Keith, T. A.; Millam, J. M. *GaussView*, Version 6; Semichem Inc.: Shawnee Mission, KS, 2016.

(50) Macrae, C. F.; Bruno, I. J.; Chisholm, J. A.; Edgington, P. R.; McCabe, P.; Pidcock, E.; Rodriguez-Monge, L.; Taylor, R.; van de Streek, J.; Wood, P. A. Mercury CSD 2.0 - new features for the visualization and investigation of crystal structures. *J. Appl. Crystallogr.* **2008**, *41*, 466−470.

https://doi.org/10.1021/acs.organomet.1c00308
Organometallics 2021, 40, 2666−2677

CHAPTER THREE

EXPERIMENTAL AND COMPUTATIONAL EVALUATION OF TANTALOCENE HYDRIDES FOR C–H ACTIVATION OF ALKANES

Abstract

While catalytic aromatic H/D exchange at the tantalocene hydrides (especially Cp_2TaH_3, where Cp = η^5-C_5H_5) was demonstrated over half a century ago, this reactivity has not been expanded to aliphatic substrates whose functionalization or homologation would give value-added products from historically underutilized substrates. In an effort to better evaluate the potential of tantalocene hydrides for processes involving aliphatic C–H activation, we have conducted a series of experimental and computational studies on the intra- and intermolecular reactivity of these complexes, including those of the homogeneous series $(^{R}Cp)_2TaH_3$ (where ^{R}Cp = η^5-C_5H_4R, with R = methyl, ethyl, *iso*-propyl, and *tert*-butyl). For complexes of the type $(^{R}Cp)_2TaH_3$, intramolecular aliphatic C—H activation could proceed via "fulvene-like" and "tuck-in like" transition states. Density functional theory (DFT) suggests that the tuck-in like pathways are energetically favored. These predictions were found to be in good agreement with *in situ* kinetics measured by ^{1}H NMR experiments. DFT calculations predict similar barriers for these experimentally observed intramolecular reactions with $(^{R}Cp)_2TaH_3$ and intermolecular C—H activation of light alkanes—including those of methane—at Cp_2TaH_3. Our efforts culminate in our demonstration of the first clear evidence of the C—H activation of unactivated aliphatic substrates of room temperature liquid alkanes.

Introduction

Worldwide reliance on petroleum products for energy production and chemical feedstocks has drawn significant controversy regarding remaining resources[1] and criticism over their potential

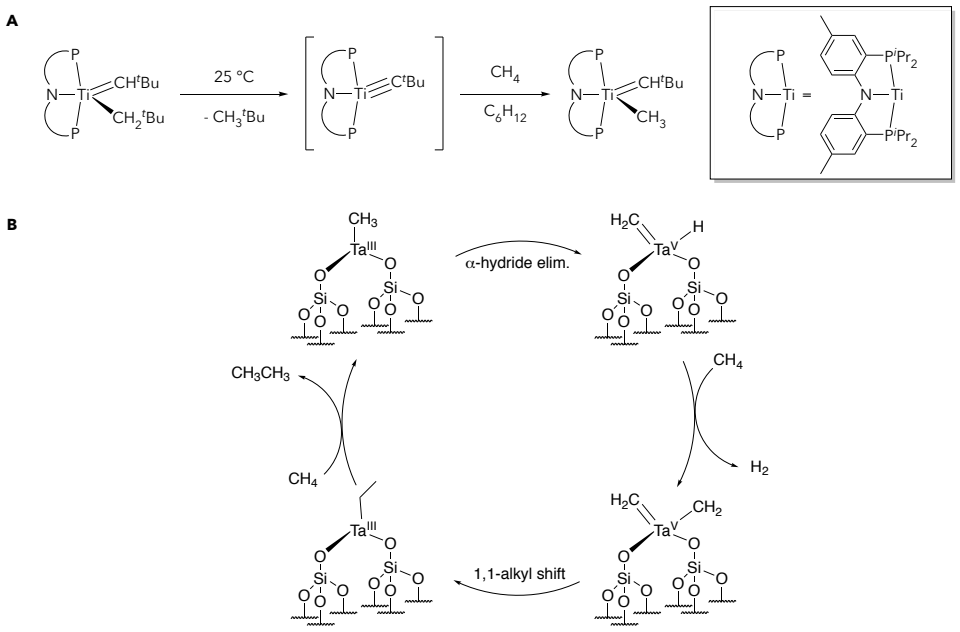
role in anthropogenic climate change.[2] While substantial progress continues to be made in technologies for their extraction, light alkanes remain underutilized due to difficulties in storage and transport originating from their high volatility. In the absence of technologies to alleviate these challenges, the lightest component of natural gas—methane—is often flared. The combustion products are either scrubbed/recaptured or vented following separation from heavier distillates at the point of extraction or refining.[3] The potential technological solution of C—H activation of light alkanes and subsequent upgrading—whether by oligimerization to produce heavier alkanes or functionalization to produce chemical feedstocks or commodity chemicals—remains a largely unfulfilled promise of molecular catalysis despite nearly a century of significant effort.[4] This persistent challenge is the result of the fundamental low reactivity of the saturated hydrocarbons, with methane the least reactive in the homologous series.[5]

Present commercial technologies for the upgrading of methane are limited to heterogeneous systems utilizing syngas (such as the Fischer-Tropsch-type processes)—a mixture of carbon monoxide and hydrogen produced from the high-temperature (>800 °C) thermolysis of methane.[6] The harsh operating conditions of these systems, however, remain a challenge in keeping the capital and operating cost of these technologies viable.[7] In contrast to the harsh conditions often employed in these heterogeneous systems, homogeneous catalysts are capable of operating at appreciably lower temperatures and pressures,[8] as well as allowing for design of well-defined catalyst structures, thereby easing mechanistic analyses and facilitating iterative design. Homogeneous catalysts for the C—H activation of alkanes are predominantly of the late transition metals[9] due to the difficulties inherent in working with the early transition metals, such as high oxophilicity[10] and reactivity, necessitating the handling of early transition metal complexes under air-free and otherwise non-coordinating conditions. The molecular chemistry of the early TM's,

however, display unique reactivity not often observed in the late TM's, such as reaction via s-bond metathesis at d^0 metal sites.[11] Alternatively, oxidative addition at low-valent oxidation state d^2 early TM complexes are often implicated in their reactivity with substrates such as molecular hydrogen and nitrogen and the C—H bonds of alkanes, alkenes, and arenes.[12]

Some of the first organometallic early TM complexes prepared were the metallocenes,[13] whose exploration continues to demonstrate their remarkable chemistry.[14] In more recent years, however, the organometallic chemistry of the early TM's has moved away from that of the cyclopentadienyl derivatives to more closely match the ligand frameworks common in late TM chemistry.[12] Previously, Baik and Mindiola demonstrated the ability of a titanium alkylidyne complex, (PNP)Ti≡C^{t}Bu to activate the C—H bonds of methane via 1,2-addition to form the alkylidene (PNP)Ti=CH^{t}Bu(CH_3) (Scheme 1A).[15] The methyl hydrogens in this alkylidene complex, interestingly, were shown to undergo slow exchange with the alkylidene hydrogens, suggesting interconversion between the alkylidene and alkylidyne species. Such early TM alkylidenes and alkylidynes have been implicated as intermediates in Basset's demonstration of the metathesis of methane to ethane with a single-site silica-supported (SSSS) tantalum hydride (Scheme 1B).[16] To date, however, a homogeneous analogue to that of Basset's SSSS tantalum hydride capable of alkane metathesis has not been realized. Moreover, alkane C—H activation by molecular early TM complexes, in particular by oxidative addition at low valent metals, remains extremely limited.[12] Inspired by Basset's work, our goal was to investigate the activity of molecular Ta(III) complexes generated in situ from Ta(V)-trihydrides toward C—H activation of hydrocarbons.

Scheme 1. C—H Activation of Methane at Early Transition Metals[15,16]



Presently, there are no examples of C—H activation of unactivated alkanes at molecular tantalum complexes, though evidence for intramolecular and aromatic C—H activation has been detected.[17,18] Intramolecular C—H activation in which the C—H bonds are more labile and biased towards reactivity due to their proximity to the metal center[17a] has been observed via the formation of various "tuck-in" complexes at the permethylcyclopentadienyl (Cp* = η^5-C_5Me_5) ligand[17b-d] and others.[17e,f] Cp_2TaH (Cp = η^5-C_5H_5), a low valent 16e$^-$ d^2 Ta(III) complex generated from the reductive elimination of dihydrogen from Cp_2TaH_3, is known to activate aromatic C—H bonds,[18] though fails to activate the benzylic C—H bonds of toluene or *p*-xylene.[18d,19] We have previously suggested this lack of reactivity is due to the competing favorability of arene π-complexation, and not the result of prohibitive energetics for benzylic C—H activation.[19] Following reductive elimination of dihydrogen from Cp_2TaH_3 to generate the monohydride Ta(III) intermediate, Cp_2TaH, arene π-complexation is computationally predicted to be stabilizing relative to the Ta(III) intermediate. This prediction matches our experimental observations with the fully permethylated

analogue. $Cp^*_2TaH_3$ was predicted to not experience the same stabilization of the Ta(III) intermediate imbued by arene π-complexation, which is in agreement with our observed lack of arene C—H activation with this complex. $Cp^*_2TaH_3$, however, undergoes hydrogen/deuterium (H/D) exchange with molecular deuterium—Despite the evidence for H/D exchange between $Cp^*_2TaH_3$ and deuterium, we observed no evidence of H/D exchange with the methyls of Cp* that would be indicative of intramolecular C—H activation. Similarly, we failed to observe the characteristic downfield ^{1}H NMR signal that would correspond to generation of the "tuck-in" complex formed from Cp^*_2TaH.[17c]

Despite our previous negative results with the lack of observed reactivity of the tantalocene hydrides at benzylic[18,19] and intramolecular C—H bonds,[19] our DFT investigations and the reactivity of tantalum observed by others[16,17] suggested an optimal tantalocene in the absence of competing π-complexation could be competent for the C—H activation of light alkanes. In this paper we detail theoretical and experimental investigations towards the C—H activation of light alkanes by tantalocene hydrides, beginning with several systems in which we bias reactivity toward the intramolecular C—H activation of primary, secondary, and tertiary aliphatic C—H bonds by tantalocenes hydrides, and culminating in our demonstration of the competency of Cp_2TaH_3 for intermolecular C—H activation of un-activated alkanes. The potential for the extension of this reactivity to methane is discussed though not yet realized.

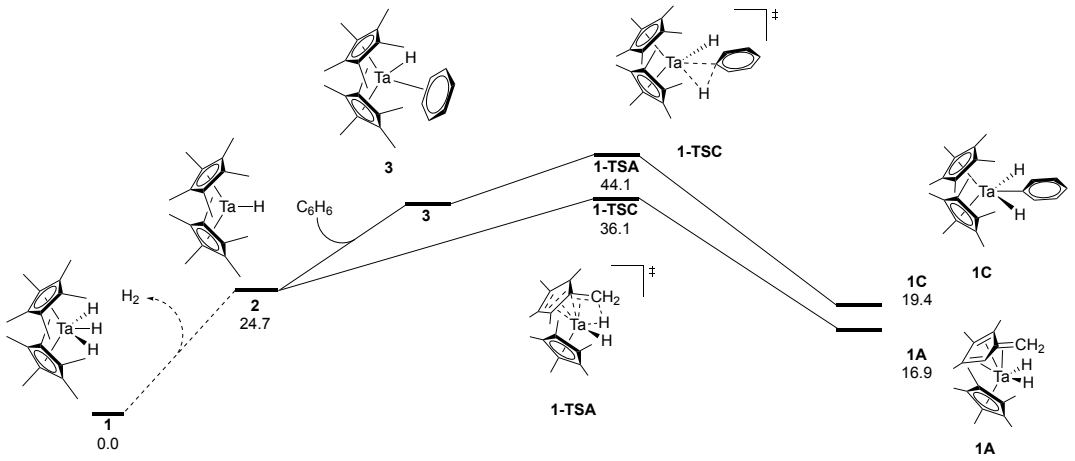
Results and Discussion

DFT calculations on intramolecular sp^3 C—H activation. Having previously failed to observe catalytic intramolecular H/D exchange between the metal center and methyl C—H bonds of $Cp^*_2TaH_3$, **1**,[19] we suspected that this complex's geometric distortion (relative to Cp_2TaH_3) imbued

by the bulkiness of the permethylation may be responsible. We conducted DFT calculations[20] to investigate the origin of this lack of observed reactivity that we found disconcerting due to the previously-demonstrated stability of the "tucked-in" complex resulting from oxidative addition of a Cp* methyl C—H bond at the stochiometrically-generated Cp^*_2TaH .[17c] Our results predict that the barrier to intramolecular C—H activation with **1** ($\Delta G^{\ddagger}$ = 36.1 kcal/mol) should not be prohibitive under experimental conditions and, in fact, may be in competition with arene C—H activation (Scheme 1). Intramolecular C—H activation and the lack of stabilization imbued by π-complexes of Cp^*_2TaH could bear equal responsibility for the lack of observed H/D exchange with deuteroarenes. Given the favorable energetics of the intramolecular C—H activation, our lack of observed intramolecular H/D exchange is likely due to the previously observed reaction depression under pressures of hydrogen and deuterium.[19]

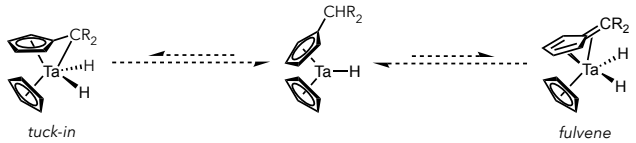
The product resulting from intramolecular C—H activation (Scheme 2, **1A**) is predicted to be more stable than the arene C—H activation product (Scheme 2, **1C)** by 2.5 kcal/mol (as well as more stable than arene C—H activation products of the previously examined Cp_2TaH_3 and $CpCp^*TaH_3$). This prediction is in agreement with the aforementioned stability of this tuck-in complex.[17c]

Scheme 2. Reaction coordinate diagram for the competing aromatic and intramolecular C—H activation pathways of **1**.



A distinction is necessary here regarding modes of intramolecular C—H activation. Intramolecular C—H activation of aliphatic substituents on a cyclopentadienyl ligand can occur through either a "tuck-in-like" or "fulvene-like" transition state and result in the corresponding "tuck-in" or "fulvene" product. As the two structures are isoelectronic and both result in abstraction of a hydrogen from the aliphatic substituent, the distinction lies in the geometric distortion of the cyclopentadienyl ring and the resulting metal-ligand binding modes.[21] In complexes that can produce both tuck-in and fulvene products, a tuck-in complex exhibits an η^5: η^1 binding mode where the C—C bond distances in the cyclopentadienyl ring are neither appreciably lengthened nor shortened relative to the parent complex and direct M—C bonding is observed with the aliphatic substituent. A fulvene product exhibits an η^4: η^2 binding mode wherein C—H bond distances in the cyclopentadienyl ring are shortened or lengthened relative to the parent complex and M—C(π) bonding is observed instead of direct M—C(σ) bonding (Scheme 3).

Scheme 3. Modes of Intramolecular C—H Activation



Our DFT calculations show that the structure of **1A** is more fulvene- than tuck-in-like. We hypothesize this is due to the strain involved in bending one of the methyl substituents of $Cp^*_2TaH_3$ sufficiently close to the metal center to facilitate direct M—C(σ) bonding.[21] (This description differs from that used by Bercaw to describe their stochiometric generation and isolation of the "tucked-in" complex (η^6-$C_5Me_4CH_2$)TaH_2.[17c]) Due the isolectronic nature of the various pentafulvene coordinate modes,[21] the distinction can feel largely semantic. As we will soon see, however, such a differentiation is representative of real mechanistic differences and is a prerequisite to understanding the mechanistic pathways leading to intramolecular aliphatic C—H activation.

With the limitations of $Cp^*_2TaH_3$ to undergo intramolecular aliphatic C—H activation apparent, we hoped similar complexes with less bulky ligands might provide the appropriate balance to allow for such reactivity. We selected four symmetrical tantalocene hydrides bearing increasingly substituted alkyl groups on their cyclopentadienyl ligands, from methyl to *tert*-butyl, such that we might examine C—H activation at aliphatic primary, secondary, and tertiary C—H bonds (Figure 1). Similar to complex **1**, the methyl-substituted complex, $(^{Me}Cp)_2TaH_3$ (^{Me}Cp = η^5-C_5H_4Me), **2**, contains only α-hydrogens for intramolecular C—H activation, whereas the ethyl- and isopropyl substituted complexes, $(^{Et}Cp)_2TaH_3$ (^{Et}Cp = η^5-C_5H_4Et), **3**, and $(^{i\text{Pr}}Cp)_2TaH_3$ ($^{i\text{Pr}}Cp$ = η^5-$C_5H_4i\text{Pr}$), **4**, contain both α- and β-hydrogens that might react intramolecularly. Given the lack of α-hydrogens in complex **5** [$(^{t\text{Bu}}Cp)_2TaH_3$, where $^{t\text{Bu}}Cp$ = η^5-$C_5H_4{}^t\text{Bu}$), only reaction at the β-hydrogens is possible.

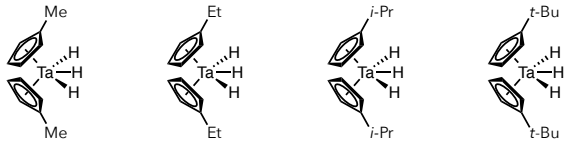


Figure 1. Homologous series of monosubstituted tantalocene hydrides used in these studies.

In contrast to our DFT work with $Cp^*_2TaH_3$, our results predict that in all cases with complexes **2**-**5** arene C—H activation is lower in energy than any competing intramolecular pathways (Schemes 4, Tables 1 and 2). For complexes **3** and **4** that react at either their α- or β-sites, α-activation is predicted to be favored due to the lower reaction enthalpy (Table 2); transition state energies are generally fairly similar. This result suggests the secondary and tertiary C—H bonds of complexes **3** and **4**, respectively, should be more reactive for intramolecular C—H activation. This result is expected as the hydrogens at the α-position to the cyclopentadienyl ring should be slightly activated and thus weaker than the primary β-C—H bonds. This prediction is further corroborated by the low barrier to activation for the primary methyl C—H bonds of complex **2**.

Scheme 4. Generalized reaction coordinate diagram of intramolecular C—H activation and intermolecular aromatic C—H activation.

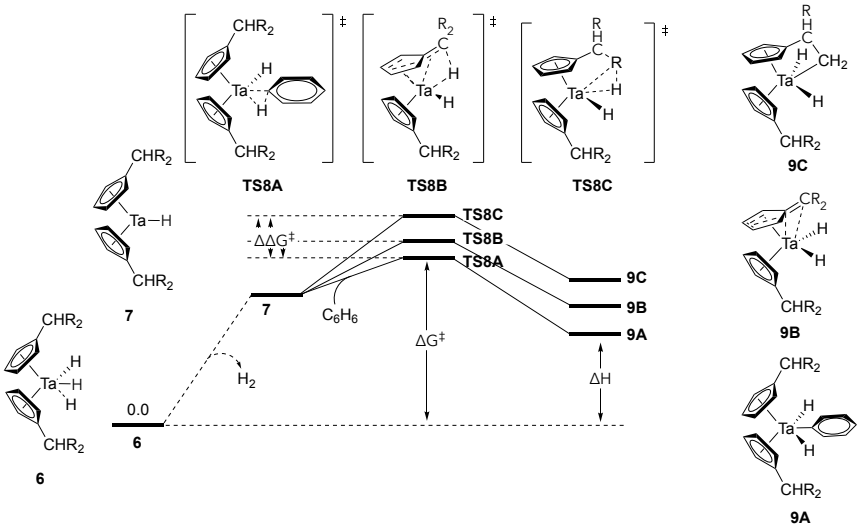


Table 1. Energetics of aromatic C—H activation by tantalocene hydrides

entry	complex	$\Delta G^{\ddagger a}$	$\Delta\Delta G^{\ddagger b}$	ΔH^{c}
1	Cp_2TaH_3 (**6**)	32.8	0.5	18.2
2	$Cp^*_2TaH_3$ (**1**)	44.1	11.8	19.4
3	$(^{Me}Cp)_2TaH_3$ (**2**)	32.6	0.3	18.5
4	$(^{Et}Cp)_2TaH_3$ (**3**)	33.8	1.5	17.8
5	$(^{iPr}Cp)_2TaH_3$ (**4**)	33.6	1.3	17.9
6	$(^{tBu}Cp)_2TaH_3$ (**5**)	32.3	0	16.4

[a] $\Delta G^{\ddagger}$ *is* measured from structures corresponding to **6** and **TS8A** in Scheme 3; [b] $\Delta\Delta G^{\ddagger}$ is measured as the difference between structures corresponding to **TS8A** in Scheme 3; [c] ΔH is measured from structures corresponding to **6** and **9A** in Scheme 3.

Table 2. Energetics of intramolecular C—H activation by tantalocene hydrides

		alpha C—H activation			beta C—H activation		
entry	complex	$\Delta G^{\ddagger a}$	$\Delta\Delta G^{\ddagger b}$	ΔH^{c}	$\Delta G^{\ddagger d}$	$\Delta\Delta G^{\ddagger e}$	ΔH^{f}
1	Cp_2TaH_3 (**6**)	(na)	(na)	(na)	(na)	(na)	(na)
2	$Cp^*_2TaH_3$ (**1**)	36.1	3.3	16.9	(na)	(na)	(na)
3	$(^{Me}Cp)_2TaH_3$ (**2**)	32.8	0	18.6	(na)	(na)	(na)
4	$(^{Et}Cp)_2TaH_3$ (**3**)	36	3.2	19.2	36.9	1.5	25.6
5	$(^{iPr}Cp)_2TaH_3$ (**4**)	36	3.2	21.1	36.6	1.2	25
6	$(^{tBu}Cp)_2TaH_3$ (**5**)	(na)	(na)	(na)	35.4	0	24

[a] $\Delta G^{\ddagger}$ *is* measured from structures corresponding to **6** and **TS8B** in Scheme 3; [b] $\Delta\Delta G^{\ddagger}$ is measured as the difference between structures corresponding to **TS8B** in Scheme 3; [c] ΔH is measured from structures corresponding to **6** and **9B** in Scheme 3; [d] $\Delta G^{\ddagger}$ *is* measured from structures corresponding to **6** and **TS8C** in Scheme 3; [e] $\Delta\Delta G^{\ddagger}$ is measured as the difference between structures corresponding to **TS8C** in Scheme 3; [f] ΔH is measured from structures corresponding to **6** and **9C** in Scheme 3.

Intramolecular sp^3 C—H activation. With promising energetics for intramolecular C—H activation predicted with each of the monosubstituted complexes **2-5**, we prepared each of them by modulation of previously described syntheses,[22] with ligand precursor preparation proving to be the most challenging aspect of their preparation (Supporting Information). Similar to our previous work[19] with Cp_2TaH_3 (Cp = η^5-C_5H_5) (**6**) $CpCp^*TaH_3$, and $Cp^*_2TaH_3$, we chose to track rates of catalysis by monitoring H/D exchange by ^{1}H NMR. We first determined the rate of tantalocene-arene H/D exchange under the same conditions we had used previously[23] such that we could compare the intermolecular reactivity with arene C—H bonds of the monosubstituted complexes to that of the unsubstituted complex, Cp_2TaH_3 (**6**). Such experiments were also necessary to confirm the catalysts are each capable of catalyzing H/D exchange with deuteroarenes such that intramolecular H/D exchange is subsequently possible. Under our experimental conditions deuterated substrate is in excess (0.20 mol % tantalocene corresponds to 500x more substrate than catalyst by molar ratio) such that the reaction is expected to be pseudo first order for catalyst "A,"

$$-\frac{d[\mathrm{A}]}{dt} = k[\mathrm{A}] \qquad \text{(Eq 1)}$$

whereby the first order rate, k, is obtained from a least squares regression of a linear plot of ln([A]) vs. t (see Supporting Information).

Our results showed that complexes **2**-**5** were all competent for catalyzing H/D exchange with deuterobenzene, with (^{Me}Cp)$_2$TaH$_3$ and (^{Et}Cp)$_2$TaH$_3$ both outperforming Cp$_2$TaH$_3$ (Table 3). In contrast to our previous findings,[19] increased catalytic activity for aromatic H/D exchange is not accompanied by a corresponding increase in catalyst decomposition; note the decreased rate of decomposition that accompanies the increased relative rates of complexes **2** and **3** (Table 3, compare Entries 2 and 3 to 1). Interestingly, our experimental rate data do not perfectly match our DFT predictions, which predicts the following order of rate of arene C—H activation, from most to least reactive: ($^{t\mathrm{Bu}}$Cp)$_2$TaH$_3$ > (^{Me}Cp)$_2$TaH$_3$ > Cp$_2$TaH$_3$ > ($^{i\mathrm{Pr}}$Cp)$_2$TaH$_3$ > (^{Et}Cp)$_2$TaH$_3$ (Table 1).

Table 3. of Decomposition and Catalysis of Arene H/D Exchange by Various Tantalocene Hydrides[a]

entry	complex	k_{decomp}[b]	k_{corr}[c]	k_{rel}[d]
1	Cp$_2$TaH$_3$	2.9(2)	44(6)	1.00
2	(^{Me}Cp)$_2$TaH$_3$ (**2**)	1.0(5)	59(3)	1.34
3	(^{Et}Cp)$_2$TaH$_3$ (**3**)	1.1(1)	44(5)	1.01
4	($^{i\mathrm{Pr}}$Cp)$_2$TaH$_3$ (**4**)	1.1(1)	23(8)	0.51
5	($^{t\mathrm{Bu}}$Cp)$_2$TaH$_3$ (**5**)	0.90(1)	19(2)	0.43

[a] All experiments were performed in triplicate, and results are an average of the collected data. Uncertainty in k_{decomp} and k_{corr} values are reported in parentheses. Reactions were followed for 6 h with heating at 100 ºC under 60 psi N$_2$; [b] k_{decomp} describes the rate of catalyst decomposition, in units of h^{-1} x 10^2; [c] k_{corr} describes the rate of catalytic H/D exchange following correction accounting for decomposition, in units of h^{-1} x 10^2; [d] k_{rel} describes relative values of k_{obs} with respect to those in entry 1.

At first glance these disparate results appeared unnerving. However, we suspected the origin of this discrepancy could be a preliminary indication of the competing intramolecular C—H activation we were seeking. Monitoring the ^{1}H NMR signals revealed only minor changes in signal shape (or the appearance of new, adjacent signals) that might be indicative of intramolecular

H/D exchange. In order to encourage more extensive intramolecular C—H activation, we repeated the experiments at an elevated temperature of 120 °C. To our delight, we observed clear evidence for intramolecular H/D exchange at each of the possible hydrogens of the alkyl substituents (Table 4, Figure 2).

Table 4. Kinetics of Catalysis of Intramolecular Aliphatic H/D Exchange by Various Tantalocene Hydrides[a]

entry	complex	position	k_{decomp}[b]	k_{obs}[c]	k_{rel}[c]
1	$(^{Me}Cp)_2TaH_3$ (**2**)	1º	7.7(4)	6.5(8)	2.47
2	$(^{Et}Cp)_2TaH_3$ (**3**)	1º	6.9(7)	2.7(4)	1.00
3	$(^{Et}Cp)_2TaH_3$ (**3**)	2º	6.9(7)	15(3)	5.78
4	$(^{iPr}Cp)_2TaH_3$ (**4**)	1º	5.1(5)	7.5(13)	2.84
5	$(^{iPr}Cp)_2TaH_3$ (**4**)	3º	5.1(5)	10(2)	3.79
6	$(^{tBu}Cp)_2TaH_3$ (**5**)	1º	3.9(4)	24(4)	9.07

[a] All experiments were performed in triplicate, and results are an average of the collected data. Uncertainty in k_{decomp} and k_{obs} values are reported in parentheses. Reactions were followed for 6 h with heating at 120 ºC under 60 psi N_2. . [b] k_{decomp} describes the rate of catalyst decomposition, in units of h^{-1} x 10^2; [c] k_{obs} describes the rate of catalytic H/D exchange without a correction for decomposition, in units of h^{-1} x 10^2; [c] k_{rel} describes relative values of k_{obs} with respect to those in entry 2.

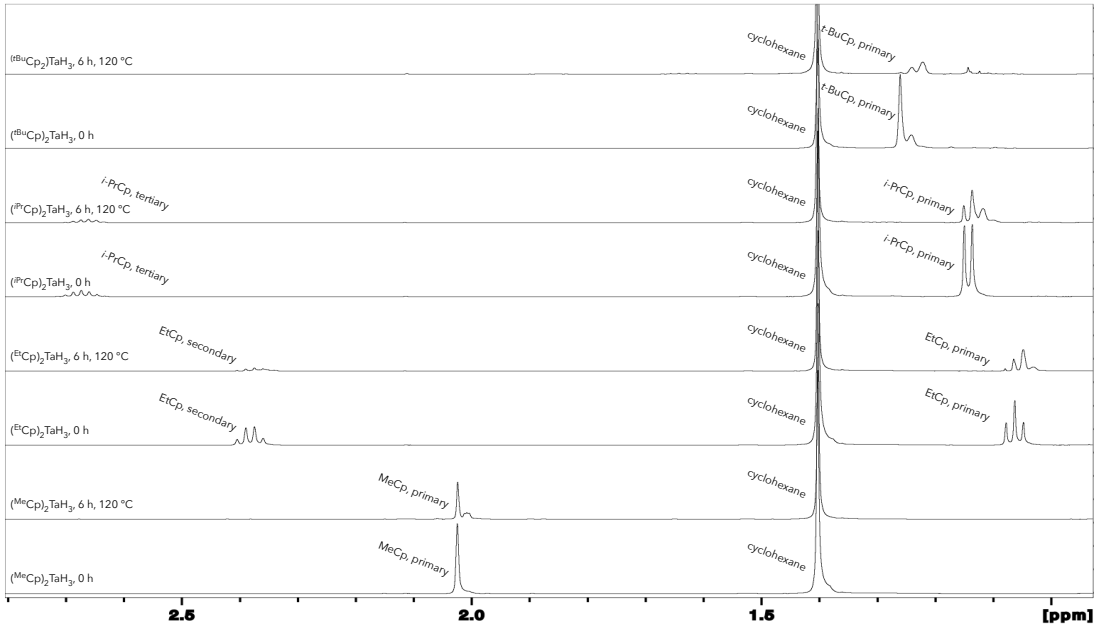
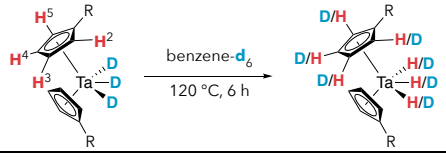


Figure 2. ^{1}H NMR signals of complexes **2**-**5** at 0 h and after 6 h at 120 °C.

Our experimental results appear to qualitatively match our DFT calculations. In cases when C—H activation can proceed through an α- or β-hydrogen (such as with complexes **3** and **4**), our computational work predicted higher barriers to the b-hydrogen pathway transition state. We experimentally observed rates of H/D exchange 5.8 and 1.3 times higher at the secondary and tertiary C—H bonds of the respective ethyl and *iso*-propyl substituents of **3** and **4** than their corresponding primary C—H bonds (Table 4, Entries 2-6). By far the highest rate of intramolecular H/D exchange was observed at the primary C—H bonds of complex **5**, $(^{t\text{Bu}}\text{Cp})_2\text{TaH}_3$, an observation that is, again, in qualitative agreement with our computational predictions given the relatively low predicted transition state energy of its tuck-in-like transition state.

Seemingly paradoxically, in the case of complexes **2** and **3**, rates of decomposition were observed to be higher than the rate of H/D exchange at primary sites (Table 4, Entries 1-2). Such an observation is anomalous as we have previously presumed a decrease in the cyclopentadienyl hydrogen signal integration values could only be representative of catalyst decomposition.[24] We suspected this unexpected observation may be indicative of a thus-far undetected intramolecular C—H activation of the cyclopentadienyl hydrogens. Sure enough—and though the subtle changes in the ^{1}H NMR cyclopentadienyl signals were alone insufficient to provide unequivocal proof—the ratio of the two alkylcyclopentadienyl hydrogen signals varies over the course of the experiments. This result is consistent with—and to our thinking, only explained by—intramolecular C—H activation of the non-alkyl hydrogens of the cyclopentadienyl ligands.

Table 5. Kinetics of Catalysis of Intramolecular Aromatic H/D Exchange by Various Tantalocene Hydrides[a]



entry	complex	position	k_{obs}[b]	k_{rel}[c]	$k_{rel,2,5}$: $k_{rel,3,4}$
1	(^{Me}Cp)$_2$TaH$_3$ (**2**)	2, 5	5.5(1)	2.64	(na)
2	(^{Me}Cp)$_2$TaH$_3$ (**2**)	3, 4	10(1)	5.02	1.00 : 1.90
3	(^{Et}Cp)$_2$TaH$_3$ (**3**)	2, 5	4.2(3)	2.02	(na)
4	(^{Et}Cp)$_2$TaH$_3$ (**3**)	3, 4	10(1)	4.85	1.00 : 2.40
5	(^{iPr}Cp)$_2$TaH$_3$ (**4**)	2, 5	3.1(2)	1.50	(na)
6	(^{iPr}Cp)$_2$TaH$_3$ (**4**)	3, 4	7.4(9)	3.59	1.00 : 2.39
7	(^{tBu}Cp)$_2$TaH$_3$ (**5**)	2, 5	2.1(1)	1.00	(na)
8	(^{tBu}Cp)$_2$TaH$_3$ (**5**)	3, 4	5.9(1)	2.82	1.00 : 2.82

[a] All experiments were performed in triplicate, and results are an average of the collected data. Uncertainty in k_{obs} values are reported in parentheses. Reactions were followed for 6 h with heating at 120 ºC under 60 psi N_2; [b] kobs describes the rate of catalytic H/D exchange, in units of h^{-1} x 10^2; [c] k_{rel} describes relative values of k_{obs} with respect to those in entry 7.

The 3,4 cyclopentadienyl C—H bonds are observed to be more reactive than the 2,5 with each of the substituted tantantalocenes. This observation is consistent with expectation given the mildly deactivating alkyl substituent wherein the 3,4 positions are nominally less electronically deactivated than the 2,5 positions. Interestingly, this trend in selectivity increases across the homologous series, with the highest and lowest selectivity observed at the tert-butyl substituted, (**5**), and methyl substituted, (**3**), complexes, respectively (Table 5, see $k_{rel,2,5}$: $k_{rel,3,4}$ ratios). This trend is likely the result of the increasing steric hindrance of the alkyl substituents increasingly favoring the aromatic C—H bonds further afield from the bulkily substituent.

While wide variability is observed in the reactivity of the various cyclopentadienyl C—H bonds, our demonstration of the propensity of the tantalocene trihydrides to catalyze aliphatic (albeit intramolecular) C—H activation is notable and suggests intermolecular aliphatic C—H activation would likely be possible under optimal conditions. The observed intermolecular

aromatic C—H activation is consistent with previous work demonstrating the importance of p-complexation preceding aromatic C—H activation.[19]

DFT calculations of intermolecular aliphatic sp^3 C—H activation. Given our success with promoting intramolecular C—H activation at the aliphatic substituents of complexes **2**-**5**, we returned to the unsubstituted complex Cp_2TaH_3, **6**, in the hope that in the absence of competing arene and intramolecular C—H activation **6** might be competent for alkane C—H activation. In addition to our past calculations with the aromatic and benzylic C—H bonds of benzene and toluene (Entries 1-2), we performed DFT calculations on C—H activation at **6** in cyclohexane (Table 6) with methane (Entry 3), the primary C—H bonds of n-butane (Entry 4), the secondary C—H bonds of propane (Entry 5), and the tertiary C—H bond of isobutane (Entry 6).

Table 6. Energetics of Activation of Various C—H Bond by Cp_2TaH_3

entry	C—H bond	σ/π-complex (kcal/mol)	ΔG‡ (kcal/mol)
1[a]	Ph**H**	20.5[d]	32.8
2[b]	PhC**H**$_3$	30.4[e]	35.2
3[c]	C**H**$_4$	30.2[e]	36.8
4[c]	C**H**$_3$(CH$_2$)$_2$C**H**$_3$	30.5[e]	36.8
5[c]	(CH$_3$)$_2$C**H**$_2$	29.2[e]	41.7
6[c]	(CH$_3$)$_3$C**H**	29.7[e]	44.2

Calculations in solvent: [a] benzene, [b] toluene, [c]cyclohexane; σ/π complex: [d] π-complex, [e] σ-complex.

The barrier to activation of methane was calculated to be only modestly higher than that of benzene ($\Delta G^{\ddagger}$ = 36.8 versus 32.8 kcal/mol), suggesting **6** may be capable of the C—H activation of methane.[25] Similar values are predicted for the primary C—H bonds of *n*-butane, though the predicted energetics increase with the increasingly substituted secondary and tertiary C—H bonds of propane and isobutane, respectively. As we have previously observed with the benzylic C—H bonds of toluene (Entry 2), σ-complexation (Figure 3) does not have the same stabilizing effect as

π-complexation; the σ-complexes of the four alkanes we investigated (Entries 3-6) are all ~ 10 kcal/mol higher in energy than the π-complex of benzene (Entry 1). While we believe the difference in energy between the σ- and π-complexes of toluene is responsible for the so-far observed lack of benzylic C—H activation (Entry 2), our results suggest that in the absence of competing pathways the C—H activation of light alkanes (including methane) by **6** may be possible.

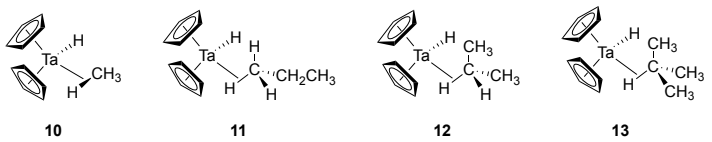


Figure 3. σ-Complexes of hydrocarbon C—H activation by **1**.

Intermolecular aliphatic sp^3 C—H activation. Encouraged by our DFT investigations predicting only a modest increase in the barrier of activation of the C—H bonds of methane versus benzene by **6** ($\Delta G^{\ddagger}$ = 36.8 versus 32.8 kcal/mol, Table 3, Entries 1 and 3) we were optimistic about the potential of **6** to activate the C—H bonds of methane. Given our predicted energetic similarity of the preceding s-complexes of methane and secondary C—H bonds (Table 3, Entries 3 and 5) and the higher energy of activation of the corresponding secondary C—H bonds, we rationalized cyclohexane may serve as a viable (i.e., less reactive than our desired substrate) solvent for the C—D bond activation of methane-d_4 by **6**.[26] Utilizing a 10 mL stainless steel pressure vessel, we screened **6** for reactivity with methane-d_4 in cyclohexane at a variety of temperatures, pressures, and reaction times.[27] Disappointingly, we were in all cases unable to produce convincing evidence for H/D exchange at the hydrides of **6** that would be indicative of C—D bond activation.

Given our promising DFT predictions, we suspected additional factors were likely contributing to the lack of desired reactivity. The low solubility of methane in aliphatic solvent seemed a likely contributor—a factor that would only be exacerbated by our elevated reaction

temperatures and the corresponding decrease in solubility. Solubility of **6** in aliphatic solvents is also appreciably lower than in aromatic solvents.

The preference for C—H bond activation (such as those at cyclohexane) over C—D bond activation (such as those at methane-d_4) also conspires against our preferred outcome. Pursuant of more favorable isotope effects, we prepared the deuteride complex Cp_2TaD_3 (**6-*d*$_3$**)[28], and repeated our previous methane activation experiments in cyclohexane-d_{12} under protiomethane. Monitoring the metal hydride/deuteride signals by ^{1}H NMR under these conditions we observed a dramatic change in the signal shape indicative of exchange of hydrogen for the deuteride ligands—just the sort of signal change expected for methane C—H activation. A control experiment with **6**-d_3 in cyclohexane-d_{12} and pressure of dueteromethane, however, revealed the same change in signal shape. It seems likely the H/D exchange observed is the results of intramolecular C—H activation of the cyclopentadienyl hydrogens. We believe the origin of this discrepancy between our theoretical predictions and experiment remains the poor solubility of methane-d_4 in aliphatic solvents and may only be achievable at appreciable pressures—and certainly not at conditions that might be considered mild.

If the limited solubility of methane (or—a related obstacle—our limited instrumentation for high-pressure chemistry) was the greatest impediment to its C—H activation in our system, we hoped C—D activation at **6** may still be favorable in more concentrated deuteroalkanes. Unlike the substrates explored computationally (Table 6—all low-boiling [b.p.'s below room temperature] alkanes), we rationalized the most reasonable substrates to start with would be deuteroalkanes with moderate boiling points (for our purposes, boiling points near 100 ° C).[29] Gratifyingly, our initial screenings of **6** with cyclohexane-d_{12} (b.p. = 81° C) and octane-d_{18} (b.p. = 120° C) at their boiling points (for 6 h at 0.20 mol % catalyst and 60 psi N_2) both showed definitive evidence of H/D

exchange at the hydrides of **1** (Figure 4)! We hoped we might be able to further probe the regioselectivity of **6** for different C—H bonds. The low catalyst concentration and low availability of hydrogen for H/D exchange at the deuteroalkanes gave correspondingly low quantities of H/D exchange at the deuteroalkanes that prohibit analysis of the preference of **6** for the primary or secondary C—D bonds of octane-d_{18}.

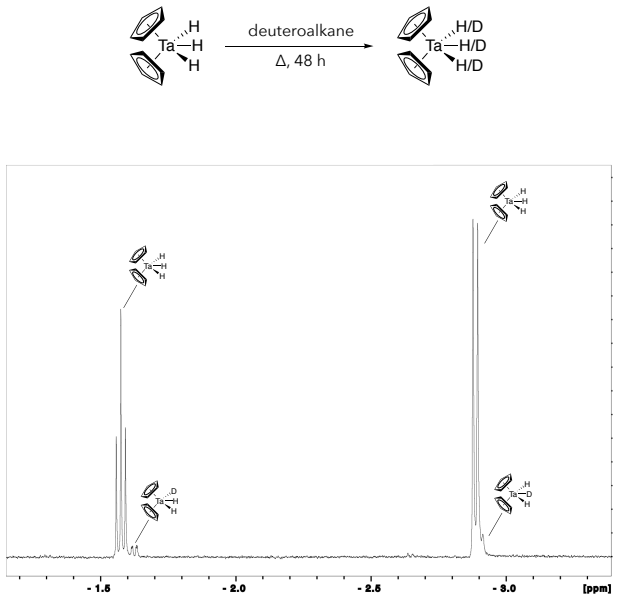
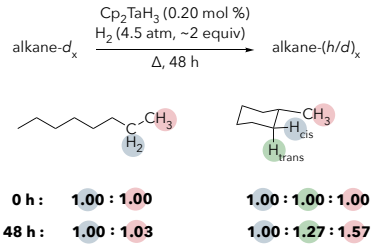


Figure 4. ^{1}H Evidence for H/D exchange at the hydrides of **6**.

To investigate the selectivity of **6** for differing C—D bonds, we turned to performing these reactions in deuteroalkanes under an atmosphere of hydrogen such that H/D exchange between **6** and the perdeuterated substrate would be significant enough for us to monitor the reaction by observing an increase in the deuteroalkane ^{1}H NMR signal integrations.[30] This objective required that we move away from our high-pressure NMR tubes to a larger volume pressure reaction vessel such that we might approach a modest 2:1 alkane-hydrogen molar ratio at elevated pressures (~ 4.5 atm).[31] Gratifyingly, when we performed these experiments with methylcyclohexane-d_{14}, and octane-d_{18} we were to observe changes in the relative signal integrations (Scheme 5).

Scheme 5. Catalytic H/D Exchange at Several Deuteroalkanes by Cp_2TaH_3[a]



[a] All reactions performed in an 88 mL glass pressure reaction vessel over 48 h at the b.p. of the substrate (80 °C and 100 °C for *n*-octane-d_{18} and methycyclohexane-d_{14}, respectively), utilizing ~2.0 mL deuteroalkane, Cp_2TaH_3 catalyst (0.20 mol %), cyclohexane internal standard (0.20 mol %), and under pressure of hydrogen (~4.5 atm, ~2:1 alkane – hydrogen ratio). Ratios are reported as the increase relative to the initial (0 h) ^{1}H NMR signal ratios of unity.

After 48 h, increases in the relative signal integrations were observed for the primary C—H bonds of both *n*-octane and methylcyclohexane—an observation that is consistent with our predicted energies of activation (Table 6). The difference in reactivity observed between the hydrogens *cis* and *trans* to the methyl substituent of methylcyclohexane are in agreement with the expected steric hinderance of the *cis*-hydrogens.

Given our demonstration of the C—D activation of moderate boiling point alkanes at **1**, the lack of reactivity towards methane-d_4 (or methane with **1-*d*$_3$**) remains particularly puzzling. Given the favorable energetics for this transformation, the most likely explanation seems to be the indiscriminate nature of **1** for various C—H bonds, such that in a high concentration of our solvent and low concentration of methane the pathway to methane activation is heavily statistically disfavored. Methane C—H activation in this system remains a possibility at higher pressures than those explored, though given the propensity of these catalysts to undertake intramolecular C—H activation we expect their utility as catalysts for this reaction will remain limited.

Conclusion

Through this work we have demonstrated the propensity of the tantalocene hydrides to activate aliphatic C—H bonds under conditions where the C—H bonds are sufficiently biased towards the metal center by proximity—whether as a result of their incorporation into the cyclopentadienyl ligand itself or by substrate concentration. Our observation of intramolecular H/D exchange from the Ta—H/D hydride/deuteride to the primary, secondary, and tertiary aliphatic C—H bonds of complexes **2**-**5** exemplifies this ability of these complexes reacted with unactivated aliphatic C—H bonds. The unexpected H/D exchange observed at the aromatic cyclopentadienyl hydrogens further demonstrates the high reactivity of the Ta(III) hydrides. Our failure to realize the C—H activation of methane with Cp_2TaH_3 (**6**)—despite our extensive efforts—is perhaps surprising given the accessible energetics predicted by density functional theory calculations. Our demonstration of the ability of **6** to catalyze H/D exchange at the deuteroalkanes cyclohexane-d_{12}, methylcyclohexane-d_{14}, and *n*-octane-d_{18} is suggestive that under sufficiently high pressures of methane (and corresponding high concentrations), its activation remains likely, though yet unrealized.

Experimental Section

General Materials and Methods. Lithium aluminum hydride, methylcyclopentadiene dimer (dimethyldicyclopentadiene), *n*-hexadecane, pyridine, and *tert*-butylamine were obtained from Acros Organics and used as received. Pyrrolidine and sodium bis(2-methoxyethoxy)aluminum hydride (70 % w/w in toluene) were obtained from Acros organics in ACROSeal bottles and used as received. Cyclopentadiene dimer (dicyclopentadiene) was obtained from Acros Organics and passed across a short silica plug to remove water and stabilizer prior to use. Sodium metal (foil-wrapped sticks in mineral oil) was obtained from Acros Organics and washed with copious

hexanes prior to use. Sodium hydride (60 % w/w dispersion in mineral oil) was obtained from Acros Organics and washed under airfree conditions with copious pentanes prior to use. Tantalum pentachloride ($TaCl_5$) was obtained from Acros Organics and purified by sublimation prior to use. Sodium metasilicate (anhydrous) was obtained from Alfa Aesar and used as received. Isotopically labeled compounds (C_6D_6, $CDCl_3$, DMSO-d_6, cyclohexane-d_{12}, methylcyclohexane-d_{12}, octane-d_{18}) were obtained from Cambridge Isotopes and degassed and stored over 3 Å molecular sieves. Acetic acid, acetone, magnesium sulfate (anhydrous), methanol, sodium bicarbonate, and sodium chloride were received from Fisher Chemical and used as received. Dichloromethane, diethyl ether (Et_2O), *n*-hexane, pentanes, tetrahydrofuran (THF), and toluene were obtained from Fisher Chemical and degassed and dried on a JC Meyer solvent system prior to use. Tri-*n*-butyltin chloride was obtained from Oakwood Chemical and used as received. Ethylcyclopentadiene dimer (diethyldicyclopentadiene) was obtained from Sigma-Aldrich and used as received. Methyl lithium (1.6 M in Et2O) and *n*-butyl lithium (2.5 M in hexanes) were obtained from Sigma-Aldrich in Sure/Seal bottles and used as received. Unless otherwise noted, all operations were performed in a nitrogen-filled glovebox or using airfree techniques in oven-dried glassware. NMR spectra were recorded at 298 K on a Bruker DRX 500 MHz (500.233 MHz for ^1H, 125.795 MHz for ^{13}C) spectrometer. Elevated-pressure ^1H NMR experiments were performed in 9-inch Wilmad Glass medium-walled high-pressure precision NMR tubes. ^1H and ^{13}C NMR chemical shifts are reported in parts per million (ppm) relative to TMS, with the residual solvent peak used as an internal reference [^1H: $CHCl_3$ (7.26 ppm), C_6D_5H (7.16 ppm), or DMSO-d_5 (2.50 ppm); ^{13}C: $CDCl_3$ (77.16 ppm), C_6D_6 (128.06 ppm), or DMSO-d_5 (39.52 ppm)]. Multiplicities are reported as follows: singlet (s), doublet (d), triplet (t), quartet (q), sextet (sext), septet (sept), and multiplet or multiple overlapping signals (m).

General Procedure for Measuring H/D Exchange Rates by ^{1}H NMR. In a 4 mL vial within a nitrogen-filled glovebox, tantalocene trihydride (freshly-sublimed, 0.2 mol % relative to substrate) was fully dissolved in a solution of deuterated substrate (1.80 mL) containing cyclohexane (0.2 mol % relative to arene). The resulting solution was divided equally (0.60 mL each) into three medium-wall high-pressure precision NMR tubes (Wilmad, 9" length, 3.46 mm internal diameter) and the tubes were sealed with Teflon stopcocks and removed from the glovebox. One at a time, the tubes were connected to a Schlenk line and pressurized to 60 psi (4.14 bar) nitrogen. Initial 1H NMR spectra (500 MHz, 32 scans, D1 relaxation delay = 10 s) were obtained of each sample (time = 0 h) and the samples were heated in a Chemglass NMR tube reaction heating block for a total of six hours (not including breaks for acquiring NMR spectra). NMR spectra were acquired approximately every hour (exact times were recorded and used during analysis of the results). During processing, the integration values of all signals were standardized relative to the cyclohexane signal (the cyclohexane signal integration was set to 10). Integration values were then normalized by multiplying the integral by a scalar value to correct for the actual initial concentrations at t = 0.

Synthesis of Na(^{Me}Cp): With cooling to 0 ºC, methyl-cyclopentadiene monomer (7.61 g, 94.9 mmol, distilled twice through glass helices from the freshly-cracked monomer to eliminate cyclopentadiene contamination) was added to a mixture of sodium hydride (2.28 g, 94.9 mmol) in Et_2O and allowed to slowly warm to room temperature and stirred for 16 h. An arduous filtration gave a solution that was concentrated to give a pale pink solid (2.07 g, 20.3 mmol, 21 % yield). ^{1}H NMR (500 MHz, DMSO-d_6, δ): 5.13 (t, 2.2 Hz, 2H), 5.11 (d, 2.3 Hz, 2H), 2.05 (s, 3H).

Synthesis of Ta(=NCMe$_3$)Cl$_3$(py)$_2$: The title compound was prepared according to a procedure adapted from the literature.[22d] *Tert*-butylamine (5.9 mL, 56 mmol) and pyridine (20.0 mL, 250

mmol) were added sequentially to a stirred heterogeneous mixture of freshly-sublimed $TaCl_5$ (10.00 g, 27.9 mmol,) and Na_2SiO_3 (6.84 g, 56.0 mmol) in toluene (80 mL) and Et_2O (20 mL). The mixture was stirred for 18 h, after which it was filtered over Celite. The Celite plug was washed with toluene, and the combined filtrates were concentrated in vacuo to give an opaque yellow solid. Recrystallization from dichloromethane:pentane at –25 °C gave large yellow crystals after 5 d (8.04 g, 56% yield). Additional product can be obtained from the same recrystallization liquor with additional time and pentane additions. Spectral data are consistent with those previously reported.[22d]

Synthesis of $(^{Me}Cp)_2Ta(=NCMe_3)Cl$: The title compound was prepared according to a procedure adapted from the literature.[22c] With cooling to – 84 ºC, a solution of $Na(^{Me}Cp)$ (2.37 g, 23.2 mmol) in Et_2O (70 mL) and THF (17 mL) was added to a solution of $Ta(=NCMe_3)Cl_2(py)_2$ in Et_2O (340 mL) and the mixture allowed to slowly warm to room temperature and stirred for 24 h. Solvent removal in vacuo gave a red oil that was extracted into pentane (3 x 100 mL), with concentration of the combined extracts giving a red solid (2.99 g, 6.7 mmol, 67 % yield) that was used without further purification or characterization.

Synthesis of $(^{Me}Cp)_2TaH_3$ (2): The title compound was prepared according to a procedure adapted from the literature.[22e] With cooling to – 84 ºC, a solution of $(^{Me}Cp)_2Ta(=NCMe_3)Cl$ (2.99 g, 6.7 mmol) in Et_2O (65 mL) was added to a suspension of $LiAlH_4$ (1.03 g, 27.2 mmol) in Et_2O (65 mL) and the mixture allowed to slowly warm to room temperature and stirred for 12 h. The mixture was cooled to 0 ºC and degassed, deionized water (2.0 mL, 111.0 mmol) added dropwise. The mixture was allowed to warm slowly to room temperature and to stir until the suspension was free-flowing. Extraction into Et_2O (3 x 60 mL) and concentration of the combined extracts in vacuo gave an off-white solid (0.76 g, 2.2 mmol, 33 % yield) showing a ~ 1 % contamination by

(MeCp)CpTaH$_3$. ^{1}H NMR (500 MHz, C_6D_6, δ): 4.83 (t, 2.5 Hz, 4H), 4.69 (t, 2.5 Hz, 4H), 2.02 (s, 6H), -0.65 (t, 10.6 Hz, 1H), -2.21 (d, 10.6 Hz, 2H); ^{13}C NMR (126 MHz, C_6D_6, δ): 106.4, 88.1, 84.8, 16.3.

Synthesis of Na(^{Et}Cp): Ethylcyclopentadiene dimer (3.77 g, 20.0 mmol) was added dropwise to a stirred suspension of sodium hydride (0.8690 g, 36.0 mmol) in hexadecane (40 mL) and heated at 195 °C for 16 h. After this time the mixture was allowed to cool to room temperature, the product collected via vacuum filtration, and washed with copious cold pentanes to give a white solid (4.12 g, 35.5 mmol, 98 % yield) with an apparent ~6% remaining undecane impurity by 1H NMR. Additional washing with pentanes or *n*-hexane resulted in reduced yield without appreciable decrease in hexadecane impurity. ^{1}H NMR (500 MHz, DMSO-d_6, δ): 5.14 (t, 1.6 Hz, 4H), 2.41 (q, 7.5 Hz, 2H), 1.05 (t, 7.5 Hz, 3H). (Note: this procedure differs significantly from that of the methyl analogue in that, here, the monomer is "cracked" alongside the NaH in high-boiling hexadecane instead of prior to its addition. This modification was undertaken to avoid the difficulties associated with cracking and distilling small quantities of the expensive ethylcyclopentadiene dimer. The increased solubility imbued by the ethyl group, however, dramatically increases its solubility in hydrocarbon solvents and makes complete removal of hexadecane difficult.)

Synthesis of (^{Et}Cp)$_2$Ta(=NCMe$_3$)Cl: The title compound was prepared according to a procedure adapted from the literature.[22c] With cooling to – 84 ºC, a solution of Na(^{Et}Cp) (2.74 g, 23.2 mmol) in Et_2O (70 mL) and THF (17 mL) was added to a mixture of Ta(=NCMe$_3$)Cl$_3$(py)$_2$ (5.16 g, 10.0 mmol) in Et_2O (340 mL) and the mixture allowed to slowly warm to room temperature and stirred for 16 h. After this time solvent was removed in vacuo to give a pasty solid that was extracted into pentane (3 x 50 mL). Concentration of the combined extracts gave a red oil (4.20 g, 8.9 mmol, 89 % yield) that was used without further purification or characterization.

Synthesis of $(^{Et}Cp)_2TaH_3$ (3): The title compound was prepared according to a procedure adapted from the literature.[22e] With cooling to – 84 ºC, a solution of $(^{Et}Cp)_2Ta(=NCMe_3)Cl$ (4.20 g, 8.9 mmol) in Et_2O (85 mL) was added to mixture of $LiAlH_4$ (1.36 g, 35.9 mmol) in Et_2O (85 mL) and the mixture allowed to slowly warm to room temperature and stirred for 16 h. After this time the mixture was cooled to 0 ºC and degassed, deionized water (2.6 mL, 144.3 mmol) added dropwise. The mixture was allowed to warm slowly to room temperature and to stir until the suspension was free-flowing. Extraction into Et_2O (2 x 80 mL) and concentration of the combined extracts gave a pale yellow solid with appreciable hexadecane contamination originating from $Na(^{Et}Cp)$. This contaminant co-distills alongside sublimation of $(^{Et}Cp)_2TaH_3$, and so was removed by a poor-yielding washing on silica gel with pentane and elution in Et_2O. Concentration of the Et_2O eluent gave of pale yellow solid (0.62 g, 1.68 mmol, 19 % yield) in agreement with the expected structure by ^1H and ^{13}C NMR. ^1H NMR (500 MHz, C_6D_6, δ): 4.79 (t, 2.6 Hz, 4H), 4.71 (t, 2.6 Hz, 4H), 2.38 (q, 7.4 Hz, 4H), 1.06 (t, 7.4 Hz, 6H), -0.87 (t, 10.5 Hz, 1H), -2.42 (d, 10.5 Hz, 2H); ^{13}C NMR (126 MHz, C_6D_6, δ): 114.9, 85.7, 84.4, 23.8, 15.9.

Synthesis of 6,6'-dimethylfulvene: The title compound was prepared according to a procedure adapted from the literature.[32] Without the use of airfree techniques and with cooling to 0 ºC, pyrrollidine (13.2 mL, 160.7 mmol) was added to a solution of cyclopentadiene (8.0 mL, 95.1 mmol, freshly "cracked") in acetone (6.0 mL, 81.0 mmol) and methanol (20 mL), giving an immediate color change from colorless to bright yellow. The mixture was allowed to warm to room temperature and stirred for 2 h, after which water (40 mL) and Et_2O (40 mL) were added and the mixture acidified (pH = 6.8) with acetic acid. The ethereal and aqueous phases were separated, and the aqueous phase extracted into Et_2O (2 x 40 mL). The combined ethereal extracts were washed with saturated aqueous $NaHCO_3$ (4 x 40 mL), water (20 mL) and saturated aqueous NaCl

(20 mL). The ethereal solution was dried with $MgSO_4$, filtered, and concentrated by rotary evaporation to give a bright yellow-orange liquid (7.80 g, 73.5 mmol, 77 % yield). Spectral data are consistent with those previously reported.[32]

Synthesis of 5-(1-methlethyl)-1,3-cyclopentadiene: With cooling to 0 ºC, a solution of 6,6'-dimethylfulvene (6.37 g, 60.0 mmol) in Et_2O (75 mL) was added to a mixture of $LiAlH_4$ (1.14 g, 30.0 mmol) in Et_2O (75 mL) and the mixture slowly allowed to warm to room temperature and stirred for 18 h. The mixture was cooled to 0 ºC and degassed, deionized water (15 mL) added slowly and the mixture slowly allowed to warm to room temperature and stirred until the mixture was free-flowing. Filtration, washing with pentane (2 x 30 mL), and the combined filtrates dried over $MgSO_4$ and concentrated by rotary evaporation to give a pale yellow liquid (5.08 g, 46.9 mmol, 78 % yield), shown by ^{1}H NMR to be a mixture of isomers with some residual Et_2O and pentane. This solvent-containing material was used without further purification.

Synthesis of Li($^{i\text{-Pr}}$Cp): With cooling to – 84 ºC, *n*-BuLi (18.0 mL 2.5 M solution in hexanes, 45.0 mmol) was added to a solution of 5-(1-methylethyl)-1,3-cyclopentadiene (4.86 g, 45.0 mmol) in Et_2O (45 mL) and the mixture slowly allowed to warm to room temperature. Upon warming, the formation of copious white solid was such that it inhibited stirring—the solution apparently being far too concentrated. After sitting for 16 h, the solid was collected by vacuum filtration, washed with copious pentane, and dried in vacuo to give a white solid (4.67 g, 41.0 mmol, 91 % yield) with a small quantity of pentane persisting even after lengthy drying. $_1$H NMR (500 MHz, DMSO-d_6, δ): 5.17 (t, 2.4 Hz, 2H), 5.12 (t, 2.4 Hz, 2H), 2.72 (sept, 6.7 Hz, 1H), 1.07 (d, 6.7 Hz, 6H).

Synthesis of *n*-Bu_3Sn($^{i\text{-Pr}}$Cp): The title compound was prepared according to a procedure adapted from the literature. *n*-Bu_3SnCl (6.0 mL, 22.1 mmol) was added to a mixture of Li($^{i\text{-Pr}}$Cp) (2.52 g, 22.1 mmol) in toluene (150 mL) and the mixture stirred at room temperature for 3 d. A difficult

filtration across Celite gave a yellow solution whose concentration gave a yellow oil (7.75 g, 19.5 mmol, 88 % yield). ^{1}H NMR (500 MHz, $CDCl_3$, δ): 6.21 (t, 1.6 Hz, 2H), 5.35 (t, 1.6 Hz, 2H), 2.77 (sept, 6.8 Hz, 1H), 1.46 (m, 6H), 1.29 (sext, 7.2 Hz, 6 H), 1.19 (d, 6.8 Hz, 6H), 0.89 (t, 7.2 Hz, 9H), 0.76 (m, 6H).

Synthesis of $(^{i\text{-Pr}}Cp)_2TaCl_2$: The title compound was prepared according to a procedure adapted from the literature.[22a] *n*-$Bu_3Sn(^{i\text{-Pr}}Cp)$ (7.75 g, 19.5 mmol) was added to a mixture of $TaCl_5$ (2.02 g, 5.63 mmol, freshly-sublimed) and dichloromethane (50 mL), giving a rapid color change from colorless to orange-red. The mixture was stirred for 7 d, during which it became a green-brown color. This mixture was concentrated to a volume of ~ 20 mL, layered with pentane, and chilled at – 25 ºC for 2 d. After this time a solid was collected by vacuum filtration, washed with pentane, and dried in vacuo to give a fine brown solid (1.99 g) that was used without further purification or characterization.

Synthesis of $(^{i\text{-Pr}}Cp)_2TaH_3$ (4): The title compound was prepared according to procedures adapted from the literature.[22a,b] Sodium bis(2-methoxyethoxy)aluminum hydride (2.9 mL 70 % w/w [~3.5 M] in toluene, 10.2 mmol) was added to a mixture of $(^{i\text{-Pr}}Cp)_2TaCl_2$ (1.99 g, 4.3 mmol) in toluene (40 mL) and the solution stirred 1 h. After this time, it was cooled to 0 ºC and degassed, deionized water (2,1 mL, 116.6 mmol) was added dropwise and the mixture allowed to slowly warm to room temperature and stirred until the viscous mixture became free-flowing. The red solution was separated from the precipitate and concentrated in vacuo to give a brown solid. Extraction into hexanes (65 ml) and cooling to – 84 ºC for 1 h gave an off-white solid that was collected and dried in vacuo (0.35 g, 0.89 mmol, 21 % yield). ^{1}H NMR (500 MHz, C_6D_6, δ): 4.77 (t, 2.5 Hz, 4H), 4.69 (t, 2.5 Hz, 4H), 2.67 (sept, 6.7 Hz, 2H), 1.14 (d, 6.7 Hz, 12H), -1.06 (t, 10.2 Hz, 1H), -2.57 (d, 10.2 Hz, 2H); ^{13}C NMR (126 MHz, C_6D_6, δ): 121.7, 83.9, 83.8, 28.8, 24.5.

Synthesis of Li($^{t\text{-Bu}}$Cp): With cooling to 0 ºC, MeLi (20.0 mL 1.6 M solution in Et_2O, 32.00 mmol) was added to a solution of 6,6'-dimethylfulvene (3.40 g, 32.0 mmol) in Et_2O (150 mL) and slowly allowed to warm to room temperature and stirred 18 h, during which a white solid formed and the bright yellow color faded. The white solid was collected by vacuum filtration, washed with copious pentane, and dried in vacuo to give a white solid (3.35, 26.2 mmol, 82 % yield). ^{1}H NMR (500 MHz, DMSO-d_6, δ): 5.20 (t, 2.6 Hz, 2H), 5.10 (t, 2.6 H, 2H), 1.13 (s, 9H).

Synthesis of n-Bu_3Sn($^{t\text{-Bu}}$Cp): The title compound was prepared according to a procedure adapted from the literature.[33] *n*-Bu_3SnCl (7.0 mL, 25.8 mmol) was added to a mixture of Li($^{t\text{-Bu}}$Cp) (3.31 g, 25l8 mmol) in toluene (160 mL) and the mixture stirred at room temperature for 2 d. After this time the mixture was filtered across Celite, washed with toluene, and the combined filtrates concentrated in vacuo to give a yellow oil (9.80 g, 23.8 mmol, 92 %). ^{1}H NMR (500 MHz, $CDCl_3$, δ): 6.35 (t, 1.6 Hz, 2H), 5.25 (t, 1.6 Hz, 2H), 1.46 (m, 6H), 1.30 (sext, 7.2 Hz, 6 H), 1.22 (s, 9H), 0.89 (t, 7.2 Hz, 9H), 0.76 (m, 6H).

Synthesis of ($^{t\text{-Bu}}$Cp)$_2$$TaCl_2$: The title compound was prepared according to a procedure adapted from the literature.[22a] *n*-Bu_3Sn($^{t\text{-Bu}}$Cp) (7.97 g, 19.38 mmol) was added to a mixture of $TaCl_5$ (2.00 g, 5.6 mmol, freshly-sublimed) in dichloromethane (50 mL), giving a rapid color change from colorless to deep red. The mixture was stirred at room temperature to 7 d, during which it became a deep green. This mixture was concentrated to a volume of ~ 20 mL, layered with pentane, and chilled at – 25 ºC for 1 d. After this time a solid was collected by vacuum filtration, washed with pentane, and dried in vacuo to give a fine brown solid (1.73 g) that was used without further purification or characterization.

Synthesis of ($^{t\text{-Bu}}$Cp)$_2$$TaH_3$ (5): The title compound was prepared according to procedures adapted from the literature.[22a,b] Sodium bis(2-methoxyethoxy)aluminum hydride (2.4 mL 70 % w/w [~3.5

M] in toluene, 8.4 mmol) was added to a mixture of (t-^{Bu}Cp)$_2$TaCl$_2$ (1.73 g, 3.5 mmol) in toluene (35 mL) and the solution stirred 1 h. After this time it was cooled to 0 ºC and degassed, deionized water (1.7 mL, 94.4 mmol) was added dropwise and the mixture allowed to slowly warm to room temperature and stirred until the viscous mixture became free-flowing. The orange solution was separated from the precipitate and concentrated in vacuo to give an orange solid. Extraction into pentane (25 ml) and cooling to – 84 ºC for 1 h gave a white microcrystalline solid that was collected and dried in vacuo (0.27 g, 0.64 mmol, 18 % yield). ^{1}H NMR (500 MHz, C_6D_6, δ): 4.73 (t, 2.5 Hz, 4H), 4.63 (t, 2.5 Hz, 4H), 1.26 (s, 18H), -1.37 (t, 9.8 Hz, 1H), -2.78 (d, 9.8 Hz, 2H); ^{13}C NMR (126 MHz, C_6D_6, δ): 83.0, 82.1, 31.9, 30.6.

Synthesis of NaCp · 1/3 THF: The title compound was prepared according to a procedure adapted from the literature.[34] Sodium (2.00 g, 87.0 mmol) was added to dicyclopentadiene (160 mL) and the mixture was heated at 160 °C for 24 h until hydrogen evolution ceased and no sodium remained. The copious white solid was collected by vacuum filtration. This solid was heated in toluene (60 mL) and THF (6 mL) at reflux for 1 h, after which it was collected by vacuum filtration, washed with copious pentane, and dried in vacuo to give a free-flowing off-white solid (6.78 g, 60.5 mmol, 69% yield). Spectral data are consistent with those previously reported.[34]

Synthesis of Cp$_2$Ta(=NCMe$_3$)Cl: The title compound was prepared according to a procedure adapted from the literature.[22c] While cooling to –84 ºC, a solution of NaCp • 1/3 THF (1.88 g, 16.88 mmol, 2.1 equiv) in Et$_2$O (60 mL) and THF (15 mL) was added to a heterogeneous solution of Ta(=NCMe$_3$)Cl$_3$(py)$_2$ (4.13 g, 8.00 mmol, 1.0 equiv) in Et$_2$O (270 mL). The mixture was allowed to slowly warm to room temperature and stirred for 18 h, after which solvent removal in vacuo gave an opaque red solid. Extraction into pentane (3 x 50 mL) and concentration of the

combined extracts gave a deep red oily-to-waxy product (2.79 g, 83% yield). Spectral data are consistent with those previously reported.[22c]

Synthesis of Cp_2TaH_3 (6). The title compound was prepared according to a procedure adapted from the literature.[22e] While cooling to –84 ºC, a solution of $Cp_2Ta(=NCMe_3)Cl$ (2.79 g, 6.68 mmol, 1.0 equiv) in Et_2O (65 mL) was added to a suspension of $LiAlH_4$ (1.02 g, 26.8 mmol, 4.0 equiv) in Et_2O (65 mL). The mixture was allowed to slowly warm to room temperature and stirred for 18 h, after which it was cooled to 0 ºC and degassed deionized water was added dropwise (1.96 mL, 108 mmol, 16 equiv). Extraction of the mixture into Et_2O (3 x 50 mL) and concentration of the combined extracts gave an off-white solid (0.90 g, 43% yield). Spectral data are consistent with those previously reported.[22e]

Computational Section

Calculations were performed with Gaussian 16[35]. An ultrafine integration grid and the keyword 5d were used for all calculations. Except when evaluating other methods as specified in the Supporting Information, geometry optimizations of the stationary points were carried out in the gas phase with the M06L[36] functional with BS1 (BS1 = the LANL2DZ pseudo-potential for Ta and the 6-31+G(d,p) basis for all other atoms). Frequency analyses were carried out at the same level to evaluate the zero-point vibrational energy and thermal corrections at 298 K. The nature of the stationary points was determined in each case according to the appropriate number of negative eigenvalues of the Hessian matrix. Forward and reverse intrinsic reaction coordinate calculations were carried out on the optimized transition structures to ensure that they indeed connect the appropriate reactants and products.[37] Multiple conformations and configurations were considered for all structures, and the lowest energy structures are reported. Unless otherwise specified in the Supporting Information, single point energy calculations were performed with the M06[38]

functional with BS2 (BS2 = the SDD pseudopotential for Ta and the 6-311++G(2d,p) basis set for all other atoms). Bulk solvent effects in benzene for computations in Schemes 2 and 3 and Tables 1, 2, and 6 (Entry 1 only), toluene for computations in Table 6 (Entry 2 only), and cyclohexane for Table 6 (Entries 3-6) were considered implicitly in the single point energy calculations through the CPCM solvation model.[39] Bond lengths were measured using Gaussview 5.0[40] and cyclopentadienyl plane angles were measured using Mercury 3.0.[41] 3D images of structures were prepared with Cylview.[42]

References

1. (a) McGlade, C.E. A review of the uncertainties in estimates of global oil resources. *Energy* **2012**, *47*, 262-270; (b) McGlade, C. & Ekins, P. The geographical distribution of fossil fuels unused when limiting global warming to 2 °C. *Nature* **2015**, *517*, 187-190.
2. Montzka, S.A.; Blugokencky, E.J.; Butler, J.H. Non-CO2 greenhouse gases and climate change. *Nature* **2011***, 476*, 43-50.
3. (a) Soltanieh, M.; Zohrabian, A.; Gholipour, M.J.; Kalnay, E. A review of global gas flaring and venting and impact on the environment: Case study of Iran. *Int. J. Greenhouse Gas Control* **2016**, *49*, 488-509; (b) Du, F.; Nojabaei, B. A Review of Gas Injection in Shale Reservoirs: Enhanced Oil/Gas Recovery Approaches and Greenhouse Gas Control. *Energies* **2019**, *12*, 2355-2387.
4. Crabtree, R.H. Alkane C–H activation and functionalization with homogeneous transition metal catalysts: a century of progress—a new millennium in prospect. *J. Chem. Soc, Dalton Trans.* **2001**, 2437-2450.
5. Gunsalas, N.J.; Koppaka, A.; Park, S.H.; Bischof, S.M.; Hashiguchi, B.G.; Periana, R.A. Homogeneous functionalization of methane. *Chem. Rev.* **2017**, *117*, 8521-8573.
6. Hodala, J.L; Moon, D.J.; Reddy, K.R.; Reddy, C.V.; Kumar, T.N.; Ahamed, M.I.; Raghu, A.V. Catalyst design for maximizing C5+ yields during Fischer-Tropsch synthesis. *Int. J. Hydrogen Energy* **2021**, *46*, 3289-3301.
7. Arakaweau,, H.; Aresta, M.; Armor, J.N.; Barteau, M.A.; Beckman, E.J.; Bell, A.T.; Bercaw, J.E.; Creutz, C.; Dinjus, E.; Dixon, D.A.; Domen, K.; DuBois, D.L.; Eckert, J.; Fujita, E.; Gibson, D.H.; Goddard, W.A.; Goodman, D.W.; Keller, J.; Kubas, G.J.; Kung, H.H.; Lyons, J.E.; Manzer, L.E.; Marks, T.J.; Morokuma, K.; Nicholas, K.M.; Periana, R.; Que, L.; Rostrup-Nielson, J.; Sachtler, W.M.H.; Schmidt, L.D.; Sen, A.; Somorjai, G.A.; Stair, P.C.; Stults, B.R.; Tumas, W. Catalysis Research of Relevance to Carbon Management: Progress, Challenges, and Opportunities. *Chem. Rev.* **2011,** *101*, 953-996.
8. (a) Crabtree, R.H. The organometallic chemistry of alkanes. *Chem. Rev.* **1985**, *85*, 245-269; (b) Gunsalus, N.J.; Koppaka, A.; Park, S.H.; Bischof, S.M.; Hashiguchi, B.G.; Periana, R.A. Homogeneous functionalization of methane. *Chem. Rev.* **2017**, *117*, 8521-8573.
9. (a) Stahl, S. S.; Labinger, J. A.; Bercaw, J. E. Homogeneous Oxidation of Alkanes by Electrophilic Late Transition Metals. *Angew. Chem., Int. Ed*. **1998**, *37*, 2180−2192; (b) Lersch, M.; Tilset, M. Mechanistic Aspects of C−H Activation by Pt Complexes. *Chem. Rev*. **2005**, *105*, 2471−2526.
10. Kepp, K.P. A quantitative scale of oxophilicity and thiophilicity. *Inorg. Chem.* **2016**, *55*, 9461-9470.
11. For the seminal example, see: (a) Watson, P.L., Methane Exchange Reactions of Lanthanide and Early-Transition-Metal Methyl Complexes. *J. Am. Chem. Soc.* **1983**, *105*, 6491-6493; For a modern review on the subject, see: (b) Waterman, R. σ-Bond Metathesis: A 30-Year Retroscpective. *Organometallics* **2013**, *32*, 7249-7263.
12. Beaumier, E.P.; Pearce, A.J.; See, X.Y.; Tonks, I.A., Modern applications of low-valent early transition metals in synthesis and catalysis, *Nat. Chem. Rev.* **2019**, *3*, 15-34.
13. For a personal and entertaining account of the early days of the metallocene chemistry (including early TM metallocene chemistry), see: Cotton, F.A., Cyclopentadienyl–metal

chemistry in the Wilkinson Group, Harvard, 1952–1955. *J. Organomet. Chem.* **2001**, *637-639*, 18-26.

14. For an engaging account focused on the specific history and modern chemistry of the titanocenes, see: Chirik, P.J. Group 4 Transition Metal Sandwich Complexes: Still Fresh after Almost 60 Years. *Organometallics* **2010**, *29*, 1500-1517.
15. (a) Bailey, B.C.; Fan, H.; Baum, E.W.; Huffman, J.C.; Baik, M.-H.; Mindiola, D.J. Intermolecular C-H Bond Activation Promoted by a Titanium Alkylidyne. *J. Am. Chem. Soc.* **2005**, *127*, 16016-16017; (b) Flores, J.A.; Cavaliere, V.N.; Buck, D.; Pinter, B.; Chen. G.; Crestani, M.G.; Baik, M.-H.; Mindiola, D.J. Methane activation and exchange by titanium-carbon multiple bonds. *Chem. Sci.* **2011,** *2*, 1457-1462.
16. For C—H activation at unactivated alkanes see: (a) Vidal, V.; Theólier, A.; Thivolle-Cazet, J.; Basset, J-M. Activation and Functionalisation of the C-H Bonds of Methane and Higher Alkanes by a Silica-supported Tantalum Hydride Complex. *J. Chem. Soc. Commun.* ***1995,*** 991-992; for alkane sigma-bond metathesis see: (b) Vidal, V.; Theolier, A.; Thivolle-Cazat, J.; Basset, J.-M. Metathesis of Alkanes Catalyzed by Silica-Supported Transition Metal Hydrides. *Science* **1997**, *276*, 99; (c) Thieuleux, C.; Copéret, C.; Dufaud, V.;Marangelli, C.; Kuntz, E.; Basset, J.-M. Heterogeneous well-defined catalysts for metathesis of inert and not so inert bonds. *J. Mol. Catal. A* **2004**, *213*, 47-57; (d) Basset, J. M.; Copéret, C.; Lefort, L.; Maunders, B. M.; Maury, O.; Le Roux, E.; Saggio, G.; Soignier, S.; Soulivong, D.; Sunley, G. J.; Taoufik, M.; Thivolle-Cazat J., Primary Products and Mechanistic Considerations in Alkane Metathesis. *J. Am. Chem. Soc*. **2005**, *127*, 8604-8605; (e) Le Roux, E.; Taoufik, M.; Copéret, C.; de Mallmann, A.; Thivolle-Cazat, J.; Basset, J.-M.; Maunders, B. M.; Sunley, G. Development of Tungsten-Based Heterogeneous Alkane Metathesis Catalysts Through a Structure–Activity Relationship. *J. Angew. Chem., Int. Ed*. **2005**, *44*, 6755-6758; for non-oxidative coupling of methane see: (f) Soulivong, D.; Norsic, S.; Taoufik, M.; Copéret, C.; Thivolle-Cazat, J., Chakka, S.; Basset, J-M. Non-Oxidative Coupling Reaction of Methane to Ethane and Hydrogen Catalyzed by the Silica-Supported Tantalum Hydride: $(SiO)_2Ta$-H. *J. Am. Chem. Soc.* **2008**, *130*, 5044-5045.
17. For a review on intramolecular C—H activation, see: (a) Ryabov, A.D. Mechanisms of intramolecular activation of carbon-hydrogen bonds in transition-metal complexes. *Chem. Rev.* **1990**, *90*, 403-424. For intramolecular C—H activation by tantalocenes of the C—H bonds of the Cp* ligand, see: (b) Parkin, G.; Bunel, E.; Burger, B.J.; Trimmer, M.S.; Van Asselt, A.; Bercaw, J.E. Alpha- and beta-migratory insertion and elimination processes for alkyl complexes of permethyl-scandocene and permethyltantalocene. *J. Mol. Catal.* **1987**, *41*, 21-39; (c) Antonelli, D. M.; Schaefer, W. P.; Parkin, G.; Bercaw, J.E. Synthesis and characterization of $(\eta^5\text{-}C_5Me_5)_2TaCl(THF)$, a useful synthetic precursor for the preparation of oxo, imido and methylidene derivatives of permethyltantalocene. *J. Organomet. Chem.* **1993**, *462*, 213-220; (d) Riley, P.N.; Parker, J.R.; Fanwick, P.E.; Rothwell, I.P. Formation of Tantalum "Tuck-in" Complexes by Activation of Methyl C-H Bonds in Pentamethylcyclopentadiene Groups by Carbazole Ligation. *Organometallics* **1999**, *18*, 3579-3583. For other examples of intramolecular C—H activation catalyzed by organometallic tantalum complexes, see: (e) Ballard, K.R.; Gardiner, I.M.; Wigley, D.W. Evidence for intramolecular carbon-hydrogen bond activation and the formation of a tucked-in complex of hexamethylbenzene at a tantalum(III) center. *J. Am. Chem. Soc.* **1989**, *111*, 2159-2162; (f) Vilardo, J.S.; Lockwood, M.A.; Hanson, L.G.; Clark, J.R.; Parkin, B.C.; Fanwick, P.E.; Rothwell, I.P. Intramolecular activation of aromatic C–H bonds at tantalum(V) metal centers:

evaluating cyclometallation 'resistant' and 'immune' aryloxide ligation. *J. Chem. Soc., Dalton Trans.* **1997**, 3353-3362.

18. (a) Barefield, E.K.; Parshall, G.W.; Tebbe, F.N. Catalysis of Aromatic Hydrogen-Deuterium Exchange by Metal Hydrides. *J. Am. Chem. Soc.* **1970**, *92*, 5234-5235; (b) Parshall, G.W. Intramolecular aromatic substitution in transition metal complexes. *Acc. Chem. Res.* **1970**, *3*, 139-144; (c) Tebbe, F.N. and Parshall, G.W. Hydride Derivatives of Niobocene and Tantalocene. *J. Am. Chem. Soc.* **1971**, *93*, 3793-3795; (d) Klabunde, U. and Parshall, G.W. Activation of Aromatic Carbon-Hydrogen Bonds by Transition Metal Complexes. II. Substituted Benzenes. *J. Am. Chem. Soc.* **1972**, *94*, 9081-9087; (e) Foust, D.F.; Rogers, R.D.; Rausch, M.D.; Atwood, J.L. Photoinduced Reactions of $(\eta^5\text{-}C_5H_5)_2M(CO)H$ (M = Nb, Ta) and the Molecular Structure of $(\eta^5\text{-}C_5H_5)_2Ta(CO)H$. *J. Am. Chem. Soc*. **1982**, *104*, 5646-5650; (f) Shilov, A.E. *Activation of Saturated Hydrocarbons by Transition Metal Complexes*; Reidel: Boston, 1984.
19. Rehbein, S.R.; Kania, M.J.; Neufeldt, S.R. Experimental and Computational Evaluation of Tantalocene Hydrides for C–H Activation of Arenes. *Organometallics* **2021**, *40*, 2666-2677.
20. Calculations were performed at the CPCM(benzene)-MO6L/BS2//MO6L/BS1 level, where BS1 = 6-31G(d,p) for C, H, D and LANL2DZ for Ta and BS2 = SDD for Ta and 6-311++G(d,p) for all other elements. Calculations were performed using Gaussian 16: Frisch, M. J.; Trucks, G. W.; Schlegel, H. B.; Scuseria, G. E.; Robb, M. A.; Cheeseman, J. R.; Scalmani, G.; Barone, V.; Petersson, G. A.; Nakatsuji, H.; Li, X.; Caricato, M.; Marenich, A. V.; Bloino, J.; Janesko, B. G.; Gomperts, R.; Mennucci, B.; Hratchian, H. P.; Ortiz, J. V.; Izmaylov, A. F.; Sonnenberg, J. L.; Williams-Young, D.; Ding, F.; Lipparini, F.; Egidi, F.; Goings, J.; Peng, B.; Petrone, A.; Henderson, T.; Ranasinghe, D.; Zakrzewski, V. G.; Gao, J.; Rega, N.; Zheng, G.; Liang, W.; Hada, M.; Ehara, M.; Toyota, K.; Fukuda, R.; Hasegawa, J.; Ishida, M.; Nakajima, T.; Honda, Y.; Kitao, O.; Nakai, H.; Vreven, T.; Throssell, K.; Montgomery, J. A., Jr.; Peralta, J. E.; Ogliaro, F.; Bearpark, M. J.; Heyd, J. J.; Brothers, E. N.; Kudin, K. N.; Staroverov, V. N.; Keith, T. A.; Kobayashi, R.; Normand, J.; Raghavachari, K.; Rendell, A. P.; Burant, J. C.; Iyengar, S. S.; Tomasi, J.; Cossi, M.; Millam, J. M.; Klene, M.; Adamo, C.; Cammi, R.; Ochterski, J. W.; Martin, R. L.; Morokuma, K.; Farkas, O.; Foresman, J. B.; Fox, D. J. Gaussian 16; Gaussian Inc.: Wallingford CT, 2016.
21. For a recent review, see: Beckhaus, R. Pentafulvene complexes of group four metals: Versatile organometallic building blocks. *Coord. Chem. Rev*. **2018**, *376*, 467-477.
22. (a) Green, M.L.H. & Jousseaume, B. Bis(η-isopropylcyclopentadienyl)tantalum chemistry: some hydride, carbonyl, alkyl, al-kyne and tertiaryphosphine derivatives, and an improved synthesis of dichlorobiscyclopentadienylniobium. *J. Organomet. Chem*. **1980**, *193*, 339-344; (b) Leblanc, J.-C.; Reynoud, J.-F.; Moise, C. Complexes bis cyclopentadienyles substitues du tantale: synthese et reactivite de dichlorures, de tri- et de monohydrures. *C. R. Acad. Sc. Paris* **1982**, *295*, 755-757; (c) Schmidt, S.; Sundermeyer, J. Höhervalente derivate der d-metall-säuren X. Imidokomplexe des fünf- und vierwertigen niobs und tantals mit halbsandwich- und metallocen- struktur *J. Organomet. Chem*. **1994**, *472*, 127-138; (d) Korolev, A.V.; Rheingold, A.L.; Williams, D.W. A General Route to Labile Niobium and Tantalum d^0 Monoimides. Discussion of Metal-Nitrogen Vibrational Modes. *Inorg. Chem*. **1997**, *36*, 2647-2655; (e) Findlay, A.E.; Leelasubcharoen, S.; Kuzmina, L.G.; Howard, J.A.K.; Nikonov, G.I. Phosphido-bridged Ta/Rh bimetallic complex: synthesis, structure, and catalytic hydrosilylation of acetophenone. *Dalton Trans*. **2010**, *39*, 9264-9269.

23. ^{1}H NMR kinetics experiments involving arene H/D exchange were done in Wilmad nine-inch medium-walled high-pressure NMR tubes in benzene-d_6 (0.60 mL) under nitrogen (60 psi) with 0.20 mol % catalyst and 0.20 mol % cyclohexane as an internal standard at 100 °C over 6 h. Cyclohexane's efficacy as an inert standard in arene H/D exchange experiments has been previously validated with Cp_2TaH_3 (0.20 mol %) in a benzene and cyclohexane-d_{12} (0.20 mol %) reaction mixture (100 °C, 60 psi N2, 14 h), after which no deuterium incorporation was observed that would indicate C—D activation of cyclohexane-d_{12}.
24. With the unsubstituted complex, Cp_2TaH_3 (**6**), the ^{1}H NMR cyclopentadienyl hydrogens appear as a singlet due to equivalency resulting from rapid ligand rotation. In the case of the alkyl-substituted complexes, however, the cyclopentadienyl hydrides produce two ^{1}H NMR signals (HMQC and HMBC NMR spectroscopy allowed for the unequivocal assignment of the two signals), which has allowed us to monitor not only the sum of these two signals as an indicator of catalyst decomposition but also the ratio of these two signals, which we have used to monitor the intramolecular C—H activation of these hydrogens.
25. The values reported in Table 6 are all the result of oxidative addition by tantalum into the relevant C—H bond. The alternate σ-bond metathesis pathways have been investigated from both the d^0 Ta(V) species, **1**, and the reactive d^2 Ta(III) species, **1-H1**, and in all instances transition states found to either be much higher in energy or reaction coordinates nonconvergent.
26. Cyclohexane has been successfully employed as the solvent in the early transition metal-catalyzed C—H activation of methane (see Reference 15).
27. Reaction conditions investigated included 0.20 mol % **1** in 2.0 mL cyclohexane at temperatures of 80, 100, and 120° C, at pressures as high as 200 psi methane-d_4, and reaction times of 24 and 48 h.
28. Deutsch, P.P.; Maguire, J.A.; Jones, W.D.; Eisenberg, R. Hydride Abstraction. The Reaction of IrX(CO)(dppe) with Cp_2TaH_3. *Inorg. Chem*. **1990**, *29*, 686-690.
29. We were, of course, further constrained by the commercial availability of perdeuterated aliphatic substrates.
30. Our initial hope was to use cyclohexane alongside the deuteroalkane substrates as an internal standard such that we could quantify the rates of reaction at each of the C—D bonds of the substrates. This means of analysis, however, was plagued by poor reproducibility that we were unable to resolve even after significant effort. We believe the origin of the lack of reproducibility is the difficulty in maintaining the initial ratio of deuteroalkane to cyclohexane—minute changes in which give outsized and likely misleading measurements of reactivity. Ultimately, we have chosen to report changes in the relative signal integrations after the reaction time, which at the beginning are taken to be unity. This means of analysis precludes or analysis of cyclohexane-d_{12} due to its single ^{1}H NMR signal.
31. Reactions were performed in a Fisher-Porter tube over 48 h at the boiling point of the particular deuteroalkane with 0.20 mol % 1. In a typical experiment a 0.20 mol % catalyst solution was prepared with 0.5 v/v internal standard (either cyclohexane or tetraethylsilane, chosen to avoid signal overlap), an initial ^{1}H NMR spectrum acquired, and—with cooling to -195° C—the vessel containing the reaction mixture three times evacuated-refilled to 1 atm hydrogen (corresponding to 4.52, 4.65, and 4.78 atm H_2 at the reaction temperatures for cyclohexane-d_{12}, methylcyclohexane-d_{14}, and octane-d_{18}, respectively). The tube was heated in an oil bath at the boiling point of the alkane for 48 h, after which the mixture was cooling and a final ^{1}H

NMR spectrum obtained. Deuteroalkane signal increases were determined as a percent increase of their original value.

32. Coşkun, N. and Erden, I., An efficient catalytic method for fulvene synthesis. *Tetrahedron* **2011**, *67*, 8607-8614.
33. Sanner, R.D.; Carter, S.T.; Bruton, Jr., W.J. The preparation of mono(η^5-pentamethylcyclopentadienyl) compounds of tantalum(V). *J. Organomet. Chem*. **1982**, *240*, 157-162.
34. Tay, B.Y.; Wang, C.; Stubbs, L.P.; Jacob, C.; van Meurs, M., Deuterated dimethyl sulfoxide as a good NMR solvent for the characterization of alkali metal cyclopentadienides, amides, alkoxides and phenoxides. *J. Organomet. Chem*. **2011**, *686*, 3431-3435.
35. Frisch, M. J.; Trucks, G. W.; Schlegel, H. B.; Scuseria, G. E.; Robb, M. A.; Cheeseman, J. R.; Scalmani G., Barone, V.; Petersson, G. A.; Nakatsuji, H.; Li, X.; Caricato, M.; Marenich, A. V.; Bloino, J.; Janesko, B. G.; Gomperts, R.; Mennucci, B.; Hratchian, H. P.; Ortiz, J. V.; Izmaylov, A. F.; Sonnenberg, J. L.; Williams-Young, D.; Ding, F.; Lipparini, F.; Egidi, F.; Goings, J.; Peng, B.; Petrone, A.; Henderson, -T.; Ranasinghe, D.; Zakrzewski, V. G.; Gao, J.; Rega, N.; Zheng, G.; Liang, W.; Hada, M.; Ehara, M.; Toyota, K.; Fukuda, R.; Hasegawa, J.; Ishida, M.; Nakajima, T.; Honda, Y.; Kitao, O.; Nakai, H.; Vreven, T.; Throssell, K.; Montgomery, J. A. Jr.; Peralta, J. E.; Ogliaro, F.; Bearpark, M. J.; Heyd, J. J.; Brothers, E. N.; Kudin, K. N.; Staroverov, V. N.; Keith, T. A.; Kobayashi, R.; Normand, J.; Raghavachari, K.; Rendell, A. P.; Burant, J. C.; Iyengar, S. S.; Tomasi, J.; Cossi, M.; Millam, J. M.; Klene, M.; Adamo, C.; Cammi, R.; Ochterski, J. W.; Martin, R. L.; Morokuma, K.; Farkas, O.; Foresman, J. B.; and Fox, D. J. *Gaussian 16*; Gaussian, Inc., Wallingford CT, 2016.
36. Zhao, Y.; Truhlar, D. G. A New Local Density Functional for Main-Group Thermochemistry, Transition Metal Bonding, Thermo-chemical Kinetics, and Noncovalent Interactions. *J. Chem. Phys*. **2006**, *125*, 194101.
37. (a) Gonzalez, C.; Schlegel, H. B. An Improved Algorithm for Reaction Path Following. *J. Chem. Phys*. **1989**, *90*, 2154−2161; (b) Gonzalez, C.; Schlegel, H. B. Reaction Path Following in Mass-Weighted Internal Coordinates. *J. Phys. Chem*. **1990**, *94*, 5523−5527; (c) Fukui, K. The Path of Chemical Reactions - the IRC Approach. *Acc. Chem. Res*. **1981**, *14*, 363−368
38. Zhao, Y.;Truhlar, D. G. The M06 suite of density functionals for main group thermochemistry, thermochemical kinetics, noncovalent interactions, excited states, and transition elements: two new functionals and systematic testing of four M06-class functionals and 12 other functionals. *Theor. Chem. Acc*., **2008**, *120*, 215–241.
39. Cossi, M.; Rega, N.; Scalmani, G.; Barone, V. Energies, structures, and electronic properties of molecules in solution with the CPCM solvation model. *J. Comput. Chem*. **2003**, *24*, 669−681.
40. GaussView, Version 6, Dennington, Roy; Keith, Todd A.; Millam, John M. Semichem Inc., Shawnee Mission, KS, 2016.
41. Macrae, C. F.; Bruno, I. J.; Chisholm, J. A.; Edgington, P. R.; McCabe, P.; Pidcock, E.; Rodriguez-Monge, L.; Taylor, R.; van de Streek, J.; Wood, P. A., Mercury CSD 2.0 - new features for the visualization and investigation of crystal structures. *Journal of Applied Crystallography* **2008**, *41*, 466-470.
42. Legault, C. Y. *CYLview, 1.0b*; Universitéde Sherbrooke, 2009 http://www.cylview.org.

CHAPTER FOUR

SOLVENT COORDINATION TO PALLADIUM CAN INVERT THE SELECTIVITY OF OXIDATIVE ADDITION

Contribution of Authors and Co-Authors

Manuscript in Chapter Four
Co-First Author: Steven M. Rehbein
Contributions: Data curation, formal analysis, investigation, methodology, validation, visualization, writing – original draft

Co-First Author: Emily K. Elias
Contributions: Data curation, formal analysis, investigation, methodology, visualization, writing – original draft

Co-Author: Sharon R. Neufeldt
Contributions: Conceptualization, data curation, formal analysis, funding acquisition, investigation, methodology, project administration, supervision, visualization, writing – original draft; writing – review and editing.

Manuscript Information

Emily K. Elias, Steven M. Rehbein, Sharon R. Neufeldt
Organometallics
Status of Manuscript:
____ Prepared for submission to a peer-reviewed journal
____ Officially submitted to a peer-reviewed journal
____ Accepted by a peer-reviewed journal
__X_ Published in a peer-reviewed journal

Chemical Science
Submitted October 25, 2021
Published online December 22, 2021
Published in issue *(awaiting assignment)*
DOI: 10.1039/D1SC05862B

Check for updates

View Article Online
View Journal

Chemical Science

Accepted Manuscript

This article can be cited before page numbers have been issued, to do this please use: E. K. Elias, S. M. Rehbein and S. R. Neufeldt, *Chem. Sci.*, 2022, DOI: 10.1039/D1SC05862B.



This is an Accepted Manuscript, which has been through the Royal Society of Chemistry peer review process and has been accepted for publication.

Accepted Manuscripts are published online shortly after acceptance, before technical editing, formatting and proof reading. Using this free service, authors can make their results available to the community, in citable form, before we publish the edited article. We will replace this Accepted Manuscript with the edited and formatted Advance Article as soon as it is available.

You can find more information about Accepted Manuscripts in the Information for Authors.

Please note that technical editing may introduce minor changes to the text and/or graphics, which may alter content. The journal's standard Terms & Conditions and the Ethical guidelines still apply. In no event shall the Royal Society of Chemistry be held responsible for any errors or omissions in this Accepted Manuscript or any consequences arising from the use of any information it contains.

Please do not adjust margins

View Article Online
DOI: 10.1039/D1SC05862B

ARTICLE

Solvent coordination to palladium can invert the selectivity of oxidative addition

Received 00th January 20xx,
Accepted 00th January 20xx

DOI: 10.1039/x0xx00000x

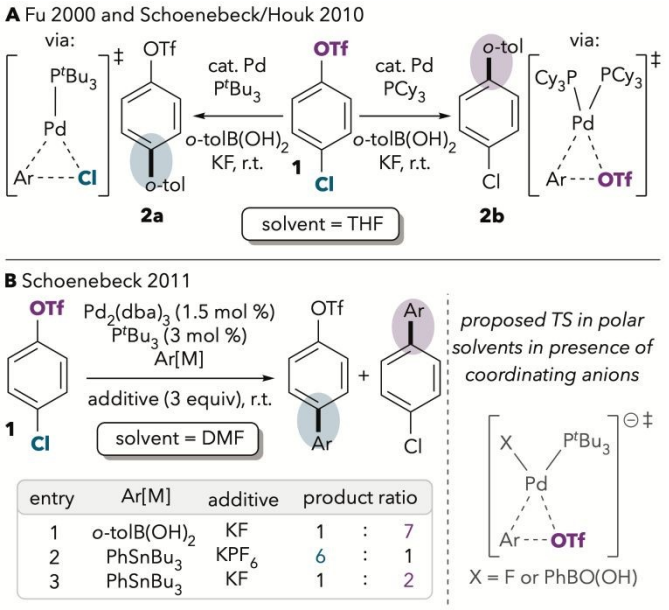
Emily K. Elias,‡[a] Steven M. Rehbein,‡[a] Sharon R. Neufeldt[a]*

Reaction solvent was previously shown to influence the selectivity of Pd/P^{t}Bu$_3$-catalyzed Suzuki-Miyaura cross-couplings of chloroaryl triflates. The role of solvents has been hypothesized to relate to their polarity, whereby polar solvents stabilize anionic transition states involving [Pd(P^{t}Bu$_3$)(X)]$^-$ (X = anionic ligand) and nonpolar solvents do not. However, here we report detailed studies that reveal a more complicated mechanistic picture. In particular, these results suggest that the selectivity change observed in certain solvents is primarily due to solvent coordination to palladium. Polar coordinating and polar noncoordinating solvents lead to dramatically different selectivity. In coordinating solvents, preferential reaction at triflate is likely catalyzed by Pd(P^{t}Bu$_3$)(solv), whereas noncoordinating solvents lead to reaction at chloride through monoligated Pd(P^{t}Bu$_3$). The role of solvent coordination is supported by stoichiometric oxidative addition experiments, density functional theory (DFT) calculations, and catalytic cross-coupling studies. Additional results suggest that anionic [Pd(P^{t}Bu$_3$)(X)]$^-$ is also relevant to triflate selectivity in certain scenarios, particularly when halide anions are available in high concentrations.

Oxidative addition is a key elementary step in diverse transformations catalyzed by transition metals.[1] For instance, this step is common to traditional cross-coupling reactions, which are among the most widely used methods for small molecule synthesis. During the oxidative addition step of cross-coupling reactions, a low valent metal [usually Pd(0)] inserts into a C—X bond with concomitant oxidation of the metal by two electrons. The "X" group of the C—X bond is commonly a halogen or triflate. Despite a wealth of research into this step,[2,3,4,5] uncertainties remain about its mechanistic nuances. The mechanistic details are especially pertinent to issues of selectivity that arise when substrates contain more than one potentially reactive C—X bond.[6]

One of the best-studied examples of divergent selectivity at the oxidative addition step is the case of Pd-catalyzed Suzuki couplings of chloroaryl triflates. In 2000, Fu reported that a combination of Pd(0) and P^{t}Bu$_3$ in tetrahydrofuran (THF) effects selective coupling of **1** with *o*-tolylB(OH)$_2$ via C—Cl cleavage, resulting in retention of the triflate substituent in the final product **2a** (Scheme 1A).[7] In contrast, the use of PCy$_3$[7] or most other phosphines[8] provides complementary selectivity (product **2b**) under similar conditions. The unique selectivity imparted by P^{t}Bu$_3$ was later attributed to this ligand's ability to promote a monoligated oxidative addition transition state on account of its bulkiness.[5,8] Smaller ligands, on the other hand, favor bisligated palladium, which prefers to react at triflate. The relationship between palladium's ligation state and chemoselectivity has been rationalized by Schoenebeck and Houk through a distortion/interaction analysis.[5] In brief, the selectivity preference of PdL$_2$ is dominated by a strong interaction between the electron-rich Pd and the more electrophilic site (C—OTf). On the other hand, PdL is less electron-rich and its selectivity preference mainly relates to minimizing unfavorable distortion energy by reacting at the more easily-distorted C—Cl bond.

Proutiere and Schoenebeck later discovered that replacing THF with dimethylformamide (DMF, Scheme 1B, entry 1) or acetonitrile caused a change in selectivity for the Pd/P^{t}Bu$_3$



entry	Ar[M]	additive	product ratio
1	*o*-tolB(OH)$_2$	KF	1 : 7
2	PhSnBu$_3$	KPF$_6$	6 : 1
3	PhSnBu$_3$	KF	1 : 2

Scheme 1. Seminal Reports on the Effects of Ligands and Solvents on the Selectivity of Cross-Coupling of a Chloroaryl Triflate[5,7,9]

[a] *Department of Chemistry and Biochemistry, Montana State University, Bozeman, Montana 59717, United States.*
‡ These authors contributed equally.
Electronic Supplementary Information (ESI) available: Experimental and computational details; NMR spectra; calculated energies; cartesian coordinates of minimum-energy calculated structures. See DOI: 10.1039/x0xx00000x

Open Access Article. Published on 22 December 2021. Downloaded on 12/26/2021 4:50:53 PM.
This article is licensed under a Creative Commons Attribution-NonCommercial 3.0 Unported Licence.

Chemical Science Accepted Manuscript

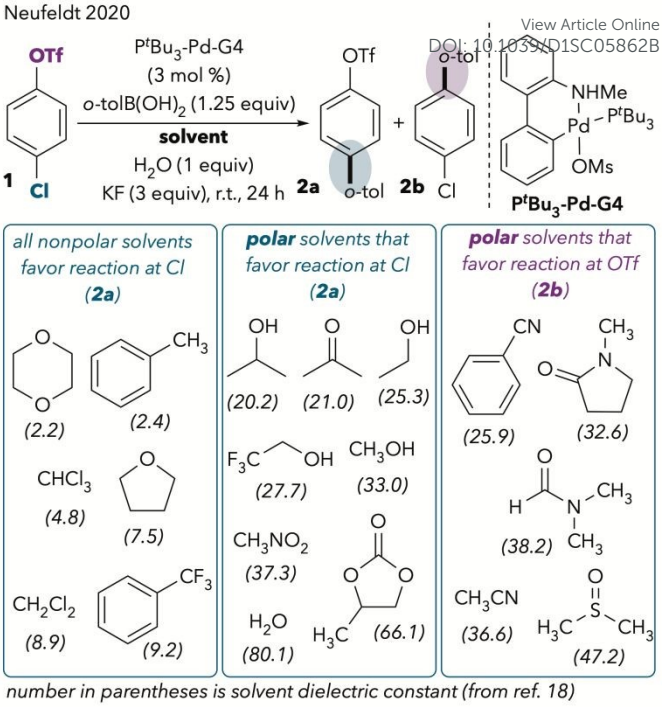
Please do not adjust margins

View Article Online
DOI: 10.1039/D1SC05862B

system.[9,10] In these two polar solvents, preferential reaction at triflate was observed, and P^{t}Bu$_3$ no longer displayed its unique chloride selectivity. The possibility of solvent coordination to Pd was considered, as bisligated Pd(P^{t}Bu$_3$)(solv) would be expected to favor reaction at triflate. However, solvent coordination was ruled out on the basis of two intriguing studies. First, DFT calculations using the functional B3LYP suggested that solvent-coordinated transition states are prohibitively high in free energy (about 16 kcal/mol higher than the lowest-energy monoligated transition structure). Second, the same solvent effect was not observed in a Pd/P^{t}Bu$_3$-catalyzed base-free Stille coupling in DMF (Scheme 1B, entry 2). Instead, the Stille coupling was reported to favor reaction at chloride despite the use of a polar solvent. This result appears inconsistent with the possibility that solvent coordination induces triflate-selectivity, as coordination of DMF to Pd should be possible in both the Stille and Suzuki conditions, if it happens at all. Instead, it was proposed that the key difference between the Suzuki and Stille conditions was the absence of coordinating anions in the latter (unlike traditional Suzuki couplings, Stille couplings do not necessarily require basic additives such as KF to promote transmetalation). Indeed, when KF or CsF was added to the Stille reaction in DMF, selectivity shifted to favor reaction at triflate (Scheme 1B, entry 3), thereby displaying the same behavior as the Suzuki coupling in this solvent. On the basis of this and the DFT studies, it was proposed that polar solvents induce a switch in chemoselectivity if coordinating anions like fluoride are available by stabilizing anionic bisligated transition structures (Scheme 1B, right).

However, our recent extended solvent effect studies produced confounding results.[11] In a Pd/ P^{t}Bu$_3$-catalyzed Suzuki cross-coupling of chloroaryl triflate **1**, we observed no correlation between solvent polarity and chemoselectivity (Scheme 2). Although some polar solvents such as MeCN, DMF, and dimethylsulfoxide (DMSO) favor reaction at triflate, a number of other polar solvents provide the same results as nonpolar solvents by favoring reaction at chloride. For example, cross-coupling primarily takes place through C—Cl cleavage when the reaction is conducted in highly polar solvents like methanol, water, acetone, and propylene carbonate. In fact, the only solvents that promote reaction at triflate are ones that are commonly thought of as "coordinating" in the context of late transition metal chemistry.[12] These are solvents containing nitrogen, sulfur, or electron-rich oxygen lone pairs (nitriles, DMSO, and amides). The observed solvent effects were upheld for a variety of chloroaryl triflates and aryl boronic acids.[11]

We have sought to reconcile these observations with the earlier evidence[9] against solvent coordination. Herein we report detailed mechanistic studies indicating that *coordinating solvents alone are sufficient to induce the observed selectivity switch*. In solvents like DMF and MeCN, stoichiometric oxidative addition is favored at C—OTf even in the absence of anionic additives. The apparent contradiction between our observations and the previously-reported DFT calculations and base-free Stille couplings is reconciled by a reevaluation of those studies. In particular, when dispersion is considered in



Scheme 2. Expanded Solvent Effect Studies in the Pd/P^{t}Bu$_3$-Catalyzed Suzuki Coupling[11]

DFT calculations, neutral solvent-coordinated transition structures involving Pd(P^{t}Bu$_3$)(solv) become energetically feasible. Furthermore, we find that the selectivity analysis in the Stille couplings is convoluted by low yields, the formation of side products, and temperature effects. When these factors are disentangled, the Stille coupling in DMF displays selectivity similar to the Suzuki coupling in the same coordinating solvent. In light of these new results, anionic bisligated [Pd(P^{t}Bu$_3$)(X)]$^-$ does not appear to be the dominant active catalyst in nonpolar or polar solvents unless special measures are taken to increase the concentration of free halide, such as adding tetraalkylammonium halide salts or crown ethers.

Results and Discussion

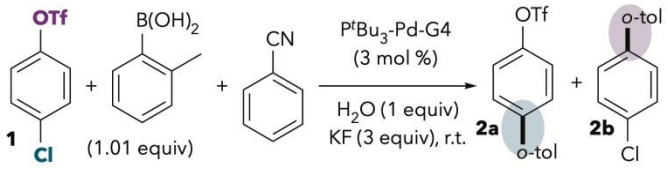
Based on the observed solvent trends in Scheme 2, we hypothesized that selectivity depends on the solvent's ability to coordinate to palladium during oxidative addition. In this scenario, oxidative addition of triflate in solvents such as DMF would not necessarily involve anionic [Pd(P^{t}Bu$_3$)(X)]$^-$, but rather would involve neutral solvent-bound palladium such as Pd(P^{t}Bu$_3$)(DMF). The experiments described below support this hypothesis. We also considered the hypothesis that selectivity could relate to the solvent's ability to solubilize the base (KF). In solvents in which KF is more soluble, a higher concentration of anions [F$^-$, HO$^-$, or ArBO(OH)$^-$] would be available to promote formation of anionic palladium. However, we found no correlation between KF solubility and selectivity (see Electronic Supplementary Information for details on this and other alternative hypotheses).

Open Access Article. Published on 22 December 2021. Downloaded on 12/26/2021 4:50:53 PM.
This article is licensed under a Creative Commons Attribution-NonCommercial 3.0 Unported Licence.
Chemical Science Accepted Manuscript

This journal is © The Royal Society of Chemistry 20xx

View Article Online
DOI: 10.1039/D1SC05362B

Table 1. Effect of Benzonitrile on Selectivity[a]



entry	solvent	PhCN (equiv)	**1** (%)	**2a** (%)	**2b** (%)	**2a**:**2b**
1	THF	0	20	74	<1	>74:1
2	THF	0.5	39	55	4	14:1
3	PhCN	(solvent)	27	7	53	1:8

[a]GC yields calibrated against undecane as the internal standard. Average of at least three trials. ≤4% yield of the diarylated product was detected in all trials.

Effect of Benzonitriles on Selectivity. Nitriles, including acetonitrile and benzonitrile, were observed to promote reaction at triflate (Scheme 2). Because nitriles are common σ-donor ligands for Pd, we were interested in whether the use of nitriles as substoichiometric additives rather than solvents would still provoke a change in selectivity. To answer this question, the Suzuki reaction was conducted under our standard optimized conditions with THF as solvent in the presence or absence of 0.5 equiv of benzonitrile (Table 1). This small amount of benzonitrile, corresponding to <3% of the solvent volume, should have a minimal effect on the polarity of the reaction medium. Our optimized conditions use Buchwald's air-stable P^{t}Bu$_3$-Pd-G4 precatalyst (see Scheme 2) for convenience of handling. Importantly, the use of the Buchwald precatalyst does not impact selectivity when compared to Fu's original system using $Pd_2(dba)_3$ (see reference 11 and ESI).[7,13] One equivalent of water was routinely added to the Suzuki couplings because this leads to better reproducibility. Small amounts of water are needed to promote transmetallation, and our lab is located in a particularly dry climate where adventitious water can be negligible. However, the addition of 1 equiv of water does not impact observed selectivities (see ESI). All results reported herein are the average of at least 2 trials (see ESI for results of individual replicates). The estimated uncertainty in total mass balance for each catalytic trial is about ±3% due to measurement and instrument error (see ESI).

Consistent with the hypothesis that benzonitrile can coordinate to palladium and influence selectivity, even a substoichiometric amount of PhCN (0.5 equiv) in THF leads to erosion of chloride-selectivity when compared to the reaction without PhCN. Although the reaction gives >70 : 1 selectivity for **2a** in the absence of PhCN (Table 1, entry 1), the addition of 0.5 equiv of PhCN leads to a lower selectivity of 14 : 1 (**2a** : **2b**, entry 2). For comparison, the use of PhCN as solvent provides a complete reversal of selectivity, affording **2a** and **2b** in a ratio of 1 : 8 (entry 3). Analysis of other ratios of PhCN:THF reveals that selectivity inverts when PhCN comprises 10-25% of the total solvent volume, and that small amounts of PhCN lead to lower conversion than observed in either neat THF or PhCN (see ESI for details and discussion).

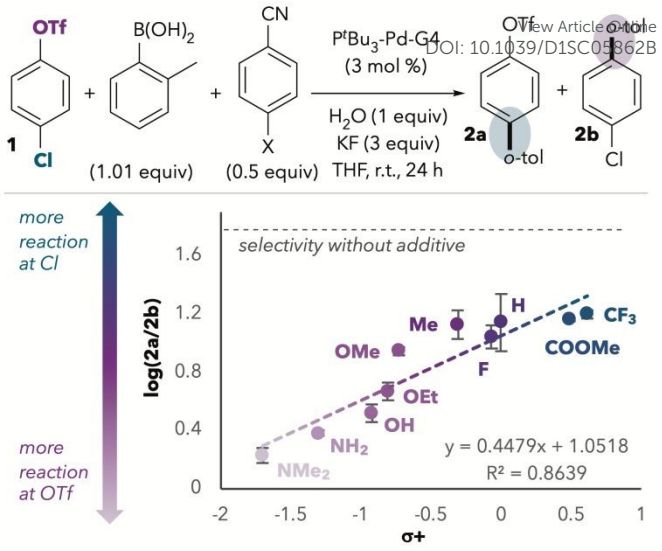


Figure 1. Hammett-type plot shows a correlation between benzonitrile donor ability and increasing reaction at triflate. Each data point represents the average of three trials, and the error bars represent standard deviation.

We next repeated this experiment using a series of substituted benzonitriles, inspired by a similar experiment performed by Watson and coworkers.[14] This study led to a linear free energy relationship plot that revealed a positive correlation between Hammett σ$^+$ values and preference for reaction at chloride (Figure 1).[15] Benzonitriles bearing more electron-donating groups in the para position are expected to be better σ-donors (better ligands) for palladium. Indeed, more reaction at triflate is observed with more electron-rich benzonitriles, consistent with the hypothesis that σ-donation of the nitrile to palladium during oxidative addition promotes reaction at triflate. However, even the most electron-deficient benzonitriles lead to more reaction at triflate compared to the results in the absence of benzonitrile additives (horizontal dashed line in Figure 1).

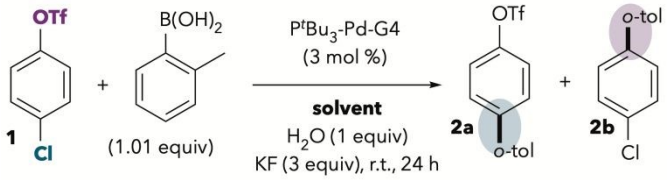
Solvent Variants with Modified Coordinating Ability. Like benzonitrile, acetonitrile also promotes reaction at triflate. We hypothesized that a more electron-deficient derivative of acetonitrile would coordinate more poorly to palladium, and thereby display less of a preference for triflate selectivity than acetonitrile itself. Indeed, the use of fluoroacetonitrile leads to poor selectivity (**2a** : **2b** = 1 : 2; Table 2, entry 2), whereas MeCN strongly favors reaction at triflate (entry 1). This observation is consistent with weaker coordination of fluoroacetonitrile to palladium, resulting in a lower concentration of Pd(P^{t}Bu$_3$)(solv) and less reaction at triflate.

We also compared DMSO to sulfolane. DMSO, a highly polar sulfoxide, can coordinate to soft metals through sulfur's lone electron pair.[16] The use of DMSO as solvent strongly favors reaction at triflate (Table 2, entry 3). Sulfolane has a similar polarity to DMSO, but because it is a sulfone (no lone pair on sulfur) it cannot coordinate to metals in the same manner as DMSO. Consistent with coordinating ability being a critical solvent feature, the use of sulfolane as solvent provides the opposite selectivity as DMSO (entry 4).[17]

Open Access Article. Published on 22 December 2021. Downloaded on 12/26/2021 4:50:53 PM.
This article is licensed under a Creative Commons Attribution-NonCommercial 3.0 Unported Licence.

Chemical Science Accepted Manuscript

Table 2. Modifying the Coordinating Ability of Common Solvents Leads to Changes in Selectivity[a]



entry	solvent	ε [b]	**2a** (%)	**2b** (%)	**2a** : **2b**
1	CH_3CN	36.6	2	77	1 : 39
2	CH_2FCN	~36	4	10	1 : 2
3		47.2	1	45	1 : 45
4		42.2	44	11	4 : 1

[a]GC yields calibrated against undecane as the internal standard. Average of two trials. ≤3% yield of the diarylated product was detected in all trials. [b]Dielectric constants from reference 18 (entries 1, 3, 4) and reference 19 (entry 2).

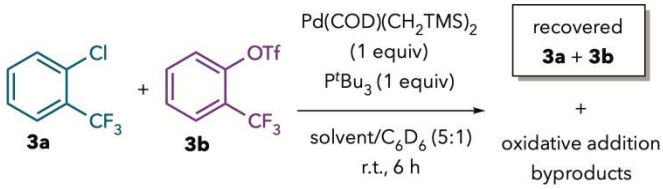
Stoichiometric Oxidative Addition Studies. The observed solvent trends in the Suzuki coupling support the hypothesis that solvent coordination to Pd during oxidative addition can lead to a switch in chemoselectivity. To eliminate confounding factors, we next sought to study the oxidative addition step in isolation. We conducted NMR studies on the reaction of Pd(P^tBu_3) with competing aryl chloride and aryl triflate electrophiles, **3a** and **3b**.[20] These fluorinated substrates were chosen so that their consumption could be monitored by ^{19}F NMR. The putative Pd^0 complex Pd(P^tBu_3) was generated in situ from a 1:1 mixture of Pd(COD)($CH_2TMS)_2$ and P^tBu_3.[21,22] C_6D_6 was added to the reactions to facilitate locking the NMR samples.

The reaction in the noncoordinating solvents toluene, THF, acetone, sulfolane, and propylene carbonate leads to consumption of **3a** (Table 3, entries 1-5, 8, 9), and the known complex (P^tBu_3)Pd(2-$CF_3C_6H_4$)(Cl) is detected by ^{19}F and ^{31}P NMR in most of these solvents.[23] In contrast, nearly all of the aryl triflate **3b** remains unreacted. This result is consistent with the high selectivity for C—Cl activation observed in the catalytic Suzuki coupling of **1** in these solvents. The lower reactivity in toluene at room temperature (entry 1) is ascribed to the formation of Pd($P^tBu_3)_2$, which can be detected by ^{31}P NMR and has been shown previously to react sluggishly with aryl chlorides.[2a,b]

In contrast to the results in non-coordinating solvents, the use of MeCN or DMF leads to preferential consumption of **3b** via C—OTf activation. In MeCN, **3b** is nearly fully consumed after 6 h at room temperature (entry 6), with concomitant formation of palladium black,[24,25,26] an intractable mixture of trifluoromethyl-containing by-products, and a new ^{19}F signal at -77.5 ppm assigned to "free" triflate anion by comparison to the chemical shift of NBu_4OTf in the same solvent mixture. Similar results are observed in DMF (entry 7), albeit with lower conversion and lower selectivity compared to MeCN.[27]

Table 3. Solvent Effect on Selectivity of Stoichiometric Oxidative Addition

View Article Online
DOI: 10.1039/D1SC05862B



		recovered (%)[a]		reacted
entry	solvent	**3a**	**3b**	**3a** : **3b**
1	toluene	89	≥99	≥ 11 : 1
2[b]	toluene	52	98	24 : 1
3	THF	55	97	15 : 1
4	acetone	71	98	15 : 1
5	MeOH	70	≥99	≥ 30 : 1
6	MeCN	97	1	1 : 33
7	DMF	78	44	1 : 3
8	sulfolane	86	95	3 : 1
9	PC[c]	83	94	3 : 1
10[d]	MeCN	≥99	≥99	--
11[d]	DMF	≥99	≥99	--
12[e]	MeCN	n.a.	3	--
13[e]	DMF	n.a.	28	--

[a] ^{19}F NMR yields calibrated against C_6H_5F as an internal standard. Average of two trials. [b]Heated to 80 °C for 2 h. [c]PC = propylene carbonate. [d]Pd(COD)($CH_2TMS)_2$ was omitted from the reaction mixture. [e]**3a** was omitted from the reaction mixture (n.a. = not applicable).

Interestingly, the ^{31}P NMR spectrum of the reaction in DMF reveals a signal at ~75 ppm that is not detected in any of the other solvents. This signal is also observed when **3a** is omitted from the reaction mixture (entry 13). Monitoring the reaction over time reveals that a signal at ~64 ppm is also present at early time points, but is completely replaced by the ~75 ppm signal within 3 h (see ESI). The ~64 ppm signal can also be detected at 6 h when the reaction is run at 0 ºC (see ESI). We hypothesize that these two signals, which are unique to the reaction in DMF, represent DMF-coordinated species such as [ArPd(P^tBu_3)($DMF)_2$]OTf, resulting from oxidative addition of the triflate. Analogous signals are not observed in MeCN, despite its strong coordinating ability. MeCN-bound oxidative addition adducts may decompose more readily due to the smaller sterics of MeCN. For example, NMR and GCMS data indicate that one decomposition pathway under these conditions involves Heck coupling with COD (see ESI), and coordination of COD to Pd(II) may be less favored in the presence of bulkier DMF ligands compared to MeCN ligands.

Importantly, palladium-free control studies demonstrate that the substrates do not decompose in the absence of Pd (entries 10-11). Furthermore, the presence of **3a** is not necessary for reaction of **3b** to take place in coordinating solvents, suggesting that formation of an anionic species like [Pd(P^tBu_3)(Cl)]$^-$ via initial C—Cl activation of **3a**, is not a prerequisite for C—OTf activation in these experiments (entries 12-13).[28]

The results of these stoichiometric studies provide strong evidence that coordinating solvents alone—in the absence of anionic ligands for Pd—can promote a switch in the

Open Access Article. Published on 22 December 2021. Downloaded on 12/26/2021 4:50:53 PM. This article is licensed under a Creative Commons Attribution-NonCommercial 3.0 Unported Licence.

Chemical Science Accepted Manuscript

This journal is © The Royal Society of Chemistry 20xx

Please do not adjust margins

chemoselectivity of oxidative addition compared to the use of noncoordinating solvents. Based on the known preference for bisligated Pd to react at triflate over chloride, the most likely explanation for the observed selectivity in coordinating solvents is involvement of Pd(P^tBu_3)(solv) during oxidative addition. We next turned to computational studies to further evaluate the feasibility of solvent-bound species.

View Article Online
DOI: 10.1039/D1SC05862B

Open Access Article. Published on 22 December 2021. Downloaded on 12/26/2021 4:50:53 PM.
This article is licensed under a Creative Commons Attribution-NonCommercial 3.0 Unported Licence.

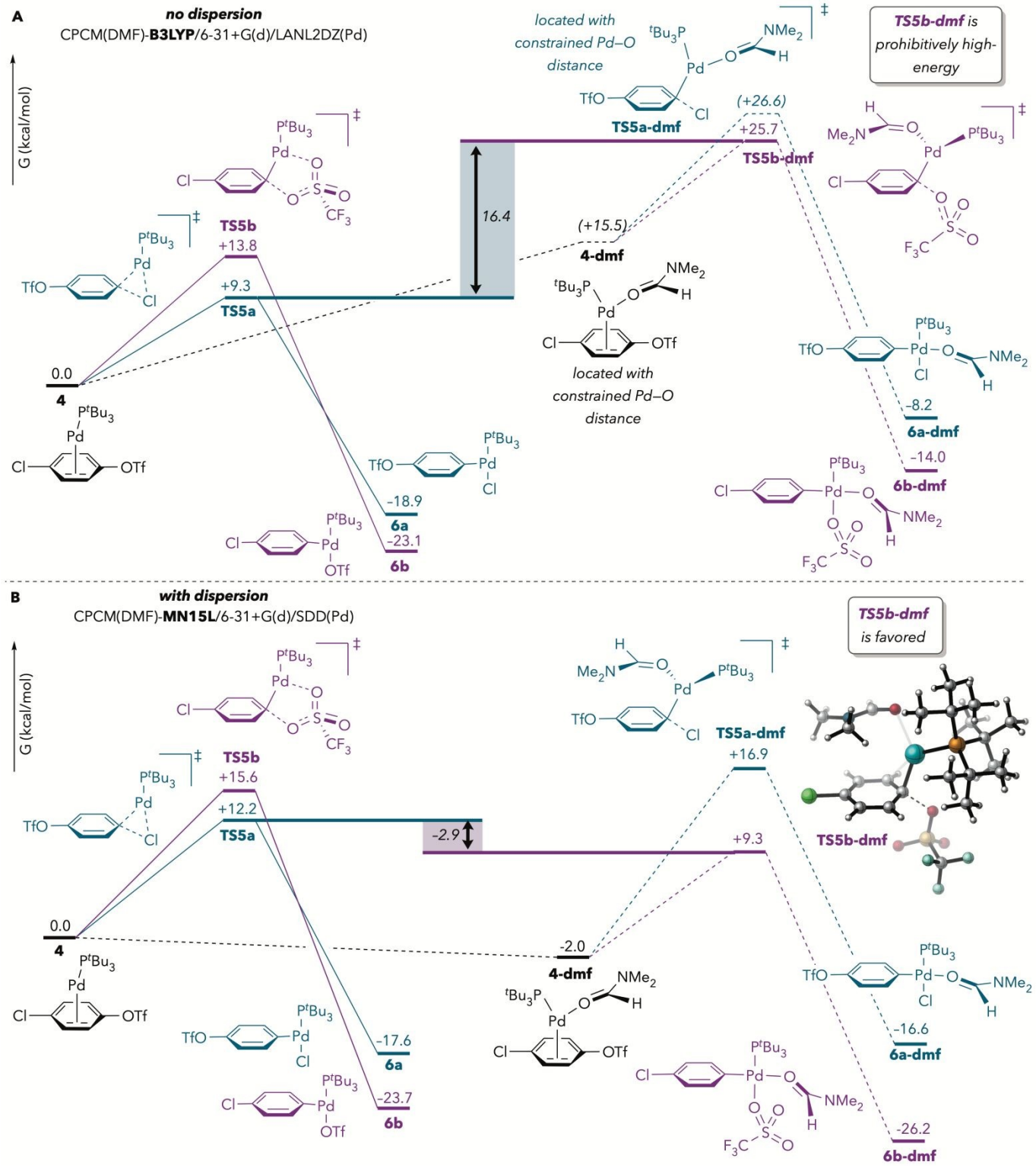


Figure 2. Effect of dispersion on the stability of DMF-coordinated oxidative addition transition structures. Free energy values are corrected for concentration (DMF:Pd = 765:1) and are reported after applying Cramer and Truhlar's[29] and Head-Gordon's[30] quasi-harmonic approximations to vibrational entropy and enthalpy, respectively.[31,32]

Chemical Science Accepted Manuscript

Please do not adjust margins

View Article Online
DOI: 10.1039/D1SC05862B

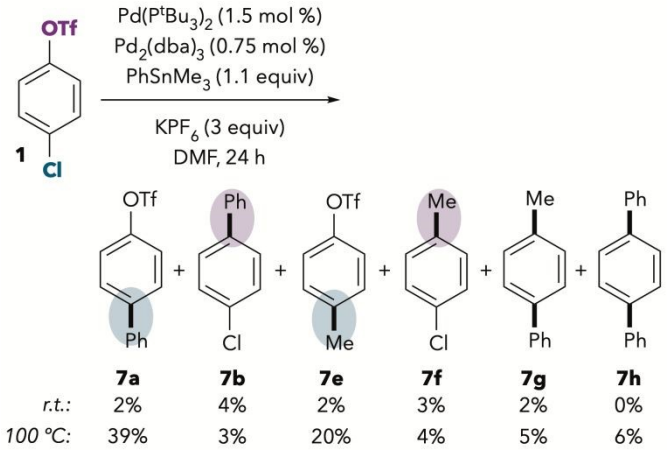
Open Access Article. Published on 22 December 2021. Downloaded on 12/26/2021 4:50:53 PM.
This article is licensed under a Creative Commons Attribution-NonCommercial 3.0 Unported Licence.

DFT Studies. In the earlier report by Proutiere and Schoenebeck, solvent coordination to Pd during oxidative addition at C—OTf was tentatively ruled out, in part on the basis of the high energy values that were calculated for such transition structures.[9] The prior DFT results had indicated that solvent-coordinated transition structures involving Pd(P^tBu_3)(solv) were prohibitively high-energy compared to monoligated transition structures with Pd(P^tBu_3). However, those calculations were conducted with a DFT method (B3LYP)[33] that does not take dispersion into account. Schoenebeck and others have since demonstrated that, in general, the computed energies of crowded structures are significantly lower when dispersion is considered.[34,35]

Therefore, we reevaluated the energetics of solvent coordination to Pd using methods that include dispersion. Figure 2 compares the results of calculations performed with B3LYP (no dispersion) and with MN15L[36] (accounts for dispersion) using the CPCM solvation model for DMF. When dispersion is not considered (Figure 2A), the DMF-coordinated transition structure for oxidative addition at triflate (**TS5b-dmf**) is about 16 kcal/mol higher in energy than the lowest-energy monoligated transition structure (**TS5a**), suggesting that **TS5b-dmf** is unfeasible. However, use of MN15L leads to very different results: **TS5b-dmf** is now predicted to be favored over **TS5a** (Figure 2B).[37] At minimum, these results demonstrate that solvent coordination should not be ruled out on the basis of DFT calculations. Instead, solvent coordination to palladium is likely to be energetically feasible during oxidative addition, especially under experimental conditions in which solvent is in large excess relative to Pd and substrate.

Stille Cross-couplings. Although the Pd/P^tBu_3-catalyzed Suzuki coupling of **1** in DMF favors reaction at triflate, the analogous base-free Stille coupling was reported to favor reaction at chloride in this solvent (see Scheme 1b, entry 2). This result is perplexing, because Suzuki and Stille couplings are thought to proceed through the same oxidative addition step, and our stoichiometric NMR studies indicate that oxidative addition of triflate is preferred in DMF even in the absence of anionic additives.

To understand this contradiction, we examined the Stille coupling between **1** and $PhSnMe_3$ in DMF (Scheme 3).[38,39] Poor conversion is observed at room temperature,[40] but **7b** is slightly favored over **7a**. Methylated products **7e** and **7f** were also detected in the reaction mixture.[41] Overall, the ratio of chloride:triflate activation under these conditions is approximately 4 : 7 [(**7a** + **7e**): (**7b** + **7f**)], which is qualitatively consistent with the triflate selectivity observed in the Suzuki coupling and in the stoichiometric oxidative addition studies. These results suggest that there may not be a discrepancy between the behavior of Pd/P^tBu_3 in the catalytic Suzuki vs. Stille couplings in DMF. However, the low conversion in the Stille coupling calls into question the accuracy of selectivity analysis for at least two reasons. First, measurement errors may be introduced when integrating small product peaks on a GC



Scheme 3. Base-Free Stille Coupling of **1** Catalyzed by Pd/P^tBu_3. GC yields calibrated against dodecane as an internal standard. Results are the average of two trials. Leftover **1**: 83% at r.t., 4% at 100 °C.

chromatogram or when isolating small quantities of materials. More importantly, the low conversion suggests a very sluggish rate of cross-coupling. If cross-coupling is slow, it is possible for undesired processes like catalyst decomposition to compete with coupling, which could lead to different catalyst speciation compared to the much faster Suzuki coupling system.[42]

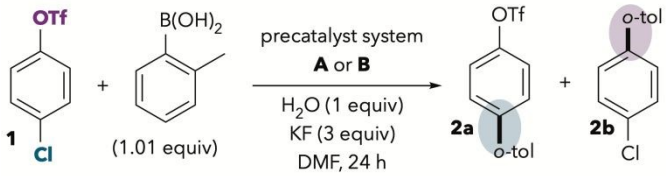
In an effort to increase the conversion of the Stille coupling, the reaction was heated to 100 °C. Slightly higher yields were observed at this temperature, and, interestingly, reaction at chloride becomes preferred. The ratio of chloride:triflate activation under these conditions is approximately 59 : 7 [(**7a** + **7e**): (**7b** + **7f**)]. The chloride preference under these conditions is consistent with the prior report.[9] However, further examination suggests that the selectivity at 100 °C should not be compared to the selectivity at room temperature. We observe an analogous change in selectivity upon heating the Suzuki coupling of **1** in DMF. At 100 °C, selectivity is eroded when using Buchwald's P^tBu_3-Pd-G4 catalyst (Table 4, compare entries 1 and 2). Furthermore, selectivity actually inverts at 100 °C when using a mixture of $Pd_2(dba)_3$ and Pd(P^tBu_3)$_2$ (entries 3 and 4).[43] High temperatures are expected to disfavor bisligated Pd (i.e., reaction at triflate) for entropic reasons. However, the observation that precatalyst influences the selectivity at 100 °C indicates that the increased formation of **2a** may reflect more than simply an entropic penalty. We hypothesize that the palladium catalyst is transformed at high temperature into a species that displays different selectivity than the active catalyst at room temperature.[44,45] As such, a high-temperature Stille coupling is not comparable to a room-temperature Suzuki coupling or to the room-temperature oxidative addition studies. For these reasons, and in order to achieve a faster rate for the room temperature Stille coupling, we next examined the use of a more reactive substrate, **8**.[46]

Chemical Science Accepted Manuscript

This journal is © The Royal Society of Chemistry 20xx

View Article Online
DOI: 10.1039/D1SC05862B

Table 4. Effect of Temperature on the Selectivity of the Pd/P^{t}Bu$_3$-Catalyzed Suzuki Coupling of **1**[a]

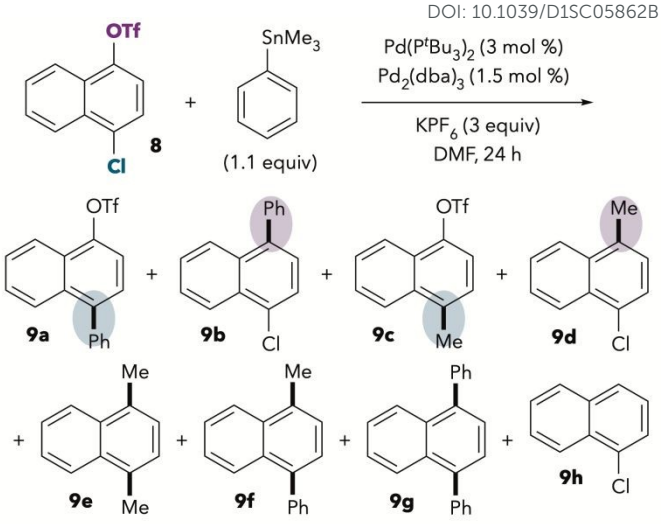


precatalyst system **A**: P^{t}Bu$_3$-Pd-G4 (3 mol %)
precatalyst system **B**: $Pd_2(dba)_3$ (0.75 mol %), $Pd(P^tBu_3)_2$ (1.5 mol %)

entry	cat.	temp (°C)	**1** (%)	**2a** (%)	**2b** (%)	ratio **2a**:**2b**
1	A	r.t.	23	10	60	1 : 6.0
2	A	100	2	21	30	1 : 1.4
3	B	r.t.	17	11	67	1 : 6.1
4	B	100	7	33	23	1.4 : 1

[a]GC yields calibrated against undecane as an internal standard. Results are the average of at least two trials. ≤2% yield of the diarylated product was detected in all trials.

Table 5. Base-Free Stille Coupling of **8** Catalyzed by Pd/P^{t}Bu$_3$[a]



entry	temp	**8**	**9a**	**9b**	**9c**	**9d**	**9e**	**9f**	**9g**	**9h**
1	r.t.	24	1	**9**	3	**42**	1	1	1	1
2	100 °C	1	**13**	4	**33**	12	1	8	9	1

[a]GC yields calibrated against undecane as an internal standard. Results are the average of two trials. No other products derived from **8** could be identified by GCMS.

The room-temperature Stille coupling between $PhSnMe_3$ and chloronaphthol derivative **8** proceeds to higher conversion compared to the reaction of 1 (Table 5, entry 1). After 24 h, only 24% of **8** remained unreacted, and numerous products were detected by GCMS. The two major products are **9b** and **9d**, resulting from triflate activation. Overall, the ratio of chloride:triflate activation is ~4 : 52 [(**9a** + **9c**) : (**9b** + **9d** + **9h**)]. Again, these results show that the Stille coupling displays the same oxidative addition preference as the Suzuki coupling in DMF. Consistent with earlier observations, more reaction at chloride is observed upon heating (entry 2). At 100 °C, the ratio of chloride:triflate activation is ~46 : 17 [(**9a** + **9c**) : (**9b** + **9d** + **9h**)]. Similar selectivity trends are observed when using $PhSn^nBu_3$ instead of $PhSnMe_3$ (see ESI).

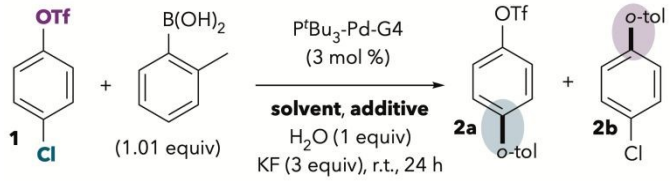
Taken together, our studies indicate that the selectivity of oxidative addition is similar under stoichiometric, catalytic Suzuki, and base-free Stille conditions at room temperature in DMF. This conclusion is consistent with the hypothesis that DMF coordinates to palladium and promotes C—OTf oxidative addition at a bisligated Pd(P^{t}Bu$_3$)(DMF) complex.

Role of Anions on Selectivity. The evidence presented thus far strongly suggests that coordinating solvents can promote oxidative addition at triflate through solvent-ligated transition states. As such, it is not necessary to invoke anionic[Pd(P^{t}Bu$_3$)(X)]$^-$ to explain the selectivity of Suzuki couplings of chloroaryl triflates in coordinating solvents. However, oxidative addition of PhOTf at [PdL(X)]$^-$ in the presence of quaternary ammonium chloride and bromide salts has been described by Hartwig [L = P(*o*-tolyl)$_3$)].[47] Oxidative addition at anionic palladium complexes bearing electron-deficient phosphines or in the absence of phosphines or other strong ancillary ligands has also been proposed.[48] Furthermore, DFT calculations suggest that if [Pd(P^{t}Bu$_3$)(X)]$^-$ participates in oxidative addition, it would preferentially react at triflate as seen for other PdL_2 complexes.[9,11] We speculated that transition states involving [Pd(P^{t}Bu$_3$)(X)]$^-$ might be primarily responsible for triflate selectivity under some conditions.

To evaluate this possibility, we subjected substrate **1** to Suzuki coupling conditions in THF in the presence of a variety of anionic additives (Table 6). As previously reported, reaction at chloride is strongly favored in the absence of extra additives, despite the use of KF (a source of fluoride anion) as a base (entry 1). This suggests that bisligated palladium is not the active catalyst under these conditions. However, addition of 18-crown-6, a chelator for K^+, induces a reversal of selectivity (entry 2). Alternatively, replacing potassium with a noncoordinating tetrabutylammonium cation also promotes reaction at triflate, albeit with significant substrate decomposition (entry 3). These results suggest that increased availability of free fluoride facilitates reaction at triflate through a mechanism involving [Pd(P^{t}Bu$_3$)(X)]$^-$. A similar effect is observed with added tetrabutylammonium salts of Cl^- and Br^- (entries 4 and 5). Because chloride and bromide are not basic, their effect on selectivity is unlikely to result from an increase in concentration of hydroxide (from water) or deprotonated boronic acid. Instead, it is reasonable to conclude that these salts promote reaction at triflate through formation of [Pd(PtBu$_3$)(Cl)]$^-$ or [Pd(P^{t}Bu$_3$)(Br)]$^-$. The quaternary ammonium salt of a non-coordinating anion (NBu_4OTf) does not have the same effect as the halide salts (entry 6), suggesting that the selectivity change with NBu_4F, NBu_4Cl, and NBu_4Br is not due to a medium effect. In the polar noncoordinating solvents ^{i}PrOH and propylene carbonate, the addition of 18-crown-6 also leads to a reversal

Open Access Article. Published on 22 December 2021. Downloaded on 12/26/2021 4:50:53 PM.
This article is licensed under a Creative Commons Attribution-NonCommercial 3.0 Unported Licence.
Chemical Science Accepted Manuscript

Table 6. Effect of Additives on the Selectivity of the Suzuki Cross-Coupling[a]



entry	solvent	additive (equiv)	1 (%)	2a (%)	2b (%)	ratio 2a:2b
1	THF	--	20	74	<1	>74 : 1
2	THF	18-crown-6 (3)	0	1	76	1 : 38
3[b]	THF	NBu_4F (3)	<1	<1	13	<1 : 13
4	THF	NBu_4Cl (1)	20	4	69	1 : 17
5	THF	NBu_4Br (1)	3	2	91	1 : 46
6	THF	NBu_4OTf (1)	26	70	3	23 : 1
7	PC	--	15	71	5	14 : 1
8	PC	18-crown-6 (3)	5	1	11	1 : 11
7	^{i}PrOH	--	2	87	1	87 : 1
8	^{i}PrOH	18-crown-6 (3)	0	0	3	<1 : 3
11	DMF	--	20	10	61	1 : 6
12	DMF	18-crown-6 (3)	0	0	47	<1 : 47

[a]GC yields calibrated against undecane as the internal standard. Average at least of two runs. ≤2% yield of the diarylated product was detected in all trials except entry 2 (8% yield of diarylated product). PC = propylene carbonate. [b]KF was omitted from the reaction mixture.

of selectivity with an increase in the total yield of **2b** (entries 7-10). However, poor mass balance is observed, likely due to an enhanced rate of triflate hydrolysis under the more basic conditions. The preexisting triflate selectivity appears to be enhanced in DMF upon the addition of 18-crown-6 (compare entries 11 and 12), although the overall quantity of **2b** produced is lower and the poor mass balance complicates interpretation of the selectivity. Taken together, the results in Table 6 show that higher concentrations of "naked" anions promote reaction at triflate. This observation is consistent with the involvement of $[Pd(P^tBu_3)(X)]^-$ under specific conditions that provide free anions in high concentration.

Conclusions

A series of studies were conducted to understand the observed solvent effects in the Pd/P^tBu_3-catalyzed Suzuki coupling of chloroaryl triflates. The results provide strong evidence for solvent coordination to Pd during triflate-selective cross-coupling. A summary of the key results is as follows: the use of coordinating solvents including nitriles, amides, and sulfoxides leads to Suzuki coupling through C—OTf bond cleavage. Conversely, nonpolar solvents as well as polar solvents that are poorly coordinating to palladium, such as propylene carbonate, alcohols, and sulfolane, favor reaction at chloride. Addition of substoichiometric amounts of benzonitrile derivatives to the Suzuki reaction in THF leads to erosion of chloride selectivity, and a correlation is observed between benzonitrile donating ability and increased reaction at triflate. The solvent-dependent selectivity observed in the stoichiometric reaction between Pd/P^tBu_3 and a competing aryl chloride and triflate mirrors that of the catalytic Suzuki coupling. DFT calculations reveal that dispersion dramatically lowers the predicted barrier to oxidative addition at Pd(P^tBu_3)(solv). Although previous results suggested that the Pd/P^tBu_3-catalyzed Stille coupling in a coordinating solvent leads to different selectivity than the corresponding Suzuki coupling, we find that the selectivity of these two reactions is approximately identical after controlling for convoluting factors such as low yields, formation of side products, and catalyst decomposition.

To our knowledge, this work represents the first compelling evidence for involvement of a solvent ligand during Ar–X oxidative addition at homogeneous Pd in the presence of a phosphine.[49] Taken together, the studies reported herein are consistent with the following mechanistic paradigm: In the presence of P^tBu_3, preferential reaction of chloride proceeds through an oxidative addition transition state involving monoligated PdL (L = P^tBu_3), as previously established. This selectivity for chloride is observed in non-coordinating solvents in the absence of a high concentration of "naked" halide ions. In coordinating solvents, however, palladium prefers to react at triflate through a transition state involving PdL(solv). Anionic bisligated $[PdL(X)]^-$, where X = halide, also reacts preferentially at triflate. However, this anionic species does not appear to be the dominant active catalyst, even in polar solvents, unless extra measures are taken to increase the concentration of free halide. Such measures include the addition of a crown ether to chelate potassium from KF (a common base in Suzuki couplings) or the addition of quaternary ammonium halide salts.

Author Contributions

EKE: data curation, formal analysis, investigation, methodology, visualization, writing – original draft; SMR: data curation, formal analysis, investigation, methodology, validation, visualization, writing – original draft; SRN: conceptualization, data curation, formal analysis, funding acquisition, investigation, methodology, project administration, supervision, visualization, writing – original draft; writing – review and editing.

Conflicts of interest

There are no conflicts to declare.

Acknowledgements

These studies are based upon work supported by NSF CAREER (CHE-1848090) and a Cottrell Scholar Award from the Research Corporation for Science Advancement (#26808). Calculations were performed on Comet and Expanse at SDSC and on Bridges-2 at the Pittsburgh Supercomputing Center through XSEDE (CHE-170089), which is supported by NSF (ACI-1548562). Support for MSU's NMR Center and the 400 MHz NMR spectrometer used in this research has been provided by the National Science Foundation (Grant No. NSF-MRI:CHE-2018388) and MSU's office of the Vice President for Research and Economic Development, and support for the 500 MHz NMR

View Article Online DOI: 10.1039/D1SC05868B
Open Access Article. Published on 22 December 2021. Downloaded on 12/26/2021 4:50:53 PM. This article is licensed under a Creative Commons Attribution-NonCommercial 3.0 Unported Licence.
Chemical Science Accepted Manuscript

View Article Online
DOI: 10.1039/D1SC05862B

spectrometer was provided by the NSF (NSF-MRI:DBI-1532078) and the Murdock Charitable Trust Foundation (2015066:MNL). We are grateful to Emily Entz, Oliver Jackson, Nate Larson, Jérome Lépeule, and John Russell for evaluating reproducibility, to Emma Baumgardner for assistance in the laboratory, and to Professor Thomas Livinghouse for helpful conversations.

Open Access Article. Published on 22 December 2021. Downloaded on 12/26/2021 4:50:53 PM.
This article is licensed under a Creative Commons Attribution-NonCommercial 3.0 Unported Licence.

Notes and references

1 (a) J. A. Labinger, *Organometallics*, 2015, **34**, 4784; (b) J. J. Hartwig in *Organotransition Metal Chemistry: From Bonding to Catalysis,* University Science Books, Sausalito, CA, 2010.
2 Selected experimental mechanistics studies with implications for oxidative addition at Pd(0) ligated by bulky monodentate phosphines: (a) A. H. Roy and J. F. Hartwig, *J. Am. Chem. Soc.,* 2001, **123**, 1232; (b) J. P. Stambuli, C. D. Incarvito, M. Bühl, and J. F. Hartwig, *J. Am. Chem. Soc.* 2004, **126**, 1184; (c) E. Galardon, S. Rhamdeehul, J. M. Brown, A. Cowley, K. K. Hii, and A. Jutand, *Angew. Chem., Int. Ed.* 2002, **41**, 1760; (d) F. Barrios Landeros, B. P. Carrow, and J. F. Hartwig, *J. Am. Chem. Soc.* 2009, **131**, 8141.
3 Selected computational studies: (a) H. M. Senn and T. Ziegler, *Organometallics*, 2004, **26**, 758; (b) K. C. Lam, T. B. Marder, and Z. Lin, *Organometallics*, 2007, **26**, 758; (c) M. Besora and F. Maseras, *Dalton Trans.*, 2019, **48**, 16242; (d) J. Joy, T. Stuvyer, and S. Shaik, *J. Am. Chem. Soc.*, 2020, **142**, 3836.
4 Selected reviews: (a) C. Amatore and A. Jutand, *J. Organomet. Chem.* 1999, **576**, 254; (b) L. Xue and Z. Lin, *Chem. Soc. Rev.* 2010, **39**, 1692; (c) M. García-Melchor, A. A. C. Braga, A. Lledós, G. Ujaque, and F. Masaras, *Acc. Chem. Res.* 2013, **46**, 2626; (d) K. J. Bonney and F. Schoenebeck, *Chem. Soc. Rev.* 2014, **43**, 6609; (e) D. J. Jones, M. Lautens, and G. P. McGlacken, *Nature Cat.* 2019, **2**, 843; (f) M. C. D'Alterio, É. Casals-Cruańas, N. V. Tzouras, G. Talarico, S. P. Nolan, and A. Poater, *Chem. Eur. J.* 2021, **27**, 13481.
5 F. Schoenebeck and K. N. Houk, *J. Am. Chem. Soc.* 2010, **132**, 2496.
6 Selected reviews: (a) J. Mahatthananchai, A. M. Dumas, and J. W. Bode, *Angew. Chem. Int*., Ed. 2012, **51**, 10954; (b) J. Almond-Thynne, D. C. Blakemore, D. C. Pryde, and A. C. Spivey, *Chem. Sci*., 2017, **8i**, 40; (c) E. K. Reeves, E. D. Entz, and S. R. Neufeldt, *Chem. Eur. J*. 2021, **27**, 6161; (d) M. Cao and H. Xie, *Chinese. Chem. Lett*. 2021, **32**, 319; (e) V. Palani, M. A. Perea, and R. Sarpong, *Chem. Rev*. 2021, *Article ASAP*. DOI: 10.1021/acs.chemrev.1c00513.
7 A. F. Littke, C. Dai, and G. C. Fu, *J. Am. Chem. Soc*. 2000, **122**, 4020.
8 Z. L. Niemeyer, A. Milo, D. P. Hickey, and M. S. Sigman, *Nat. Chem*. 2016, **8**, 610.
9 F. Proutiere and F. Schoenebeck, *Angew. Chem., Int. Ed.*, 2011, **50**, 8192.
10 F. Proutiere and F. Schoenebeck *Synlett* 2012, **23**, 645.
11 E. K. Reeves, O. R. Bauman, G. B. Mitchem, and S. R. Neufeldt, *Isr. J. Chem*. 2020, **60**, 406.
12 To our knowledge, none of the published solvent coordinative ability scales closely match the observed trends. However, none of these scales have been developed specifically for soft, late transition metals like palladium. For a review, see: S. Alvarez, *Chem. Eur. J*., 2020, **26**, 4350.
13 Anecdotally, we have sometimes encountered worse reproducibility with $Pd_2(dba)_3$, likely due to challenges with controlling its purity: S. S. Zalesskiy and V. P. Ananikov, *Organometallics*, 2012, **31**, 2302.
14 Q. Zhou, H. D. Srinivas, S. Zhang, and M. P. Watson, *J. Am. Chem. Soc*. 2016, **138**, 11989.
15 The correlation to σ^+ is a little stronger than to σ, see ESI for details.
16 For examples, see: (a) T. Diao, P. White, I. Guzei, and S. S. Stahl, *Inorg. Chem*. 2012, **51**, 11898; (b) F. Schroeter, J. Soellner, and T. Strassner, *ACS Catal*. 2017, **7**, 3004.
17 We also examined the use of tetrahydrothiophene (THT), a sulfur analog of THF with a similar dielectric constant. However, as a softer atom, sulfur is generally a better ligand for palladium compared to oxygen. Consistent with a coordination hypothesis, THT and THF promote opposite chemoselectivities, but the reaction in THT gives extremely poor conversion (~2% yield of **2b**, the only product observed). The low yield in THT may be due to its very strong coordinating ability, leading to catalyst poisoning (see ESI).
18 C. Wohlfarth in *CRC Handbook of Chemistry and Physics*, eds. J. Rumble Jr., D. Lide, and T. Bruno, CRC Press, Boca Raton, FL, 2020, Permittivity (Dielectric Constant) of Liquids.
19 K. Suzuki, M. Shinya, Y. Ono, T. Matsumoto, N. Nanbu, M. Takehara, M. Ue, and Y. Sasaki,. *Electrochemistry* 2007, **75**, 611.
20 An intermolecular competition between **3a** and **3b** under the catalytic Suzuki coupling conditions yields similar selectivities as observed under stoichiometric conditions (see ESI). Compared to **3a**/**3b**, the *para* substituted analogues of these substrates give similar results in catalytic and stoichiometric studies, but with increased decomposition (see ESI).
21 The reaction of $Pd(COD)(CH_2TMS)_2$ with ArI + P^tBu_3 in toluene at room temperature has been shown to yield the oxidative addition adduct (P^tBu3)Pd(Ar)(I): T. L. Andersen, S. D. Friis, H. Audrain, P. Nordeman, G. Antoni, and T. Skrydstrup, *J. Am. Chem. Soc*. 2015, **137**, 1548.
22 For other examples of the use of $Pd(COD)(CH_2SiR_3)_2$ as a precursor to LnPd(Ar)(X) oxidative addition complexes (n = 1 or 2, X = halide); see: (a) B. P. Fors, D. A. Watson, M. R. Biscoe, and S. L. Buchwald, *J. Am. Chem. Soc*. 2008, **130**, 13552; (b) D. A. Watson, M. Su, G. Teverovskiy, Y. Zhang, J. Garcia-Fortanet, T. Kinzel, and S. L. Buchwald, *Science* 2009, **325**, 1661; (c) A. G. Sergeev, T. Schultz, C. Torborg, A. Spannenberg, H. Neumann, and M. Beller, Angew. Chem., Int. Ed. 2009, **48**, 7595; (d) P. Larini, C. E. Kefalidis, R. Jazzar, A. Renaudat, E. Clot, and O. Baudoin, *Chem. Eur. J*. 2012, **18,** 1932; (e) P. J. Milner, Y. Yang, and S. L. Buchwald, *Organometallics* 2015, **34**, 4775−4775.
23 This complex has been previously reported as a dimer in the solid state and a monomer in solution: see reference 2d.
24 A. L. Casado, P. Espinet, A. M. Gallego, *J. Am. Chem. Soc.* **2000**, *122*, 11771.
25 We observe formation of Pd black during the stoichiometric reactions in all solvents, typically after about 30-60 minutes or longer. This can partly be attributed to decomposition of the Pd triflate oxidative addition adduct (see ref. 2b). Although stable palladium complexes $ArPd(PPh_3)_2(OTf)$ and $ArPd(PPh_3)_2(THF)$ have been previously reported (see ref 24), we see no evidence of inner-sphere Pd(OTf) in any solvents nor evidence for THF-stabilized cationic palladium complexes under our conditions with P^tBu_3.
26 The route to formation of Pd black involves clusters and nanoparticles, and the selectivity of such intermediate multinuclear species during oxidative addition is a topic of ongoing study in our group.

Chemical Science Accepted Manuscript

View Article Online
DOI: 10.1039/D1SC05862B

Open Access Article. Published on 22 December 2021. Downloaded on 12/26/2021 4:50:53 PM.
This article is licensed under a Creative Commons Attribution-NonCommercial 3.0 Unported Licence.

27 The ^{31}P NMR spectra for the DMF reactions in entries 7 and 13 display a unique signal that may correspond to a solvent-bound cationic oxidative addition product from the reaction of **3b** (see ESI).
28 We also considered, and tentatively ruled out, the possibility that autocatalysis mediated by P^tBu_3•HCl is primarily responsible for the triflate selectivity observed in coordinating sol-vents (see ESI). Autocatalysis has previously been reported in the oxidative addition of PhBr to $Pd(P^tBu_3)_2$: F. Barrios-Landeros, B. P. Carrow, and J. F. Hartwig, *J. Am. Chem. Soc*. 2008, **130**, 5842.
29 R. F. Ribeiro, A. V. Marenich, C. J. Cramer, D. G. Truhlar, *J. Phys. Chem. B*. 2011, **115**, 14556.
30 Y.-P. Li, J. Gomes, S. M. Sharada, A. T. Bell, M. Head-Gordon, *J. Phys. Chem. C* 2015, **119**, 1840.
31 3D image was prepared using CYLview, 1.0b; Legault, C. Y., Université de Sherbrooke, 2009 (http://www.cylview.org)
32 All thermodynamic quantities were computed with the GoodVibes code (298.15 K): G. Luchini, J. V. Alegre-Requena, I. Funes-Ardoiz, R. S. Paton, GoodVibes: Automated Thermochemistry for Heterogeneous Computational Chemistry Data. *F1000Res*. 2020, **9**, 291.
33 (a) A. D. Becke, *Phys. Rev. A* 1998, **38**, 3098; (b) A. D. Becke, *J. Chem. Phys.* 1993, **98**, 5648; (c) A. D. Becke, *J. Chem. Phys.* 1993, **98**, 1372.
34 E. Lyngvi, I. A. Sanhueza, F. Schoenebeck, *Organometallics* 2015, **34**, 805.
35 Examples: (a) Y. Zhao, D. G. Truhlar, *Org. Lett.* 2007, **9**, 1967; (b) D. Benitez, E. Tkatchouk, W. A. Goddard III, *Chem. Commun.* 2008, 6194; (c) C. L. McMullin, J. Jover, J. N. Harvey, N. Fey, *Dalton Trans.* 2010, **39**, 10833; (d) M. S. G. Ahlquist, P-O. Norrby, *Angew. Chem. Int. Ed.* 2011, **50**, 11794; (e) S. O. N. Lill, P. Ryberg, T. Rein, E. Bennström, P-O. Norrby, *Chem. Eur. J.* 2012, **18**, 1640. (f) C. McMullin, N. Fey, J. N. Harvey, *Dalton Trans.* 2014, **43**, 13545. (g) J. Zhu, Y. Liang, L. Wang, Z.-B. Zheng, K. N. Houk, Y. Tang, *J. Am. Chem. Soc.* 2014, **136**, 6900. (h) M. Xie, W. Lu, *RSC Adv.* 2018, **8**, 2240. (i) L. V. Hooker, S. R. Neufeldt, *Tetrahedron* 2018, **74**, 6717.
36 H. S. Yu, X. He, and D. G. Truhlar, *J. Chem. Theory Comput*. 2016, **12**, 1280.
37 Results are similar with LANL2DZ instead of SDD for Pd; see ESI.
38 The room-temperature reaction of **1** with $PhSn^nBu_3$ is low-yielding. See the ESI for full details of our analysis of this cross-coupling.
39 The attempted Stille coupling of **1** with $PhSnMe_3$ in other coordinating solvents (MeCN and DMSO) gives only trace yields of **7a** and **7b** at room temperature.
40 The poor conversion in the absence of a base is consistent with a previous report under slightly different conditions: A. F. Littke, L. Schwarz, G. C. Fu, *J. Am. Chem. Soc*. 2002, **124**, 6343.
41 Aryl group transfer is usually favored over alkyl group transfer from tin in Stille couplings, but, in at least one example, methylation was observed as the major product from a Stille coupling using $PhSnMe_3$: E. Gomez-Bengoa, A. M. Echavarren, *J. Org. Chem*. 1991, **56**, 3497.
42 Replacing KPF_6 with KF in the room temperature reaction in Scheme 3 leads to 18% yield of **7a** and 45% of **7b**, with 33% of **1** remaining after 24 h. The clear preference for **7b** under these conditions is consistent with the prior report (reference 9). We hypothesize that fluoride accelerates the slow transmetallation step, allowing the desired cross-coupling to outcompete catalyst speciation changes (decomposition). For an example of the accelerating effect of fluoride on a Pd/PtBu3-catalyzed Stille cross-coupling of aryl chlorides, see reference 40.
43 Other precatalyst systems give similar results to system **B**. See ESI for details.
44 For example, palladium clusters and monomeric Pd have been found to promote different selectivity in cross-coupling reactions of 2,4-dibromopyridine: N. W. J. Scott, M. J. Ford, N. Jeddi, A. Eyles, L. Simon, A. C. Whitwood, T. Tanner, C. E. Willans, I. J. S. Fairlamb, *J. Am. Chem. Soc*. 2021, **143**, 9682.
45 Attempts to recycle the catalyst after using it in a 100 °C Suzuki coupling in DMF provides results that are consistent with catalyst decomposition to a species that preferentially reacts at chloride in DMF (see ESI).
46 M. Tobisu and N. Chatani, *Acc. Chem. Res*. 2015, **48**, 1717.
47 A. H. Roy and J. F. Hartwig, *Organometallics*, 2004, **23**, 194.
48 (a) C. Amatore and A. Jutand, *Acc. Chem. Res.* 2000, **33**, 314; (b) A. H. M. De Vries, F. J. Parlevliet, L. Schmieder-van de Vondervoort, J. H. Mommers, H. J. W. Henderickx, M. A. M. Walet, J. G. De Vries, *Adv. Synth. Catal*., 2002, **344**, 996; (c) L. J. Gooßen, D. Koley, H. L. Hermann, W. Thiel, *J. Am. Chem. Soc*. 2005, **127**, 11102; (d) S. Kozuch, C. Amatore, A. Jutand, and S. Shaik, *Organometallics* 2005, **24**, 2319; (e) M. Ahlquist, P. Fristrup, D. Tanner, P.-O. Norrby, *Organometallics* **2006**, *25*, 2066; (f) M. Ahlquist, P.-O. Norrby, *Organometallics* **2007**, *26*, 550; (g) B. P. Carrow and J. F. Hartwig, *J. Am. Chem. Soc*. **2010**, *132*, 79; (h) F. Schroeter, J. Soellner, T. Strassner, *ACS Catal*. 2017, **7**, 3004.
49 For examples of other solvent effects on Pd-catalyzed cross-couplings, see: J. Sherwood, J. H. Clark, I. J. S. Fairlamb, and J. M. Slattery, *Green Chem*., 2019, **21**, 2164.

Chemical Science Accepted Manuscript

This journal is © The Royal Society of Chemistry 20xx

CHAPTER FIVE

CONCLUSIONS AND PERSPECTIVE

C—H Activation at Early Transition Metals

Chapters 2 and 3 explored the factors controlling aromatic and aliphatic C—H activation at tantalocene hydrides, culminating in our demonstration of the extension of this reactivity from intermolecular aromatic C—H activation to intermolecular aliphatic C—H activation. Despite our efforts and some success with liquid hydrocarbons, however, this reactivity could not be extended to the C—H activation of methane. Several obstacles remain to be overcome before such a reaction might be realized.

Our computational work suggests that the activation of methane C—H bonds by the simplest tantalocene hydride, Cp_2TaH_3, should be energetically comparable to the primary, secondary, and tertiary C—H activation of heavier hydrocarbons such as *n*-butane and *iso*-butane. While we have not specifically examined C—H activation of butane, we have observed aliphatic C—H activation of similar substrates including cyclohexane, *n*-octane, and methylcyclohexane.

If our DFT calculations are correct, then the lack of observed methane activation seems likely to be the result of solvent outcompeting methane under our reaction conditions. At the highest pressures of methane we have explored (200 psi) there is still approximately four times more solvent (cyclohexane or cyclohexane-d_{12}) than methane (or methane-d_4) by molar ratio; there is approximately twelve times more solvent C—H bonds than methane C—H bonds in the reaction mixture (note that the real concentrations of methane in solution are likely lower than this owing to the poor solubility of methane in aliphatic solvents and the elevated experiment temperatures). As such, aliphatic C—H activation of the cyclohexane solvent likely outcompetes the reaction with methane.

The methane pressures we have explored are much lower than those that could be achieved with specialized equipment. Further increases in methane pressure would give a proportional increase in dissolved methane. An increase to 800 psi methane would give a ~1:1 molar ratio of methane to cyclohexane under our reaction conditions; an increase to 2500 psi methane would be necessary to achieve a ~1:1 molar ratio of methane C—H bonds to cyclohexane C—H bonds. The possibility remains that the only practical barrier to methane C—H activation at Cp_2TaH_3 is one of reaching sufficiently high pressures of methane.

In addition to methane activation, the homologation step of our proposed catalytic cycle (Scheme 1.2) also remains unrealized, though similar hydrocarbon homologation chemistry was recently demonstrated at a molecular diruthenium carbide.[1] Exploration of this step from an isolated tantalum alkylidene (rather than one generated catalytically, as proposed in Scheme 1.1) would be more pragmatic than pursuing this chemistry under the aforementioned high-pressure conditions. If such a homologation from a tantalocene alkylidene were demonstrated then the work of coupling the two processes under high pressures of methane could begin.

Given our demonstration of both intermolecular aromatic and aliphatic C—H activation at the substituted tantalocenes, $(^{R}Cp)_2TaH_3$, it appears that a particular impediment to the further utilization of the tantalocene hydrides as catalysts for C—H activation is their indiscriminate nature. Though aromatic and aliphatic C—H activation can be achieved with these complexes, it seems likely these desirable transformations are in direct competition with intramolecular reactions. These intramolecular reactions may be kinetically favored by the constant proximity of the ligand C—H bonds to the metal center. Our efforts focused on ligand modulation—whether by permethylation or alkyl substitution—have led to only modest improvements in catalytic competence for C—H activation.

The size of the cyclopentadienyl ligands themselves seems to be primarily responsible for the deleterious intramolecular pathways; ligand C—H bonds are always within reach of the metal center. As such, it seems evident that moving to a ligand scaffold with fewer proximal reactive bonds would be advantageous. This necessarily precludes the use of any of the ligands related to cyclopentadienyl ligands such as indenyl or fluorenyl. The main advantages of such ligands are the stabilization imbued by their π-backbonding and their high number of electrons for bonding such that an eighteen-electron complex is accessible from a d^5 metal. The latter is difficult to achieve with other familiar ligand frameworks, though given the electropositivity of the early transition metals this is less of a prerequisite than later in the *d*-block. Pincer ligand frameworks may be well-suited to the task given their planarity and ease of modulation. Below are a few theoretical amine- and imine-based tantalum hydrides with their oxidation states, *d*-electron counts, valence electron counts, and metal-ligand MLX formalism.[2] Many similar pincer or scorpionate ligands exist with a variety of carbon, nitrogen, oxygen, and phosphorus coordinating moieties.

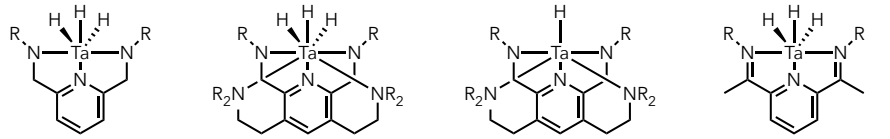


Figure 1. Theoretical amine- and imine-based tantalum pincer complexes.

Similarly, in moving away from the tantalocene hydrides we need not limit ourselves only to tantalum. We initially considered both niobocene and tantalocene hydrides for our investigations into C—H activation chemistry. Disappointingly, however, the niobocene hydrides do not give well-resolved ^{1}H NMR signals for their hydrides like those observed with the tantalocene hydrides (Figures 2.1, 2.2).[3,4] As we had initially planned to monitor the *individual* ^{1}H NMR signals

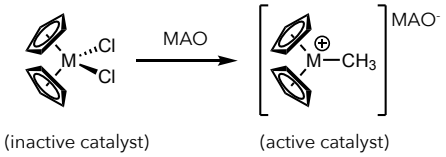
associated with each isotopologue resulting from hydridic H/D exchange we chose to focus on the tantalocenes; however, we soon moved to integral monitoring of the sum of all hydride signals—a method that could have been employed just as easily with the niobocene hydrides. Due to the lanthanide contraction, second and third row transition metals (such as niobium and tantalum) are often quite similar in their chemical properties (the atomic radii of niobium and tantalum are *nearly* identical).[5] Despite this predicted similarity, past reports affirm that higher activity for aromatic C—H activation was observed with the niobocenes than with tantalocenes. As such a reexamination of niobocene hydrides may be in order.

Interestingly, a so-called "diagonal relationship" has been noted for the reactivity of organometallic transition metal complexes, whereby similar catalytic capabilities are observed in metals on a descending diagonal upon going across the periodic table (i.e. at scandium-zirconium-tantalum or titanium-niobium-tungsten, for example).[6] Such a relationship would suggest the next metal to examine might be zirconium. Organometallic complexes of zirconium (and hafnium) are more numerous than those of niobium and tantalum in large part due to their importance as Ziegler-Natta catalysts for olefin polymerization—certainly they're *the* poster child for industrially relevant homogeneous chemistry of the early transition metals.

Curiously, many of the original homogeneous Ziegler-Natta catalysts were metallocenes whose successful implementation does not seem to have been inhibited by deleterious intramolecular reactions. The high reactivity of the olefinic substrates likely bears at least partial responsibility for the lack of intramolecular C—H activation. However, the means of catalyst activation also differs dramatically between the Group(V) metallocene hydrides and the Group(IV) metallocene chlorides employed as Ziegler-Natta catalysts. With the niobocene and tantalocene trihydrides, the trihydride is essentially a precatalyst, i.e. thermal or photochemical reductive

elimination of dihydrogen furnishes the active low-valent monohydride. With the Ziegler-Natta catalysts, the precatalyst is typically a metallocene chloride that is activated by the addition of methylaluminoxane (MAO) that serves to convert the halide (or dihalide) to a cationic metallocenium metal-methyl species (Scheme 1).

Scheme 1. Ziegler-Natta polymerization catalyst activation.



To our knowledge a similar means of catalyst activation for the Group V chlorides has not been explored within the context of C—H activation catalysis. Though a path involving reductive elimination/oxidative addition would not be feasible from a M(V) species, perhaps a stable M(III) chloride would be amenable to this type of catalyst activation and competent for reductive elimination/oxidative addition chemistry. Additionally, it is unclear if a cationic M(III) species might be stabilized by σ-complexation of a C—H bond *en route* to oxidative addition to a greater extent than for the M(III) monohydrides. It remains likely that many complexes prepared in the pursuit of Ziegler-Natta-type catalysis were underexplored for C—H activation chemistry; their reexamination may provide new classes of catalysts or means of catalyst activation.

Alternatively—and as a direct analogue to the single-site supported catalysts employed by Basset and coworkers—it may be possible to employ silsesquioxane ligands at tantalum and niobium for the homogeneous homologation of methane. Such ligands have occasionally been employed to mimic the chemistry of silica-supported catalysts.[7] The potential drawbacks of the silsesquioxane ligands are their large size and difficulty in modulation, though if the goal is simply to do homogeneous chemistry in analogy to that of the tantalum single-site silica-supported catalysts this may well do the trick.

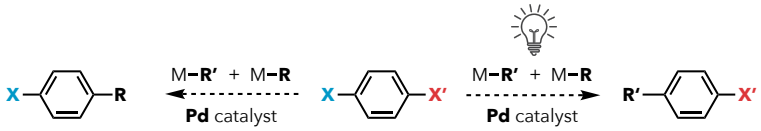
In summary, though our goal of light alkane C—H activation at early transition metal complexes remains unfulfilled, numerous potential routes remain unexplored. While simply going to higher pressures of methane may result in the desired outcome, modulation of ligand framework and transition metal identity may provide catalysts capable at operating at more moderate gas pressures which may be more amenable to development of a coupled catalytic process for alkane homologation.

Cross-Coupling Reactions Catalyzed by Late Transition Metals

Chemodivergence at the substrate 4-chlorophenyl triflate has been well explored. Previous work has demonstrated the importance of ligand choice in chemoselectivity,[8] whereby a bulkier ligand enforces a monoligated transition state during oxidative addition whereas less bulky ligands favor a bisligated transition state (Scheme 4.1).[9] In our work in Chapter 4 we have presented compelling evidence that coordinating solvents can enforce a bisligated transition state via solvent-metal coordination during oxidative addition in the palladium-catalyzed Suzuki and Stille cross couplings. Solvent selection can thus be tailored to effect the desired outcome in analogous cross-coupling reactions. Given the myriad ways to control chemodivergence in cross coupling (ligand choice, solvent choice, additives, etc.) what other means of reaction outcome control might be desirable?

One stimulus we have long been interested in exploring to control chemodivergence is reaction irradiation. We have envisioned a scenario where a reaction gives one outcome under irradiation and the opposite in its absence (Scheme 2).

Scheme 2. Photochemical chemodivergence in cross-coupling.



Given our success in effecting chemodivergence originating from solvent coordinating versus noncoordinating ability, it may be possible to design a photoswitchable additive that would be coordinating under one set of photochemical conditions and noncoordinating under another set of photochemical conditions. Several potential candidates from the many photoswitchable molecules are highlighted below (Figure 2).

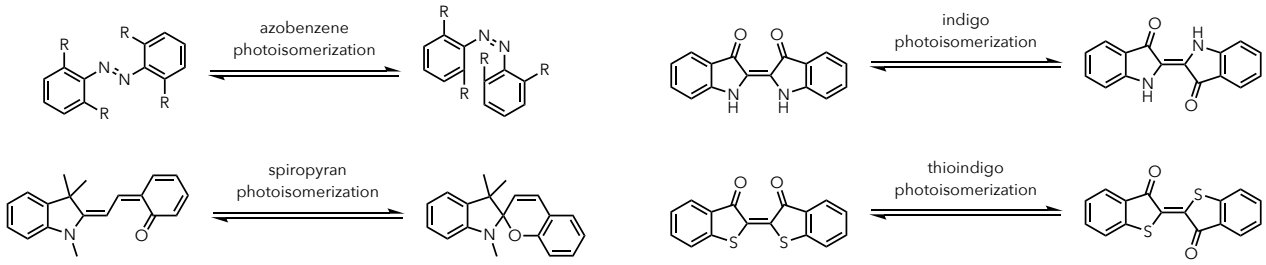


Figure 2. Molecules with potentially differing coordinating ability or denticity upon photoswitching.

Azobenzenes are perhaps the most well-known molecular photoswitches, undergoing a *trans-cis* isomerization upon irradiation. Such a molecule could be employed as a photoswitchable ligand by aromatic substitution of the azobenzene with coordinating moieties that would be more or less available for coordination based on which isomer was present. In a similar approach, an azobenzene bearing coordinating moieties might be photoswitchable between monodentate and bidentate. Alternatively, the azo group itself might act as a coordinating moiety with greater propensity for coordination in the *cis*- than *trans*-isomer.

Many photoswitchable molecules are known beyond the azobenzenes. The spiropyrans may act as a bidentate ligand in the "open" form and as a poor or monodentate ligand in their "closed" spiro form. Photoisomerable indigoids—such as those derived from indigo and

thioindigo— bear potentially coordinating moieties whose isomerization will likely give ligands of variable denticity. The use of strategically placed sterically hindering groups may be advantageous with either the spiropyrans or indigoids to enforce the desired coordination mode so long as it does not inhibit forward or reverse photoisomerization.

Many other photoswitchable molecules are known. The results from our investigation into the role of solvent coordination in chemodivergent cross-coupling suggest a substochiometric quantity of coordinating additive can be sufficient to affect a switch in selectivity. A screen of the effect of photoswitchable materials bearing coordinating moieties under irradiative and nonirradiative conditions in cross-coupling would be facile and provide insight into what additive classes are worth exploring further. It is our hope that photoswitchable ligands of the type discussed here might be employed for photoswitchable cross-couplings and in other divergent chemical processes.

References

1. Ohata, J.; Teramoto, A.; Fujita, H.; Takemoto, S.; Matsuzaka, H. Linear Hydrocarbon Chain Growth from a Molecular Diruthenium Carbide Platform. *J. Am. Chem. Soc.* **2021**, *143*, 16105-16112.
2. Parkin, G. Classification of Organotransition Metal Compounds. In *Comprehensive Organometallic Chemistry*, Third Edition. Michael, D., Mingos, P., Crabtree, R.H.; Elsevier Science: 2007; pp 1-57.
3. (a) Parshall, G. W.; Tebbe, F. N. Hydride Derivatives of Niobocene and Tantalocene. *J. Am. Chem. Soc.* **1971**, *93*, 3793−3795; (b) Klabunde, U.; Parshall, G. W. Activation of Aromatic Carbon-Hydrogen Bonds by Transition Metal Complexes. II. Substituted Benzenes. *J. Am. Chem. Soc.* **1972**, *94*, 9081−9087.
4. Antiñolo, A.; Carrillo-Hermosilla, F.; Fajardo, M.; Fernándex-Baeza, J.; García-Yuste, S.; Otero, A. Advances in the chemistry of bis-cyclopentadienyl hydride derivatives of niobium and tantalum. *Coord. Chem. Rev.* **1999**, *193-195*, 43-72.
5. Clementi, E.; Raimond, D. L.; Reinhardt, W. P. Atomic Screening Constants from SCF Functions. II. Atoms with 37 to 86 Electrons. *J. Chem. Phys*. **1967,** *47*, 1300–1307.
6. Mashima, K. Diagonal Relationship among Organometallic Transition-Metal Complexes. *Organometallics.* **2021**, *40*, 3497-3505.
7. Cho, H.M.; Weissman, H.; Wilson, S.R.; Moore, J.S. A Mo(VI) Alkylidyne Complex with Polyhedral Oligomeric Silsesquioxane Ligands: Homogeneous Analogue of a Silica-Supported Alkyne Metathesis Catalyst. *J. Am. Chem. Soc.* **2006**, *128*, 14742-14743.
8. Littke, A.F.; Dai, C.; Fu, G.C. Versatile Catalysts for the Suzuki Cross-Coupling of Arylboronic Acids with Aryl and Vinyl Halides and Triflates under Mild Conditions. *J. Am. Chem. Soc.* **2000**, *122*, 4020-4028.
9. Schoenebeck, F.; Houk, K.N. Ligand-Controlled Regioselectivity in Palladium-Catalyzed Cross Coupling Reactions. *J. Am. Chem. Soc.* **2010**, *132*, 2496-2497.

REFERENCES

Almond-Thynne, J.; Blakemore, D. C.; Pryde, D. C.; Spivey, A. C. Site-selective Suzuki–Miyaura coupling of heteroaryl halides – understanding the trends for pharmaceutically important classes. *Chem. Sci.* **2017**, *8i, 40-62.*

Alvarez, S. Coordinating Ability of Anions, Solvents, Amino Acids, and Gases towards Alkaline and Alkaline-Earth Elements, Transition Metals, and Lanthanides. *Chem. Eur. J.* **2020**, *26*, 4350–4377.

Amatore, C.; Jutand, A. Anionic Pd(0) and Pd(II) Intermediates in Palladium-Catalyzed Heck and Cross-Coupling Reactions. *Acc. Chem. Res.* **2000**, *33*, 314-321.

Amatore, C.; Jutand, A. Mechanistic and kinetic studies of palladium catalytic systems. *J. Organomet. Chem.* **1999**, *576*, 254-278.

Andersen, T. L.; Friis, S. D.; Audrain, H.; Nordeman, P.; Antoni, G.; Skrydstrup, T. Efficient ^{11}C-Carbonylation of Isolated Aryl Palladium Complexes for PET: Application to Challenging Radiopharmaceutical Synthesis. *J. Am. Chem. Soc.* **2015**, *137*, 1548−1555.

Antonelli, D. M.; Schaefer, W. P.; Parkin, G.; Bercaw, J.E. Synthesis and characterization of (η^5-$C_5Me_5)_2TaCl(THF)$, a useful synthetic precursor for the preparation of oxo, imido and methylidene derivatives of permethyltantalocene. *J. Organomet. Chem*. **1993**, *462*, 213-220.

Antiñolo, A.; Carrillo-Hermosilla, F.; Fajardo, M.; Fernándex-Baeza, J.; García-Yuste, S.; Otero, A. Advances in the chemistry of bis-cyclopentadienyl hydride derivatives of niobium and tantalum. *Coord. Chem. Rev.* **1999**, *193-195*, 43-72.

Arakaweau,, H.; Aresta, M.; Armor, J.N.; Barteau, M.A.; Beckman, E.J.; Bell, A.T.; Bercaw, J.E.; Creutz, C.; Dinjus, E.; Dixon, D.A.; Domen, K.; DuBois, D.L.; Eckert, J.; Fujita, E.; Gibson, D.H.; Goddard, W.A.; Goodman, D.W.; Keller, J.; Kubas, G.J.; Kung, H.H.; Lyons, J.E.; Manzer, L.E.; Marks, T.J.; Morokuma, K.; Nicholas, K.M.; Periana, R.; Que, L.; Rostrup-Nielson, J.; Sachtler, W.M.H.; Schmidt, L.D.; Sen, A.; Somorjai, G.A.; Stair, P.C.; Stults, B.R.; Tumas, W. Catalysis Research of Relevance to Carbon Management: Progress, Challenges, and Opportunities. *Chem. Rev.* **2011,** *101*, 953-996.

Bailey, B.C.; Fan, H.; Baum, E.W.; Huffman, J.C.; Baik, M.-H.; Mindiola, D.J. Intermolecular C-H Bond Activation Promoted by a Titanium Alkylidyne. *J. Am. Chem. Soc.* **2005**, *127*, 16016-16017.

Ballard, K.R.; Gardiner, I.M.; Wigley, D.W. Evidence for intramolecular carbon-hydrogen bond activation and the formation of a tucked-in complex of hexamethylbenzene at a tantalum(III) center. *J. Am. Chem. Soc*. **1989,** *111,* 2159-2162.

Barefield, E.K.; Parshall, G.W.; Tebbe, F.N. Catalysis of Aromatic Hydrogen-Deuterium Exchange by Metal Hydrides. *J. Am. Chem. Soc*. **1970**, *92*, 5234-5235.

Barrios-Landeros, F.; Carrow, B. P.; Hartwig, J. F. Autocatalytic Oxidative Addition of PhBr to $Pd(P^tBu_3)_2$ via $Pd(P^tBu_3)_2(H)(Br)$ *J. Am. Chem. Soc.* **2008**, *130*, 5842-5843.
Barrios-Landeros, F.; Carrow, B. P.; Hartwig, J. F. Effect of Ligand Steric Properties and Halide Identity on the Mechanism for Oxidative Addition of Haloarenes to Trialkylphosphine Pd(0) Complexes. *J. Am. Chem. Soc.* **2009**, *131*, 8141-8154.

Basset, J. M.; Copéret, C.; Lefort, L.; Maunders, B. M.; Maury, O.; Le Roux, E.; Saggio, G.; Soignier, S.; Soulivong, D.; Sunley, G. J.; Taoufik, M.; Thivolle-Cazat, J. Primary Products and Mechanistic Considerations in Alkane Metathesis. *J. Am. Chem. Soc*. **2005**, *127*, 8604-8605.

Baynham, R.F.G.; Chetwynd-Talbot, J.; Grebenik, P.; Perutz, R.N.; Powell, M.H.A. Photochemistry of $M(\eta^5\text{-}C_5H_5)_2(H)CO$ and $M(\eta^5\text{-}C_5H_5)_2H_3$ (M = Nb, Ta) in low temperature matrices. *J. Organomet. Chem.* **1985**, *284*, 229-242.

Beaumier, E.P.; Pearce, A.J.; See, X.Y.; Tonks, I.A. Modern applications of low-valent early transition metals in synthesis and catalysis. *Nat. Chem. Rev.* **2019**, *3*, 15-34.

Becke, A. D. A new mixing of Hartree–Fock and local density-functional theories. *J. Chem. Phys.* **1993**, *98*, 1372.

Becke, A. D. Density-functional exchange-energy approximation with correct asymptotic behavior. *Phys. Rev. A* **1998**, *38*, 3098.

Becke, A. D. Density-functional thermochemistry. III. The role of exact exchange. *J. Chem. Phys.* **1993**, *98*, 5648.

Beckhaus, R. Pentafulvene complexes of group four metals: Versatile organometallic building blocks. *Coord. Chem. Rev*. **2018**, *376*, 467-477.

Benitez, D.; Tkatchouk, E.; Goddard, III, W. A. Relevance of cis- and trans-dichloride Ru intermediates in Grubbs-II olefin metathesis catalysis ($H_2IMesCl_2Ru$=CHR). *Chem. Commun.* **2008**, 6194-6196.

Bercaw, J.E.; Brintzinger, H.H. Bis(pentamethylcyclopentadienyl)titanium(II). Isolation and Reactions with Hydrogen, Nitrogen, and Carbon Monoxide. *J. Am. Chem. Soc.* **1971**, *93*, 2045-2046.

Besora, M.; Maseras, F. The diverse mechanisms for the oxidative addition of C–Br bonds to $Pd(PR_3)$ and $Pd(PR_3)_2$ complexes. *Dalton Trans.* **2019**, *48*, 16242-16248.

Bonney, K. J.; Schoenebeck, F. Experiment and computation: a combined approach to study the reactivity of palladium complexes in oxidation states 0 to IV. *Chem. Soc. Rev.* **2014**, *43*, 6609-6638.

Bregel, D.C.; Oldham, S.M.; Eisenberg, R. Mechanistic Studies on the Addition of Dihydrogen to Tantalocene Complexes. *J. Am. Chem. Soc.* **2002**, *124*, 13827-13832.

Brookes, N. J.; Ariafard, A.; Stranger, R.; Yates, B. F., Scission of Carbon Monoxide Using TaR_3, R = (N(tBu)Ph) or $OSi(tBu)_3$): A DFT Investigation. *Chem. Eur. J.* **2010**, *16*, 8117-8132.
Buckner, S.W.; MacMahon, T.J.; Byrd, G.D.; Freiser, B.S. Gas-phase reactions of niobium(1+) and tantalum(1+) with alkanes and alkenes. Carbon-hydrogen bond activation and ligand-coupling mechanisms. *Inorg. Chem.* **1989**, *28*, 3511-3518.

Burford, R.J.; Yeo, A.; Fryzuk, M.D. Dinitrogen activation by group 4 and group 5 metal complexes supported by phosphine-amido containing ligand manifolds. *Coord. Chem. Rev.* **2017**, *334*, 84-89.

Cao, M.; Xie, H. Recent advances in theoretical studies on ligand-controlled selectivity of nickel- and palladium-catalyzed cross-coupling reactions. *Chinese. Chem. Lett.* **2021**, *32*, 319-327.
Carrow, B. P.; Hartwig, J. F. Ligandless, Anionic, Arylpalladium Halide Intermediates in the Heck Reaction *J. Am. Chem. Soc.* **2010**, *132*, 79−81.

Chirik, P.J. Group 4 Transition Metal Sandwich Complexes: Still Fresh after Almost 60 Years. *Organometallics* **2010**, *29*, 1500-1517.

Cho, H.M.; Weissman, H.; Wilson, S.R.; Moore, J.S. A Mo(VI) Alkylidyne Complex with Polyhedral Oligomeric Silsesquioxane Ligands: Homogeneous Analogue of a Silica-Supported Alkyne Metathesis Catalyst. *J. Am. Chem. Soc.* **2006**, *128*, 14742-14743.

Clementi, E.; Raimond, D. L.; Reinhardt, W. P. Atomic Screening Constants from SCF Functions. II. Atoms with 37 to 86 Electrons. *J. Chem. Phys*. **1967,** *47*, 1300–1307.

Collins, R.A.; Russell, A.F.; Mountford, P., Group 4 metal complexes for homogeneous olefin polymerisation: a short tutorial review. *Appl. Petrochem. Res.* **2015**, *5*, 153-171.
Coşkun, N. and Erden, I., An efficient catalytic method for fulvene synthesis. *Tetrahedron* **2011**, *67*, 8607-8614.

Cossi, M.; Rega, N.; Scalmani, G.; Barone, V. Energies, structures, and electronic properties of molecules in solution with the C-PCM solvation model. *J. Comput. Chem*. **2003**, *24*, 669−681.

Cotton, F.A., Cyclopentadienyl–metal chemistry in the Wilkinson Group, Harvard, 1952–1955. *J. Organomet. Chem.* **2001**, *637-639*, 18-26

Crabtree, R.H. Alkane C–H activation and functionalization with homogeneous transition metal catalysts: a century of progress—a new millennium in prospect. *J. Chem. Soc, Dalton Trans.* **2001**, 2437-2450.

Crabtree, R.H. The organometallic chemistry of alkanes. *Chem. Rev.* **1985**, *85*, 245-269.

Crabtree, R.H., The Organometallic Chemistry of the Transition Metals, Seventh Edition; John Wiley & Sons Inc: Hoboken, New Jersey, 2019.

Cramer, C. J.; Truhlar, D. G., Density functional theory for transition metals and transition metal chemistry. *Phys. Chem. Chem. Phys.* **2009,** *11*, 10757-10816.

Curtis, D.M.; Bell, L.G.; Butler, W.M. C—H Activation. Synthesis of Silyl Derivatives of Niobocene and Tantalocene Hydrides, Their H/D Exchange Reactions with C_6D_6, and the Structure of $Cp_2Ta(H)_2SiMe_2Ph$. *Organometallics* **1985**, *4*, 701-707.
D'Alterio, M. C.; Casals-Cruañas, É.; Tzouras, N. V.; Talarico, G.; Nolan, S. P.; Poater, A. Mechanistic Aspects of the Palladium-Catalyzed Suzuki-Miyaura Cross-Coupling Reaction. *Chem. Eur. J.* **2021**, *early view* DOI: 10.1002/chem.202101880.

De Vries, A. H. M.; Parlevliet, F. J.; Schmieder-van de Vondervoort, L.; Mommers, J. H. M.; Henderickx, H. J. W.; Walet, M. A. M.; De Vries, J. G. A Practical Recycle of a Ligand-Free Palladium Catalyst for Heck Reactions. *Adv. Synth. Catal.* **2002**, *344*, 996−1002.

Deutsch, P.P.; Maguarie, J.A.; Jones, W.D.; Eisenberg, R. Hydride abstraction. The reaction of $IrX(CO)(dppe)$ with Cp_2TaH_3. *Inorg. Chem.* **1990**, *29*, 686-690.

Diao, T.; White, P.; Guzei, I.; Stahl, S. S. Characterization of DMSO Coordination to Palladium(II) in Solution and Insights into the Aerobic Oxidation Catalyst, Pd(DMSO)2(TFA)2. *Inorg. Chem.* **2012**, *51*, 11898-11909.

Dry, M.E., The Fischer-Tropsch process: 1950-2000. *Catal. Today.* **2002**, *71*, 277-241.
Eckhard, J.F.; Masubauchu, T.; Tschurl, M.; Barnett, R.N.; Landman, U.; Heix, U. Thermal Dehydrogenation of Methane Enhanced by μ^2-Oxo Ligands in Tantalum Cluster Cations $[TaxO]+$, x = 4, 5. *J. Phys. Chem. C* **2018**, *122*, 25628-25637.

Du, F.; Nojabaei, B. A Review of Gas Injection in Shale Reservoirs: Enhanced Oil/Gas Recovery Approaches and Greenhouse Gas Control. *Energies* **2019**, *12*, 2355-2387.

Elson, I.H.; Kochi, J.K.; Klabunde, U.; Manzer, L.E.; Parshall, G.W.; Tebbe, F.N. Paramagentic hydride and alkyl complexes of niobium(IV) and tantalum(IV). *J. Am. Chem. Soc.* **1974**, *96*, 7374-7376.

Findlay, A.E.; Leelasubcharoen, S.; Kuzmina, L.G.; Howard, J.A.K.; Nikonov, G.I. Phosphido-bridged Ta/Rh bimetallic complex: synthesis, structure, and catalytic hydrosilylation of acetophenone. *Dalton Trans.* **2010**, *39*, 9264-9269.

Fischer, E. O. and Pfab, W., Cyclopentadien-Metallkomplexe, ein neuer Typ metallorganischer Verbindungen. *Zeitschrift für Naturforschung B* **1952**, 7**,** 377-379.

Flores, J.A.; Cavaliere, V.N.; Buck, D.; Pinter, B.; Chen. G.; Crestani, M.G.; Baik, M.-H.; Mindiola, D.J. Methane activation and exchange by titanium-carbon multiple bonds. *Chem. Sci.* **2011,** *2*, 1457-1462.

Fors, B. P.; Watson, D. A.; Biscoe, M. R.; Buchwald, S. L. A Highly Active Catalyst for Pd-Catalyzed Amination Reactions: Cross-Coupling Reactions Using Aryl Mesylates and the Highly Selective Monoarylation of Primary Amines Using Aryl Chlorides *J. Am. Chem. Soc.* **2008**, *130*, 13552−13554.

Foust, D.F.; Rogers, R.D.; Rausch, M.D.; Atwood, J.L. Photoinduced Reactions of (η^5-$C_5H_5)_2M(CO)H$ (M = Nb, Ta) and the Molecular Structure of (η^5-$C_5H_5)_2Ta(CO)H$. *J. Am. Chem. Soc*. **1982**, *104*, 5646-5650.

Frisch, M. J.; Trucks, G. W.; Schlegel, H. B.; Scuseria, G. E.; Robb, M. A.; Cheeseman, J. R.; Scalmani G., Barone, V.; Petersson, G. A.; Nakatsuji, H.; Li, X.; Caricato, M.; Marenich, A. V.; Bloino, J.; Janesko, B. G.; Gomperts, R.; Mennucci, B.; Hratchian, H. P.; Ortiz, J. V.; Izmaylov, A. F.; Sonnenberg, J. L.; Williams-Young, D.; Ding, F.; Lipparini, F.; Egidi, F.; Goings, J.; Peng, B.; Petrone, A.; Henderson, T.; Ranasinghe, D.; Zakrzewski, V. G.; Gao, J.; Rega, N.; Zheng, G.; Liang, W.; Hada, M.; Ehara, M.; Toyota, K.; Fukuda, R.; Hasegawa, J.; Ishida, M.; Nakajima, T.; Honda, Y.; Kitao, O.; Nakai, H.; Vreven, T.; Throssell, K.; Montgomery, J. A. Jr.; Peralta, J. E.; Ogliaro, F.; Bearpark, M. J.; Heyd, J. J.; Brothers, E. N.; Kudin, K. N.; Staroverov, V. N.; Keith, T. A.; Kobayashi, R.; Normand, J.; Raghavachari, K.; Rendell, A. P.; Burant, J. C.; Iyengar, S. S.; Tomasi, J.; Cossi, M.; Millam, J. M.; Klene, M.; Adamo, C.; Cammi, R.; Ochterski, J. W.; Martin, R. L.; Morokuma, K.; Farkas, O.; Foresman, J. B.; and Fox, D. J. *Gaussian 16*; Gaussian, Inc., Wallingford CT, 2016.

Fryzuk, M.D.; Clentsmith, G.K.B.; Rettig, S.J. Coordination behavior of $LiBEt_4$ towards (η^5-$C_5H_5)_2ReH$, (η^5-$C_5H_5)_2WH_2$ and (η^5-$C_5H_5)_2TaH_3$. Solid state structure of $[(\eta^5\text{-}C_5H_5)_2TaH \cdot A1H_2(OCH_2CH_2CH_2CH_3)]_2$. *Inorg. Chim. Acta*. **1997**, *259*, 51-59.
Fryzuk, M.D.; Johnson, S.A. The continuing story of dinitrogen activation. *Coord. Chem. Rev.* **2000**, *200-202*, 379-409.

Fukui, K. The Path of Chemical Reactions - the IRC Approach. *Acc. Chem. Res*. **1981**, *14*, 363−368

Galardon, E.; Rhamdeehul, S.; Brown, J. M.; Cowley, A.; Hii, K. K.; Jutand, A. Profound Steric Control of Reactivity in Aryl Halide Addition to Bisphosphane Palladium(0) Complexes. *Angew. Chem. Int. Ed.* **2002**, *41*, 1760-1763.

García-Melchor, M.; Braga, A. A. C.; Lledós, A.; Ujaque, G.; Maseras, F. Computational Perspective on Pd-Catalyzed C–C Cross-Coupling Reaction Mechanisms. *Acc. Chem. Res.* **2013**, *46*, 2626-2634.

GaussView, Version 6, Dennington, Roy; Keith, Todd A.; Millam, John M. Semichem Inc., Shawnee Mission, KS, 2016.

Gianetti, T.L.; Bergman, R.G.; Arnold, J. Carbon–fluorine bond cleavage in fluoroarenes via a niobium(III) imido complex: from stoichiometric to catalytic hydrodefluorination. *Chem. Sci.* **2014**, *5*, 2517-2524.

Gibson, V. C.; Parkin, G.; Bercaw, J. E. Synthesis and Reactivity of Permethyltantalocene Derivatives Possessing η^3-Allyl, η^2-Butadiene, η^2-Methylallene,and η^1-Alkenylidene Ligands. Model Studies for the Role of Surface Vinylidenes in the Fischer−Tropsch Hydrocarbon-Chain-Lengthening Process. *Organometallics* **1991**, *10*, 220−231.

Gomez-Bengoa, E.; Echavarren, A. M. Synthesis of isoascididemin, a regioisomer of the marine alkaloid ascididemin. *J. Org. Chem.* **1991**, *56*, 3497-3501.

Gonzalez, C.; Schlegel, H. B. An Improved Algorithm for Reaction Path Following. *J. Chem. Phys*. **1989**, *90*, 2154−2161.
Gonzalez, C.; Schlegel, H. B. Reaction Path Following in Mass-Weighted Internal Coordinates. *J. Phys. Chem*. **1990**, *94*, 5523−5527.

Goossen, L. J.; Koley, D.; Hermann, H. L.; Thiel, W. The Palladium-Catalyzed Cross-Coupling Reaction of Carboxylic Anhydrides with Arylboronic Acids: A DFT Study *J. Am. Chem. Soc.* **2005**, *127*, 11102−11114.

Green, J.C. Bent metallocenes revisited. *Chem. Soc. Rev.* **1998**, *27*, 263-271.

Green, M.L.H. & Jousseaume, B. Bis(η-isopropylcyclopentadienyl)tantalum chemistry: some hydride, carbonyl, alkyl, al-kyne and tertiaryphosphine derivatives, and an improved synthesis of dichlorobiscyclopentadienylniobium. *J. Organomet. Chem*. **1980**, *193*, 339-344.

Grimme, S.; Antony, J.; Ehrlich, S.; Krieg, H. A consistent and accurate ab initio parametrization of density functional dispersion correction (DFT-D) for the 94 elements H-Pu. *J. Chem. Phys.* **2010**, 132, 154104-154119. (b) Grimme, S.; Ehrlich, S.; Goerigk, L. Effect of the damping function in dispersion corrected density functional theory. *J. Comput. Chem.* **2011**, *32*, 1456-1465.

Gulyás, H.; Hayano, S.; Madarász, Á.; Pápai, I.; Sxabó, M.; Bucsai, Á.; Martin, E.; Benet-Bucholz, J., Air-stable 18-electron adducts of Schrock catalysts with tuned stability constants for spontaneous release of the active species. *Commun. Chem.* **2021**, *4*, 71.

Gunsalas, N.J.; Koppaka, A.; Park, S.H.; Bischof, S.M.; Hashiguchi, B.G.; Periana, R.A. Homogeneous functionalization of methane. *Chem. Rev.* **2017**, *117*, 8521-8573.

Halpern, J. Activation of Carbon-Hydrogen Bonds by Metal Complexes: Mechanism, Kinetic, and Thermodynamic Considerations. *Inorg. Chim. Acta.* **1985**, *100*, 41-48.

Hartwig, J. J. *Organotransition Metal Chemistry: From Bonding to Catalysis*; University Science Books: Sausalito, CA, 2010.

Hodala, J.L; Moon, D.J.; Reddy, K.R.; Reddy, C.V.; Kumar, T.N.; Ahamed, M.I.; Raghu, A.V. Catalyst design for maximizing C5+ yields during Fischer-Tropsch synthesis. *Int. J. Hydrogen Energy* **2021**, *46*, 3289-3301.

Hooker, L. V.; Neufeldt, S. R. Ligation state of nickel during CeO bond activation with monodentate phosphines. *Tetrahedron* **2018**, *74*, 6717-6725.

Jia, C.; Kitamura, T.; Fujiwara, Y. Catalytic Functionalization of Arenes and Alkanes via C-H Bond Activation. *Acc. Chem. Res.* **2001**, *34*, 633-639.

Jiang, Q.; Pestana, D.C.; Carroll, P.J.; Berry, D.H. Thermochemical Aspects of Arene C-H Activation by Tantalum Silyl Complexes: Relative Ta-Si and Ta-C Bond Enthalpies. *Organometallics* **1994**, *13*, 3679-3691.
Jones, D. J.; Lautens, M.; McGlacken, G. P. The emergence of Pd-mediated reversible oxidative addition in cross coupling, carbohalogenation and carbonylation reactions. *Nature Cat.* **2019**, *2*, 843-851.

Joy, J.; Stuyver, T.; Shaik, S. Oriented External Electric Fields and Ionic Additives Elicit Catalysis and Mechanistic Crossover in Oxidative Addition Reactions. *J. Am. Chem. Soc.* **2020**, *142*, 3836-3850.

Kaplan, J; Wilzbach, K.E. Photolysis of benzene vapor. Benzvalene formation at wavelengths 2537-2370 Å. *J. Am. Chem. Soc.* **1968**, *90*, 3291-3292.

Keim, W., Oligomerization of Ethylene to α-Olefins: Discovery and Development of the Shell Higher Olefin Process (SHOP). *Angew. Chem. Int. Ed.* **2013**, *52,* 12492-12496.

Kepp, K.P. A quantitative scale of oxophilicity and thiophilicity. *Inorg. Chem.* **2016**, *55*, 9461-9470.

Klabunde, U. and Parshall, G.W. Activation of Aromatic Carbon-Hydrogen Bonds by Transition Metal Complexes. II. Substituted Benzenes. *J. Am. Chem. Soc*. **1972**, *94*, 9081-9087.

Korolev, A.V., Rheingold, A.L., and Williams, D.W. A General Route to Labile Niobium and Tantalum d^0 Monoimides. Discussion of Metal-Nitrogen Vibrational Modes. *Inorg. Chem*. **1997**, *36,* 2647-2655.

Kozuch, S.; Amatore, C.; Jutand, A.; Shaik, S. What Makes for a Good Catalytic Cycle? A Theoretical Study of the Role of an Anionic Palladium(0) Complex in the Cross-Coupling of an Aryl Halide with an Anionic Nucleophile. *Organometallics* **2005**, *24*, 2319-2330.
Kuhl, N.; Hopkins, M.H.; Wencel-Delord, J.; Glorius, F. Beyond Directing Groups: Transition-Metal-Catalyzed C—H Activation of Simple Arenes. *Angew. Chem. Int. Ed***. 2012**, *51*, 10236-10254.

Labinger, J. A. Tutorial on Oxidative Addition. *Organometallics* **2015**, *34*, 4784–4795.

Labinger, J.A. and Bercaw, J.E. Understanding and exploiting C–H bond activation. *Nature* **2002**, *417*, 507-514.

Labinger, J.A. and Wong, K.S. Mechanism of Formation of $(\eta^5\text{-}C_5H_5)_2NbH_3$ from the Reaction of $(\eta^5\text{-}C_5H_5)_2NbCl_2$ with Hydroaluminate Reducing Agents. *J. Organomet. Chem.* **1979**, *170*, 373-384.

Labinger, J.A.; Bercaw, J.E. Understanding and exploiting C—H bond activation. *Nature* **2002**, *407*, 507-514.

Lam, K. C.; Marder, T. B.; Lin, Z. DFT Studies on the Effect of the Nature of the Aryl Halide Y-C_6H_4-X on the Mechanism of Its Oxidative Addition to Pd^0L versus Pd^0L_2. *Organometallics* **2007**, *26*, 758-760.
Lapoutre, V. J. F.; Redlich, B.; van der Meer, A. F. G.; Oomens, J.; Bakker, J. M.; Sweeney, A.; Mookherjee, A.; Armentrout, P. B. Structures of the Dehydrogenation Products of Methane Activation by 5d Transition Metal Cations. *J. Phys. Chem. A* **2013**, *117*, 4115-4126.

Larini, P.; Kefalidis, C. E.; Jazzar, R.; Renaudat, A.; Clot, E.; Baudoin, O. On the Mechanism of the Palladium-Catalyzed β-Arylation of Ester Enolates. *Chem. - Eur. J.* **2012**, *18*, 1932−1944.

Le Roux, E.; Taoufik, M.; Copéret, C.; de Mallmann, A.; Thivolle-Cazat, J.; Basset, J.-M.; Maunders, B. M.; Sunley, G. Development of Tungsten-Based Heterogeneous Alkane Metathesis Catalysts Through a Structure–Activity Relationship. *Angew. Chem., Int. Ed*. **2005**, *44*, 6755-6758.

Leblanc, J.-C.; Reynoud, J.-F.; Moise, C. Complexes bis cyclopentadienyles substitues du tantale: synthese et reactivite de dichlorures, de tri- et de monohydrures. *C. R. Acad. Sc. Paris* **1982**, *295*, 755-757.

Legault, C. Y. *CYLview, 1.0b*; Universitéde Sherbrooke, 2009 http://www.cylview.org.

Lersch, M.; Tilset, M. Mechanistic Aspects of C−H Activation by Pt Complexes. *Chem. Rev*. **2005**, *105*, 2471−2526.

Li, C.; Dinoi, C.; Coppel, T.; Etienne, M., CH Bond Activation of Methane by a Transient η^2-Cyclopropene/Metallabicyclobutane Complex of Niobium. *J. Am. Chem. Soc.* **2015**, *137*, 12450-12453.

Lill, S. O. N.; Ryberg, P.; Rein, T.; Bennström, E.; Norrby, P-O. *t*Bu or not *t*Bu? *Chem. Eur. J.* **2012**, *18*, 1640-1649.

Lin, X.; Xi, Y.; Zhang, G.; Phillips, D.L.; Guo, W. A Reaction Mechanism of Methane Coupling on a Silica-Supported Single-Site Tantalum Catalyst. *Organometallics* **2014**, *33*, 2172-2181.

Littke, A. F.; Dai, C.; Fu, G. C. Versatile Catalysts for the Suzuki Cross-Coupling of Arylboronic Acids with Aryl and Vinyl Halides and Triflates under Mild Conditions. *J. Am. Chem. Soc*. **2000**, *122*, 4020−4028.

Littke, A. F.; Schwarz, L.; Fu, G. C. Pd/P(*t*-Bu)$_3$: A Mild and General Catalyst for Stille Reactions of Aryl Chlorides and Aryl Bromides. *J. Am. Chem. Soc.* **2002**, *124*, 6343-6348.

Lyngvi, E.; Sanhueza, I. A.; Schoenebeck, F. Dispersion Makes the Difference: Bisligated Transition States Found for the Oxidative Addition of $Pd(P^tBu_3)_2$ to Ar-OSO_2R and Dispersion-Controlled Chemoselectivity in Reactions with $Pd[P(^iPr)(^tBu2)]_2$. *Organometallics* **2015**, *34*, 805-812.

Macrae, C. F.; Bruno, I. J.; Chisholm, J. A.; Edgington, P. R.; McCabe, P.; Pidcock, E.; Rodriguez-Monge, L.; Taylor, R.; van de Streek, J.; Wood, P. A., Mercury CSD 2.0 - new features for the visualization and investigation of crystal structures. Journal of Applied Crystallography 2008, 41, 466-470.

Mahatthananchai, J.; Dumas, A. M.; Bode, J. W. Catalytic Selective Synthesis. *Angew. Chem. Int. Ed.* **2012**, *51*, 10954-10990.
Manabe, K.; Ohba, M.; Matsushima, Y., A Repetitive One-Step Method for Oligoarene Synthesis Using Catalyst Controlled Chemoselective Cross-Coupling. *Org. Lett.* **2011***, 13*, 2436-2439.

Margulieux, G.W.; Semproni, S.P.; Chirik, P.J. Photochemically Induced Reductive Elimination as a Route to a Zirconocene Complex with a Strongly Activated N_2 Ligand. *Angew. Chem. Int. Ed*. **2014**, *53*, 9189-9192.

Mashima, K. Diagonal Relationship among Organometallic Transition-Metal Complexes. *Organometallics.* **2021**, *40*, 3497-3505.

McGlade, C.E. A review of the uncertainties in estimates of global oil resources. *Energy* **2012**, *47*, 262-270; (b) McGlade, C. & Ekins, P. The geographical distribution of fossil fuels unused when limiting global warming to 2 °C. *Nature* **2015**, *517*, 187-190.

McLain, S.J.; Sancho, J.; Schrock, R.R. Metallacyclopentane to Metallacyclobutane Ring Contraction. *J. Am. Chem. Soc.* **1979**, *101*, 5451-5453.

McLain, S.J.; Sancho, J.; Schrock, R.R. Selective Dimerization of Monosubstituted a-Olefins by Tantalacyclopentane Catalysts. *J. Am. Chem. Soc.* **1980**, *102*, 5610-5618.

McLain, S.J.; Wood, C.D.; Schrock, R.R. Preparation and Characterization of Tantalum(III) Olefin Complexes and Tantalum(V) Metallacyclopentane Complexes Made from Acyclic a Olefins. *J. Am. Chem. Soc.* **1979**, *101*, 4558-4570.

McMullin, C.; Fey, N.; Harvey, J. N. Computed ligand effects on the oxidative addition of phenyl halides to phosphine supported palladium(0) catalysts. *Dalton Trans.* **2014**, *43*, 13545-13556.

McMullin, C. L.; Jover, J.; Harvey, J. N.; Fey, N. Accurate modelling of Pd(0) + PhX oxidative addition kinetics. *Dalton Trans.* **2010**, *39*, 10833-10836. (d) Ahlquist, M. S. G.; Norrby, P.-O. Dispersion and Back-Donation Gives Tetracoordinate $[Pd(PPh_3)_4]$. *Angew. Chem. Int. Ed.* **2011**, *50*, 11794-11797.

Millar, S.P.; Zubris, D.L.; Bercaw, J.E.; Eisenberg, R. On the Mechanism of Dihydrogen Addition to Tantalocene Complexes. *J. Am. Chem. Soc*. **1998**, *120*, 5329-5330.

Milner, P. J.; Yang, Y.; Buchwald, S. L. In-Depth Assessment of the Palladium-Catalyzed Fluorination of Five-Membered Heteroaryl Bromides. *Organometallics* **2015**, *34*, 4775−4775.

Mindiola, D.J. Oxidatively Induced Abstraction Reactions. A Synthetic Approach to Low-Coordinate and Reactive Early Transition Metal Complexes Containing Metal—Ligand Multiple Bonds. *Acc. Chem. Res.* **2006**, *39*, 813-821.

Moltved, K. A.; Kepp, K. P. Chemical Bond Energies of 3d Transition Metals Studied by Density Functional Theory. *J. Chem. Theory Comput.* **2018**, *14*, 3479–3492.

Montzka, S.A.; Blugokencky, E.J.; Butler, J.H. Non-CO2 greenhouse gases and climate change. *Nature* **2011***, 476*, 43-50.

Neese, F., A critical evaluation of DFT, including time-dependent DFT, applied to bioinorganic chemistry. *J. Biol. Inorg. Chem.* **2006,** *11*, 702-711.

Niemeyer, Z. L.; Milo, A.; Hickey, D. P.; Sigman, M. S. Parameterization of Phosphine Ligands Reveals Mechanistic Pathways and Predicts Reaction Outcomes. *Nat. Chem.* **2016**, *8*, 610−617.

Nomura, K.; Zhang, S. Design of Vanadium Complex Catalysts for Precise Olefin Polymerization. *Chem. Rev.* **2011, *111*,** 2342-2362.

Nunez-Zarur, F.; Solans-Monfort, X.; Restrepo, A., Mechanistic Insights into Alkane Metathesis Catalyzed by Silica-Supported Tantalum Hydrides: A DFT Study. *Inorg. Chem.* **2017**, *56*, 10458-10473.

Ohata, J.; Teremoto, A.; Fujita, H.; Takemoto, S.; Matsuzaka, H. Linear Hydrocarbon Chain Growth from a Molecular Diruthenium Carbide Platform. *J. Am. Chem. Soc.* **2021**, *143*, 16105-16112.

Ohki, Y.; Fryzuk, M.D. Dinitrogen Activation by Group 4 Metal Complexes. *Angew. Chem. Int. Ed.* **2007**, *46*, 3180-3183.

Okuda, J., Ferrocene – 65 Years After. *Eur. J. Inorg. Chem.* **2017**, *2*, 217-219.

Palani, V.; Perea, M. A.; Sarpong, R. Site-Selective Cross-Coupling of Polyhalogenated Arenes and Heteroarenes with Identical Halogen Groups. *Chem. Rev.* **2021**, *Article ASAP*. DOI: 10.1021/acs.chemrev.1c00513.

Parke, L.G.; Hinton, C.S.; Arementrout, P.B. Experimental and Theoretical Studies of the Activation of Methane by Ta+. *J. Phys. Chem. C* **2007**, *111*, 17773-17787.

Parkin, G.; Bunel, E.; Burger, B.J.; Trimmer, M.S.; Van Asselt, A.; Bercaw, J.E. Alpha- and beta-migratory insertion and elimination processes for alkyl complexes of permethyl-scandocene and permethyltantalocene. *J. Mol. Catal***. 1987**, *41*, 21-39.

Parkin, G. Classification of Organotransition Metal Compounds. In *Comprehensive Organometallic Chemistry*, Third Edition. Michael, D., Mingos, P., Crabtree, R.H.; Elsevier Science: 2007; pp 1-57.

Parshall, G.W. Intramolecular aromatic substitution in transition metal complexes. *Acc. Chem. Res***. 1970**, *3*, 139-144.

Pasha, F.A.; Cavallo, L.; Basset, J-M. Mechanism of n-Butane Hydrogenolysis Promoted by Ta-Hydrides Supported on Silica. *ACS Catal*. **2014,** *4*, 1868-1874.

Pfab, W.; Fisher, E.O., Zur Kristallstruktur der Di-cyclopentadienyl-verbindungen des zweiwertigen Eisens, Kobalts und Nickels. *Zeitschrift für anorganische und allgemeine Chemie* **1953**, *274*, 316-322.

Proutiere, F.; Schoenebeck, F. Orthogonal Selectivities under Pd(0) Catalysis with Solvent Polarity: An Interplay of Computational and Experimental Studies. *Synlett* **2012**, *23*, 645-648.
Proutiere, F.; Schoenebeck, F. Solvent Effect on Palladium-Catalyzed Cross-Coupling Reactions and Implications on the Active Catalytic Species. *Angew. Chem., Int. Ed.* **2011**, *50*, 8192−8195.

Rabe, G.; Roesky, H.W.; Stalke, D.; Pauer, F.; Sheldrick, G.M., The preparation and crystal structures of sodium and potassium pentamethylcyclopentadienyl pyridine solvates. *J. Organomet. Chem*. **1991**, *403*, 11-19.

Ramirez-Contreras, R.; Bhuvanesh, N.; Ozerov, O. V. Cycloaddition and C-H Activation Reactions of a Tantalum Alkylidyne*. Organometallics* **2015**, *34*, 1143-1146.

Reeves, E. K.; Bauman, O. R.; Mitchem, G. B.; Neufeldt, S. R. Solvent Effects on the Selectivity of Palladium-Catalyzed Suzuki- Miyaura Couplings. *Isr. J. Chem.* **2020**, *60*, 406−409

Reeves, E. K.; Entz, E. D.; Neufeldt, S. R. Chemodivergence between Electrophiles in Cross-Coupling Reactions. *Chem. Eur. J.* **2021**, *27*, 6161–6177.

Rehbein, S.M.; Kania, M.J.; Neufeldt, S.R., Experimental and Computational Evaluation of Tantalocene Hydrides for C–H Activation of Alkanes. *Manuscript in preparation*

Rehbein, S.R.; Kania, M.J.; Neufeldt, S.R. Experimental and Computational Evaluation of Tantalocene Hydrides for C–H Activation of Arenes. *Organometallics* **2021**, *40*, 2666-2677.

Rej, S.; Das, A.; Chatani, N. Strategic evolution in transition metal-catalyzed directed C–H bond activation and future directions. *Coord. Chem. Rev.* **2021**, *431*, 213683.

Riley, P.N.; Parker, J.R.; Fanwick, P.E.; Rothwell, I.P. Formation of Tantalum "Tuck-in" Complexes by Activation of Methyl C-H Bonds in Pentamethylcyclopentadiene Groups by Carbazole Ligation. *Organometallics* **1999**, *18,* 3579-3583.
Roy, A. H.; Hartwig, J. F. Oxidative Addition of Aryl Sulfonates to Palladium(0) Complexes of Mono- and Bidentate Phosphines. Mild Addition of Aryl Tosylates and the Effects of Anions on Rate and Mechanism. *Organometallics*, **2004**, *23*, 194-202.

Roy, A.; Hartwig, J. F. Reductive Elimination of Aryl Halides from Palladium(II). *J. Am. Chem. Soc.* **2001**, *123*, 1232-1233.

Ryabov, A.D. Mechanisms of intramolecular activation of carbon-hydrogen bonds in transition-metal complexes. *Chem. Rev*. **1990**, *90*, 403-424.

Sanner, R.D.; Carter, S.T.; Bruton, Jr., W.J. The preparation of mono(η^5-pentamethylcyclopentadienyl) compounds of tantalum(V). *J. Organomet. Chem.* **1982**, *240*, 157-162.

Schaller, C.P.; Wolczanski, P.T. Methane vs Benzene Activation via Transient $^{t}Bu_3SiNHTa(=NSi^{t}Bu_3)_2$: Structure of $(py)_2MeTa(=NSi^{t}Bu_3)_2$. *Inorg. Chem.* **1993**, *32*, 131-144.
Schmidt, S.; Sundermeyer, J. Höhervalente derivate der d-metall-säuren X. Imidokomplexe des fünf- und vierwertigen niobs und tantals mit halbsandwich- und metallocen- struktur *J. Organomet. Chem*. **1994**, *472*, 127-138.

Schoenebeck, F.; Houk, K. N. Ligand-Controlled Regioselectivity in Palladium-Catalyzed Cross-coupling Reactions. *J. Am. Chem. Soc*. **2010**, *132*, 2496−2497.

Schroeter, F.; Soellner, J.; Strassner, T. Cross-Coupling Catalysis by an Anionic Palladium Complex. *ACS Catal.* **2017**, *7*, 3004-3009.

Scott, N. W. J.; Ford, M. J.; Jeddi, N.; Eyles, A.; Simon, L.; Whitwood, A. C.; Tanner, T.; Willans, C. E.; Fairlamb, I. J. S. A Dichotomy in Cross-Coupling Site Selectivity in a Dihalogenated Heteroarene: Influence of Mononuclear Pd, Pd Clusters, and Pd Nanoparticles—the Case for Exploiting Pd Catalyst Speciation. *J. Am. Chem. Soc.* **2021**, *143*, 9682-9693.

Senn, H. M.; Ziegler, T. Oxidative Addition of Aryl Halides to Palladium(0) Complexes: A Density-Functional Study Including Solvation. *Organometallics* **2004**, *23*, 2980-2988.

Sergeev, A. G.; Schultz, T.; Torborg, C.; Spannenberg, A.; Neumann, H.; Beller, M. Palladium-Catalyzed Hydroxylation of Aryl Halides under Ambient Conditions. *Angew. Chem., Int. Ed.* **2009**, *48*, 7595−7599.

Sherwood, J.; Clark, J. H.; Fairlamb, I. J. S.; Slattery, J. M. Solvent effects in palladium catalysed cross-coupling reactions. *Green Chem.* **2019**, *21*, 2164.

Shilov, A.E. *Activation of Saturated Hydrocarbons by Transition Metal Complexes*; Reidel: Boston, 1984.

Solans-Monfort, X.; Chow, C.; Gouré, E.; Kaya, Y.; Basset, J.M.; Taoufik, M.; Alessandra Quadrelli, E.A.; Eisenstein, O. Successive Heterolytic Cleavages of H_2 Achieve N_2 Splitting on Silica-Supported Tantalum Hydrides: A DFT Proposed Mechanism. *Inorg. Chem.* **2012**, *51*, 7237-7249.

Soltanieh, M.; Zohrabian, A.; Gholipour, M.J.; Kalnay, E. A review of global gas flaring and venting and impact on the environment: Case study of Iran. *Int. J. Greenhouse Gas Control* **2016**, *49*, 488-509.

Soulivong, D.; Norsic, S.; Taoufik, M.; Copéret, C.; Thivolle-Cazat, J., Chakka, S.; Basset, J-M. Non-Oxidative Coupling Reaction of Methane to Ethane and Hydrogen Catalyzed by the Silica-Supported Tantalum Hydride: $(SiO)_2Ta$-H. *J. Am. Chem. Soc*. **2008**, *130*, 5044-5045.

Stahl, S. S.; Labinger, J. A.; Bercaw, J. E. Homogeneous Oxidation of Alkanes by Electrophilic Late Transition Metals. *Angew. Chem., Int. Ed*. **1998**, *37*, 2180−2192.

Stambuli, J. P.; Incarvito, C. D.; Bühl, M.; Hartwig, J. F. Synthesis, Structure, Theoretical Studies, and Ligand Exchange Reactions of Monomeric, T-Shaped Arylpalladium(II) Halide Complexes with an Additional, Weak Agostic Interaction. *J. Am. Chem. Soc.* **2004**, *126*, 1184-1194.

Sunley, G.J.; Waton, D.J., High productivity methanol carbonylation catalysis using iridium: The Cativa™ process for the manufacture of acetic acid. *Catal. Today* **2000**, *58*, 293-307.

Suzuki, K.; Shin-ya, M.; Ono, Y.; Matsumoto, T.; Nanbu, N.; Takehara, M.; Ue, M.; Sasaki, Y. Physical and Electrochemical Properties of Fluoroacetonitrile and Its Application to Electric Double-Layer Capacitors. *Electrochemistry* **2007**, *75*, 611-614.

Tanaka, H.; Nishibayashi, Y.; Yoshizawa, K. Interplay between Theory and Experiment for Ammonia Synthesis Catalyzed by Transition Metal Complexes. *Acc. Chem. Res.* **2016**, *49*, 987-995.

Tay, B.Y.; Wang, C.; Stubbs, L.P.; Jacob, C.; van Meurs, M., Deuterated dimethyl sulfoxide as a good NMR solvent for the characterization of alkali metal cyclopentadienides, amides, alkoxides and phenoxides. *J. Organomet. Chem*. **2011**, *686*, 3431-3435.
Tebbe, F.N. and Parshall, G.W. Hydride Derivatives of Niobocene and Tantalocene. *J. Am. Chem. Soc*. **1971**, *93*, 3793-3795.

Thieuleux, C.; Copéret, C.; Dufaud, V.;Marangelli, C.; Kuntz, E.; Basset, J.-M. Heterogeneous well-defined catalysts for metathesis of inert and not so inert bonds. *J. Mol. Catal. A* **2004**, *213*, 47-57.

Thomson, R.K; Monreal, M.J.; Masuda, J.D.; Scott, B.L.; Kiplinger, J.L. Lutetium gets a crown: Synthesis, structure and reaction chemistry of the separated ion pair complex, $[Li(12\text{-crown-}4)_2][(C_5Me_5)_2LuMe_2]$. *J. Organomet. Chem.* **2011**, *696*, 3966-3973.

Tobisu, M.; Chatani, N. Cross-Couplings Using Aryl Ethers via C–O Bond Activation Enabled by Nickel Catalysts. *Acc. Chem. Res.* **2015**, *48*, 1717-1726.

Van Asselt, A.; Burger, B.A.; Gibson, V.C.; Bercaw, J.E. Hydrido methylidene, hydrido vinylidene, hydrido oxo, and hydrido formaldehyde derivatives of bis(pentamethylcyclopentadienyl)tantalum. *J. Am. Chem. Soc*. **1986**, *108*, 5347-5349.

Vidal, V.; Theolier, A.; Thivolle-Cazat, J.; Basset, J.-M. Metathesis of Alkanes Catalyzed by Silica-Supported Transition Metal Hydrides. *Science* **1997**, *276*, 99-102.

Vidal, V.; Theólier, A.; Thivolle-Cazet, J.; Basset, J-M. Activation and Functionalisation of the C-H Bonds of Methane and Higher Alkanes by a Silica-supported Tantalum Hydride Complex. *J. Chem. Soc. Commun. **1995**,* 991-992.

Vilardo, J.S.; Lockwood, M.A.; Hanson, L.G.; Clark, J.R.; Parkin, B.C.; Fanwick, P.E.; Rothwell, I.P. Intramolecular activation of aromatic C–H bonds at tantalum(V) metal centers: evaluating cyclometallation 'resistant' and 'immune' aryloxide ligation. *J. Chem. Soc., Dalton Trans*. **1997**, 3353-3362.

Walton, J.W.; Wilkinson, L.A. π-Coordinated arene metal complexes and catalysis. In *Organometallic Chemistry: Volume 42*, Paymore, N.J., Elliot, P.P.; Royal Society of Chemistry: Cambridge, U.K., 2019: pp 125-171.

Waterman, R. σ-Bond Metathesis: A 30-Year Restrospective. *Organometallics* **2013**, *32*, 7249-7263.

Watson, D. A.; Su, M.; Teverovskiy, G.; Zhang, Y.; Garcia-Fortanet, J.; Kinzel, T.; Buchwald, S. L. Formation of ArF from LPdAr(F): Catalytic Conversion of Aryl Triflates to Aryl Fluorides. *Science* **2009**, *325*, 1661−1664.

Watson, P.L., Methane Exchange Reactions of Lanthanide and Early-Transition-Metal Methyl Complexes. *J. Am. Chem. Soc.* **1983**, *105*, 6491-6493.

Wesendrup, R. and Schwarz, H. Tantalum-Mediated Coupling of Methane and Carbon Dioxide in the Gas Phase. *Angew. Chem. Int. Ed*. **1995**, *34*, 2033-2035.

Wilkinson, G.; Rosenblum, M.C.; Whiting, M.C.; Woodward, R.B., The structure of iron bis-cyclopentadienyl. *J. Am. Chem. Soc.* **1952**, *74*, 2125-2126.

Williams, L.J.; Bhonoah, Y.; Wilkinson, L.A.; Walton, J.W. As Nice as p: Aromatic Reactions Activated by p -Coordination to Transition Metals. *Chem. Eur. J.* **2021**, *27*, 3650-3660.

Wilzbach, K.E.; Ritscher, J.S.; Kaplan, L. Benzvalene, the tricyclic valance isomer of benzene. *J. Am. Chem. Soc.* **1967**, *89*, 1031-1032.

Wohlfarth, C. "Permittivity (Dielectric Constant) of Liquids" in *CRC Handbook of Chemistry and Physics,* Rumble, Jr., J. R.; Lide, D. R.; Bruno, T. J., eds. CRC Press, Boca Raton, FL, **2020**.

Wolfsbergers, W.; Schmidbaur, H. Eine befriendegende darstellungsmethode für trimethylphosphin. *Syn. React. Inorg. Metal-Org. Chem.* **1974**, *4*, 149-156.
Woo, T.K.; Blöchl, P.E.; Ziegler, T. Monomer Capture in Brookhart's Ni(II) Diimine Olefin Polymerization Catalyst: Static and Dynamic Quantum Mechanics/Molecular Mechanics Study. *J. Phys. Chem. A.* **2000**, *104*, 121-129.

Xie, M.; Lu, W. Attraction or repulsion? Theoretical assessment of bulky alkyl groups by employing dispersion-corrected DFT. *RSC Adv.* **2018**, *8*, 2240-2247.

Xue, L.; Lin, Z. Theoretical aspects of palladium-catalysed carbon–carbon cross-coupling reactions. *Chem. Soc. Rev.* **2010**, *39*, 1692-1705.

Xue, X.S.; Ji, P.J.; Zhou, B.Y.; Cheng, J.P. The Essential Role of Bond Energetics in C—H Activation/Functionalization. *Chem. Rev.* **2017**, *117*, 8622-8648.
Yin, C.; Edy, A.; Ali, H.; Bilel, H.; Lyndon, E.; Basset, J.M. Alkane Metathesis with the Tantalum Methylidene [(≡SiO)Ta(:CH_2)Me_2]/ [(≡SiO)$_2$Ta(:CH_2)Me] Generated from Well-Defined Surface Organometallic Complex [(≡SiO)$Ta^{V}Me_4$]. *J. Am. Chem. Soc*. **2015,** *137*, 588-591.

Yu, H. S.; He, X.; Truhlar, D. G. MN15-L: A New Local Exchange-Correlation Functional for Kohn–Sham Density Functional Theory with Broad Accuracy for Atoms, Molecules, and Solids. *J. Chem. Theory Comput.* **2016**, *12*, 1280.

Zalesskiy, S. S.; Ananikov, V. P. $Pd_2(dba)_3$ as a Precursor of Soluble Metal Complexes and Nanoparticles: Determination of Palladium Active Species for Catalysis and Synthesis. *Organometallics* **2012**, *31*, 2302–2309.

Zhao, Y.; Truhlar, D. G. A New Local Density Functional for Main-Group Thermochemistry, Transition Metal Bonding, Thermo-chemical Kinetics, and Noncovalent Interactions. *J. Chem. Phys*. **2006**, *125*, 194101.

Zhao, Y.; Truhlar, D. G. Attractive Noncovalent Interactions in the Mechanism of Grubbs Second-Generation Ru Catalysts for Olefin Metathesis. *Org. Lett.* **2007**, *9*, 1967-1970.

Zhao, Y.;Truhlar, D. G. The M06 suite of density functionals for main group thermochemistry, thermochemical kinetics, noncovalent interactions, excited states, and transition elements: two new functionals and systematic testing of four M06-class functionals and 12 other functionals. *Theor. Chem. Acc.,* **2008**, *120,* 215–241.

Zhou, Q.; Srinivas, H. D.; Zhang, S.; Watson, M. P. Accessing Both Retention and Inversion Pathways in Stereospecific, Nickel-Catalyzed Miyaura Borylations of Allylic Pivalates. *J. Am. Chem. Soc.* **2016**, *138*, 11989-11995.

Zhu, J.; Liang, Y.; Wang, L.; Zheng, Z.-B.; Houk, K. N.; Tang, Y. Remote Ester Groups Switch Selectivity: Diastereodivergent Synthesis of Tetracyclic Spiroindolines. *J. Am. Chem. Soc.* **2014**, *136*, 6900-6903.

APPENDICES

APPENDIX A

CHAPTER TWO SUPPLEMENTAL

Supporting Information

for

Experimental and Computational Evaluation of Tantalocene Hydrides for C—H Activation of Arenes

Steven M. Rehbein, Matthew J. Kania, and Sharon R. Neufeldt*

Department of Chemistry and Biochemistry, Montana State University
Bozeman, MT 59717, USA

Correspondence: sharon.neufeldt@montana.edu

Table of Contents

I. Experimental Details
- **A.** Rate Studies
  - **1.** Example of Data Analysis S3
  - **2.** H/D Exchange Rate Data S4
- **B.** Benzylic H/D Exchange Experiments
  - **1.** Experiments Using Toluene-d_8 and H_2 S5
  - **2.** Experiments Using Toluene-α,α,α- d_3 S6
- **C.** UV-Vis Spectrum of Cp_2TaH_3 S7

II. Computational Details
- **A.** Graphical Guide to Numbered Compounds S8
- **B.** Energies, Entropies, and Lowest Frequencies of Minimum Energy Structures S10
- **C.** Comparison of π-Complex Energies With and Without Dispersion S12
- **D.** Discussion on the Spin State of Cp_2TaH S12
- **E.** Discussion on the Reductive Elimination of H_2 S15
- **F.** Benzene Activation on the Triplet Energy Surface S16
- **G.** σ-Bond Metathesis Mechanism for Benzene Activation S17
- **H.** Additional Pathways for Benzylic C—H Activation of Toluene S18

III. References S20

IV. NMR Spectra S22

I. Experimental Details

A. Rate Studies

1. Example of Data Analysis

For each experiment, rates of catalysis were calculated as follows:

(1) For each time point, the total integration value of the hydride regions of the NMR spectra was converted into a concentration [hydride]. These data were plotted on a graph of concentration vs. time (example in Figure S1, black circles).

(2) For each time point, the integration value of the Cp signal (or, in the case of Cp*, the Me signal) was converted into a concentration [Cp]. These data were plotted on a graph of concentration vs. time (example in Figure S1, white squares).

(3) A least squares regression line was fit to each set of points (solid black and dashed trendlines in Figure S1). The slope of the [hydride] line corresponds to the negative of the rate r_{uncorr}, while the slope of the [Cp] line corresponds to the negative of r_{decomp}.

(4) To obtain a rate for H/D exchange that corrects for other decomposition pathways (r_{corr}), the slope of the [Cp] line was subtracted from the slope of the [hydride] line. The difference between these slopes corresponds to the negative of the corrected rate r_{corr}

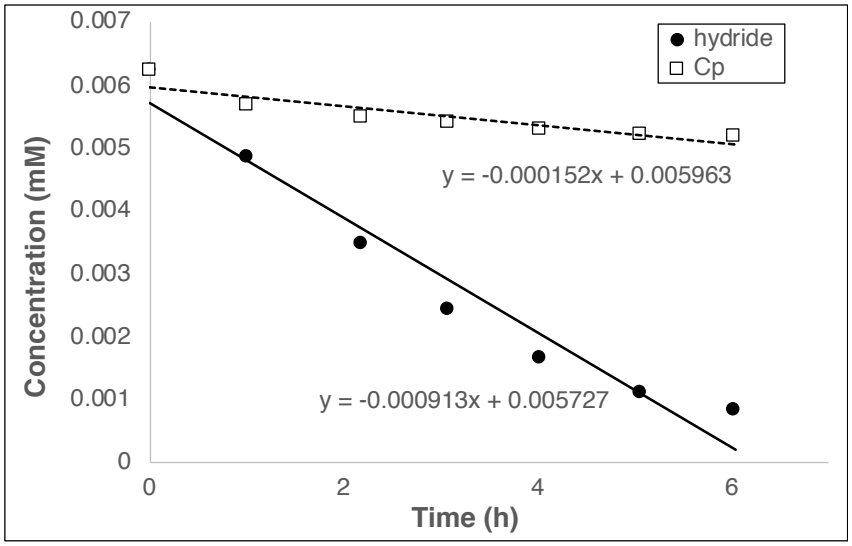


Figure S1. Sample plot of rate data.

2. *H/D Exchange Rate Data*

Each data point in Table 1 of the manuscript represents the average of three trials. The results from the individual trials are below in Table S1.

Table S1. Rate Data for Table 1.

entry from Table 1	trial	r_{uncorr} (M h^{-1} x 10^{-7})	r_{decomp} (M h^{-1} x 10^{-7})	std. error. r_{decomp} (M h^{-1} x 10^{-7})	r_{corr} (M h^{-1} x 10^{-7})	std. error. r_{corr} (M h^{-1} x 10^{-7})
1	**(Mean)**	**29.11**	**5.15**	0.09	**23.95**	0.03
	i	28.17	5.83		22.33	
	ii	30.40	4.84		25.56	
	iii	28.77	4.80		23.97	
2	**(Mean)**	**29.85**	**5.57**	0.24	**24.28**	0.06
	i	26.43	6.09		20.34	
	ii	32.98	4.35		28.63	
	iii	30.15	6.28		23.87	
3	**(Mean)**	**21.46**	**4.61**	0.06	**16.85**	0.03
	i	21.49	5.01		16.49	
	ii	20.77	4.71		16.06	
	iii	22.11	4.13		17.99	
4	**(Mean)**	**5.41**	**3.78**	0.03	**1.63**	0.16
	i	9.21	7.02		2.19	
	ii	3.58	2.41		1.17	
	iii	3.43	1.89		1.54	
5	**(Mean)**	**9.78**	**2.77**	0.02	**7.01**	0.02
	i	9.34	2.60		6.74	
	ii	9.86	2.57		7.29	
	iii	10.14	3.13		7.00	
6	**(Mean)**	**5.95**	**1.11**	0.06	**4.84**	0.02
	i	7.43	1.39		6.04	
	ii	5.46	1.25		4.20	
	iii	4.95	0.68		4.27	
7	**(Mean)**	**-0.05**	**-0.08**	0.05	**0.04**	0.06
	i	-0.72	0.05		-0.76	
	ii	-0.42	-0.44		0.01	
	iii	0.99	0.14		0.86	

B. Benzylic H/D Exchange Experiments

1. Experiments Using Toluene-d_8 and H_2

Experiments were carried out to monitor H/D exchange at the four unique sites of toluene. In a glass pressure vessel (88 mL volume), Cp_2TaH_3 (10.8 mg, 0.035 mmol, 1 equiv) was dissolved in a solution of toluene-d_8 (2.0 mL, 17.3 mmol) containing cyclohexane (1 equiv). The mixture was frozen in liquid nitrogen and the atmosphere was replaced with hydrogen (1 atm) through a series of three evacuation-refill cycles. The vessel was then heated at 100 °C in an oil bath for 6 or 24 h. The reaction mixture was allowed to cool to room temperature and ^{1}H NMR spectra were acquired and compared to a sample of the original toluene-d_8/cyclohexane stock solution. Increases in the toluene-d_8 residual solvent signals relative to cyclohexane are reported as percent increases relative to the original stock solution (Table S2).

Table S2. Change in ^{1}H NMR Signals of Toluene-d_8 After Heating with Cp_2TaH_3.

signal	δ (ppm)	% increase, 6 h	% increase, 24 h
CH (*meta*)	7.09	24	306
CH (*para*)	7.01	31	342
CH (*ortho*)	6.97	19	306
CH_3	2.08	17	67

The increases in the benzylic signal are consistently smaller than those at all other positions and are believed to be within the error of the experiment. In particular, these small increases may be due to loss of cyclohexane from solution, whose boiling point is ~30 °C below that of toluene. To resolve this uncertainty, we performed the following experiment using toluene-*a,a,a*-d_3.

2. Experiments Using Toluene-a,a,a-d_3

Experiments were carried out to monitor H/D exchange resulting from benzylic C—H activation at toluene-α,α,α-d_3. In a high-pressure NMR tube (9" length, 3.46 mm internal diameter), Cp_2TaH_3 (3.4 mg, 0.011 mmol) was dissolved in toluene-α,α,α–d_3 (0.60 mL, 5.5 mmol). The tube was pressurized with nitrogen (4 atm), and an initial ^{1}H NMR spectrum was acquired. The reaction mixture was then heated at 100 °C for 24 h, and ^{1}H NMR spectra were acquired at 0, 4, 8, and 24 h. No change in the appearance of the hydride signals was observed at any of these time points, indicating that H/D exchange between Cp_2TaH_3 and the benzylic site of toluene did not occur (Figure S2). Analogous experiments performed at 1 atm of nitrogen or under photochemical conditions (350 nm, 35 °C) also failed to produce evidence of benzylic H/D exchange.

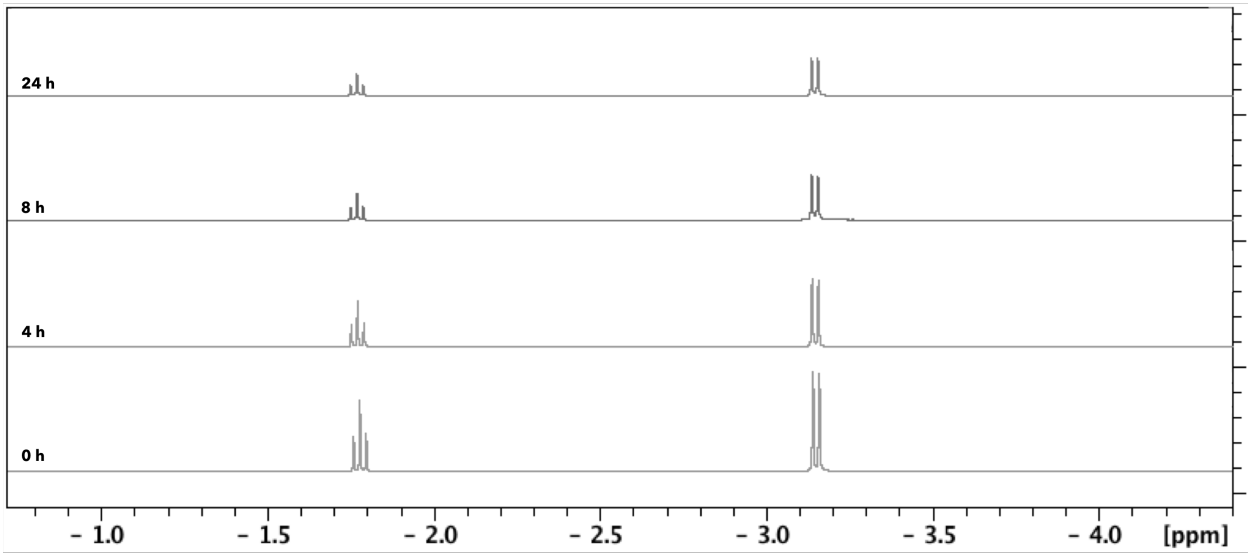


Figure S2. Lack of evidence for benzylic H/D exchange between Cp_2TaH_3 and toluene-α,α,α-d_3

C. UV-Vis Spectrum of Cp_2TaH_3

A UV-Vis spectrum of Cp_2TaH_3 (**1**) was collected in Et_2O at room temperature via dual beam UV-Vis spectroscopy on an Agilent Cary 60 spectrophotometer from 600 to 200 nm at 1 nm intervals. An absorbance maxima at 235 nm was observed (Figure S3).

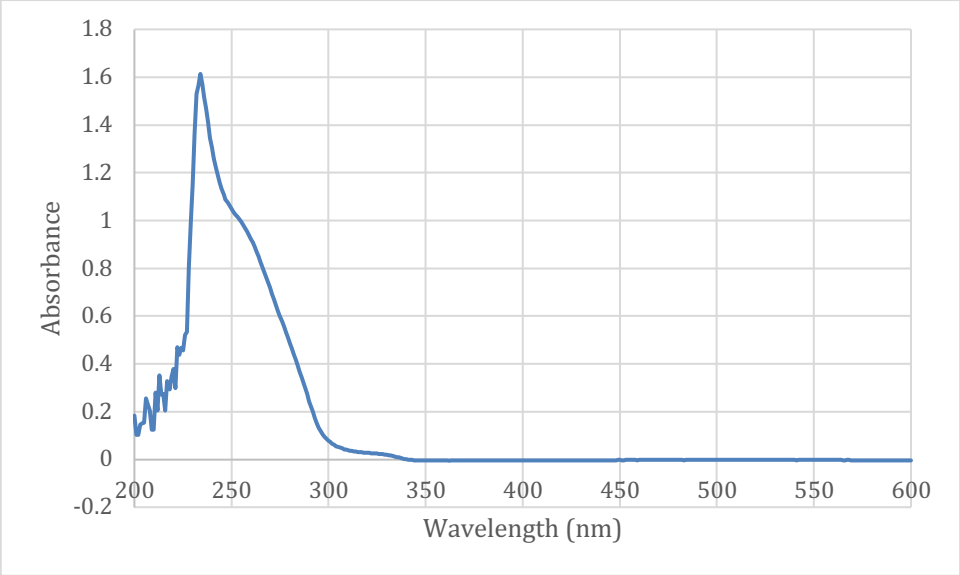
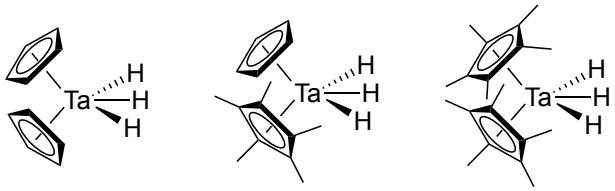


Figure S3. UV-Vis spectrum of Cp_2TaH_3.

II. Computational Details

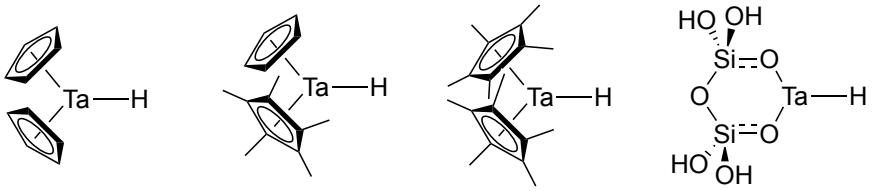
A. Graphical Guide to Numbered Compounds

Ta(V) Trihydride Complexes



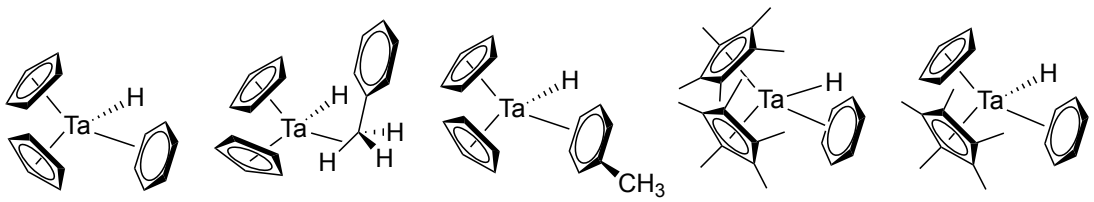
1 **8** **9**

Ta(III) Monohydride Intermediates



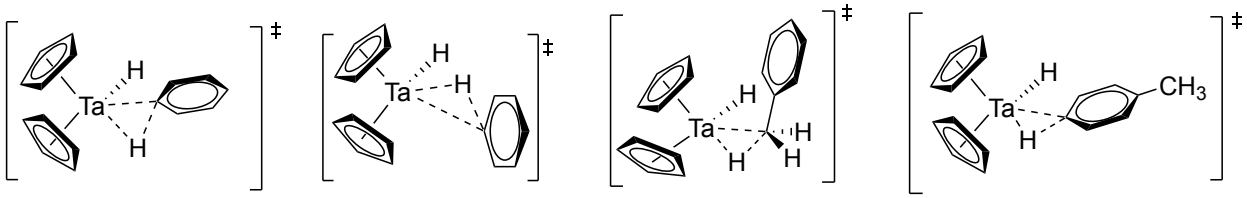
^{1}**2** and ^{3}**2** ^{1}**16** and ^{3}**16** ^{1}**17** and ^{3}**17** ^{1}**A** and ^{3}**A**

π- and σ-Complexes (Intermediates Prior to Oxidative Addition)

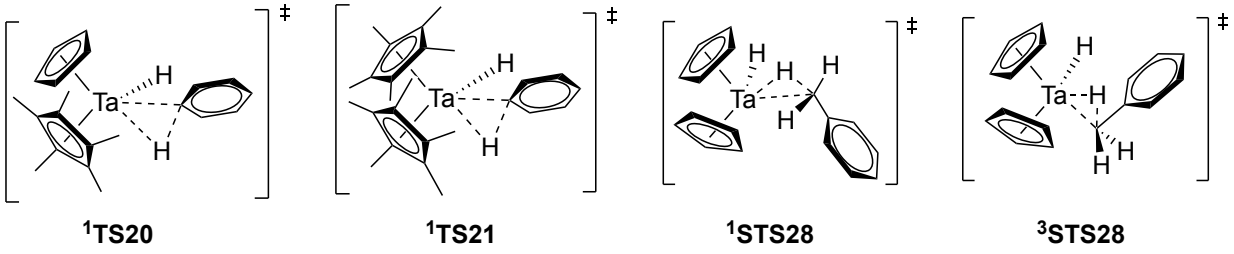


3 **10** **11** **18** **19**

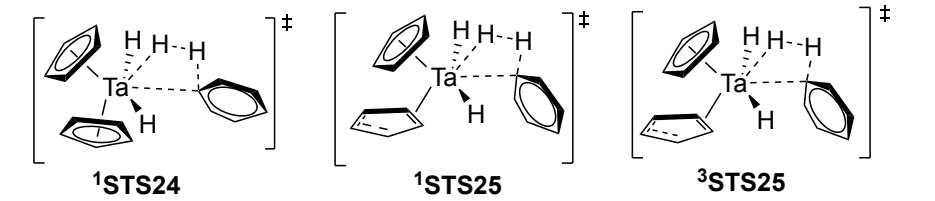
Oxidative Addition Transition Structures

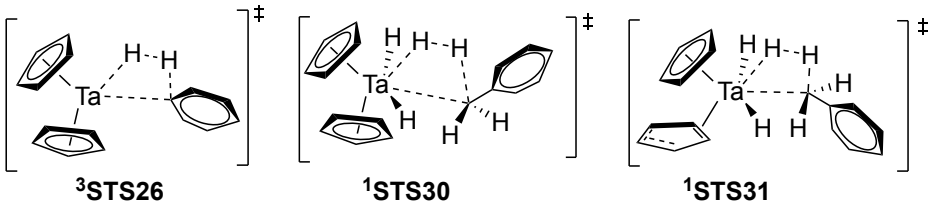


^{1}**TS4** and ^{3}**TS4** ^{1}**TS5** ^{1}**TS12** ^{1}**TS13**

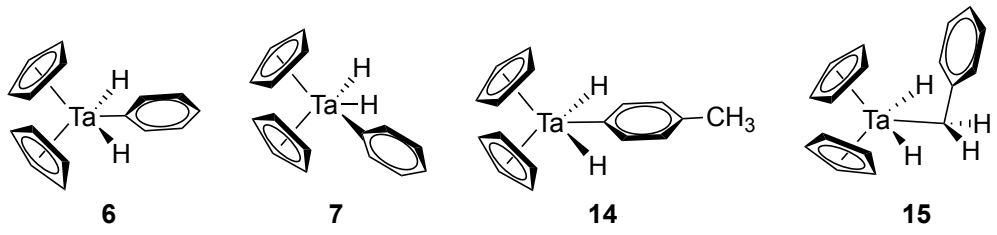


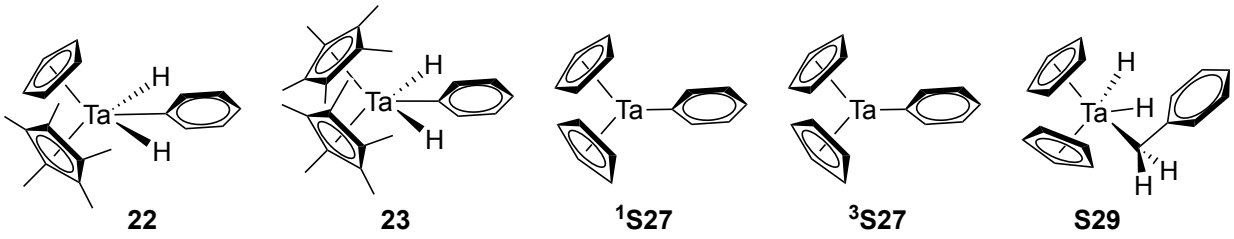
σ-Bond Metathesis Transition Structures





C-H Activation Products





B. Energies, Entropies, and Lowest Frequencies of Minimum Energy Structures

Table S3. Energies, Entropies, and Lowest Frequencies of Minimum Energy Structures in Benzene[a]

Structure	E_{elec} (Hartree)	E_{elec} + ZPE (Hartree)	H (Hartree)	S (cal mol^{-1} K^{-1})	G[b] (Hartree)	Lowest freq. (cm^{-1})
1	-445.6901403	-445.4991833	-445.4881133	99.684	-445.5354763	47.8724
^{1}2	-444.4612326	-444.2882526	-444.2773926	98.353	-444.3241236	68.5392
^{3}2	-444.474046	-444.300785	-444.289749	102.833	-444.338608	37.2295
3	-676.6113546	-676.3346626	-676.3188286	120.478	-676.3760716	53.7681
^{1}TS4	-676.5861012	-676.3139482	-676.2980912	123.025	-676.3565442	-619.6796
^{3}TS4	-676.495495	-676.228636	-676.211565	131.615	-676.274099	-369.6462
^{1}TS5	-676.58542	-676.312914	-676.297182	121.993	-676.355145	-660.7414
6	-676.6106379	-676.3359749	-676.3199679	124.421	-676.3790849	45.4516
7	-676.6103318	-676.3363238	-676.3201088	125.545	-676.3797598	30.0461
8	-642.1726581	-641.8435261	-641.8238861	136.432	-641.8887091	34.8218
9	-838.6504573	-838.1825313	-838.1545083	172.111	-838.2362843	20.9878
^{1}16	-640.943537	-640.632274	-640.612858	135.757	-640.677361	34.8992
^{3}16	-640.9556289	-640.6444429	-640.6246759	140.910	-640.6916269	27.0302
^{1}17	-837.4207911	-836.9711231	-836.9432201	171.543	-837.0247261	31.1864
^{3}17	-837.4369655	-836.9872575	-836.9590435	176.177	-837.0427515	29.3716
18	-873.0928894	-872.6774334	-872.6534364	153.443	-872.7263424	46.4056
19	-1069.549546	-1068.994607	-1068.962449	186.683	-1069.051148	36.3499
^{1}TS20	-873.0624767	-872.6516427	-872.6273987	157.350	-872.7021607	-620.4639
^{1}TS21	-1069.532544	-1068.981977	-1068.949911	188.182	-1069.039323	-661.7812
22	-873.0944717	-872.6811397	-872.6567757	159.440	-872.7325307	28.9782
23	-1069.573003	-1069.020523	-1068.988135	190.513	-1069.078654	25.4086
^{1}STS24	-677.7212478	-677.4326948	-677.4157708	129.076	-677.4770988	-1100.1406
^{1}STS25	-677.7199629	-677.4310879	-677.4142789	126.846	-677.4745469	-193.2862
^{3}STS26	-676.5140983	-676.2447213	-676.2281433	128.384	-676.2891423	-1088.8528
^{1}S27	-675.393998	-675.137674	-675.121416	127.066	-675.181789	28.2276
^{3}S27	-675.4063349	-675.1501469	-675.1338809	130.836	-675.1960449	26.9919
^{1}A	-1165.965643	-1165.886584	-1165.871515	121.512	-1165.929249	36.7948
^{3}A	-1165.96283	-1165.883215	-1165.868812	117.500	-1165.92464	66.2244

[a]Energy values calculated at the CPCM(benzene)-M06/BS2//M06L/BS1 level, where BS2 = 6-311++G(2d,p)/SDD(Ta); BS1 = 6-31+G(d,p)(C,H)/LANL2DZ(Ta). 1 Hartree = 627.51 kcal mol^{-1}. Thermal corrections at 298.15 K. [b]Solvent-corrected free energy given by G[(CPCM)/M06/BS2] = E_{elec}[(CPCM)/M06/BS2] + G_{corr} [M06L/BS1], where G_{corr} is the thermal correction to Gibbs free energy obtained in the gas phase.

Table S4. Energies, Entropies and Lowest Frequencies of Minimum Energy Structures in Toluene[a]

Structure	E_{elec} (Hartree)	E_{elec} + ZPE (Hartree)	H (Hartree)	S (cal mol^{-1} K^{-1})	G[b] (Hartree)	Lowest freq. (cm^{-1})
1	-445.6903298	-445.4993728	-445.4883028	99.684	-445.5356658	47.8724
^{1}2	-444.4615471	-444.2885671	-444.2777071	98.353	-444.3244381	68.5392
^{3}2	-444.4742082	-444.3009472	-444.2899112	102.833	-444.3387702	37.2295
10	-715.8880767	-715.5849667	-715.5669507	135.858	-715.6315017	28.8137
11	-715.906821	-715.602661	-715.585086	128.524	-715.646152	49.2489
^{1}TS12	-715.878646	-715.578352	-715.561089	131.809	-715.623716	-972.705
^{1}TS13	-715.8813348	-715.5819318	-715.5650118	128.062	-715.6258578	-678.9909
14	-715.9056348	-715.6036968	-715.5857238	136.934	-715.6507848	14.1565
15	-715.9073113	-715.6046543	-715.5873773	132.706	-715.6504303	17.9707
^{1}STS28	-715.8711355	-715.5718125	-715.5543545	131.942	-715.6170445	-1069.4981
^{3}STS28	-715.8709557	-715.5716327	-715.5541747	131.955	-715.6168707	-1069.2904
S29	-715.9069044	-715.6045244	-715.5873304	128.827	-715.6485404	46.0609
^{1}STS30	-717.0144755	-716.6965525	-716.6782535	136.462	-716.7430905	-294.6255
^{1}STS31	-717.0106977	-716.6939107	-716.6756057	136.859	-716.7406327	-352.8554

[a]Energy values calculated at the CPCM(toluene)-M06/BS2//M06L/BS1 level, where BS2 = 6-311++G(2d,p)/SDD(Ta); BS1 = 6-31+G(d,p)(C,H)/LANL2DZ(Ta). 1 Hartree = 627.51 kcal mol^{-1}. Thermal corrections at 298.15 K. [b]Solvent-corrected free energy given by G[(CPCM)/M06/BS2] = E_{elec}[(CPCM)/M06/BS2] + G_{corr} [M06L/BS1], where G_{corr} is the thermal correction to Gibbs free energy obtained in the gas phase.

C. Comparison of π-Complex Energies With and Without Dispersion

Single point energies were calculated for the Cp_2TaH(benzene) π-complex (**3**) using a variety of DFT functionals. These calculations were performed at the CPCM(benzene)/*X*/6-311++G(2d,p)/SDD(Ta)//M06L/6-31+G(d,p)(C,H)/LANL2DZ(Ta) level where *X* = the functional used for the single point energy calculation. When *X* includes dispersion, the calculations predict that formation of **3** is exergonic relative to Cp_2TaH (**^{1}2**, grey bars in Figure S4). In contrast, the use of functionals that do not contain dispersion predict that **3** is higher energy than **^{1}2** (black bars). Based on the difference between calculations with and without dispersion, it appears that stabilization of the π-complex **3** relative to Cp_2TaH is due to favorable London dispersion interactions.

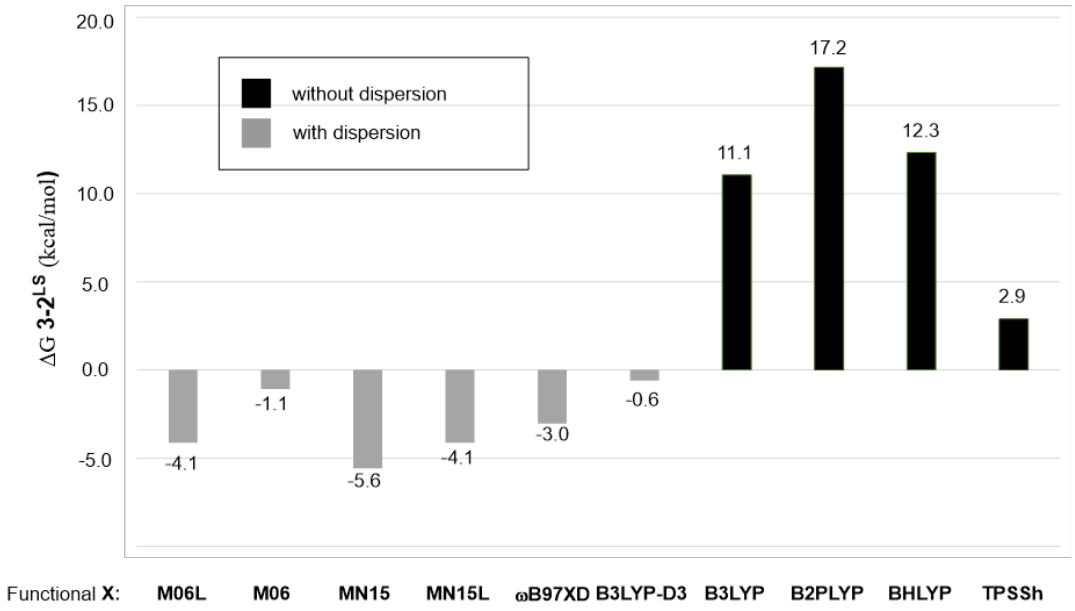
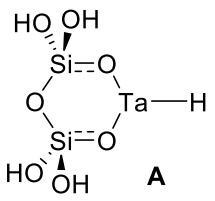


Figure S4. Comparison of the energies of π-complex **3** relative to Cp_2TaH (**^{1}2**) calculated with functionals that do and do not contain dispersion. Level of theory: CPCM(benzene)-*X*/6-311++G(2d,p)/SDD(Ta)//M06L/6-31+G(d,p)/ LANL2DZ(Ta) where *X* = the functional used.[1-9]

D. Discussion on the Spin State of Cp_2TaH



A

In at least one previous report by Basset and coworkers, a variety of DFT functionals were found to predict that the silica-supported Ta(III) monohydride **A** is more stable in the low spin electron configuration.[10,11] This result contrasts with our original calculations on Cp_2TaH using M06/BS2//M06L/BS1, as well as with other reported calculations on d^2 tantalum species,[12] which predict a triplet ground state configuration. We were interested in understanding whether the discrepancy between our spin state prediction for Cp_2TaH and Basset's prediction for silica-supported TaH is due to a difference in our DFT

methods or due to the different ligand environments for these Ta(III) species. Consequently, we calculated single point energies of **A** using a variety of methods. The results are summarized in Table S5. The functionals M06, M06L, B3LYP, B3PW91,[13] and BP86[6a,14] had been previously evaluated by Basset et al. in combination with the triple-ζ basis set TZVP[15] and the SDD[16] pseudopotential on tantalum. We repeated these single-point energy calculations on **A** (Column A, rows 1-5) using the cartesian coordinates for **A** taken from reference 10 [in this reference, **A** had been optimized using M06/TZVP/SDD(Ta)]. Unsurprisingly, we obtained the same results as previously described with these methods: **A** is predicted to have a low-spin ground state with most of these functionals (i.e., $E_{(LS-HS)}$ is a negative value, indicated by bolded red text). Adding Grimme's dispersion correction to B3LYP does not affect the energy predictions (row 6). Interestingly, like B3PW91, the newer Minnesota functionals MN15 and MN15L predict that high-spin Ta(III) is favored (rows 7-8). These results illustrate that the predicted ground state can be sensitive to the DFT functional used. Adding a solvent correction to the calculations (Column B) does not have a significant impact on the energy predictions. Use of the Pople basis set 6-311++G(2d,p) and the SDD pseudopotential on tantalum (equivalent to our "BS2") also leads to the same qualitative predictions about the stability of low-spin **A** (Columns C and D).

Importantly, when the structure of **A** was re-optimized using M06L/BS1 (the method typically used by us in this paper) prior to the single-point energy calculations, the low-spin configuration becomes destabilized, and high-spin is usually favored (Column E). As such, ground state predictions can be highly sensitive to DFT method, especially to the method used for geometry optimizations.

Table S5. Predicted Spin State for Silica-Supported Tantalum Monohydride **A**.

		$E_{(LS-HS)}$ (kcal/mol)[a]				
Functional	Row/Column[b]	A	B	C	D	E
M06	1	**-8.8**	**-7.3**	**-8.9**	**-7.5**	**-1.8**
M06L	2	**-5.5**	**-3.9**	**-5.2**	**-3.6**	+2.8
B3LYP	3	**-3.5**	**-1.4**	**-3.4**	**-1.5**	+0.7
B3PW91	4	+1.0	+3.0	+1.2	+3.1	+6.5
BP86	5	**-2.2**	**-0.3**	**-2.0**	**-0.1**	+4.2
B3LYP-D3	6	**-3.5**	**-1.4**	**-3.4**	**-1.5**	+1.5
MN15	7	+1.2	+3.1	+1.3	+3.0	+9.6
MN15L	8	+3.9	+5.5	+4.3	+5.7	+14.0

[a]Calculated electronic energy difference between the low-spin (S=0) and high-spin (S=1) electronic configurations of **A**. [b]Each column represents a different combination of basis set and solvent. The energies in Columns A–D (entries highlighted in gray) were calculated using the cartesian coordinates for **A** extracted from reference 10 (the geometry was optimized with M06/TZVP/SDD(Ta)), as follows. Column A: gas phase calculations with TZVP/SDD(Ta); Column B: CPCM(benzene) with TZVP/SDD(Ta); Column C: gas phase calculations with 6-311++G(2d,p)/SDD(Ta); Column D: CPCM(benzene) with 6-311++G(2d,p)/SDD(Ta). The energies in Column E were calculated with CPCM(benzene) and 6-311++G(2d,p)/SDD(Ta) using cartesian coordinates for **A** that were reoptimized using M06L/6-31+G(d,p)/LANL2DZ(Ta).

We next evaluated some of these DFT methods for the spin state predictions on Cp_2TaH (**2**). Unlike the results with **A**, **2** is predicted to be more stable with spin = 1 (high spin) with nearly all methods, including

when its geometry is optimized using the same method used by Basset for optimization of **A** (M06/TZVP/SDD(Ta), last column of Table S6). Taken together, these calculations suggest that the discrepancy between predicted spin state of **2** and **A** is primarily due to ligand effects. Nevertheless, it is clear that predicted ground-state electron configurations of Ta(III) are method-sensitive (especially the method used for geometry optimization).

Table S6. Predicted Spin State for Cp_2TaH (**2**).

	Functional and Basis Set for Geometry Optimizations ($E_{(LS-HS)}$ given in kcal/mol)[a]			
Functional for single point energy calculations	M06L/ 6-31+G(d,p)/ LANL2DZ(Ta)	M06L/ 6-31+G(d,p)/ SDD(Ta)	M06L/ TZVP/ SDD(Ta)	M06/ TZVP/ SDD(Ta)
M06	+10.6	+10.5	+10.5	+10.5
M06L	+9.4	+9.4	+9.4	+9.4
B3LYP	+10.6	+10.5	+10.4	+10.3
B3PW91	+11.3	+11.3	+11.2	-11.2
BP86	+9.5	+9.5	+9.4	+9.4

[a]Calculated electronic energy difference between the low-spin (S=0) and high-spin (S=1) electronic configurations of **2**. Geometry optimizations and single point energy calculations were conducted in the gas phase. Single point energies were calculated using the indicated functional and 6-311++G(2d,p)/SDD(Ta).

E. Discussion on the Reductive Elimination of H_2

Relaxed potential energy scans along the reaction coordinate on the singlet surface for H—H bond formation from Cp_2TaH_3 were carried out in search of a transition structure for reductive elimination of H_2 (example in Figure S5). Scans were conducted bringing together *cis* hydrogens as well as bringing together pseudo-*trans* hydrogens. Each scan was carried out using the 6-31+G(d,p) basis set with the LANL2DZ pseudopotential for tantalum, using the hybrid functionals M06L (Figure S5), MN15, MN15L, B3LYP, B3LYP-D3, B2PLYP, and TPSSh, as well as with the pure functionals TPSS[9a] and OPBE.[17] All scans resulted in similar outcomes: when a possible energy maximum was visible in the scan, it was very small [approximately 0.0021 Hartree (1.3 kcal/mol) above the adjacent points in the scans]. Attempts to optimize geometries from these maximum energy points failed to converge on a transition structure. As such, we conclude that there is little or no energy barrier to reductive elimination along the singlet surface.

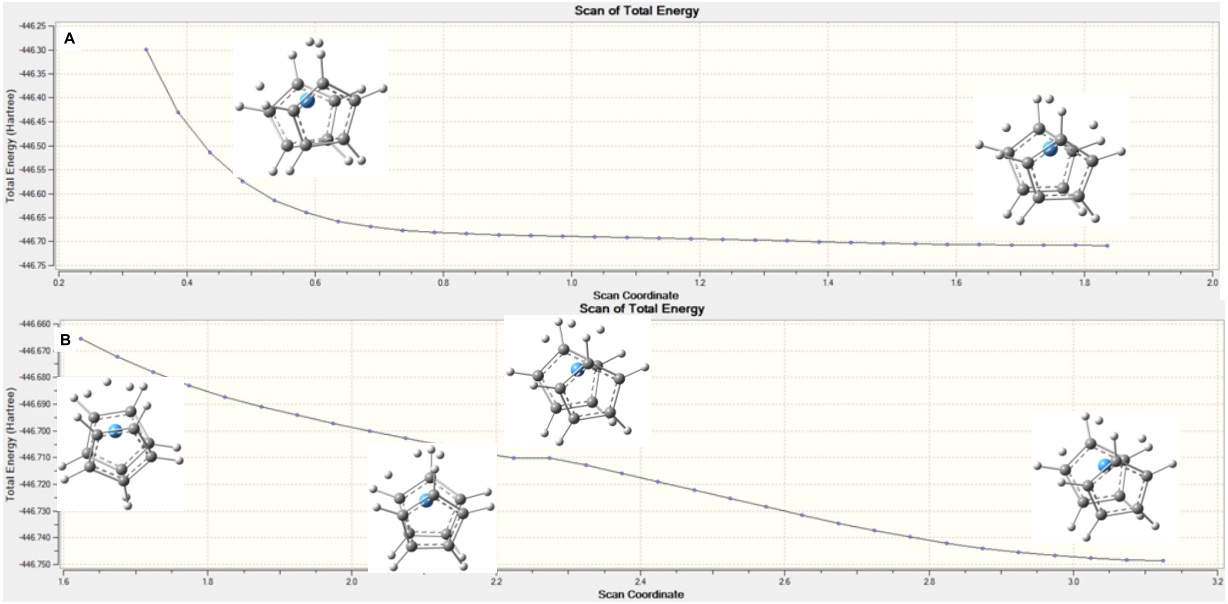


Figure S5. Relaxed scans of the potential energy along the reaction coordinate on the singlet surface for: (A) *cis*-H-H bond formation and (B) *pseudo-trans*-H-H bond formation from Cp_2TaH_3 (**1**). The starting complex **1** is shown to the right in both images. Calculated using M06L/6-31+G(d,p)/LANL2DZ(Ta).

F. Benzene Activation on the Triplet Energy Surface

Possible reaction pathways for C—H oxidative addition of benzene along the triplet energy surface were investigated for the three tantalocene monohydride complexes **2**, **16**, and **17**, generated by reductive elimination of H_2 from **1**, **8**, and **9**, respectively (Figure S6). Each of these Ta(III) complexes is predicted to be more stable in the triplet spin state compared to singlet. Interestingly, the triplet-singlet energy gap is predicted to be largest for the permethylated complex (compare ^{1}**17** and ^{3}**17**, red pathway in Figure S6). Attempted geometry optimizations of S=1 π-complexes (high spin versions of **3**, **18**, and **19**) resulted in dissociation of benzene, indicating that such complexes are unstable as triplets. This observation is consistent with the Dewar-Chatt model for bonding in the benzene π-complexes (inset in Figure S6); this model gives tantalum a formal oxidation state of +5 (zero *d*-electrons), which precludes localization of spin density on the metal.

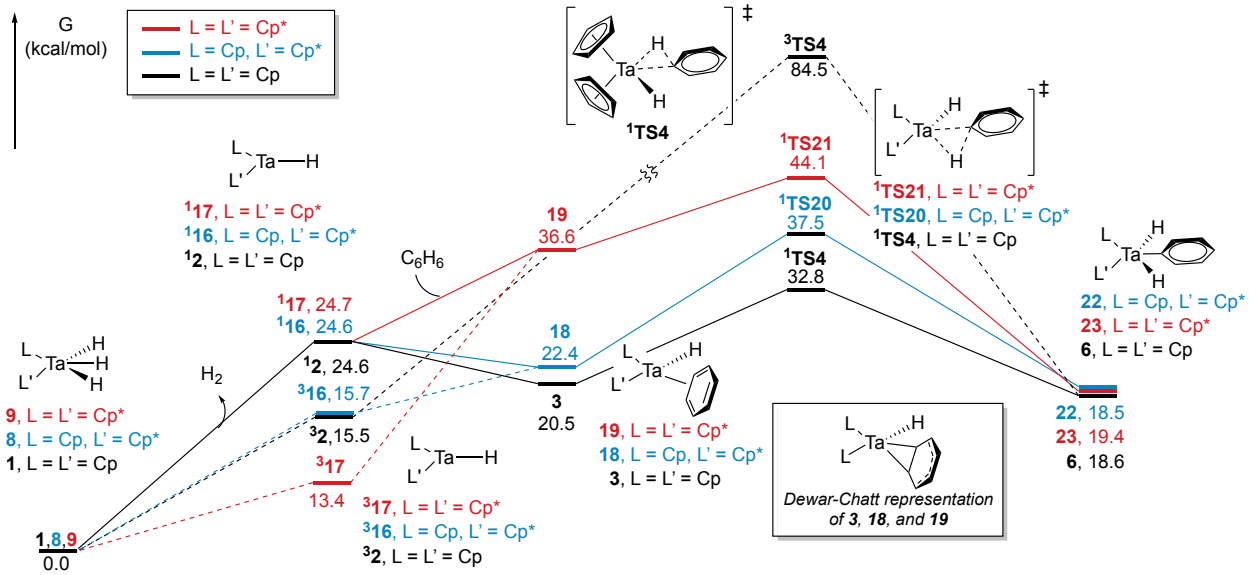


Figure S6. Comparison of oxidative addition reaction pathways found for C—H activation of benzene starting from L_2TaH_3 (L = Cp, Cp*). Calculated using CPCM(benzene)-M06/6-311++G(2d,p)/SDD(Ta)//M06L/6-31G+(d,p)/LANL2DZ(Ta).

The calculated geometries of the π-complexes are consistent with the Dewar-Chatt model. For example, the benzene C—C bond distance elongates from 1.39 Å (unbound benzene) to 1.46 Å in **3** (Figure S7). Furthermore, the carbons that are bound to tantalum appear to have sp^3-character: this is illustrated by the H—$C_{(1)}$---$C_{(4)}$ angle of 30.4°, showing that hydrogen is bent significantly out of plane of the ring. Oxidative addition of benzene along the triplet surface to place carbon at the internal position of the unmethylated complex (^{3}**TS4**) is predicted to proceed through an energy barrier of 84.5 kcal/mol relative to **1**. This barrier is 51.7 kcal/mol higher in energy than its low spin counterpart ^{1}**TS4**. An attempt to locate a S=1 oxidative addition transition state that positions carbon at the lateral position of the unmethylated complex led to a transition structure for a σ-bond metathesis mechanism for C—H activation (see section G below). High-

spin oxidative addition transition states for the penta- and decamethylated complexes did not converge during geometry optimization calculations.

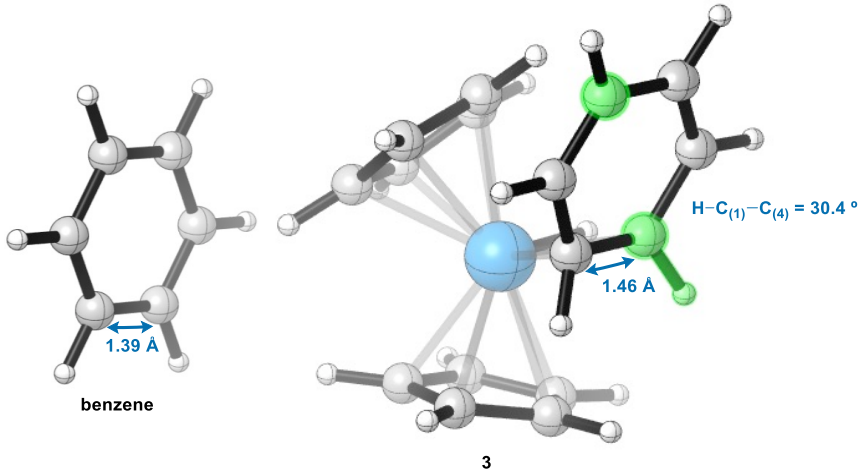


Figure S7. Optimized geometries of benzene and π-complex **3**. Complex **3** is best represented by the Dewar-Chatt model based on an elongated C—C bond as well as hydrogens that are bent out of the plane of the ring. Calculated using M06L/6-31+G(d,p)/LANL2DZ(Ta).

G. σ-Bond Metathesis Mechanism for Benzene Activation

4-Centered σ-bond metathesis transition structures for benzene activation were located along both the singlet and triplet energy surfaces starting from Cp_2TaH_3 (**1**). However, the calculated energy barriers are too high for σ-bond metathesis to be considered a significant pathway for arene activation (Figure S8). Transition structures for σ-bond metathesis at **1** along the singlet energy surface (**^{1}STS24** and **^{1}STS25**) are 32.3-33.9 kcal/mol higher in energy than the oxidative addition transition structure **^{1}TS4**. A high-spin σ-bond metathesis transition structure **^{3}STS25** was located, but it is 78.7 kcal/mol higher in energy than **^{1}TS4**. A high-spin analog to **STS24** was also located; however, we were unable to confirm that it connects Cp_2TaH_3 and $Cp_2TaH(Ph)$ via IRC calculations. A hapticity change from η^5 to η^2 in one of the cyclopentadienyl rings is observed in both **^{1}STS25** and **^{3}STS25**. IRC calculations starting from these two transition structures led to a high energy intermediate immediately following σ-bond metathesis, involving σ-complexation to dihydrogen and with retention of the η^2 bonding character for one of the Cp rings (not shown). As such, arriving at the C—H activation product **6** requires a hapticity change back to η^5 and dissociation of the newly formed dihydrogen. However, we did not pursue a complete mapping of these steps because of the prohibitively high energies of the σ-bond metathesis transition structures. Interestingly, a 4-centered transition structure resembling σ-bond metathesis (**^{3}STS26**) was also found on the triplet energy surface starting from the d^2 monohydride Cp_2TaH. The open shell d^2 product **^{3}S27** of this activation pathway is predicted to be lower in energy then its low spin **^{1}S27** counterpart by 8.9 kcal/mol. However, this pathway is also likely insignificant due to the high energy of **^{3}STS26**.

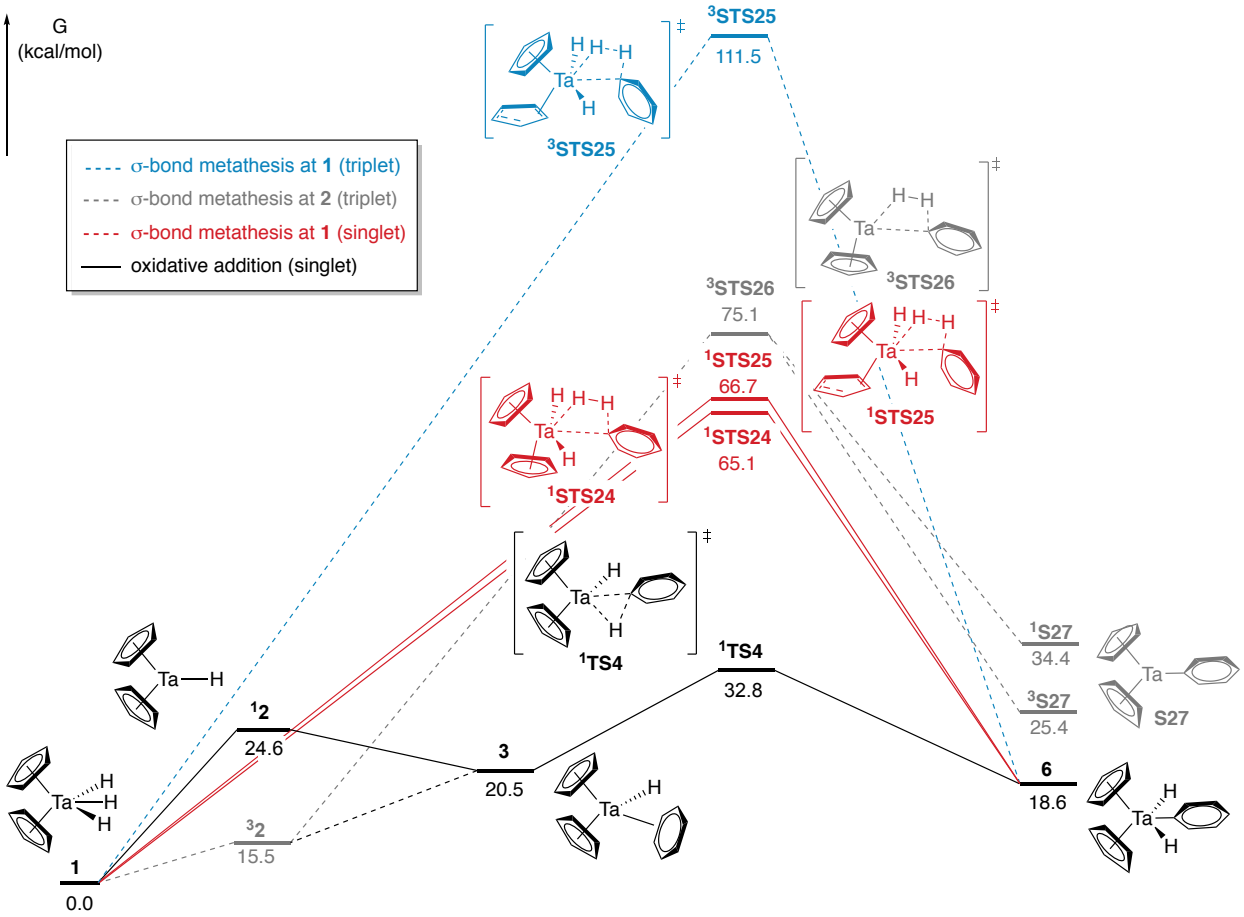


Figure S8. Reaction pathways found for benzene activation via σ-bond metathesis pathways (blue, gray, and red lines) compared to oxidative addition (black lines). Location of additional intermediates along the pathways involving **¹STS25** and **³STS25** was not pursued. Calculated using CPCM(benzene)-M06/6-311++G(2d,p)/SDD(Ta)//M06L/6-31+G(d,p)/LANL2DZ(Ta).

H. Additional Pathway for Benzylic C—H Activation of Toluene

Alternative pathways for C—H activation of toluene at the benzylic position were evaluated by DFT (Figure S9). On the singlet energy surface, oxidative addition to place carbon at the lateral position is predicted to be 1.4 kcal/mol higher in energy than oxidative addition to place carbon at the internal position (compare **¹STS28** and **¹TS12**). The resulting product with carbon at the lateral position (**S29**) is predicted to be slightly less stable than **15** by about 1.2 kcal/mol. Although a transition state for high spin oxidative addition at the internal position could not be located, a structure could be found for oxidative addition at the lateral position along the triplet spin surface (**³STS28**). However, the energy barrier is about 4.3 kcal/mol higher than **¹TS12**.

Two transition structures for benzylic C—H activation by a σ-bond metathesis mechanism were located along the singlet surface. These two pathways are predicted to be 33.1 kcal/mol and 34.7 kcal/mol higher in energy than low spin oxidative addition (compare **¹STS30** and **¹STS31** to **¹TS12**). The geometry of

^{1}STS31 displays a hapticity shift from η^5 to η^2 for one of the cyclopentadienyl ligands. IRC calculations starting from **^{1}STS31** led to a high energy intermediate immediately following σ-bond metathesis, involving σ-complexation to dihydrogen and with retention of the η^2 bonding character for one of the Cp rings (not shown). σ-Bond metathesis transition structures along the open shell triplet surface could not be confirmed as valid by IRC calculations. As such, the most likely pathway for C—H activation of the benzylic position of toluene would involve oxidative addition at the internal position along the closed shell, singlet surface due to the comparatively low activation barrier.

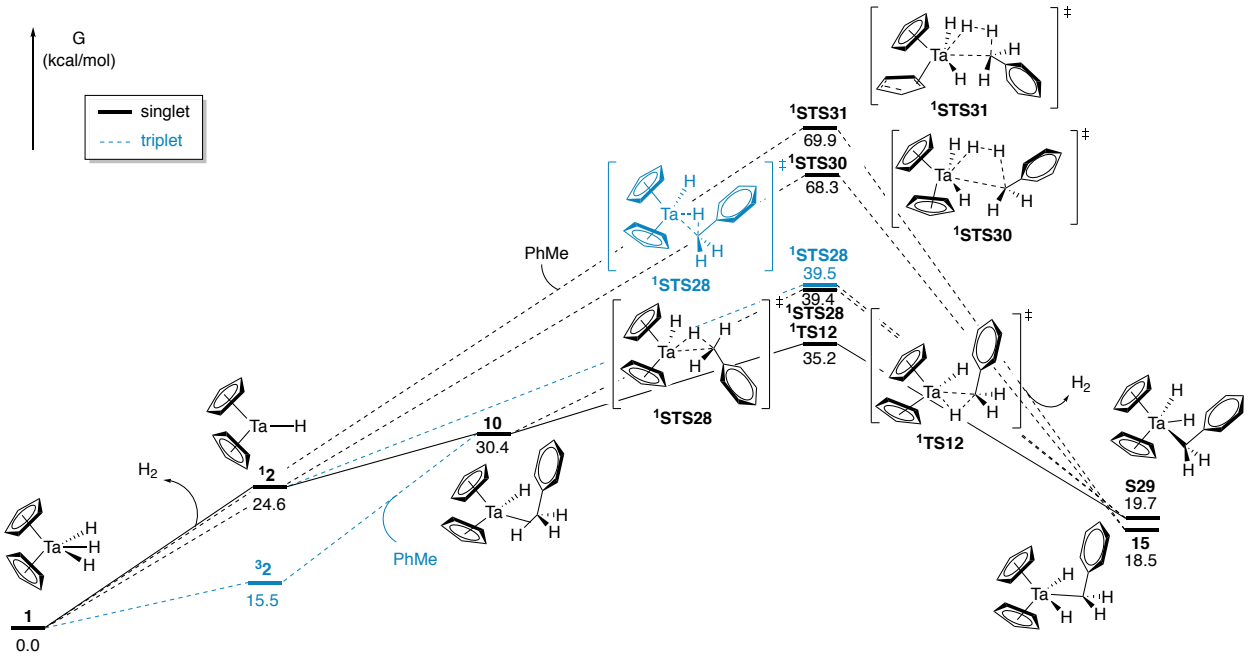


Figure S9. Reaction pathways found for benzylic activation of toluene via oxidative addition and σ-bond metathesis. Calculated using CPCM(benzene)-M06/6-311++G(2d,p)/SDD(Ta)//M06L/6-31+G(d,p)/LANL2DZ(Ta).

III. References

1. M06L: Zhao, Y.; Truhlar, D. G. A new local density functional for main-group thermochemistry, transition metal bonding, thermochemical kinetics, and noncovalent interactions. *J. Chem. Phys.,* **2006**, *125*, 194101.
2. M06: Zhao, Y.;Truhlar, D. G. The M06 suite of density functionals for main group thermochemistry, thermochemical kinetics, noncovalent interactions, excited states, and transition elements: two new functionals and systematic testing of four M06-class functionals and 12 other functionals. *Theor. Chem. Acc.,* **2008**, *120*, 215.
3. MN15: Yu, H. S.; He, X.; Li, S. L.; Truhlar, D. G. MN15: A Kohn–Sham global-hybrid exchange–correlation density functional with broad accuracy for multi-reference and single-reference systems and noncovalent interactions. *Chem. Sci.,* **2016**, *7*, 5032.
4. MN15L: Yu, H. S.; He, X.; Truhlar, D. G. MN15-L: A New Local Exchange-Correlation Functional for Kohn–Sham Density Functional Theory with Broad Accuracy for Atoms, Molecules, and Solids. *J. Chem. Theory Comput.* **2016**, *12*, 1280.
5. wB97XD: Chai, J. D.; Head-Gordon, M. Long-range corrected hybrid density functionals with damped atom–atom dispersion corrections. *Phys. Chem. Chem. Phys.*, **2008**, *10*, 6615.
6. B3LYP and BHLYP: (a) Becke, A. D. Density-functional exchange-energy approximation with correct asymptotic behavior. *Phys. Rev. A* **1998**, *38*, 3098. (b) Becke, A. D. Density-functional thermochemistry. III. The role of exact exchange. *J. Chem. Phys.* **1993**, *98*, 5648. (c) Becke, A. D. A new mixing of Hartree–Fock and local density-functional theories. *J. Chem. Phys.* **1993**, *98*, 1372.
7. B2PLYP: Grimme, S. Semiempirical hybrid density functional with perturbative second-order correlation *J. Chem. Phys.,* **2006**, *124,* 034108.
8. Dispersion: Grimme, S.; Antony, J.; Ehrlich, S.; Krieg, H. A consistent and accurate ab initio parameterization of density functional dispersion correction (DFT-D) for the 94 elements. H-Pu, *J. Chem. Phys.,* **2010**, *132*, 154104.
9. TPSSh: (a) Tao, J. M.; Perdew, J. P.; Staroverov, V. N.; Scuseria, G. E. Climbing the density functional ladder: Nonempirical meta-generalized gradient approximation designed for molecules and solids *Phys. Rev. Lett.,* **2003**, *91,* 146401. (b) Staroverov, V. N.; Scuseria, G. E.; Tao, J.; Perdew, J. P. Comparative assessment of a new nonempirical density functional: Molecules and hydrogen-bonded complexes *J. Chem. Phys.,* **2003***, 119,* 12129.
10. Pasha, F. A.; Cavallo, L.; Basset, J.-M. Mechanism of *n*-Butane Hydrogenolysis Promoted by Ta-Hydrides Supported on Silica. *ACS Catal.* **2014**, *4*, 1868.

11. See also Brookes, N. J.; Ariafard, A.; Stranger, R.; Yates, B. F., Scission of Carbon Monoxide Using TaR_3, R = (N(tBu)Ph) or $OSi(tBu)_3$): A DFT Investigation. *Chem. Eur. J.* **2010**, *16*, 8117.

12. (a) Solans-Monfort, X.; Chow, C.; Gouré, E.; Kaya, Y.; Basset, J. M.; Taoufik, M.; Alessandra Quadrelli, E.A.; Eisenstein, O. Successive Heterolytic Cleavages of H_2 Achieve N_2 Splitting on Silica-Supported Tantalum Hydrides: A DFT Proposed Mechanism. *Inorg. Chem.* **2012**, *51*, 7237. (b) Lin, X.; Xi, Y.; Zhang, G.; Phillips, D.L.; Guo, W. A Reaction Mechanism of Methane Coupling on a Silica-Supported Single-Site Tantalum Catalyst. *Organometallics* **2014**, *33*, 2172; (c) Nunez-Zarur, F.; Solans-Monfort, X.; Restrepo, A., Mechanistic Insights into Alkane Metathesis Catalyzed by Silica-Supported Tantalum Hydrides: A DFT Study. *Inorg. Chem.* **2017**, *56*, 10458.

13. B3PW91: Becke, A. D. Density-functional thermochemistry. III. The role of exact exchange. *J. Chem. Phys.* **1993**, *98*, 5648.

14. BP86: Perdew, J. P. Density-functional approximation for the correlation energy of the inhomogeneous electron gas. *Phys. Rev. B* **1986**, *33*, 8822.

15. TZVP: (a) Schafer, A.; Horn, H.; Ahlrichs, R. Fully optimized contracted Gaussian basis sets for atoms Li to Kr. *J. Chem. Phys.* **1992**, *97*, 2571. (b) Schafer, A.; Huber, C.; Ahlrichs, R. Fully optimized contracted Gaussian basis sets of triple zeta valence quality for atoms Li to Kr. *J. Chem. Phys.* **1994**, *100*, 5829.

16. SDD: Haussermann, U.; Dolg, M.; Stoll, H.; Preuss, H.; Schwerdtfeger, P.; Pitzer, R. M. Accuracy of energy-adjusted quasirelativistic *ab initio* pseudopotentials. *Mol. Phys.* **1993**, *78,* 1211.

17. (a) Handy, N. C.; Cohen, A. J. Left-right correlation energy. *Mol. Phys.,* **2001**, *99*, 403. (b) Hoe, W.-M.; Cohen, A.; Handy, N. C. Assessment of a new local exchange functional OPTX. *Chem. Phys. Lett.,* **2001,** *341*, 319. (c) Perdew, J. P.; Burke, K.; Ernzerhof, M. Generalized gradient approximation made simple. *Phys. Rev. Lett.,* **1996**, *77*, 3865. (d) Perdew, J. P.; Burke, K.; Ernzerhof, M. Errata: Generalized gradient approximation made simple. *Phys. Rev. Lett.*, **1997**, *78*, 1396.

IV. NMR Spectra

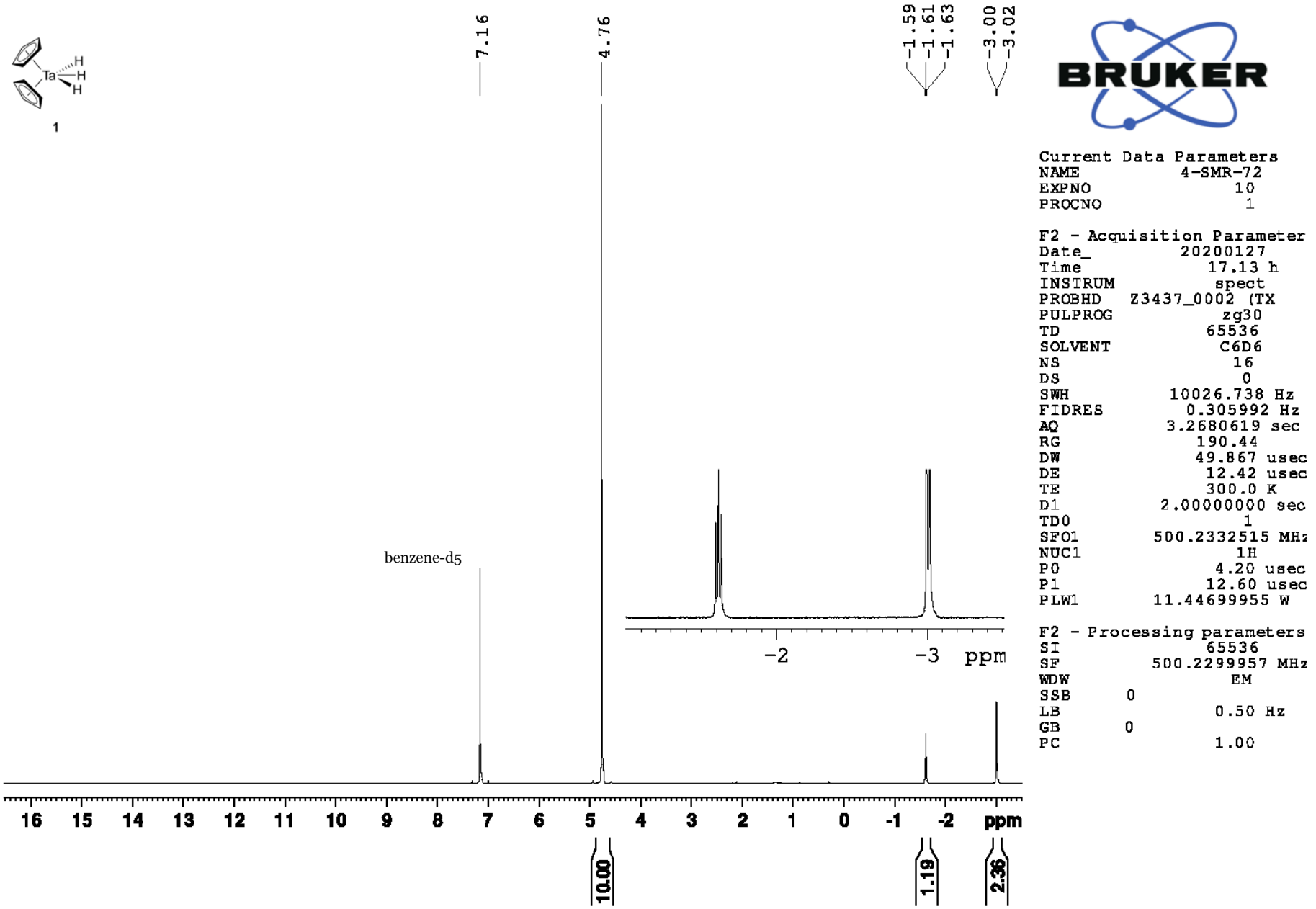
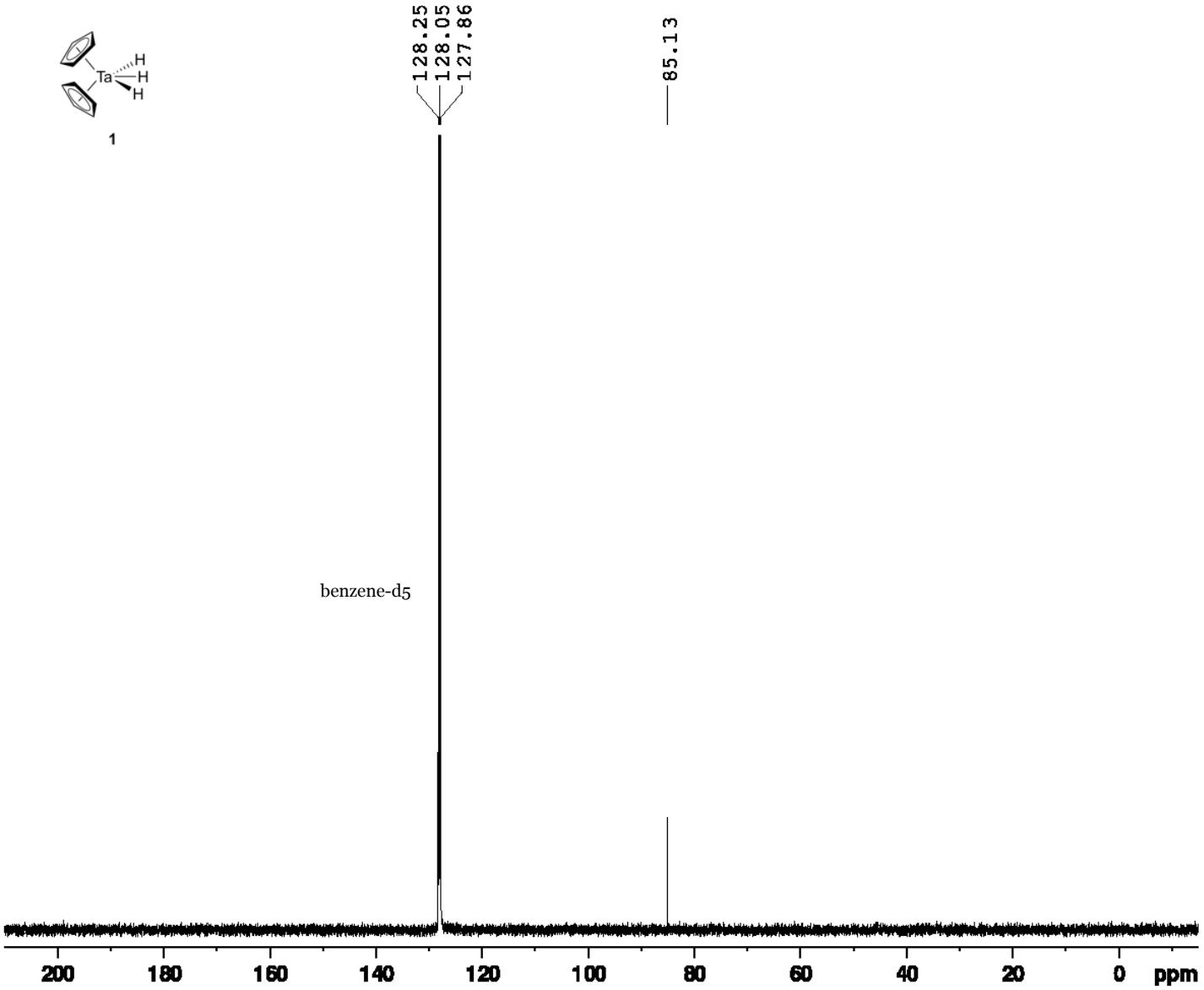


Figure S10. 1H NMR spectrum of compound 1. Inset: Magnification of the hydride region.




```
Current Data Parameters
NAME            4-SMR-72
EXPNO                 11
PROCNO                 1

F2 - Acquisition Parameter
Date_           20200127
Time              17.20 h
INSTRUM             spect
PROBHD    Z3437_0002 (TX
PULPROG           zgpg30
TD                65536
SOLVENT             C6D6
NS                  100
DS                    4
SWH           29761.904 Hz
FIDRES         0.908261 Hz
AQ            1.1010048 sec
RG                190.44
DW              16.800 usec
DE               6.50 usec
TE              300.0 K
D1           2.00000000 sec
D11          0.03000000 sec
TD0                   1
SFO1         125.7955118 MHz
NUC1                13C
P0                4.17 usec
P1               12.50 usec
PLW1         56.90299988 W
SFO2         500.2320009 MHz
NUC2                1H
CPDPRG[2         waltz65
PCPD2             80.00 usec
PLW2          0.25000000 W
PLW12         0.25000000 W
PLW13         0.12575001 W

F2 - Processing parameters
SI                 32768
SF           125.7828851 MHz
WDW                  EM
SSB       0
LB                1.00 Hz
GB        0
PC                1.40
```

Figure S11. 13C NMR spectrum of compound 1.

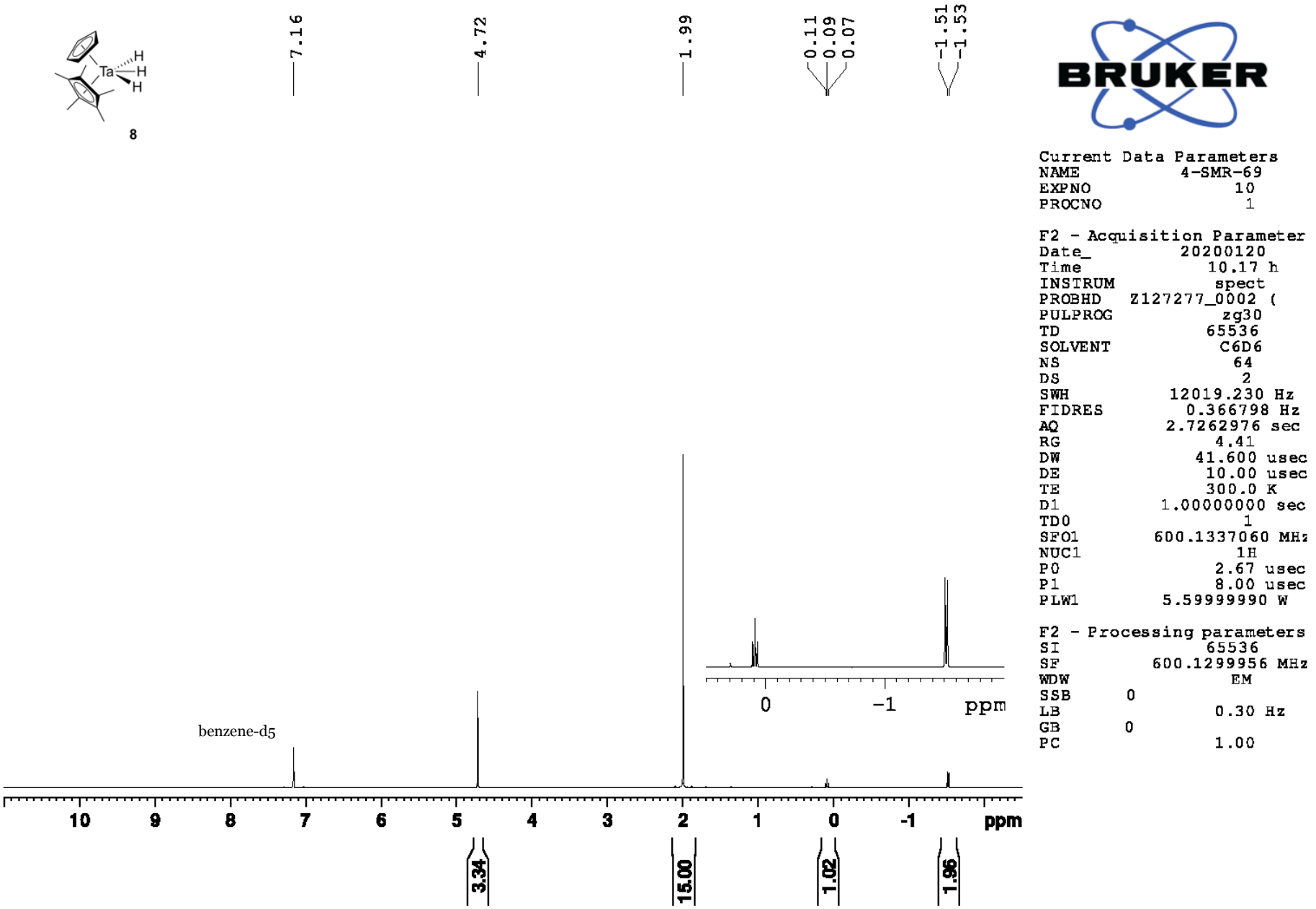
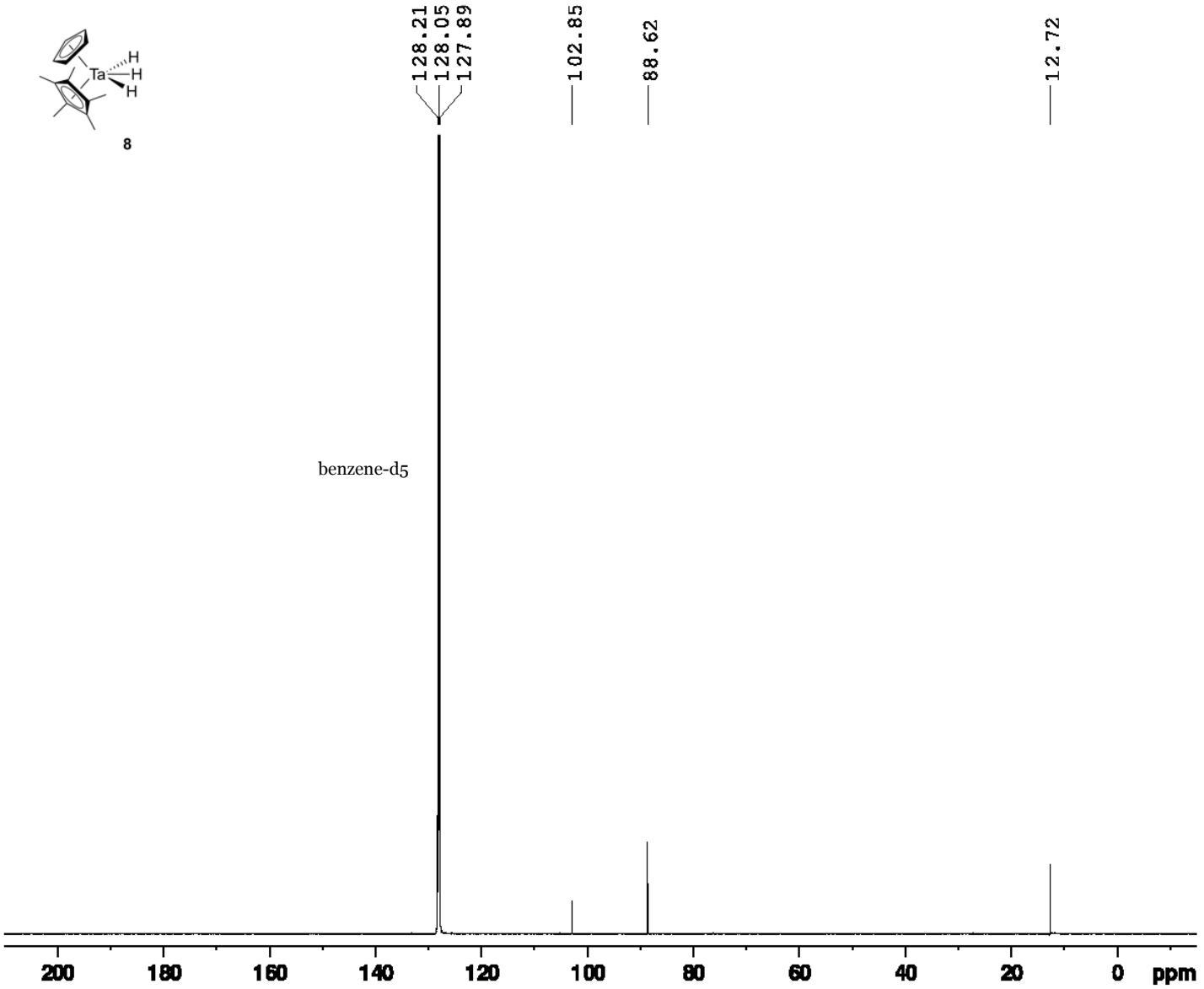


Figure S12. 1H NMR spectrum of compound 8. Inset: Magnification of the hydride region.



BRUKER

```
Current Data Parameters
NAME            4-SMR-69
EXPNO                 11
PROCNO                 1

F2 - Acquisition Parameter
Date_           20200120
Time              11.13 h
INSTRUM             spect
PROBHD    Z127277_0002 (
PULPROG           zgpg30
TD                65536
SOLVENT             C6D6
NS                  1024
DS                     4
SWH           36057.691 Hz
FIDRES         1.100393 Hz
AQ            0.9087659 sec
RG                 184.4
DW               13.867 usec
DE                18.00 usec
TE                300.0 K
D1           2.00000000 sec
D11          0.03000000 sec
TD0                    1
SFO1        150.9178981 MHz
NUC1                13C
P0                 4.00 usec
P1                12.00 usec
PLW1        91.00000000 W
SFO2        600.1324005 MHz
NUC2                1H
CPDPRG[2        waltz16
PCPD2            70.00 usec
PLW2         5.59999990 W
PLW12        0.07314300 W
PLW13        0.03679000 W

F2 - Processing parameters
SI                 32768
SF          150.9027528 MHz
WDW                   EM
SSB       0
LB                 1.00 Hz
GB        0
PC                 1.40
```

Figure S13. 13C NMR spectrum of compound 8.

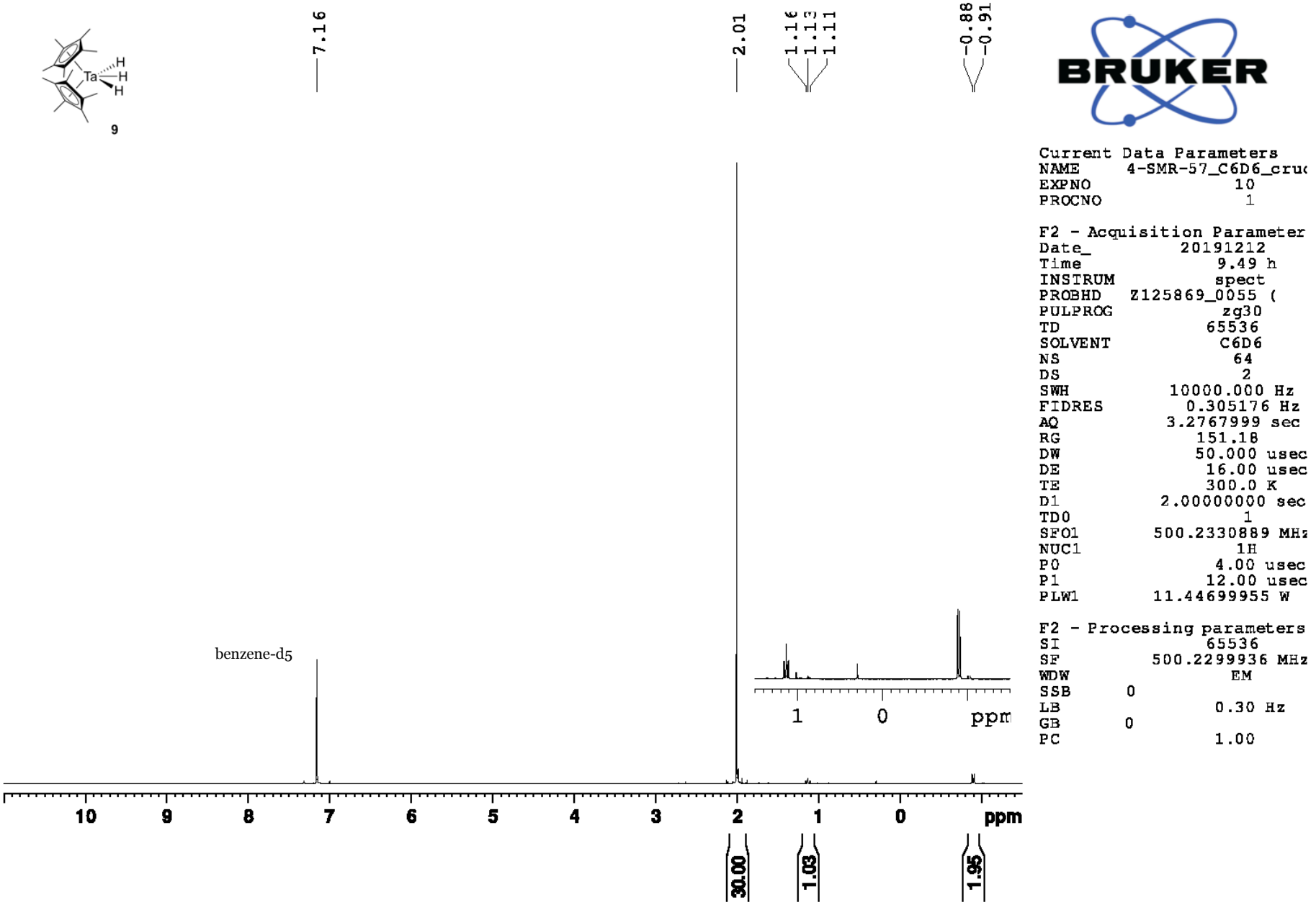
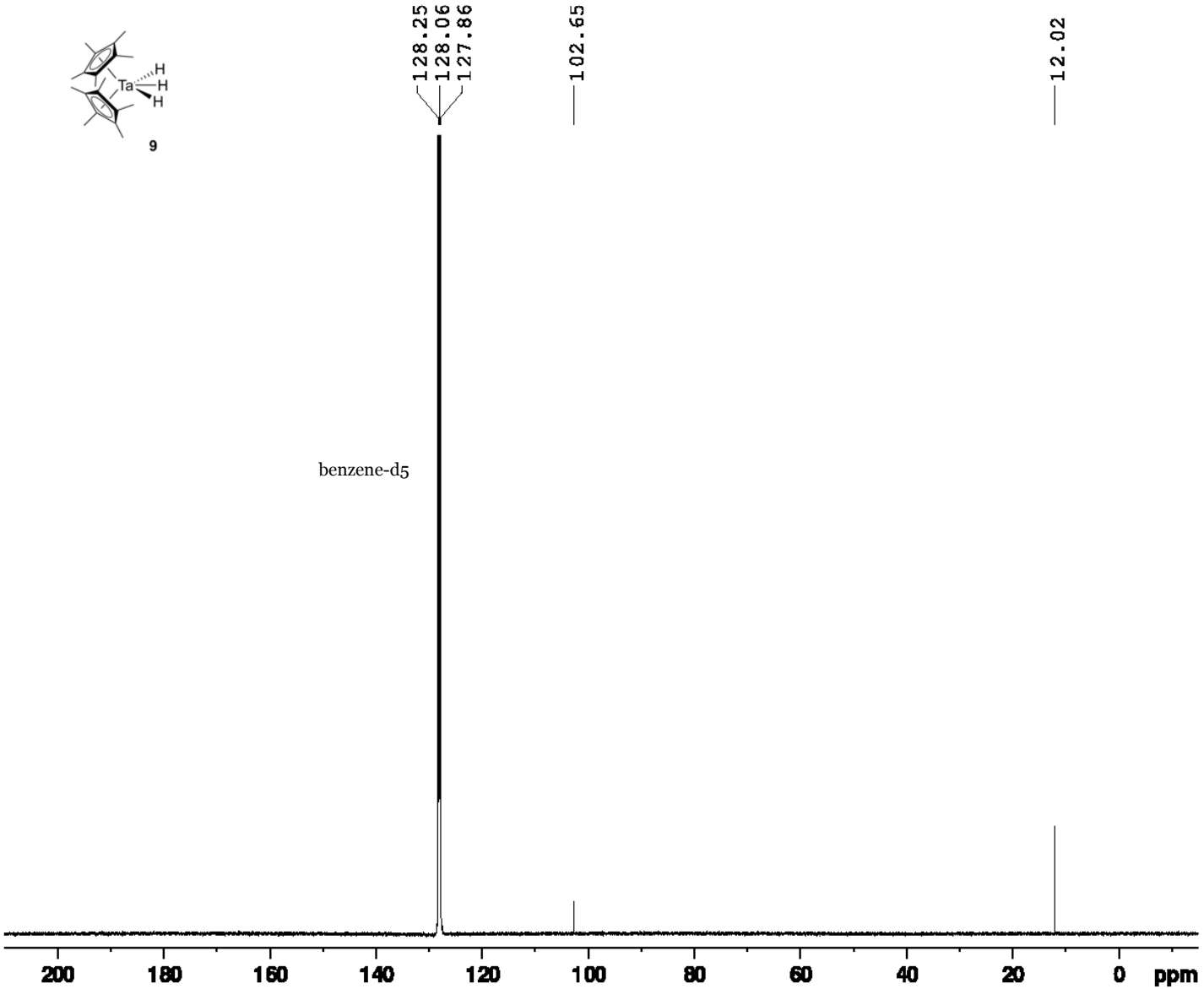


Figure S14. 1H NMR spectrum of compound 9. Inset: Magnification of the hydride region.





```
Current Data Parameters
NAME      4-SMR-57_C6D6_cru
EXPNO                    11
PROCNO                    1

F2 - Acquisition Parameter
Date_              20191212
Time                 19.48 h
INSTRUM                spect
PROBHD    Z125869_0055 (
PULPROG              zgpg30
TD                    65536
SOLVENT                C6D6
NS                     1024
DS                        4
SWH              29761.904 Hz
FIDRES            0.908261 Hz
AQ               1.1010048 sec
RG                   190.44
DW                 16.800 usec
DE                 18.00 usec
TE                 300.0 K
D1              2.00000000 sec
D11             0.03000000 sec
TD0                       1
SFO1           125.7955118 MHz
NUC1                    13C
P0                  3.33 usec
P1                 10.00 usec
PLW1           56.90299988 W
SFO2           500.2320009 MHz
NUC2                    1H
CPDPRG[2           waltz16
PCPD2               80.00 usec
PLW2           11.44699955 W
PLW12           0.25756001 W
PLW13           0.12955000 W

F2 - Processing parameters
SI                    32768
SF           125.7828852 MHz
WDW                      EM
SSB          0
LB                    1.00 Hz
GB           0
PC                    1.40
```

Figure S15. 13C NMR spectrum of compound 9.

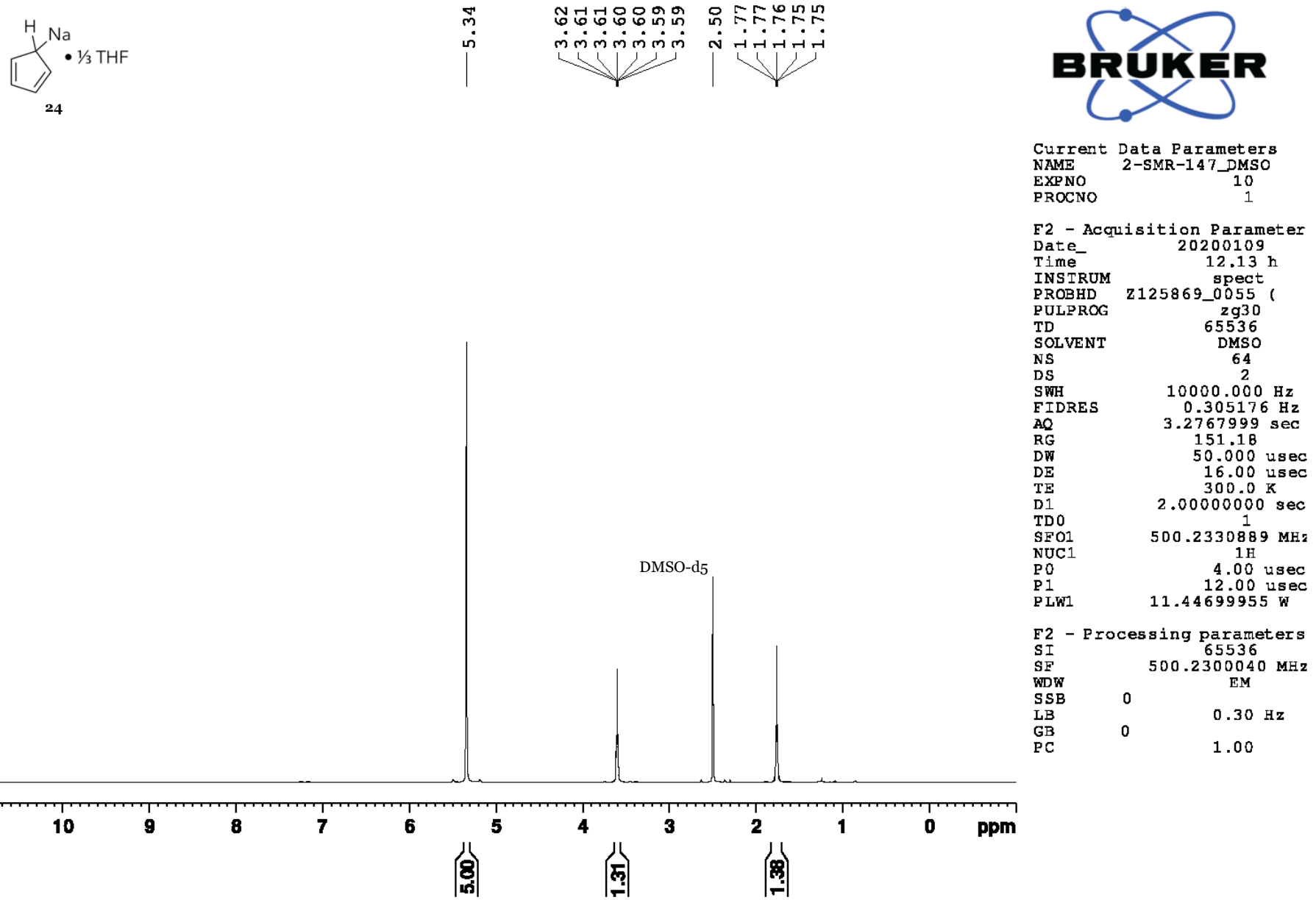


Figure S16. 1H NMR spectrum of compound 24.

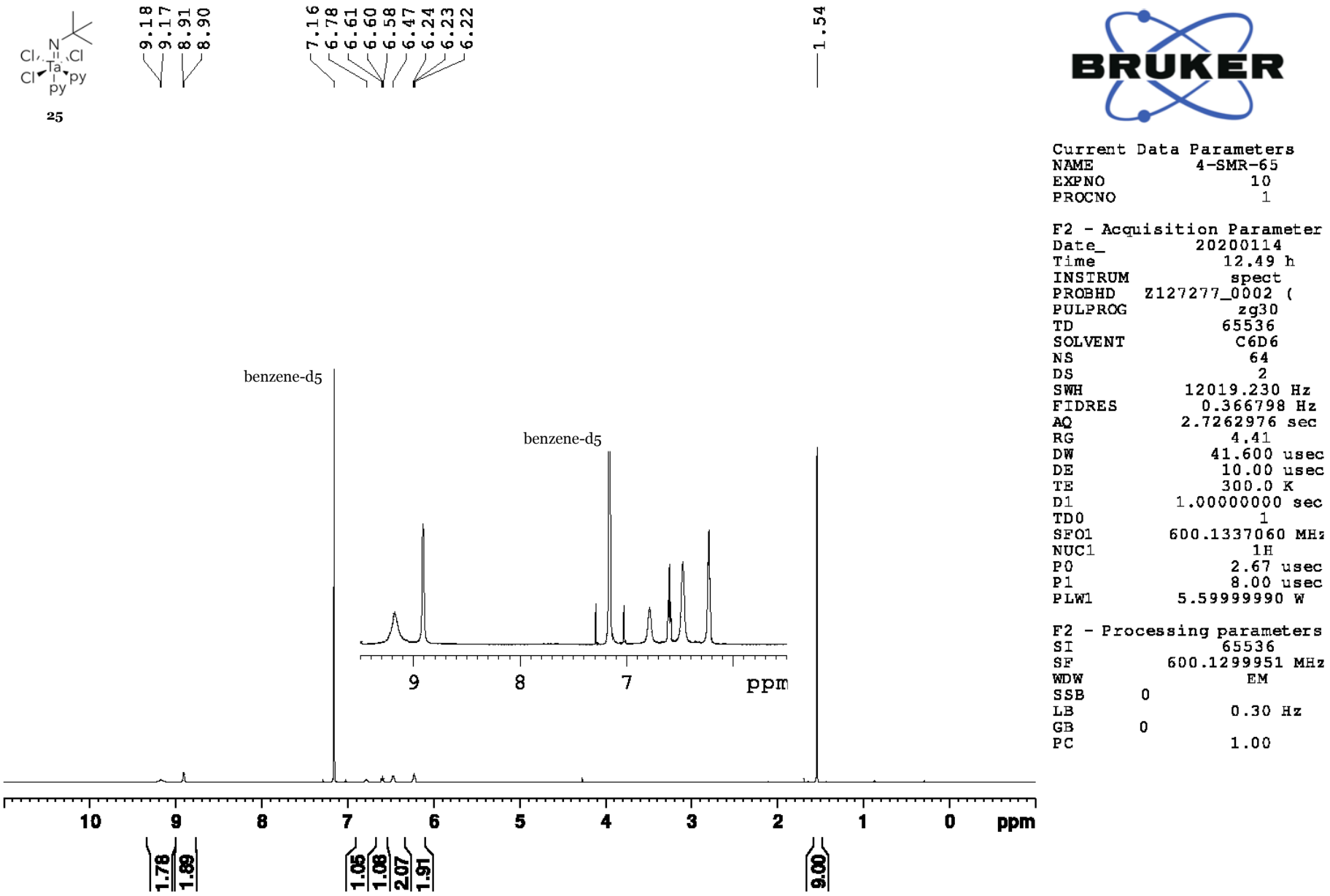


Figure S17. 1H NMR spectrum of compound 25.

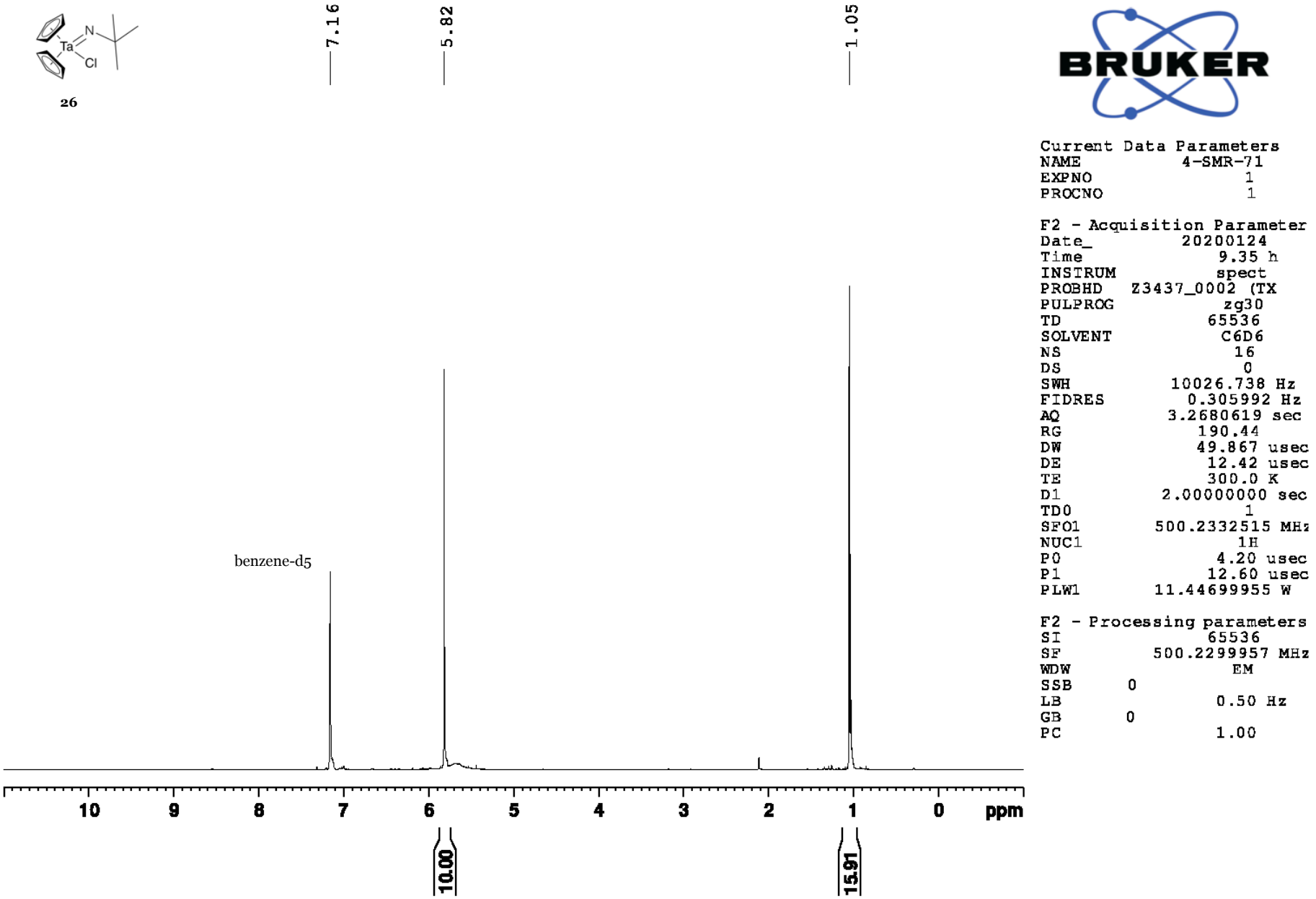


Figure S18. 1H NMR spectrum of compound 26.

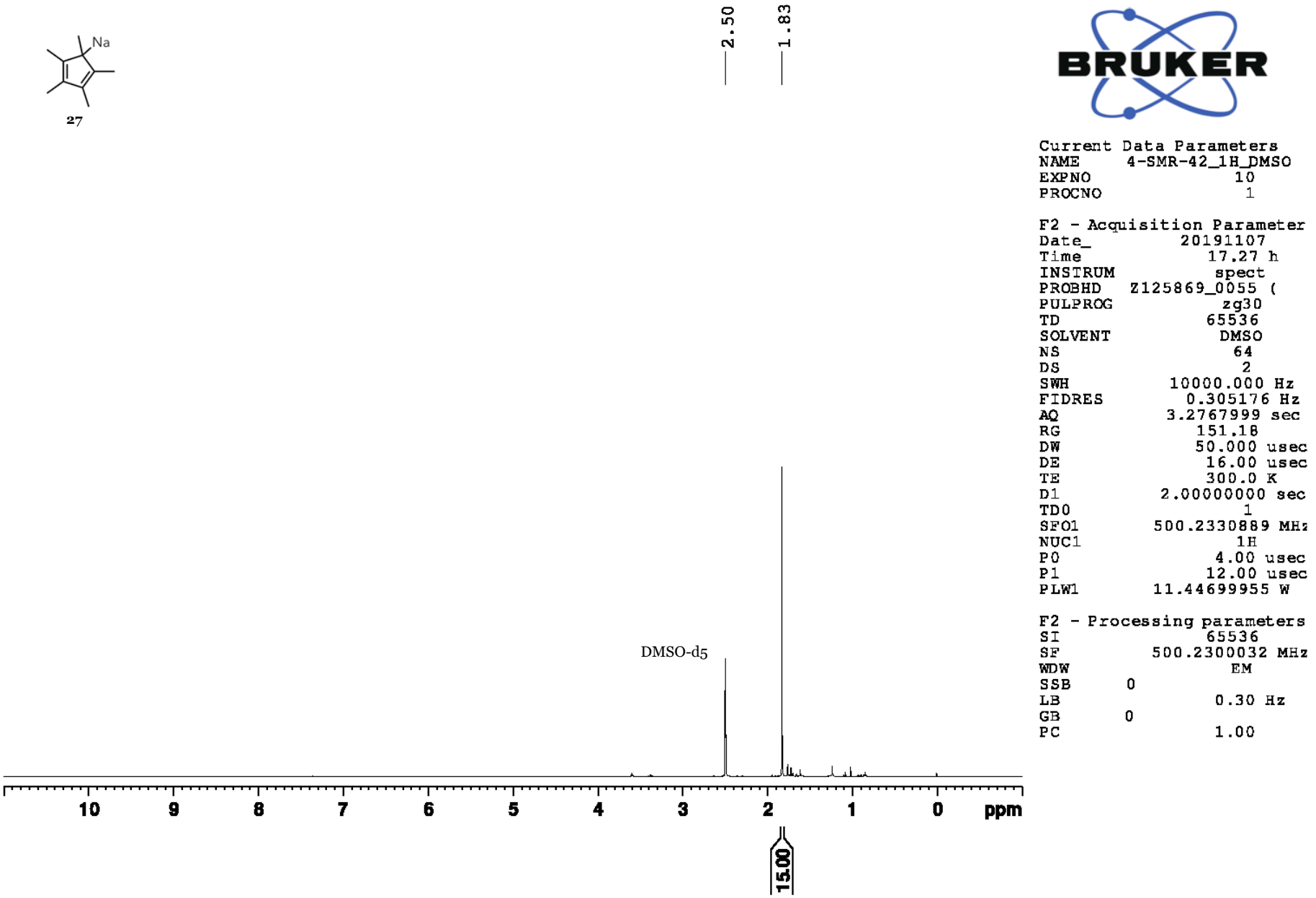


Figure S19. 1H NMR spectrum of compound 27.

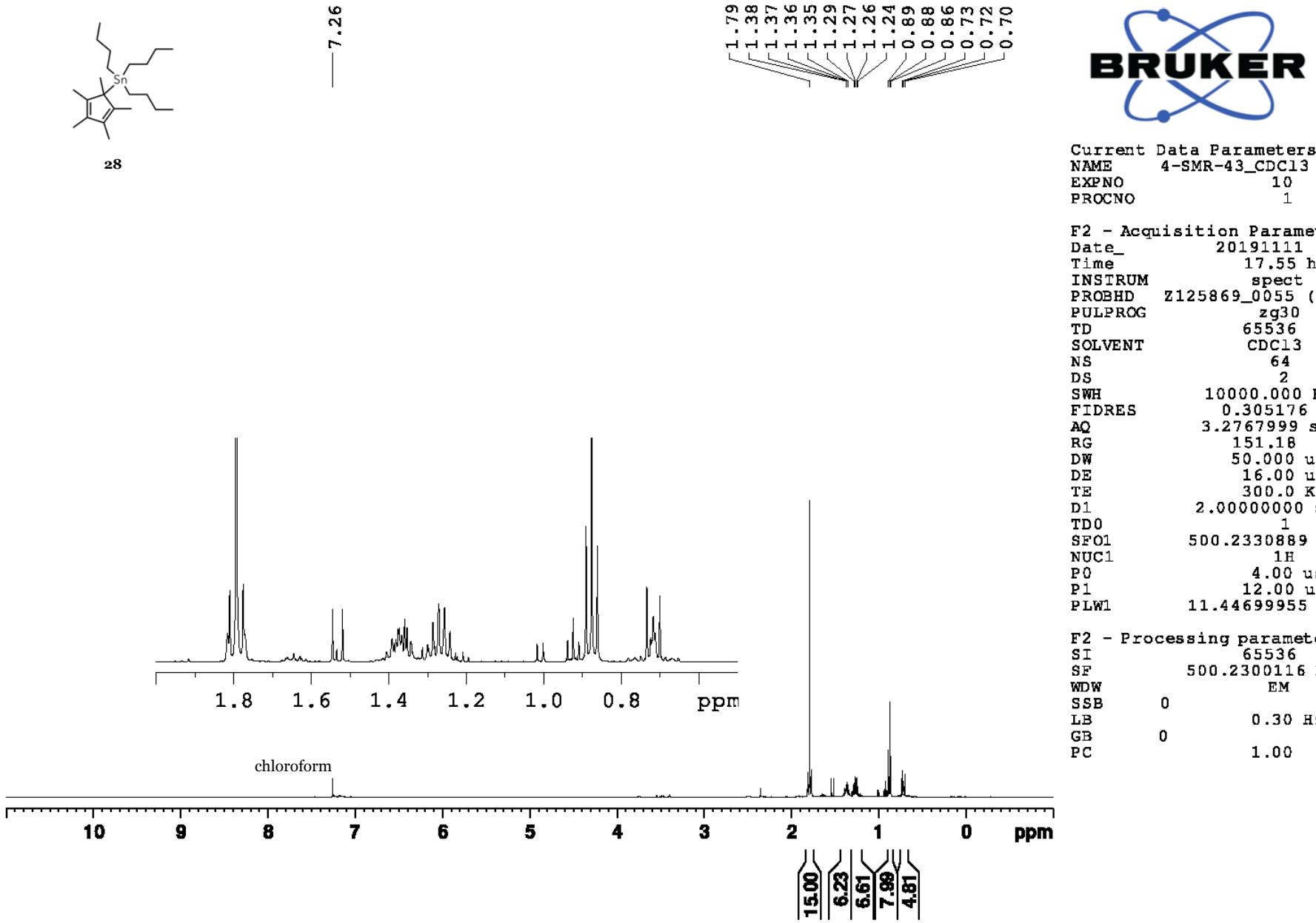


Figure S20. 1H NMR spectrum of compound 28.

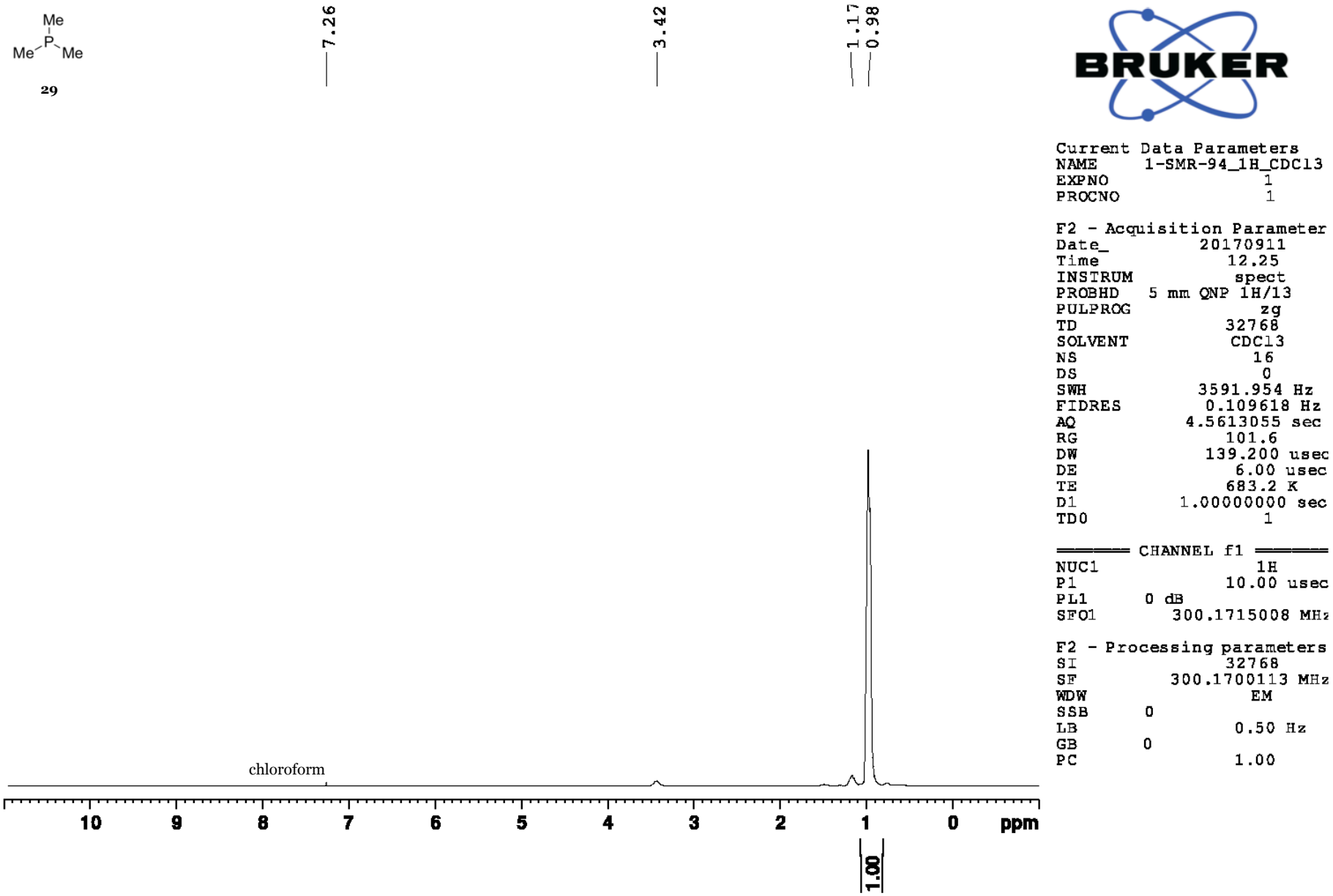


Figure S21. 1H NMR spectrum of compound 29.

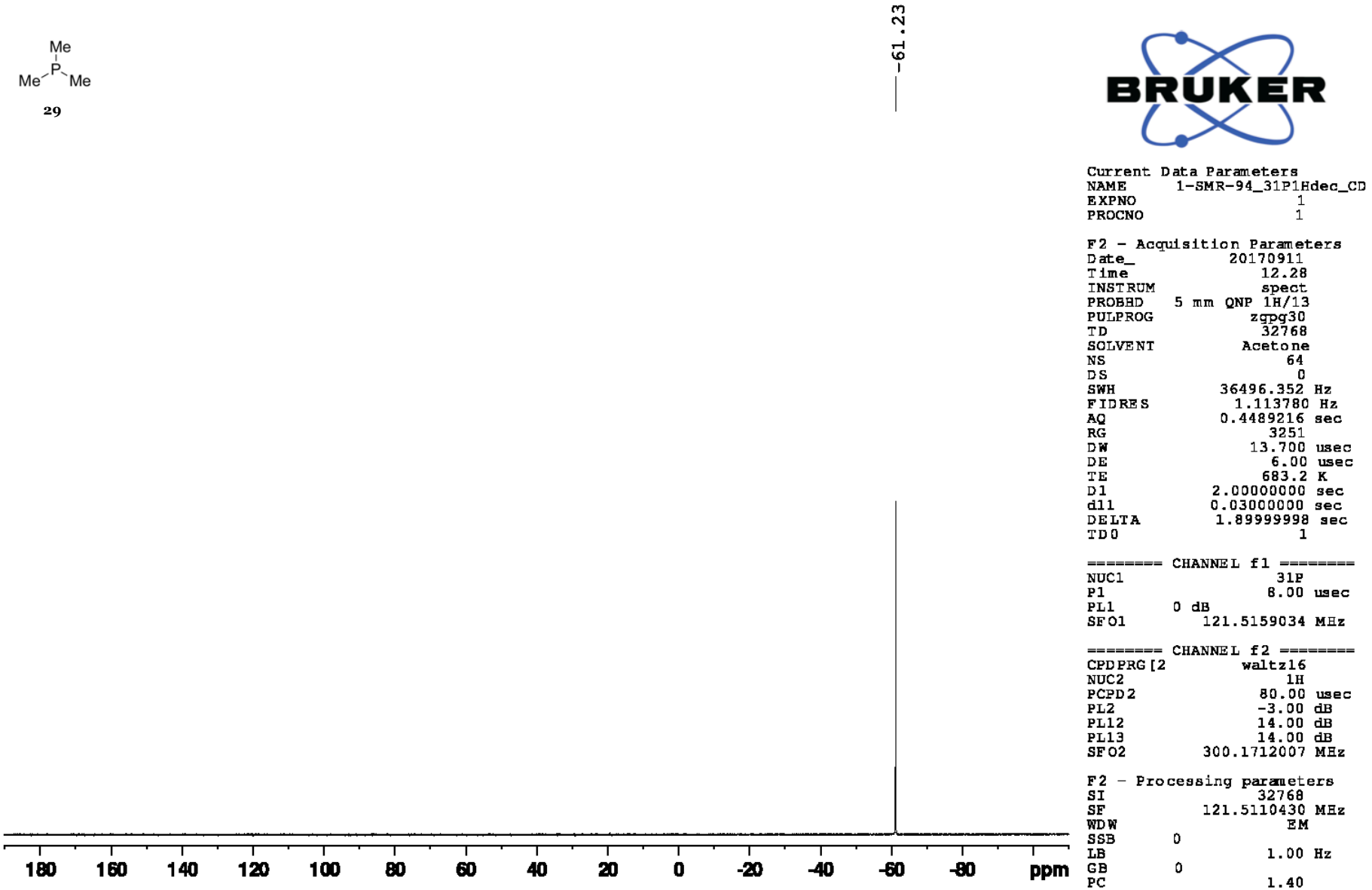


Figure S22. 31 P NMR spectrum of compound 29.

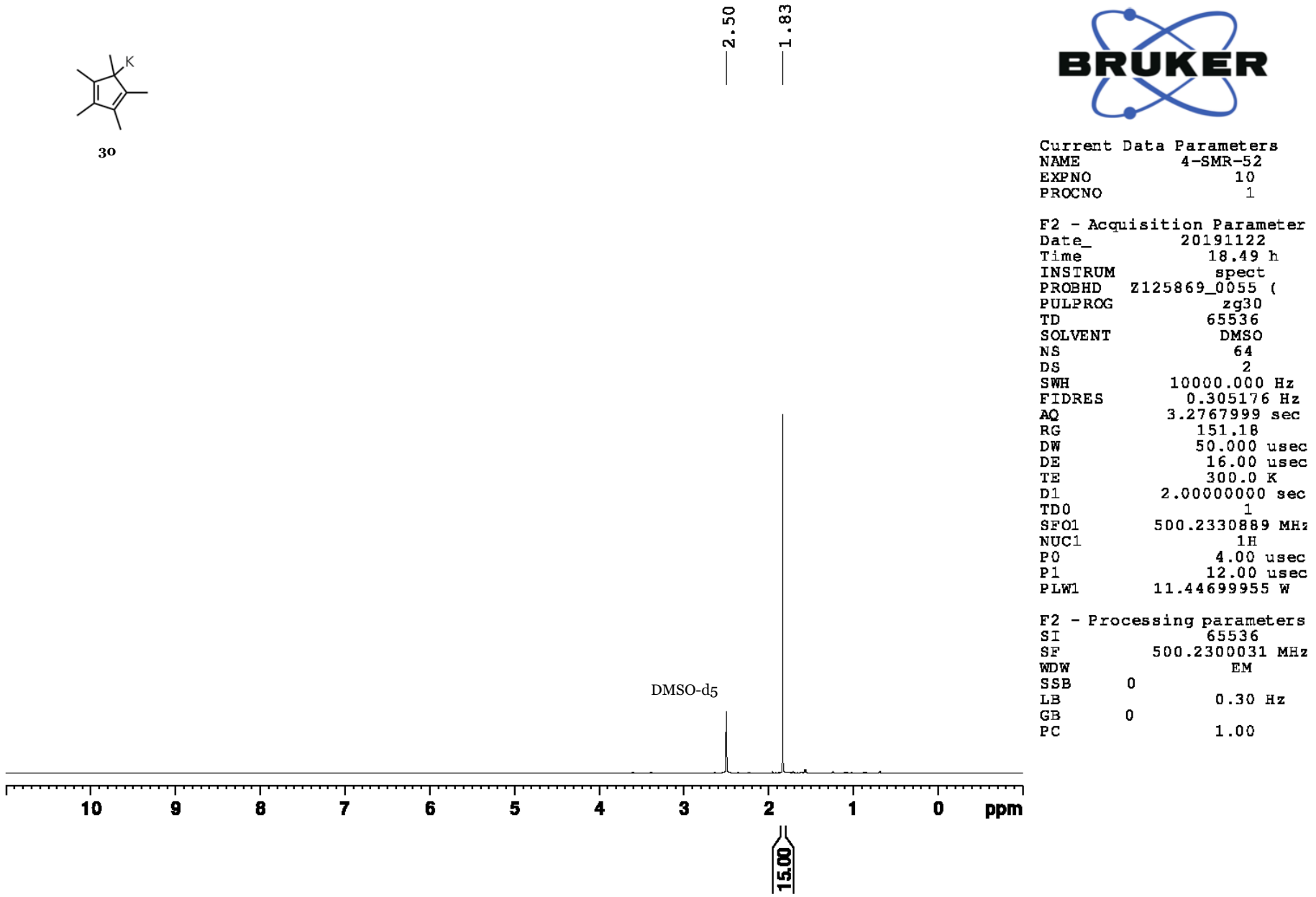


Figure S23. 1H NMR spectrum of compound 30.

APPENDIX B

CHAPTER FOUR SUPPLEMENTAL

Supporting Information

for

Solvent Coordination to Palladium Can Invert the Selectivity of Oxidative Addition

*Emily K. Elias, Steven M. Rehbein, Sharon R. Neufeldt**

Department of Chemistry and Biochemistry, Montana State University
Bozeman, MT 59717, USA

**Correspondence: sharon.neufeldt@montana.edu*

Table of Contents

I. Experimental Details
- **A.** General Materials and Methods S4
- **B.** Synthesis and Characterization of Substrates and Authentic Samples of Products S5
- **C.** Catalytic Suzuki Couplings of **1**
  - **1.** Evaluation of Precatalyst and Water Effect on Selectivity S9
  - **2.** Benzonitrile Additives (Table 1 and Figure 1) S11
  - **3.** Mixed THF/Benzonitrile Solvent S14
  - **4.** Results with Fluoroacetonitrile, Sulfolane (Table 2), and Tetrahydrothiophene S16
  - **5.** Effect of Temperature (Table 4) S17
  - **6.** Effect of Additives (Table 6) S20
  - **7.** Recycling "Decomposed" Catalyst S21
- **D.** Reactions with **3a** and **3b**
  - **1.** Catalytic Suzuki Couplings S24
  - **2.** Stoichiometric Oxidative Addition Studies (Table 3)
    - **a.** ^{19}F NMR Calibrations S25
    - **b.** ^{19}F NMR Chemical Shifts S25
    - **c.** Oxidative Addition Reactions S26
- **E.** Reactions with **S15a** and **S15b**
  - **1.** Catalytic Suzuki Couplings S32
  - **2.** Stoichiometric Oxidative Addition Studies
    - **a.** ^{19}F NMR Calibrations S33
    - **b.** ^{19}F NMR Chemical Shifts S33
    - **c.** Oxidative Addition Reactions S33
- **F.** Stille Cross-Couplings
  - **1.** Reactions of **1** (Scheme 3) S35
  - **2.** Reactions of **8** (Table 5) S36
  - **3.** Independent Reactions of an Aryl Chloride and an Aryl Triflate S37
  - **4.** Efforts to Reproduce Literature Results for the Base-Free Stille Coupling of **1** S39
- **G.** Evaluation of Alternative Hypotheses
  - **1.** Alternative Hypothesis: Is Solvent Effect Related to KF Solubility? S41
  - **2.** Alternative Hypothesis: Is Oxidative Addition Reversible (Curtin-Hammett)? S43
  - **3.** Alternative Hypothesis: "Greasy Tin Hypothesis" S45
  - **4.** Alternative Hypothesis: Effect of Bu_3SnOTf S46
  - **5.** Alternative Hypothesis: Autocatalysis in Stoichiometric Oxidative Addition? S47
- **H.** Error Analysis S49

II. Computational Details
- **A.** General Methods S51
- **B.** Reaction Free Energy Diagram Using DMF Calculated with B3LYP-D3(BJ) S52
- **C.** DFT Predictions at 100 °C S53
- **D.** Discussion of DFT Shortcomings S53
- **E.** Energies, Entropies, and Lowest Frequencies of Minimum Energy Structures S56

III. References S58

IV. NMR Spectra
- **A.** Compound Characterization S60
- **B.** Stoichiometric Oxidative Addition Studies with **3a** and **3b**
  - **1.** Experiments from Table 3 and with Deuterated Solvents S89
  - **2.** Experiments in DMF at 100 and 0 °C S120
  - **3.** Monitoring the Reaction in DMF over Time S124
  - **4.** Reactions in the Presence of Additives S136
- **C.** Stoichiometric Oxidative Addition Studies with **S15a** and **S15b** S144
- **D.** Reaction with **S11** and NBu_4OTf S154

I. Experimental Details

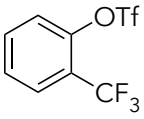
A. General Materials and Methods

NMR spectra were recorded at 298 K on Bruker DPX Avance I 300 MHz (300.130 MHz for ^{1}H, 75.468 MHz for ^{13}C, 282.404 MHz for ^{19}F, 121.495 MHz for ^{31}P), Bruker Ascend 400 MHz (400.130 MHz for ^{1}H NMR, 100.613 for ^{13}C, 376.498 for ^{19}F, 161.967 for ^{31}P), Bruker Ascend Avance III 500 MHz (500.130 for ^{1}H, 125.758 MHz for ^{13}C, 470.592 for ^{19}F, 202.478 MHz for ^{31}P), or Bruker Avance III 600 MHz (600.130 MHz for ^{1}H, 150.903 for ^{13}C) NMR spectrometers. ^{1}H and ^{13}C NMR chemical shifts are reported in parts per million (ppm) relative to TMS, with the residual solvent peak used as an internal reference [^{1}H NMR: $CHCl_3$ (7.26 ppm); ^{13}C NMR: $CDCl_3$ (77.16 ppm).] ^{19}F chemical shifts are reported in ppm relative to fluorobenzene (–113.15 ppm). Multiplicities are reported as follows: singlet (s), doublet (d), triplet (t), quartet (q), quartet of triplets (qt), triplet of triplets (tt), triplet of quintets (tqn), triplet of sextets of doublets (tsd), multiplet (m). GC data were collected using a Shimadzu GC-2010 Plus with a flame ionization detector equipped with a SH-Rxi-5ms capillary column (15 m x 0.25 mm ID x 0.25 μm df). GCMS data were collected on a Shimadzu GCMS-QP2020 NX gas chromatograph mass spectrometer. HRMS data were collected on a Bruker MicroTOF II in acetonitrile with NaCl doping. Purifications via flash chromatography were performed using a Biotage Selekt Flash Purification System. "Room temperature" reactions described herein are generally between 23–25 °C as measured by a temperature probe on the reaction stir plates.

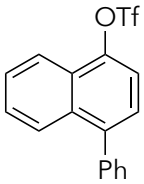
Unless otherwise noted, all commercially-obtained chemicals were used as received. Anisonitrile, dioxane, *N*,*N*-dimethylformamide, *p*-cresol, $PdCl_2$, KF, sulfolane, 4-(dimethylamino)benzonitrile, 4-chlorophenol, and 4-chlorotoluene were obtained from Acros Organics. Propylene carbonate was obtained from Aldrich Chemical. Acetonitrile, K_2CO_3, tetrahydrothiophene, P^tBu_3, and 4-methylbiphenyl were obtained from Alfa Aesar. Benzonitrile was obtained from Eastman Chemical. *p*-Xylene was obtained from Honeywell Fluka Research Chemicals. 4-Chloro-1,1′-biphenyl was obtained from Matrix Scientific. Biphenyl, methyl-4-cyanobenzoate, nitromethane, *o*-tolyl boronic acid, phenyl boronic acid, tetrabutylammonium bromide, tetrabutylammonium chloride, tetrabutylammonium fluoride hexahydrate, tetrabutylammonium trifluoromethanesulfonate, tetrabutylstannane, trifluoromethanesulfonic anhydride, 1-chloro-2-trifluoromethylbenzene, 1-naphthol, 18-crown-6, 2-bromobenzotrifluoride, 2-chlorobenzotrifluoride, 4-(trifluoromethyl)benzonitrile, 4-aminobenzonitrile, 4-ethoxybenzonitrile, 4-fluorobenzonitrile, 4-hydroxybenzonitrile, and 4-nitrobenzonitrile were obtained from Oakwood Chemical. The boronic acids were recrystallized from water prior to use. 1-Methylnaphthalene, $^{n}Bu_3SnOTf$, Me_3SnPh, and α, α, α-trifluorotoluene were obtained from Millipore Sigma. Bis(tri-t-butylphosphine)palladium(0), methanesulfonato(tri-*t*-butylphosphino)(2'-methylamino-1,1'-biphenyl-2-yl)palladium(II) (Buchwald's precatalyst P^tBu_3-Pd-G4), and Me_3SnBr were obtained from Strem Chemical. Fluoroacetonitrile, *N*-methyl-2-pyrrolidone, *p*-terphenyl, *p*-tolunitrile, 1-chloronaphthalene, 1,4-dimethylnaphthalene, 4-chlorobenzotrifluoride, 4-chloro-1-naphthol, 4-hydroxybenzotrifluoride, and 4-phenyl-1-bromonaphthalene were obtained from TCI America. KPF_6 was obtained from Alfa Aesar, Oakwood Chemical, or Millipore Sigma. $^{n}Bu_3SnPh$ was obtained from Alfa Aesar or Millipore Sigma. Tris(dibenzylideneacetone)dipalladium(0) (Pd_2dba_3) was obtained from Millipore Sigma or Strem Chemical. Compounds **1**,[1] **2a**,[1] **2b**,[1] **3a**,[1] **3b**,[1] **4b**,[2] $Pd(COD)(CH_2TMS)_2$,[3] [$Pd(P^tBu_3)$(*o*-CF_3Ph)(Cl)] (**S10**),[4] and P^tBu_3•HCl[5] were synthesized according to literature procedures.

Acetone, acetonitrile, chloroform, dichloromethane, diethyl ether, dimethyl formamide (DMF), dimethylsulfoxide (DMSO), ethanol, ethyl acetate, fluorobenzene, hexanes, isopropanol, methanol, pentane, tetrahydrofuran (THF), and toluene were obtained from Fisher Chemical. Benzene was obtained from TCI America. Solvents were used as received except for those that were used inside the glovebox. In these cases, MeCN, MeOH, DMF, toluene, and fluorobenzene were degassed and dried with a JC Meyer solvent system prior to use. The dried DMF, MeCN, toluene, and methanol were stored over molecular sieves in the glovebox. Deuterated solvents ($CDCl_3$, C_6D_6) were obtained from Cambridge Isotopes and stored over molecular sieves.

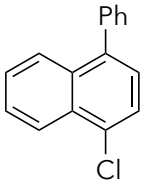
B. Synthesis and Characterization of Substrates and Authentic Samples of Products



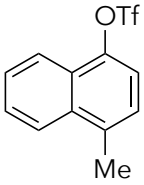
2-(Trifluoromethyl)phenyl triflate (3b): The title compound was prepared according to a modified literature procedure.[6] With cooling to 0 °C, a solution of trifluoromethanesulfonic anhydride (4.0 mL, 24.0 mmol, 1.2 equiv) in CH_2Cl_2 (10 mL) was added dropwise to a solution of 2-hydroxybenzotrifluoride (3.24 g, 20.0 mmol) and pyridine (3.23 mL, 40.0 mmol, 2 equiv) in CH_2Cl_2 (20 mL). The mixture was allowed to warm to room temperature and stirred for 1 h, after which the solution was diluted with Et_2O and acidified with aqueous 1 *M* HCl. The layers were separated, and the aqueous layer was washed with Et_2O (3 x 10 mL). The combined organic layers were washed with saturated $NaHCO_3$ and brine (aqueous NaCl), dried over $MgSO_4$, filtered, and concentrated to give a yellow oil that was purified through a short silica plug (100% hexanes) to afford **3b** as a clear, colorless oil (4.40 g, 75 % yield). Spectral data are consistent with those previously reported.[7]



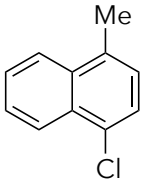
4-Phenylnaphthalen-1-yl triflate (9a). The title compound was prepared according to a modified literature procedure.[8] Pd-P^{t}Bu$_3$-G4 (7.0 mg, 0.012 mmol, 3 mol %), phenyl boronic acid (49.3 mg, 0.404 mmol, 1.01 equiv), and KF (69.7 mg, 1.20 mmol, 3 equiv) were combined in a 1-dram vial equipped with a magnetic stir bar. In rapid succession, 4-chloronaphthalen-1-yl triflate (**8**, 79 μL, 0.40 mmol), deionized water (7.2 μL, 0.40 mmol, 1 equiv), and THF (1.0 mL) were added to the vial and the mixture was immediately sparged with nitrogen for ~2 min. The vial was sealed with a PTFE-lined cap and the reaction was stirred at room temperature for 24 h. The reaction mixture was extracted with ethyl acetate, and the organic extract was filtered over a plug of celite. The filtrate was concentrated and then purified by flash column chromatography (100% hexanes) to afford **9a** as a colorless oil (40 mg, 28% yield). ^{1}H NMR (500 MHz, $CDCl_3$, δ): 8.17 (d, *J* = 8.5 Hz, 1H), 7.95 (d, *J* = 8.5, 1H), 7.69 (t, *J* = 7.6 Hz, 1H), 7.51 (multiple overlapping signals, 8H). ^{13}C{^{1}H} NMR (126 MHz, $CDCl_3$, δ): 145.2, 141.3, 139.4, 133.3, 130.1, 128.6, 128.0, 127.8, 127.6, 126.8, 126.7, 126.2, 121.1, 118.9 (q, $^1J_{CF}$ = 320 Hz), 117.4; ^{19}F (471 MHz, $CDCl_3$, δ): -73.3. HRMS (ESI/Q-TOF) *m/z*: $[M+Na]^+$ Calcd for $C_{17}H_{11}F_3NaO_3S^+$ 375.0273. Found 375.0261.



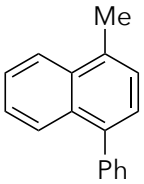
1-Chloro-4-phenylnaphthalene (9b). $PdCl_2$ (2.1 mg, 0.012 mmol, 3 mol %), phenyl boronic acid (48.8 mg, 0.40 mmol, 1 equiv), and KF (69.7 mg, 1.20 mmol, 3 equiv) were combined in a 1-dram vial equipped with a magnetic stir bar. In rapid succession, 4-chloronaphthalen-1-yl triflate (**8**, 79 μL, 0.40 mmol), deionized water (7.2 μL, 0.40 mmol, 1 equiv), and acetonitrile (750 μL) were added to the vial and the mixture was immediately sparged with nitrogen for ~2 min. The vial was sealed with a PTFE-lined cap and the reaction was stirred at room temperature for 22 h. The reaction mixture was extracted with ethyl acetate, and the organic extract was filtered over a plug of celite. The filtrate was concentrated and then purified by flash column chromatography (100% hexanes) to afford **9b** as a colorless oil (79 mg, 84% yield). Spectral data are consistent with those previously reported.[9]



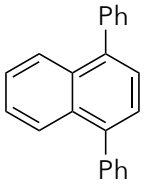
4-Methylnaphthalen-1-yl triflate (9c): In a nitrogen-filled glovebox, Pd_2dba_3 (6.9 mg, 0.0075 mmol 1.5 mol %), $Pd(P^tBu_3)_2$ (7.7 mg, 0.015 mmol, 3.0 mol %), and KPF_6 (276 mg, 1.50 mmol, 3 equiv) were combined in a 1-dram vial equipped with a magnetic stir bar. In rapid succession, 4-chloronaphthalen-1-yl triflate (**8**, 98 μL, 0.50 mmol), $PhSnMe_3$ (100 μL, 0.55 mmol, 1.1 equiv), and DMF (1.0 mL) were added. The vial was sealed with a PTFE-lined cap and the mixture was stirred at 100 °C for 24 h. The reaction mixture was extracted with ethyl acetate, and the organic extract was filtered over a plug of celite. The filtrate was concentrated and then purified by flash column chromatography (100% hexanes, dry-loaded on C18 silica gel) to afford **9c** as a white solid (52 mg, 36% yield).). ^{1}H NMR (500 MHz, $CDCl_3$, δ): 8.21-8.01 (two overlapping signals, 2H), 7.68-7.60 (two overlapping signals, 2H), 7.38-7.30 (two overlapping signals 2H), 2.71 (s, 3H); $^{13}C\{^1H\}$ NMR (126 MHz, $CDCl_3$ δ): 144.4, 135.6, 133.9, 127.6, 127.3, 126.5, 125.7, 124.7, 122.7, 118.8 (q, $^1J_{CF}$ = 320 Hz), 117.5, 19.4; ^{19}F (471 MHz, $CDCl_3$, δ): -73.4. HRMS (ESI/Q-TOF) *m/z*: $[M+Na]^+$ Calcd for $C_{12}H_9F_3NaO_3S^+$ 313.0117. Found 313.0123.



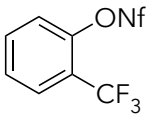
1-Chloro-4-methylnaphthalene (9d): In a nitrogen-filled glovebox, Pd_2dba_3 (6.9 mg, 0.0075 mmol 1.5 mol %), $Pd(P^tBu_3)_2$ (7.7 mg, 0.015 mmol, 3.0 mol %), and KPF_6 (276 mg, 1.50 mmol, 3 equiv) were combined in a 1-dram vial equipped with a magnetic stir bar. In rapid succession, 4-chloronaphthalen-1-yl triflate (**8**, 98 μL, 0.50 mmol), $PhSnMe_3$ (100 μL, 0.55 mmol, 1.1 equiv), and DMF (1.0 mL) were added. The vial was sealed with a PTFE-lined cap and the mixture was stirred at room temperature for 24 h. The reaction mixture was extracted with ethyl acetate, and the organic extract was filtered over a plug of celite. The filtrate was concentrated and then purified by flash column chromatography (100% hexanes, dry-loaded on C18 silica gel) to afford **9d** as a white solid (31 mg, 35% yield). Spectral data are consistent with those previously reported,[10] but higher resolution data are included here. ^{1}H NMR (400 MHz, $CDCl_3$, δ): 8.30 (dd, *J* = 7.6 Hz, 1H), 8.0 (dd, 7.5 Hz, 1H), 7.70-7.57 (two overlapping signals, 2H), 7.46 (d, 7.7 Hz, 1H), 7.23 (d, 7.7 Hz, 1H, overlaps with solvent), 2.67 (s, 3H); $^{13}C\{^1H\}$ NMR (101 MHz, $CDCl_3$ δ): 133.8, 133.7, 130.8, 130.2, 130.0, 128.5, 126.8 (d, *J* = 7.2 Hz), 126.5, 125.9, 124.1, 124.7, 19.4.



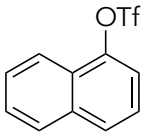
1-Methyl-4-phenylnaphthalene (9f): The title compound was prepared according to a modified literature procedure.[8] Pd-P^{t}Bu$_3$-G4 (7.0 mg, 0.012 mmol, 3 mol %), phenyl boronic acid (49.3 mg, 0.404 mmol, 1.01 equiv), and KF (69.7 mg, 1.20 mmol, 3 equiv) were combined in a 1-dram vial equipped with a magnetic stir bar. In rapid succession, 1-bromo-4-methylnaphthalene (63 μl, 0.40 mmol), deionized water (7.2 μL, 0.40 mmol, 1 equiv), and THF (1.0 mL) were added to the vial and the mixture was immediately sparged with nitrogen for ~ 2 min. The vial was sealed with a PTFE-lined cap and the reaction was stirred at room temperature for 24 h. The reaction mixture was extracted with ethyl acetate, and the organic extract was filtered over a plug of celite. The filtrate was concentrated and then purified by flash column chromatography (100% hexanes) to afford **9f** as a white solid (76 mg, 87% yield). Spectral data are consistent with those previously reported.[11]



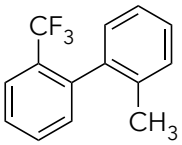
1,4-Diphenylnaphthalene (9g): The title compound was prepared according to a modified literature procedure.[8] Pd-P^{t}Bu$_3$-G4 (7.0 mg, 0.012 mmol, 3 mol %), phenyl boronic acid (49.3 mg, 0.404 mmol, 1.01 equiv), KF (69.7 mg, 1.20 mmol, 3 equiv), and 1-bromo-4-phenylnaphthalene (113.3 mg, 0.40 mmol) were combined in a 1-dram vial equipped with a magnetic stir bar. In rapid succession, deionized water (7.2 μL, 0.40 mmol, 1 equiv) and THF (1.0 mL) were added to the vial and the mixture was immediately sparged with nitrogen for ~ 2 min. The vial was sealed with a PTFE-lined cap and the reaction was stirred at room temperature for 24 h. The reaction mixture was extracted with ethyl acetate, and the organic extract was filtered over a plug of celite. The filtrate was concentrated and then purified by flash column chromatography (100% hexanes) to afford **9g** as a white solid (45 mg, 40% yield). Spectral data are consistent with those previously reported.[11]



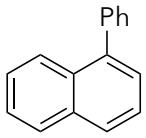
2-(Trifluoromethyl)phenyl nonaflate (S11). The title compound was prepared according to a modified literature procedure.[12] To an oven-dried 50 mL round bottom flask was added 2-(trifluoromethyl)phenol (0.68 g, 4.2 mmol, 1 equiv), K_2CO_3 (0.87 g, 6.3 mmol, 1.5 equiv), and acetonitrile (8.3 mL, 0.5 *M*). The resulting slurry was stirred rapidly while perfluorobutanesulfonyl fluoride (1.26 g, 5.0 mmol, 1.2 equiv) was added via Pasteur pipette. The solution was allowed to stir at room temperature for 16 h, after which the slurry was filtered over a pad of silica gel and rinsed thoroughly with hexanes. The filtrate was concentrated under vacuum to yield **S11** as a clear, colorless oil (1.39 g, 75% yield). ^{1}H NMR (600 MHz, $CDCl_3$, δ): 7.77 (d, *J* = 7.6 Hz, 1H), 7.67 (t, *J* = 8.2 Hz, 1H), 7.53 (d, *J* = 8.2 Hz, 1H), 7.50 (t, *J* = 7.6 Hz, 1H). ^{13}C{^{1}H} NMR (151 MHz, $CDCl_3$, δ): 146.4, 134.2, 128.4, 128.2 (q, *J* = 5.5 Hz), 123.6 (q, *J* = 33.1 Hz), 122.6, 122.2 (q, *J* = 272.7 Hz), 117.5, (qt, *J* = 295.6, 33.1 Hz), 114.7 (tt, *J* = 295.6, 33.1), 110.1 (tqn, *J* = 272.7, 31.8 Hz), 108.7 (tsd, *J* = 272.7, 31.8, 5.5 Hz). ^{19}F NMR (282 MHz, $CDCl_3$, δ): -60.9, -80.7, -109.3, -120.9, -125.9. HRMS (EI/Q-TOF) *m*/*z*: $[M]^+$ Calcd for $C_{11}H_4F_{12}O_3S^+$ 443.9690. Found 443.9686.



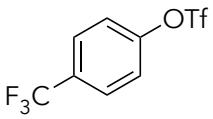
Naphthalen-1-yl triflate (S12): The title compound was prepared according to a modified literature procedure.[6] With cooling to 0 °C, trifluoromethanesulfonic anhydride (1.0 mL, 6.0 mmol, 1.2 equiv) was added dropwise to a solution of 1-naphthol (0.72 g, 5.0 mmol) and pyridine (0.81 mL, 10.0 mmol, 2 equiv) in CH_2Cl_2 (10 mL). The mixture was allowed to warm to room temperature and stirred for 1 h, after which the solution was diluted with Et_2O and acidified with aqueous 1 N HCl. The layers were separated, and the aqueous layer was washed with Et_2O (3 x 5 mL). and the combined organics washed with saturated $NaHCO_3$ and NaCl brine. The combined organic layers were washed with saturated $NaHCO_3$ and brine (aqueous NaCl), dried over $MgSO_4$, filtered, and concentrated to give a yellow oil that was purified through a short silica plug (100% hexanes) to afford **S12** as a clear, colorless oil (1.05 g, 76 % yield). Spectral data are consistent with those previously reported.[7]



2-Methyl-2'-(trifluoromethyl)biphenyl (S13). The title compound was prepared according to a modified literature procedure.[8] Pd-P^{t}Bu$_3$-G4 (7.0 mg, 0.012 mmol, 3 mol %), *ortho*-tolylboronic acid (54.9 mg, 0.404 mmol, 1.01 equiv), and KF (69.7 mg, 1.20 mmol, 3 equiv) were combined in a 1-dram vial equipped with a magnetic stir bar. In rapid succession, deionized water (7.2 μL, 0.40 mmol, 1 equiv), 2-chlorobenzotrifluoride (54 μL, 0.40 mmol), and toluene (1.0 mL) were added to the vial and the mixture was immediately sparged with nitrogen for ~2 min. The vial was sealed with a PTFE-lined cap and the reaction was stirred at room temperature for 24 h. The reaction mixture was extracted with ethyl acetate, and the organic extract was filtered over a plug of celite. The filtrate was concentrated and then purified by flash column chromatography (100% hexanes) to afford **S13** as a colorless oil (45 mg, 48 % yield).). ^{1}H NMR (500 MHz, $CDCl_3$, δ): 7.79 (d, *J* = 7.8 Hz, 1H), 7.59 (dd, *J* = 7.7, 7.7 Hz, 1H), 7.52 (dd, *J* = 7.6, 7.6 Hz, 1H), 7.37-7.23 (multiple signals, 4H, overlaps with solvent), 7.16 (d, *J* = 7.5 Hz, 1H), 2.06 (s, 3H). ^{13}C{^{1}H} NMR (126 MHz, $CDCl_3$ δ): 140.8, 139.0, 136.1, 131.7, 131.4, 129.7, 129.6, 128.9 (q, $^2J_{CF}$ = 29 Hz), 128.0, 127.4, 126.1 (q, $^3J_{CF}$ = 5 Hz), 125.0, 124.1 (q, $^1J_{CF}$ = 276 Hz), 20.2. ^{19}F (471 MHz, $CDCl_3$, δ): -59.2. HRMS (ESI/Q-TOF) *m/z*: $[M+Na]^+$ Calcd for $C_{14}H_{11}F_3Na^+$ 259.0705. Found 259.0711 .



1-Phenylnaphthalene (S14): The title compound was prepared according to a modified literature procedure.[8] Pd-P^{t}Bu$_3$-G4 (7.0 mg, 0.012 mmol, 3 mol %), phenyl boronic acid (49.3 mg, 0.404 mmol, 1.01 equiv), and KF (69.7 mg, 1.20 mmol, 3 equiv) were combined in a 1-dram vial equipped with a magnetic stir bar. In rapid succession, deionized water (7.2 μL, 0.40 mmol, 1 equiv), 1-chloronaphthalene (55 μL, 0.40 mmol, 1 equiv), and THF (1.0 mL) were added to the vial and the mixture was immediately sparged with nitrogen for ~ 2 min.. The vial was sealed with a PTFE-lined cap and the reaction was stirred at room temperature for 24 h. The reaction mixture was extracted with ethyl acetate, and the organic extract was filtered over a plug of celite. The filtrate was concentrated and then purified by flash column chromatography (100% hexanes) to afford **S14** as a viscous, colorless oil (6 mg, 7% yield). Spectral data are consistent with those previously reported.[13]



4-(Trifluoromethyl)phenyl triflate (S15b): The title compound was prepared according to a modified literature procedure.[14] With cooling to 0 °C, a solution of trifluoromethanesulfonic anhydride (4.0 mL, 24.0 mmol, 1.2 equiv) in CH_2Cl_2 (10 mL) was added dropwise to a solution of 4-hydroxybenzotrifluoride (3.24 g, 20.0 mmol) and pyridine (3.25 mL, 40.3 mmol, 2 equiv) in CH_2Cl_2 (20 mL). The mixture was allowed to warm to room temperature and stirred for 1 h, after which the solution was diluted with Et_2O and acidified with aqueous 1 *M* HCl. The layers were separated, and the aqueous layer was washed with Et_2O (3 x 10 mL). The combined organic layers were washed with saturated $NaHCO_3$ and brine (aqueous NaCl), dried over $MgSO_4$, filtered, and concentrated to give a yellow oil that was purified through a short silica plug (100% hexanes) to afford **S15b** as a clear, colorless oil (4.53 g, 77% yield). Spectral data are consistent with those previously reported.[15]

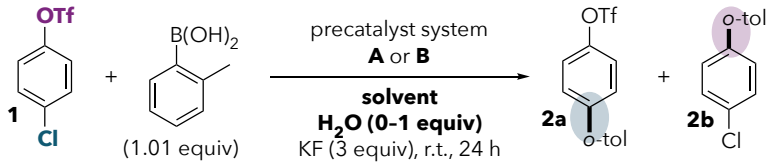
C. Catalytic Suzuki Couplings of 1

1. Evaluation of Precatalyst and Water Effect on Selectivity

General Procedure with Precatalyst System A: Without exclusion of air or moisture, P^tBu_3-Pd-G4 (1.5 mg, 0.0026 mmol, 3 mol %), *o*-tolyl boronic acid (11.0 mg, 0.081 mmol, 1.01 equiv), and KF (13.9 mg, 0.24 mmol, 3 equiv) were combined in a 1-dram vial equipped with a magnetic stir bar. In rapid succession, water (0–1.4 μL, 0–0.08 mmol, 0–1 equiv), 4-chlorophenyl triflate (14 μL, 0.08 mmol, 1 equiv), and solvent (150 μL) were added to the vial and the mixture was immediately sparged with nitrogen for two minutes. The sparging needle and septum was quickly replaced with a PTFE-lined cap and the reaction was stirred vigorously at room temperature for 24 h. Undecane (7.5 μL) was added to the reaction mixture as an internal standard, and the mixture was diluted with EtOAc. A small aliquot was removed and filtered through celite, and the celite was washed with additional EtOAc. The filtrate was analyzed by gas chromatography.

General Procedure for Precatalyst System B: In a nitrogen filled glovebox, Pd_2dba_3 (0.5 mg, 0.0006 mmol, 0.75 mol %), $Pd(PtBu_3)_2$ (0.6 mg, 0.0012 mmol, 1.5 mol %) , *o*-tolyl boronic acid (11.0 mg, 0.081 mmol, 1.01 equiv), and KF (13.9 mg, 0.24 mmol, 3 equiv) were combined in a 1-dram vial equipped with a magnetic stir bar. The vial was sealed with a PTFE-lined cap and removed from the glovebox. Outside of the glovebox, the cap was removed and, in rapid succession, water (0–1.4 μL, 0–0.08 mmol, 0–1 equiv), 4-chlorophenyl triflate (14 μL, 0.08 mmol, 1 equiv), and solvent (150 μL) were added to the vial and the mixture was immediately sparged with nitrogen for two minutes. The sparging needle and septum cap was quickly replaced with a PTFE-lined cap and the reaction was stirred vigorously at room temperature for 24 h. Undecane (7.5 μL) was added to the reaction mixture as an internal standard, and the mixture was diluted with EtOAc. A small aliquot was removed and filtered through celite, and the celite was washed with additional EtOAc. The filtrate was analyzed by gas chromatography.

Table S1. Effect of Precatalyst and Water on Selectivity[a]



precatalyst system **A**: P^tBu_3-Pd-G4 (3 mol %)
precatalyst system **B**: $Pd_2(dba)_3$ (0.75 mol %), $Pd(P^tBu_3)_2$ (1.5 mol %)

entry	solvent	precatalyst	H_2O (equiv)	trial	**1** (%)	**2a** (%)	**2b** (%)
1	THF	**A**	0	1	25	79	1
2	THF	**A**	0	2	21	79	1
3	THF	**A**	0	Average	23	79	1
4	THF	**A**	1	1	5	63	<1
5	THF	**A**	1	2	23	72	<1
6	THF	**A**	1	3	26	68	1
7	THF	**A**	1	4	25	71	1
8	THF	**A**	1	5	27	75	1
9	THF	**A**	1	6	24	79	1
10	THF	**A**	1	7	20	78	1
11	THF	**A**	1	8	18	79	1
12	THF	**A**	1	Average	20	74	<1
13	THF	**B**	1	1	28	72	1
14	THF	**B**	1	2	19	75	1
15	THF	**B**	1	Average	24	74	1
16	MeOH	**A**	1	1	0	68	3
17	MeOH	**A**	1	2	0	65	2
18	MeOH	**A**	1	Average	0	67	2
19	MeOH	**B**	1	1	35	19	2
20	MeOH	**B**	1	2	36	21	2
21	MeOH	**B**	1	Average	35	19	2
22	DMF	**A**	0	1	65	6	30
23	DMF	**A**	0	2	63	7	31
24	DMF	**A**	0	Average	64	7	30
25	DMF	**A**	1	1	16	9	58
26	DMF	**A**	1	2	19	9	61
27	DMF	**A**	1	3	24	11	59
28	DMF	**A**	1	4	26	11	59
29	DMF	**A**	1	5	16	12	66
30	DMF	**A**	1	6	20	11	62
31	DMF	**A**	1	7	18	9	66
32	DMF	**A**	1	8	46	7	46
33	DMF	**A**	1	Average	23	10	60
34	DMF	**B**	1	1	49	7	42
35	DMF	**B**	1	2	23	10	62
36	DMF	**B**	1	Average	36	9	52
37	MeCN	**A**	1	1	8	2	75
38	MeCN	**A**	1	2	8	2	78
39	MeCN	**A**	1	Average	8	2	77
40	MeCN	**B**	1	1	16	4	72
41	MeCN	**B**	1	2	19	4	71
42	MeCN	**B**	1	Average	17	4	72
43	propylene carbonate	**A**	1	1	9	57	6

Table S2 Continued

44	propylene carbonate	**A**	1	2	23	68	6
45	propylene carbonate	**A**	1	3	12	75	5
46	propylene carbonate	**A**	1	4	19	68	6
47	propylene carbonate	**A**	1	Average	16	67	6
48	propylene carbonate	**B**	1	1	22	52	6
49	propylene carbonate	**B**	1	2	20	55	5
50	propylene carbonate	**B**	1	Average	21	53	6

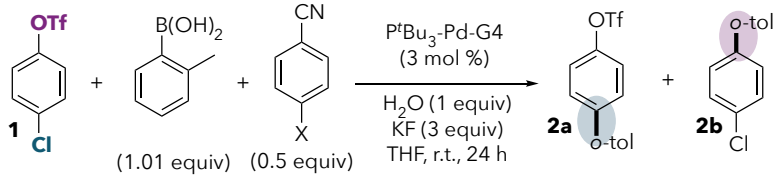
[a]GC yields calibrated against undecane as an internal standard. Diarylated product observed in ≤5% yield in all cases.

Discussion: The addition of 1 equiv water does not significantly impact selectivity (compare entries 3 vs 12, and 24 vs 33). Precatalyst systems **A** and **B** provide very similar selectivity in all solvents examined, although in some cases precatalyst **A** affords somewhat higher yields. Precatalyst **A** has the added advantage that it can be handled open to air.

2. Benzonitrile Additives (Table 1 and Figure 1)

General Procedure: Without exclusion of air or moisture, P^tBu_3-Pd-G4 (1.5 mg, 0.0026 mmol, 3 mol %), *o*-tolyl boronic acid (11.0 mg, 0.081 mmol, 1.01 equiv), and KF (13.9 mg, 0.24 mmol, 3 equiv) were combined in a 1-dram vial equipped with a magnetic stir bar. In rapid succession, water (1.4 μL, 0.08 mmol, 1 equiv), 4-chlorophenyl triflate (14 μL, 0.08 mmol, 1 equiv), benzonitrile additive (0.04 mmol, 0.5 equiv, if applicable), and solvent (usually THF, 150 μL) were added to the vial and the mixture was immediately sparged with nitrogen for two minutes. The sparging needle and septum was quickly replaced with a PTFE-lined cap and the reaction was stirred vigorously at room temperature for 24 h. Undecane (7.5 μL) was added to the reaction mixture as an internal standard, and the mixture was diluted with EtOAc. A small aliquot was removed and filtered through celite, and the celite was washed with additional EtOAc. The filtrate was analyzed by gas chromatography.

Table S3. Effect of Benzonitrile Additives on Selectivity[a]



entry	X	σ_p	σ_p^+	trial	**1** (%)	**2a** (%)	**2b** (%)	log (**2a**/**2b**)	std. dev.[b]
1[c]	--	--	--	1	5	63	<1	>1.80	
2[c]	--	--	--	2	23	72	<1	>1.86	
3[c]	--	--	--	3	26	68	1	1.83	
4[c]	--	--	--	4	25	71	1	1.85	
5[c]	--	--	--	5	27	75	1	1.88	
6[c]	--	--	--	6	24	79	1	1.90	
7[c]	--	--	--	7	20	78	1	1.89	
8[c]	--	--	--	8	18	79	1	1.90	
9[c]	--	--	--	Average	20	74	<1	>1.87	0.03
10	NMe2	-0.83	-1.70	1	46	28	15	0.27	
11	NMe2	-0.83	-1.70	2	47	29	20	0.16	

Table S4 Continued

12	NMe2	-0.83	-1.70	3	37	36	21	0.23	
13	NMe2	-0.83	-1.70	Average	44	31	18	0.24	0.06
14	NH2	-0.66	-1.30	1	29	46	19	0.38	
15	NH2	-0.66	-1.30	2	29	45	20	0.35	
16	NH2	-0.66	-1.30	3	36	43	17	0.40	
17	NH2	-0.66	-1.30	Average	31	45	19	0.37	0.03
18	OH	-0.37	-0.92	1	38	50	16	0.49	
19	OH	-0.37	-0.92	2	28	53	14	0.58	
20	OH	-0.37	-0.92	3	33	46	16	0.46	
21	OH	-0.37	-0.92	Average	33	50	15	0.52	0.06
22	OEt	-0.24	-0.81	1	35	47	10	0.67	
23	OEt	-0.24	-0.81	2	41	45	8	0.75	
24	OEt	-0.24	-0.81	3	48	42	10	0.62	
25	OEt	-0.24	-0.81	Average	42	45	10	0.65	0.06
26	OMe	-0.27	-0.73	1	72	26	3	0.94	
27	OMe	-0.27	-0.73	2	56	18	2	0.95	
28	OMe	-0.27	-0.73	3	62	32	4	0.90	
29	OMe	-0.27	-0.73	Average	63	26	3	0.94	0.03
30	Me	-0.17	-0.31	1	65	35	2	1.24	
31	Me	-0.17	-0.31	2	66	25	2	1.10	
32	Me	-0.17	-0.31	3	69	28	2	1.15	
33	Me	-0.17	-0.31	Average	67	29	2	1.16	0.07
34	F	0.06	-0.07	1	40	51	5	1.01	
35	F	0.06	-0.07	2	71	30	2	1.18	
36	F	0.06	-0.07	3	46	50	5	1.00	
37	F	0.06	-0.07	Average	52	44	4	1.04	0.10
38	H	0	0	1	37	53	3	1.25	
39	H	0	0	2	43	53	6	0.95	
40	H	0	0	3	38	59	3	1.29	
41	H	0	0	Average	39	55	4	1.14	0.19
42	COOMe	0.45	0.49	1	56	41	3	1.14	
43	COOMe	0.45	0.49	2	55	44	3	1.17	
44	COOMe	0.45	0.49	3	55	41	3	1.14	
45	COOMe	0.45	0.49	Average	55	42	3	1.15	0.02
46	CF3	0.54	0.61	1	44	45	3	1.18	
47	CF3	0.54	0.61	2	46	49	3	1.21	
48	CF3	0.54	0.61	3	49	44	3	1.17	
49	CF3	0.54	0.61	Average	46	46	3	1.19	0.02
50	NO2	0.78	0.79	1	63	32	8	0.60	
51	NO2	0.78	0.79	2	49	38	8	0.68	
52	NO2	0.78	0.79	3	59	35	6	0.77	
53	NO2	0.78	0.79	Average	57	35	7	0.70	0.08
54[d]	--	--	--	1	27	7	54	-0.89	
55[d]	--	--	--	2	26	7	53	-0.88	
56[d]	--	--	--	Average	27	7	53	-0.88	0.01

[a]GC yields calibrated against undecane as an internal standard. Diarylated product observed in ≤5% yield in all cases. Sigma values from reference 16. [b]Standard deviation of the log(**2a**/**2b**) values. [b]No benzonitrile derivatives were added. [c]PhCN was used as the reaction solvent (no additional benzonitrile derivatives were added).

Discussion: Table S2 entries 10-49 were used to create Figure 1 in the manuscript, which shows a good correlation between σ_p^+ and log(**2a**/**2b**), with an R^2 value of 0.8639. The correlation to σ_p is not quite as strong (Figure S1). Unusual results were observed with 4-nitrobenzonitrile (entry 53). With this additive, the **2a**/**2b** ratio was much

smaller than expected based on the trend with all of the other substituted benzonitriles (Figure S2). This particularly electron-poor nitrile is expected to coordinate to Pd(0) as a π-acceptor, and we speculate that the increased reaction at OTf may be due to this coordination mode. There is no evidence that nitro groups in isolation promote reaction at triflate. For example, high selectivity for reaction at chloride is observed in the catalytic Suzuki coupling using 3-nitrophenylboronic acid in MeOH and THF,[8] and running the reaction shown in Table S2 with $PhNO_2$ as the solvent leads exclusively to product **2a** from reaction at chloride.

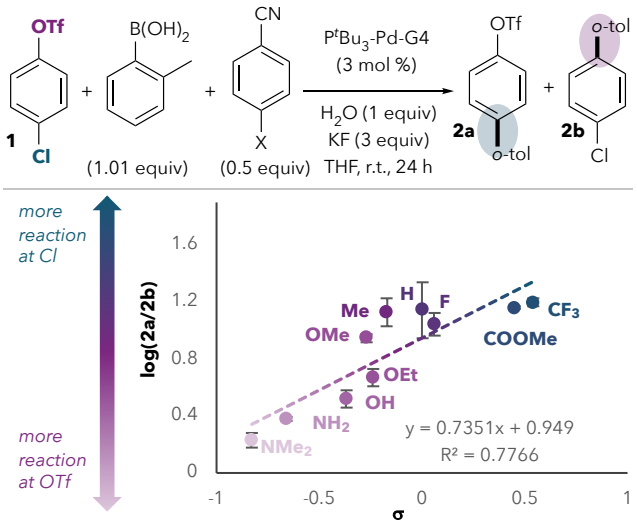


Figure S1. Hammett-type plot using σ shows slightly worse correlation than the plot using σ+.

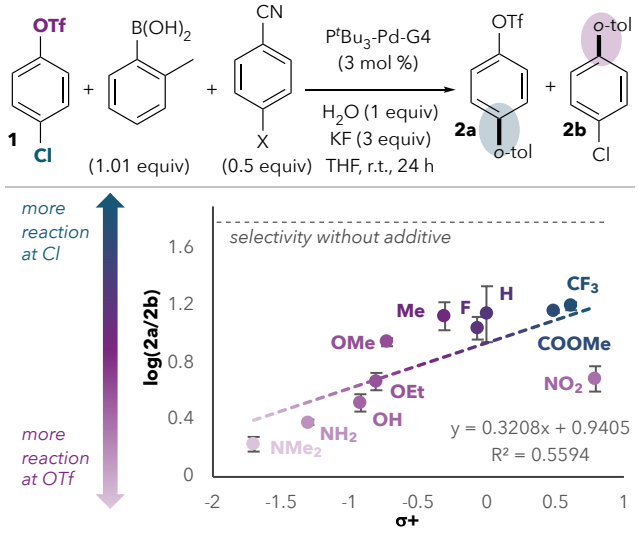
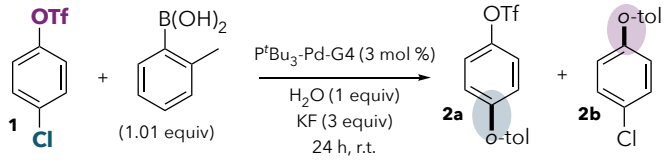


Figure S2. NO_2 is an outlier in the Hammett-type plot correlating benzonitrile donor ability and increased reaction at triflate.

3. Mixed THF/Benzonitrile Solvent

General Procedure: Without exclusion of air or moisture, P^tBu_3-Pd-G4 (1.5 mg, 0.0026 mmol, 3 mol %), *o*-tolyl boronic acid (11.0 mg, 0.081 mmol, 1.01 equiv), and KF (13.9 mg, 0.24 mmol, 3 equiv) were combined in a 1-dram vial equipped with a magnetic stir bar. In rapid succession, water (1.4 μL, 0.08 mmol, 1 equiv), 4-chlorophenyl triflate (14 μL, 0.08 mmol, 1 equiv), and solvent(s) (total of 150 μL) were added to the vial and the mixture was immediately sparged with nitrogen for two minutes. The sparging needle and septum was quickly replaced with a PTFE-lined cap and the reaction was stirred vigorously at room temperature for 24 h. Undecane (7.5 μL) was added to the reaction mixture as an internal standard, and the mixture was diluted with EtOAc. A small aliquot was removed and filtered through celite, and the celite was washed with additional EtOAc. The filtrate was analyzed by gas chromatography.

Table S5. Effect of Mixed PhCN/THF Solvent on Selectivity[a]



PhCN (% of total solvent volume)	THF (% of total solvent volume)	trial	**1** (%)	**2a** (%)	**2b** (%)	total yield **2a** + **2b**	ratio **2a** : **2b**
0	100	1	5	63	<1	63	>63 : 1
0	100	2	23	72	<1	72	>72 : 1
0	100	3	26	68	1	69	68 : 1
0	100	4	25	71	1	72	71 : 1
0	100	5	27	75	1	76	75 : 1
0	100	6	24	79	1	80	79 : 1
0	100	7	20	78	1	79	78 : 1
0	100	8	18	79	1	80	79 : 1
0	100	average	21	74	1	75	74 : 1
1	99	1	33	56	2	58	28 : 1
1	99	2	19	74	2	76	37 : 1
1	99	average	26	65	2	67	33 : 1
5	95	1	58	30	6	36	5 : 1
5	95	2	45	41	9	50	5 : 1
5	95	average	51	35	7	43	5 : 1
10	90	1	39	33	17	50	2 : 1
10	90	2	38	36	19	55	2 : 1
10	90	average	39	35	18	53	2 : 1
25	75	1	26	25	38	63	1 : 2
25	75	2	21	26	38	64	1 : 2
25	75	average	24	25	38	63	1 : 2
50	50	1	13	15	48	63	1 : 3
50	50	2	17	13	52	65	1 : 4
50	50	average	15	14	50	64	1 : 4
75	25	1	18	12	56	68	1: 5
75	25	2	27	10	44	54	1 : 4
75	25	average	22	11	50	61	1 : 5
100	0	1	27	7	54	61	1 : 8
100	0	2	26	7	53	60	1 : 8
100	0	average	27	7	53	60	1 : 8

[a]GC yields calibrated against undecane as an internal standard.

Discussion: The data in Table S3 show that selectivity inverts between 10-25% PhCN, as illustrated in Figure S3. Interestingly, small amounts of PhCN (5% and 10% of total volume) lead to lower conversion than observed in neat THF or with larger amounts of PhCN (≥25% of total volume). This phenomenon is illustrated in Figure S4. The unusual shape of the curve in Figure S4 may relate to solvent polarity. Small quantities of PhCN begin to suppress reaction at chloride because Pd is more likely to be bisligated. Reaction at triflate increases with small quantities of PhCN, but it increases even more with larger quantities of PhCN because of increased polarity of the reaction medium. Aryl triflates are known to undergo faster oxidative addition at bisligated palladium in more polar media.[17]

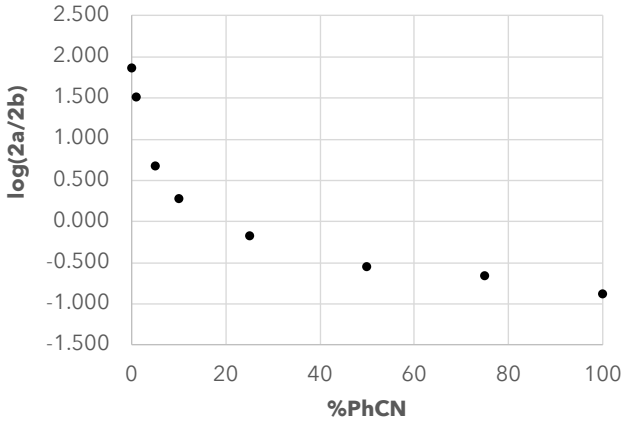


Figure S3. Effect of PhCN/THF ratio on product ratio.

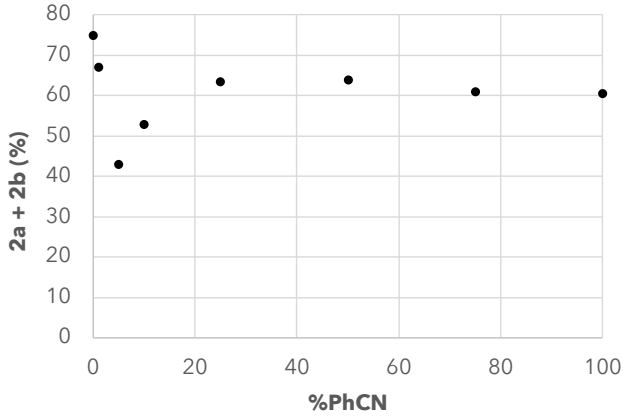
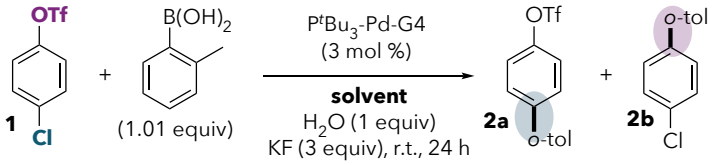


Figure S4. Effect of PhCN/THF ratio on the total yield of **2a** + **2b**.

4. Results with Fluoroacetonitrile, Sulfolane (Table 2), and Tetrahydrothiophene

General Procedure: Without exclusion of air or moisture, P^tBu_3-Pd-G4 (1.5 mg, 0.0026 mmol, 3 mol %), *o*-tolyl boronic acid (11.0 mg, 0.081 mmol, 1.01 equiv), and KF (13.9 mg, 0.24 mmol, 3 equiv) were combined in a 1-dram vial equipped with a magnetic stir bar. In rapid succession, water (1.4 μL, 0.08 mmol, 1 equiv), 4-chlorophenyl triflate (14 μL, 0.08 mmol, 1 equiv), and solvent (150 μL) were added to the vial and the mixture was immediately sparged with nitrogen for two minutes. The sparging needle and septum was quickly replaced with a PTFE-lined cap and the reaction was stirred vigorously at room temperature for 24 h. Undecane (7.5 μL) was added to the reaction mixture as an internal standard, and the mixture was diluted with EtOAc. A small aliquot was removed and filtered through celite, and the celite was washed with additional EtOAc. The filtrate was analyzed by gas chromatography.

Table S6. Modifying the Coordinating Ability of Common Solvents Leads to Changes in Selectivity[a]



entry	solvent	ε^b	trial	**1** (%)	**2a** (%)	**2b** (%)
1	CH_3CN	36.6	1	8	2	75
2	CH_3CN	36.6	2	8	2	78
3	CH_3CN	36.6	Average	8	2	77
4	CH_2FCN	~36	1	85	4	10
5	CH_2FCN	~36	2	88	3	9
6	CH_2FCN	~36	Average	86	4	10
7	DMSO	47.2	1	61	1	26
8	DMSO	47.2	2	25	1	64
9	DMSO	47.2	Average	43	1	45
10	sulfolane	42.2	1	41	44	12
11	sulfolane	42.2	2	41	43	10
12	sulfolane	42.2	Average	41	44	11
13	THF	7.5	1	5	63	<1
14	THF	7.5	2	23	72	<1
15	THF	7.5	3	26	68	1
16	THF	7.5	4	25	71	1
17	THF	7.5	5	27	75	1
18	THF	7.5	6	24	79	1
19	THF	7.5	7	20	78	1
20	THF	7.5	8	18	79	1
21	THF	7.5	Average	20	74	<1
22	tetrahydrothiophene	8.6	1	92	0	2
23	tetrahydrothiophene	8.6	2	105	0	1
24	tetrahydrothiophene	8.6	Average	99	0	2

[a]GC yields calibrated against undecane as an internal standard. Results are the average of at least two trials. Diarylated product observed in ≤3% yield in all cases. [b]Dielectric constants from references 18 and 19.

Discussion: Although reaction in THF provides **2a** as the major product (Table S4, entry 21), the only product observed in tetrahydrothiophene (THT) is **2b** (entry 24). This is consistent with THT acting as a coordinating ligand during oxidative addition. However the yield is so low that selectivity cannot be reliably interpreted. The low yield is likely due to the strong coordinating ability of sulfides to palladium, effectively poisoning it as a catalyst. For a discussion of entries 1-12, see the manuscript.

5. Effect of Temperature (Table 4)

General Procedure with Precatalyst System A: Without exclusion of air or moisture, P^tBu_3-Pd-G4 (1.5 mg, 0.0026 mmol, 3 mol %), *o*-tolyl boronic acid (11.0 mg, 0.081 mmol, 1.01 equiv), and KF (13.9 mg, 0.24 mmol, 3 equiv) were combined in a 1-dram vial equipped with a magnetic stir bar. In rapid succession, water (1.4 μL, 0.08 mmol, 1 equiv), 4-chlorophenyl triflate (14 μL, 0.08 mmol, 1 equiv), and solvent (150 μL) were added to the vial and the mixture was immediately sparged with nitrogen for two minutes. The sparging needle and septum was quickly replaced with a PTFE-lined cap and the reaction was stirred vigorously at the indicated temperature for 24 h. Undecane (7.5 μL) was added to the reaction mixture as an internal standard, and the mixture was diluted with EtOAc. A small aliquot was removed and filtered through celite, and the celite was washed with additional EtOAc. The filtrate was analyzed by gas chromatography.

General Procedure for Precatalyst Systems B-E: In a nitrogen filled glovebox, the following reagents were combined with *o*-tolyl boronic acid (11.0 mg, 0.081 mmol, 1.01 equiv) and KF (13.9 mg, 0.24 mmol, 3 equiv) in a 1-dram vial equipped with a magnetic stir bar:

Precatalyst System B: Pd_2dba_3 (0.5 mg, 0.0006 mmol, 0.75 mol %), $Pd(PtBu_3)_2$ (0.6 mg, 0.0012 mmol, 1.5 mol %)

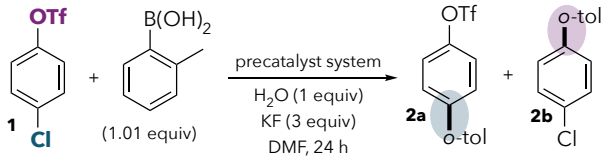
Precatalyst System C: Pd_2dba_3 (1.1 mg, 0.0012 mmol, 1.5 mol %), $PtBu_3$ (0.5 mg, 0.0024 mmol, 3.0 mol %)

Precatalyst System D: $Pd(OAc)_2$ (0.7 mg, 0.0024 mmol, 3.0 mol %), $PtBu_3$ (0.5 mg, 0.0024 mmol, 3.0 mol %)

Precatalyst System E: $Pd(COD)(CH_2TMS)_2$ (0.9 mg, 0.0024 mmol, 3.0 mol %), $PtBu_3$ (0.5 mg, 0.0024 mmol, 3.0 mol %)

The vial was sealed with a PTFE-lined cap and removed from the glovebox. Outside of the glovebox, the cap was removed and, in rapid succession, water (1.4 μL, 0.08 mmol, 1 equiv), 4-chlorophenyl triflate (14 μL, 0.08 mmol, 1 equiv), and solvent (150 μL) were added to the vial and the mixture was immediately sparged with nitrogen for two minutes. The sparging needle and septum was quickly replaced with a PTFE-lined cap and the reaction was stirred vigorously at the indicated temperature for 24 h. Undecane (7.5 μL) was added to the reaction mixture as an internal standard, and the mixture was diluted with EtOAc. A small aliquot was removed and filtered through celite, and the celite was washed with additional EtOAc. The filtrate was analyzed by gas chromatography.

Table S7. Effect of Reaction Temperature of Suzuki Selectivity[a]



precatalyst system **A**: P^tBu_3-Pd-G4 (3 mol %)
precatalyst system **B**: $Pd_2(dba)_3$ (0.75 mol %), $Pd(P^tBu_3)_2$ (1.5 mol %)
precatalyst system **C**: $Pd_2(dba)_3$ (1.5 mol %), P^tBu_3 (3 mol %)
precatalyst system **D**: $Pd(OAc)_2$ (3 mol %), P^tBu_3 (3 mol %)
precatalyst system **E**: $Pd(COD)(CH_2TMS)_2$ (3 mol %), P^tBu_3 (3 mol %)

entry	solvent	precatalyst	temperature	trial	**1** (%)	**2a** (%)	**2b** (%)	$\Delta\Delta G^{\ddagger}$
1	THF	**A**	r.t.	1	5	63	<1	>2.4
2	THF	**A**	r.t.	2	23	72	<1	>2.5
3	THF	**A**	r.t.	3	26	68	1	2.5
4	THF	**A**	r.t.	4	25	71	1	2.5
5	THF	**A**	r.t.	5	27	75	1	2.6
6	THF	**A**	r.t.	6	24	79	1	2.6
7	THF	**A**	r.t.	7	20	78	1	2.6
8	THF	**A**	r.t.	8	18	79	1	2.6
9	THF	**A**	r.t.	Average	20	74	<1	>2.5
10	THF	**A**	100 °C	1	9	77	0	>2.6
11	THF	**A**	100 °C	2	10	87	1	2.6
12	THF	**A**	100 °C	Average	10	82	<1	>2.6
13	THF	**B**	r.t.	1	17	79	1	2.6
14	THF	**B**	r.t.	2	16	78	0	2.6
15	THF	**B**	r.t.	Average	17	79	1	2.6
16	THF	**B**	100 °C	1	7	75	<1	>2.6
17	THF	**B**	100 °C	2	5	72	<1	>2.5
18	THF	**B**	100 °C	Average	6	73	<1	>2.5
19	DMF	**A**	r.t.	1	16	9	58	-1.1
20	DMF	**A**	r.t.	2	19	9	61	-1.1
21	DMF	**A**	r.t.	3	24	11	59	-1.0
22	DMF	**A**	r.t.	4	26	11	59	-1.0
23	DMF	**A**	r.t.	5	16	12	66	-1.0
24	DMF	**A**	r.t.	6	20	11	62	-1.0
25	DMF	**A**	r.t.	7	18	9	66	-1.2
26	DMF	**A**	r.t.	8	46	7	46	-1.1
27	DMF	**A**	r.t.	Average	23	10	60	-1.1
28	DMF	**A**	100 °C	1	2	24	29	-0.1
29	DMF	**A**	100 °C	2	3	19	31	-0.3
30	DMF	**A**	100 °C	Average	2	21	30	-0.2
31	DMF	**B**	r.t.	1	17	11	67	-1.1
32	DMF	**B**	r.t.	2	17	11	67	-1.1
33	DMF	**B**	r.t.	Average	17	11	67	-1.1
34	DMF	**B**	100 °C	1	6	33	24	0.2
35	DMF	**B**	100 °C	2	9	34	22	0.3
36	DMF	**B**	100 °C	Average	7	33	23	0.2
37	DMF	**C**	r.t.	1	101	0	1	--
38	DMF	**C**	r.t.	2	75	3	23	-1.2

Table S8 Continued

39	DMF	**C**	r.t.	Average	88	2	12	-1.1
40	DMF	**C**	100 °C	1	10	38	19	0.4
41	DMF	**C**	100 °C	2	42	30	19	0.3
42	DMF	**C**	100 °C	Average	26	34	19	0.3
43	DMF	**D**	r.t.	1	48	1	42	-2.2
44	DMF	**D**	r.t.	2	39	7	44	-1.1
45	DMF	**D**	r.t.	Average	44	4	43	-1.4
46	DMF	**D**	100 °C	1	12	20	18	0.1
47	DMF	**D**	100 °C	2	11	8	14	-0.3
48	DMF	**D**	100 °C	Average	11	14	16	-0.1
49	DMF	**E**	r.t.	1	60	4	33	-1.2
50	DMF	**E**	r.t.	2	39	6	47	-1.2
51	DMF	**E**	r.t.	Average	50	5	40	-1.2
52	DMF	**E**	100 °C	1	9	26	20	0.2
53	DMF	**E**	100 °C	2	9	38	20	0.4
54	DMF	**E**	100 °C	Average	9	32	20	0.3

[a]GC yields calibrated against undecane as an internal standard. [b]Calculated difference in activation barriers to forming products (**2b** – **2a**) based on $\Delta\Delta G^{\ddagger} = RT\ln(\mathbf{2a}/\mathbf{2b})$.

Discussion: In DMF, more reaction at chloride is observed at 100 °C compared to room temperature. However, the 100 °C product ratios vary somewhat depending on precatalyst source. This difference is most prominent for precatalyst system **A** compared to the other precatalyst systems. As shown in Table S6, the change in $\Delta\Delta G^{\ddagger}$ when going from room temperature to 100 °C is smaller for this system than for the other systems.

Table S9. Effect of Reaction Temperature of Suzuki Selectivity[a]

precatalyst	$\Delta\Delta G_{(\mathbf{2b}-\mathbf{2a})}^{\ddagger}$ at r.t.	$\Delta\Delta G_{(\mathbf{2b}-\mathbf{2a})}^{\ddagger}$ at 100 °C	change in $\Delta\Delta G^{\ddagger}$ from r.t. to 100 °C
A	-1.1	-0.2	0.9
B	-1.1	+0.2	1.3
C	-1.1	+0.3	1.4
D	-1.4	-0.1	1.3
E	-1.2	+0.3	1.5

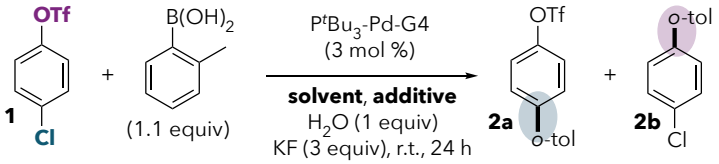
[a]Data are taken from Table S5.

The difference in selectivity between different precatalyst systems at 100 °C is inconsistent with hypotheses that (a) the temperature effect is solely due to entropy (where higher temperature disfavors a bisligated oxidative addition transition state) or (b) that oxidative addition is reversible at this temperature and selectivity is based on thermodynamics or on the rate of a subsequent step of the catalytic cycle. Instead, these observations are consistent with catalyst decomposition at 100 °C leading to a species that favors chloride activation. Different precatalysts may decompose at different rates. However, further study is needed to generate higher quality data to support or refute this hypothesis. In THF, no significant temperature effect is observed with either precatalyst system, and the reaction is selective for chloride at both temperatures.

6. Effect of Additives (Table 6)

General Procedure: Without exclusion of air or moisture, P^tBu_3-Pd-G4 (1.5 mg, 0.0026 mmol, 3 mol %), *o*-tolyl boronic acid (11.0 mg, 0.081 mmol, 1.01 equiv), KF (13.9 mg, 0.24 mmol, 3 equiv), and other additives (0–3 equiv) were combined in a 1-dram vial equipped with a magnetic stir bar. In rapid succession, water (1.4 μL, 0.08 mmol, 1 equiv), 4-chlorophenyl triflate (14 μL, 0.08 mmol, 1 equiv), and solvent (150 μL) were added to the vial and the mixture was immediately sparged with nitrogen for two minutes. The sparging needle and septum was quickly replaced with a PTFE-lined cap and the reaction was stirred vigorously at room temperature for 24 h. Undecane (7.5 μL) was added to the reaction mixture as an internal standard, and the mixture was diluted with EtOAc. A small aliquot was removed and filtered through celite, and the celite was washed with additional EtOAc. The filtrate was analyzed by gas chromatography.

Table S10. Additive Effects[a]



entry	solvent	additive (equiv)	trial	**1** (%)	**2a** (%)	**2b** (%)
1	THF	--	1	5	63	<1
2	THF	--	2	23	72	<1
3	THF	--	3	26	68	1
4	THF	--	4	25	71	1
5	THF	--	5	27	75	1
6	THF	--	6	24	79	1
7	THF	--	7	20	78	1
8	THF	--	8	18	79	1
9	THF	--	Average	20	74	<1
10	THF	18-crown-6 (3)	1	0	2	77
11	THF	18-crown-6 (3)	2	0	1	76
12	THF	18-crown-6 (3)	Average	0	1	76
13[b]	THF	NBu_4F (3)	1	<1	<1	17
14[b]	THF	NBu_4F (3)	2	<1	<1	9
15[b]	THF	NBu_4F (3)	Average	<1	<1	13
16	THF	NBu_4Cl (1)	1	20	4	70
17	THF	NBu_4Cl (1)	2	21	4	69
18	THF	NBu_4Cl (1)	Average	20	4	69
19	THF	NBu_4Br (1)	1	1	4	90
20	THF	NBu_4Br (1)	2	5	1	91
21	THF	NBu_4Br (1)	Average	3	2	91
22	THF	NBu_4OTf (1)	1	27	72	3
23	THF	NBu_4OTf (1)	2	26	67	3
24	THF	NBu_4OTf (1)	Average	26	70	3
25	^{i}PrOH	--	1	4	79	1
26	^{i}PrOH	--	2	1	95	1
27	^{i}PrOH	--	Average	2	87	1
28	^{i}PrOH	18-crown-6 (3)	1	0	0	5
29	^{i}PrOH	18-crown-6 (3)	2	0	0	1
30	^{i}PrOH	18-crown-6 (3)	Average	0	0	3

Table S11 Continued

31	PC	--	1	12	75	5
32	PC	--	2	19	68	6
33	PC	--	Average	15	71	5
34	PC	18-crown-6 (3)	1	5	2	14
35	PC	18-crown-6 (3)	2	5	1	8
36	PC	18-crown-6 (3)	Average	5	1	11
37	DMF	--	1	16	9	58
38	DMF	--	2	19	9	61
39	DMF	--	3	24	11	59
40	DMF	--	4	26	11	59
41	DMF	--	5	16	12	66
42	DMF	--	6	20	11	62
43	DMF	--	7	18	9	66
44	DMF	--	8	46	7	46
45	DMF	--	Average	23	10	60
46	DMF	18-crown-6 (3)	1	0	0	45
47	DMF	18-crown-6 (3)	2	0	0	50
48	DMF	18-crown-6 (3)	Average	0	0	47

[a]GC yields calibrated against undecane as an internal standard. Diarylated product observed in ≤4% yield in all cases except entry 12 (8%). [b]KF was omitted from the reaction mixture.

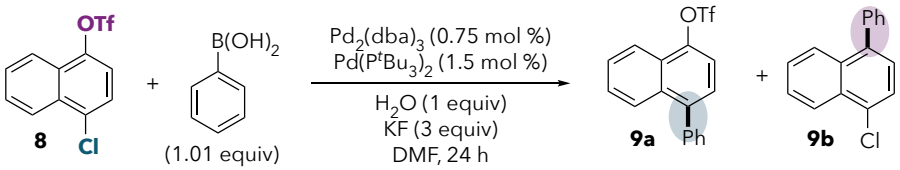
7. Recycling "Decomposed" Catalyst

Hypothesis: The results in Tables 3-5 of the manuscript show that heating either the Stille or Suzuki coupling in DMF leads to increased reaction at chloride. One hypothesis is that, upon heating, the catalyst decomposes to a new catalytically active species that preferentially reacts at chloride. If this is the case, then we would expect that the 'decomposed' catalyst would continue to demonstrate chloride-selectivity when it is recycled. To test this hypothesis, we conducted a Suzuki coupling of **1** at 100 °C for 4 h, then added a second substrate (**8**) and a second boronic acid and stirred for an additional 100 °C at either room temperature or 100 °C (Table S9). In order to interpret the results, it was necessary to establish the baseline selectivity of the Suzuki cross-coupling of **8** at both room temperature and 100 °C (Table S8).

General Procedure for Table S8: In a nitrogen filled glovebox, Pd_2dba_3 (0.5 mg, 0.0006 mmol, 0.75 mol %), $Pd(Pt\text{-}Bu_3)_2$ (0.6 mg, 0.0012 mmol, 1.5 mol %) , and KF (13.9 mg, 0.24 mmol, 3 equiv) were combined in a 1-dram vial equipped with a magnetic stir bar. The vial was sealed with a PTFE-lined cap and removed from the glovebox. Outside of the glovebox, the cap was removed and, in rapid succession, water (1.4 μL, 0.08 mmol, 1 equiv), 4-chlorophenyl triflate (14 μL, 0.08 mmol, 1 equiv), phenylboronic acid (9.9 mg, 0.081 mmol, 1.01 equiv), and DMF (150 μL) were added to the vial and the mixture was immediately sparged with nitrogen for two minutes, then resealed with a PTFE-lined cap. The reaction was stirred vigorously at the indicated temperature for 24 h. Undecane (7.5 μL) was added to the reaction mixture as an internal standard, and the mixture was diluted with EtOAc. A small aliquot was removed and filtered through celite, and the celite was washed with additional EtOAc. The filtrate was analyzed by gas chromatography.

General Procedure for Table S9: In a nitrogen filled glovebox, Pd_2dba_3 (0.5 mg, 0.0006 mmol, 0.75 mol %), Pd(Pt-$Bu_3)_2$ (0.6 mg, 0.0012 mmol, 1.5 mol %) , *o*-tolyl boronic acid (11.0 mg, 0.081 mmol, 1.01 equiv), and KF (13.9 mg, 0.24 mmol, 3 equiv) were combined in a 1-dram vial equipped with a magnetic stir bar. The vial was sealed with a PTFE-lined cap and removed from the glovebox. Outside of the glovebox, the cap was removed and, in rapid succession, water (1.4 μL, 0.08 mmol, 1 equiv), 4-chlorophenyl triflate (14 μL, 0.08 mmol, 1 equiv), and DMF (150 μL) were added to the vial and the mixture was immediately sparged with nitrogen for two minutes, then resealed with a PTFE-lined cap and the reaction stirred vigorously at 100 °C for 4 h. The reaction was allowed to cool to room temperature, then briefly uncapped (~10 seconds) and phenylboronic acid (9.9 mg, 0.081 mmol, 1.01 equiv) and 4-chloronaphthyl triflate (16 μL, 0.08 mmol) were quickly added. The reaction mixture was immediately sparged with nitrogen for two minutes through a septum cap. The sparging needle and septum cap were quickly replaced with a PTFE-lined cap and the reaction was stirred vigorously at the indicated temperature for an additional 24 h. Undecane (7.5 μL) and dodecane (8.0 μL) were added to the reaction mixture as internal standards, and the mixture was diluted with EtOAc. A small aliquot was removed and filtered through celite, and the celite was washed with additional EtOAc. The filtrate was analyzed by gas chromatography.

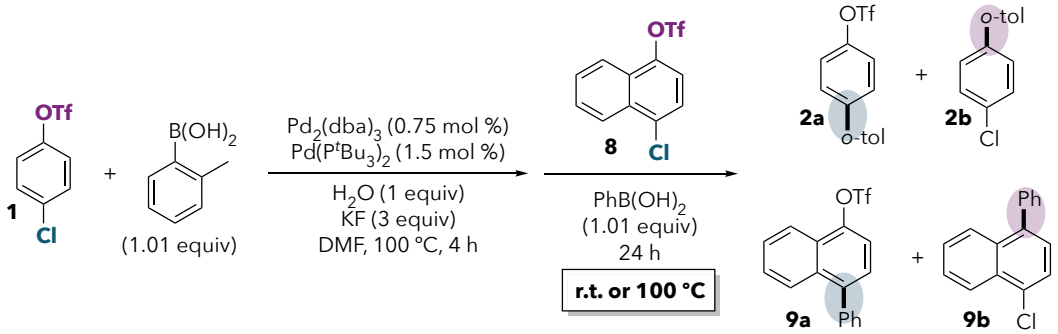
Table S12. Effect of Temperature on Selectivity of Suzuki Coupling of Substrate **8**[a]



entry	temperature	trial	**8** (%)	**9a** (%)	**9b** (%)
1	r.t.	1	7	3	52
2	r.t.	2	16	4	43
3	r.t.	Average	11	4	47
4	100 °C	1	0	1	31
5	100 °C	2	0	2	30
6	100 °C	Average	0	1	30

[a]GC yields calibrated against undecane as an internal standard.

Table S13. Recycling Thermally Decomposed Catalyst[a]



entry	temperature	trial	**1** (%)	**2a** (%)	**2b** (%)	**8** (%)	**9a** (%)	**9b** (%)
1	r.t.	1	19	44	22	87	1	7
2	r.t.	2	25	40	21	89	1	4
3	r.t.	Average	22	42	21	88	1	5
4	100 °C	1	17	29	17	24	22	13
5	100 °C	2	17	40	20	25	29	20
6	100 °C	Average	17	35	18	25	26	17

[a]GC yields calibrated against undecane as an internal standard.

Discussion: As shown in Table S8, substrate **8** does *not* exhibit the same switch in selectivity at 100 °C as seen for substrate **1** in Table 4 of the manuscript. The major product of Suzuki coupling of **8** is **9b**, from reaction at triflate, at both room temperature and at 100 °C. This observation may be rationalized by the higher reactivity of substrate **8**. If Suzuki coupling is fast, then it can outcompete slower decomposition of catalyst. Notably, the mass balance is poor at both temperatures, suggesting that this substrate is prone to decomposition (e.g., by hydrolysis of the triflate).

When the catalyst is recycled, very poor conversion of **8** is observed at room temperature (Table S9, entry 3). Under these conditions, the major product remains the one resulting from triflate activation (**9b**), albeit in only 5% yield. On the other hand, the use of recycled catalyst at 100 °C leads to preferential reaction at chloride, giving **9a** as the major product in 26% yield (entry 6). Critically, this chloride selectivity is different from the triflate-selectivity observed in the high-temperature Suzuki reaction of **8** using fresh catalyst (Table S8, entry 6). A comparison of Table S8, entry 6 and Table S9, entry 6 demonstrates that high temperature alone is *not* sufficient to cause chloride-selective cross-coupling of **8**. Instead, prior heat treatment of the catalyst (hypothesized to cause decomposition) is necessary before chloride-selectivity can be observed.

These results are consistent with the following scenario: Using fresh catalyst, the Suzuki reaction of **8** is fast enough at 100 °C to outcompete catalyst decomposition. Thus, Suzuki coupling of **8** using fresh catalyst favors triflate activation at both room temperature and 100 °C (Table S8). The active catalytic species is expected to be [Pd(P^{t}Bu$_3$)(DMF)] prior to decomposition. Heating to 100 °C for 4 h in the presence of Suzuki coupling reagents (including **1**) leads to decomposition of most of the catalyst to an unidentified species that exhibits chloride

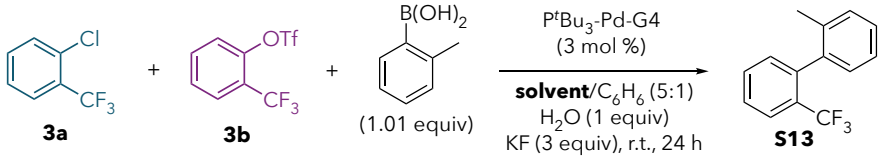
selectivity. When this decomposed catalyst is recycled at room-temperature for the reaction of **8**, poor yield is observed because the decomposed catalyst is not active at low temperature (i.e., the barrier to one or more steps of the catalytic cycle with this catalytic species is too high to be overcome at room temperature). Instead, the small amount of cross-coupling that does occur at room temperature is catalyzed by residual [Pd(P^tBu_3)(DMF)]. However, the decomposed catalyst *is* active at 100 °C, and leads primarily to chloride activation (Table S9, entry 2).

D. Reactions with 3a and 3b

1. Catalytic Suzuki Couplings

General Procedure: Without exclusion of air or moisture, P^tBu_3-Pd-G4 (1.5 mg, 0.0026 mmol, 3 mol %), *o*-tolyl boronic acid (11.0 mg, 0.081 mmol, 1.01 equiv), and KF (13.9 mg, 0.24 mmol, 3 equiv) were combined in a 1-dram vial equipped with a magnetic stir bar. In rapid succession, water (1.4 μL, 0.08 mmol, 1 equiv), 1-chloro-2-trifluoromethylbenzene (6.5 μL, 0.08 mmol, 1 equiv), 2-trifluoromethylphenyl triflate (14.8 μL, 0.08 mmol, 1 equiv), and a 5:1 mixture of solvent:benzene (150 μL) were added to the vial and the mixture was immediately sparged with nitrogen for two minutes. The sparging needle and septum was quickly replaced with a PTFE-lined cap and the reaction was stirred vigorously at room temperature for 24 h. Undecane (7.5 μL) was added to the reaction mixture as an internal standard, and the mixture was diluted with EtOAc. A small aliquot was removed and filtered through celite, and the celite was washed with additional EtOAc. The filtrate was analyzed by gas chromatography.

Table S14. Intermolecular Competition Between **3a** and **3b** in the Catalytic Suzuki Coupling[a]



entry	solvent	trial	**3a** (%)	**3b** (%)	**S13**(%)
1	toluene	1	11	88	91
2	toluene	2	13	92	90
3	toluene	Average	12	90	91
4	THF	1	20	90	86
5	THF	2	20	90	84
6	THF	Average	20	90	85
7	acetone	1	22	82	84
8	acetone	2	13	78	92
9	acetone	Average	17	80	88
10	MeOH	1	3	52	94
11	MeOH	2	2	43	88
12	MeOH	Average	3	48	91
13	MeCN	1	92	18	67
14	MeCN	2	93	17	66
15	MeCN	Average	92	18	66
16	DMF	1	77	11	88
17	DMF	2	79	15	81

Table S15 Continued

37	DMF	Average	78	13	84
19	sulfolane	1	55	61	50
20	sulfolane	2	64	58	37
21	sulfolane	Average	59	60	43
22	PC	1	30	80	75
23	PC	2	26	77	84
24	PC	Average	28	78	79

[a]GC yield calibrated against undecane as an internal standard.

Discussion: The catalytic cross-coupling selectivity shown in Table S10 qualitatively matches the selectivity observed in the stoichiometric oxidative addition studies (Table 3). However, the mass balance is poor in polar solvents. For example, 91% yield of **S13** is observed in MeOH, but 149% of the starting material is consumed (97% of **3a** and 52% of **3b**). The poor mass balance in polar solvents is likely due to hydrolysis of the electron-deficient aryl triflate **3b**.

2. Stoichiometric Oxidative Addition Studies (Table 3)

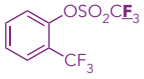
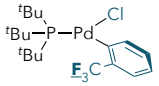
a. 19F NMR Calibrations

Representative Procedure: Inside a nitrogen-filled glovebox, P^tBu_3 (5.5 mg, 0.027 mmol, 1 equiv) was measured into a 1-dram scintillation vial. In a separate vial, a solution was prepared of **3a** (3.6 μL, 0.027 mmol, 1 equiv), **3b** (5.0 μL, 0.027 mmol, 1 equiv), and C_6H_5F (7.6 μL, 0.081 mmol, 3 equiv) in C_6D_6 (100 μL). 500 μL of the indicated solvent was added to the vial containing P^tBu_3, followed by the entire volume of the substrate solution. The vial was capped and shaken briefly, and then the solution was transferred via Pasteur pipette into an NMR tube. The tube was capped tightly, removed from the glovebox, and the sample was immediately analyzed by ^{19}F NMR. The observed ratio of substrate to C_6H_5F signals at this "time=0" was used to define the expected ratios for 100% calibrated yield of recovered substrates in the subsequent intermolecular competition reactions run for 6 h. For **3b**, yields were calculated separately based on each of its two fluorine signals and then averaged together.

b. ^{19}F NMR Chemical Shifts

Peaks corresponding to **3a**, **3b**, and 'free' triflate were assigned by comparison to the spectra of authentic samples of **3a**, **3b**, and NBu_4OTf in 600 μL of a mixture of solvent:C_6D_6 (5:1 v/v). Chemical shifts were referenced to fluorobenzene (set to -113.15 ppm regardless of solvent). The ^{19}F NMR signals corresponding to **S10** were assigned by comparison to the spectra of an authentic sample prepared by a literature procedure and/or by analogy to the published spectral data for this compound and the spectra in other solvents.[4] Relevant chemical shifts in the different solvent mixtures are assigned as follows:

Table S16. ^{19}F Chemical Shifts of Relevant Species by Solvent: *ortho*-CF_3 Substrates

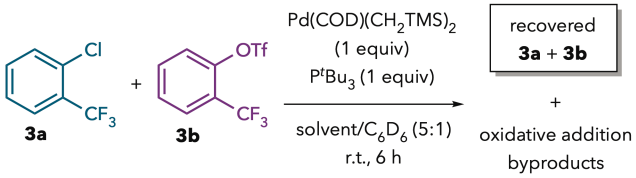
	 **3a**	 **3b**	 **3b**	OTf⁻ anion (NBu_4OTf)	 **S10**
toluene	-62.9	-61.2	-74.7	-78.4	-55.3[b]
THF	-62.2	-60.3	-74.0	-78.1	-54.7[c]
acetone	-61.6	-59.7	-73.5	-77.4	-54.1[c]
MeOH[a]	-61.9	-60.0	-73.6	-78.0	-54.3[b]
MeCN	-61.5	-59.5	-73.1	-77.5	-54.1[b]
DMF	-61.1	-59.4	-73.3	-77.4	-53.9[b]
sulfolane	-59.8	-61.7	-73.5	-80.0	*n.d.*[d]
PC	-59.5	-61.1	-73.1	-77.7	-54.1[c]

[a]In a control reaction in this solvent in the absence of palladium, a small amount of decomposition of **3b** to form 2-$CF_3C_6H_4OH$ and free OTf was observed. [b]Chemical shift was identified by analysis of the authentic material, prepared by a literature procedure,[4] in the indicated solvent. [c]Chemical shift was identified in the oxidative addition reactions by analogy to the chemical shift observed of this compound in other solvents. [d]n.d. = not determined.

c. Oxidative Addition Reactions

Representative Procedure: Inside a nitrogen-filled glovebox, P^tBu_3 (5.5 mg, 0.027 mmol, 1 equiv) and $Pd(COD)(CH_2TMS)_2$ (10.5 mg, 0.027 mmol, 1 equiv) were combined in a 1-dram vial equipped with a stir bar. In a separate vial, a solution was prepared of **3a** (3.6 μL, 0.027 mmol, 1 equiv), **3b** (5.0 μL, 0.027 mmol, 1 equiv), and C_6H_5F (7.6 μL, 0.081 mmol, 3 equiv) in C_6D_6 (100 μL). 500 μL of the indicated solvent was added to the vial containing P^tBu_3 and $Pd(COD)(CH_2TMS)_2$, followed by the entire volume of the substrate solution. The vial was sealed with a PTFE-lined cap and the reaction was allowed to stir for 6 h at room temperature. The reaction mixture was transferred via Pasteur pipette into an NMR tube. The tube was capped tightly, removed from the glovebox, and immediately analyzed by ^{19}F NMR.

Table S17. Stoichiometric oxidative addition reactions of **3a** and **3b**.



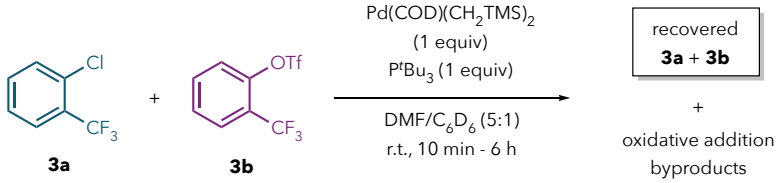
entry	solvent	trial	recovered (%)[a] **3a**	**3b**	reacted **3a** : **3b**
1	toluene	1	90	≥99	≥ 10 : 1
2	toluene	2	89	≥99	≥ 11 : 1
3	toluene	Average	89	≥99	≥ 11 : 1
4[b]	toluene	1	64	≥99	≥ 36 : 1
5[b]	toluene	2	40	91	7 : 1
6[b]	toluene	Average	52	98	24 : 1
7	THF	1	61	≥99	≥39 : 1
8	THF	2	52	≥99	≥48 : 1
9	THF	3	51	92	6 : 1
10	THF	Average	55	97	15 : 1
11	acetone	1	69	91	3 : 1

Table S18 Continued

12	acetone	2	73	≥99	≥27 : 1
13	acetone	Average	71	98	15 : 1
14	MeOH	1	66	≥99	≥36 : 1
15	MeOH	2	74	≥99	≥26 : 1
16	MeOH	Average	70	≥99	≥30 : 1
17	MeCN	1	94	0	1 : 16
18	MeCN	2	96	3	1 : 24
19	MeCN	3	≥99	0	≤1 : 100
20	MeCN	4	≥99	0	≤1 : 100
21	MeCN	Average	97	1	1 : 33
22	DMF	1	88	57	1 : 4
23	DMF	2	87	57	1 : 3
24	DMF	3	76	33	1 : 3
25	DMF	4	63	29	1 : 2
26	DMF	Average	78	44	1 : 3
27	sulfolane	1	82	93	3 : 1
28	sulfolane	2	90	98	5 : 1
29	sulfolane	Average	86	95	3 : 1
30	PC[c]	1	74	93	4 : 1
31	PC[c]	2	79	95	4 : 1
32	PC[c]	3	98	97	1 : 2
33	PC[c]	4	80	92	3 : 1
34	PC[c]	Average	83	94	3 : 1
35[d]	MeCN	1	>99	≥99	--
36[d]	DMF	1	>99	≥99	--
37[e]	MeCN	1	n.a.	5	--
38[e]	MeCN	2	n.a.	3	--
39[e]	MeCN	3	n.a.	0	--
40[e]	MeCN	Average	n.a.	3	--
41[e]	DMF	1	n.a.	23	--
42[e]	DMF	2	n.a.	25	--
43[e]	DMF	3	n.a.	36	--
44[e]	DMF	Average	n.a.	28	--
45	Toluene-d_8	1	74	97	9 : 1
46	Toluene-d_8	2	85	≥99	≥15 : 1
47	Toluene-d_8	Average	79	98	11 : 1
48	MeCN-d_3	1	87	0	1 : 8
49	MeCN-d_3	2	87	1	1 : 8
50	MeCN-d_3	Average	87	1	1 : 8
51	DMF-d_7	1	91	40	1 : 7
52	DMF-d_7	2	93	52	1 : 7
53	DMF-d_7	Average	92	46	1 : 7
54[f]	DMF	1	36	34	1 : 1
55[f]	DMF	2	47	45	1 : 1
56[f]	DMF	Average	42	39	1 : 1
57[g]	DMF	1	94	86	1 : 2
58[g]	DMF	2	98	83	1 : 8
59[g]	DMF	Average	96	83	1 : 4

[a] ^{19}F NMR yields calibrated against C_6H_5F as an internal standard. [b]Heated to 80 °C for 2 h. [c]PC = propylene carbonate. [d]Pd(COD)(CH_2TMS)$_2$ was omitted from the reaction mixture. [e]**3a** was omitted from the reaction mixture (n.a. = not applicable). [f] Heated at 100°C. [g]Cooled to 0 °C.

Table S19. Stoichiometric oxidative addition reactions of **3a** and **3b** in DMF tracked over time.[a]



entry	time	recovered (%)[b] **3a**	**3b**	reacted **3a** : **3b**
1	10 min	99	94	1 : 3
2	20 min	≥99	95	<1 : 5
3	30 min	99	93	1 : 7
4	1 h	98	88	1 : 6
5	3 h	98	82	1 : 9
6	6 h	97	74	1 : 9

[a]The reaction setup differed from the Representative Procedure in that the reaction was run in an NMR tube (without stirring) instead of in a vial with a stir bar. [b] ^{19}F NMR yields calibrated against C_6H_5F as an internal standard.

Analysis of Variable Temperature and Time Studies for the Reaction in DMF

Three main signals are observed in the ^{31}P NMR spectrum of the DMF reaction after 6 h at room temperature: 85 ppm [assigned to $Pd(P^tBu_3)_2$], ~75 ppm, and 53 ppm (assigned to cationic HP^tBu_3). At 0 °C, the phosphonium signal is absent, but there is an additional signal at ~64 ppm. Finally, at 100 °C there are around a dozen signals. One small signal corresponds to $Pd(P^tBu_3)_2$, but none of the other signals match those seen at r.t. or 0 °C. Figure S5 illustrates the ^{31}P NMR spectra of these reactions, which correspond to entries 26, 56, and 59 in Table S12. The signals at ~74 and ~64 are tentatively assigned as products resulting from oxidative addition of aryl triflate **3b**. The following observations are worth noting:

- The signal at 64 ppm is observable within 10 minutes at room temperature (Table S13 and Figure S6), but is slowly replaced by the signal at 74 ppm. By 3 h reaction time, the 64 ppm signal is gone but the 74 ppm signal remains at 6 h.
- The signal at 64 ppm is detected even at 6 h when the reaction is run at cold temperature (0 °C).
- The signal at 74 ppm is detected even in the absence of **3a**, so it is not derived from **3a**.

Two signals in the ^{19}F NMR spectra for the time studies in DMF display a pattern of growth and disappearance that matches those of the signals in the ^{31}P NMR spectra. These are labeled in Figure S7 with the same labels used in Figure S6.

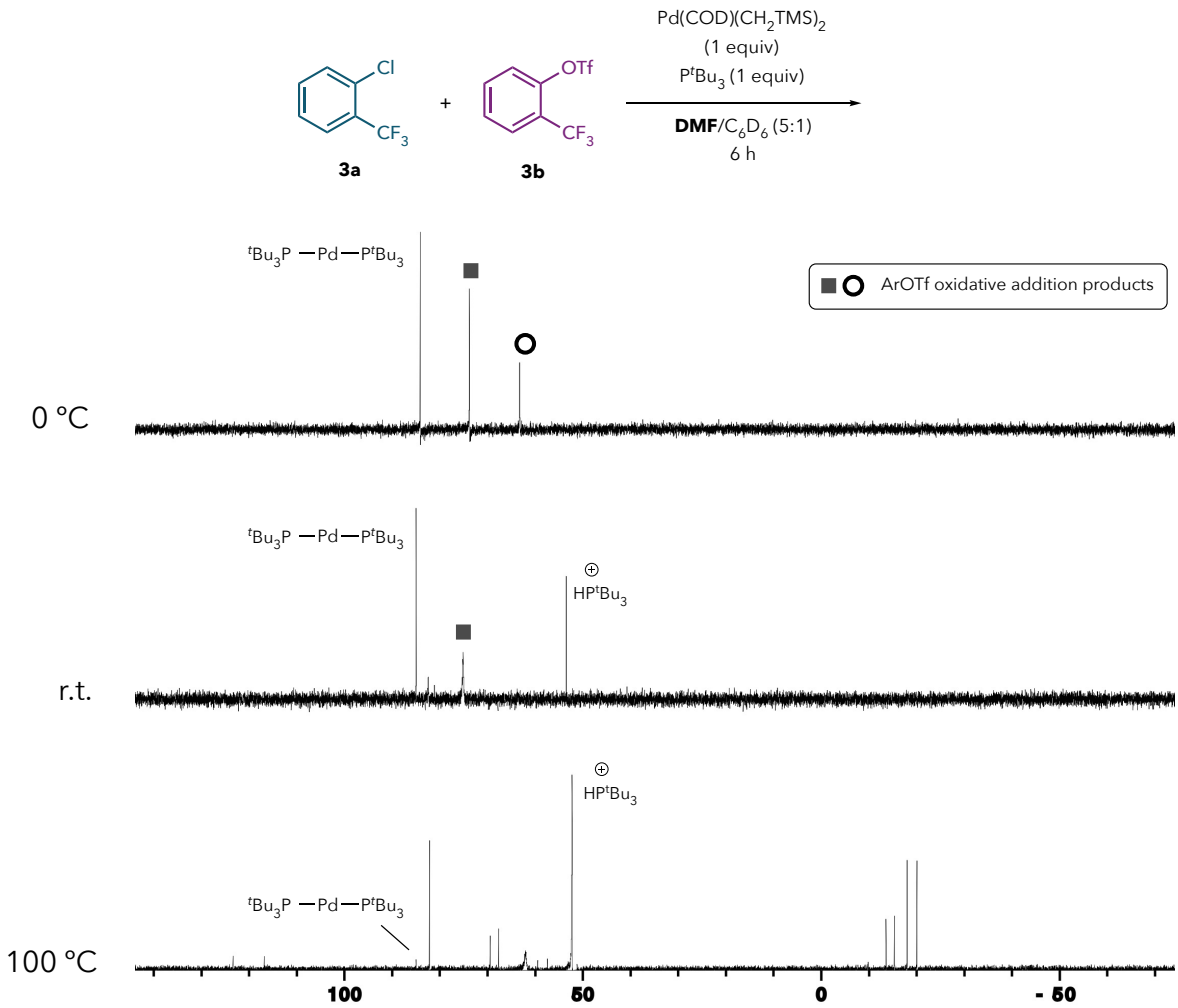


Figure S5. Stacked ^{31}P NMR spectra for the reaction of **3a** and **3b** in DMF at three temperatures.

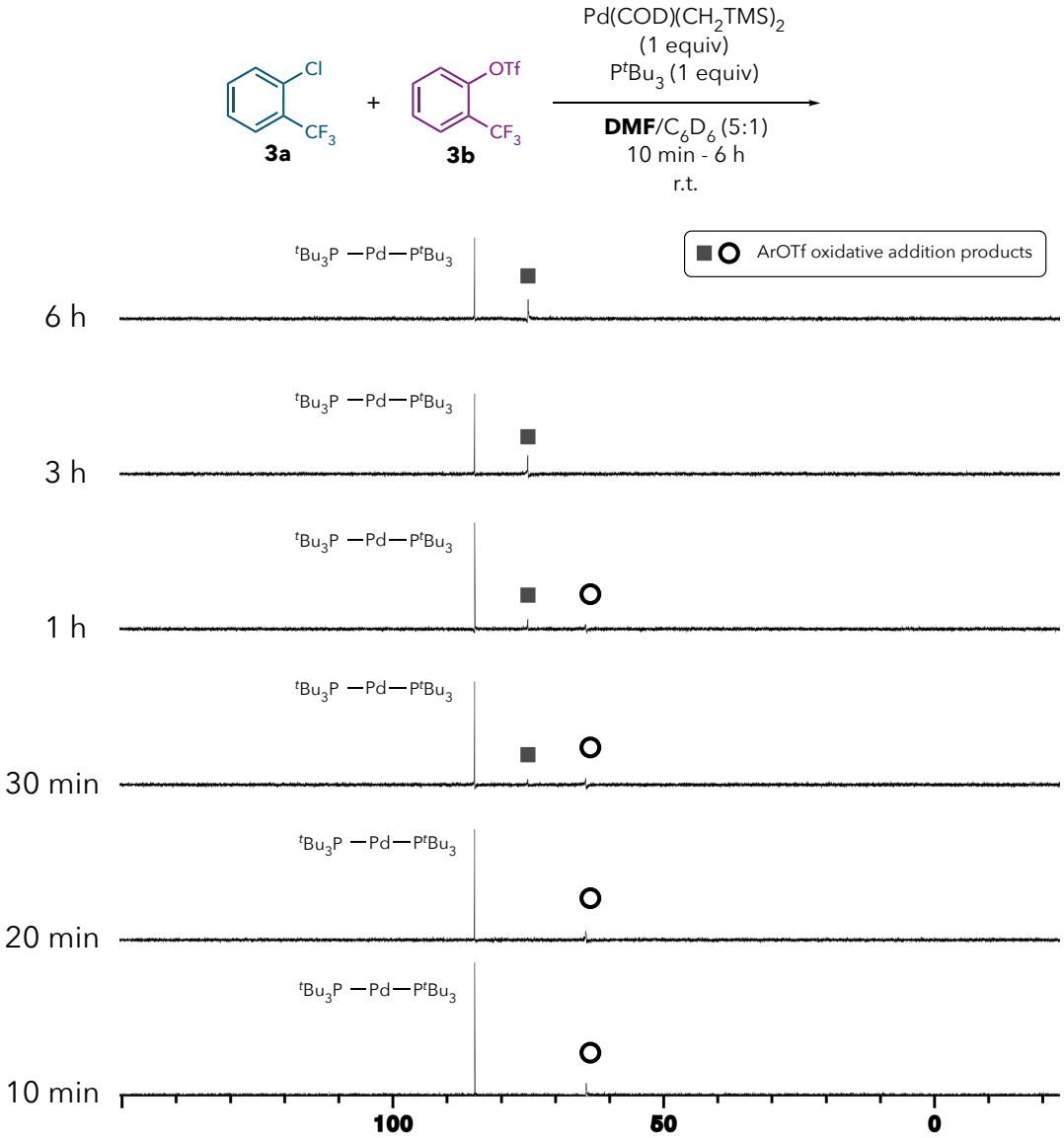


Figure S6. Stacked ^{31}P NMR spectra for the reaction of **3a** and **3b** tracked over time.

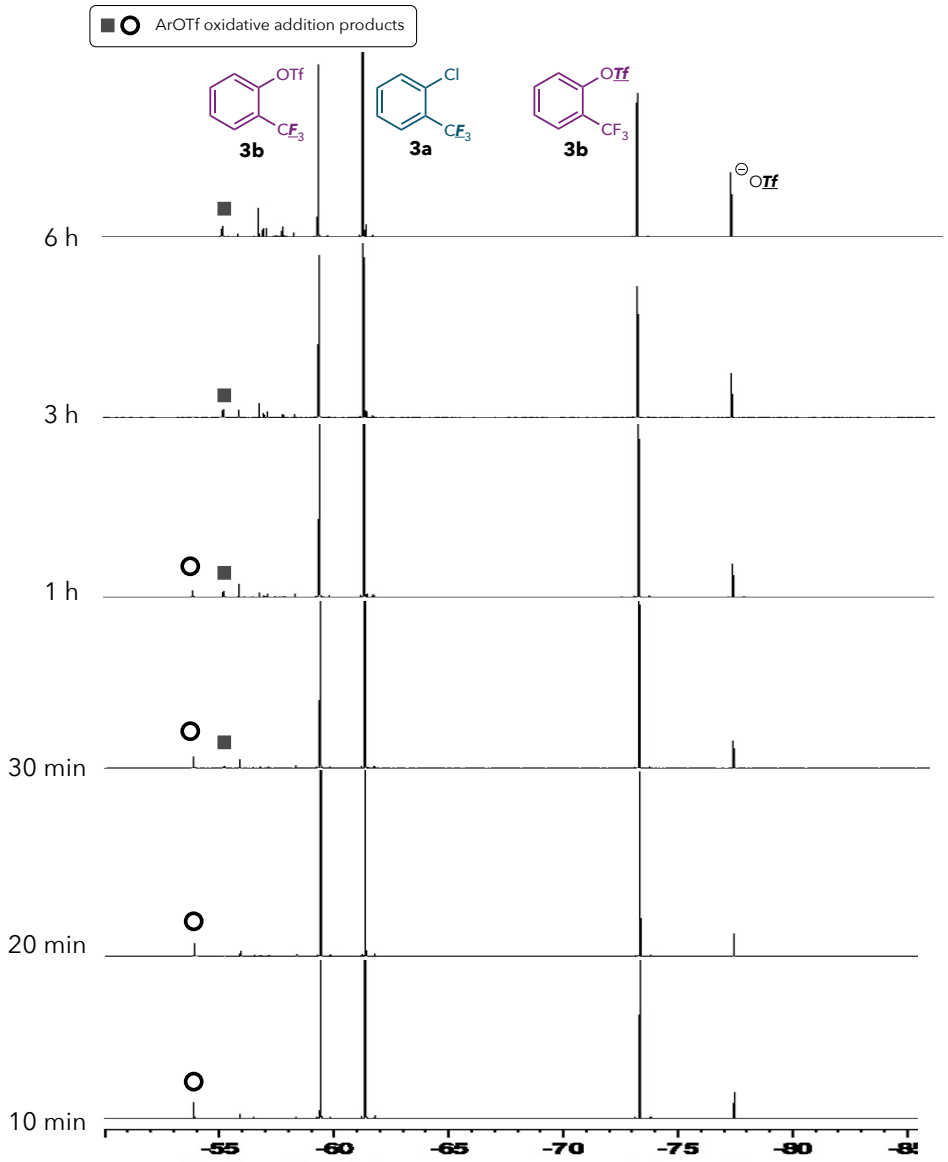
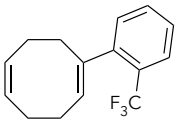


Figure S7. Stacked ^{19}F NMR spectra for the reaction of **3a** and **3b** tracked over time.

See pages S91-S135 for additional representative NMR spectra corresponding to the stoichiometric experiments with **3a** and **3b** (spectra are provided for a single replicate of each experiment, although most experiments were repeated multiple times).

Analysis of Decomposition Products of Oxidative Addition Adducts

The stoichiometric reaction of **3a** and **3b** was repeated in deuterated toluene, acetonitrile, and DMF (i.e., repeats of entries 3, 21, and 26 of Table S12 using deutero instead of protio solvents). The results were analyzed by ^{1}H NMR as well as by GCMS. The primary compounds detected by GCMS have m/z = 252, which is consistent with Heck coupling products resulting from reaction of Pd(Ar) oxidative addition adducts with COD. Indeed, ^{1}H NMR reveals the presence of alkene signals that do not correspond to COD itself (see S92, S102, and S107).



and isomers
Exact Mass: 252.11

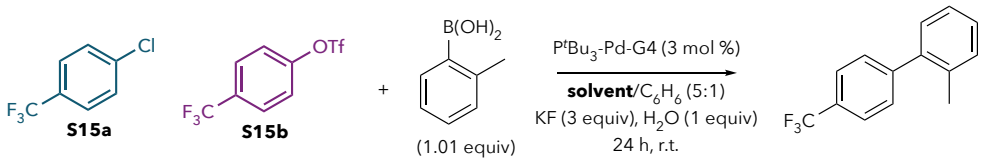
GCMS was also used to analyze the reactions of the stoichiometric oxidative additions performed in THF and propylene carbonate (PC). Heck products were detected in THF but not in PC.

E. Reactions with S15a and S15b

1. Catalytic Suzuki Couplings

General Procedure: Without exclusion of air or moisture, P^tBu_3-Pd-G4 (1.5 mg, 0.0026 mmol, 3 mol %), *o*-tolyl boronic acid (11.0 mg, 0.081 mmol, 1.01 equiv), and KF (13.9 mg, 0.24 mmol, 3 equiv) were combined in a 1-dram vial equipped with a magnetic stir bar. In rapid succession, water (1.4 μL, 0.08 mmol, 1 equiv), 1-chloro-4-trifluoromethylbenzene (10.8 μL, 0.08 mmol, 1 equiv), 4-trifluoromethylphenyl triflate (14.8 μL, 0.08 mmol, 1 equiv), and a 5:1 mixture of solvent:benzene (150 μL) were added to the vial and the mixture was immediately sparged with nitrogen for two minutes. The sparging needle and septum was quickly replaced with a PTFE-lined cap and the reaction was stirred vigorously at room temperature for 24 h. Undecane (7.5 μL) was added to the reaction mixture as an internal standard, and the mixture was diluted with EtOAc. A small aliquot was removed and filtered through celite, and the celite was washed with additional EtOAc. The filtrate was analyzed by gas chromatography.

Table S20. Intermolecular Competition Between **S15a** and **S15b** in the Catalytic Suzuki Coupling[a]



entry	trial	solvent	recovered **S15a** (%)	recovered **S15b** (%)	total conversion **S15a** + **S15b** (%)	reacted **S15a** : **S15b**
1	1	THF	18	89	92	7.7 : 1
2	2	THF	2	88	110	8.3 : 1
3	average	THF	10	89	101	8.0 : 1
4	1	MeCN	68	1	131	1 : 3.1
5	2	MeCN	53	1	147	1 : 2.1
6	average	MeCN	60	1	139	1 : 2.5
7	1	DMF	60	48	92	1 : 1.3
8	2	DMF	58	52	90	1 : 1.2
9	average	DMF	59	50	91	1 : 1.2
10	1	PC	4	61	135	2.4 : 1
11	2	PC	7	64	129	2.6 : 1
12	average	PC	6	62	132	2.5 : 1

[a]GC yield calibrated against undecane as an internal standard.

Discussion: The catalytic cross-coupling selectivities shown in Table S14 qualitatively match the selectivity observed in the stoichiometric oxidative additions and catalytic couplings of **3a**/**3b** and **1**. However, it is clear that one or both of the substrates is decomposing in a non-productive pathway based on the >100% conversion observed in some cases. Hydrolysis of the electron-deficient aryl triflate **S15b** is likely taking place.

2. Stoichiometric Oxidative Addition Studies

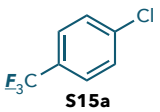
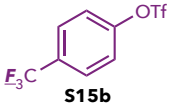
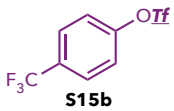
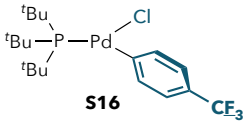
a. ^{19}F NMR Calibrations

Representative Procedure: Inside a nitrogen-filled glovebox, P^tBu_3 (5.5 mg, 0.027 mmol, 1 equiv) was measured into a 1-dram scintillation vial. In a separate vial, a solution was prepared of **S15a** (3.6 μL, 0.027 mmol, 1 equiv), **S15b** (5.0 μL, 0.027 mmol, 1 equiv), and C_6H_5F (7.6 μL, 0.081 mmol, 3 equiv) in C_6D_6 (100 μL). 500 μL of the indicated solvent was added to the vial containing P^tBu_3, followed by the entire volume of the substrate solution. The vial was capped and shaken briefly, and then the solution was transferred via Pasteur pipette into an NMR tube. The tube was capped tightly, removed from the glovebox, and the sample was immediately analyzed by ^{19}F NMR. The observed ratio of substrate to C_6H_5F signals at this "time=0" was used to define the expected ratios for 100% calibrated yield of recovered substrates in the subsequent intermolecular competition reactions run for 6 h. For **S15b**, yields were calculated separately based on each of its two fluorine signals and then averaged together.

b. ^{19}F NMR Chemical Shifts

Peaks corresponding to **S15a**, **S15b**, and unbound triflate were assigned by comparison to the spectra of authentic samples of **S15a**, **S15b**, and NBu_4OTf in 600 μL of a mixture of solvent:C_6D_6 (5:1 v/v). Chemical shifts were referenced to fluorobenzene (set to -113.15 ppm regardless of solvent). The ^{19}F NMR signals corresponding to the putative complex **S16** were assigned by comparison to the spectra obtained by reacting **S15a** in the absence of **S15b** in THF. Relevant chemical shifts in the different solvent mixtures are assigned as follows:

Table S21. ^{19}F Chemical Shifts of Relevant Species by Solvent: *para*-CF_3 Substrates [a]

	 **S15a**	 **S15b**	 **S15b**	OTf- anion (NBu_4OTf)	 **S16**
THF	-62.3	-62.3	-73.2	-78.2	-62.8[b]
MeCN	-61.5	-61.6	-72.2	-77.6	-60.9[b]
DMF	-61.4	-61.4	-72.6	-77.4	n.d.
PC	-61.4	-61.5	-72.3	-77.7	-60.7[b]

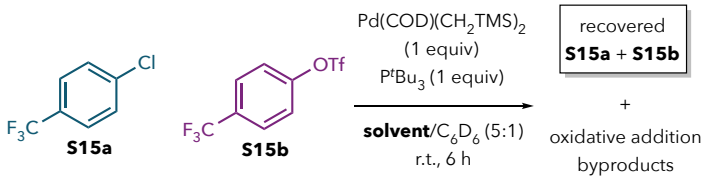
[a]The chemical shifts of the Ar-CF_3 groups of **S15a** and **S15b** are very close. In each of the 4 solvents examined, the ^{19}F signal for **S15a** is slightly further downfield than **S15b**. n.d. = not determined. [b]Tentative assignment; the chemical shift of **S16** was assigned by analogy to **S10** and by corroboration with ^{31}P NMR.

c. Oxidative Addition Reactions

Representative Procedure: Inside a nitrogen-filled glovebox, P^tBu_3 (5.5 mg, 0.027 mmol, 1 equiv) and $Pd(COD)(CH_2TMS)_2$ (10.5 mg, 0.027 mmol, 1 equiv) were combined in a 1-dram vial equipped with a stir bar. In a

separate vial, a solution was prepared of **S15a** (3.6 μL, 0.027 mmol, 1 equiv), **S15b** (5.0 μL, 0.027 mmol, 1 equiv), and C_6H_5F (7.6 μL, 0.081 mmol, 3 equiv) in C_6D_6 (100 μL). 500 μL of the indicated solvent was added to the vial containing P^tBu_3 and $Pd(COD)(CH_2TMS)_2$, followed by the entire volume of the substrate solution. The vial was sealed with a PTFE-lined cap and the reaction was allowed to stir for 6 h at room temperature. The reaction mixture was transferred via Pasteur pipette into an NMR tube. The tube was capped tightly, removed from the glovebox, and immediately analyzed by ^{19}F NMR.

Table S22. Solvent effect on selective of stochiometric oxidative addition



entry	trial	solvent	recovered (%)[a] **S15a**	recovered (%)[a] **S15b**	total conversion **S15a** + **S15b** (%)	reacted **S15a** : **S15b**
1	1	THF	50	>99	50	> 50 : 1
2	2	THF	28	99	72	>72 : 1
3	Average	THF	39	>99	61	>61 : 1
4	1	MeCN	71	7	122	1 : 3
5	2	MeCN	51	9	140	1 : 2
6	Average	MeCN	61	8	131	1 : 2
7	1	DMF	62	14	124	1 : 2
8	2	DMF	50	11	139	1 : 2
9	Average	DMF	56	13	131	1 : 2
10	1	PC[b]	52	98	50	24 : 1
11	2	PC[b]	51	91	60	6 : 1
12	Average	PC[b]	51	95	54	10 : 1
13[c]	1	DMF	>99	>99	<1	--
14[c]	1	MeCN	89	>99	11	>11 : 1
15[c]	2	MeCN	93	95	12	1 : 1
16[c]	Average	MeCN	91	>99	9	> 9 : 1
17[c,d]	1	MeCN	97	96	7	1 : 1
18[c,d]	2	MeCN	85	97	18	5 : 1
19[c,d]	Average	MeCN	91	97	12	3 : 1
20[d]	1	MeCN	89	35	76	1 : 6
21[d]	2	MeCN	87	18	95	1 : 6
22[d]	Average	MeCN	88	27	85	1 : 6

[a] ^{19}F NMR yields calibrated against C_6H_5F as an internal standard. [b]PC = propylene carbonate. [c]$Pd(COD)(CH_2TMS)_2$ was omitted from the reaction mixture. [d]Reaction time = 1 h.

Discussion: The selectivities shown in Table S16 qualitatively match the selectivity observed in the stoichiometric oxidative additions of **3a**/**3b** and **1**. However, more reaction of chloride (**S15a**) is observed in MeCN (entry 6) than expected based on the results with **3a**/**3b** (i.e., the selectivity in MeCN appears much worse for the *p*-CF_3 substrates compared to the *o*-CF_3 substrates). The selectivity is better at shorter reaction time (1 h, entry 22). On closer examination it appears that the substrates, especially **S15a**, undergo a background reaction in the absence of

palladium (see entries 14-19). The ^{31}P NMR spectra reveals at least 2 new signals (Figure S8), suggesting that the substrate(s) can react with P^tBu_3, a process that is apparently hindered by *ortho* substituents in **3a** and **3b** (comparable signals are never detected in the reactions of **3a** and **3b**).

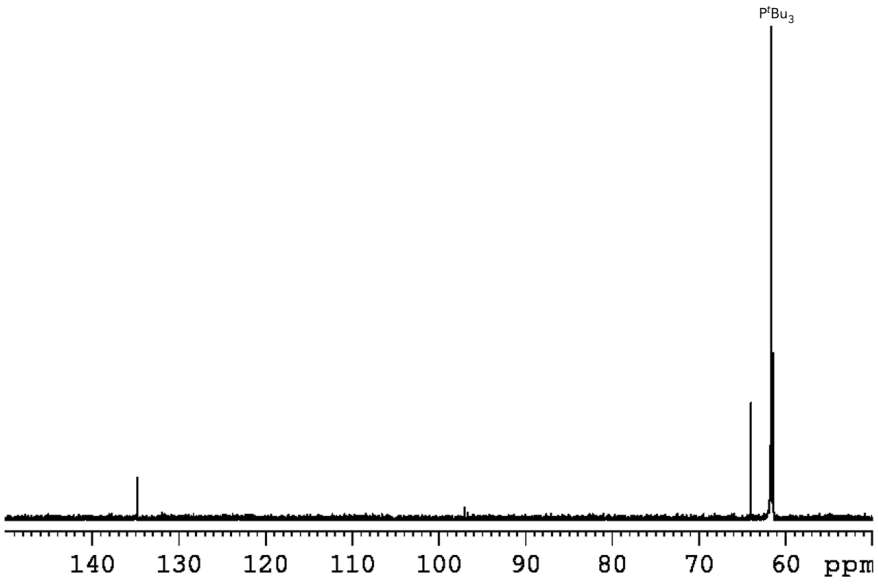


Figure S8. ^{31}P NMR spectrum of Pd-free control reaction of **S15a** + **S15b** with P^tBu_3 in MeCN.

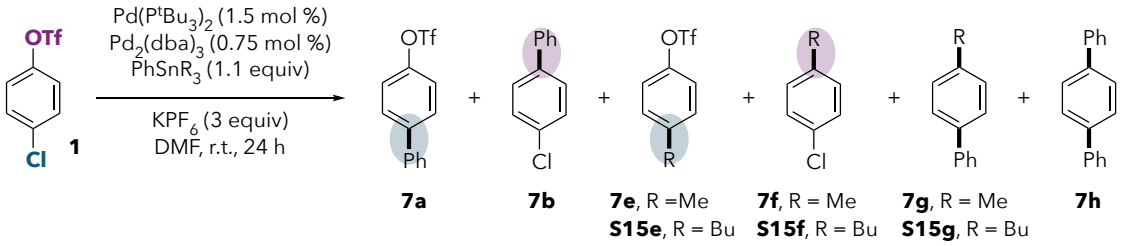
See pages S144-S153 for the NMR spectra corresponding to the experiments in Table S16.

F. Stille Cross-Couplings

1. Reactions of 1 (Scheme 3)

In a nitrogen filled glovebox, Pd_2dba_3 (0.5 mg, 0.0006 mmol, 0.75 mol %), $Pd(PtBu_3)_2$ (0.6 mg, 0.0012 mmol, 1.5 mol %), and KPF_6 (44.2 mg, 0.24 mmol, 3 equiv) were combined in a 1-dram vial equipped with a magnetic stir bar. Trialkylphenyl stannane (0.088 mmol, 1.1 equiv), **1** (14 μL, 0.08 mmol, 1 equiv), and DMF (150 μL) were added. The vial was immediately sealed with a PTFE-lined cap and removed from the glovebox, and the reaction was stirred at the indicated temperature for 24 h. Dodecane (8.0 μL) was added to the reaction mixture as an internal standard, and the mixture was diluted with EtOAc. A small aliquot was removed and filtered through celite, and the celite was washed with additional EtOAc. The filtrate was analyzed by gas chromatography. (Safety Note: Organostannanes and their byproducts are toxic and should be handled in a fumehood or glovebox. For reactions utilizing fluoride bases, quenching crude reaction mixtures via acidification[20] prior to disposal is undesirable due to the additional hazard of generating hydrogen fluoride.)

Table S23. Base-Free Stille Coupling of **1**[a]



S15g *was identified based on MS but has not been isolated.* ***S15e*** *and* ***S15f*** *are hypothetical and were not detected.*

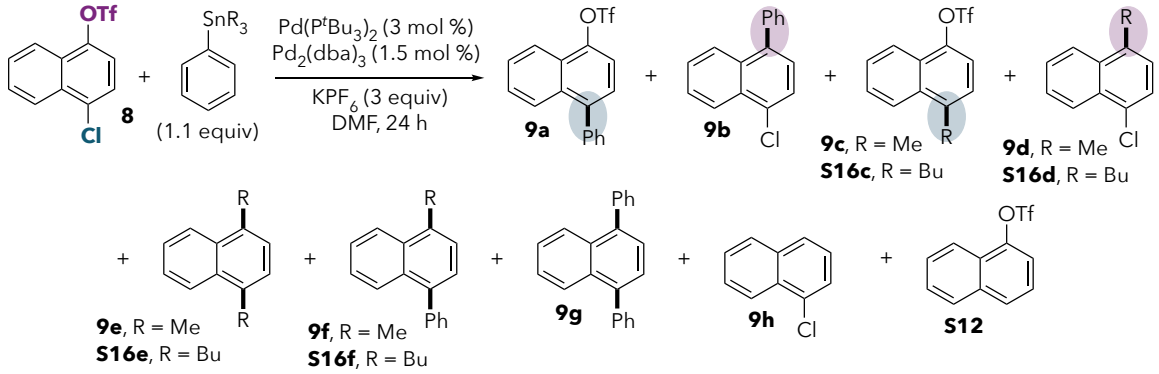
entry	Trial	R	temperature	**1** (%)	**7a** (%)	**7b** (%)	**e** (%)	**f** (%)	**g** (%)	**7h** (%)
1	1	*n*-Bu	r.t.	86	5	4	n.d.	n.d.	trace	0
2	2	*n*-Bu	r.t.	80	4	4	n.d.	n.d.	trace	0
3	Average	*n*-Bu	r.t.	83	5	4	n.d.	n.d.	trace	0
4	1	*n*-Bu	100 °C	71	14	2	n.d.	n.d.	trace	0
5	2	*n*-Bu	100 °C	76	14	2	n.d.	n.d.	trace	0
6	Average	*n*-Bu	100 °C	74	14	2	n.d.	n.d.	trace	0
7	1	Me	r.t.	87	2	4	2	2	2	0
8	2	Me	r.t.	80	3	4	2	3	2	0
9	Average	Me	r.t.	83	2	4	2	3	2	0
10	1	Me	100 °C	7	42	5	20	4	4	5
11	2	Me	100 °C	1	36	4	21	4	6	7
12	Average	Me	100 °C	4	39	3	20	4	5	6

[a]GC yields calibrated against dodecane as an internal standard. Trace = a minor signal with the expected mass for this compound was detected by GCMS, although no authentic material was available for calibration. n.d. = not detected by GCMS.

2. Reactions of 8 (Table 5)

General Procedure: In a nitrogen filled glovebox, Pd_2dba_3 (1.1 mg, 0.0012 mmol, 1.5 mol %), $Pd(P^tBu_3)_2$ (1.2 mg, 0.0024 mmol, 3.0 mol %), and KPF_6 (44.2 mg, 0.24 mmol, 3 equiv) were combined in a 1-dram vial equipped with a magnetic stir bar. Trialkylphenyl stannane (0.088 mmol, 1.1 equiv), **8** (16 μL, 0.08 mmol, 1 equiv), and DMF (150 μL) were added. The vial was immediately sealed with a PTFE-lined cap and removed from the glovebox, and the reaction was stirred at the indicated temperature for 24 h. Undecane (7.5 μL) was added to the reaction mixture as an internal standard, and the mixture was diluted with EtOAc. A small aliquot was removed and filtered through celite, and the celite was washed with additional EtOAc. The filtrate was analyzed by gas chromatography.

Table S24. Base-Free Stille Coupling of **8**[a]



S16c *and* ***S16f*** *were identified based on MS but have not been isolated.* ***S16d*** *and* ***S16e*** *are hypothetical and were not detected.*

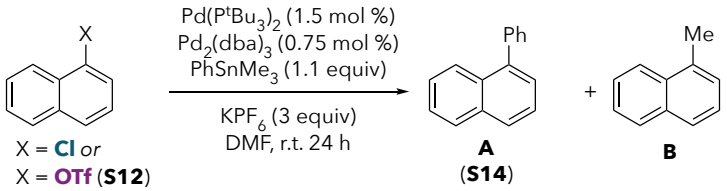
entry	trial	R	temperature	**8** (%)	**9a** (%)	**9b** (%)	**c** (%)	**d** (%)	**e** (%)	**f** (%)	**9g** (%)	**9h** (%)	**S12** (%)
1	1	*n*-Bu	r.t.	79	4	5	trace	n.d.	n.d.	trace	1	1	<1
2	2	*n*-Bu	r.t.	80	4	5	trace	n.d.	n.d.	trace	1	1	<1
3	Average	*n*-Bu	r.t.	80	4	5	trace	n.d.	n.d.	trace	1	1	<1
4	1	*n*-Bu	100 °C	15	19	11	trace	n.d.	n.d.	trace	10	1	<1
5	2	*n*-Bu	100 °C	39	30	8	trace	n.d.	n.d.	trace	4	1	<1
6	Average	*n*-Bu	100 °C	27	25	10	trace	n.d.	n.d.	trace	7	1	<1
7	1	Me	r.t.	24	1	10	3	39	1	1	1	1	<1
8	2	Me	r.t.	24	1	9	3	37	1	1	1	1	<1
9	Average	Me	r.t.	24	1	9	3	42	1	1	1	1	<1
10	1	Me	100 °C	2	14	5	31	12	2	8	8	1	<1
11	2	Me	100 °C	1	13	4	35	12	1	9	9	1	<1
12	Average	Me	100 °C	1	13	4	33	12	1	8	9	1	<1
13[b]	1	Me	r.t.	11	1	12	4	54	12	1	1	8	<1
14[b]	2	Me	r.t.	11	2	12	4	50	13	1	1	4	<1
15[b]	Average	Me	r.t.	11	1	12	4	52	12	1	1	6	<1

[a]GC yields calibrated against undecane as an internal standard. Average of two runs. Trace = a minor signal with the expected mass for this compound was detected by GCMS, although no authentic material was available for calibration. n.d. = not detected by GCMS. [b]KPF_6 was omitted from the reaction mixture.

3. Independent Reactions of an Aryl Chloride and an Aryl Triflate

General Procedure: In a nitrogen filled glovebox, Pd_2dba_3 (0.5 mg, 0.0006 mmol, 0.75 mol %), $Pd(P^tBu_3)_2$ (0.6 mg, 0.0012 mmol, 1.5 mol %), and KPF_6 (44.2 mg, 0.24 mmol, 3 equiv) were combined in a 1-dram vial equipped with a magnetic stir bar. Trimethylphenyl stannane (16 μL, 0.088 mmol, 1.1 equiv), 1-substituted naphthalene substrate (0.08 mmol, 1 equiv), and DMF (150 μL) were added. The vial was immediately sealed with a PTFE-lined cap and removed from the glovebox, and the reaction was stirred at the indicated temperature for 24 h. Undecane (7.5 μL) was added to the reaction mixture as an internal standard, and the mixture was diluted with EtOAc. A small aliquot was removed and filtered through celite, and the celite was washed with additional EtOAc. The filtrate was analyzed by gas chromatography.

Table S25. Stille Cross-Couplings of 1-Chloronaphthalene and **S12** Tracked Over Time[a]



entry	X	temp (°C)	time (h)	**A** (%)	**B** (%)	**ratio A/B**	**total product (A+B)**
1	**Cl**	r.t.	2	2	0	--	2
2	**Cl**	r.t.	4	2	0	--	2
3	**Cl**	r.t.	8	2	1	2.0	3
4	**Cl**	r.t.	16	3	2	1.5	5
5	**Cl**	r.t.	24	3	3	1.0	6
6	**Cl**	100	2	35	31	1.1	66
7	**Cl**	100	4	42	34	1.2	76
8	**Cl**	100	8	36	35	1.0	71
9	**Cl**	100	16	42	31	1.4	73
10	**Cl**	100	24	45	37	1.2	82
11	**OTf**	r.t.	2	3	2	1.5	5
12	**OTf**	r.t.	4	3	3	1.0	6
13	**OTf**	r.t.	8	5	6	0.8	11
14	**OTf**	r.t.	16	9	11	0.8	20
15	**OTf**	r.t.	24	10	11	0.9	21
16	**OTf**	100	2	44	38	1.2	82
17	**OTf**	100	4	44	37	1.2	81
18	**OTf**	100	8	51	40	1.3	91
19	**OTf**	100	16	50	39	1.3	89
20	**OTf**	100	24	47	42	1.1	89

[a]GC yields calibrated against undecane as an internal standard. Results of a single trial.

Discussion: The results suggest that an aryl triflate reacts with faster initial rate than an aryl chloride at both room temperature and at 100 °C in the base-free Stille cross-coupling in DMF. There is no clear trend in the ratio of phenylation versus methylation.

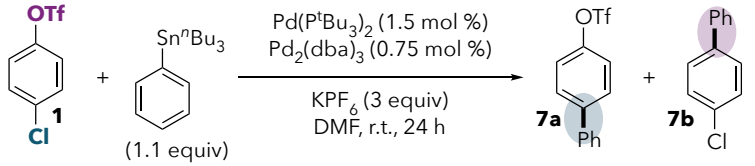
4. Efforts to Reproduce Literature[21] Results for the Base-Free Stille Coupling of 1

For the room-temperature base-free coupling of **1** with $PhSnBu_3$ catalyzed by $Pd_2(dba)_3/P^tBu_3$, the literature reports a **1**:**7a**:**7b** ratio of 45:47:8. We have been unable to reproduce this ratio. In an effort to control for possible variables, we evaluated different sources of most reagents (Table S20). Additionally, six different chemists across three different labs, including our own, set up the reaction using the exact conditions reported (e.g., same scale, same Pd and ligand source, same reaction time; Table S21). As shown below, none of these efforts enabled us to reproduce the literature report.

Procedure for Table S20: In a nitrogen filled glovebox, Pd_2dba_3 (0.5 mg, 0.0006 mmol, 0.75 mol %), $Pd(P^tBu_3)_2$ (0.6 mg, 0.0012 mmol, 1.5 mol %), and KPF_6 (44.2 mg, 0.24 mmol, 3 equiv) were combined in a 1-dram vial equipped with a magnetic stir bar. Tributylphenyl stannane (28μL, 0.088 mmol, 1.1 equiv), **1** (14 μL, 0.08 mmol), and DMF (150 μL) were added. The vial was immediately sealed with a PTFE-lined cap and removed from the glovebox, and the reaction was stirred at room temperature for 24 h. Dodecane (8.0 μL) was added to the reaction mixture as an internal standard, and the mixture was diluted with EtOAc. A small aliquot was removed and filtered through celite, and the celite was washed with additional EtOAc. The filtrate was analyzed by gas chromatography.

Procedure for Table S21: Six chemists in three organometallic chemistry research groups were recruited to attempt to reproduce the literature results of the base-free Stille coupling of **1** by following the procedure described in Table 3, entry 1 of reference 21, on the same scale described in the literature (0.65 mmol of **1**). The only alterations to the reported procedure are as follows: (1) an aqueous workup was not performed for entries 1 and 4-8 in Table S14 below, and (2) dodecane was used as the internal standard for calibrated GC yields instead of mesitylene, the standard reported in the literature. Dodecane was added to the reaction mixture after the 38-hour reaction time. For the table entries without an aqueous workup, the mixture was diluted with EtOAc. A small aliquot was removed and filtered through celite, and the celite was washed with additional EtOAc. The filtrate was analyzed by gas chromatography. The preparation method for **1** is noted below. The chemists outside of our own laboratory ordered new bottles of all commercial reagents for use in these studies.

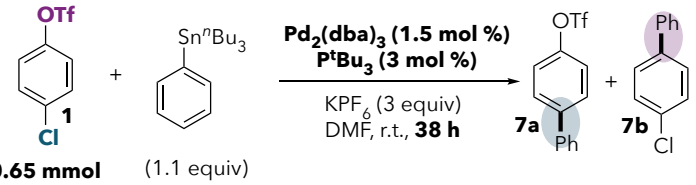
Table S26. Varying Material Sources in Stille Cross-Coupling of **1**[a]



entry	Pd_2dba_3 source	Pd_2dba_3 purity[b]	KPF_6 source	Bu_3SnPh source	literature procedure used to prepare **1**	DMF source	trial	**1**	**7a**	**7b**
1	Aldrich	31%	Oakwood	Aldrich	ref. 6	solvent system	1	84	4	3
2	Aldrich	31%	Oakwood	Aldrich	ref. 6	solvent system	2	88	3	3
3	Aldrich	31%	Oakwood	Aldrich	ref. 6	solvent system	Average	86	4	3
4	Aldrich	30%	Oakwood	Aldrich	ref. 6	solvent system	1	88	4	3
5	Aldrich	30%	Oakwood	Aldrich	ref. 6	solvent system	2	88	4	4
6	Aldrich	30%	Oakwood	Aldrich	ref. 6	solvent system	Average	88	4	3
7	Aldrich	30 %	Oakwood	Alfa Aesar	ref. 6	solvent system	1	88	3	3
8	Aldrich	30 %	Oakwood	Alfa Aesar	ref. 6	solvent system	2	88	4	3
9	Aldrich	30 %	Oakwood	Alfa Aesar	ref. 6	solvent system	Average	88	3	3
10	Aldrich	69%	Oakwood	Alfa Aesar	ref. 6	solvent system	1	87	4	3
11	Aldrich	69%	Oakwood	Alfa Aesar	ref. 6	solvent system	2	89	3	3
12	Aldrich	69%	Oakwood	Alfa Aesar	ref. 6	solvent system	Average	89	4	3
13	Strem	63%	Oakwood	Alfa Aesar	ref. 6	solvent system	1	88	3	3
14	Strem	63%	Oakwood	Alfa Aesar	ref. 6	solvent system	2	88	3	3
15	Strem	63%	Oakwood	Alfa Aesar	ref. 6	solvent system	Average	88	3	3
16	prepared in-house (ref. 22)	27%	Oakwood	Alfa Aesar	ref. 6	solvent system	1	88	3	3
17	prepared in-house (ref.22)	27%	Oakwood	Alfa Aesar	ref. 6	solvent system	2	88	4	3
18	prepared in-house (ref.22)	27%	Oakwood	Alfa Aesar	ref. 6	solvent system	Average	88	3	3
19	Aldrich	30%	Aldrich[c]	Alfa Aesar	ref. 6	solvent system	1	92	3	3
20	Aldrich	30%	Aldrich[c]	Alfa Aesar	ref. 6	solvent system	2	88	3	3
21	Aldrich	30%	Aldrich[c]	Alfa Aesar	ref. 6	solvent system	Average	90	3	3
22	Aldrich	30%	Alfa Aesar	Alfa Aesar	ref. 6	solvent system	1	92	3	3
23	Aldrich	30%	Alfa Aesar	Alfa Aesar	ref. 6	solvent system	2	89	3	3
24	Aldrich	30%	Alfa Aesar	Alfa Aesar	ref. 6	solvent system	Average	90	3	3
25	Aldrich	30%	Oakwood	Alfa Aesar	ref. 6	new, sealed[d]	1	89	4	4
26	Aldrich	30%	Oakwood	Alfa Aesar	ref. 6	new, sealed[d]	2	89	4	4
27	Aldrich	30%	Oakwood	Alfa Aesar	ref. 6	new, sealed[d]	Average	89	4	4
28	Aldrich	30%	Oakwood	Alfa Aesar	ref. 21	solvent system	1	89	1	2
29	Aldrich	30%	Oakwood	Alfa Aesar	ref. 21	solvent system	2	90	2	2
30	Aldrich	30%	Oakwood	Alfa Aesar	ref. 21	solvent system	Average	89	1	2

[a] GC yields calibrated against undecane as an internal standard. Average of two runs. [b] Purity was determined by ^1H NMR in $CDCl_3$ by the method in reference 23. [c] 99.5 % trace metals basis KPF_6. [d] Newly-opened bottle of DMF in an AcroSeal bottle from Acros Organics was used.

Table S27. Impact of Chemist and Workup Procedure in Stille Cross-Coupling of **1**[a]



entry	chemist	literature procedure used to prepare **1**	workup chemist	aqueous workup?[b]	extra additive?	**1**	**7a**	**7b**
1	A	ref. 21	A	no	no	89	2	2
2	A	ref. 21	A	yes	no	76	3	2
3	A	ref. 21	A	yes	mesitylene (1 equiv)[c]	84	3	2
4	B	ref. 6	B	no	no	85	6	3
5	C	ref. 6	C	no	no	94	2	2
6	D	ref. 21	D	no	no	86	6	3
7	E	ref. 21	A	no	no	77	10	6
8	F	ref. 21	A	no	no	89	3	3

[a]GC yields calibrated against dodecane as an internal standard. Results of a single run. [b]When indicated, the aqueous workup was performed after adding internal standard (dodecane) and followed the procedure described in reference 21. [c]Mesitylene, which is the internal GCMS standard used in reference 21, was added with the other liquid reagents prior to the start of the reaction.

Discussion: As shown in Table S20, the Pd source and its purity, the KPF_6 source, the Bu_3SnPh source, the DMF source, and the preparation method for **1** did not have a significant effect on the reaction yields in our hands. Furthermore, there was little variation among the different chemists (Table S21). The total yield of products **7a** + **7b** ranged from 4–16% yield, and the remaining starting material ranged from 77–94% based on calibrated GC.

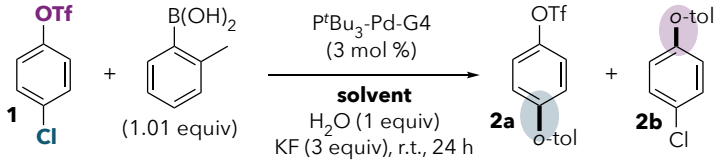
G. Evaluation of Alternative Hypotheses

1. Alternative Hypothesis: Is Solvent Effect Related to KF Solubility?

Hypothesis: We evaluated an alternative hypothesis for the observed solvent effect wherein better solubility of KF promotes formation of anionic bisligated $[Pd(P^tBu_3)(F)]^-$, which in turn favors reaction at triflate.

General Procedure: Without exclusion of air or moisture, P^tBu_3-Pd-G4 (1.5 mg, 0.0026 mmol, 3 mol %), *o*-tolyl boronic acid (11.0 mg, 0.081 mmol, 1.01 equiv), and KF (13.9 mg, 0.24 mmol, 3 equiv) were combined in a 1-dram vial equipped with a magnetic stir bar. In rapid succession, water (1.4 μL, 0.08 mmol, 1 equiv), 4-chlorophenyl triflate (14 μL, 0.08 mmol, 1 equiv), and solvent (150 μL) were added to the vial and the mixture was immediately sparged with nitrogen for two minutes. The sparging needle and septum was quickly replaced with a PTFE-lined cap and the reaction was stirred vigorously at the indicated temperature for 24 h. Undecane (7.5 μL) was added to the reaction mixture as an internal standard, and the mixture was diluted with EtOAc. A small aliquot was removed and filtered through celite, and the celite was washed with additional EtOAc. The filtrate was analyzed by gas chromatography.

Table S28. Comparing Selectivity to KF Solubility.[a]



entry	solvent	KF solubility (g KF/100 g solvent, 20-25 °C)[b]	reference for solubility data	trial	**1** (%)	**2a** (%)	**2b** (%)
1	H_2O	102	24	1	22	55	0
2	H_2O	102	24	2	35	64	0
3	H_2O	102	24	Average	28	59	0
4	THF	0.85	25	1	5	63	<1
5	THF	0.85	25	2	23	72	<1
6	THF	0.85	25	3	26	68	1
7	THF	0.85	25	4	25	71	1
8	THF	0.85	25	5	27	75	1
9	THF	0.85	25	6	24	79	1
10	THF	0.85	25	7	20	78	1
11	THF	0.85	25	8	18	79	1
12	THF	0.85	25	Average	20	74	<1
13	DMF	7.0×10^{-3}	24	1	16	9	58
14	DMF	7.0×10^{-3}	24	2	19	9	61
15	DMF	7.0×10^{-3}	24	3	24	11	59
16	DMF	7.0×10^{-3}	24	4	26	11	59
17	DMF	7.0×10^{-3}	24	5	16	12	66
18	DMF	7.0×10^{-3}	24	6	20	11	62
19	DMF	7.0×10^{-3}	24	Average	23	10	60
20	MeCN	3.6×10^{-3}	24	1	8	2	75
21	MeCN	3.6×10^{-3}	24	2	8	2	78
22	MeCN	3.6×10^{-3}	24	Average	8	2	77
23	acetone	2.2×10^{-5}	24	1	16	72	3
24	acetone	2.2×10^{-5}	24	2	26	63	4
25	acetone	2.2×10^{-5}	24	Average	21	68	4
26	propylene carbonate (PC)	2.0×10^{-7}	26	1	9	57	6
27	propylene carbonate (PC)	2.0×10^{-7}	26	2	23	68	6
28	propylene carbonate (PC)	2.0×10^{-7}	26	3	12	75	5
29	propylene carbonate (PC)	2.0×10^{-7}	26	4	19	68	6
30	propylene carbonate (PC)	2.0×10^{-7}	26	Average	16	67	6

[a]GC yields calibrated against undecane as an internal standard. Diarylated product observed in ≤4% yield in all cases.

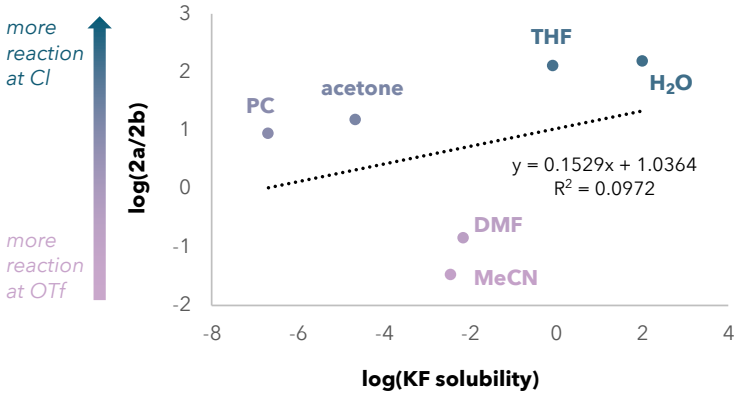
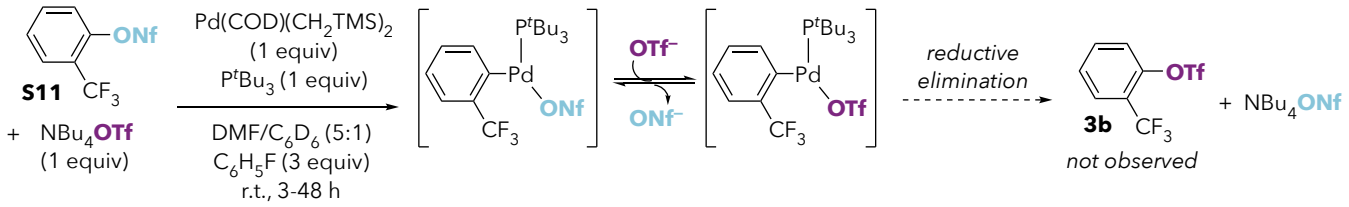


Figure S9. No correlation between KF solubility and selectivity is observed in six representative solvents.

Discussion: Solubility data and selectivity were plotted on a linear free energy relationship diagram (Table S22 and Figure S9). For six representative solvents, in which KF solubility is known, there is no trend between solubility and selectivity. As such, it does not appear that fluoride availability is responsible for the observed solvent effects.

2. Alternative Hypothesis: Is Oxidative Addition Reversible (Curtin-Hammett)?

Hypothesis: We considered a scenario in which the previously reported difference between the Suzuki and Stille selectivities[21] relates to reversible oxidative addition. If transmetallation with organostannane reagents is sufficiently slow, and oxidative addition is reversible, then the Stille reaction kinetics would fall into a Curtin-Hammett regime wherein transmetallation would actually be the selectivity-determining step. For this scenario to serve as an explanation for why chloride-selectivity was reported in the base-free Stille coupling in DMF, despite the observation that stoichiometric oxidative addition occurs preferentially at C—OTf in this solvent, oxidative addition of triflate must be reversible and transmetallation at $P^tBu_3Pd(Ar)Cl$ must be faster than at a putative $P^tBu_3Pd(Ar)OTf$ intermediate. To evaluate this hypothesis, we conducted an experiment using an aryl nonaflate in the presence of triflate anion designed to look for reversible oxidative addition of fluorinated sulfonates. Successful oxidative addition of **S11**, followed by exchange of $^-$ONf for $^-$OTf at palladium and C—O bond-forming reductive elimination would result in product **3b**. We hypothesized that this process could be tracked by ^{19}F NMR, since NBu_4OTf (-77.4 ppm) would be consumed and peaks corresponding to product **3b** (diagnostic signal at -73.3 ppm) would appear.



Procedure: Inside a nitrogen-filled glovebox, P^tBu_3 (5.5 mg, 0.027 mmol, 1 equiv), $Pd(COD)(CH_2TMS)_2$ (10.5 mg, 0.027 mmol, 1 equiv), and NBu_4OTf (10.6 mg, 0.027 mmol, 1 equiv) were combined in a 1-dram vial equipped with a stir bar. In a separate vial, a solution was prepared of **S11** (0.027 mmol, 1 equiv), C_6H_5F (7.6 μL, 0.081 mmol, 3 equiv) in C_6D_6 (100 μL). DMF (500 μL) was added to the vial containing Pd, followed by the entire volume of the substrate solution. The vial was sealed with a PTFE-lined cap and the reaction was allowed to stir for 3-48 h at room temperature. The reaction mixture was transferred via Pasteur pipette into an NMR tube. The tube was capped tightly, removed from the glovebox, and immediately analyzed by ^{19}F NMR.

Results and Discussion: The NMR spectra from these experiments show evidence of oxidative addition of **S11** based on decrease in the signals corresponding to this compound, but **3b** is not detected after 3 hours, nor after extended reaction time (up to 48 h). We conclude from these results that reductive elimination of C—OTf is unlikely to occur in polar coordinating solvent at room temperature. As such, a Curtin-Hammett scenario involving rapid equilibrium between oxidative addition adducts [Pd(P^tBu_3)(Ar)(Cl)] and [Pd(P^tBu_3)(Ar)(OTf)] is not feasible. This conclusion is consistent with the dearth of literature examples of $C_{(sp2)}$—O reductive elimination from Pd(II). Furthermore, DFT calculations suggest that oxidative addition of both C—OTf and C—Cl at [Pd(P^tBu_3)] is highly exergonic and unlikely to be reversible based on the calculated free energy barriers for the reverse reaction (see Figure 2 of the manuscript).

See pages S154-S155 for the ^{19}F NMR spectra corresponding to these experiments.

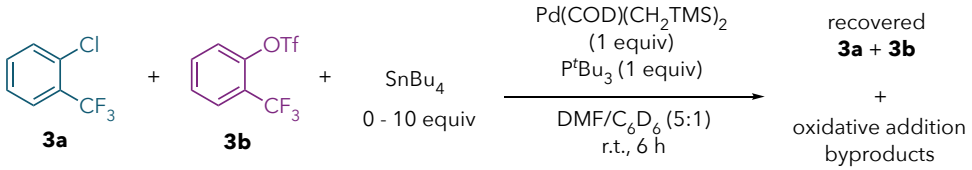
3. Alternative Hypothesis: "Greasy Tin Hypothesis"

Hypothesis: We considered an alternative hypothesis to explain the previously-reported anomalous solvent effects in the Stille coupling. In this hypothesis, we envisioned that the greasy organostannane reagents could modulate the polarity of the reaction medium (for example, oxidative addition could take place within nonpolar micelles rather than within the bulk reaction medium). To test this hypothesis, stoichiometric oxidative addition studies were conducted in DMF at room temperature in the presence of $SnBu_4$ (a reagent that is structurally similar to Bu_3SnPh but is unlikely to undergo transmetallation).

Procedure: Inside a nitrogen-filled glovebox, P^tBu_3 (5.5 mg, 0.027 mmol, 1 equiv) and $Pd(COD)(CH_2TMS)_2$ (10.5 mg, 0.027 mmol, 1 equiv) were combined in a 1-dram vial equipped with a stir bar. In a separate vial, a solution was prepared of **3a** (3.6 μL, 0.027 mmol, 1 equiv), **3b** (5.0 μL, 0.027 mmol, 1 equiv), C_6H_5F (7.6 μL, 0.081 mmol, 3 equiv), and $SnBu_4$ (8.9 μL – 88.9 μL, 0.027 – 0.27 mmol, 1-10 equiv) in C_6D_6 (100 μL). DMF (500 μL) was added to the vial containing Pd, followed by the entire volume of the substrate solution. The vial was sealed with a PTFE-lined cap and the reaction was allowed to stir for 6 h at room temperature. The reaction mixture was transferred via Pasteur pipette into an NMR tube. The tube was capped tightly, removed from the glovebox, and immediately analyzed by ^{19}F NMR.

Results:

Table S29. Effect of $SnBu_4$ on Stoichiometric Selectivity[a]



entry	additive (equiv)	recovered (%) **3a**	recovered (%) **3b**	reacted **3a** : **3b**
1	(none)	87	57	1 : 3
2	$SnBu_4$ (1 equiv)	86	26	1 : 5
3	$SnBu_4$ (2 equiv)	73	16	1 : 3
4	$SnBu_4$ (10 equiv)	76	23	1 : 3

Discussion: $SnBu_4$ did not have a significant effect on the selectivity of oxidative addition, even when used in large excess. C—OTf oxidative addition continues to occur preferentially.

See pages S136-S138 for the ^{19}F NMR spectra corresponding to these experiments.

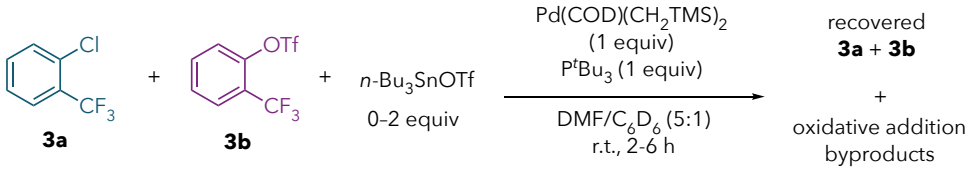
4. Alternative Hypothesis: Effect of n-Bu$_3$SnOTf

Hypothesis: We speculated that the byproduct of transmetallation with organotin reagents might influence the selectivity of oxidative addition in subsequent catalyst turnovers. In a coordinating solvent like DMF, which favors oxidative addition at triflate, the formal byproduct of transmetallation with PhSnR$_3$ would be R$_3$SnOTf (R = ^{n}Bu or Me). In this compound, tin has Lewis acidic character, and we envisioned that the Lewis acidic tin might activate an Ar—Cl bond toward oxidative addition through interaction with lone pairs on Cl. We evaluated this hypothesis through stoichiometric oxidative addition studies in DMF in the presence of added Bu$_3$SnOTf.

Procedure: Inside a nitrogen-filled glovebox, P^{t}Bu$_3$ (5.5 mg, 0.027 mmol, 1 equiv) and Pd(COD)(CH$_2$TMS)$_2$ (10.5 mg, 0.027 mmol, 1 equiv) were combined in a 1-dram vial equipped with a stir bar. In a separate vial, a solution was prepared of **3a** (3.6 μL, 0.027 mmol, 1 equiv), **3b** (5.0 μL, 0.027 mmol, 1 equiv), C$_6$H$_5$F (7.6 μL, 0.081 mmol, 3 equiv), and *n*-Bu$_3$SnOTf (0.027–0.054 mmol, 1-2 equiv) in C$_6$D$_6$ (100 μL). DMF (500 μL) was added to the vial containing Pd, followed by the entire volume of the substrate solution. The vial was sealed with a PTFE-lined cap and the reaction was allowed to stir for 2-6 h at room temperature. The reaction mixture was transferred via Pasteur pipette into an NMR tube. The tube was capped tightly, removed from the glovebox, and immediately analyzed by ^{19}F NMR.

Results:

Table S30. Effect of *n*-Bu$_3$SnOTf on Stoichiometric Selectivity[a]



entry	Bu$_3$SnOTf (equiv)	recovered (%) **3a**	**3b**	reacted **3a** : **3b**
1	0	87	57	1 : 3
2	1	88	64	1 : 3
3	2	86	65	1 : 3

[a] ^{19}F NMR yields calibrated against C$_6$H$_5$F as an internal standard.

Discussion: The addition of *n*-Bu$_3$SnOTf does not influence the observed selectivity. Thus the previously reported difference between Stille and Suzuki selectivity in DMF should not be attributed to the formation of the byproduct *n*-Bu$_3$SnOTf.

See pages S139-S140 for the ^{19}F NMR spectra corresponding to these experiments.

5. Alternative Hypothesis: Autocatalysis in Stoichiometric Oxidative Addition?

Hypothesis: Hartwig has previously observed autocatalytic oxidative addition of PhBr to $Pd(P^tBu_3)_2$ through the proposed mechanism illustrated below in Figure S10.[27] In this mechanism, a side product of the initial reaction is $(P^tBu_3)_2Pd(H)(Br)$ (the proton is derived from C—H activation of a phosphine ligand). This complex undergoes reductive elimination to form $[H—P^tBu_3][Pd(P^tBu_3)(Br)]$, which contains anionic Pd(0). The anionic Pd(0) is believed to undergo much more rapid oxidative addition into PhBr than the original neutral $Pd(P^tBu_3)_n$ species.

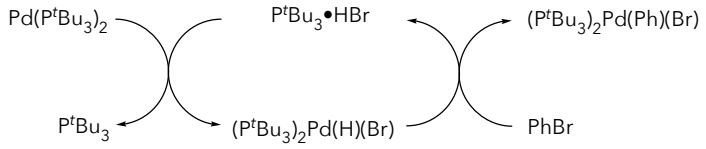
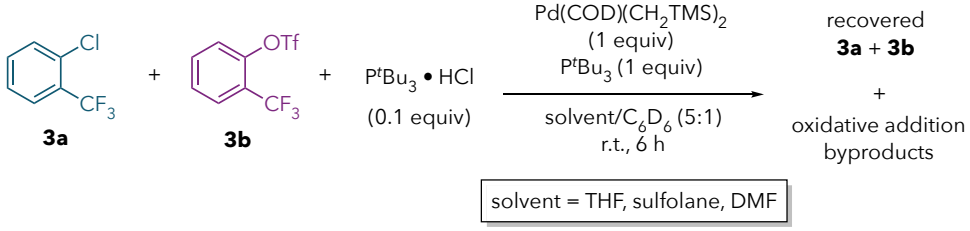


Figure S10. Previously reported autocatalytic oxidative addition of PhBr mediated by phosphonium salt.[27]

We considered the possibility that, in our stoichiometric oxidative addition reactions between $[Pd(P^tBu_3)]$ and **3a**/**3b**, an analogous process could occur that would generate highly reactive $[Pd(P^tBu_3)(Cl)]^-$. This anionic bisligated Pd(0) species would be expected to preferentially react at C—OTf, as proposed by Proutiere and Schoenebeck.[21] Because the envisioned autocatalytic cycle would be mediated by P^tBu_3•HCl, by analogy to Figure S4, we evaluated this hypothesis by using P^tBu_3•HCl as an additive in our stoichiometric studies. If this species promotes a catalytic cycle involving anionic bisligated $[Pd(P^tBu_3)(Cl)]^-$, we would expect to see a change in selectivity toward increased reaction at triflate.

Procedure: Inside a nitrogen-filled glovebox, P^tBu_3 (5.5 mg, 0.027 mmol, 1 equiv), $Pd(COD)(CH_2TMS)_2$ (10.5 mg, 0.027 mmol, 1 equiv), and P^tBu_3•HCl (0.7 mg, 0.0027 mmol, 0.1 equiv) were combined in a 1-dram vial equipped with a stir bar. In a separate vial, a solution was prepared of **3a** (3.6 μL, 0.027 mmol, 1 equiv), **3b** (5.0 μL, 0.027 mmol, 1 equiv), and C_6H_5F (7.6 μL, 0.081 mmol, 3 equiv) in C_6D_6 (100 μL). 500 μL of the indicated solvent was added to the vial containing Pd, followed by the entire volume of the substrate solution. The vial was sealed with a PTFE-lined cap and the reaction was allowed to stir for 6 h at room temperature. The reaction mixture was transferred via Pasteur pipette into an NMR tube. The tube was capped tightly, removed from the glovebox, and immediately analyzed by ^{19}F NMR.

Table S31. Effect of Phosphonium Chloride on Stoichiometric Selectivity



entry	solvent	P^tBu_3.HCl (equiv)	trial	recovered (%)[a] **3a**	**3b**	reacted **3a** : **3b**
1	THF	0	1	61	≥99	≥39 : 1
2	THF	0	2	52	≥99	≥48 : 1
3	THF	0	3	51	92	6 : 1
4	THF	0	Average	55	97	**15 : 1**
5	THF	0.1	1	60	94	7 : 1
6	THF	0.1	2	62	96	10 : 1
7	THF	0.1	Average	61	95	8 : 1
8	sulfolane	0	1	82	93	3 : 1
9	sulfolane	0	2	90	98	5 : 1
10	sulfolane	0	Average	86	95	3 : 1
11	sulfolane	0.1	1	91	96	2 : 1
12	sulfolane	0.1	2	90	94	2 : 1
13	sulfolane	0.1	Average	90	95	2 : 1
14	DMF	0	1	88	57	1 : 4
15	DMF	0	2	87	57	1 : 3
16	DMF	0	3	76	33	1 : 3
17	DMF	0	4	63	29	1 : 2
18	DMF	0	Average	78	44	1 : 3
19	DMF	0.1	1	76	31	1 : 3
20	DMF	0.1	2	81	44	1 : 3
21	DMF	0.1	Average	79	37	1 : 3

[a] ^{19}F NMR yields calibrated against C_6H_5F as an internal standard.

Discussion: The addition of 10 mol % of P^tBu_3•HCl led to some selectivity deterioration in THF and sulfolane. However, addition of this quantity of phosphonium salt was insufficient to result in an inversion of selectivity in these solvents. There was no change to the observed selectivity in DMF. These results suggest that, under the standard stoichiometric conditions in the absence of added P^tBu_3•HCl, it is unlikely that bisligated anionic $[Pd(P^tBu_3)(Cl)]^-$ is primarily responsible for the preferential triflate selectivity that is observed in coordinating solvents.

Additionally, there are other observations that contradict the hypothesis that triflate selectivity in DMF/MeCN is due to the involvement of $[Pd(P^tBu_3)(Cl)]^-$ under the stoichiometric conditions. (1) While it makes sense to consider that this anionic species would be better stabilized in polar solvents, preferential reaction at triflate is *not* observed in polar noncoordinating solvents like sulfolane and propylene carbonate (see Table 3 of the manuscript, entries 8-9). (2) Hartwig observed autocatalysis in the oxidative addition of PhBr in the nonpolar solvents toluene and THF, in addition to the polar non-coordinating solvent 2-butanone. If a similar mechanism occurred in our stoichiometric

studies, we would expect to see preferential reaction at triflate (via [Pd(P^tBu_3)(Cl)]$^-$) in toluene, THF, and acetone, but instead we see preferential selectivity for reaction of chloride in these solvents (Table 3, entries 1-4). (3) Control studies show that the presence of a **3a** as a chloride source is not necessary to observe reaction of **3b** in MeCN and DMF (Table 3, entries 12-13).

See pages S141-S143 for the ^{19}F NMR spectra corresponding to these experiments.

H. Error Analysis

Possible sources of error in GC yields include measurements of reagents and internal standard (typically undecane) and instrument error. To analyze measurement error, substrate **1** and undecane were measured out by volume in the same manner used for reaction set up, and the masses of the measured volumes were weighed by injecting the volume into an empty tared vial. In particular, 7.5 µL of undecane was measured with a 10 µL syringe (marked with 0.2 µL gradations), and 14 µL of **1** was measured with a 25 µL syringe (marked with 0.5 µL gradations). This process was repeated 5x for each compound. The results are summarized in Tables S26 and S27 below. To analyze error in GC analysis, the same reaction sample was analyzed by GC 5x (Table S28).

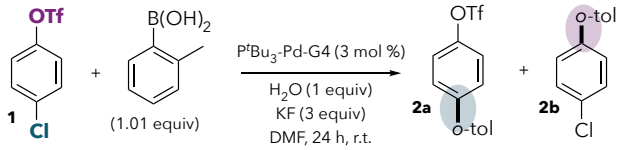
Table S32. Undecane measurement error.

trial	mass
1	5.8 mg
2	5.7 mg
3	5.5 mg
4	5.6 mg
5	5.7 mg
Average	5.66 mg
Std. dev.	0.11 mg
Std. dev. as % of avg	±1.9%

Table S33. Substrate **1** measurement error.

trial	mass
1	21.8 mg
2	21.9 mg
3	21.6 mg
4	21.9 mg
5	21.7 mg
Average	21.78 mg
Std. dev.	0.13 mg
Std. dev. as % of avg	±0.6%

Table S34. Instrument error: GC yields based on 5 GC runs of the same sample.



trial	**1** (%)	**2a** (%)	**2b** (%)
1	21.018	9.039	60.442
2	21.151	9.168	60.546
3	21.225	9.399	60.106
4	20.917	9.390	60.323
5	21.449	9.655	60.716
Average (%)	21.152	9.330	60.427
Std. dev. (%)	0.204	0.237	0.230

Discussion:

The standard deviation of the measured quantity of undecane is ±1.9% of the average. The standard deviation of the measured quantity of substrate is ±0.6% of the average. The standard deviation of the yields of **2a** and **2b** determined by GC analysis is ±0.2% of the average. As such, measurement error of both substrate and (especially) standard are expected to contribute to the most error in calculated yields. Instrument variation is associated with only a small amount of error. Overall, the estimated error in the total mass balance throughout the manuscript is about ±3% based on the standard deviations of the measurements in this error analysis. Importantly, this error is expected to influence the yields of the two products in the same direction (e.g., under-measuring undecane would increase the yield of both **2a** and **2b**, leading to a relatively minor effect on calculated ratio). Additional variation in yields can be attributed to factors including other measurement errors (e.g., of precatalyst), minor variations in room temperature, heterogeneity of particle size of solid reagents, and variations in the amount of residual O_2 in the reaction vessel.

II. Computational Details

A. General Methods

Calculations were performed with Gaussian 16.[28] An ultrafine integration grid and the keyword 5d were used for all calculations. Geometry optimizations of stationary points were carried out in implicit solvent using the CPCM continuum solvation model[29] with the indicated functional (B3LYP or MN15L[30]) and basis sets (either LANL2DZ[31] o r SDD for Pd and 6-31+G(d) for all other atoms). Frequency analyses were carried out at the same level to evaluate the zero-point vibrational energy and thermal corrections at 298.15 K. Unless otherwise indicated, Gibbs free energy values are reported after applying Cramer and Truhlar's quasi-harmonic approximation to vibrational entropy[32] and Head-Gordon's quasi-harmonic approximation to vibrational enthalpy[33] to frequencies that are less than 100 cm^{-1}. All thermodynamic quantities were computed with the GoodVibes code.[34] The nature of the stationary points was determined in each case according to the appropriate number of negative eigenvalues of the Hessian matrix. Forward and reverse intrinsic reaction coordinate (IRC) calculations were carried out on the optimized transition structures to ensure that the TSs indeed connect the appropriate reactants and products.[35] Multiple conformations were considered for all structures, and the lowest energy conformations are reported. It is worth noting that the lowest-energy π-complexes are not necessarily directly connected to the oxidative addition transition structures on the potential energy surfaces (i.e., in some cases the IRC calculations lead to different higher-energy π complexes than the lowest-energy structures reported). This factor is unimportant to the overall energetics, assuming that the barrier to interconverting π-complexes is low (e.g., by palladium ring-walking or by rotation of the triflate group). 3D images of optimized structures were generated with CYLview.[36] Where indicated, Grimme's D3(BJ) empirical dispersion correction with Becke-Johnson damping was added to the B3LYP energies using the empiricaldispersion=GD3BJ keyword.[37]

B. Reaction Free Energy Diagram Using DMF Calculated with B3LYP-D3(BJ)

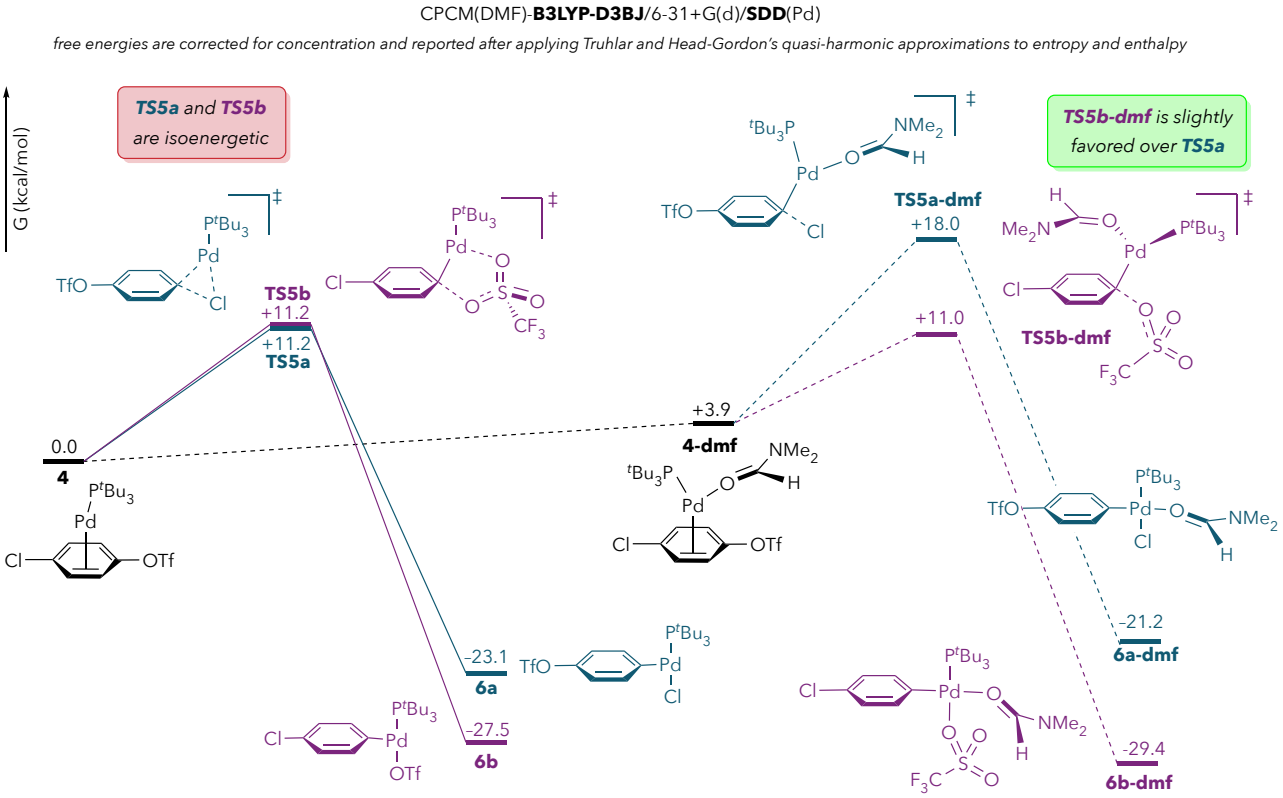


Figure S11. Reaction free energy diagrams in DMF calculated with B3LYP-D3(BJ).

Discussion: Although the functional B3LYP does not consider London dispersion forces, dispersion corrections can be added. Here we applied Grimme's D3(BJ) empirical dispersion correction with Becke-Johnson damping to the DFT energies using the empiricaldispersion=GD3BJ keyword.[38] The results are similar to those obtained using MN15L in that **TS5b-dmf** becomes much more favorable than it appears without dispersion. However, this level of theory also predicts that **TS5b** and **TS5a** should be isoenergetic, which contradicts the well-established preference for monoligated Pd to react at chloride.[1,39,40,41] As such, MN15L appears to perform better than B3LYP-D3BJ for these calculations. This observation is consistent with prior benchmarking studies with transition metals.[42]

C. DFT Predictions at 100 °C

Applying thermal corrections at 373.15 K to the calculations performed at the CPCM(DMF)-MN15L/6-31+G(d)/SDD(Pd) level of theory predicts lower selectivity for triflate, (Figure S12). This is expected because **TS5b-dmf** is less entropically favorable than **TS5a**.

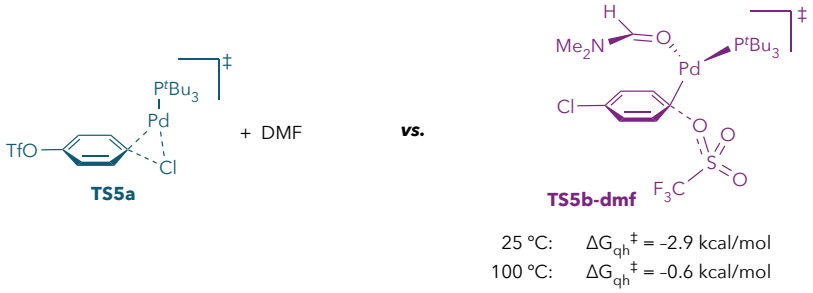
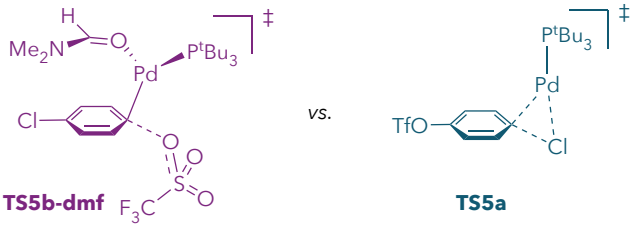


Figure S12. DFT predictions at 100 °C using CPCM(DMF)-MN15L/6-31+G(d)/SDD(Pd).

D. Discussion of DFT Shortcomings

Our DFT calculations, at minimum, suggest that solvent coordination should not be ruled out on the basis of dispersion-free DFT calculations. In particular, they show that the energy of **TS5b-dmf** is similar in energy to **TS5a**. However, even when dispersion is included, the DFT methods used in this work fall short of being able to reproduce the expected coordinating ability trends of different solvents to palladium. For example, the expected order of solvent cordinating ability is MeCN > DMF > THF > benzene, but DFT predicts different trends that vary with method. These results are summarized in Tables S29-S31.

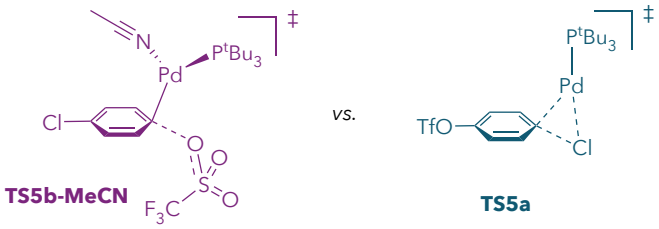
Table S35. Differences in energy between **TS5b-dmf** and **TS5a** calculated in implicit DMF[a]



	TS5b–dmf — TS5a			
Method	ΔE	ΔH_{qh}	ΔG	ΔG_{qh}
CPCM(DMF)-B3LYP/6-31+G(d)/LANL2DZ(Pd)	+6.3	+6.3	+16.2	+16.4
CPCM(DMF)-B3LYP-D3(BJ)/6-31+G(d)/LANL2DZ(Pd)	−9.3	−8.2	+0.9	+0.7
CPCM(DMF)-B3LYP-D3(BJ)/6-31+G(d)/SDD(Pd)	−10.6	−10.3	−0.1	−0.1
CPCM(DMF)-MN15L/6-31+G(d)/LANL2DZ(Pd)	−13.0	−12.7	−1.7	−2.4
CPCM(DMF)-MN15L/6-31+G(d)/SDD(Pd)	−13.7	−12.7	−2.0[c]	−2.9

[a]Thermal corrections at 298.15 K. All energies reported in kcal/mol. Free energies are corrected for concentration (ratio of DMF:Pd = 765:1). Enthalpy (ΔH_{qh}) is reported after applying Head-Gordon's quasi-harmonic approximation to vibrational enthalpy. The free energy value labeled with ΔG_{qh} is reported after applying Cramer and Truhlar's and Head-Gordon's quasi-harmonic approximations to vibrational entropy and enthalpy, while the value labeled as ΔG does not include the quasi-harmonic approximations.

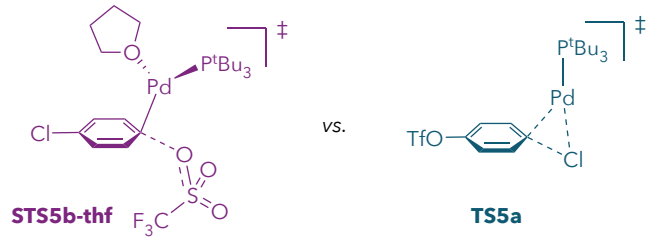
Table S36. Differences in energy between **TS5b-MeCN** and **TS5a** calculated in implicit MeCN[a]



	TS5b–dmf — TS5a			
Method	ΔE	ΔH	ΔG	$\Delta G_{corrected}$
CPCM(MeCN)-MN15L/6-31+G(d)/LANL2DZ(Pd)	−7.2	−7.3	+0.3	+0.1
CPCM(MeCN)-MN15L/6-31+G(d)/SDD(Pd)	−7.4	−7.4	+0.3	0.0

[a]Thermal corrections at 298.15 K. All energies reported in kcal/mol. Free energies are corrected for concentration (ratio of DMF:Pd = 1,118:1). Enthalpy (ΔH_{qh}) is reported after applying Head-Gordon's quasi-harmonic approximation to vibrational enthalpy. The free energy value labeled with ΔG_{qh} is reported after applying Cramer and Truhlar's and Head-Gordon's quasi-harmonic approximations to vibrational entropy and enthalpy, while the value labeled as ΔG does not include the quasi-harmonic approximations.

Table S37. Differences in energy between **TS5b-thf** and **TS5a** calculated in implicit THF[a]



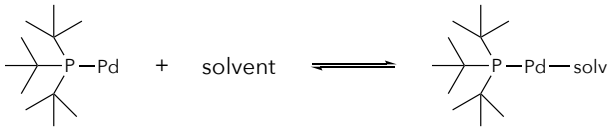
	TS5b–dmf — TS5a			
Method	ΔE	ΔH	ΔG	$\Delta G_{corrected}$
CPCM(THF)-B3LYP-D3(BJ)/6-31+G(d)/LANL2DZ(Pd)	−9.1	−8.8	+0.8	+1.4
CPCM(MeCN)-MN15L/6-31+G(d)/SDD(Pd)	−11.2	−10.9	0.0	−1.0

[a]Thermal corrections at 298.15 K. All energies reported in kcal/mol. Free energies are corrected for concentration (ratio of DMF:Pd = 718:1). Enthalpy (ΔH_{qh}) is reported after applying Head-Gordon's quasi-harmonic approximation to vibrational enthalpy. The free energy value labeled with ΔG_{qh} is reported after applying Cramer and Truhlar's and Head-Gordon's quasi-harmonic approximations to vibrational entropy and enthalpy, while the value labeled as ΔG does not include the quasi-harmonic approximations.

Using CPCM(solvent)-MN15L/6-31+G(d)/LANL2DZ(Pd), we also attempted to evaluate coordinating strength of several different solvents at both Pd(0) and Pd(II) by calculating the energies of the species depicted in Schemes S1 and S2. The free energy values in these schemes are reported after applying a standard state concentration assuming that Pd is 0.017 *M* in solvent, and with quasi-harmonic approximations to vibrational enthalpy and entropy. However, as shown, DFT at this level of theory suggests that the order of coordinating ability to 12 e^- Pd(0) should be benzene > MeCN > DMF > THF, which does not match the expected order of MeCN > DMF > THF > benzene. When considering coordination to 14 e^- Pd(II), the calculations indicate that solvent coordination is unfavorable in all cases, and the energetics suggest the following order of coordinating ability to Pd(II): benzene > DMF ≈ MeCN > THF. Moreover, in the optimized structures of the solvato complexes with THF and benzene, the solvent molecule is very far away from Pd (≥3.65 Å). The failure of DFT to discriminate between coordinating ability of these solvents indicates that this level of theory is not adequate for describing the strength of weak dative bonds. It is possible that

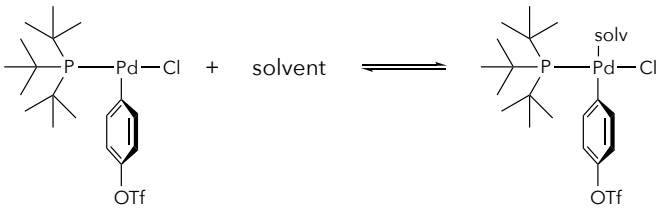
more useful information may be gleaned using different functionals or larger basis sets; alternatively, molecular dynamics simulations may contribute to a more accurate representation of solvent coordination.

Scheme S1. Calculating favorability of solvent coordination to 12 e^- Pd(0).



MeCN (σ-type): -9.2 kcal/mol
MeCN (π-type): -9.0 kcal/mol
DMF: -6.9 kcal/mol
THF: -6.2 kcal/mol
benzene: -13.1 kcal/mol

Scheme S2. Calculating favorability of solvent coordination to 14 e^- Pd(II).



MeCN (σ-type): +3.9 kcal/mol
DMF: +4.0 kcal/mol
THF: +3.4 kcal/mol
benzene: +0.9 kcal/mol

E. Energies, Entropies, and Lowest Frequencies of Minimum Energy Structures

Table S38. Calculations at the CPCM(DMF)-B3LYP/6-31+G(d)/LANL2DZ(Pd) level of theory.[a]

Structure	E_{elec} (Hartree)	ZPE (Hartree)	H_{qh} (Hartree)[c]	G[d] (Hartree)	G_{qh}[e] (Hartree)	Imaginary Freq[f]
4	-2594.348615	0.479968	-2593.838126	-2593.939812	-2593.935128	
TS5a	-2594.33273	0.478858	-2593.823409	-2593.925542	-2593.920232	-206.2301
TS5b	-2594.325045	0.47793	-2593.816619	-2593.916959	-2593.913175	-259.9956
6a	-2594.380785	0.481617	-2593.868329	-2593.967968	-2593.965253	
6b	-2594.388147	0.481944	-2593.875515	-2593.97488	-2593.97189	
(4-dmf)[b]	-2842.870244	0.583401	-2842.251221	-2842.367065	-2842.362175	-14.5954
(TS5a-dmf)[b]	-2842.851507	0.583269	-2842.232268	-2842.350003	-2842.34438	-179.6848
TS5b-dmf	-2842.853054	0.582742	-2842.234138	-2842.351143	-2842.345837	-260.8251
6a-dmf	-2842.911073	0.586476	-2842.28799	-2842.404586	-2842.39992	
6b-dmf	-2842.919852	0.586244	-2842.297336	-2842.41364	-2842.409048	
DMF	-248.530317	0.102799	-248.420798	-248.45138	-248.451688	

[a]1 Hartree = 627.51 kcal mol^{-1}. Thermal corrections at 298.15 K, with concentration = 13 *M* for DMF and 0.017 *M* for all other species. [b]Optimized with a constrained Pd—O distance; so these are unlikely to represent a true minimum-energy structure at this level of theory. [c]Enthalpy reported after application of Head-Gordon's quasi-harmonic approximation to vibrational enthalpy. [d]Solvent-corrected free energy given by $G = E_{elec} + G_{corr}$, where G_{corr} is the thermal correction to Gibbs free energy. [e]Solvent-corrected free energy given by $G_{qh} = E_{elec} + G_{corr*}$, where G_{corr*} is the thermal correction to Gibbs free energy obtained after applying Cramer and Truhlar's and Head-Gordon's quasi-harmonic approximations. [f]The single imaginary frequency is reported for the structures that have one (i.e., the transition structures; and **4-dmf** (optimized with constrained Pd-O distance) also has one imaginary frequency).

Table S39. Calculations at the CPCM(DMF)-MN15L/6-31+G(d)/SDD(Pd) level of theory. [a]

Structure	E_{elec} (Hartree)	ZPE (Hartree)	H_{qh} (Hartree)[b]	G[c] (Hartree)	G_{qh}[d] (Hartree)	Imaginary Freq[e]
4	-2593.644346	0.481345	-2593.133222	-2593.228452	-2593.227671	
TS5a	-2593.625463	0.480954	-2593.114724	-2593.210282	-2593.2083	-171.5502
TS5b	-2593.616729	0.478692	-2593.108203	-2593.205818	-2593.202853	-228.3686
6a	-2593.675812	0.483879	-2593.161958	-2593.257676	-2593.255789	
6b	-2593.685169	0.483386	-2593.17171	-2593.266324	-2593.265437	
4-dmf	-2841.934404	0.586643	-2841.312338	-2841.419651	-2841.419805	
TS5a-dmf	-2841.902557	0.585601	-2841.281456	-2841.391212	-2841.389741	-137.2208
TS5b-dmf	-2841.914925	0.585201	-2841.294157	-2841.402029	-2841.401882	-246.0247
6a-dmf	-2841.959897	0.588859	-2841.33526	-2841.446021	-2841.443004	
6b-dmf	-2841.974739	0.588358	-2841.350582	-2841.459279	-2841.45836	
DMF	-248.26759	0.10276	-248.158125	-248.188622	-248.188946	

[a]1 Hartree = 627.51 kcal mol^{-1}. Thermal corrections at 298.15 K, with concentration = 13 *M* for DMF and 0.017 *M* for all other species. [b]Enthalpy reported after application of Head-Gordon's quasi-harmonic approximation to vibrational enthalpy. [c]Solvent-corrected free energy given by $G = E_{elec} + G_{corr}$, where G_{corr} is the thermal correction to Gibbs free energy. [d]Solvent-corrected free energy given by $G_{qh} = E_{elec} + G_{corr*}$, where G_{corr*} is the thermal correction to Gibbs free energy obtained after applying Cramer and Truhlar's and Head-Gordon's quasi-harmonic approximations. [e]The single imaginary frequency is reported for the structures that have one (i.e., the transition structures).

Table S40. Calculations at the CPCM(DMF)-B3LYP-D3BJ/6-31+G(d)/SDD(Pd) level of theory.[a]

Structure	E_{elec} (Hartree)	ZPE (Hartree)	H_{qh} (Hartree)[b]	G[c] (Hartree)	G_{qh}[d] (Hartree)	Imaginary Freq[e]
4	-2595.688612	0.481727	-2595.176572	-2595.276064	-2595.272339	
TS5a	-2595.670641	0.481266	-2595.159196	-2595.257293	-2595.254542	-143.4386
TS5b	-2595.66856	0.479359	-2595.158894	-2595.258514	-2595.254518	-291.4703
6a	-2595.728252	0.48407	-2595.213709	-2595.311295	-2595.309183	
6b	-2595.735645	0.484165	-2595.221073	-2595.318547	-2595.316219	
4-dmf	-2844.243619	0.586633	-2843.621117	-2843.734454	-2843.731391	
TS5a-dmf	-2844.220638	0.586291	-2843.598437	-2843.71181	-2843.708974	-101.0273
TS5b-dmf	-2844.231449	0.585406	-2843.610018	-2843.722351	-2843.720012	-320.8933
6a-dmf	-2844.286863	0.589193	-2843.661374	-2843.775281	-2843.771396	
6b-dmf	-2844.298688	0.588445	-2843.674178	-2843.788233	-2843.784421	
DMF	-248.543978	0.10288	-248.434389	-248.464973	-248.46527	

[a]1 Hartree = 627.51 kcal mol^{-1}. Thermal corrections at 298.15 K, with concentration = 13 *M* for DMF and 0.017 *M* for all other species. [b]Enthalpy reported after application of Head-Gordon's quasi-harmonic approximation to vibrational enthalpy. [c]Solvent-corrected free energy given by $G = E_{elec} + G_{corr}$, where G_{corr} is the thermal correction to Gibbs free energy. [d]Solvent-corrected free energy given by $G_{qh} = E_{elec} + G_{corr*}$, where G_{corr*} is the thermal correction to Gibbs free energy obtained after applying Cramer and Truhlar's and Head-Gordon's quasi-harmonic approximations. [e]The single imaginary frequency is reported for the structures that have one (i.e., the transition structures).

III. References

1. Reeves, E. K.; Humke, J. N.; Neufeldt, S. R. *J. Org. Chem.* **2019**, *84*, 11789-11812.
2. Gill, D.; Hester, A. J.; Lloyd-Jones, G. C. *Org. Biomol. Chem.* **2004**, *2*, 2547-2548.
3. Andersen, T. L.; Kramer, S.; Overgaard, J.; Skrydstrup, T. *Organometallics* **2017**, *36*, 2058-2066.
4. Barrios-Landeros, F.; Carrow, B. P.; Hartwig, J. F. *J. Am. Chem. Soc.* **2009**, *131*, 8141-8154.
5. Morozova, V.; Mayer, P.; Berionni, G. *Angew. Chem. Int. Ed.* **2015**, *54*, 14508-14512.
6. Gooβen, L.J.; Rodríguez, N.; Linder, C. *J. Am. Chem. Soc.* **2008**, *130*, 15248-15249.
7. Onodera, S.; Kochi, T.; Kakiuchi, F. *J. Org. Chem.* **2019**, *84*, 6508-6515
8. Reeves, E.K.; Bauman, O.R.; Mitchem, G.B.; Neufeldt, S.R. *Isr. J. Chem.* **2020**, *60*, 406-409.
9. Entz, E. D.; Russell, J. E. A.; Hooker, L. V. *J. Am. Chem. Soc.* **2020**, *142*, 15454-15463.
10. Bartoli, G.; Bosco, M. *Synthesis* **1980**, *8*, 616-617.
11. Viswanathan, G.S.; Wang, M.; Li, C.J. *Angew. Chem. Int. Ed.* **2002**, *41*, 2138-2141.
12. Shekhar, S.; Dunn, T. B.; Kotecki, B. J.; Montavon, D. K.; Cullen, S. C. *J. Org. Chem.* **2011**, *76*, 4552-4563.
13. Zhang, Z.; Wang, Z. *J. Am. Chem. Soc.* **2006**, *71*, 7485-7487.
14. Gooβen, L.J.; Rodríguez, N.; Linder, C. *J. Am. Chem. Soc.* **2008**, *130*, 15248-15249.
15. Gill, D.; Hester, A.J.; Lloyd-Jones, G.C. *Org. & Biomol. Chem.* **2004**, *2*, 2547-2548.
16. Hansch, C.; Leo, A.; Taft, R.W. *Chem. Rev.* **1991**, *91*, 165-195.
17. Roy, A. H.; Hartwig, J. F. *Organometallics* **2004**, *23*, 194-202.
18. Wohlfarth, C. "Permittivity (Dielectric Constant) of Liquids" in CRC Handbook of Chemistry and Physics, Rumble, Jr., J. R.; Lide, D. R.; Bruno, T. J., eds. CRC Press, Boca Raton, FL, 2020.
19. Suzuki, K.; Shin-ya, M.; Ono, Y.; Matsumoto, T.; Nanbu, N.; Takehara, M.; Ue, M.; Sasaki, Y. *Electrochemistry* **2007**, *75*, 611-614.
20. Salmon, C. J.; Danelon, G. O.; Mascaretti, O. A. *J. Org. Chem.* **2000**, *65*, 9220-9222.
21. Proutiere, F.; Schoenebeck, F. *Angew. Chem. Int. Ed.* **2011**, *50*, 8192-9195.
22. Fairlamb, I.J.S.; Kapdi, A.R.; Lee, A.F. *J. Am. Chem. Soc.* **2004**, *6*, 4435-4438,
23. Zalesskiy, S.S.; Ananikov, V.P. *Organometallics* **2012**, *13*, 2302-2309.
24. National Institute of Health PubChem. Potassium fluoride. https://pubchem.ncbi.nlm.nih.gov/compound/522689 (accessed Sep 30, 2020).
25. Wynn, D. A.; Roth, M. M.; Pollard, B. D. Talanta **1984**, *31*, 1036-1040.
26. Peruzzi, N.; Lo Nostro, P.; Ninham, B. W.; Baglioni, P. *J. Solution Chem.* **2015**, *44*, 1224-1239.
27. Barrios-Landeros, F.; Carrow, B. P.; Hartwig, J. F. *J. Am. Chem. Soc.* **2008**, *130*, 5842-5843
28. Gaussian 16, Revision C.01, Frisch, M. J.; Trucks, G. W.; Schlegel, H. B.; Scuseria, G. E.; Robb, M. A.; Cheeseman, J. R.; Scalmani, G.; Barone, V.; Petersson, G. A.; Nakatsuji, H.; Li, X.; Caricato, M.; Marenich, A. V.; Bloino, J.; Janesko, B. G.; Gomperts, R.; Mennucci, B.; Hratchian, H. P.; Ortiz, J. V.; Izmaylov, A. F.; Sonnenberg, J. L.; Williams-Young, D.; Ding, F.; Lipparini, F.; Egidi, F.; Goings, J.; Peng, B.; Petrone, A.; Henderson, T.; Ranasinghe, D.; Zakrzewski, V. G.; Gao, J.; Rega, N.; Zheng, G.; Liang, W.; Hada, M.; Ehara, M.; Toyota, K.; Fukuda, R.; Hasegawa, J.; Ishida, M.; Nakajima, T.; Honda, Y.; Kitao, O.; Nakai, H.; Vreven, T.; Throssell, K.; Montgomery, J. A., Jr.; Peralta, J. E.; Ogliaro, F.; Bearpark, M. J.; Heyd, J. J.; Brothers, E. N.; Kudin, K. N.; Staroverov, V. N.; Keith, T. A.; Kobayashi, R.; Normand, J.; Raghavachari, K.; Rendell, A. P.; Burant, J. C.; Iyengar, S. S.; Tomasi, J.; Cossi, M.; Millam, J. M.; Klene, M.; Adamo, C.; Cammi, R.;

Ochterski, J. W.; Martin, R. L.; Morokuma, K.; Farkas, O.; Foresman, J. B.; Fox, D. J. Gaussian, Inc., Wallingford CT, 2016

29. Cossi, M.; Rega, N.; Scalmani, G.; Barone, V. *J. Comput. Chem.* **2003**, *24*, 669.
30. Yu, H. S.; He, X.; Truhlar, D. G. *J. Chem. Theory Comput.* **2016**, *12*, 1280.
31. Hay, P. J.; Wadt, W. R. *J. Chem. Phys.* **1985**, *82*, 299.
32. Ribeiro, R.F.; Marenich, A.V.; Cramer, C.J.; Truhlar, D.G. *J. Phys. Chem. B.* **2011**, *115*, 14556.
33. Li, Y.-P.; Gomes, J.; Sharada, S. M.; Bell, A.T.; Head-Gordon, M. *J. Phys. Chem. C* **2015**, *119*, 1840
34. Luchini, G.; Alegre-Requena, J. V.; Funes-Ardoiz, I.; Paton, R. S. GoodVibes: Automated Thermochemistry for Heterogeneous Computational Chemistry Data. *F1000Research*, **2020**, *9*, 291.
35. (a) Gonzalez, C.; Schlegel, H. B. *J. Chem. Phys.* **1989**, *90*, 2154; (b) Gonzalez, C.; Schlegel, H.B. *J. Phys. Chem.* **1990**, *94*, 5523; (c) Fukui, K. *Acc. Chem. Res.* **1981**, *14*, 363.
36. CYLview, 1.0b; Legault CY, Université de Sherbrooke, 2009 (http://www.cylview.org)

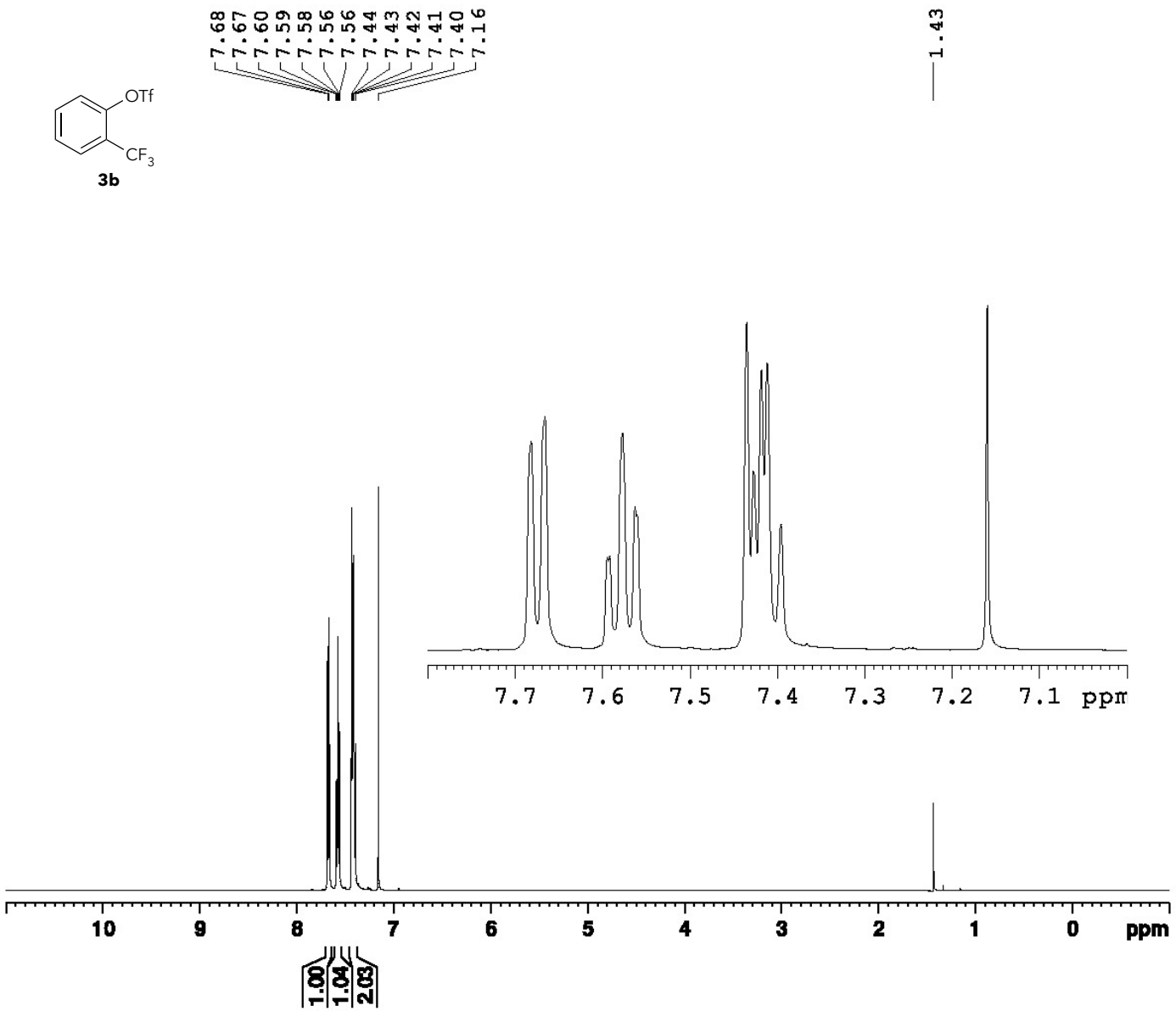
37 (a) Grimme, S.; Antony, J.; Ehrlich, S.; Krieg, H. *J. Chem. Phys.* **2010**, 132, 154104-154119. (b) Grimme, S.; Ehrlich, S.; Goerigk, L. *J. Comput. Chem.* **2011**, *32*, 1456-1465.

38 (a) Grimme, S.; Antony, J.; Ehrlich, S.; Krieg, H. *J. Chem. Phys.* **2010**, 132, 154104-154119. (b) Grimme, S.; Ehrlich, S.; Goerigk, L. *J. Comput. Chem.* **2011**, *32*, 1456-1465.

39. Schoenebeck, F.; Houk, K. N. *J. Am. Chem. Soc.* **2010**, 132, 2496.
40. Niemeyer, Z. L.; Milo, A.; Hickey, D. P.; Sigman, M. S. *Nat. Chem.* **2016**, *8*, 610.
41. So, C. M.; Yuen, O. Y.; Ng, S. S.; Chen, Z. *ACS Catal.* **2021**, *11*, 7820/
42. Moltved, K. A.; Kepp, K. P. *J. Chem. Theory Comput.* **2018**, *14*, 3479.

IV. NMR Spectra

A. Compound Characterization

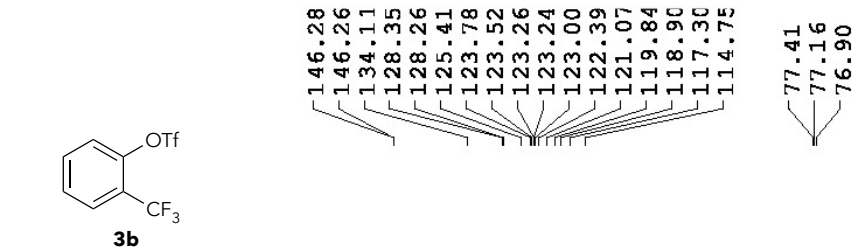


BRUKER

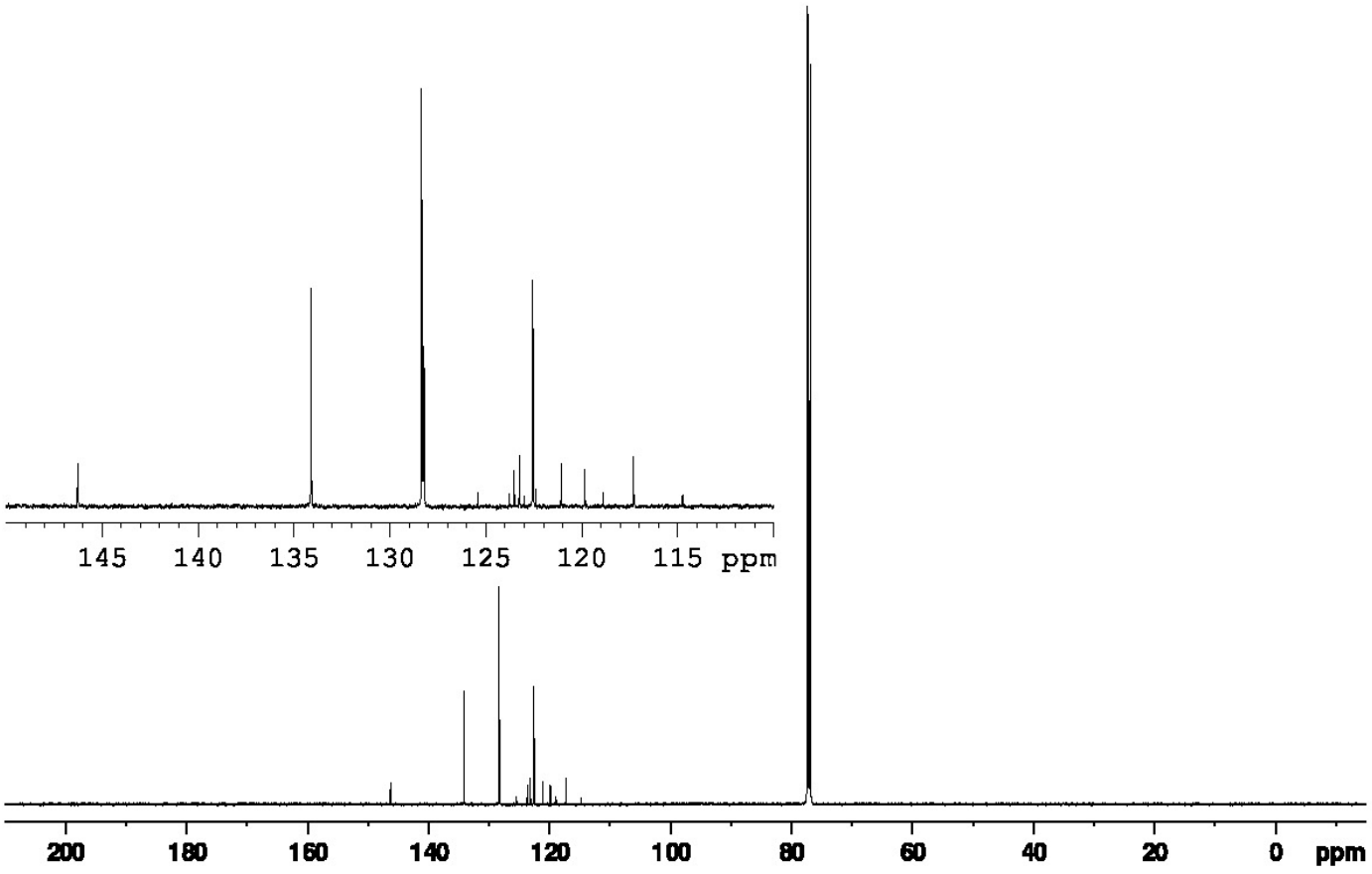
```
Current Data Parameters
NAME            5-SMR-74
EXPNO                 20
PROCNO                 1

F2 - Acquisition Parameter
Date_           20211009
Time              12.37 h
INSTRUM             spect
PROBHD   Z125869_0055 (
PULPROG             zg30
TD                 65536
SOLVENT             CDCl3
NS                    64
DS                     2
SWH           10000.000 Hz
FIDRES         0.305176 Hz
AQ             3.2767999 sec
RG                151.18
DW                50.000 usec
DE                16.00 usec
TE                298.0 K
D1             2.00000000 sec
TD0                    1
SFO1          500.2330889 MHz
NUC1                  1H
P0                4.00 usec
P1                12.00 usec
PLW1          11.44699955 W

F2 - Processing parameters
SI                 65536
SF            500.2300620 MHz
WDW                   EM
SSB       0
LB                0.30 Hz
GB        0
PC                1.00
```



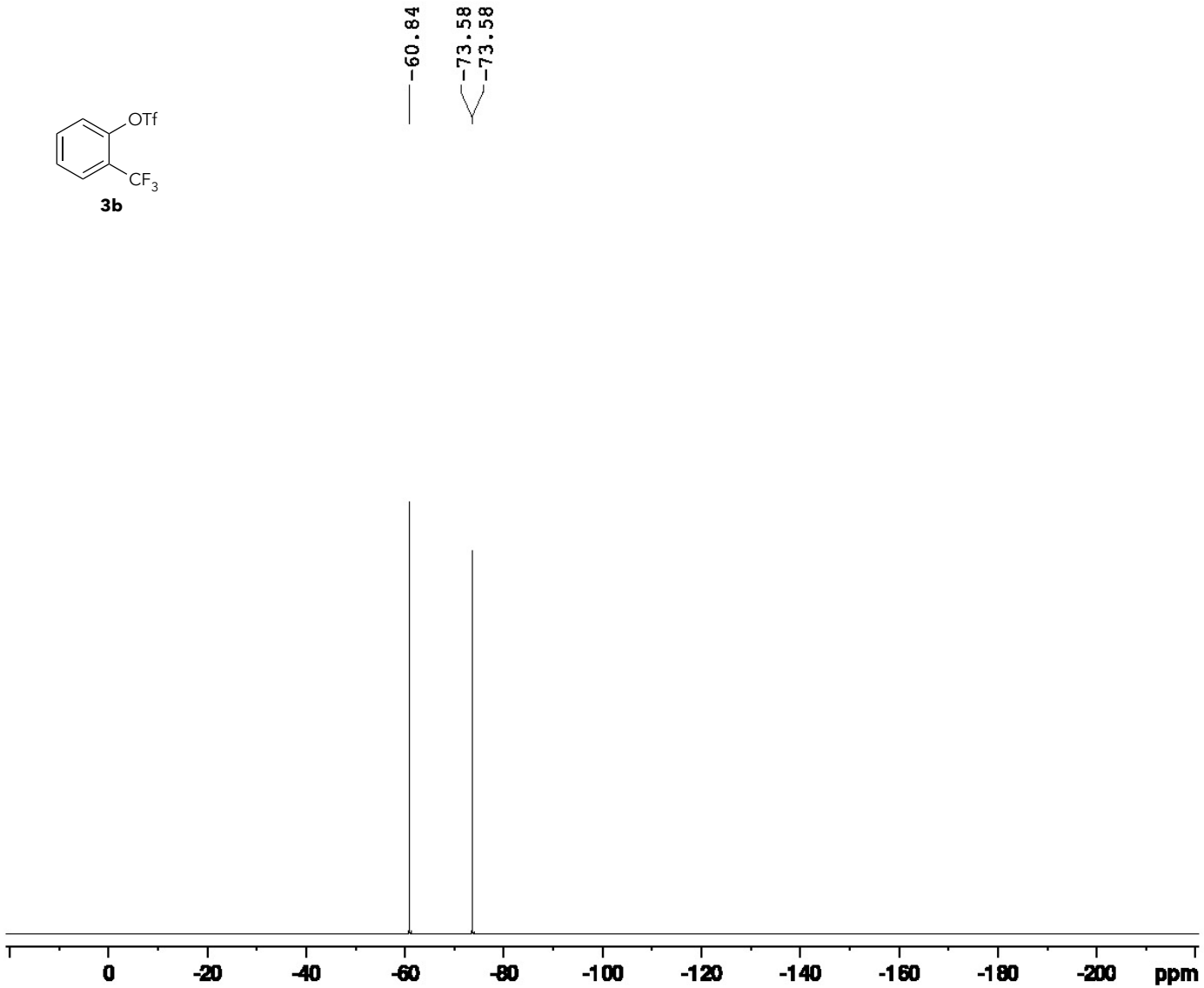
3b




```
Current Data Parameters
NAME                  5-SMR-74
EXPNO                       22
PROCNO                       1

F2 - Acquisition Parameter
Date_                 20211009
Time                     13.35 h
INSTRUM                  spect
PROBHD   Z125869_0055 (
PULPROG                 zgpg30
TD                       65536
SOLVENT                  CDCl3
NS                        1024
DS                           4
SWH                  29761.904 Hz
FIDRES                0.908261 Hz
AQ                   1.1010048 sec
RG                       190.44
DW                     16.800 usec
DE                     18.00 usec
TE                     298.0 K
D1                   2.00000000 sec
D11                  0.03000000 sec
TD0                          1
SFO1               125.7955118 MHz
NUC1                        13C
P0                     3.33 usec
P1                     10.00 usec
PLW1               56.90299988 W
SFO2               500.2320009 MHz
NUC2                        1H
CPDPRG[2                waltz16
PCPD2                  80.00 usec
PLW2               11.44699955 W
PLW12               0.25756001 W
PLW13               0.12955000 W

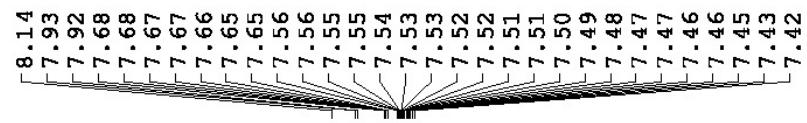
F2 - Processing parameters
SI                       32768
SF                 125.7829153 MHz
WDW                         EM
SSB                  0
LB                      1.00 Hz
GB                   0
PC                      1.40
```

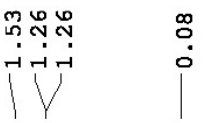


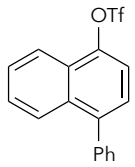
Current Data Parameters
NAME 5-SMR-74
EXPNO 21
PROCNO 2

F2 - Acquisition Parameter
Date_ 20211009
Time 12.39 h
INSTRUM spect
PROBHD Z125869_0055 (
PULPROG zgflqn
TD 130892
SOLVENT CDCl3
NS 16
DS 4
SWH 113636.367 Hz
FIDRES 1.736338 Hz
AQ 0.5759248 sec
RG 15.61
DW 4.400 usec
DE 18.00 usec
TE 298.0 K
D1 1.00000000 sec
TD0 1
SFO1 470.6394024 MHz
NUC1 19F
P1 15.00 usec
PLW1 11.70800018 W

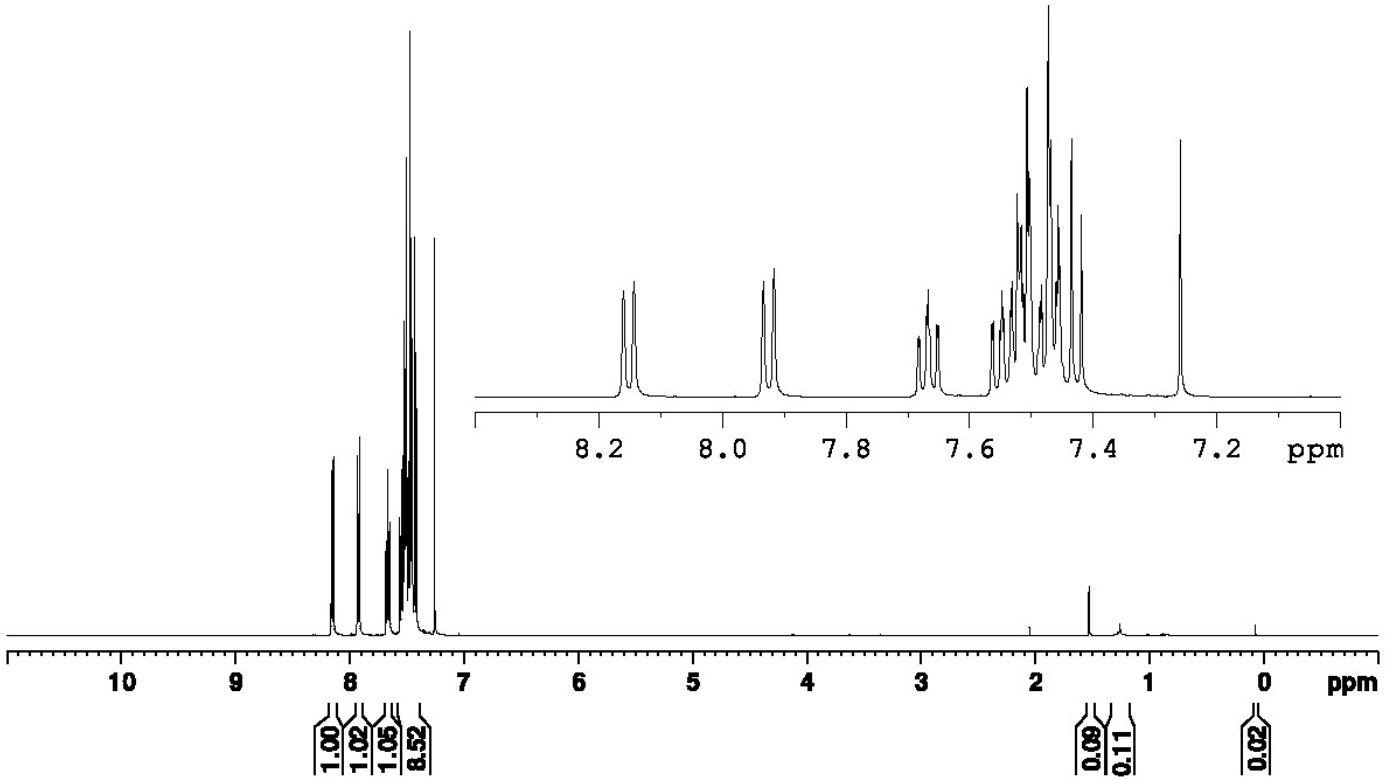
F2 - Processing parameters
SI 65536
SF 470.6864712 MHz
WDW EM
SSB 0
LB 0.30 Hz
GB 0
PC 1.00







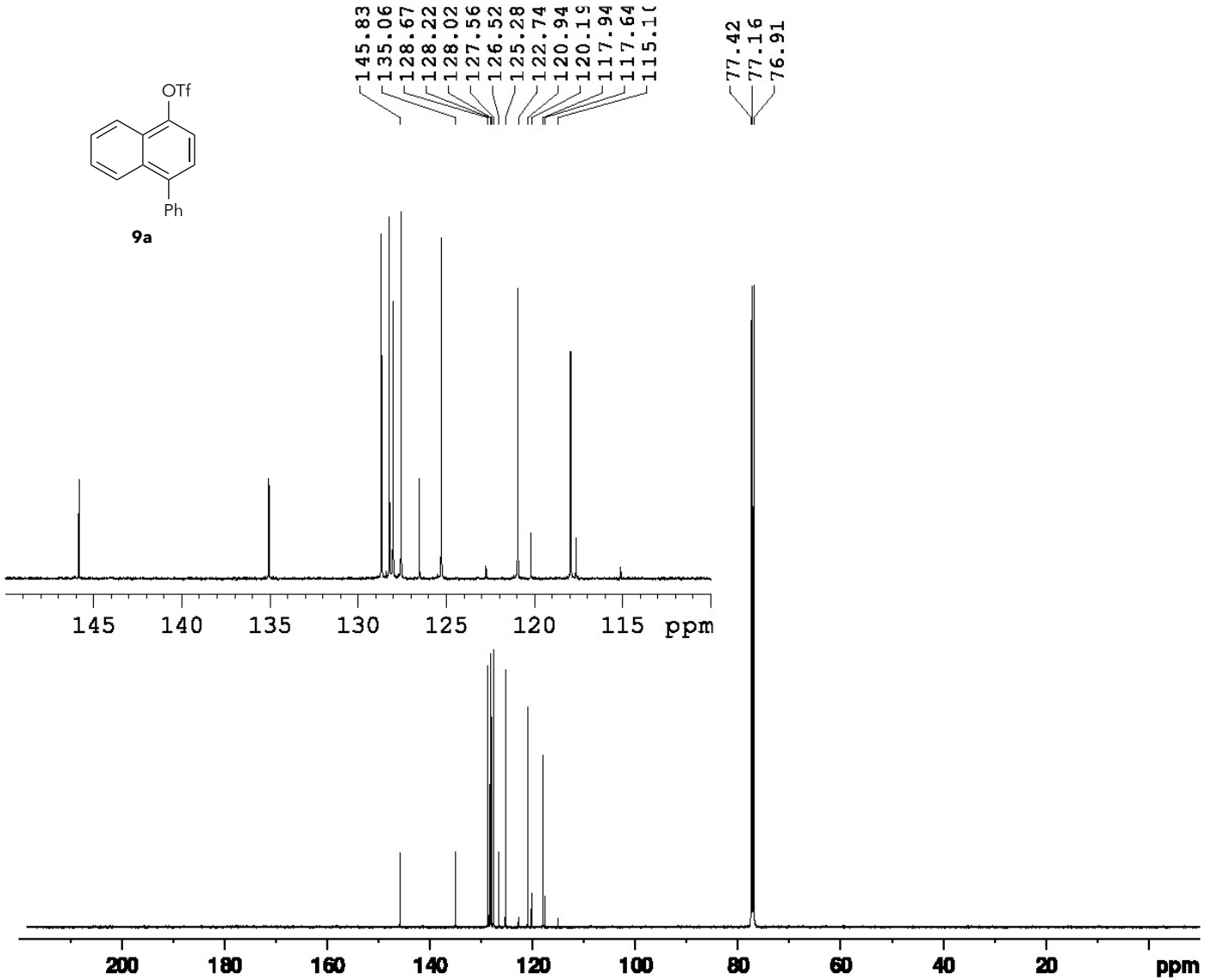
9a




```
Current Data Parameters
NAME          EKB-1-188
EXPNO                20
PROCNO                1

F2 - Acquisition Parameter
Date_          20211006
Time              15.56 h
INSTRUM           spect
PROBHD   Z125869_0055 (
PULPROG           zg30
TD               65536
SOLVENT          CDCl3
NS                  64
DS                   2
SWH          10000.000 Hz
FIDRES         0.305176 Hz
AQ            3.2767999 sec
RG               151.18
DW               50.000 usec
DE               16.00 usec
TE               298.0 K
D1           2.00000000 sec
TD0                  1
SFO1         500.2330889 MHz
NUC1                1H
P0               4.00 usec
P1               12.00 usec
PLW1        11.44699955 W

F2 - Processing parameters
SI               65536
SF          500.2300126 MHz
WDW                 EM
SSB      0
LB                0.30 Hz
GB       0
PC                1.00
```

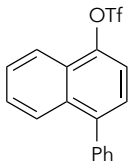


BRUKER

```
Current Data Parameters
NAME          EKB-1-184
EXPNO                22
PROCNO                1

F2 - Acquisition Parameter
Date_          20211007
Time              12.53 h
INSTRUM            spect
PROBHD   Z125869_0055 (
PULPROG          zgpg30
TD                65536
SOLVENT           CDCl3
NS                 1024
DS                    4
SWH           29761.904 Hz
FIDRES         0.908261 Hz
AQ            1.1010048 sec
RG               190.44
DW               16.800 usec
DE               18.00 usec
TE               298.0 K
D1            2.00000000 sec
D11           0.03000000 sec
TD0                   1
SFO1         125.7955118 MHz
NUC1                 13C
P0                3.33 usec
P1               10.00 usec
PLW1         56.90299988 W
SFO2         500.2320009 MHz
NUC2                 1H
CPDPRG[2         waltz16
PCPD2             80.00 use
PLW2         11.44699955 W
PLW12         0.25756001 W
PLW13         0.12955000 W

F2 - Processing parameters
SI                32768
SF          125.7829156 MHz
WDW                  EM
SSB       0
LB                1.00 Hz
GB        0
PC                1.40
```

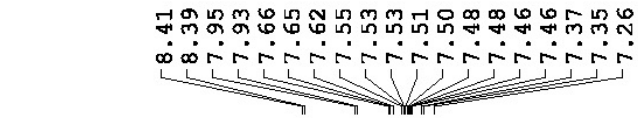


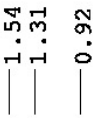
9a

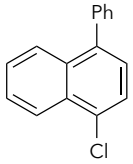

```
Current Data Parameters
NAME          EKB-1-188
EXPNO                21
PROCNO                2

F2 - Acquisition Parameter
Date_          20211006
Time              15.59 h
INSTRUM            spect
PROBHD   Z125869_0055 (
PULPROG           zgflqn
TD                130892
SOLVENT             CDCl3
NS                    16
DS                     4
SWH          113636.367 Hz
FIDRES         1.736338 Hz
AQ             0.5759248 sec
RG                 15.61
DW                4.400 usec
DE                18.00 usec
TE                298.0 K
D1           1.00000000 sec
TD0                    1
SFO1         470.6394024 MHz
NUC1                 19F
P1                15.00 usec
PLW1         11.70800018 W

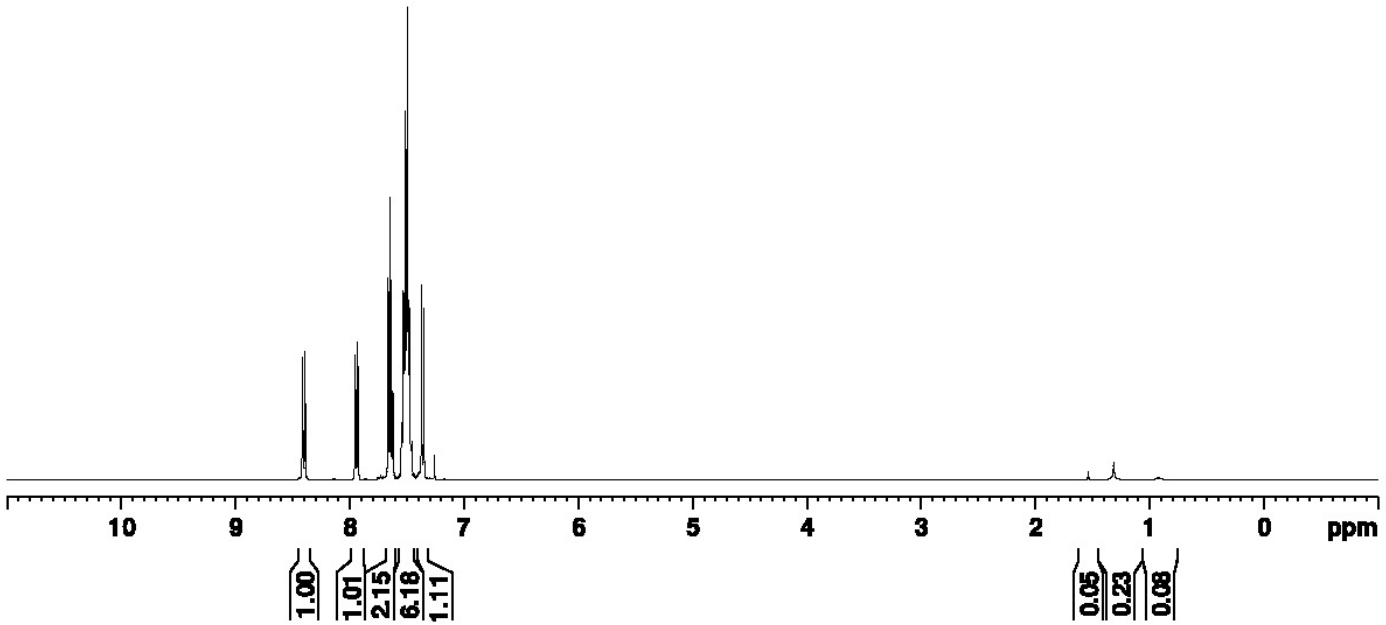
F2 - Processing parameters
SI                 65536
SF           470.6864712 MHz
WDW                   EM
SSB       0
LB                 0.30 Hz
GB        0
PC                 1.00
```







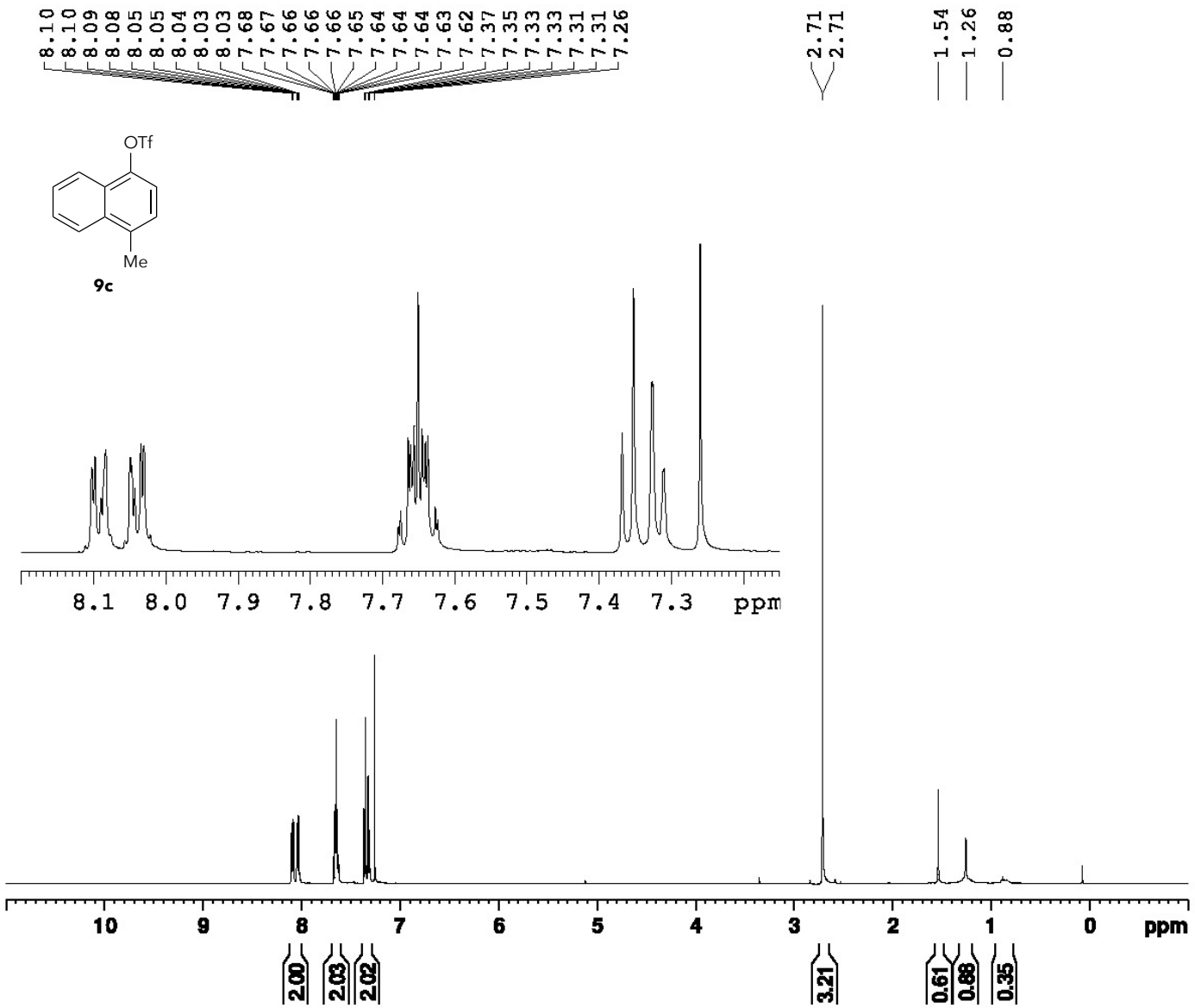
9b




```
Current Data Parameters
NAME      5-SMR-147-final
EXPNO                  10
PROCNO                  1

F2 - Acquisition Parameter
Date_           20210902
Time              16.06 h
INSTRUM       Avance Neo
PROBHD   Z152088_0031 (
PULPROG             zg30
TD                 65536
SOLVENT             CDCl3
NS                     16
DS                      2
SWH             8196.722 Hz
FIDRES           0.250144 Hz
AQ              3.9976959 sec
RG                 79.9054
DW                 61.000 usec
DE                 13.89 usec
TE                 298.2 K
D1              1.00000000 sec
TD0                     1
SFO1          400.1324708 MHz
NUC1                   1H
P0                 2.67 usec
P1                 8.00 usec
PLW1          24.03499985 W

F2 - Processing parameters
SI                 65536
SF            400.1300097 MHz
WDW                   EM
SSB       0
LB                 0.30 Hz
GB        0
PC                 1.00
```

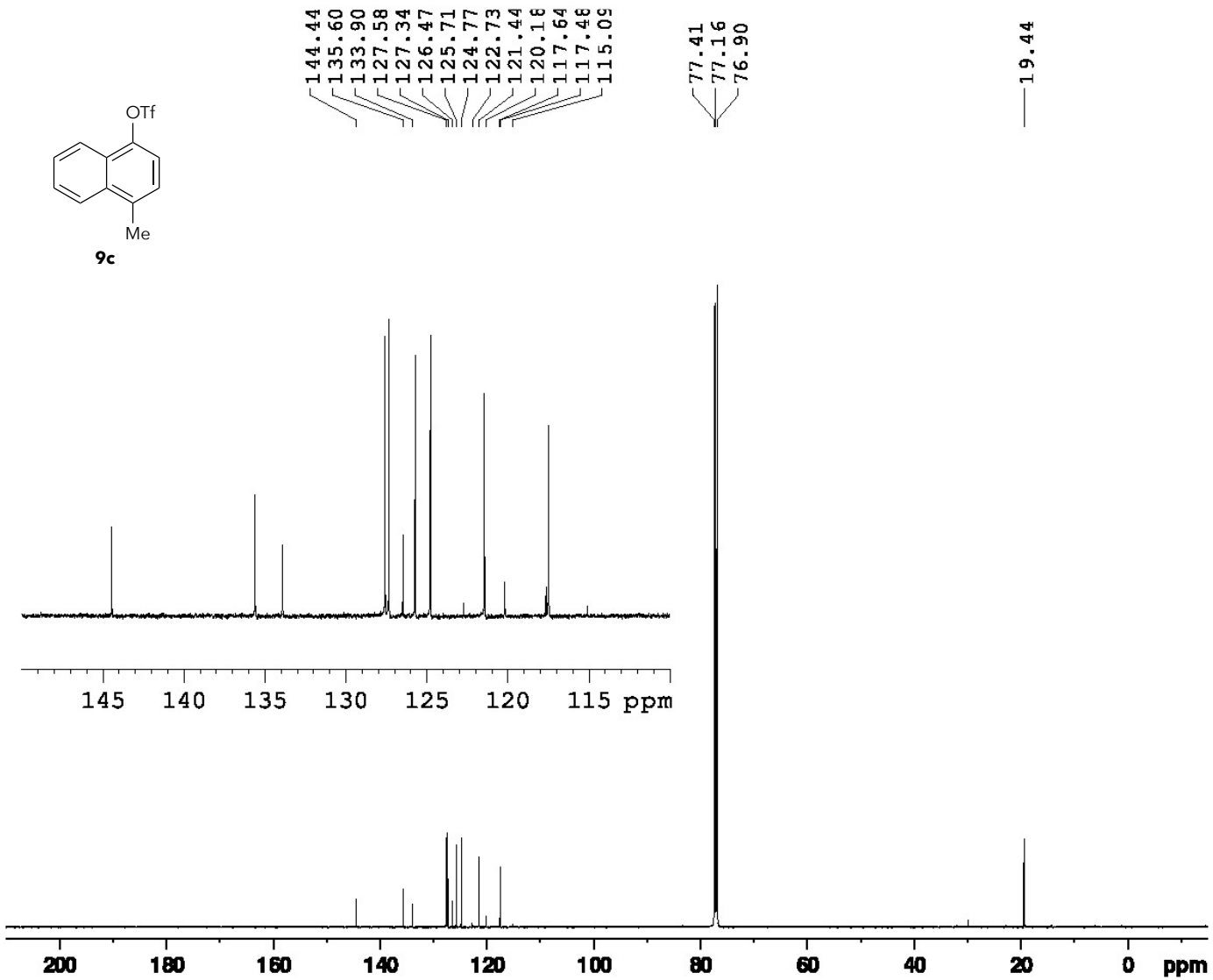





```
Current Data Parameters
NAME          5-SMR-181
EXPNO                20
PROCNO                1

F2 - Acquisition Parameter
Date_          20211007
Time              18.30 h
INSTRUM           spect
PROBHD   Z125869_0055 (
PULPROG           zg30
TD               65536
SOLVENT          CDCl3
NS                  64
DS                   2
SWH          10000.000 Hz
FIDRES         0.305176 Hz
AQ           3.2767999 sec
RG                151.18
DW             50.000 usec
DE             16.00 usec
TE               298.0 K
D1           2.00000000 sec
TD0                  1
SFO1         500.2330889 MHz
NUC1                1H
P0             4.00 usec
P1             12.00 usec
PLW1        11.44699955 W

F2 - Processing parameters
SI               65536
SF          500.2300124 MHz
WDW                 EM
SSB       0
LB              0.30 Hz
GB        0
PC              1.00
```

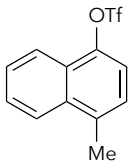


BRUKER

```
Current Data Parameters
NAME          5-SMR-181
EXPNO                21
PROCNO                1

F2 - Acquisition Parameter
Date_          20211007
Time              20.21 h
INSTRUM             spect
PROBHD   Z125869_0055 (
PULPROG           zgpg30
TD                65536
SOLVENT            CDCl3
NS                 2048
DS                    4
SWH           29761.904 Hz
FIDRES         0.908261 Hz
AQ            1.1010048 sec
RG                190.44
DW              16.800 usec
DE              18.00 usec
TE              298.0 K
D1           2.00000000 sec
D11          0.03000000 sec
TD0                   1
SFO1        125.7955118 MHz
NUC1                 13C
P0               3.33 usec
P1              10.00 usec
PLW1         56.90299988 W
SFO2        500.2320009 MHz
NUC2                 1H
CPDPRG[2         waltz16
PCPD2            80.00 usec
PLW2         11.44699955 W
PLW12         0.25756001 W
PLW13         0.12955000 W

F2 - Processing parameters
SI                32768
SF          125.7829158 MHz
WDW                  EM
SSB       0
LB                1.00 Hz
GB        0
PC                1.40
```

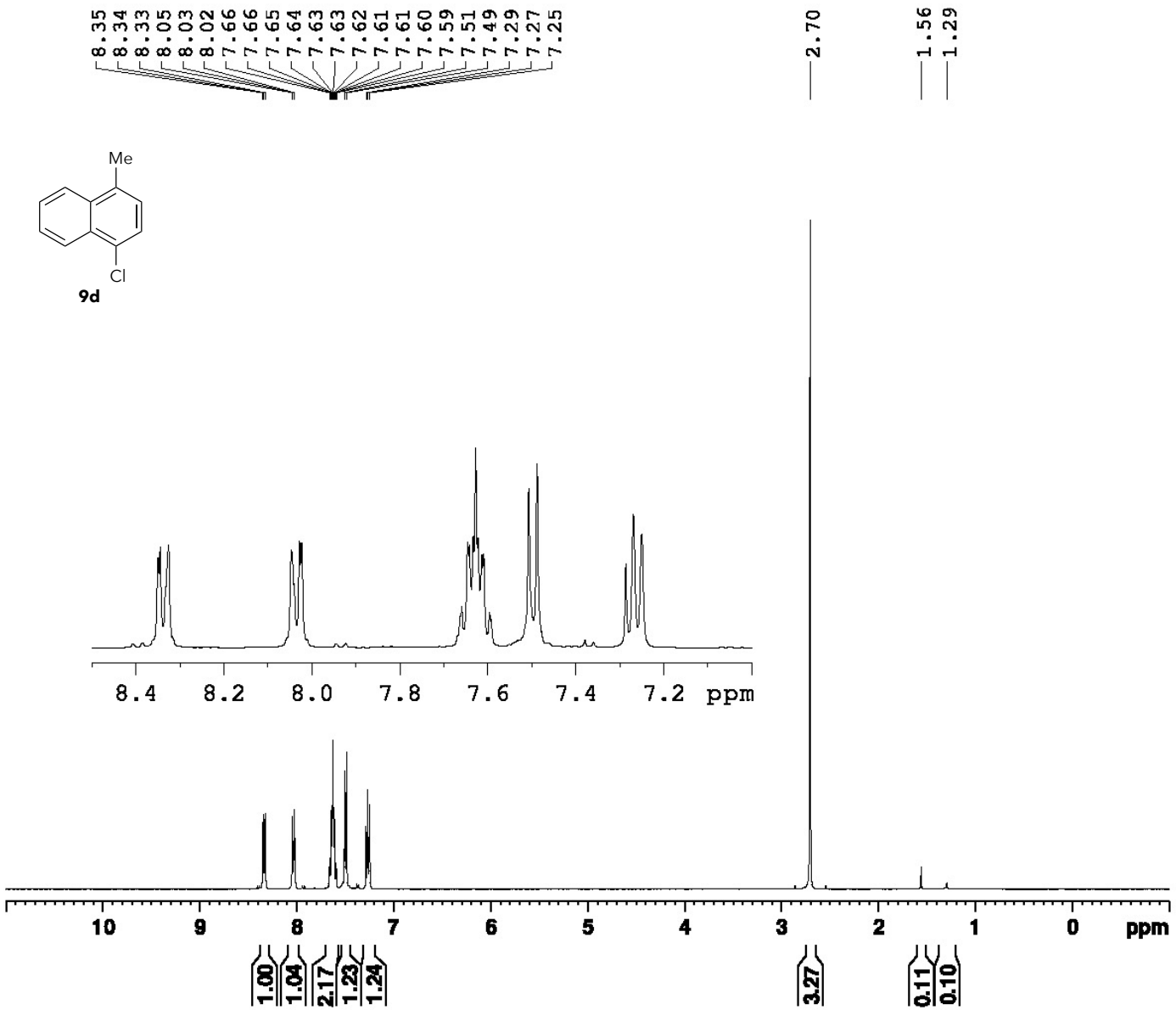


9c


```
Current Data Parameters
NAME          5-SMR-181
EXPNO                22
PROCNO                2

F2 - Acquisition Parameter
Date_          20211007
Time              20.23 h
INSTRUM             spect
PROBHD   Z125869_0055 (
PULPROG           zgflqn
TD                130892
SOLVENT             CDCl3
NS                    16
DS                     4
SWH           113636.367 Hz
FIDRES          1.736338 Hz
AQ             0.5759248 sec
RG                 15.61
DW                4.400 usec
DE                18.00 usec
TE                298.0 K
D1            1.00000000 sec
TD0                    1
SFO1         470.6394024 MHz
NUC1                 19F
P1                15.00 usec
PLW1         11.70800018 W

F2 - Processing parameters
SI                 65536
SF           470.6864712 MHz
WDW                  EM
SSB       0
LB                0.30 Hz
GB        0
PC                1.00
```

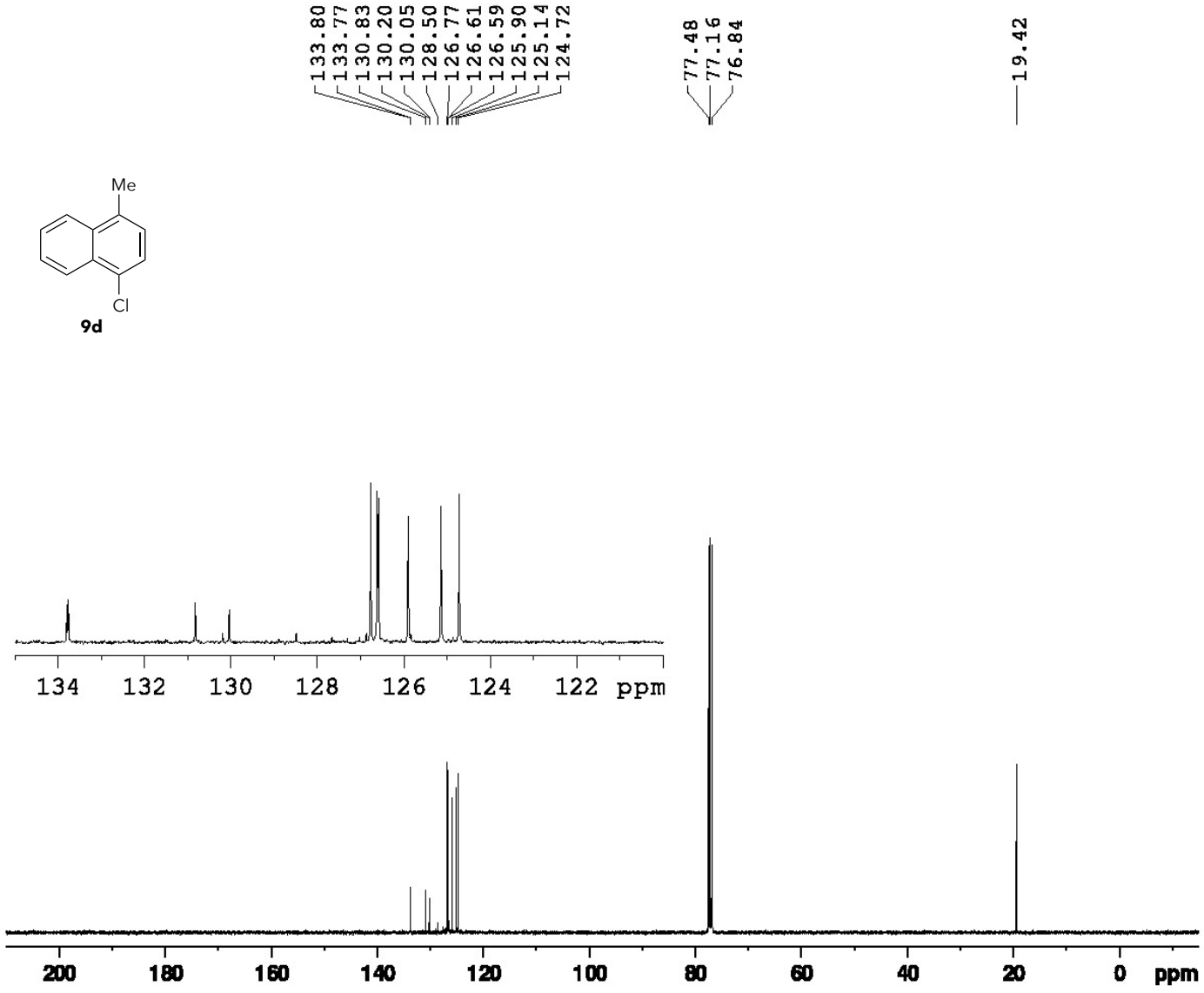


BRUKER

```
Current Data Parameters
NAME      5-SMR-156-final
EXPNO                  10
PROCNO                  1

F2 - Acquisition Parameter
Date_           20210902
Time              17.12 h
INSTRUM       Avance Neo
PROBHD   Z152088_0031 (
PULPROG             zg30
TD                 65536
SOLVENT             CDCl3
NS                     16
DS                      2
SWH             8196.722 Hz
FIDRES           0.250144 Hz
AQ              3.9976959 sec
RG                    101
DW                 61.000 usec
DE                 13.89 usec
TE                 298.2 K
D1             1.00000000 sec
TD0                     1
SFO1          400.1324708 MHz
NUC1                   1H
P0                 2.67 usec
P1                 8.00 usec
PLW1          24.03499985 W

F2 - Processing parameters
SI                 65536
SF            400.1299991 MHz
WDW                    EM
SSB       0
LB                 0.30 Hz
GB        0
PC                 1.00
```

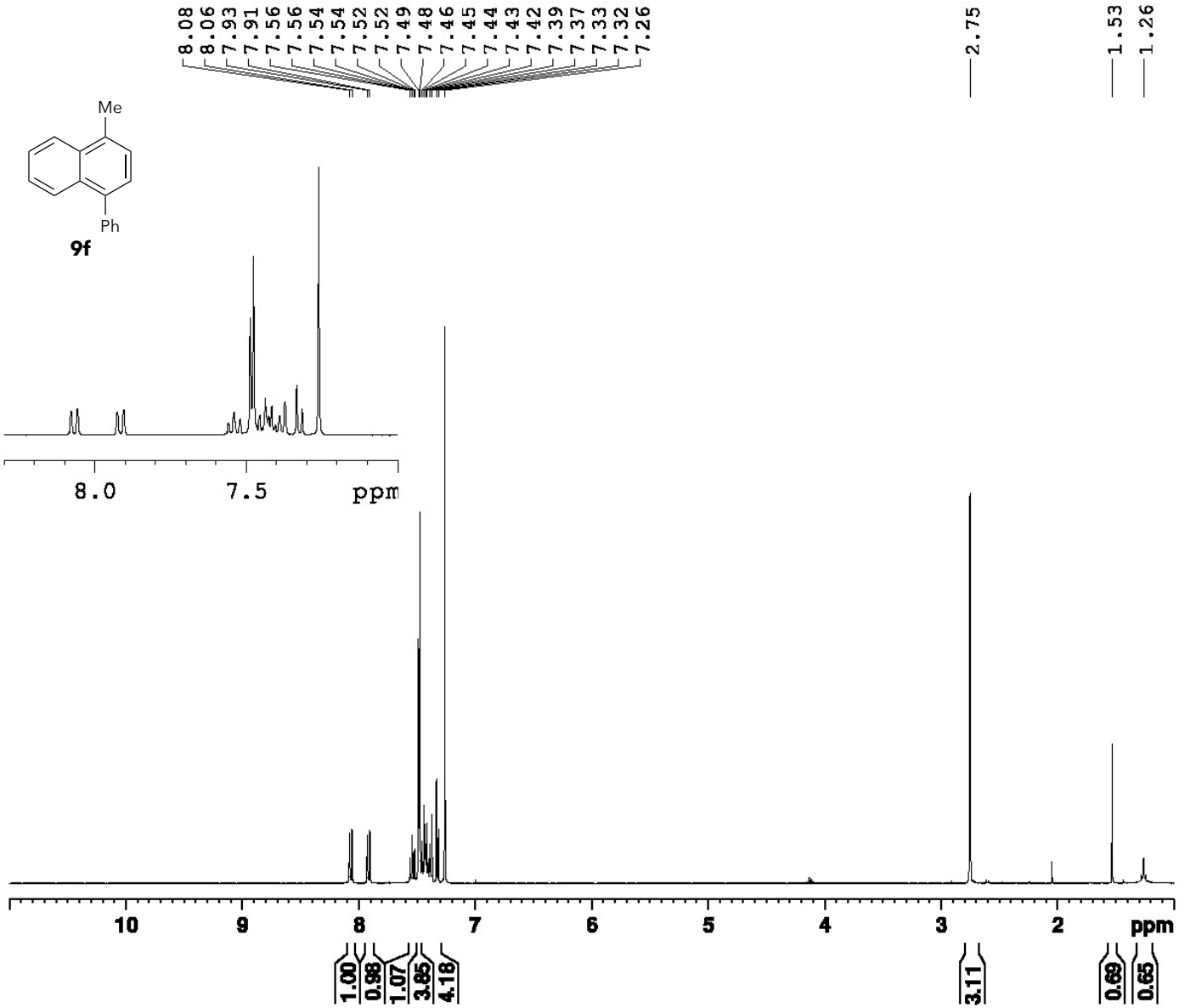


BRUKER

```
Current Data Parameters
NAME      5-SMR-156-final
EXPNO                  11
PROCNO                  1

F2 - Acquisition Parameter
Date_           20210902
Time              18.12 h
INSTRUM       Avance Neo
PROBHD   Z152088_0031 (
PULPROG           zgpg30
TD                65536
SOLVENT           CDCl3
NS                 1024
DS                    4
SWH          23809.523 Hz
FIDRES        0.726609 Hz
AQ           1.3762560 sec
RG                8.125
DW             21.000 usec
DE              6.50 usec
TE              298.2 K
D1           2.00000000 sec
D11          0.03000000 sec
TD0                   1
SFO1         100.6228298 MHz
NUC1                 13C
P0                2.67 usec
P1                8.00 usec
PLW1         86.55400085 W
SFO2         400.1316005 MHz
NUC2                 1H
CPDPRG[2         waltz65
PCPD2             90.00 use
PLW2         24.03499985 W
PLW12         0.18990999 W
PLW13         0.09552100 W

F2 - Processing parameters
SI                32768
SF          100.6127555 MHz
WDW                  EM
SSB       0
LB                1.00 Hz
GB        0
PC                1.40
```

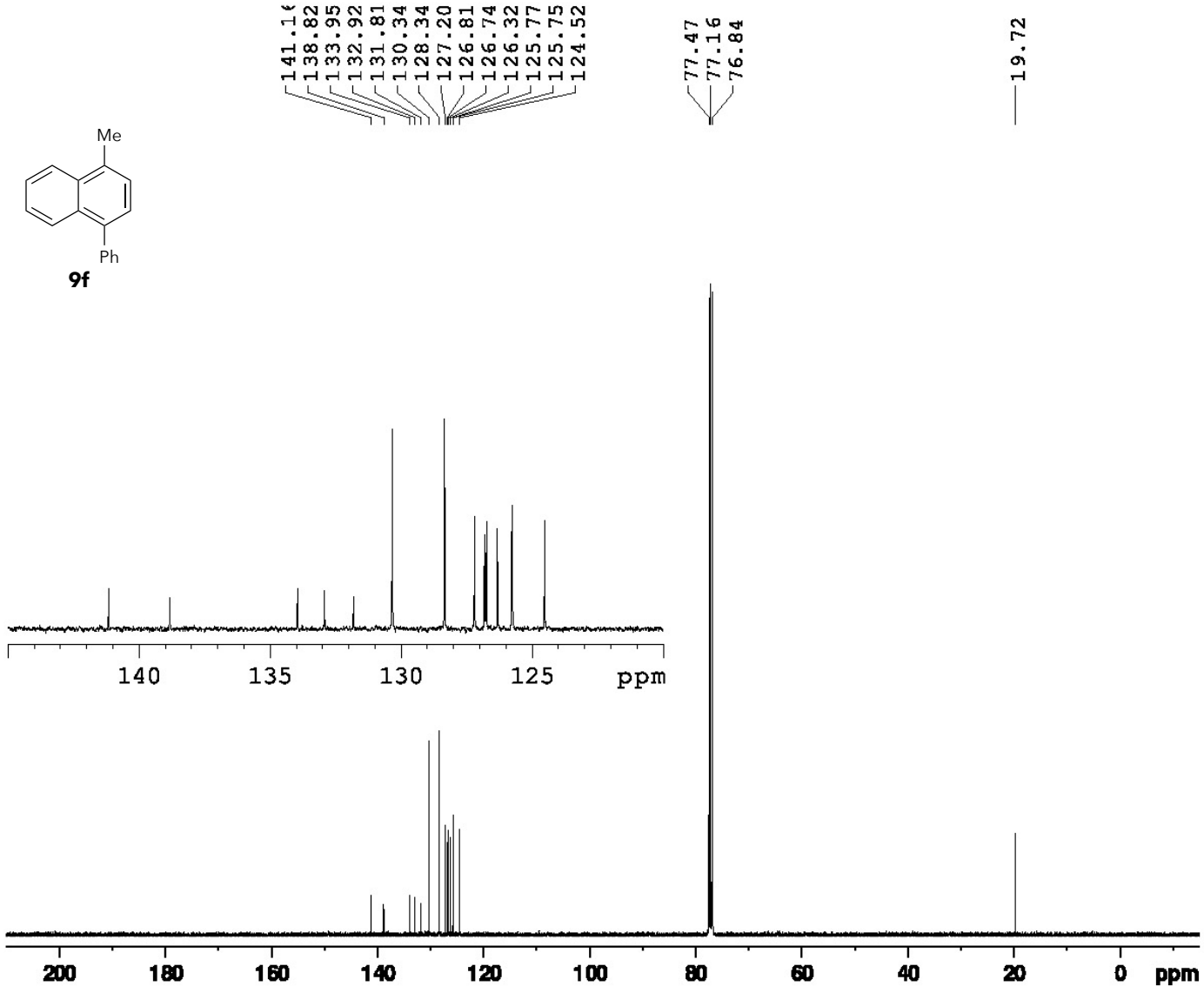


BRUKER

```
Current Data Parameters
NAME          5-SMR-149
EXPNO                10
PROCNO                1

F2 - Acquisition Parameter
Date_          20210803
Time              14.52 h
INSTRUM       Avance Neo
PROBHD   Z152088_0031 (
PULPROG             zg30
TD                 65536
SOLVENT             CDCl3
NS                    16
DS                     2
SWH             8196.722 Hz
FIDRES           0.250144 Hz
AQ              3.9976959 sec
RG                   101
DW                61.000 usec
DE                13.89 usec
TE                298.1 K
D1             1.00000000 sec
TD0                    1
SFO1          400.1324708 MHz
NUC1                  1H
P0                 2.67 usec
P1                 8.00 usec
PLW1          24.03499985 W

F2 - Processing parameters
SI                 65536
SF            400.1300093 MHz
WDW                   EM
SSB       0
LB                0.30 Hz
GB        0
PC                1.00
```

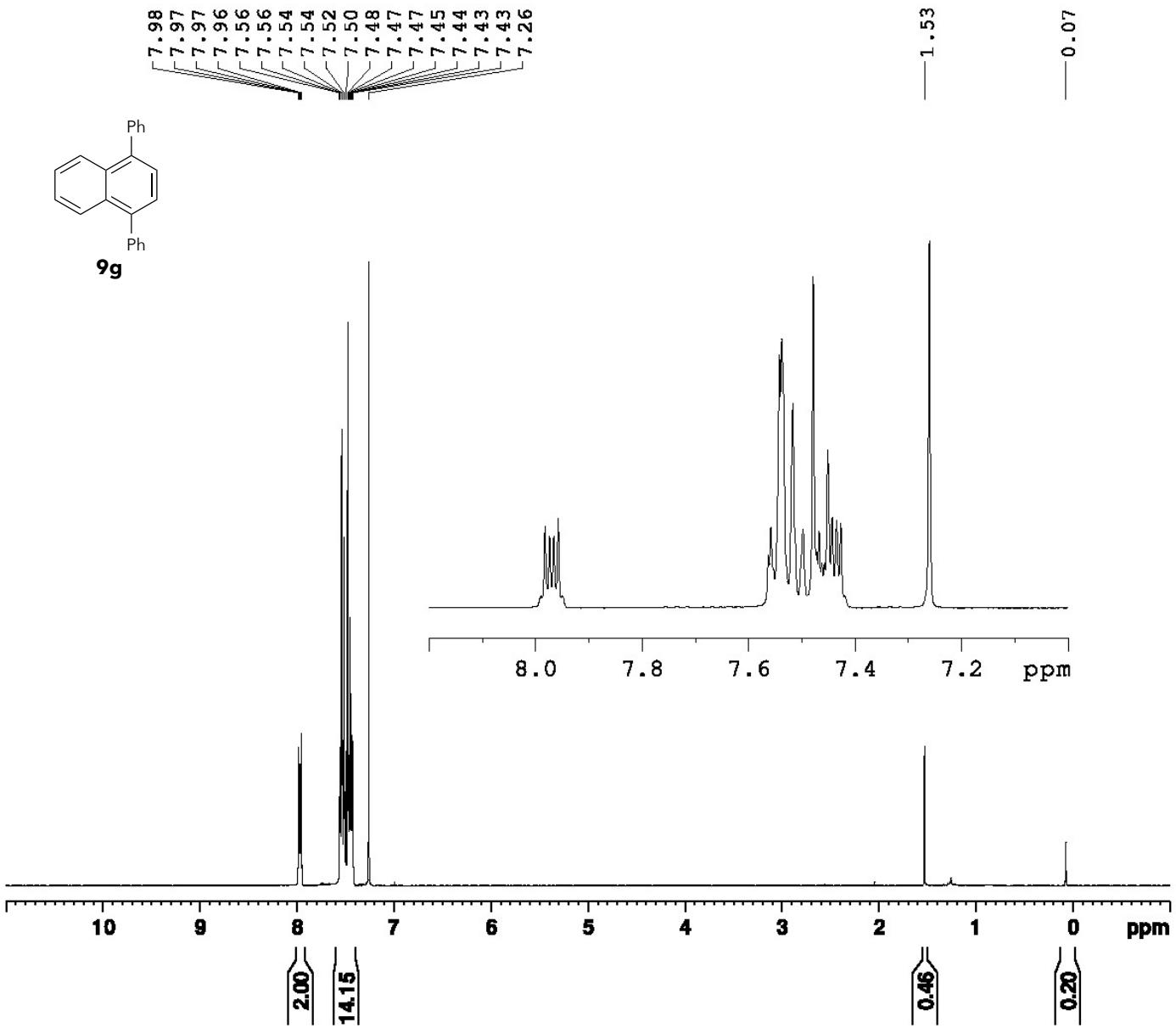




```
Current Data Parameters
NAME          5-SMR-149
EXPNO                12
PROCNO                1

F2 - Acquisition Parameter
Date_          20210906
Time             14.20 h
INSTRUM      Avance Neo
PROBHD   Z152088_0031 (
PULPROG          zgpg30
TD                65536
SOLVENT           CDCl3
NS                 1024
DS                    4
SWH          23809.523 Hz
FIDRES         0.726609 Hz
AQ             1.3762560 sec
RG                8.125
DW               21.000 usec
DE                6.50 usec
TE               298.2 K
D1             2.00000000 sec
D11            0.03000000 sec
TD0                   1
SFO1         100.6228298 MHz
NUC1                 13C
P0                2.67 usec
P1                8.00 usec
PLW1         86.55400085 W
SFO2         400.1316005 MHz
NUC2                 1H
CPDPRG[2         waltz65
PCPD2             90.00 use
PLW2         24.03499985 W
PLW12         0.18990999 W
PLW13         0.09552100 W

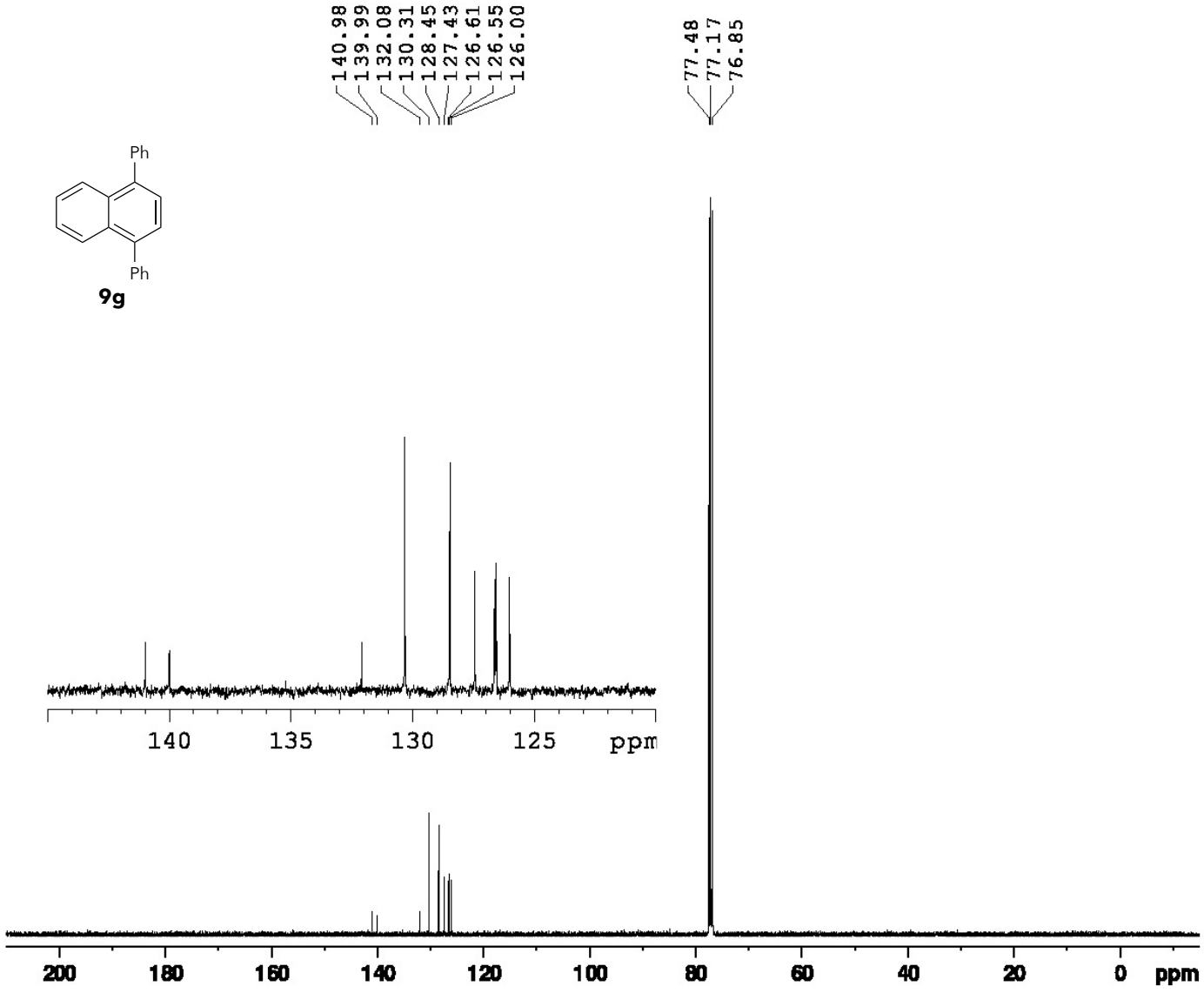
F2 - Processing parameters
SI                32768
SF          100.6127551 MHz
WDW                  EM
SSB       0
LB                1.00 Hz
GB        0
PC                1.40
```



Current Data Parameters
NAME 5-SMR-163-full
EXPNO 10
PROCNO 1

F2 - Acquisition Parameter
Date_ 20210906
Time 14.26 h
INSTRUM Avance Neo
PROBHD Z152088_0031 (
PULPROG zg30
TD 65536
SOLVENT CDCl3
NS 16
DS 2
SWH 8196.722 Hz
FIDRES 0.250144 Hz
AQ 3.9976959 sec
RG 101
DW 61.000 usec
DE 13.89 usec
TE 298.2 K
D1 1.00000000 sec
TD0 1
SFO1 400.1324708 MHz
NUC1 1H
P0 2.67 usec
P1 8.00 usec
PLW1 24.03499985 W

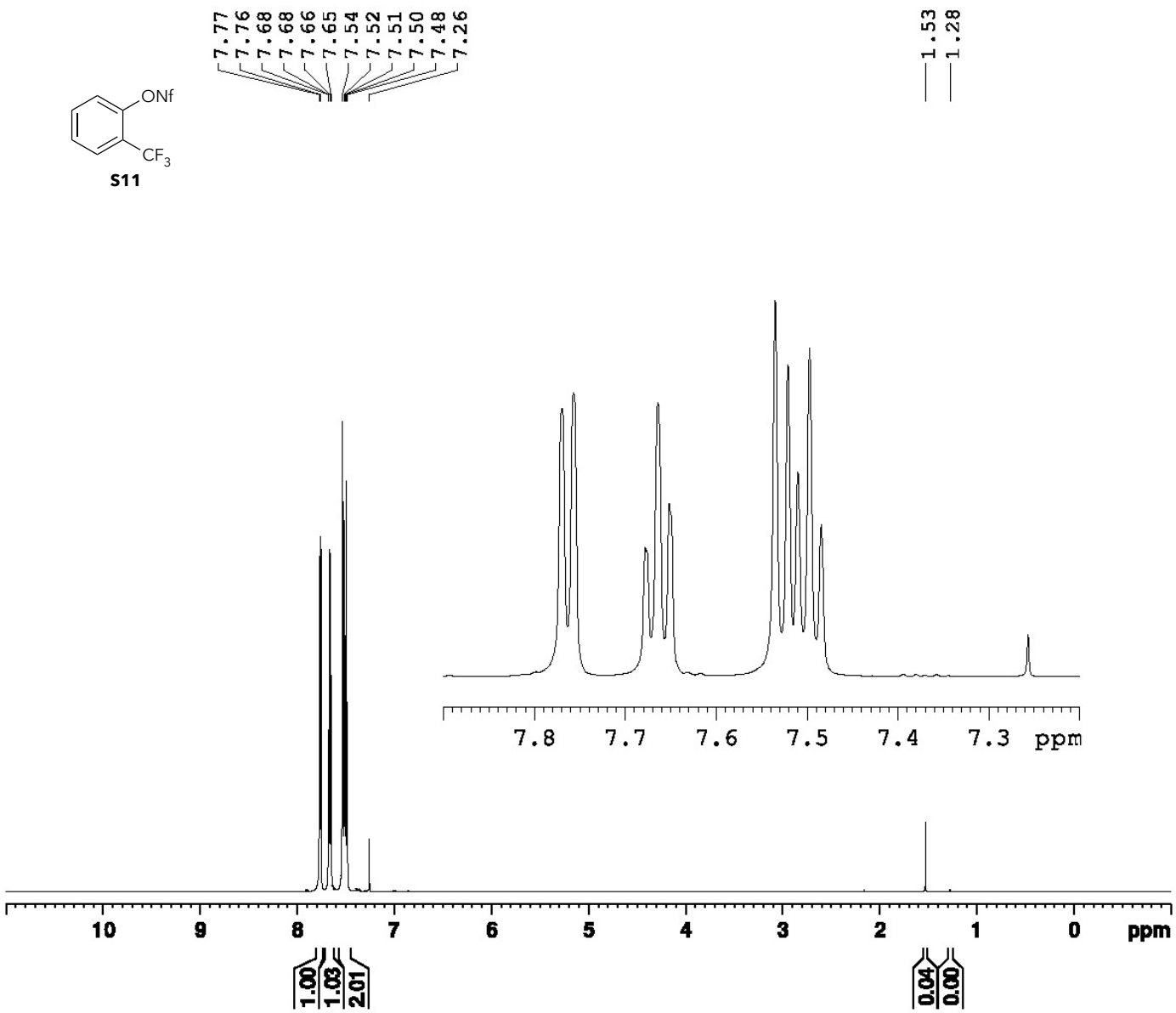
F2 - Processing parameters
SI 65536
SF 400.1300095 MHz
WDW EM
SSB 0
LB 0.30 Hz
GB 0
PC 1.00



Current Data Parameters
NAME 5-SMR-163-full
EXPNO 12
PROCNO 1

F2 - Acquisition Parameter
Date_ 20210906
Time 15.27 h
INSTRUM Avance Neo
PROBHD Z152088_0031 (
PULPROG zgpg30
TD 65536
SOLVENT CDCl3
NS 1024
DS 4
SWH 23809.523 Hz
FIDRES 0.726609 Hz
AQ 1.3762560 sec
RG 8.125
DW 21.000 usec
DE 6.50 usec
TE 298.2 K
D1 2.00000000 sec
D11 0.03000000 sec
TD0 1
SFO1 100.6228298 MHz
NUC1 13C
P0 2.67 usec
P1 8.00 usec
PLW1 86.55400085 W
SFO2 400.1316005 MHz
NUC2 1H
CPDPRG[2 waltz65
PCPD2 90.00 use
PLW2 24.03499985 W
PLW12 0.18990999 W
PLW13 0.09552100 W

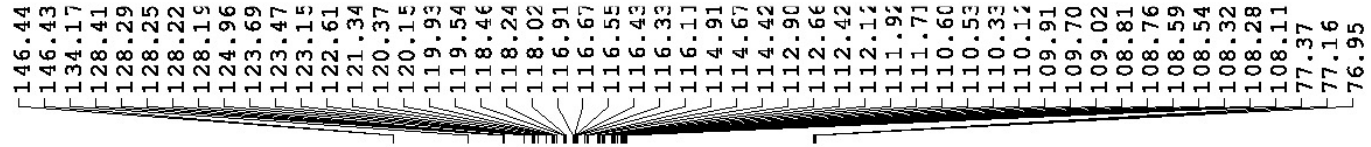
F2 - Processing parameters
SI 32768
SF 100.6127534 MHz
WDW EM
SSB 0
LB 1.00 Hz
GB 0
PC 1.40

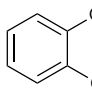


Current Data Parameters
NAME ER-6-CF3PhONf
EXPNO 10
PROCNO 1

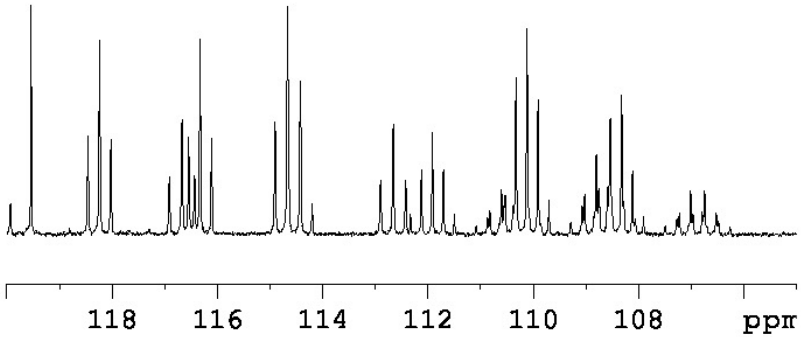
F2 - Acquisition Parameter
Date_ 20200709
Time 15.43 h
INSTRUM spect
PROBHD Z127277_0002 (
PULPROG zg30
TD 65536
SOLVENT CDCl3
NS 64
DS 2
SWH 12019.230 Hz
FIDRES 0.366798 Hz
AQ 2.7262976 sec
RG 4.41
DW 41.600 usec
DE 10.00 usec
TE 300.0 K
D1 1.00000000 sec
TD0 1
SFO1 600.1337060 MHz
NUC1 1H
P0 2.67 usec
P1 8.00 usec
PLW1 5.59999990 W

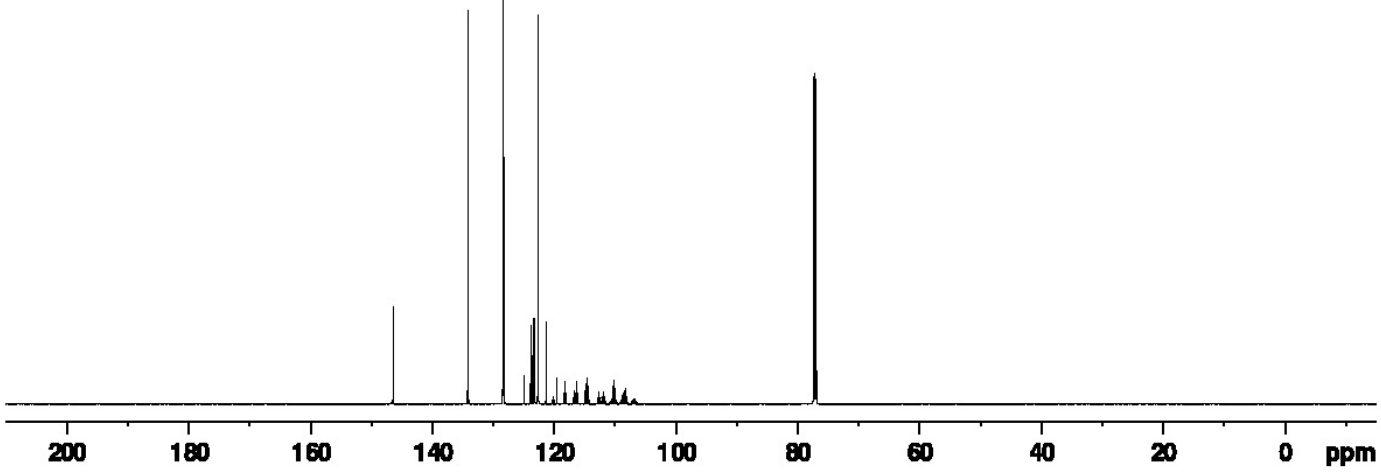
F2 - Processing parameters
SI 65536
SF 600.1300162 MHz
WDW EM
SSB 0
LB 0.30 Hz
GB 0
PC 1.00





S11

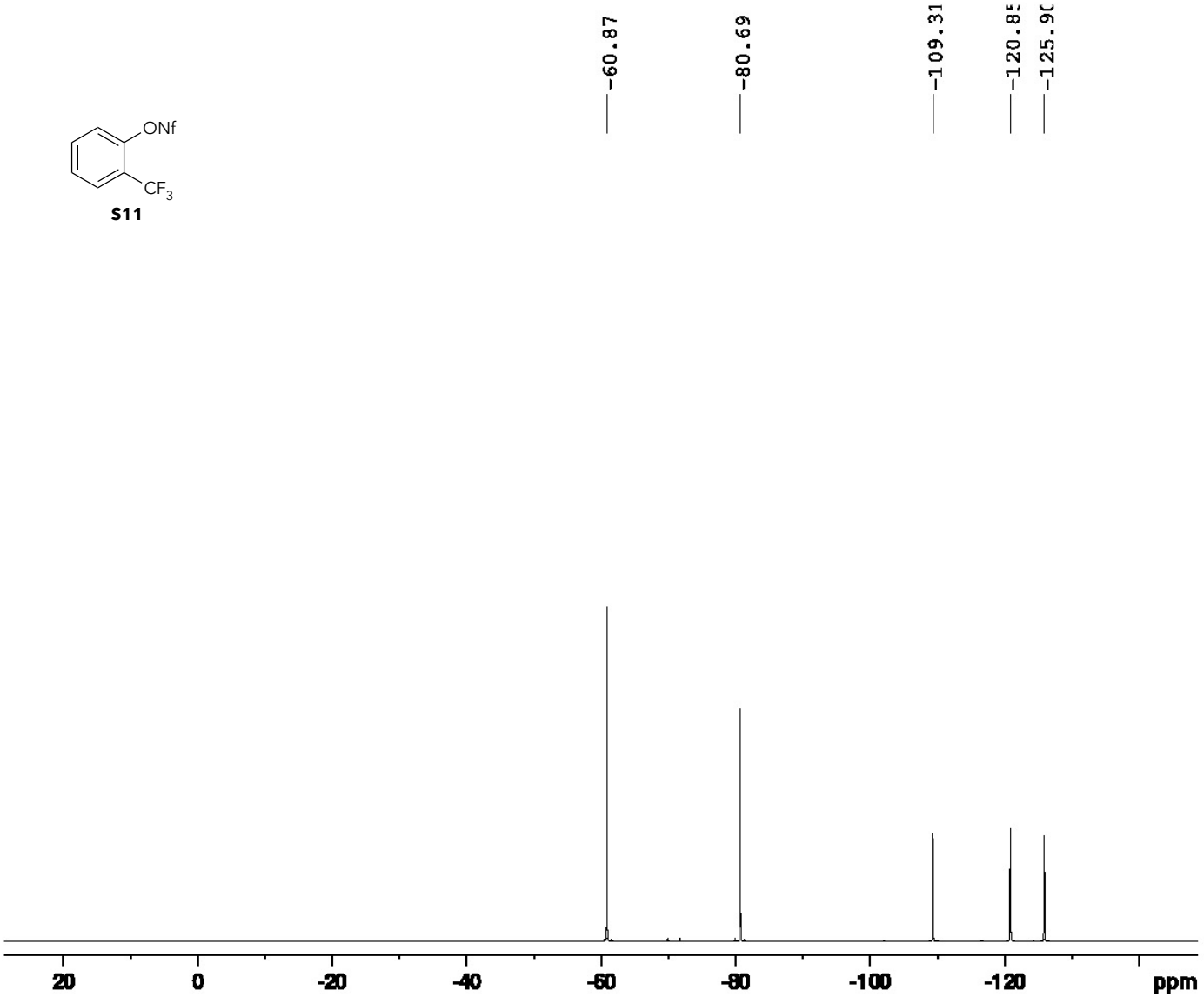





```
Current Data Parameters
NAME      ER-6-CF3PhONf
EXPNO              11
PROCNO              1

F2 - Acquisition Parameter
Date_          20200709
Time             16.35 h
INSTRUM           spect
PROBHD   Z127277_0002 (
PULPROG          zgpg30
TD               65536
SOLVENT           CDCl3
NS                1024
DS                   4
SWH          36057.691 Hz
FIDRES         1.100393 Hz
AQ           0.9087659 sec
RG                184.4
DW              13.867 usec
DE              18.00 usec
TE              300.0 K
D1           2.00000000 sec
D11          0.03000000 sec
TD0                  1
SFO1        150.9178981 MHz
NUC1               13C
P0              4.00 usec
P1              12.00 usec
PLW1        91.00000000 W
SFO2        600.1324005 MHz
NUC2               1H
CPDPRG[2        waltz16
PCPD2           70.00 use
PLW2         5.59999990 W
PLW12        0.07314300 W
PLW13        0.03679000 W

F2 - Processing parameters
SI                32768
SF          150.9027731 MHz
WDW                EM
SSB       0
LB              1.00 Hz
GB        0
PC              1.40
```



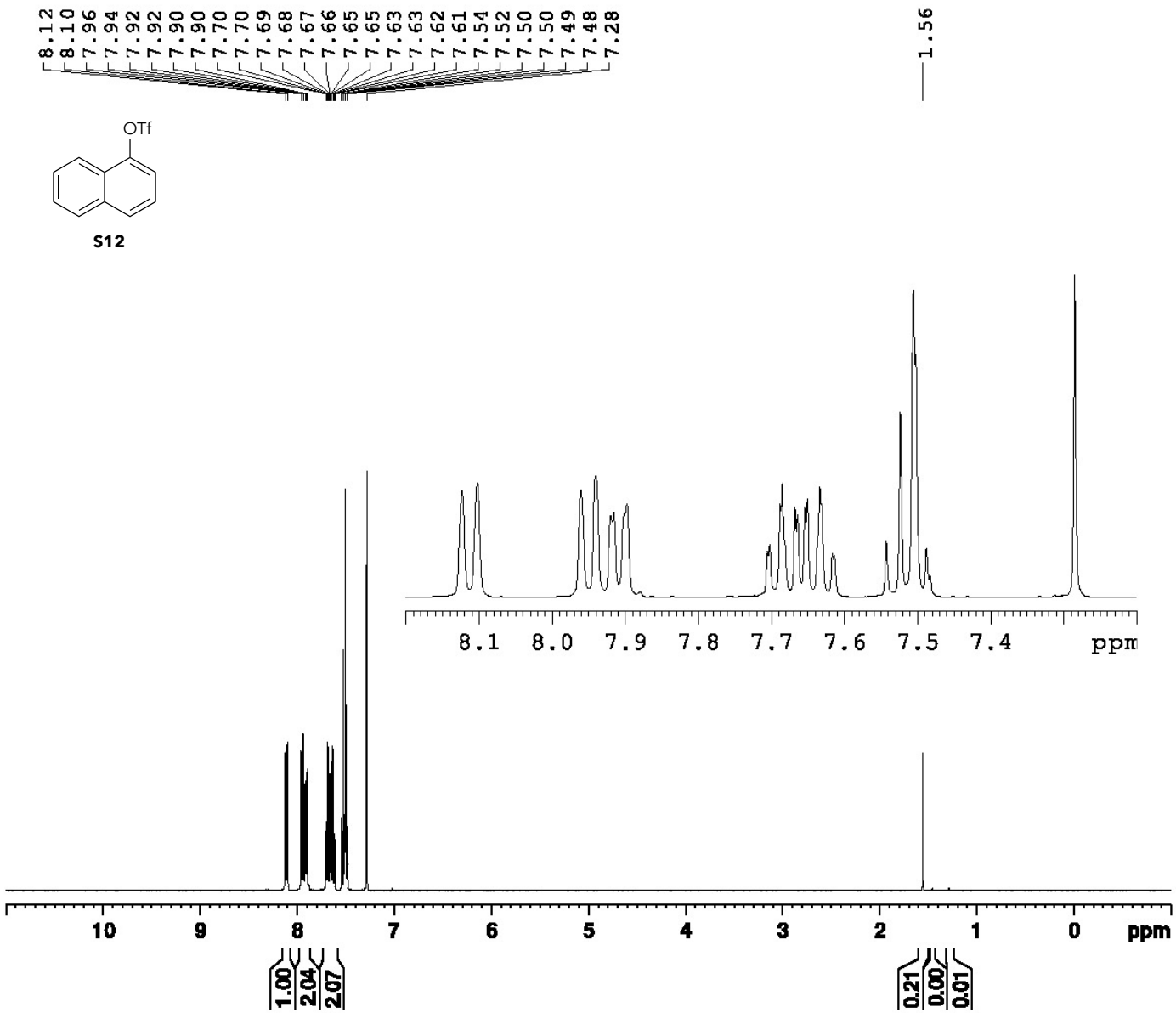
BRUKER

```
Current Data Parameters
NAME      ER-6-CF3PhONf
EXPNO                 4
PROCNO                1

F2 - Acquisition Parameter
Date_          20201005
Time               7.13
INSTRUM           spect
PROBHD   5 mm QNP 1H/13
PULPROG          zgflqn
TD              32768
SOLVENT            C6D6
NS                   64
DS                    0
SWH           50125.312 Hz
FIDRES         1.529703 Hz
AQ            0.3268608 sec
RG                645.1
DW              9.975 usec
DE              6.00 usec
TE              683.2 K
D1           1.50000000 sec
TD0                   1

====== CHANNEL f1 ======
NUC1                 19F
P1                9.00 usec
PL1       0 dB
SFO1        282.4250465 MHz

F2 - Processing parameters
SI                65536
SF          282.4419930 MHz
WDW                  EM
SSB       0
LB                0.30 Hz
GB        0
PC                1.00
```

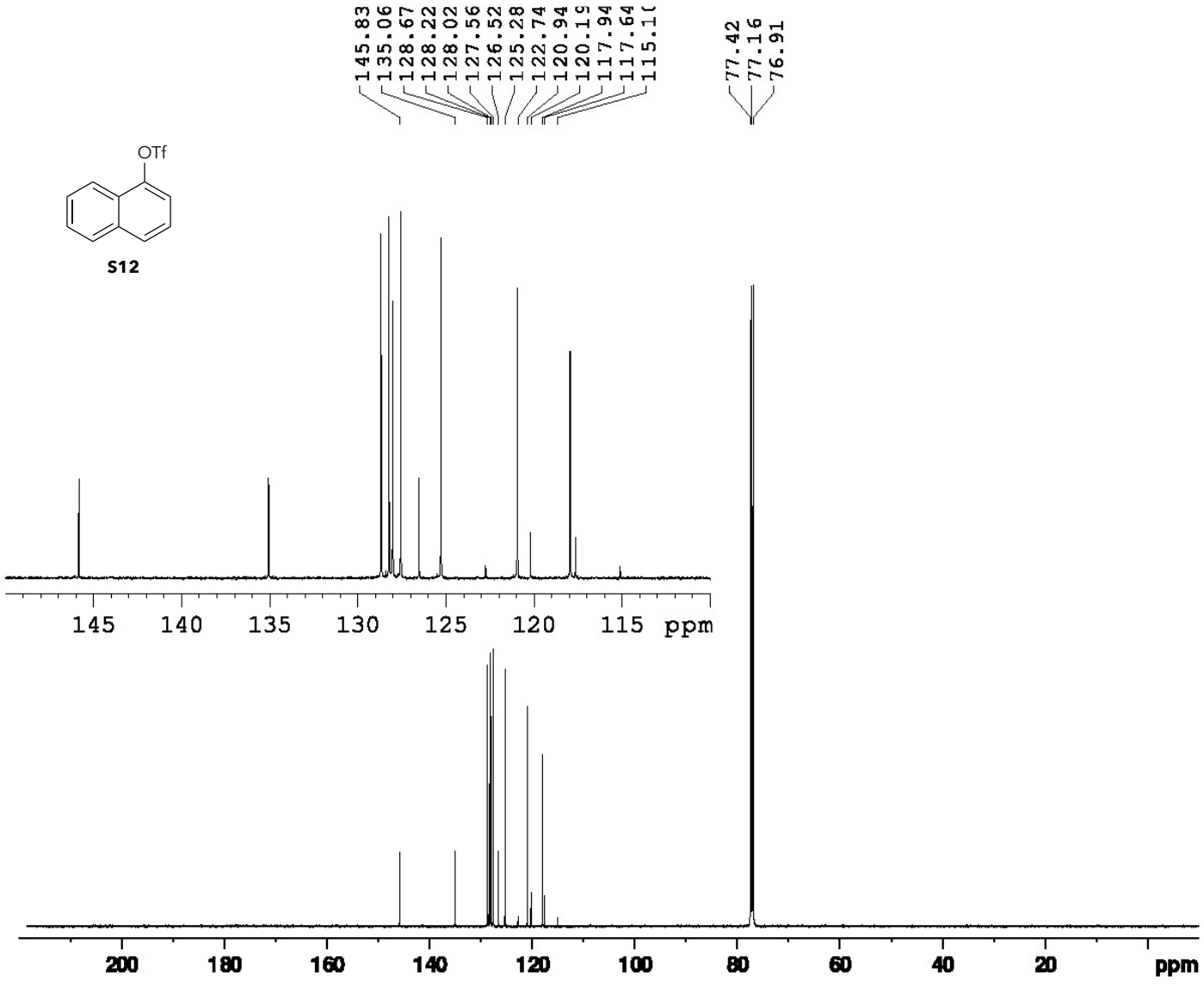


BRUKER

Current Data Parameters
NAME EKB-1-184
EXPNO 10
PROCNO 1

F2 - Acquisition Parameter
Date_ 20210702
Time 12.05 h
INSTRUM Avance Neo
PROBHD Z152088_0031 (
PULPROG zg30
TD 65536
SOLVENT CDCl3
NS 16
DS 2
SWH 8196.722 Hz
FIDRES 0.250144 Hz
AQ 3.9976959 sec
RG 101
DW 61.000 usec
DE 13.89 usec
TE 298.0 K
D1 1.00000000 sec
TD0 1
SFO1 400.1324708 MHz
NUC1 1H
P0 2.67 usec
P1 8.00 usec
PLW1 24.03499985 W

F2 - Processing parameters
SI 65536
SF 400.1300000 MHz
WDW EM
SSB 0
LB 0.30 Hz
GB 0
PC 1.00

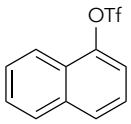


BRUKER

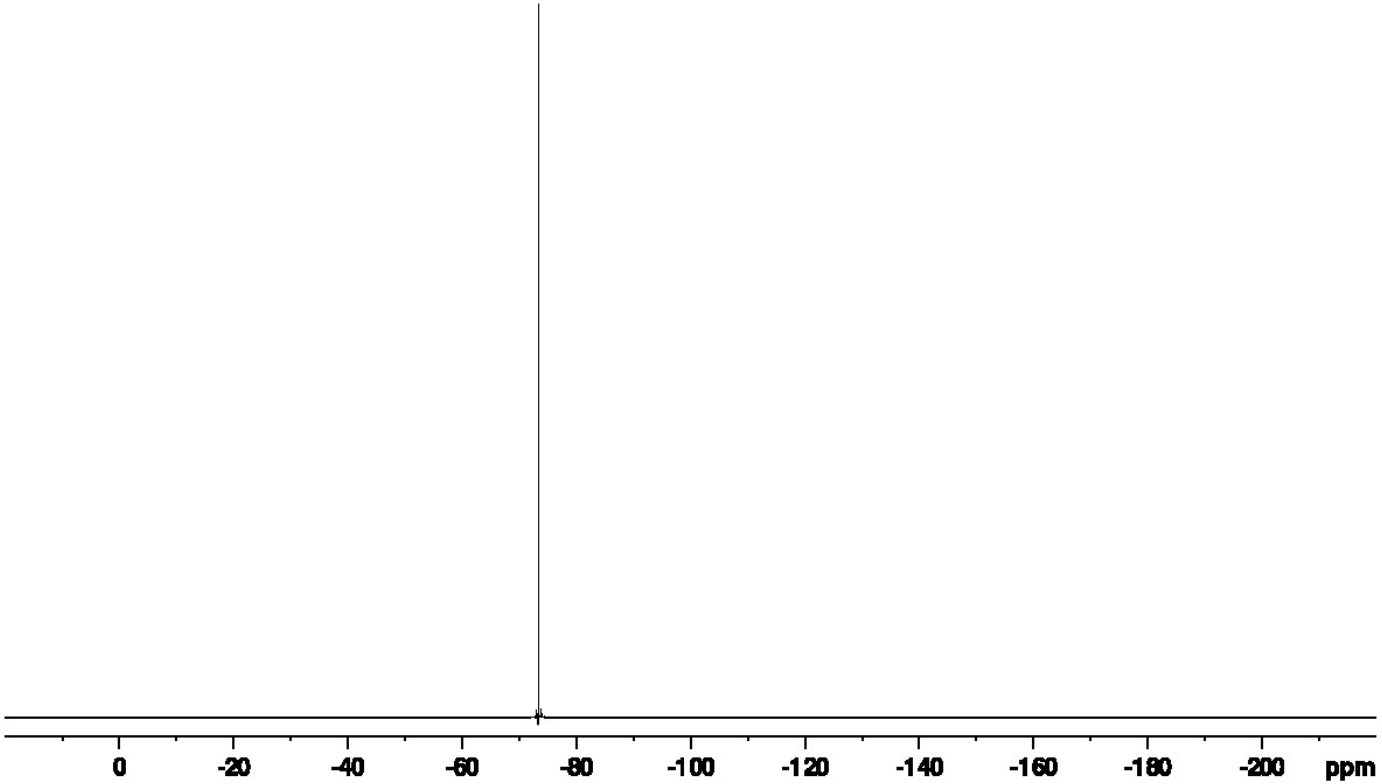
```
Current Data Parameters
NAME          EKB-1-184
EXPNO                22
PROCNO                1

F2 - Acquisition Parameter
Date_          20211007
Time              12.53 h
INSTRUM           spect
PROBHD   Z125869_0055 (
PULPROG          zgpg30
TD                65536
SOLVENT           CDCl3
NS                 1024
DS                    4
SWH           29761.904 Hz
FIDRES         0.908261 Hz
AQ            1.1010048 sec
RG               190.44
DW              16.800 usec
DE              18.00 usec
TE              298.0 K
D1            2.00000000 sec
D11           0.03000000 sec
TD0                   1
SFO1         125.7955118 MHz
NUC1                 13C
P0               3.33 usec
P1              10.00 usec
PLW1         56.90299988 W
SFO2         500.2320009 MHz
NUC2                 1H
CPDPRG[2         waltz16
PCPD2             80.00 use
PLW2         11.44699955 W
PLW12         0.25756001 W
PLW13         0.12955000 W

F2 - Processing parameters
SI                32768
SF          125.7829156 MHz
WDW                  EM
SSB       0
LB                1.00 Hz
GB        0
PC                1.40
```



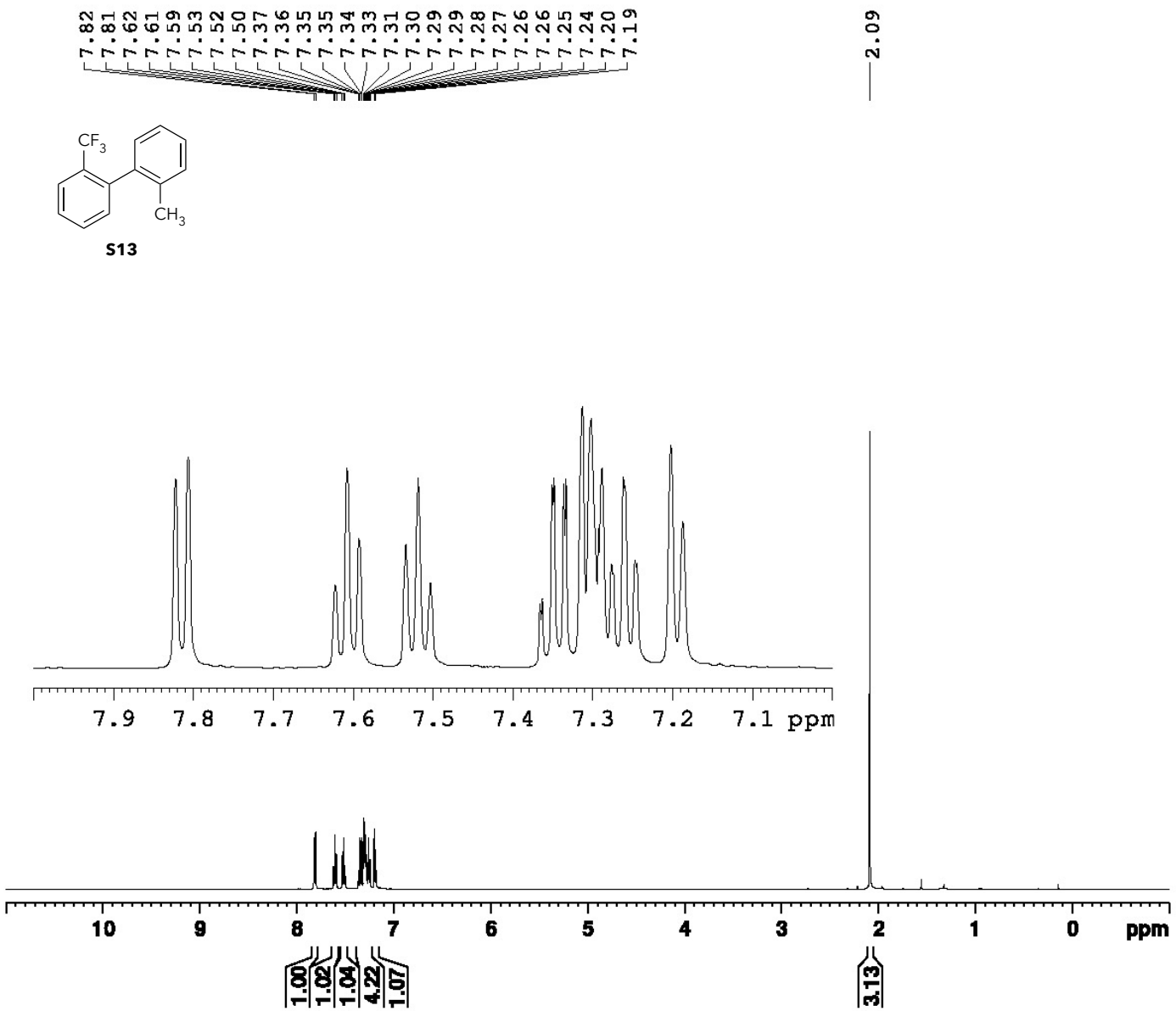
S12




```
Current Data Parameters
NAME          EKB-1-184
EXPNO                11
PROCNO                2

F2 - Acquisition Parameter
Date_          20210702
Time              12.13 h
INSTRUM       Avance Neo
PROBHD   Z152088_0031 (
PULPROG           zgig
TD              130892
SOLVENT           CDCl3
NS                   16
DS                    4
SWH           90909.094 Hz
FIDRES         1.389070 Hz
AQ            0.7199060 sec
RG                  101
DW                5.500 usec
DE                6.50 usec
TE                298.1 K
D1           1.00000000 sec
D11          0.03000000 sec
TD0                   1
SFO1        376.4607164 MHz
NUC1               19F
P1                12.00 usec
PLW1        31.08900070 W
SFO2        400.1316005 MHz
NUC2               1H
CPDPRG[2        waltz16
PCPD2             90.00 usec
PLW2        24.03499985 W
PLW12        0.18990999 W

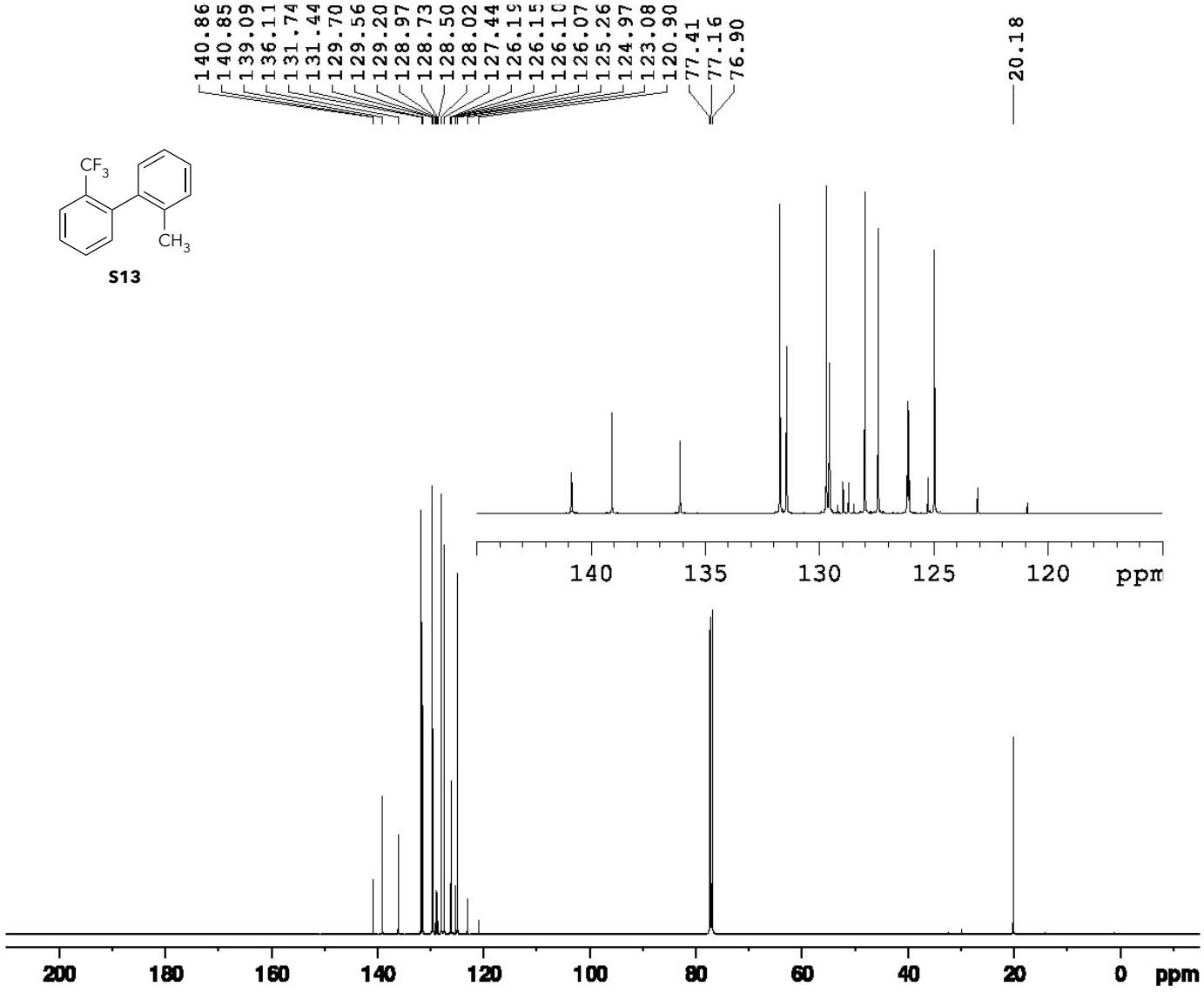
F2 - Processing parameters
SI                65536
SF          376.4983662 MHz
WDW                  EM
SSB       0
LB                0.30 Hz
GB        0
PC                1.00
```




```
Current Data Parameters
NAME                  6-SMR-4
EXPNO                      30
PROCNO                      1

F2 - Acquisition Parameter
Date_              20211008
Time                  15.37 h
INSTRUM                spect
PROBHD    Z125869_0055 (
PULPROG                 zg30
TD                     65536
SOLVENT                CDCl3
NS                        64
DS                         2
SWH               10000.000 Hz
FIDRES             0.305176 Hz
AQ                3.2767999 sec
RG                     37.93
DW                  50.000 usec
DE                  16.00 usec
TE                  298.0 K
D1               2.00000000 sec
TD0                        1
SFO1           500.2330889 MHz
NUC1                      1H
P0                  4.00 usec
P1                  12.00 usec
PLW1           11.44699955 W

F2 - Processing parameters
SI                     65536
SF             500.2299955 MHz
WDW                       EM
SSB          0
LB                  0.30 Hz
GB           0
PC                     1.00
```

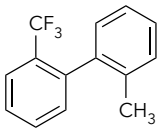




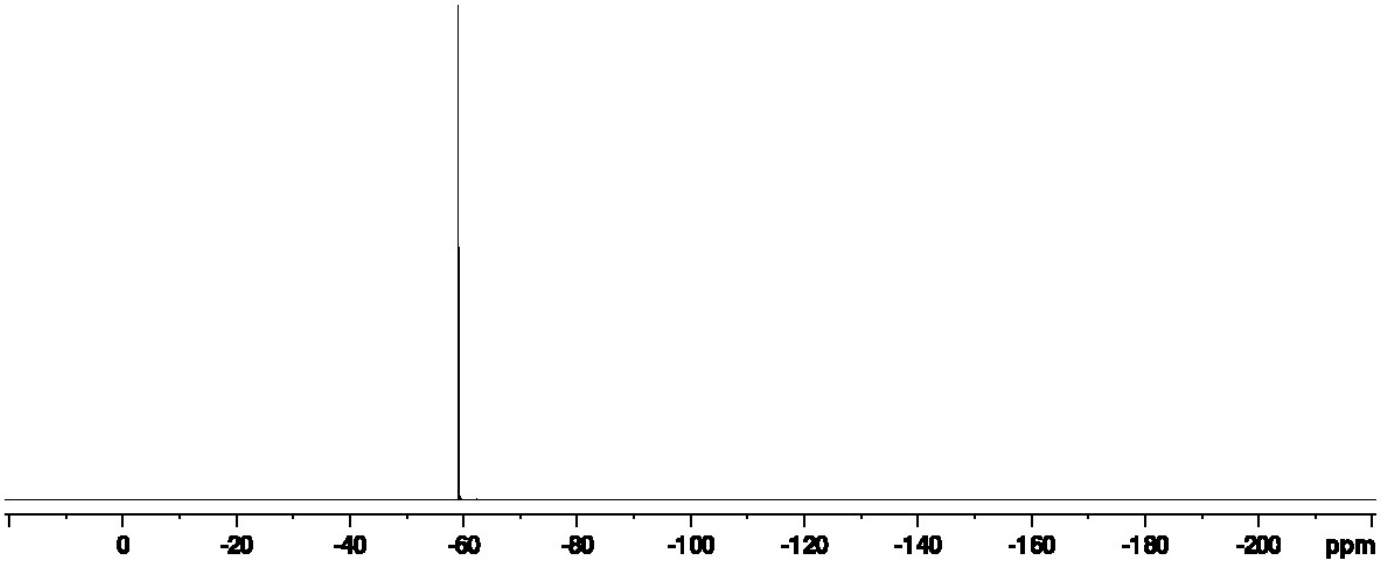
```
Current Data Parameters
NAME                  6-SMR-4
EXPNO                      32
PROCNO                      1

F2 - Acquisition Parameter
Date_              20211008
Time                 17.31 h
INSTRUM                spect
PROBHD   Z125869_0055 (
PULPROG                zgpg30
TD                     65536
SOLVENT                CDCl3
NS                      2048
DS                         4
SWH               29761.904 Hz
FIDRES             0.908261 Hz
AQ                1.1010048 sec
RG                    190.44
DW                  16.800 usec
DE                  18.00 usec
TE                  298.0 K
D1                2.00000000 sec
D11               0.03000000 sec
TD0                        1
SFO1             125.7955118 MHz
NUC1                     13C
P0                   3.33 usec
P1                  10.00 usec
PLW1             56.90299988 W
SFO2             500.2320009 MHz
NUC2                     1H
CPDPRG[2              waltz16
PCPD2                80.00 usec
PLW2             11.44699955 W
PLW12             0.25756001 W
PLW13             0.12955000 W

F2 - Processing parameters
SI                       32768
SF               125.7829185 MHz
WDW                         EM
SSB          0
LB                    1.00 Hz
GB           0
PC                    1.40
```



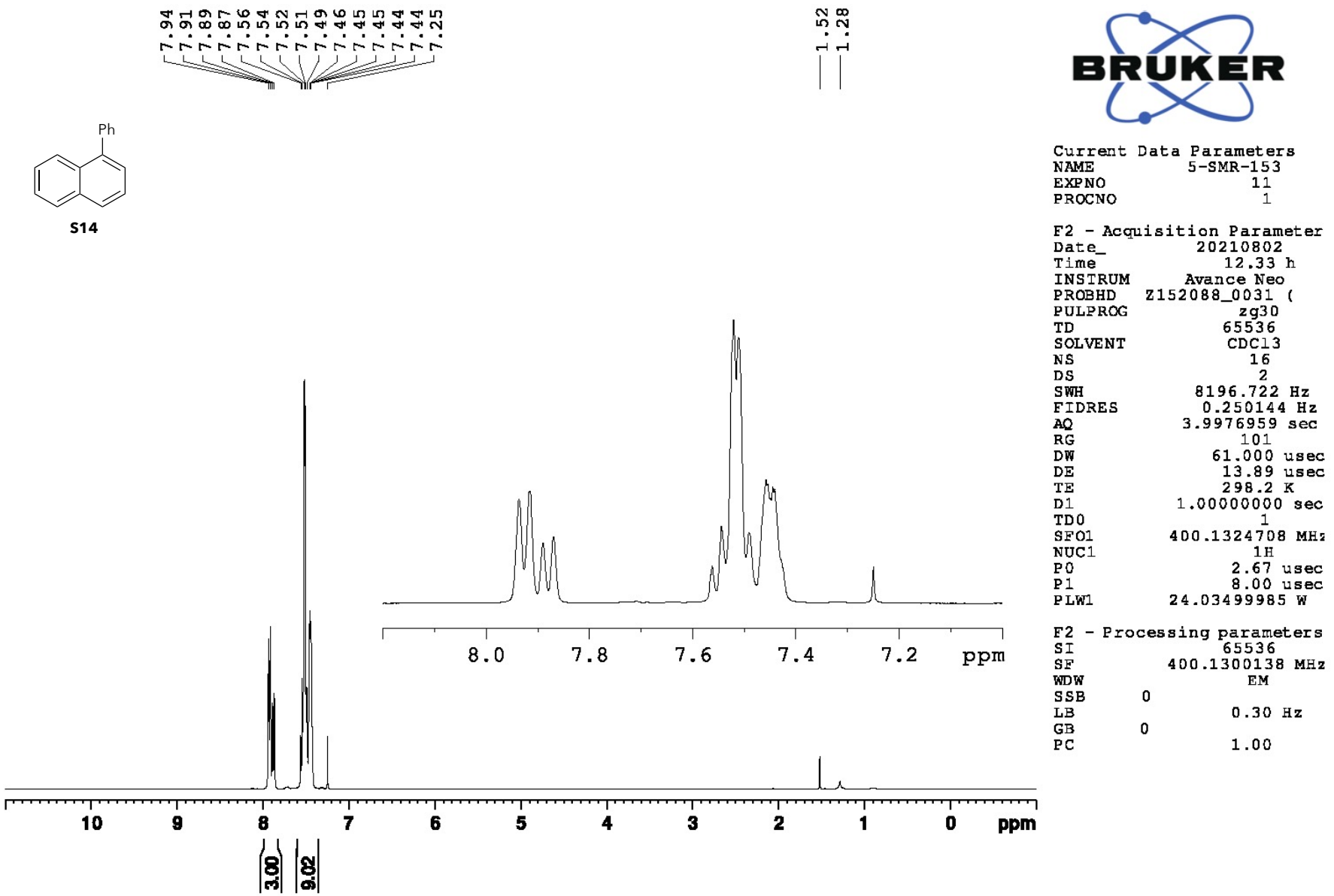
S13




```
Current Data Parameters
NAME                  6-SMR-4
EXPNO                      31
PROCNO                      2

F2 - Acquisition Parameter
Date_              20211008
Time                 15.39 h
INSTRUM                spect
PROBHD   Z125869_0055 (
PULPROG                zgflqn
TD                     130892
SOLVENT                 CDCl3
NS                         16
DS                          4
SWH               113636.367 Hz
FIDRES              1.736338 Hz
AQ                 0.5759248 sec
RG                      17.98
DW                     4.400 usec
DE                     18.00 usec
TE                     298.0 K
D1                1.00000000 sec
TD0                         1
SFO1              470.6394024 MHz
NUC1                      19F
P1                     15.00 usec
PLW1              11.70800018 W

F2 - Processing parameters
SI                      65536
SF                470.6864712 MHz
WDW                       EM
SSB       0
LB                     0.30 Hz
GB        0
PC                      1.00
```

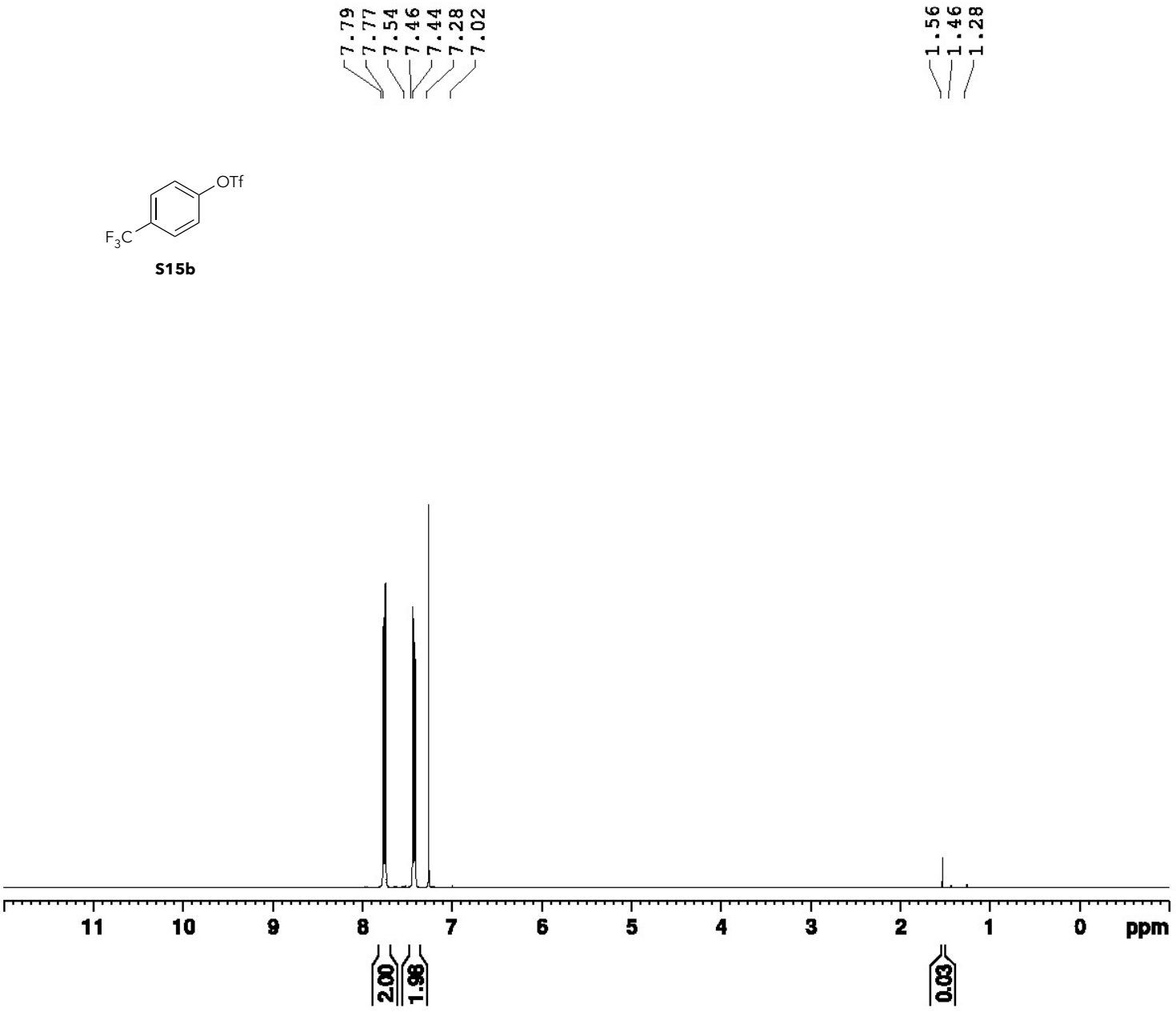


BRUKER

Current Data Parameters
NAME 5-SMR-153
EXPNO 11
PROCNO 1

F2 - Acquisition Parameter
Date_ 20210802
Time 12.33 h
INSTRUM Avance Neo
PROBHD Z152088_0031 (
PULPROG zg30
TD 65536
SOLVENT CDCl3
NS 16
DS 2
SWH 8196.722 Hz
FIDRES 0.250144 Hz
AQ 3.9976959 sec
RG 101
DW 61.000 usec
DE 13.89 usec
TE 298.2 K
D1 1.00000000 sec
TD0 1
SFO1 400.1324708 MHz
NUC1 1H
P0 2.67 usec
P1 8.00 usec
PLW1 24.03499985 W

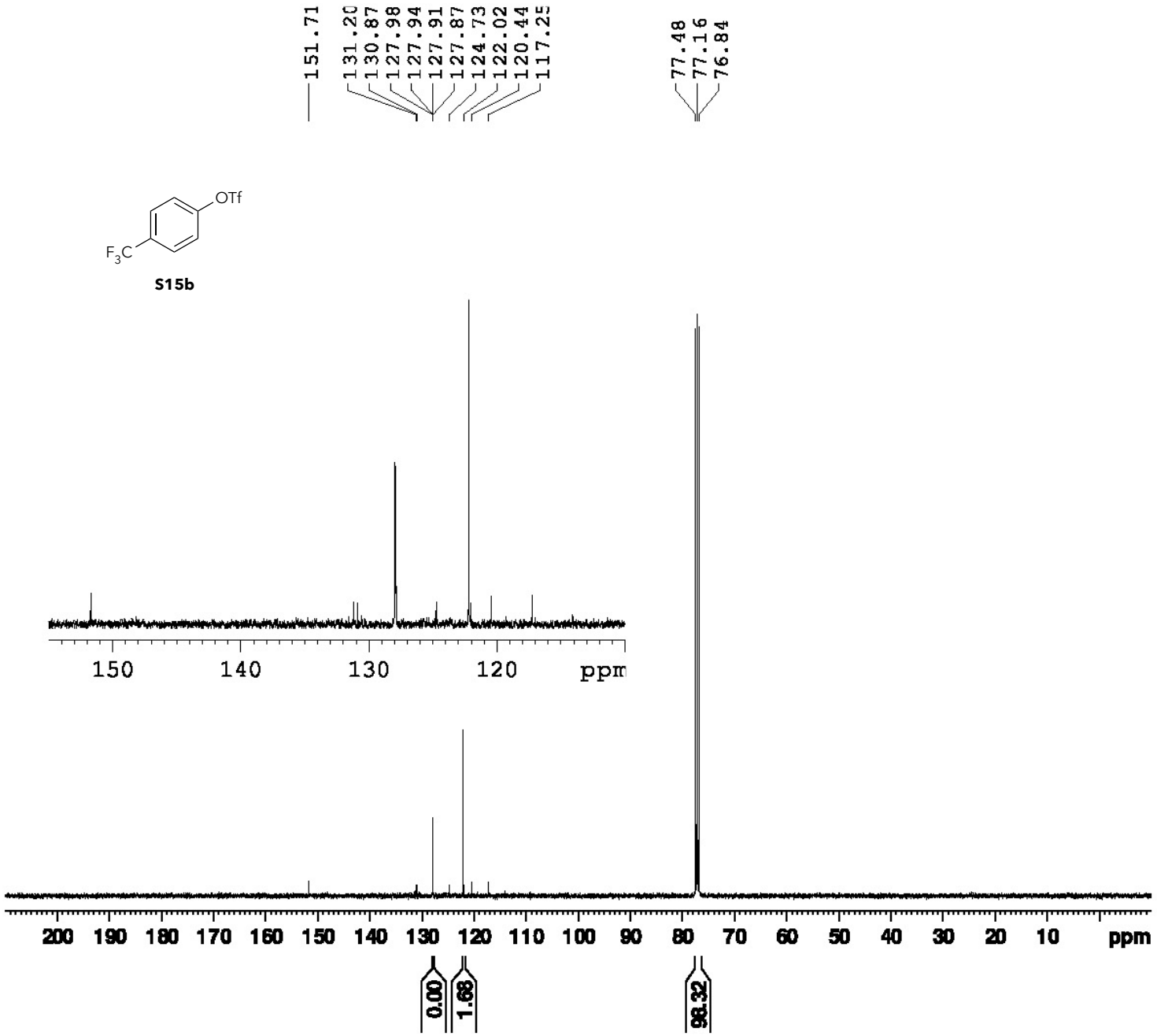
F2 - Processing parameters
SI 65536
SF 400.1300138 MHz
WDW EM
SSB 0
LB 0.30 Hz
GB 0
PC 1.00



Current Data Parameters
NAME 6-SMR-25
EXPNO 10
PROCNO 1

F2 - Acquisition Parameter
Date_ 20211105
Time 20.28 h
INSTRUM Avance Neo
PROBHD Z152088_0031 (
PULPROG zg30
TD 65536
SOLVENT CDCl3
NS 16
DS 2
SWH 8196.722 Hz
FIDRES 0.250144 Hz
AQ 3.9976959 sec
RG 101
DW 61.000 usec
DE 13.89 usec
TE 298.0 K
D1 1.00000000 sec
TD0 1
SFO1 400.1324708 MHz
NUC1 1H
P0 2.67 usec
P1 8.00 usec
PLW1 24.03499985 W

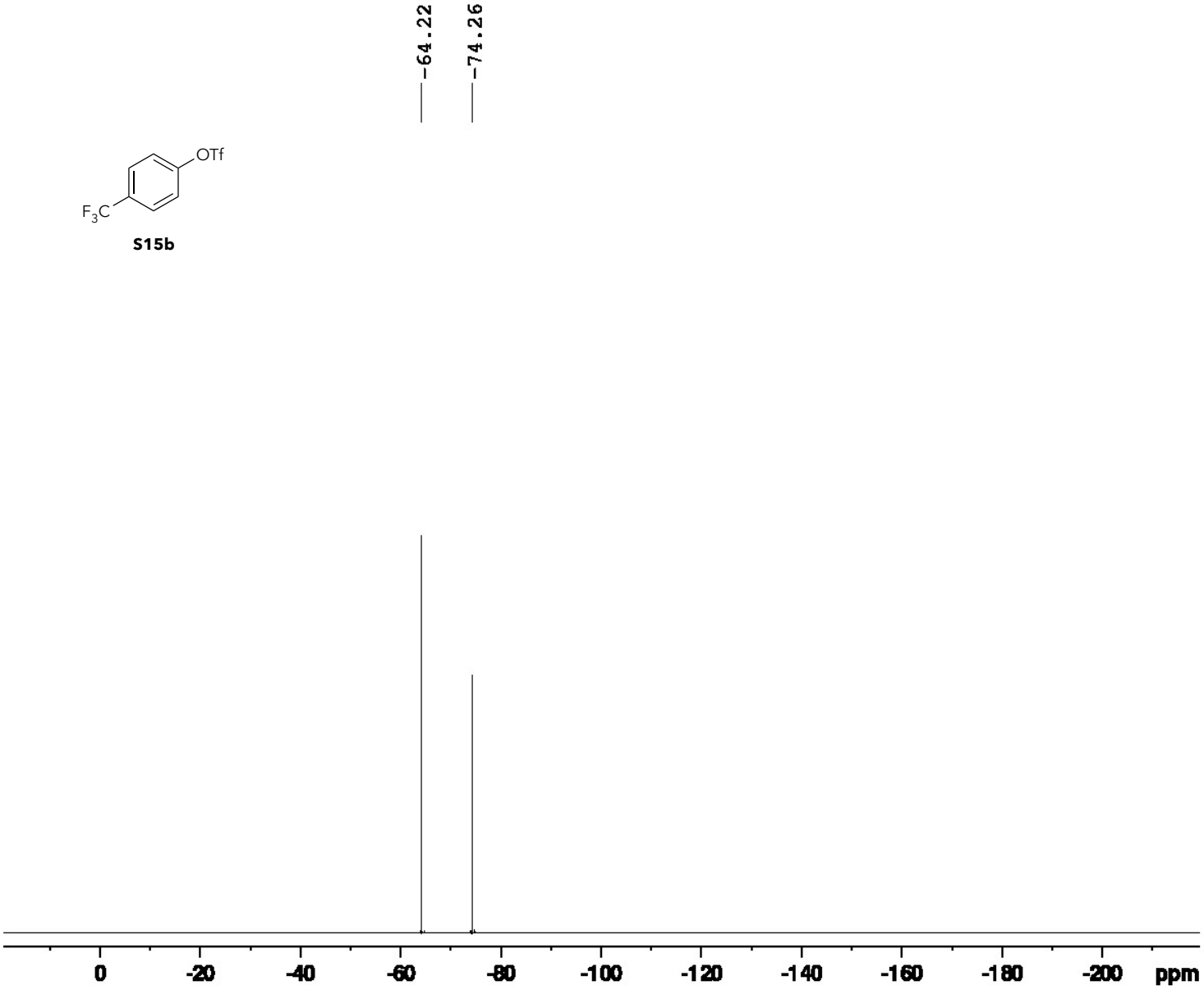
F2 - Processing parameters
SI 65536
SF 400.1300097 MHz
WDW EM
SSB 0
LB 0.30 Hz
GB 0
PC 1.00




```
Current Data Parameters
NAME                  6-SMR-25
EXPNO                       11
PROCNO                       1

F2 - Acquisition Parameter
Date_                 20211105
Time                     21.29 h
INSTRUM               Avance Neo
PROBHD           Z152088_0031 (
PULPROG                 zgpg30
TD                       65536
SOLVENT                  CDCl3
NS                        1024
DS                           4
SWH                  23809.523 Hz
FIDRES                0.726609 Hz
AQ                    1.3762560 sec
RG                        8.125
DW                       21.000 usec
DE                        6.50 usec
TE                       298.0 K
D1                    2.00000000 sec
D11                   0.03000000 sec
TD0                          1
SFO1                100.6228298 MHz
NUC1                        13C
P0                        2.67 usec
P1                        8.00 usec
PLW1                86.55400085 W
SFO2                400.1316005 MHz
NUC2                        1H
CPDPRG[2                waltz65
PCPD2                    90.00 usec
PLW2                24.03499985 W
PLW12                0.18990999 W
PLW13                0.09552100 W

F2 - Processing parameters
SI                       32768
SF                  100.6127535 MHz
WDW                         EM
SSB                  0
LB                        1.00 Hz
GB                   0
PC                        1.40
```



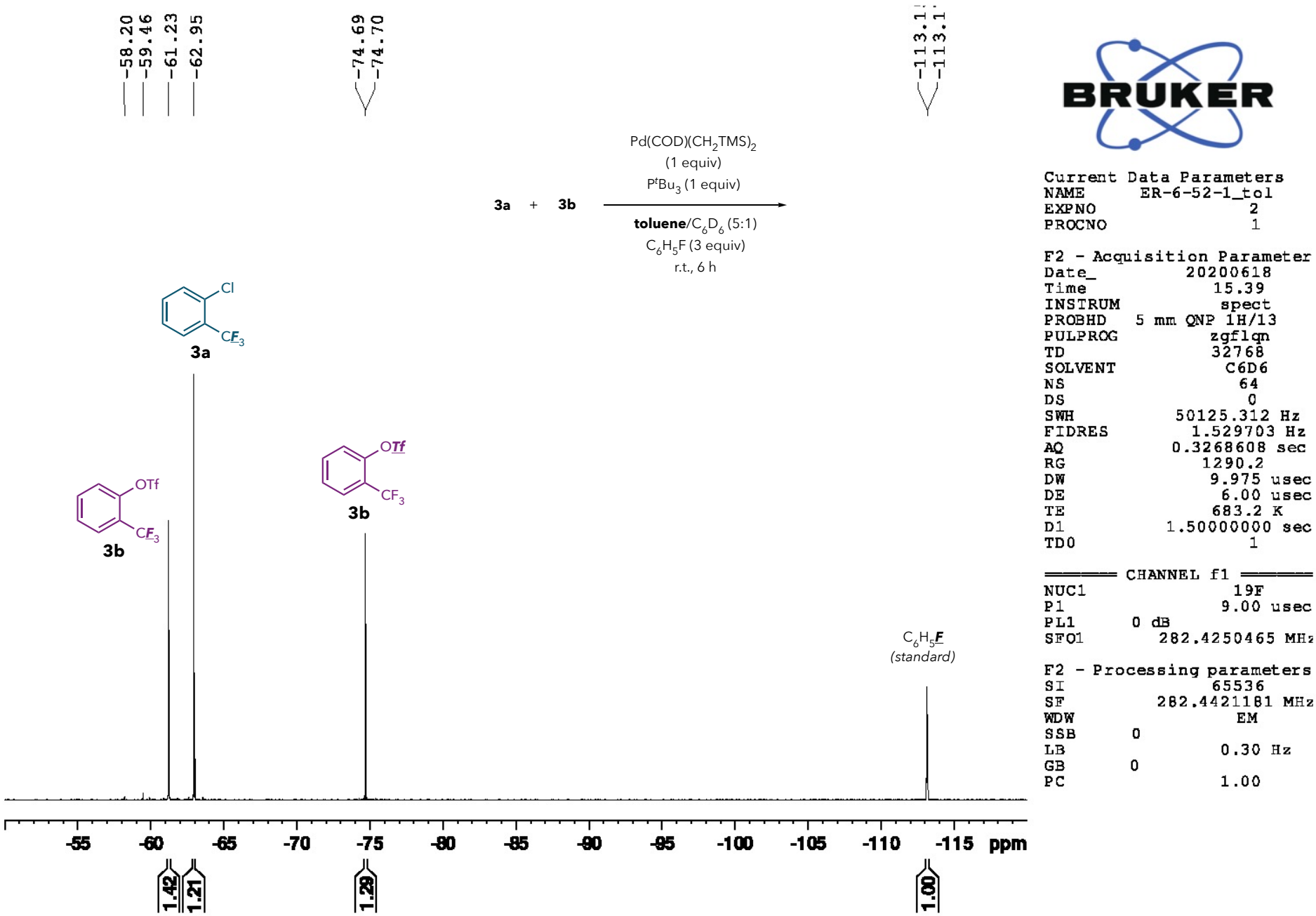

```
Current Data Parameters
NAME            6-SMR-25
EXPNO                 12
PROCNO                 1

F2 - Acquisition Parameter
Date_           20211105
Time              21.32 h
INSTRUM       Avance Neo
PROBHD    Z152088_0031 (
PULPROG               zg
TD                131072
SOLVENT             CDCl3
NS                    16
DS                     4
SWH           90909.094 Hz
FIDRES         1.387163 Hz
AQ            0.7208960 sec
RG                   101
DW                5.500 usec
DE                6.50 usec
TE                298.0 K
D1           1.00000000 sec
TD0                    1
SFO1         376.4607164 MHz
NUC1                 19F
P1                12.00 usec
PLW1         31.08900070 W

F2 - Processing parameters
SI                 65536
SF           376.4989587 MHz
WDW                  EM
SSB       0
LB                0.30 Hz
GB        0
PC                1.00
```

B. Stoichiometric Oxidative Addition Studies with 3a and 3b

1. Experiments from Table 3 and with Deuterated Solvents

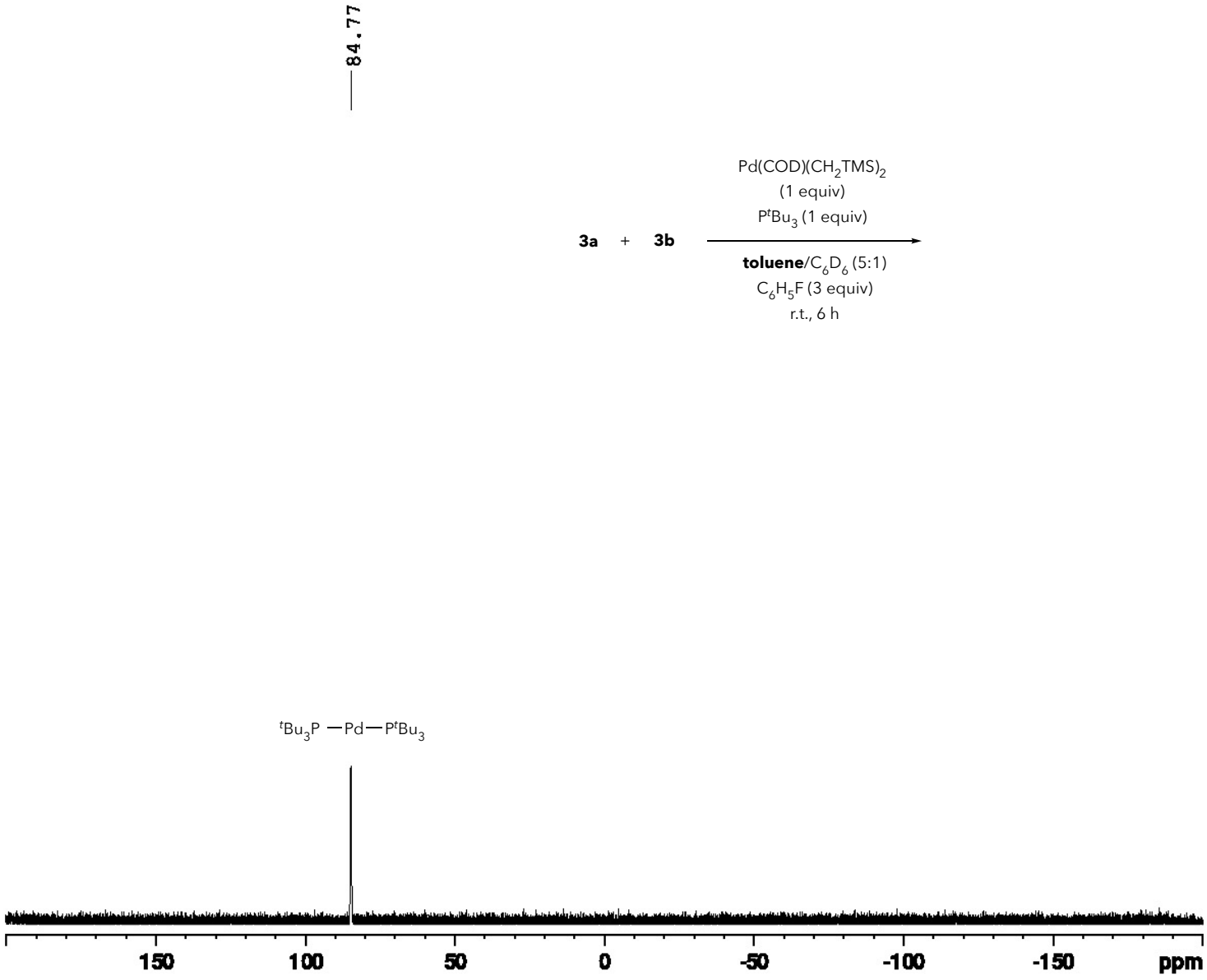



```
Current Data Parameters
NAME      ER-6-52-1_tol
EXPNO                2
PROCNO               1

F2 - Acquisition Parameter
Date_          20200618
Time              15.39
INSTRUM           spect
PROBHD   5 mm QNP 1H/13
PULPROG          zgflqn
TD                32768
SOLVENT            C6D6
NS                   64
DS                    0
SWH           50125.312 Hz
FIDRES         1.529703 Hz
AQ            0.3268608 sec
RG               1290.2
DW                9.975 usec
DE                6.00 usec
TE                683.2 K
D1           1.50000000 sec
TD0                  1

====== CHANNEL f1 ======
NUC1                19F
P1                9.00 usec
PL1       0 dB
SFO1        282.4250465 MHz

F2 - Processing parameters
SI                65536
SF          282.4421181 MHz
WDW                EM
SSB       0
LB                0.30 Hz
GB        0
PC                1.00
```

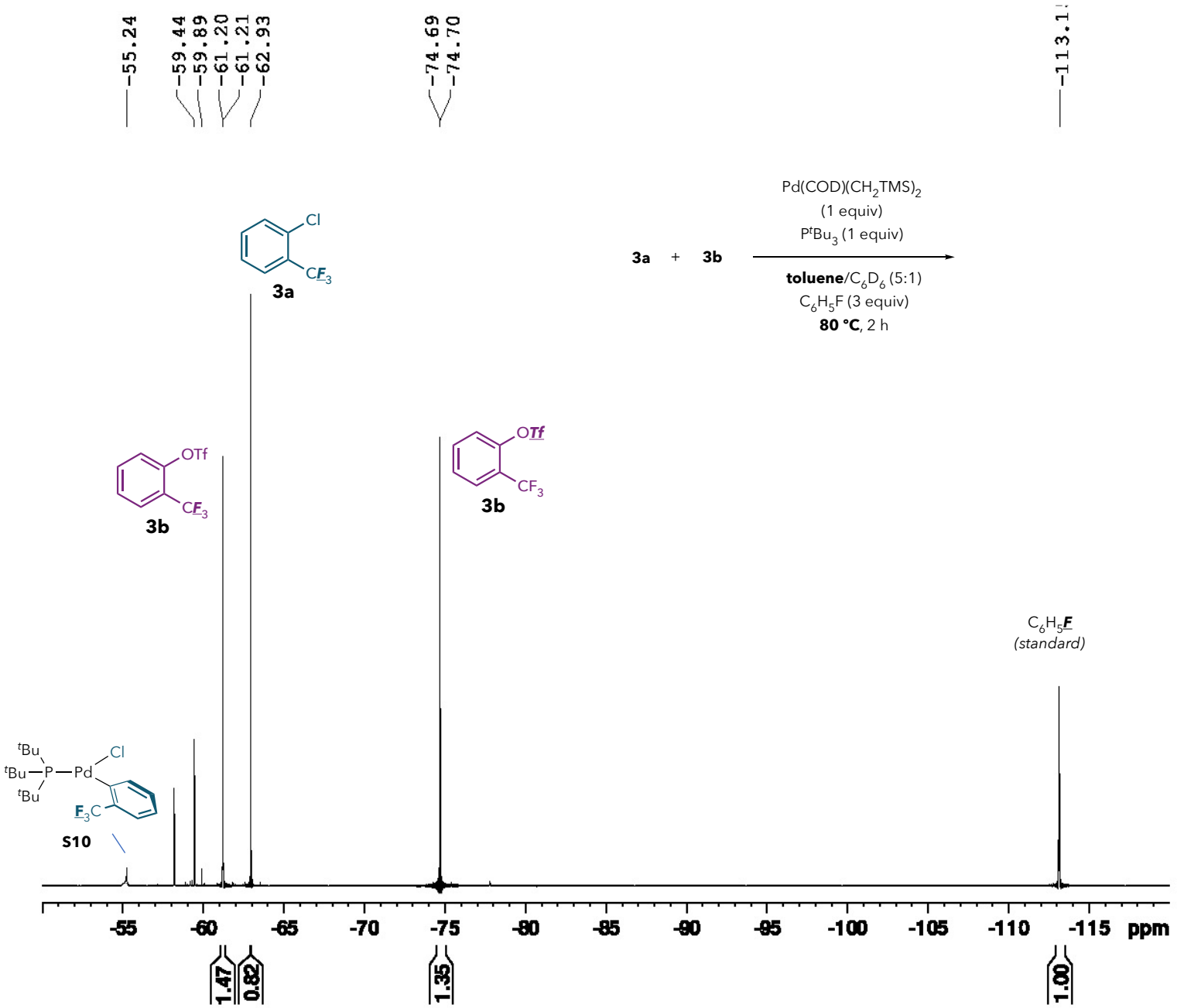


Current Data Parameters
NAME ER-6-55-1_toluene
EXPNO 2
PROCNO 1

F2 - Acquisition Parameter
Date_ 20200513
Time 7.30
INSTRUM spect
PROBHD 5 mm QNP 1H/13
PULPROG zg
TD 32768
SOLVENT Acetone
NS 32
DS 0
SWH 48661.801 Hz
FIDRES 1.485040 Hz
AQ 0.3366912 sec
RG 14596.5
DW 10.275 usec
DE 6.00 usec
TE 683.2 K
D1 2.00000000 sec
TD0 1

====== CHANNEL f1 ======
NUC1 31P
P1 8.00 usec
PL1 0 dB
SFO1 121.5110430 MHz

F2 - Processing parameters
SI 32768
SF 121.5110430 MHz
WDW EM
SSB 0
LB 1.00 Hz
GB 0
PC 1.40

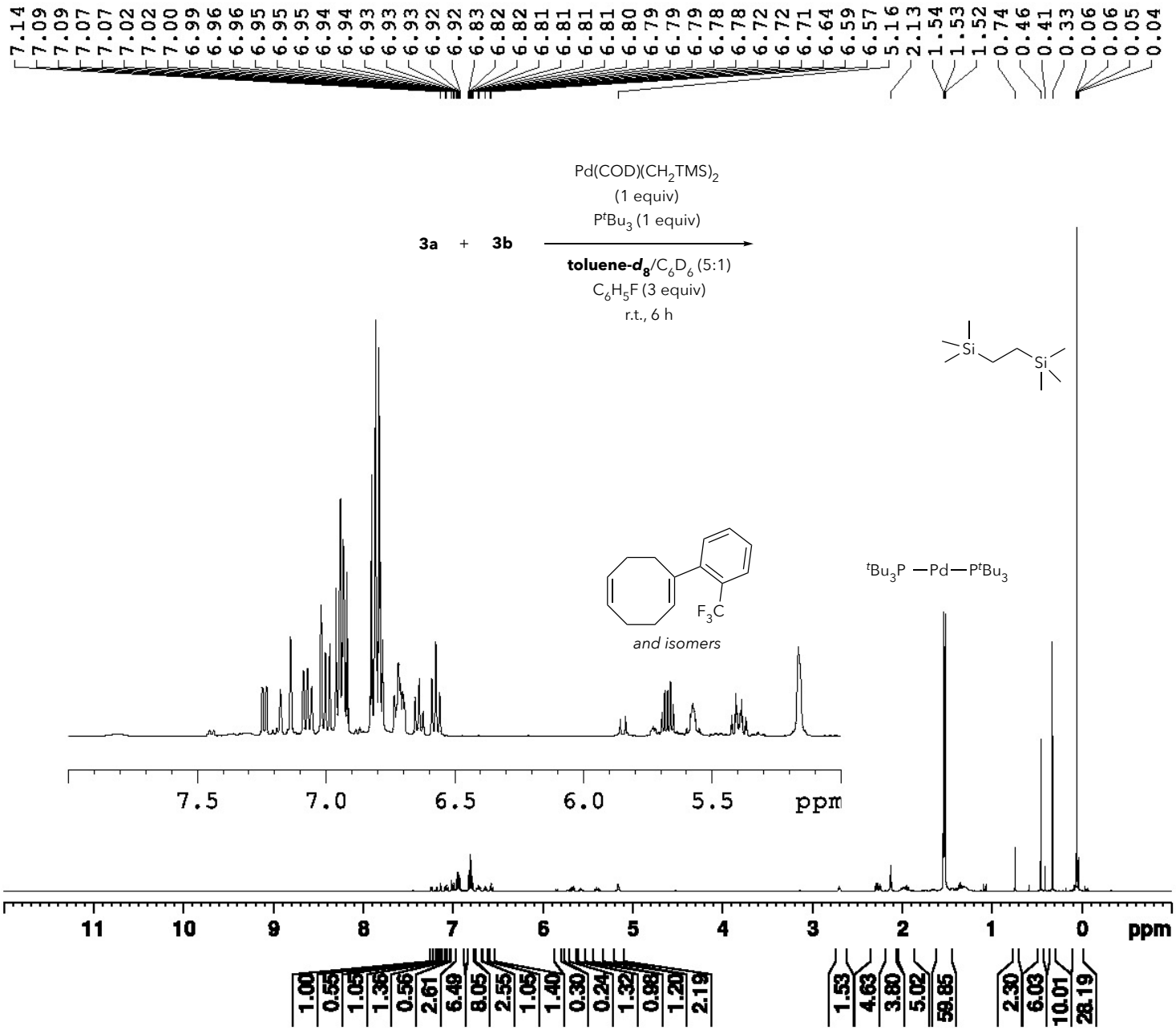



```
Current Data Parameters
NAME      ER-6-55-1_toluene_80
EXPNO                        1
PROCNO                       1

F2 - Acquisition Parameters
Date_              20200707
Time                   7.51
INSTRUM               spect
PROBHD    5 mm QNP 1H/13
PULPROG             zgflqn
TD                   32768
SOLVENT               C6D6
NS                      64
DS                       0
SWH              50125.312 Hz
FIDRES            1.529703 Hz
AQ               0.3268608 sec
RG                  1625.5
DW                   9.975 usec
DE                   6.00 usec
TE                  683.2 K
D1              1.50000000 sec
TD0                      1

======== CHANNEL f1 ========
NUC1                   19F
P1                  9.00 usec
PL1        0 dB
SFO1          282.4250465 MHz

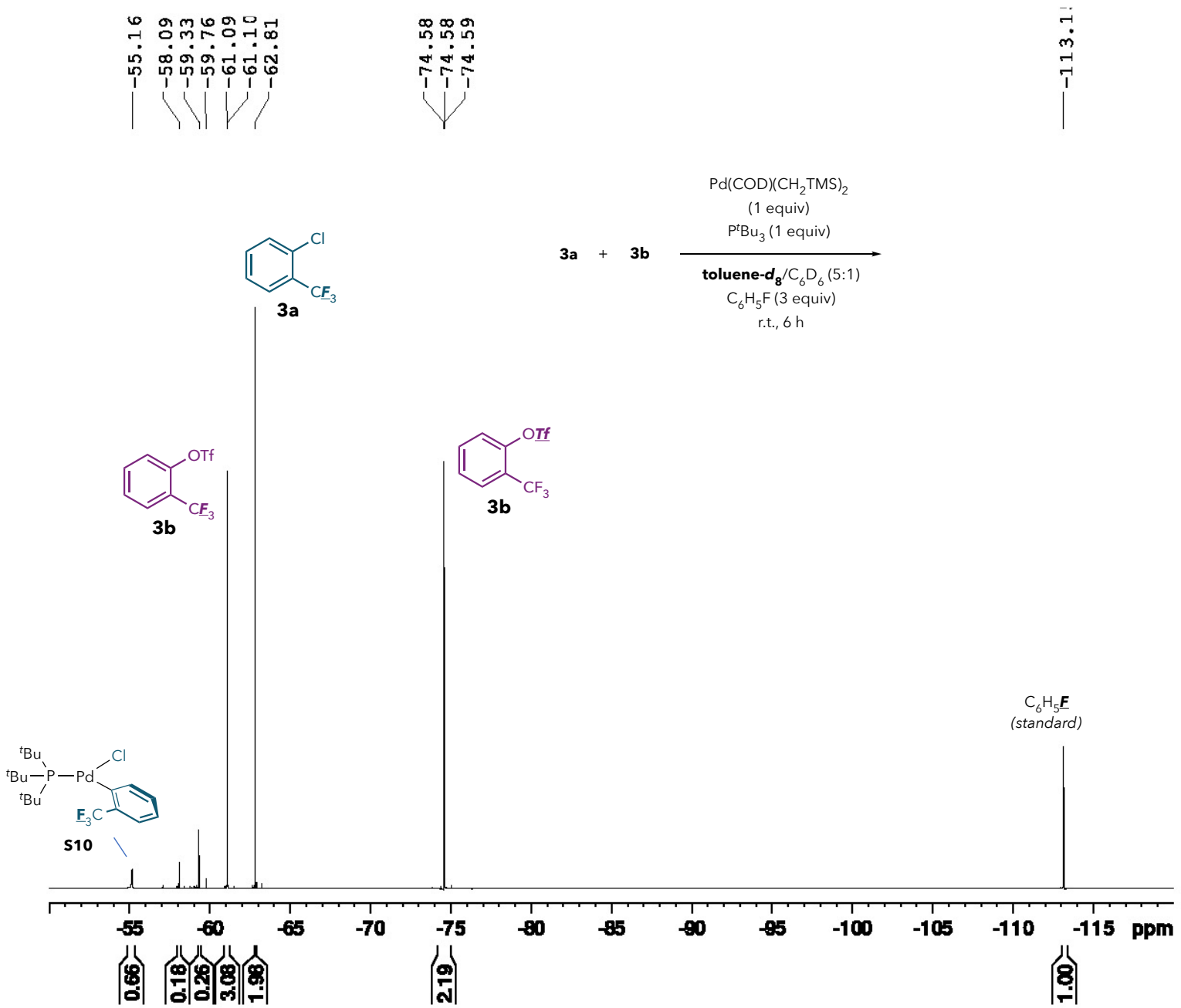
F2 - Processing parameters
SI                   65536
SF            282.4421250 MHz
WDW                    EM
SSB        0
LB                  0.30 Hz
GB         0
PC                  1.00
```




```
Current Data Parameters
NAME          6-SMR-41-3
EXPNO                 10
PROCNO                 1

F2 - Acquisition Parameter
Date_          20211116
Time             15.16 h
INSTRUM            spect
PROBHD   Z125869_0055 (
PULPROG            zg30
TD                65536
SOLVENT             Tol
NS                   64
DS                    2
SWH          10000.000 Hz
FIDRES         0.305176 Hz
AQ           3.2767999 sec
RG                30.54
DW              50.000 usec
DE              16.00 usec
TE              298.0 K
D1           2.00000000 sec
TD0                   1
SFO1        500.2330889 MHz
NUC1                 1H
P0              4.00 usec
P1              12.00 usec
PLW1        11.44699955 W

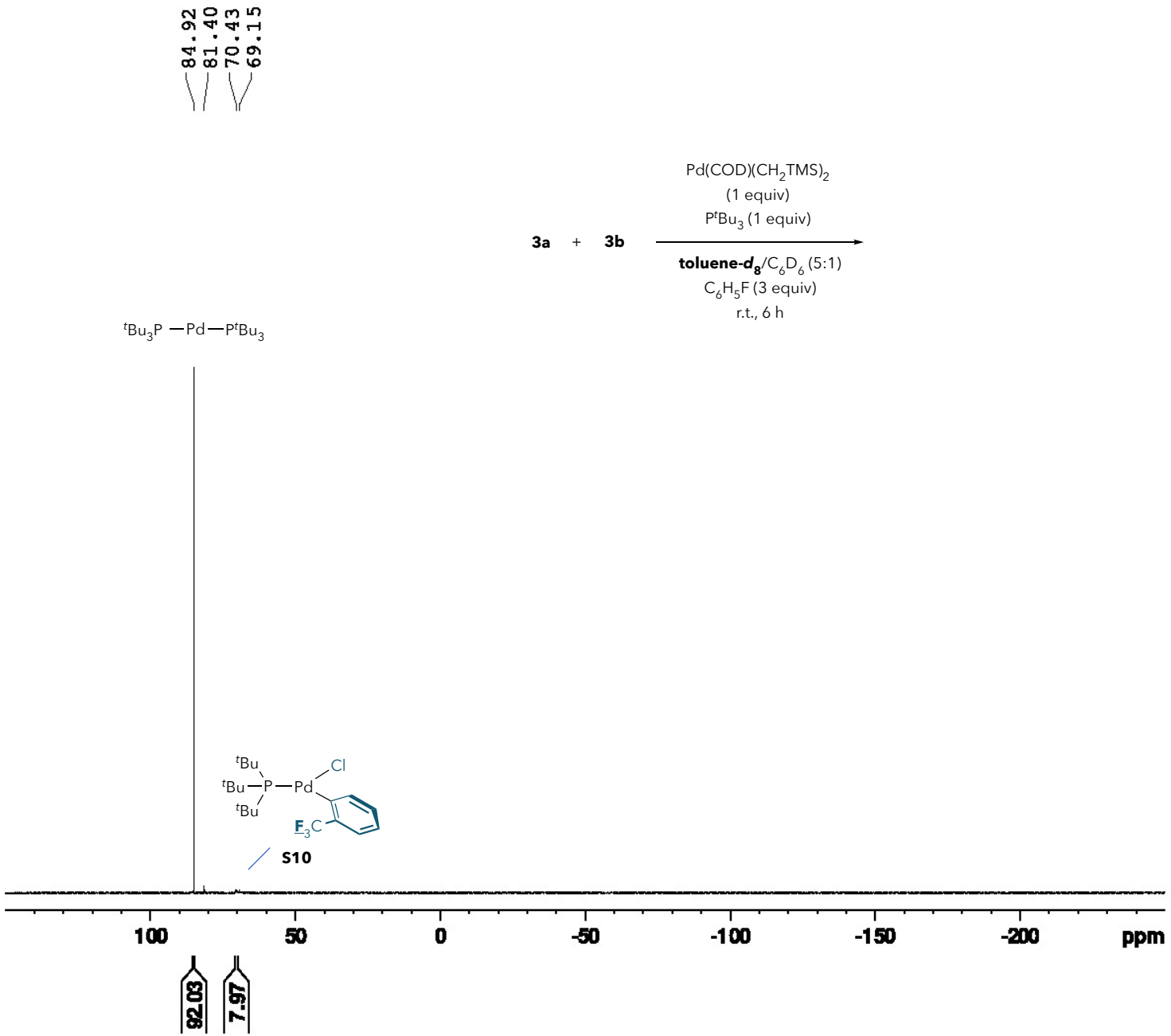
F2 - Processing parameters
SI                65536
SF          500.2300000 MHz
WDW                  EM
SSB       0
LB              0.30 Hz
GB        0
PC              1.00
```




```
Current Data Parameters
NAME          6-SMR-41-3
EXPNO                 11
PROCNO                 2

F2 - Acquisition Parameter
Date_          20211116
Time             15.18 h
INSTRUM            spect
PROBHD   Z125869_0055 (
PULPROG           zgflqn
TD                131072
SOLVENT              Tol
NS                    16
DS                     4
SWH          113636.367 Hz
FIDRES         1.733953 Hz
AQ            0.5767168 sec
RG                 15.61
DW                4.400 usec
DE                18.00 usec
TE                298.0 K
D1           1.00000000 sec
TD0                    1
SFO1         470.6394024 MHz
NUC1                 19F
P1                15.00 usec
PLW1         11.70800018 W

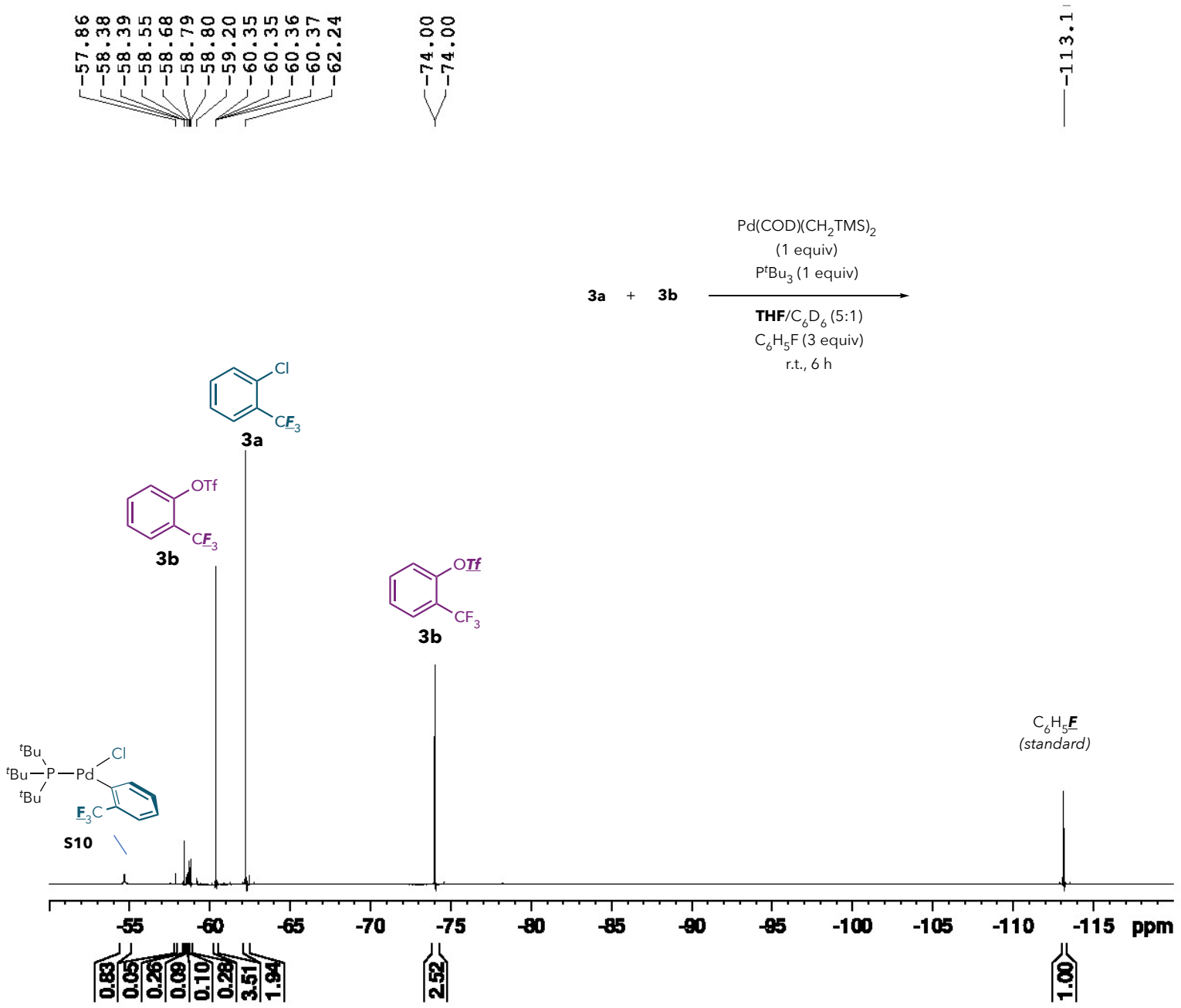
F2 - Processing parameters
SI                 65536
SF           470.6866398 MHz
WDW                  EM
SSB       0
LB                0.30 Hz
GB        0
PC                1.00
```




```
Current Data Parameters
NAME          6-SMR-41-3
EXPNO                 12
PROCNO                 1

F2 - Acquisition Parameter
Date_          20211116
Time              15.21 h
INSTRUM            spect
PROBHD   Z125869_0055 (
PULPROG           zgpg30
TD                65536
SOLVENT             Tol
NS                   16
DS                    4
SWH           81521.742 Hz
FIDRES         2.487846 Hz
AQ            0.4019541 sec
RG                190.44
DW                6.133 usec
DE                18.00 usec
TE                298.0 K
D1           2.00000000 sec
D11          0.03000000 sec
TD0                   1
SFO1        202.4866909 MHz
NUC1                31P
P0                4.00 usec
P1                12.00 usec
PLW1        40.26200104 W
SFO2        500.2320009 MHz
NUC2                1H
CPDPRG[2         waltz16
PCPD2             80.00 usec
PLW2        11.44699955 W
PLW12        0.25756001 W
PLW13        0.12955000 W

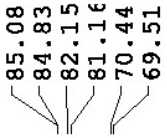
F2 - Processing parameters
SI                 32768
SF          202.4968157 MHz
WDW                  EM
SSB       0
LB                1.00 Hz
GB        0
PC                1.40
```

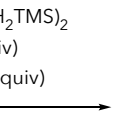


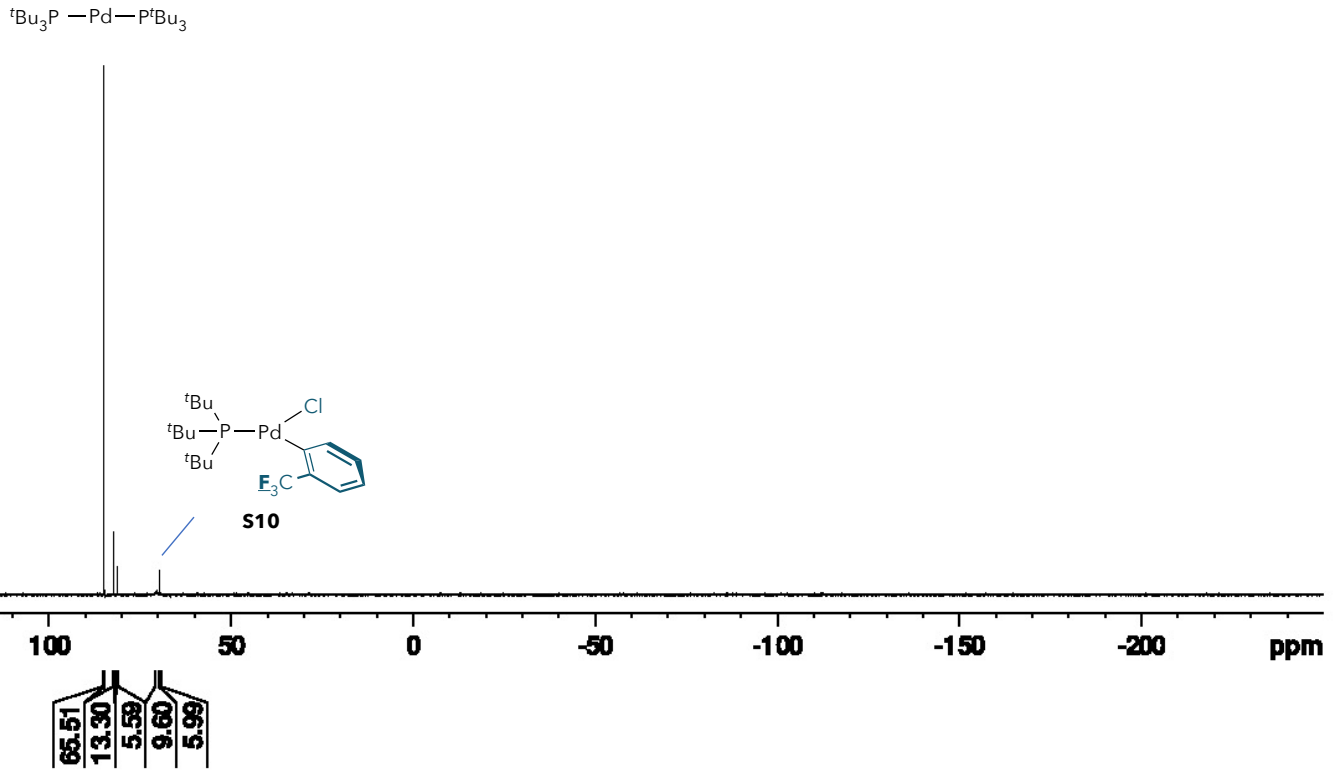

```
Current Data Parameters
NAME          6-SMR-39-3
EXPNO                 10
PROCNO                 2

F2 - Acquisition Parameter
Date_          20211115
Time             15.47 h
INSTRUM       Avance Neo
PROBHD   Z152088_0031 (
PULPROG            zgig
TD               131072
SOLVENT            C6D6
NS                   16
DS                    4
SWH           90909.094 Hz
FIDRES         1.387163 Hz
AQ            0.7208960 sec
RG                  101
DW              5.500 usec
DE              6.50 usec
TE              298.1 K
D1           1.00000000 sec
D11          0.03000000 sec
TD0                   1
SFO1         376.4607164 MHz
NUC1                19F
P1               12.00 usec
PLW1         31.08900070 W
SFO2         400.1316005 MHz
NUC2                1H
CPDPRG[2         waltz16
PCPD2             90.00 usec
PLW2         24.03499985 W
PLW12         0.18990999 W

F2 - Processing parameters
SI                 65536
SF           376.4979704 MHz
WDW                  EM
SSB       0
LB               0.30 Hz
GB        0
PC               1.00
```





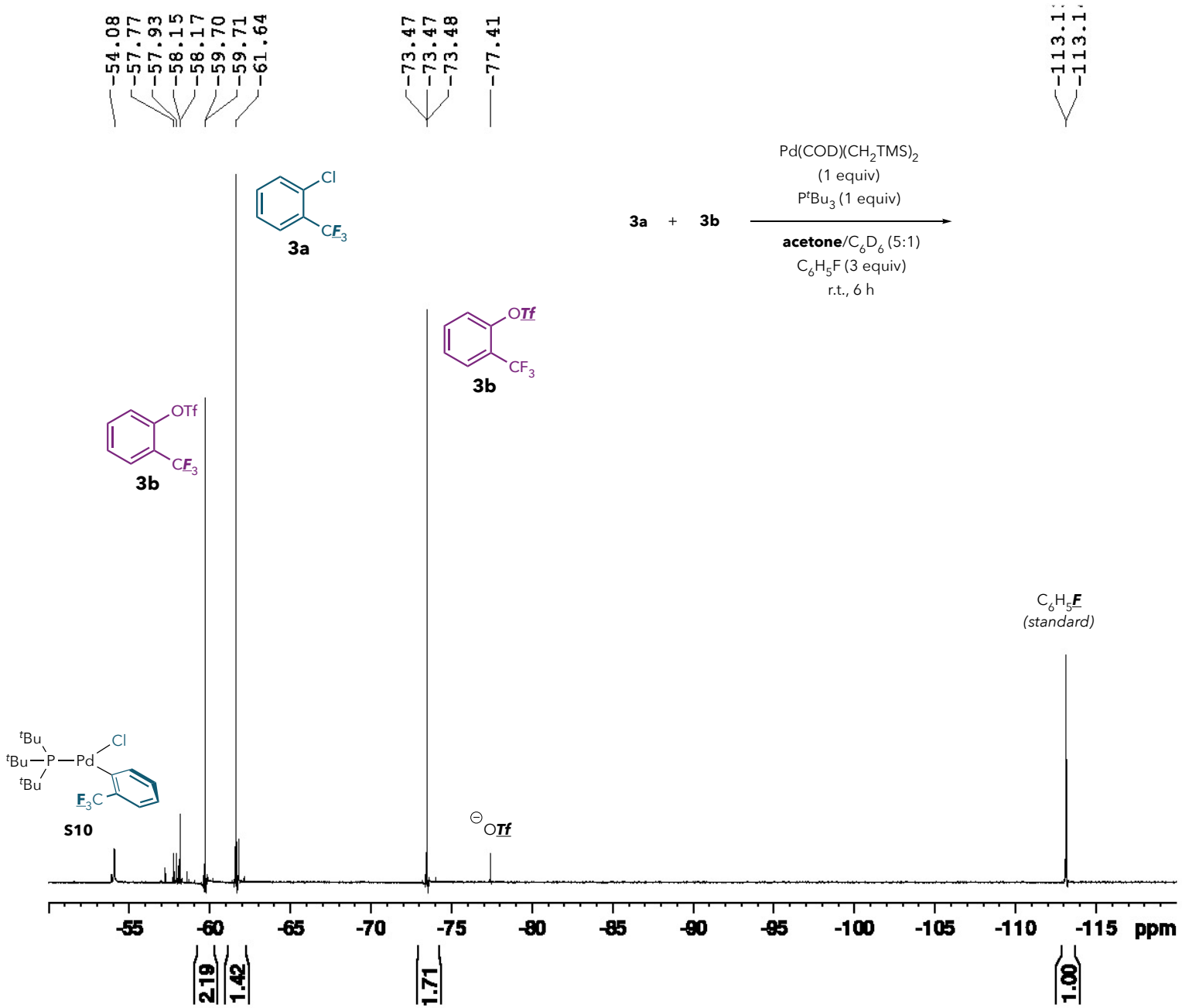





```
Current Data Parameters
NAME          6-SMR-39-3
EXPNO                 11
PROCNO                 1

F2 - Acquisition Parameter
Date_          20211115
Time              15.50 h
INSTRUM       Avance Neo
PROBHD   Z152088_0031 (
PULPROG           zgpg30
TD                65536
SOLVENT             C6D6
NS                    32
DS                     4
SWH           65789.477 Hz
FIDRES          2.007735 Hz
AQ            0.4980736 sec
RG                   101
DW                7.600 usec
DE                6.50 usec
TE                298.0 K
D1           2.00000000 sec
D11          0.03000000 sec
TD0                    1
SFO1        161.9674942 MHz
NUC1                 31P
P0                2.67 usec
P1                8.00 usec
PLW1         45.86100006 W
SFO2        400.1316005 MHz
NUC2                 1H
CPDPRG[2         waltz16
PCPD2             90.00 usec
PLW2         24.03499985 W
PLW12         0.18990999 W
PLW13         0.09552100 W

F2 - Processing parameters
SI                 32768
SF          161.9755930 MHz
WDW                   EM
SSB       0
LB                1.00 Hz
GB        0
PC                1.40
```

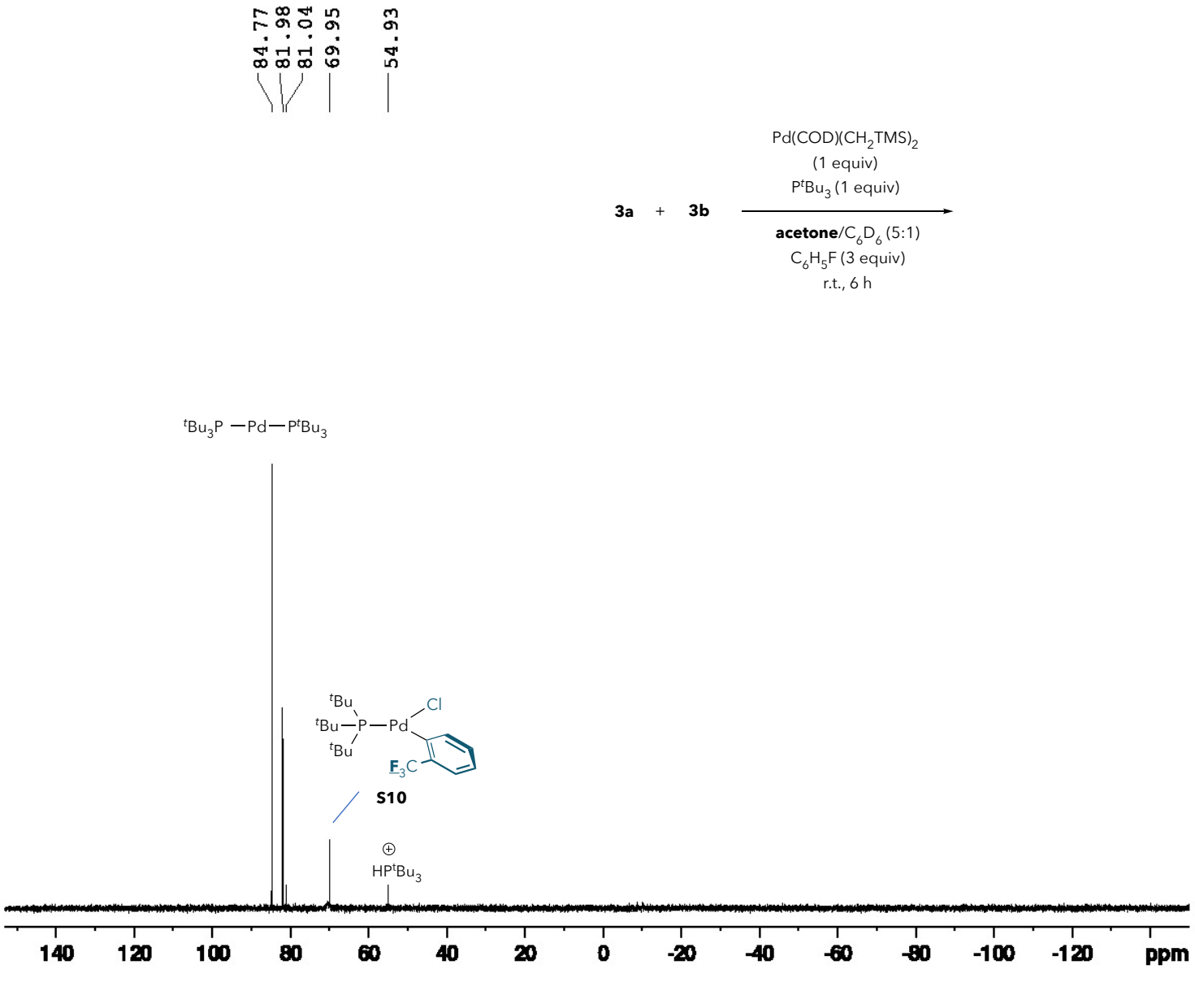




```
Current Data Parameters
NAME          6-SMR-5-7
EXPNO                12
PROCNO                2

F2 - Acquisition Parameter
Date_          20210911
Time             22.06 h
INSTRUM       Avance Neo
PROBHD   Z152088_0031 (
PULPROG              zg
TD               130892
SOLVENT            C6D6
NS                   16
DS                    4
SWH          90909.094 Hz
FIDRES        1.389070 Hz
AQ           0.7199060 sec
RG                  101
DW              5.500 usec
DE              6.50 usec
TE              298.0 K
D1           1.00000000 sec
TD0                   1
SFO1        376.4607164 MHz
NUC1               19F
P1              12.00 usec
PLW1        31.08900070 W

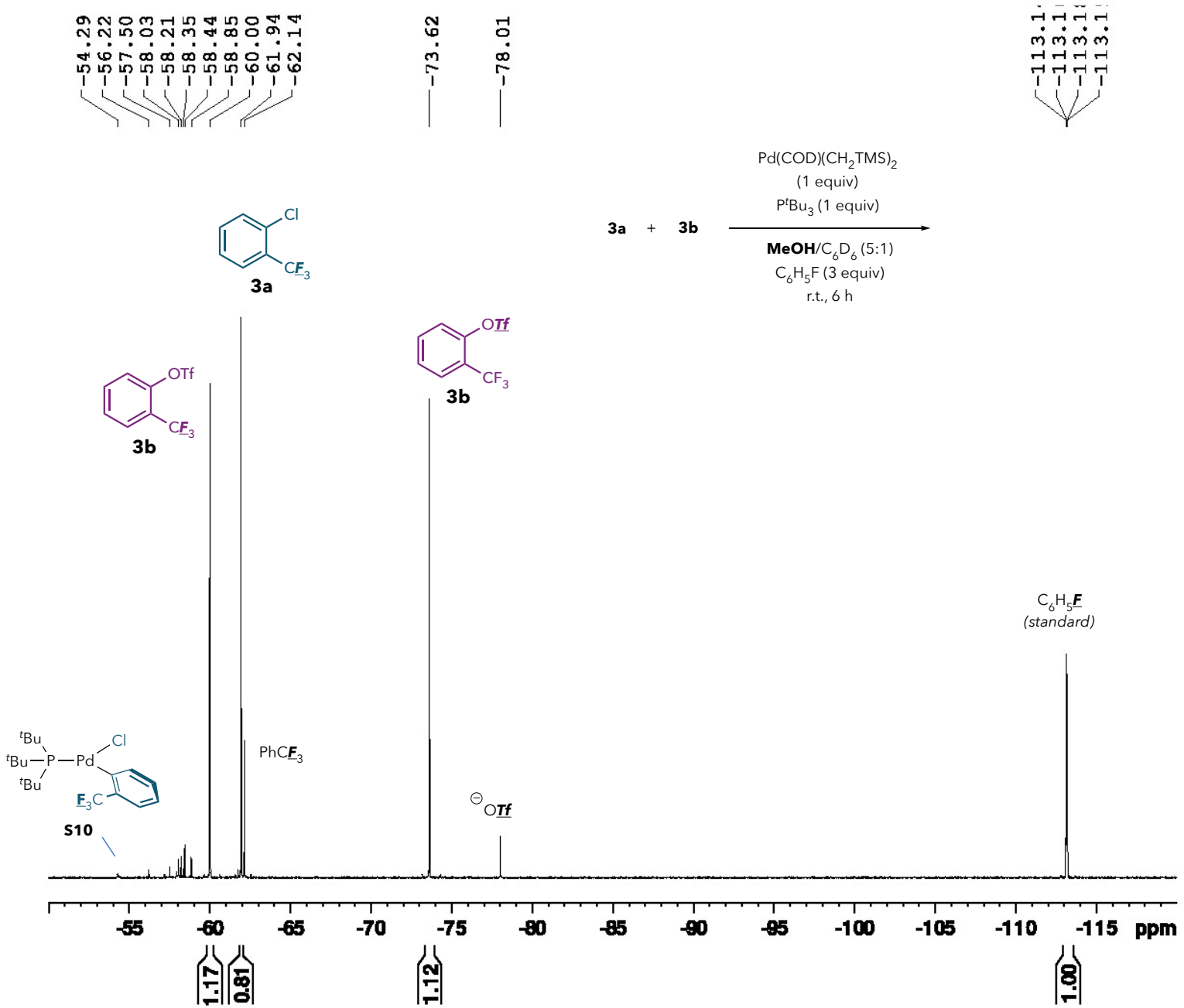
F2 - Processing parameters
SI                65536
SF          376.4978043 MHz
WDW                  EM
SSB       0
LB                0.30 Hz
GB        0
PC                1.00
```



Current Data Parameters
NAME 6-SMR-5-7
EXPNO 13
PROCNO 2

F2 - Acquisition Parameter
Date_ 20210911
Time 22.10 h
INSTRUM Avance Neo
PROBHD Z152088_0031 (
PULPROG zgpg30
TD 65536
SOLVENT C6D6
NS 32
DS 4
SWH 65789.477 Hz
FIDRES 2.007735 Hz
AQ 0.4980736 sec
RG 101
DW 7.600 usec
DE 6.50 usec
TE 298.0 K
D1 2.00000000 sec
D11 0.03000000 sec
TD0 1
SFO1 161.9674942 MHz
NUC1 31P
P0 2.67 usec
P1 8.00 usec
PLW1 45.86100006 W
SFO2 400.1316005 MHz
NUC2 1H
CPDPRG[2 waltz16
PCPD2 90.00 usec
PLW2 24.03499985 W
PLW12 0.18990999 W
PLW13 0.09552100 W

F2 - Processing parameters
SI 32768
SF 161.9755930 MHz
WDW EM
SSB 0
LB 1.00 Hz
GB 0
PC 1.40

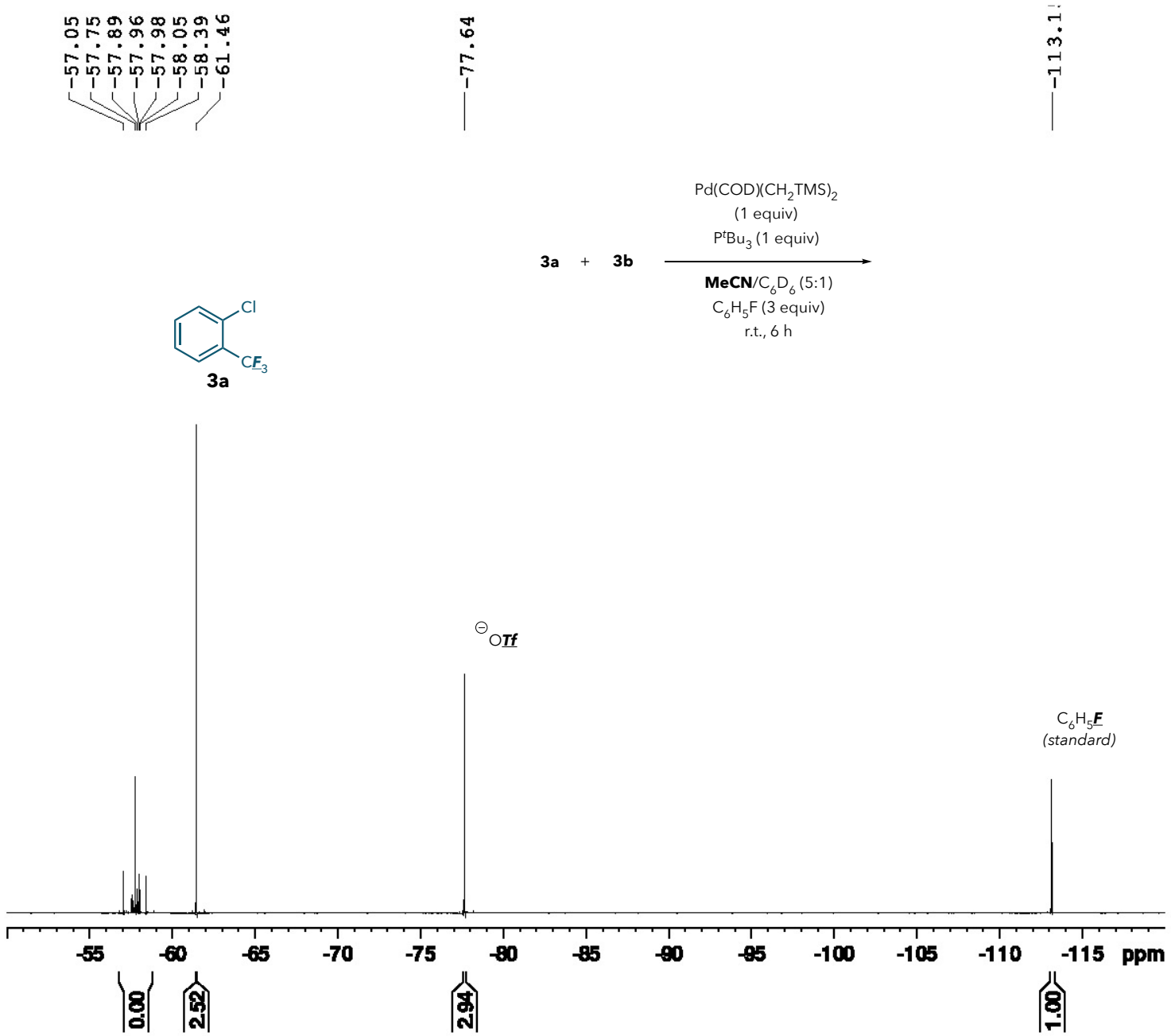



```
Current Data Parameters
NAME      ER-6-52-2_MeOH_new
EXPNO                      1
PROCNO                     1

F2 - Acquisition Parameter
Date_              20200618
Time                 15.46
INSTRUM              spect
PROBHD    5 mm QNP 1H/13
PULPROG              zgflqn
TD                   32768
SOLVENT              C6D6
NS                     64
DS                      0
SWH              50125.312 Hz
FIDRES            1.529703 Hz
AQ               0.3268608 sec
RG                  2580.3
DW                   9.975 usec
DE                   6.00 usec
TE                   683.2 K
D1               1.50000000 sec
TD0                        1

====== CHANNEL f1 ======
NUC1                    19F
P1                   9.00 usec
PL1        0 dB
SFO1          282.4250465 MHz

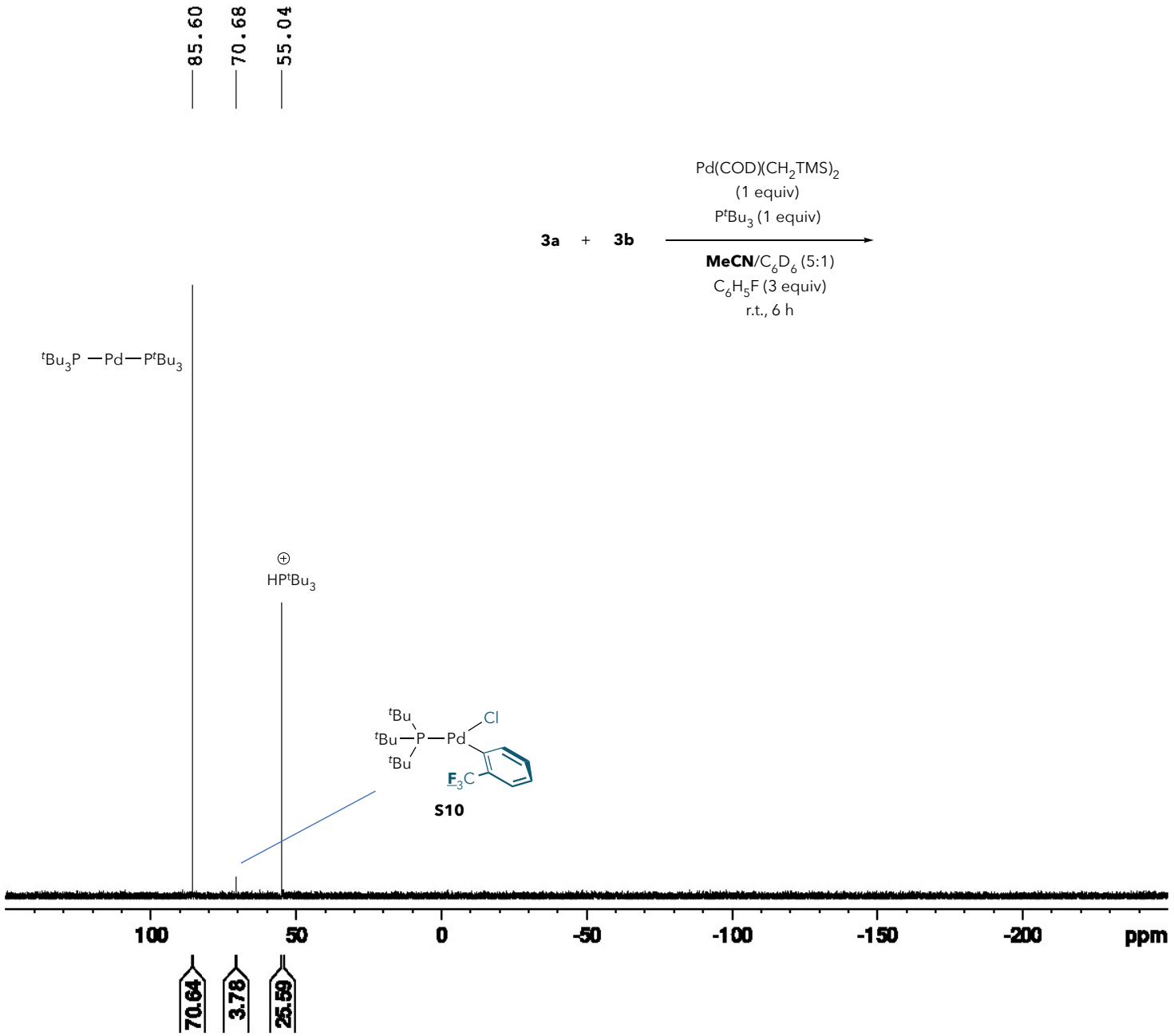
F2 - Processing parameters
SI                      65536
SF             282.4414859 MHz
WDW                     EM
SSB        0
LB                   0.30 Hz
GB         0
PC                   1.00
```




```
Current Data Parameters
NAME          6-SMR-39-7
EXPNO                 10
PROCNO                 2

F2 - Acquisition Parameter
Date_          20211115
Time             16.20 h
INSTRUM       Avance Neo
PROBHD   Z152088_0031 (
PULPROG            zgig
TD               131072
SOLVENT            C6D6
NS                   16
DS                    4
SWH           90909.094 Hz
FIDRES         1.387163 Hz
AQ            0.7208960 sec
RG                  101
DW              5.500 usec
DE              6.50 usec
TE              298.1 K
D1            1.00000000 sec
D11           0.03000000 sec
TD0                   1
SFO1         376.4607164 MHz
NUC1                 19F
P1              12.00 usec
PLW1         31.08900070 W
SFO2         400.1316005 MHz
NUC2                 1H
CPDPRG[2         waltz16
PCPD2             90.00 usec
PLW2         24.03499985 W
PLW12         0.18990999 W

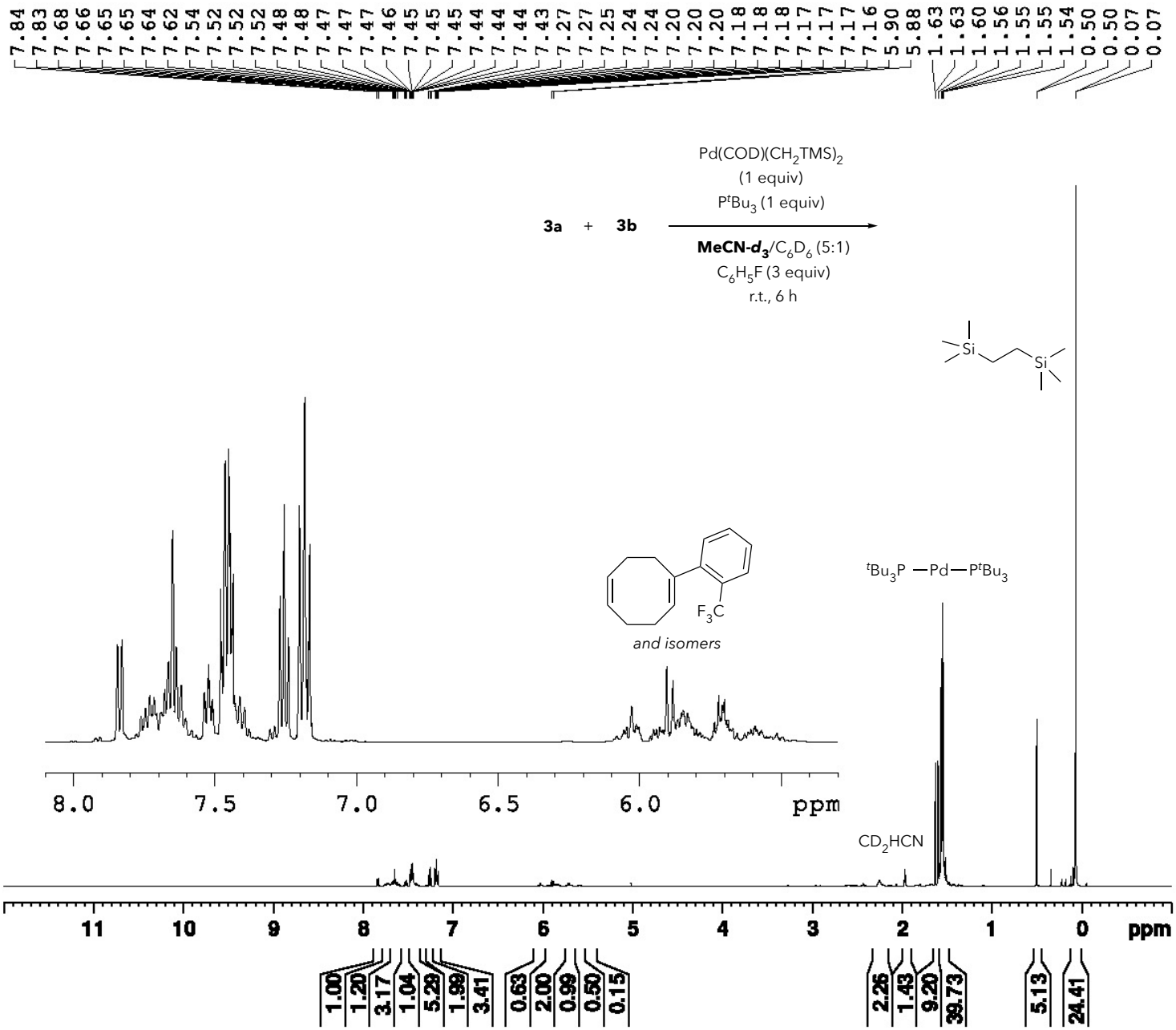
F2 - Processing parameters
SI                65536
SF           376.4977327 MHz
WDW                  EM
SSB       0
LB                0.30 Hz
GB        0
PC                1.00
```




```
Current Data Parameters
NAME          6-SMR-39-7
EXPNO                 11
PROCNO                 1

F2 - Acquisition Parameter
Date_          20211115
Time             16.23 h
INSTRUM       Avance Neo
PROBHD   Z152088_0031 (
PULPROG          zgpg30
TD                65536
SOLVENT           C6D6
NS                   32
DS                    4
SWH           65789.477 Hz
FIDRES          2.007735 Hz
AQ            0.4980736 sec
RG                  101
DW                7.600 usec
DE                6.50 usec
TE                298.0 K
D1           2.00000000 sec
D11          0.03000000 sec
TD0                   1
SFO1        161.9674942 MHz
NUC1               31P
P0                2.67 usec
P1                8.00 usec
PLW1         45.86100006 W
SFO2        400.1316005 MHz
NUC2               1H
CPDPRG[2        waltz16
PCPD2            90.00 usec
PLW2         24.03499985 W
PLW12         0.18990999 W
PLW13         0.09552100 W

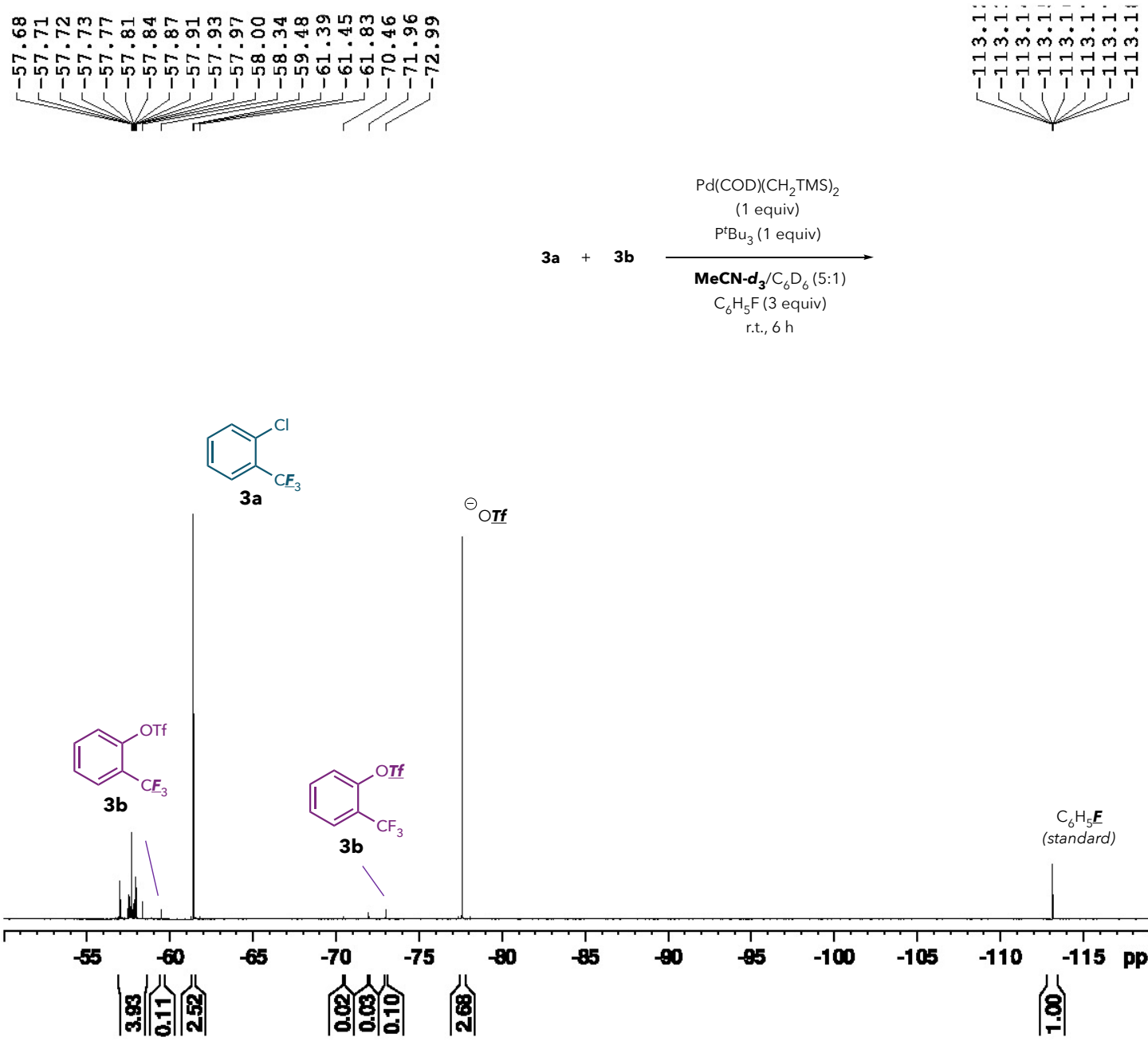
F2 - Processing parameters
SI                32768
SF          161.9755930 MHz
WDW                EM
SSB       0
LB                1.00 Hz
GB        0
PC                1.40
```




```
Current Data Parameters
NAME          6-SMR-41-6
EXPNO                 10
PROCNO                 1

F2 - Acquisition Parameter
Date_          20211116
Time              15.46 h
INSTRUM             spect
PROBHD   Z125869_0055 (
PULPROG             zg30
TD                 65536
SOLVENT             CD3CN
NS                    64
DS                     2
SWH           10000.000 Hz
FIDRES         0.305176 Hz
AQ            3.2767999 sec
RG                 35.18
DW               50.000 usec
DE               16.00 usec
TE                298.0 K
D1            2.00000000 sec
TD0                    1
SFO1         500.2330889 MHz
NUC1                  1H
P0               4.00 usec
P1               12.00 usec
PLW1         11.44699955 W

F2 - Processing parameters
SI                 65536
SF          500.2300000 MHz
WDW                   EM
SSB       0
LB                0.30 Hz
GB        0
PC                1.00
```

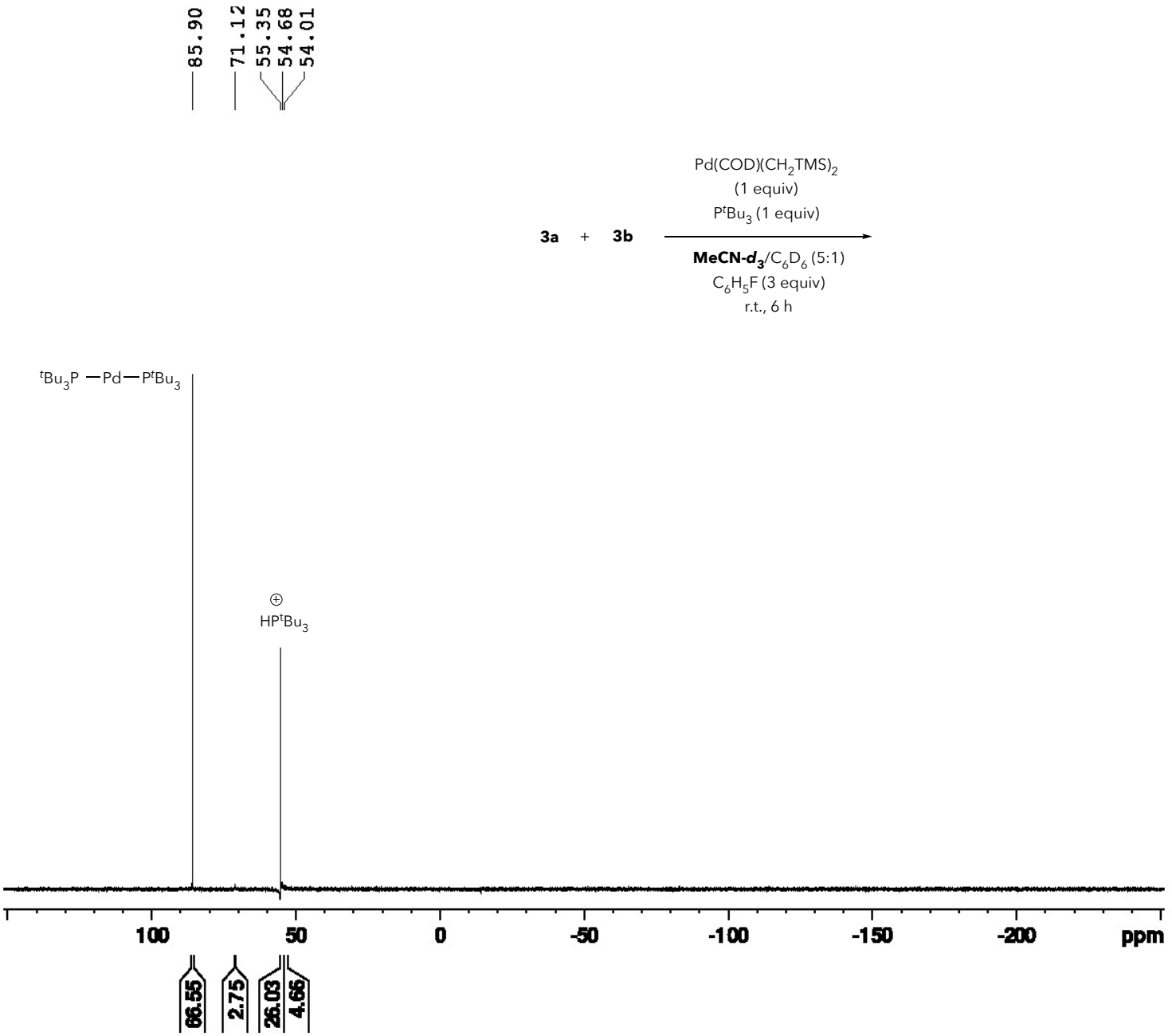


BRUKER

```
Current Data Parameters
NAME          6-SMR-41-6
EXPNO                 11
PROCNO                 2

F2 - Acquisition Parameter
Date_          20211116
Time              15.48 h
INSTRUM            spect
PROBHD   Z125869_0055 (
PULPROG           zgflqn
TD                131072
SOLVENT             CD3CN
NS                    16
DS                     4
SWH           113636.367 Hz
FIDRES          1.733953 Hz
AQ             0.5767168 sec
RG                 15.61
DW                4.400 usec
DE                18.00 usec
TE                298.0 K
D1             1.00000000 sec
TD0                    1
SFO1          470.6394024 MHz
NUC1                 19F
P1                15.00 usec
PLW1          11.70800018 W

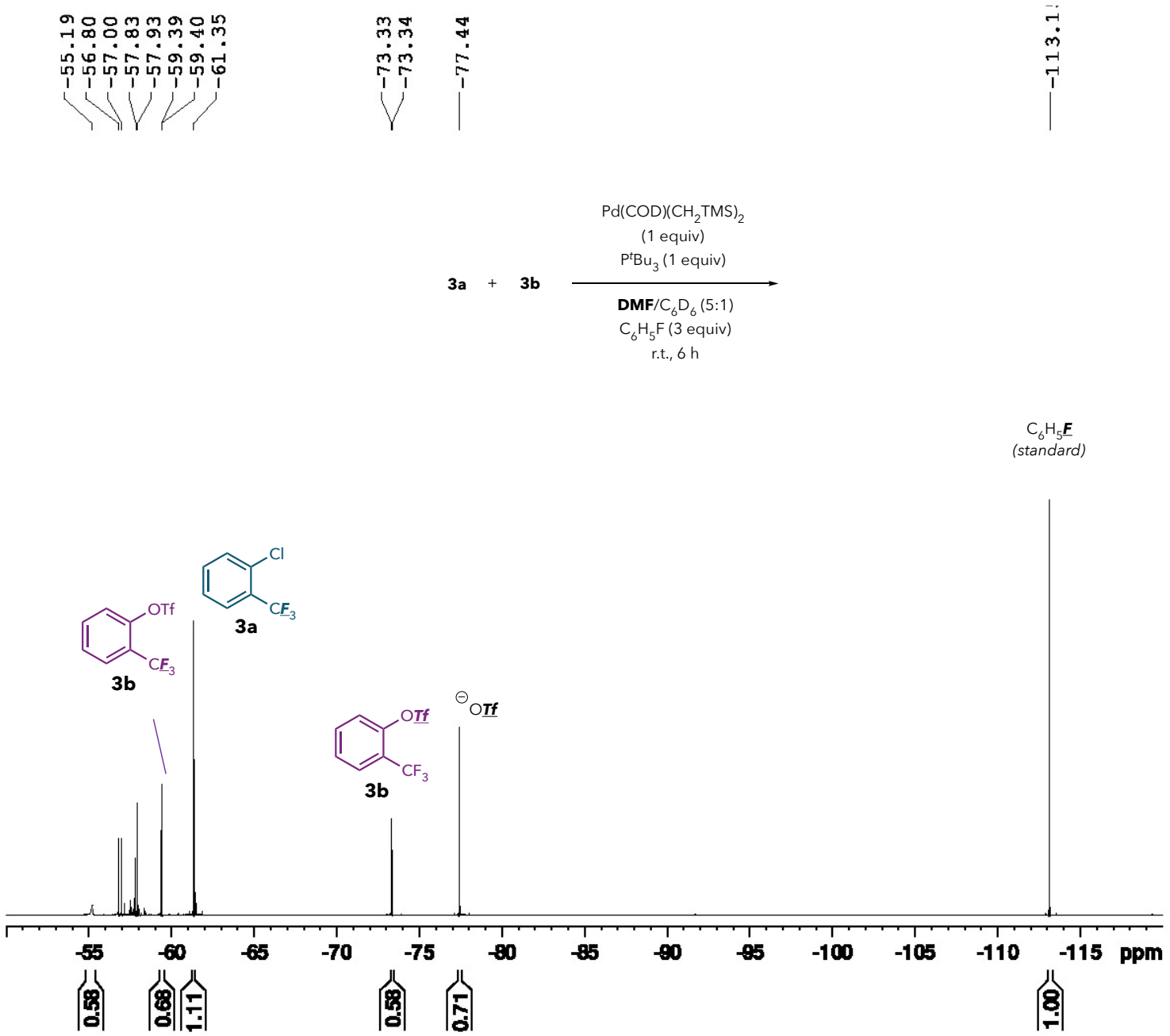
F2 - Processing parameters
SI                 65536
SF            470.6857814 MHz
WDW                  EM
SSB       0
LB                0.30 Hz
GB        0
PC                1.00
```




```
Current Data Parameters
NAME          6-SMR-41-6
EXPNO                 12
PROCNO                 1

F2 - Acquisition Parameter
Date_          20211116
Time              15.51 h
INSTRUM             spect
PROBHD   Z125869_0055 (
PULPROG           zgpg30
TD                65536
SOLVENT            CD3CN
NS                    16
DS                     4
SWH           81521.742 Hz
FIDRES          2.487846 Hz
AQ            0.4019541 sec
RG                190.44
DW                6.133 usec
DE                18.00 usec
TE                298.0 K
D1           2.00000000 sec
D11          0.03000000 sec
TD0                    1
SFO1         202.4866909 MHz
NUC1                  31P
P0                4.00 usec
P1               12.00 usec
PLW1         40.26200104 W
SFO2         500.2320009 MHz
NUC2                  1H
CPDPRG[2         waltz16
PCPD2             80.00 usec
PLW2         11.44699955 W
PLW12         0.25756001 W
PLW13         0.12955000 W

F2 - Processing parameters
SI                 32768
SF           202.4968157 MHz
WDW                   EM
SSB       0
LB                1.00 Hz
GB        0
PC                1.40
```

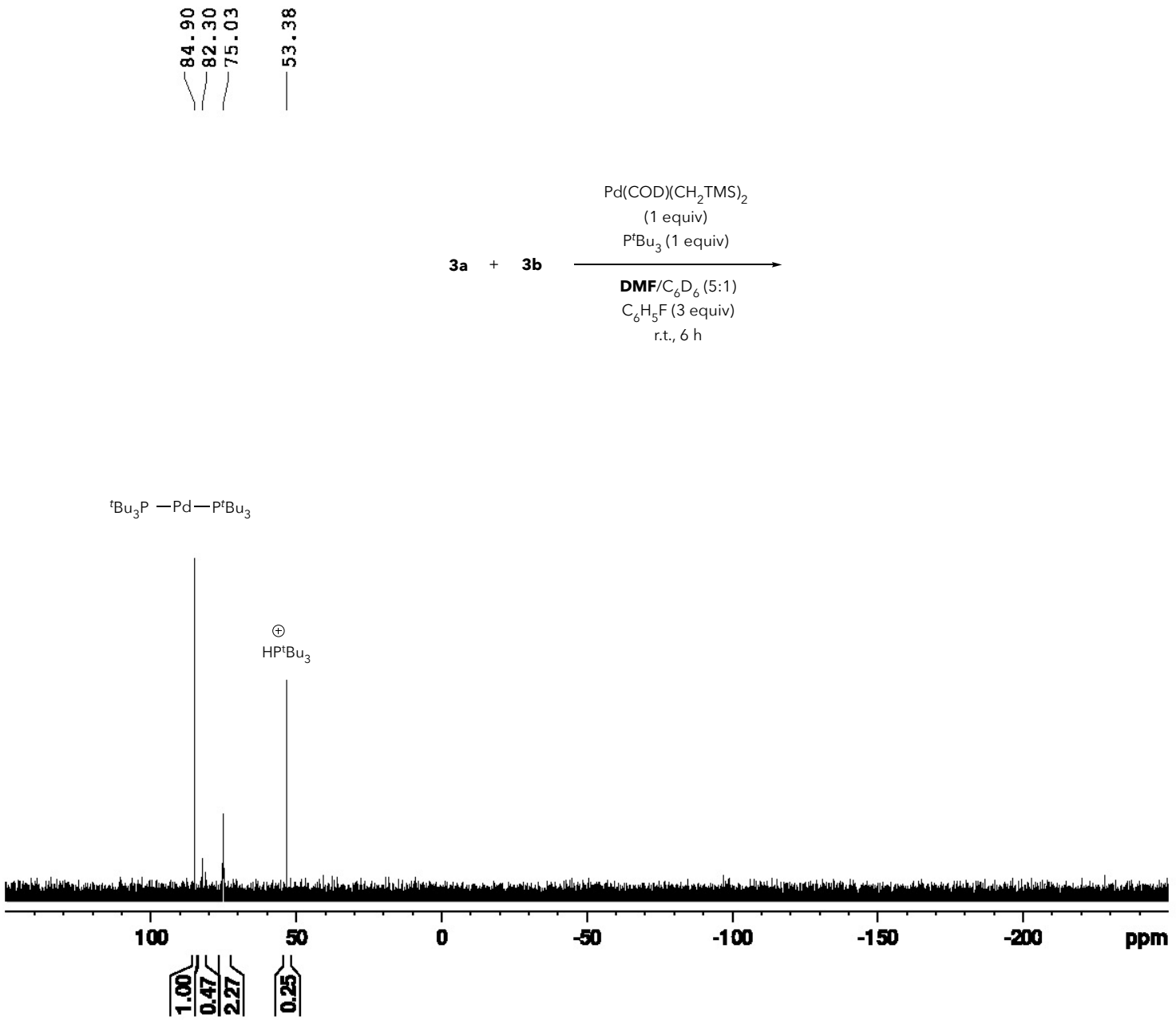


BRUKER

```
Current Data Parameters
NAME          6-SMR-39-11
EXPNO                  10
PROCNO                  2

F2 - Acquisition Parameter
Date_           20211115
Time              16.46 h
INSTRUM       Avance Neo
PROBHD    Z152088_0031 (
PULPROG             zgig
TD                131072
SOLVENT             C6D6
NS                    16
DS                     4
SWH           90909.094 Hz
FIDRES         1.387163 Hz
AQ            0.7208960 sec
RG                   101
DW               5.500 usec
DE               6.50 usec
TE               298.1 K
D1            1.00000000 sec
D11           0.03000000 sec
TD0                    1
SFO1          376.4607164 MHz
NUC1                 19F
P1                12.00 usec
PLW1          31.08900070 W
SFO2          400.1316005 MHz
NUC2                 1H
CPDPRG[2         waltz16
PCPD2             90.00 usec
PLW2          24.03499985 W
PLW12          0.18990999 W

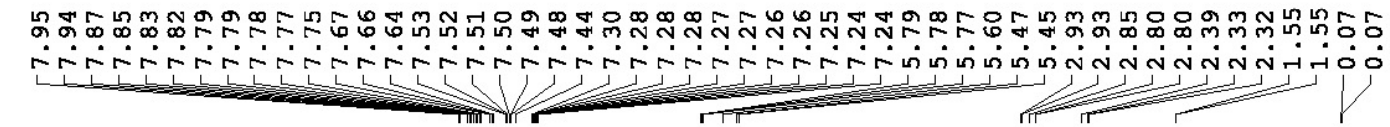
F2 - Processing parameters
SI                  65536
SF            376.4978850 MHz
WDW                    EM
SSB       0
LB                0.30 Hz
GB        0
PC                1.00
```

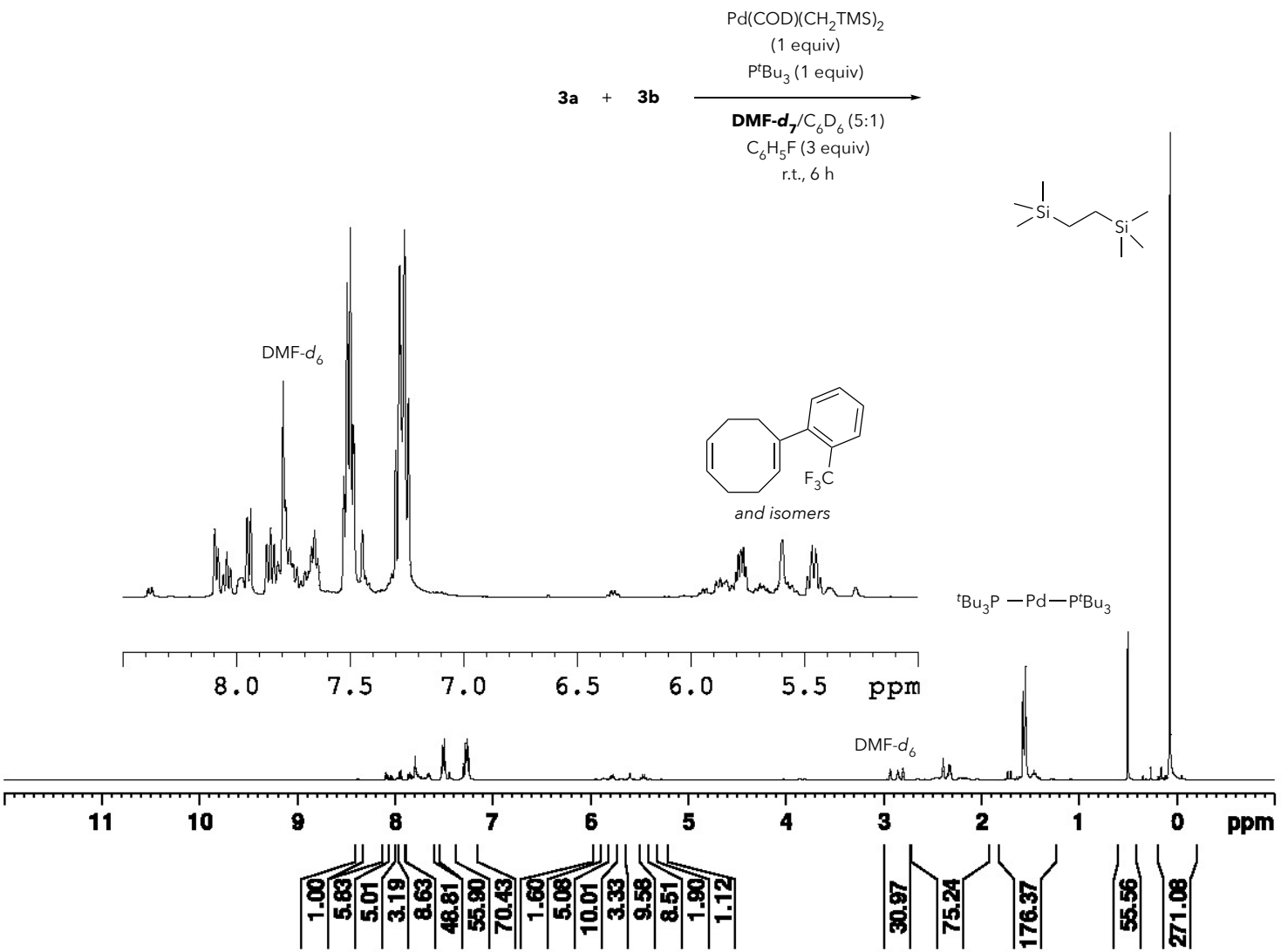


Current Data Parameters
NAME 6-SMR-39-11
EXPNO 11
PROCNO 1

F2 - Acquisition Parameter
Date_ 20211115
Time 16.50 h
INSTRUM Avance Neo
PROBHD Z152088_0031 (
PULPROG zgpg30
TD 65536
SOLVENT C6D6
NS 32
DS 4
SWH 65789.477 Hz
FIDRES 2.007735 Hz
AQ 0.4980736 sec
RG 101
DW 7.600 usec
DE 6.50 usec
TE 298.0 K
D1 2.00000000 sec
D11 0.03000000 sec
TD0 1
SFO1 161.9674942 MHz
NUC1 31P
P0 2.67 usec
P1 8.00 usec
PLW1 45.86100006 W
SFO2 400.1316005 MHz
NUC2 1H
CPDPRG[2 waltz16
PCPD2 90.00 usec
PLW2 24.03499985 W
PLW12 0.18990999 W
PLW13 0.09552100 W

F2 - Processing parameters
SI 32768
SF 161.9755930 MHz
WDW EM
SSB 0
LB 1.00 Hz
GB 0
PC 1.40



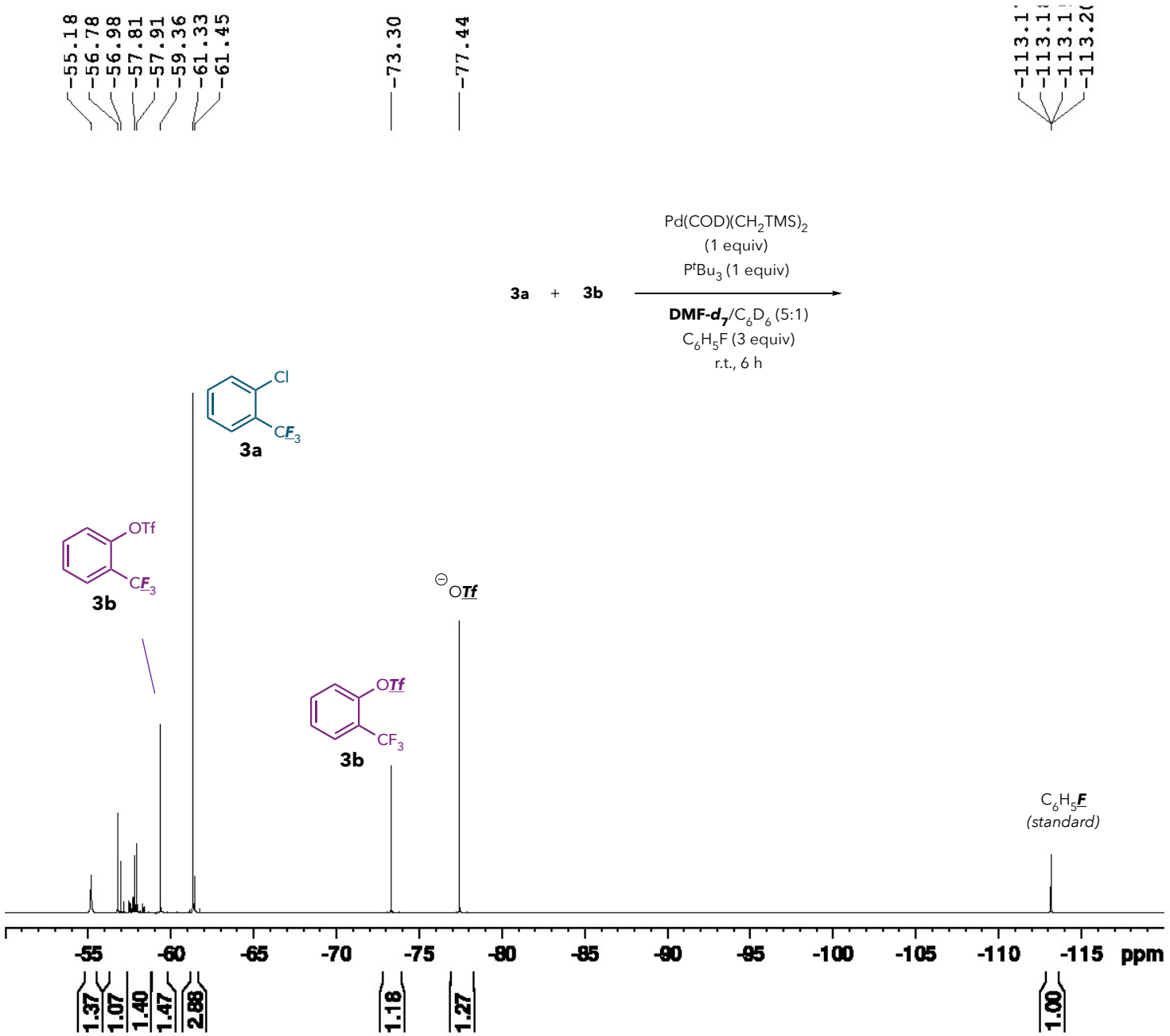


BRUKER

```
Current Data Parameters
NAME          6-SMR-41-11
EXPNO                  10
PROCNO                  1

F2 - Acquisition Parameter
Date_           20211116
Time              16.15 h
INSTRUM             spect
PROBHD    Z125869_0055 (
PULPROG             zg30
TD                 65536
SOLVENT              DMF
NS                    64
DS                     2
SWH           10000.000 Hz
FIDRES         0.305176 Hz
AQ            3.2767999 sec
RG                 37.93
DW               50.000 usec
DE               16.00 usec
TE                298.0 K
D1           2.00000000 sec
TD0                    1
SFO1         500.2330889 MHz
NUC1                  1H
P0               4.00 usec
P1               12.00 usec
PLW1         11.44699955 W

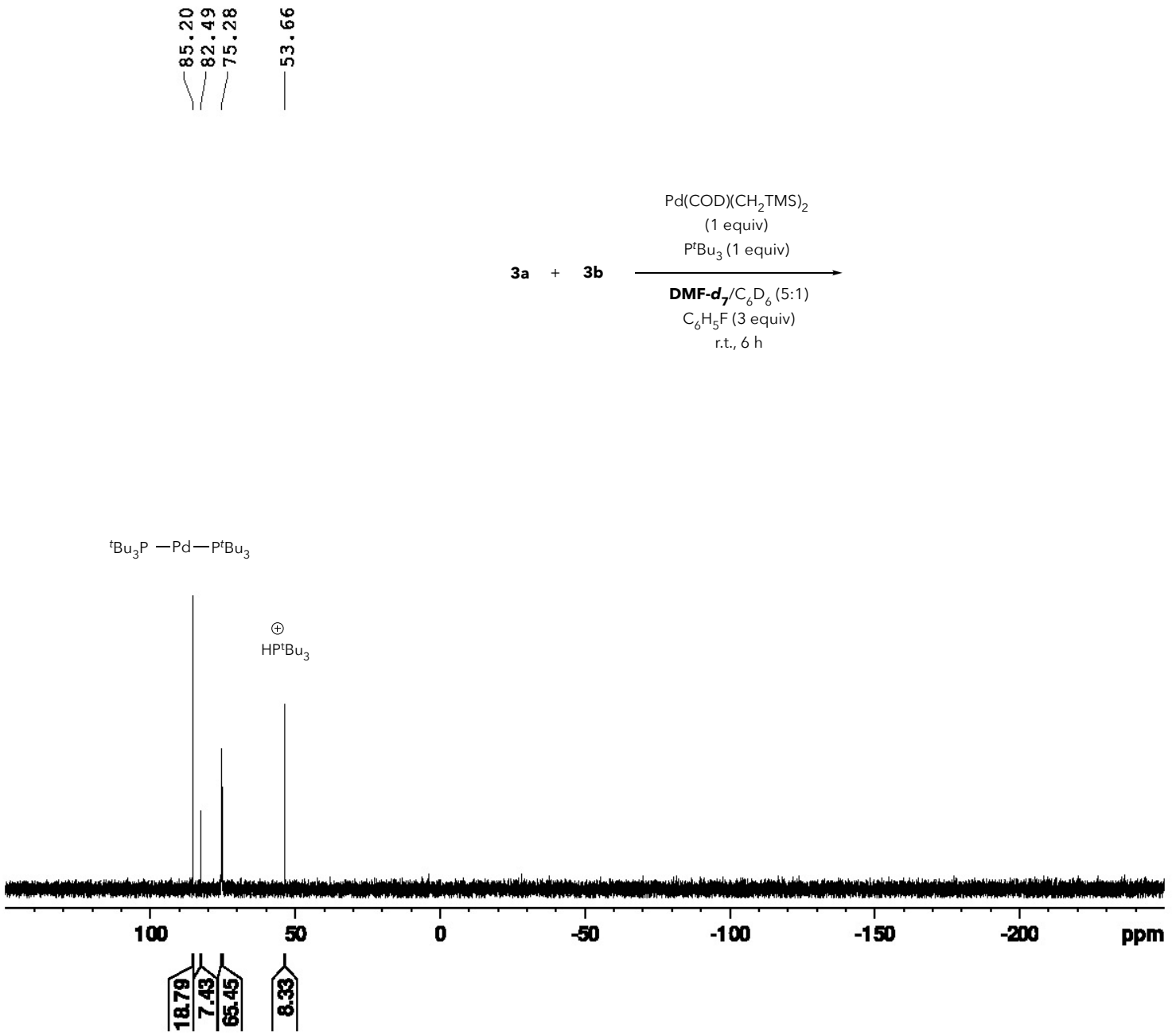
F2 - Processing parameters
SI                 65536
SF           500.2300000 MHz
WDW                   EM
SSB       0
LB                0.30 Hz
GB        0
PC                1.00
```




```
Current Data Parameters
NAME         6-SMR-41-11
EXPNO                 11
PROCNO                 2

F2 - Acquisition Parameter
Date_          20211116
Time             16.17 h
INSTRUM            spect
PROBHD   Z125869_0055 (
PULPROG            zgflqn
TD                131072
SOLVENT              DMF
NS                    16
DS                     4
SWH           113636.367 Hz
FIDRES          1.733953 Hz
AQ             0.5767168 sec
RG                 15.61
DW                4.400 usec
DE                18.00 usec
TE                298.0 K
D1             1.00000000 sec
TD0                    1
SFO1          470.6394024 MHz
NUC1                 19F
P1                15.00 usec
PLW1          11.70800018 W

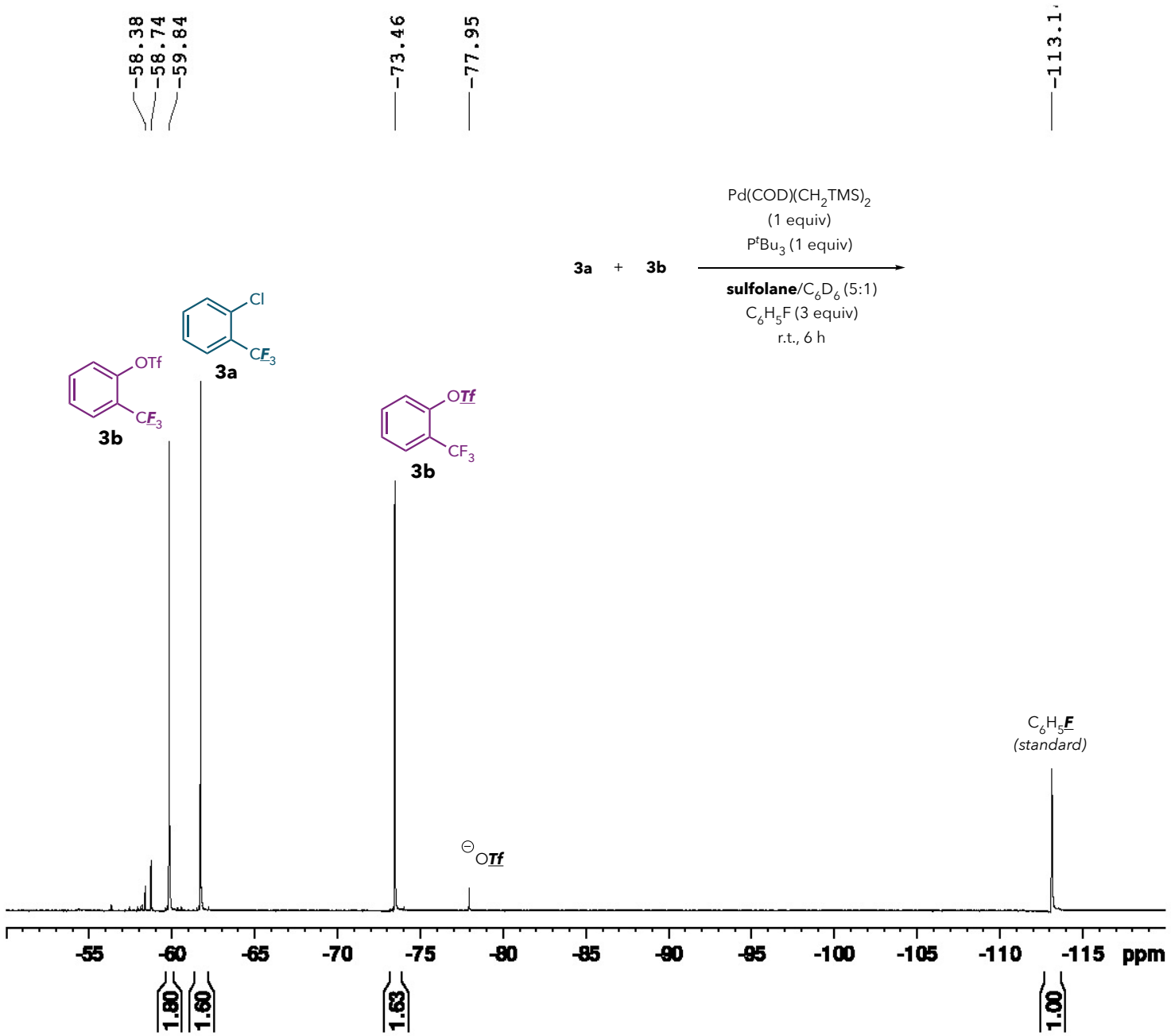
F2 - Processing parameters
SI                 65536
SF            470.6859888 MHz
WDW                  EM
SSB       0
LB                0.30 Hz
GB        0
PC                1.00
```



Current Data Parameters
NAME 6-SMR-41-11
EXPNO 12
PROCNO 1

F2 - Acquisition Parameter
Date_ 20211116
Time 16.19 h
INSTRUM spect
PROBHD Z125869_0055 (
PULPROG zgpg30
TD 65536
SOLVENT DMF
NS 16
DS 4
SWH 81521.742 Hz
FIDRES 2.487846 Hz
AQ 0.4019541 sec
RG 190.44
DW 6.133 usec
DE 18.00 usec
TE 298.0 K
D1 2.00000000 sec
D11 0.03000000 sec
TD0 1
SFO1 202.4866909 MHz
NUC1 31P
P0 4.00 usec
P1 12.00 usec
PLW1 40.26200104 W
SFO2 500.2320009 MHz
NUC2 1H
CPDPRG[2 waltz16
PCPD2 80.00 usec
PLW2 11.44699955 W
PLW12 0.25756001 W
PLW13 0.12955000 W

F2 - Processing parameters
SI 32768
SF 202.4968157 MHz
WDW EM
SSB 0
LB 1.00 Hz
GB 0
PC 1.40

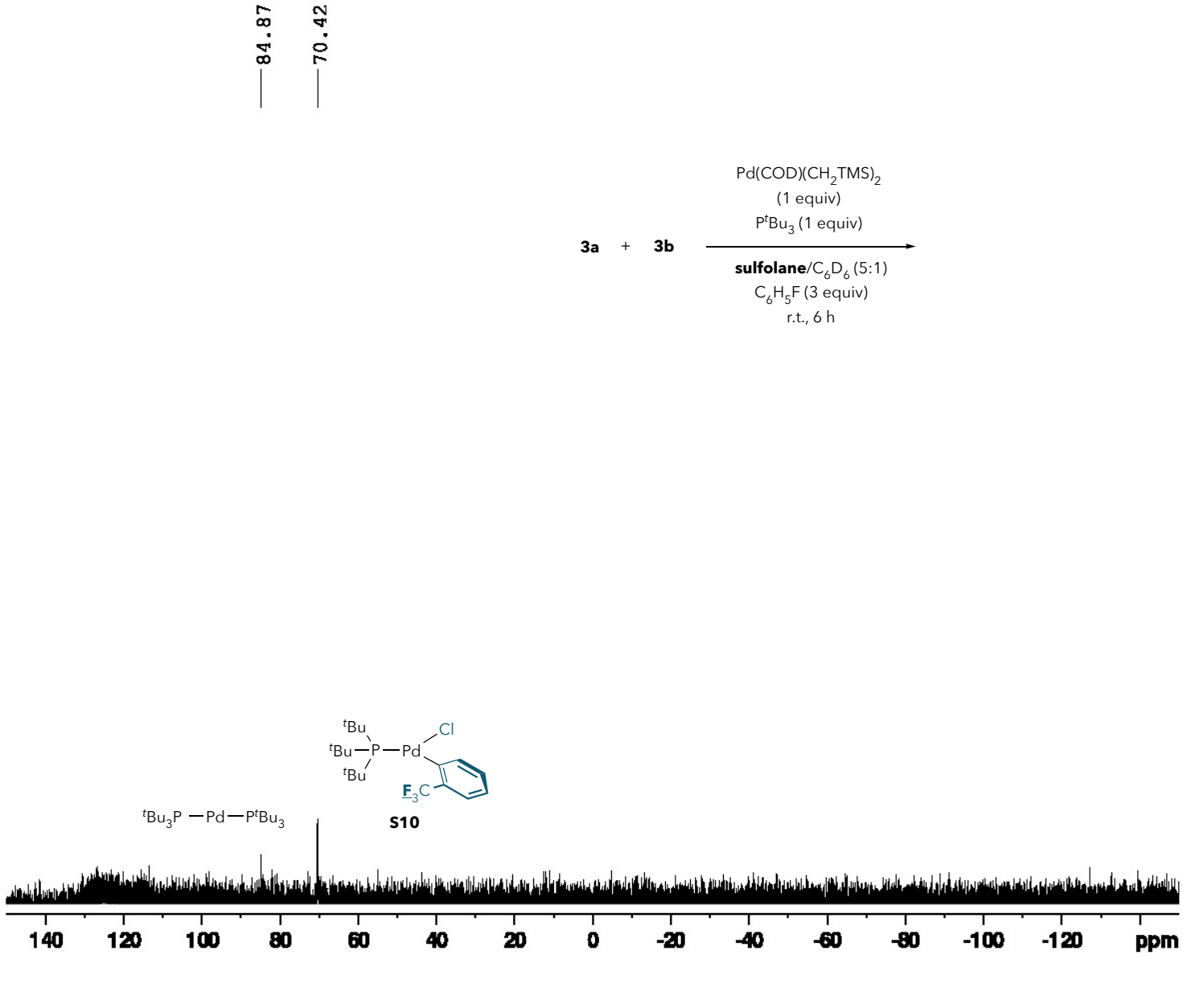


BRUKER

```
Current Data Parameters
NAME          6-SMR-5-15
EXPNO                 10
PROCNO                 2

F2 - Acquisition Parameter
Date_          20210911
Time             20.34 h
INSTRUM       Avance Neo
PROBHD   Z152088_0031 (
PULPROG               zg
TD                130892
SOLVENT             C6D6
NS                    16
DS                     4
SWH           90909.094 Hz
FIDRES          1.389070 Hz
AQ            0.7199060 sec
RG                   101
DW               5.500 usec
DE                6.50 usec
TE                298.0 K
D1           1.00000000 sec
TD0                    1
SFO1         376.4607164 MHz
NUC1                 19F
P1               12.00 usec
PLW1         31.08900070 W

F2 - Processing parameters
SI                 65536
SF           376.4982209 MHz
WDW                   EM
SSB       0
LB                0.30 Hz
GB        0
PC                1.00
```

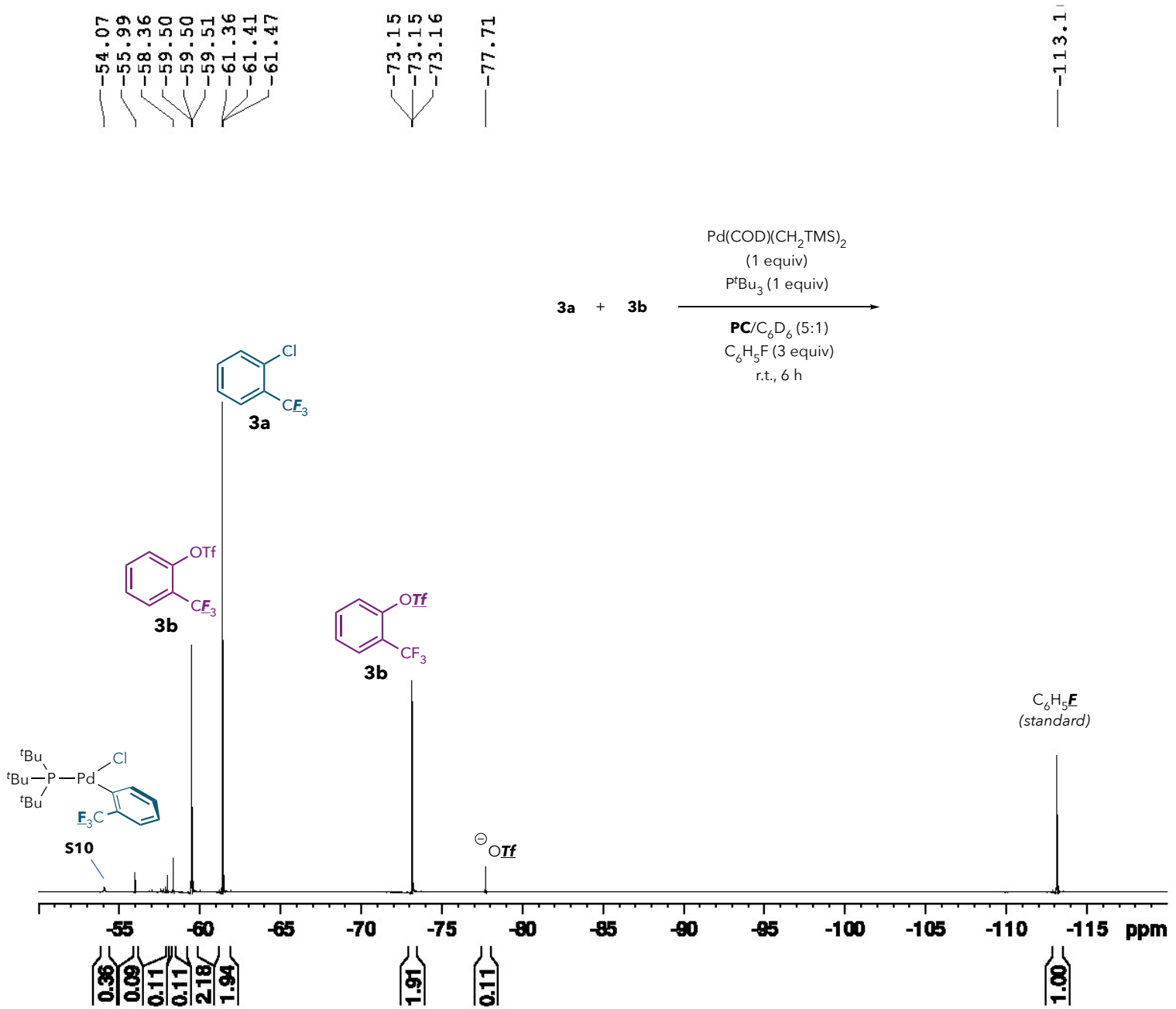


BRUKER

```
Current Data Parameters
NAME          6-SMR-5-15
EXPNO                 11
PROCNO                 2

F2 - Acquisition Parameter
Date_          20210911
Time             20.38 h
INSTRUM      Avance Neo
PROBHD   Z152088_0031 (
PULPROG          zgpg30
TD                65536
SOLVENT           C6D6
NS                   32
DS                    4
SWH           65789.477 Hz
FIDRES         2.007735 Hz
AQ            0.4980736 sec
RG                  101
DW                7.600 usec
DE                6.50 usec
TE                298.0 K
D1           2.00000000 sec
D11          0.03000000 sec
TD0                   1
SFO1        161.9674942 MHz
NUC1               31P
P0                2.67 usec
P1                8.00 usec
PLW1         45.86100006 W
SFO2        400.1316005 MHz
NUC2               1H
CPDPRG[2        waltz16
PCPD2            90.00 usec
PLW2         24.03499985 W
PLW12         0.18990999 W
PLW13         0.09552100 W

F2 - Processing parameters
SI                 32768
SF          161.9755930 MHz
WDW                EM
SSB       0
LB                1.00 Hz
GB        0
PC                1.40
```

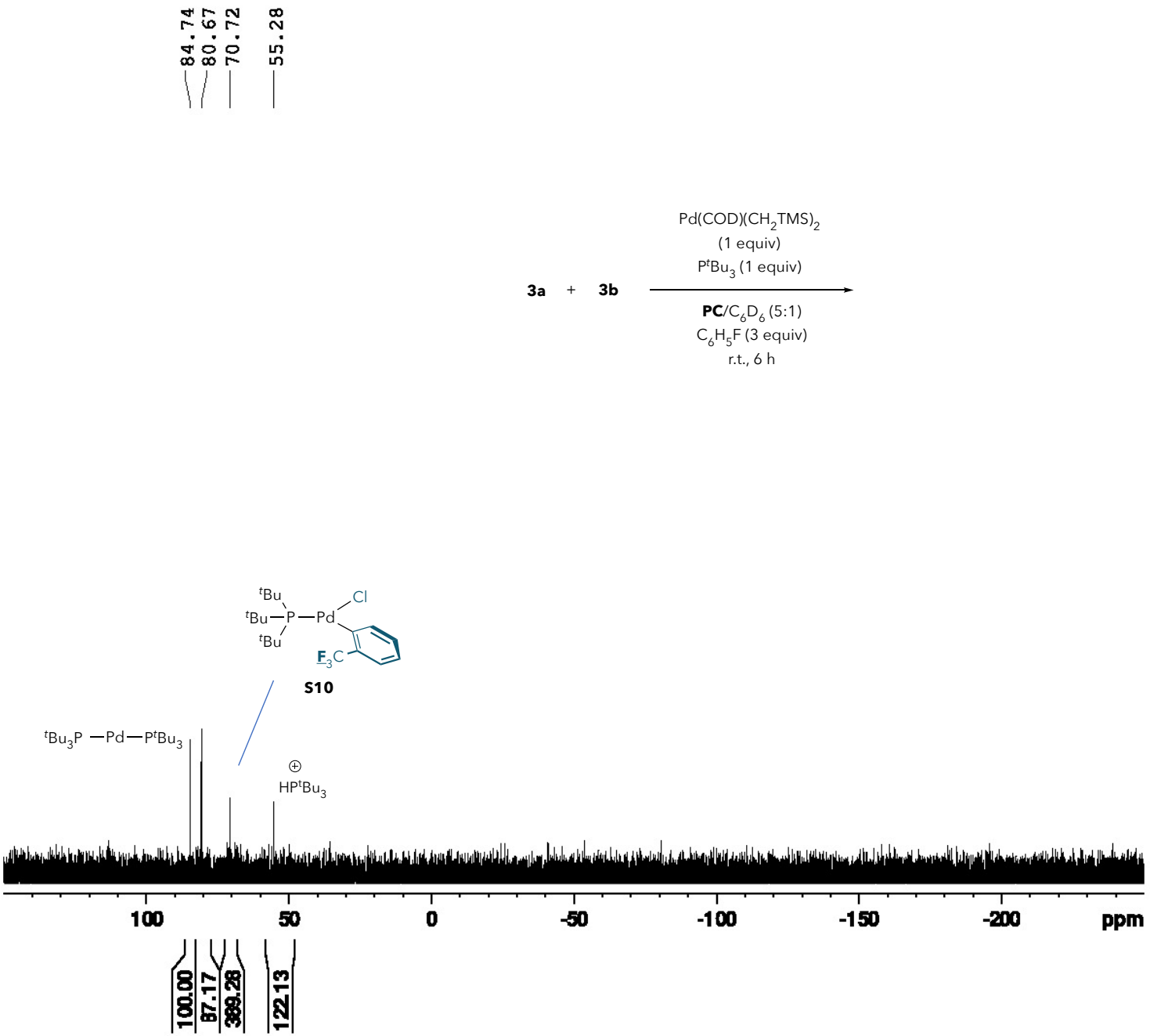




```
Current Data Parameters
NAME          6-SMR-39-15
EXPNO                  10
PROCNO                  2

F2 - Acquisition Parameter
Date_           20211115
Time              17.06 h
INSTRUM       Avance Neo
PROBHD    Z152088_0031 (
PULPROG            zgig
TD               131072
SOLVENT            C6D6
NS                   16
DS                    4
SWH           90909.094 Hz
FIDRES         1.387163 Hz
AQ            0.7208960 sec
RG                  101
DW              5.500 usec
DE              6.50 usec
TE              298.1 K
D1           1.00000000 sec
D11          0.03000000 sec
TD0                   1
SFO1         376.4607164 MHz
NUC1               19F
P1              12.00 usec
PLW1         31.08900070 W
SFO2         400.1316005 MHz
NUC2               1H
CPDPRG[2        waltz16
PCPD2            90.00 usec
PLW2         24.03499985 W
PLW12         0.18990999 W

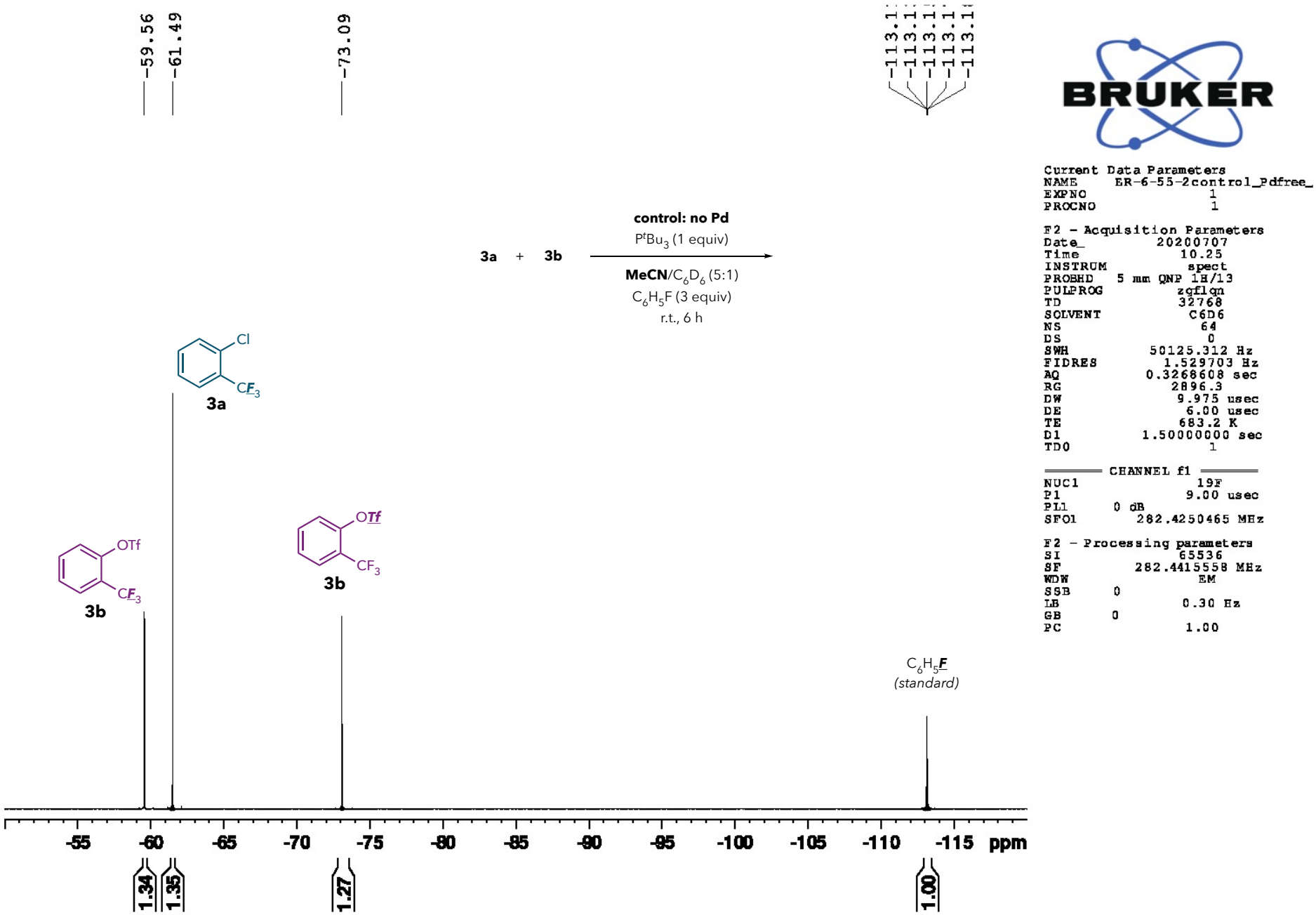
F2 - Processing parameters
SI                 65536
SF           376.4979014 MHz
WDW                  EM
SSB       0
LB              0.30 Hz
GB        0
PC              1.00
```




```
Current Data Parameters
NAME         6-SMR-39-15
EXPNO                 11
PROCNO                 1

F2 - Acquisition Parameter
Date_          20211115
Time             17.09 h
INSTRUM       Avance Neo
PROBHD   Z152088_0031 (
PULPROG          zgpg30
TD                65536
SOLVENT            C6D6
NS                   32
DS                    4
SWH           65789.477 Hz
FIDRES          2.007735 Hz
AQ            0.4980736 sec
RG                  101
DW                7.600 usec
DE                6.50 usec
TE                298.0 K
D1           2.00000000 sec
D11          0.03000000 sec
TD0                   1
SFO1         161.9674942 MHz
NUC1                31P
P0                2.67 usec
P1                8.00 usec
PLW1         45.86100006 W
SFO2         400.1316005 MHz
NUC2                1H
CPDPRG[2         waltz16
PCPD2             90.00 usec
PLW2         24.03499985 W
PLW12         0.18990999 W
PLW13         0.09552100 W

F2 - Processing parameters
SI                 32768
SF           161.9755930 MHz
WDW                  EM
SSB       0
LB                1.00 Hz
GB        0
PC                1.40
```

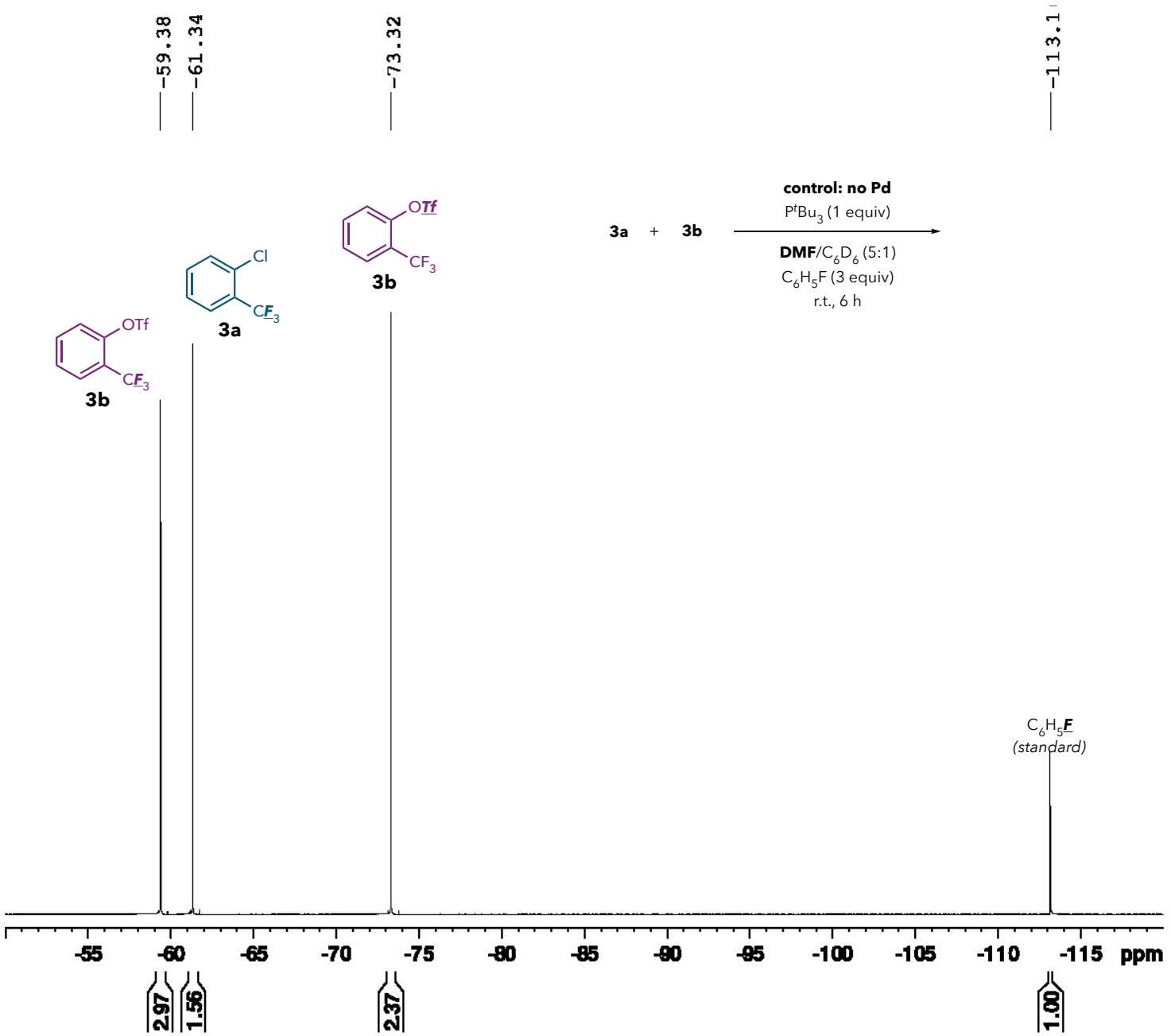



```
Current Data Parameters
NAME      ER-6-55-2control_Pdfree_
EXPNO                1
PROCNO               1

F2 - Acquisition Parameters
Date_          20200707
Time             10.25
INSTRUM          spect
PROBHD   5 mm QNP 1H/13
PULPROG          zgflqn
TD               32768
SOLVENT          C6D6
NS                  64
DS                   0
SWH          50125.312 Hz
FIDRES        1.529703 Hz
AQ           0.3268608 sec
RG              2896.3
DW               9.975 usec
DE                6.00 usec
TE               683.2 K
D1           1.50000000 sec
TD0                  1

======== CHANNEL f1 ========
NUC1               19F
P1                9.00 usec
PL1       0 dB
SFO1        282.4250465 MHz

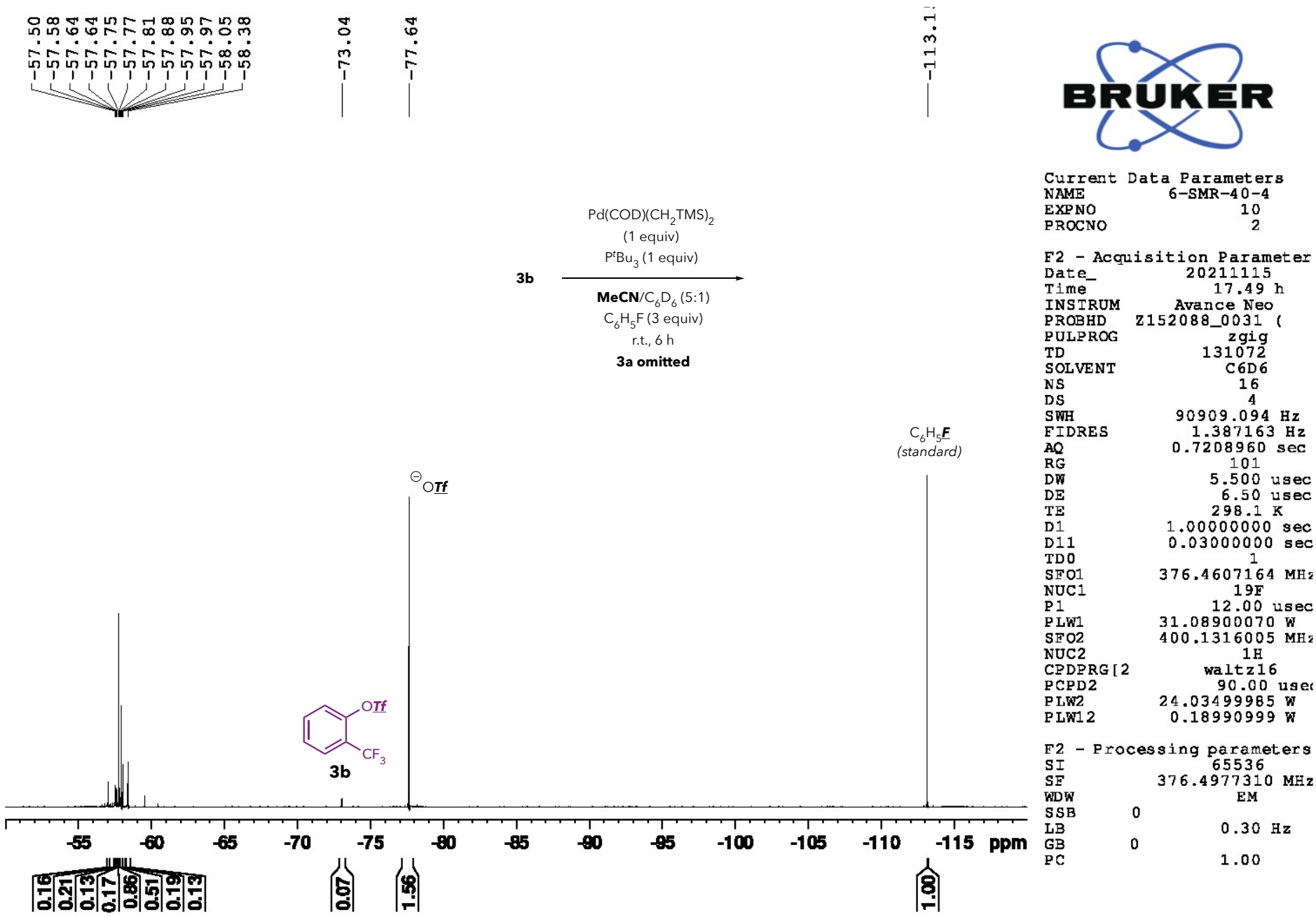
F2 - Processing parameters
SI                65536
SF          282.4415558 MHz
WDW                EM
SSB       0
LB              0.30 Hz
GB        0
PC              1.00
```




```
Current Data Parameters
NAME          5-SMR-95-1
EXPNO                 10
PROCNO                 2

F2 - Acquisition Parameter
Date_          20210519
Time             17.06 h
INSTRUM            spect
PROBHD   Z125869_0055 (
PULPROG          zgflqn
TD               130892
SOLVENT            C6D6
NS                   16
DS                    4
SWH          113636.367 Hz
FIDRES         1.736338 Hz
AQ           0.5759248 sec
RG                15.61
DW               4.400 usec
DE               18.00 usec
TE               300.0 K
D1           1.00000000 sec
TD0                   1
SFO1         470.6394024 MHz
NUC1                 19F
P1               15.00 usec
PLW1         11.70800018 W

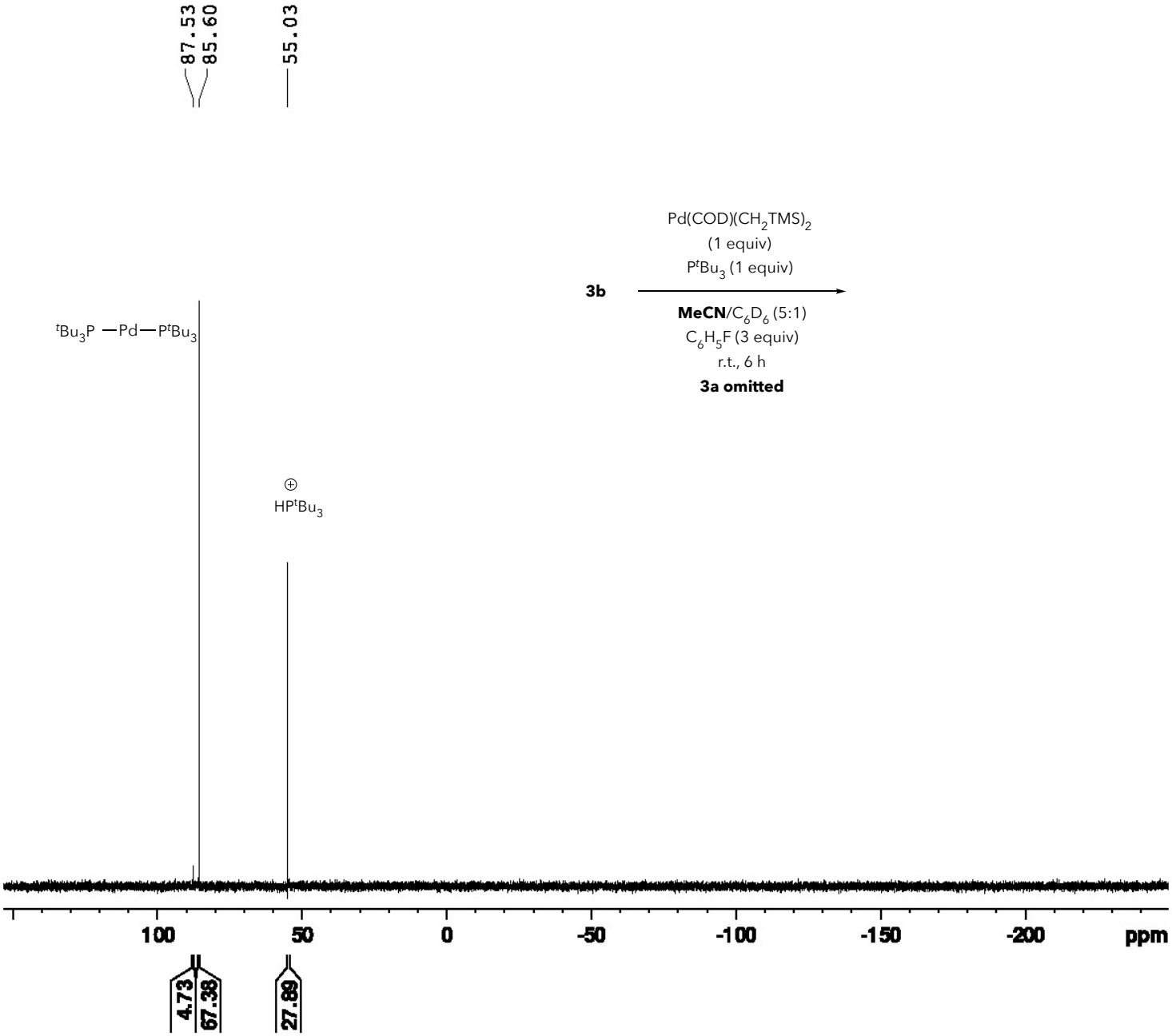
F2 - Processing parameters
SI                65536
SF           470.6858616 MHz
WDW                  EM
SSB       0
LB               0.30 Hz
GB        0
PC               1.00
```




```
Current Data Parameters
NAME          6-SMR-40-4
EXPNO                 10
PROCNO                 2

F2 - Acquisition Parameter
Date_          20211115
Time              17.49 h
INSTRUM       Avance Neo
PROBHD    Z152088_0031 (
PULPROG            zgig
TD               131072
SOLVENT            C6D6
NS                   16
DS                    4
SWH           90909.094 Hz
FIDRES         1.387163 Hz
AQ            0.7208960 sec
RG                  101
DW              5.500 usec
DE              6.50 usec
TE              298.1 K
D1           1.00000000 sec
D11          0.03000000 sec
TD0                   1
SFO1         376.4607164 MHz
NUC1                19F
P1              12.00 usec
PLW1         31.08900070 W
SFO2         400.1316005 MHz
NUC2                1H
CPDPRG[2         waltz16
PCPD2             90.00 usec
PLW2         24.03499985 W
PLW12         0.18990999 W

F2 - Processing parameters
SI                 65536
SF           376.4977310 MHz
WDW                  EM
SSB       0
LB              0.30 Hz
GB        0
PC              1.00
```

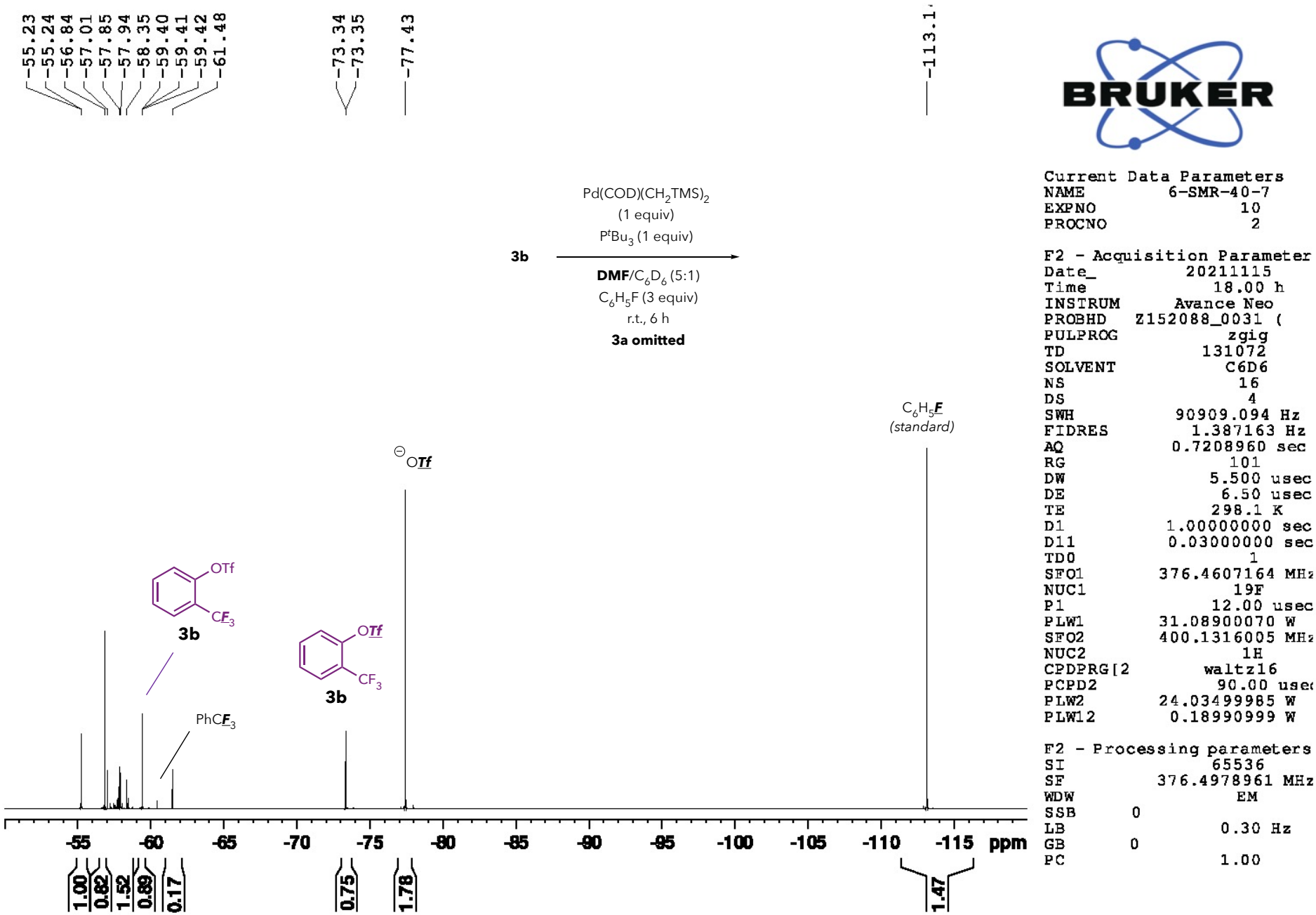





```
Current Data Parameters
NAME          6-SMR-40-4
EXPNO                 11
PROCNO                 1

F2 - Acquisition Parameter
Date_          20211115
Time              17.52 h
INSTRUM       Avance Neo
PROBHD   Z152088_0031 (
PULPROG           zgpg30
TD                65536
SOLVENT             C6D6
NS                    32
DS                     4
SWH           65789.477 Hz
FIDRES          2.007735 Hz
AQ            0.4980736 sec
RG                   101
DW                7.600 usec
DE                6.50 usec
TE                298.0 K
D1           2.00000000 sec
D11          0.03000000 sec
TD0                    1
SFO1         161.9674942 MHz
NUC1                 31P
P0                2.67 usec
P1                8.00 usec
PLW1         45.86100006 W
SFO2         400.1316005 MHz
NUC2                 1H
CPDPRG[2         waltz16
PCPD2             90.00 usec
PLW2         24.03499985 W
PLW12         0.18990999 W
PLW13         0.09552100 W

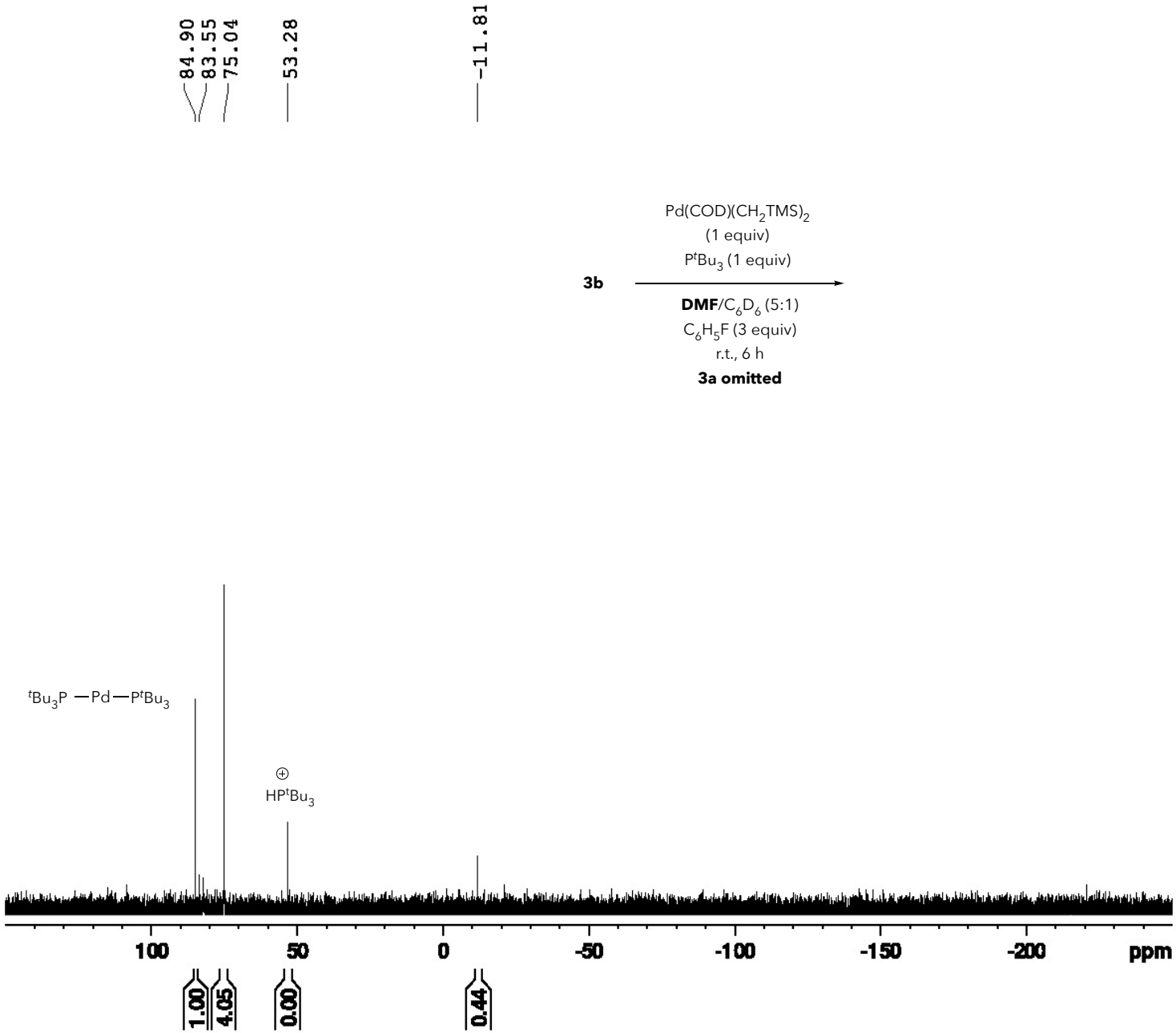
F2 - Processing parameters
SI                 32768
SF           161.9755930 MHz
WDW                   EM
SSB       0
LB                1.00 Hz
GB        0
PC                1.40
```




```
Current Data Parameters
NAME          6-SMR-40-7
EXPNO                 10
PROCNO                 2

F2 - Acquisition Parameter
Date_          20211115
Time             18.00 h
INSTRUM       Avance Neo
PROBHD   Z152088_0031 (
PULPROG            zgig
TD               131072
SOLVENT            C6D6
NS                   16
DS                    4
SWH           90909.094 Hz
FIDRES         1.387163 Hz
AQ            0.7208960 sec
RG                  101
DW                5.500 usec
DE                6.50 usec
TE                298.1 K
D1           1.00000000 sec
D11          0.03000000 sec
TD0                   1
SFO1         376.4607164 MHz
NUC1                 19F
P1                12.00 usec
PLW1         31.08900070 W
SFO2         400.1316005 MHz
NUC2                 1H
CPDPRG[2         waltz16
PCPD2             90.00 usec
PLW2         24.03499985 W
PLW12         0.18990999 W

F2 - Processing parameters
SI                65536
SF           376.4978961 MHz
WDW                  EM
SSB       0
LB                0.30 Hz
GB        0
PC                1.00
```

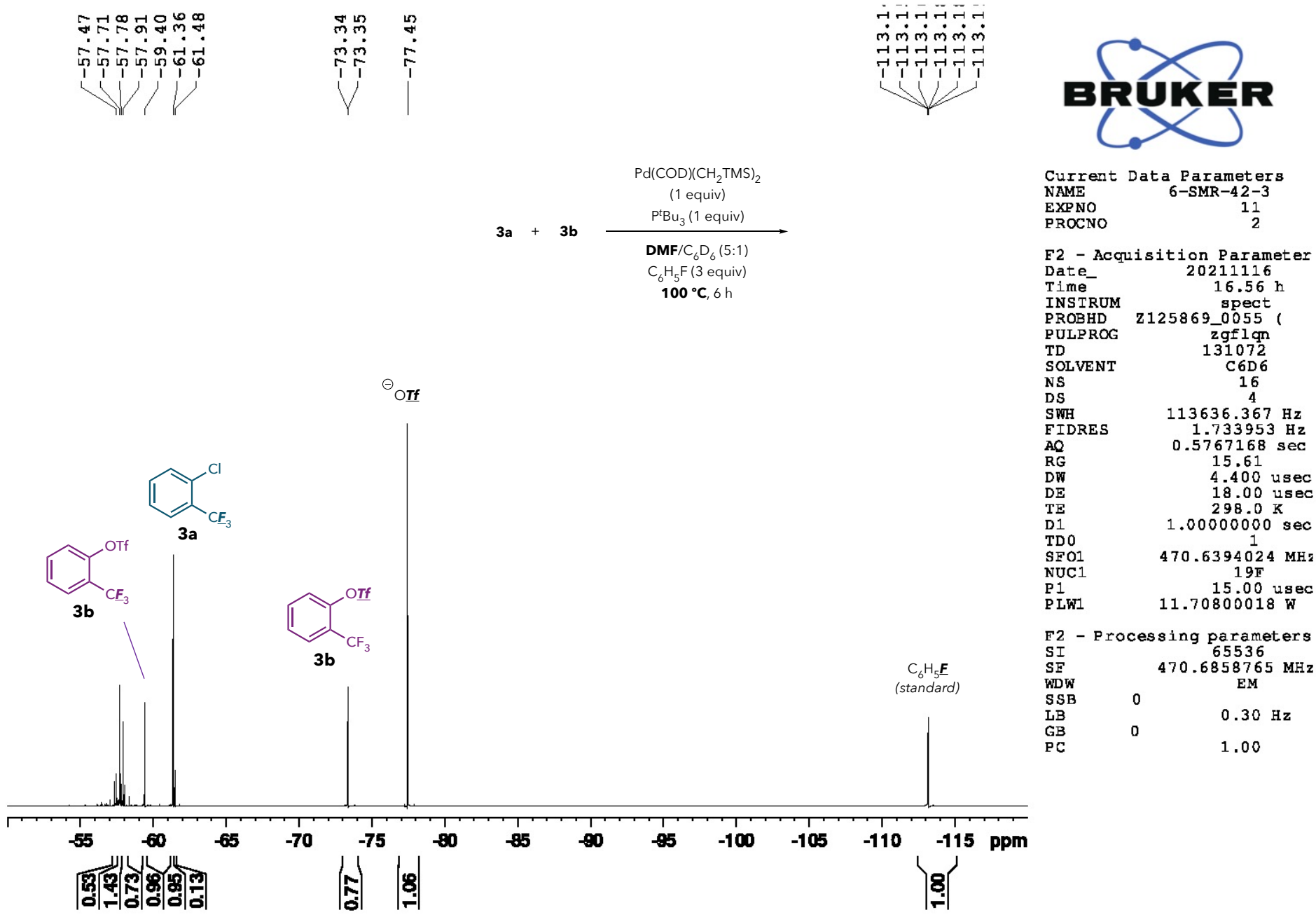



```
Current Data Parameters
NAME          6-SMR-40-7
EXPNO                 11
PROCNO                 1

F2 - Acquisition Parameter
Date_          20211115
Time             18.04 h
INSTRUM       Avance Neo
PROBHD   Z152088_0031 (
PULPROG          zgpg30
TD                65536
SOLVENT           C6D6
NS                   32
DS                    4
SWH           65789.477 Hz
FIDRES          2.007735 Hz
AQ            0.4980736 sec
RG                  101
DW                7.600 usec
DE                6.50 usec
TE                298.0 K
D1           2.00000000 sec
D11          0.03000000 sec
TD0                   1
SFO1        161.9674942 MHz
NUC1               31P
P0                2.67 usec
P1                8.00 usec
PLW1         45.86100006 W
SFO2        400.1316005 MHz
NUC2               1H
CPDPRG[2        waltz16
PCPD2            90.00 usec
PLW2         24.03499985 W
PLW12         0.18990999 W
PLW13         0.09552100 W

F2 - Processing parameters
SI                32768
SF          161.9755930 MHz
WDW                EM
SSB       0
LB                1.00 Hz
GB        0
PC                1.40
```

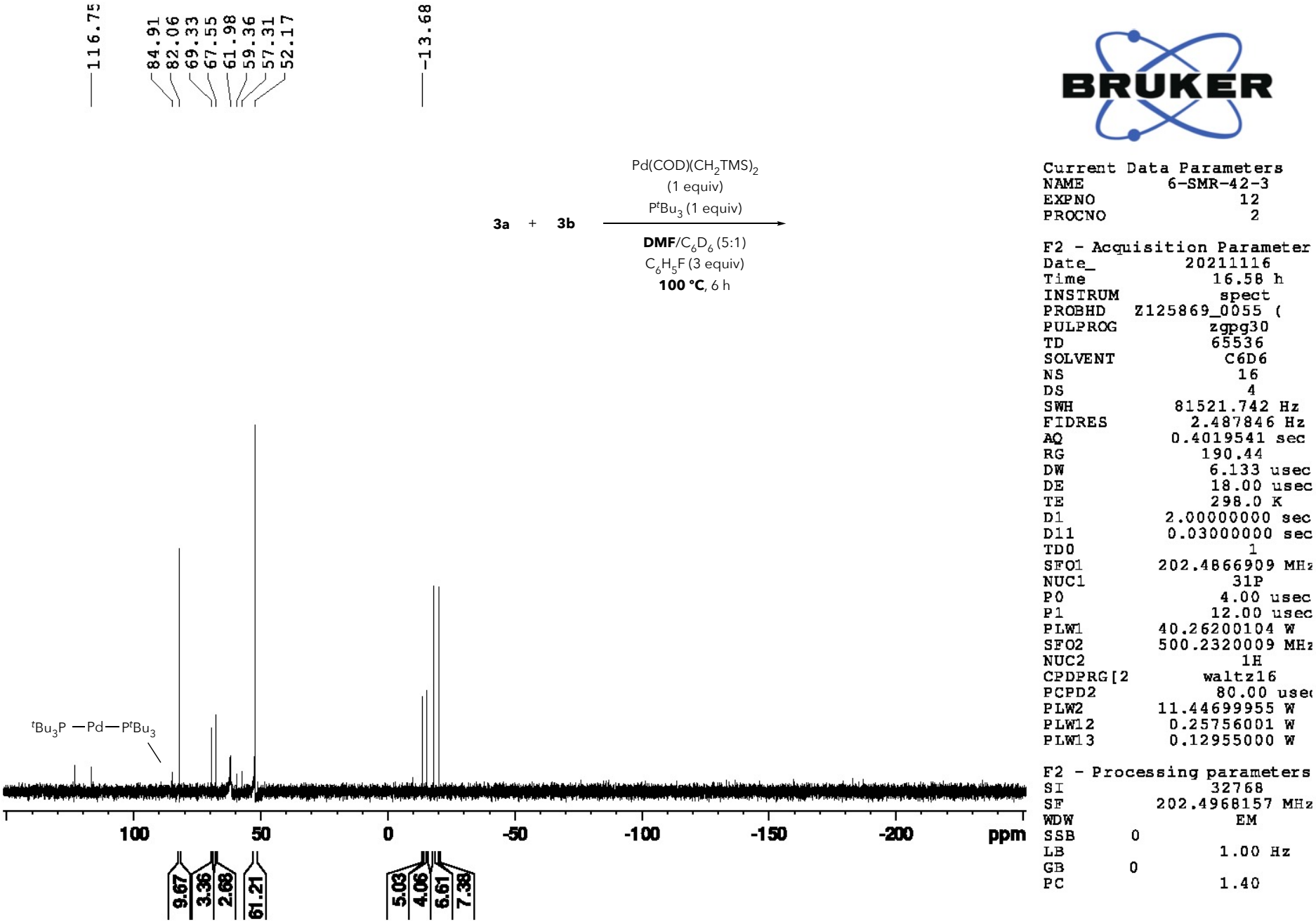
2. Experiments in DMF at 100 and 0 ºC




```
Current Data Parameters
NAME          6-SMR-42-3
EXPNO                 11
PROCNO                 2

F2 - Acquisition Parameter
Date_          20211116
Time             16.56 h
INSTRUM            spect
PROBHD   Z125869_0055 (
PULPROG            zgflqn
TD                131072
SOLVENT             C6D6
NS                    16
DS                     4
SWH          113636.367 Hz
FIDRES         1.733953 Hz
AQ           0.5767168 sec
RG                 15.61
DW                4.400 usec
DE                18.00 usec
TE                298.0 K
D1           1.00000000 sec
TD0                    1
SFO1         470.6394024 MHz
NUC1                 19F
P1                15.00 usec
PLW1         11.70800018 W

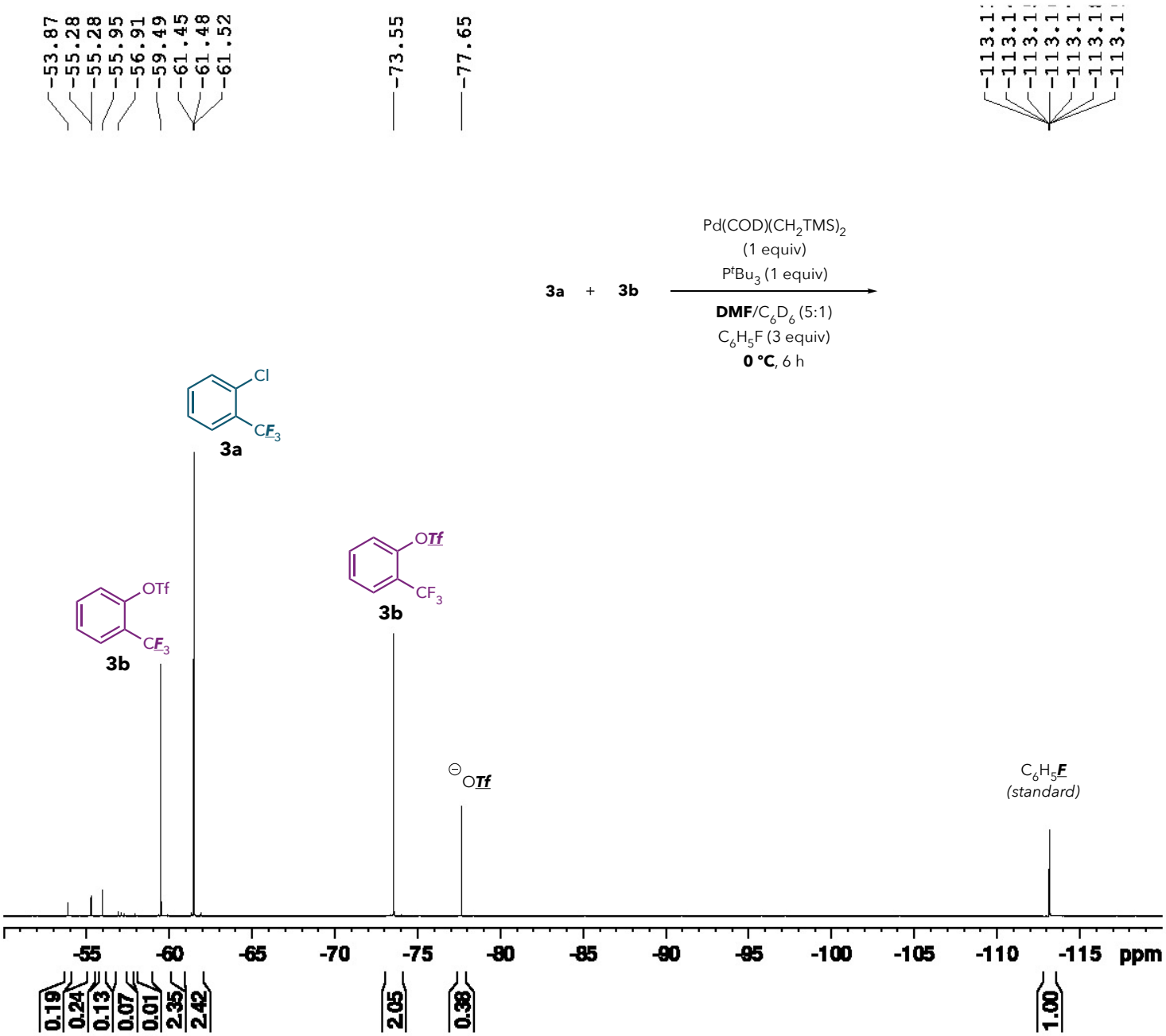
F2 - Processing parameters
SI                 65536
SF           470.6858765 MHz
WDW                   EM
SSB       0
LB                0.30 Hz
GB        0
PC                1.00
```




```
Current Data Parameters
NAME          6-SMR-42-3
EXPNO                 12
PROCNO                 2

F2 - Acquisition Parameter
Date_          20211116
Time             16.58 h
INSTRUM            spect
PROBHD   Z125869_0055 (
PULPROG           zgpg30
TD                65536
SOLVENT             C6D6
NS                    16
DS                     4
SWH           81521.742 Hz
FIDRES          2.487846 Hz
AQ            0.4019541 sec
RG                190.44
DW                6.133 usec
DE                18.00 usec
TE                298.0 K
D1           2.00000000 sec
D11          0.03000000 sec
TD0                    1
SFO1        202.4866909 MHz
NUC1                 31P
P0                4.00 usec
P1               12.00 usec
PLW1         40.26200104 W
SFO2        500.2320009 MHz
NUC2                 1H
CPDPRG[2         waltz16
PCPD2             80.00 usec
PLW2         11.44699955 W
PLW12         0.25756001 W
PLW13         0.12955000 W

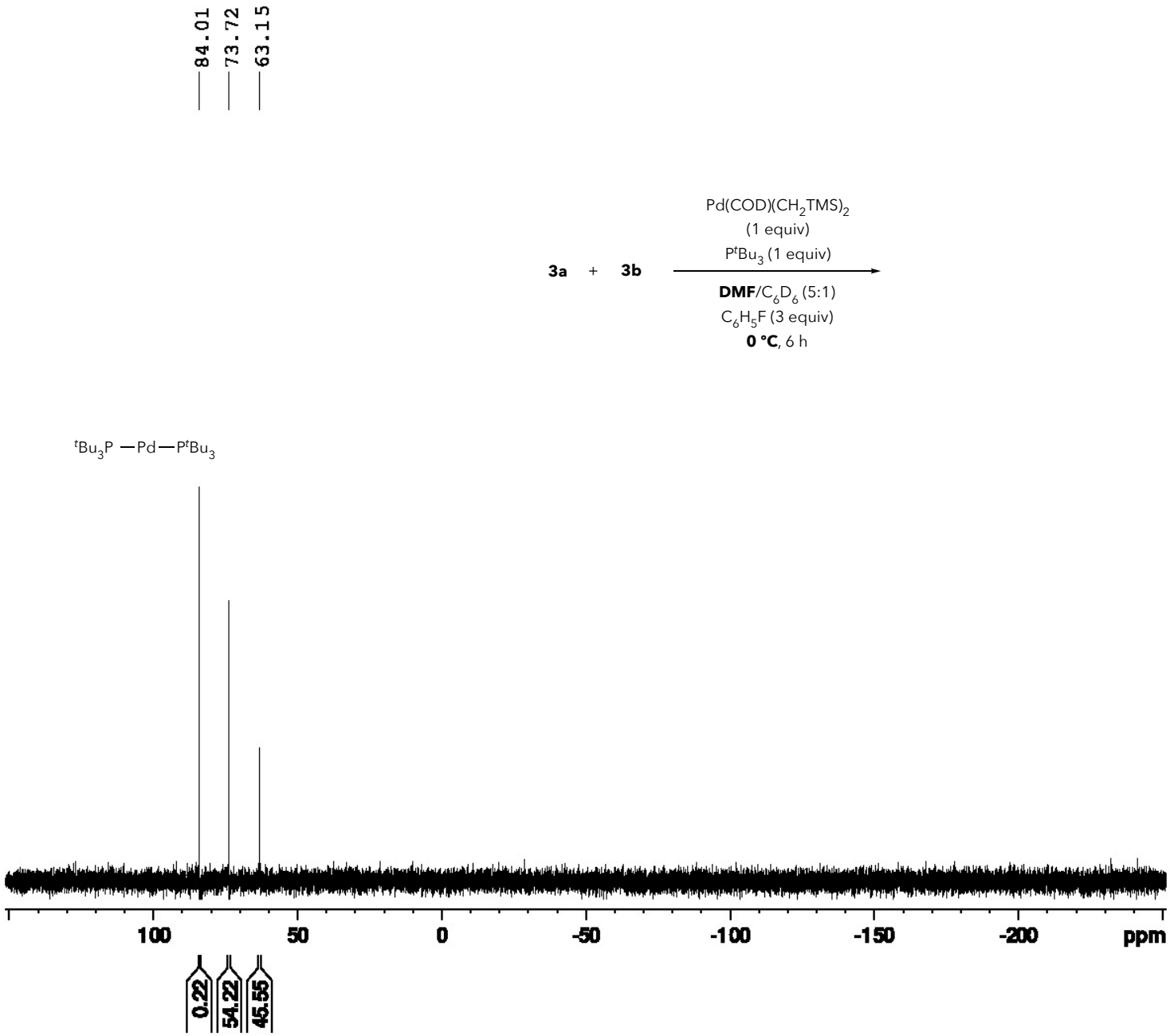
F2 - Processing parameters
SI                 32768
SF          202.4968157 MHz
WDW                   EM
SSB       0
LB                1.00 Hz
GB        0
PC                1.40
```




```
Current Data Parameters
NAME          6-SMR-42-8
EXPNO                 11
PROCNO                 1

F2 - Acquisition Parameter
Date_          20211117
Time             15.39 h
INSTRUM            spect
PROBHD   Z125869_0055 (
PULPROG            zgflqn
TD                131072
SOLVENT             C6D6
NS                    16
DS                     4
SWH           113636.367 Hz
FIDRES          1.733953 Hz
AQ             0.5767168 sec
RG                 15.61
DW                4.400 usec
DE                18.00 usec
TE                273.0 K
D1             1.00000000 sec
TD0                    1
SFO1          470.6394024 MHz
NUC1                 19F
P1                15.00 usec
PLW1          11.70800018 W

F2 - Processing parameters
SI                 65536
SF            470.6859023 MHz
WDW                  EM
SSB       0
LB                0.30 Hz
GB        0
PC                1.00
```

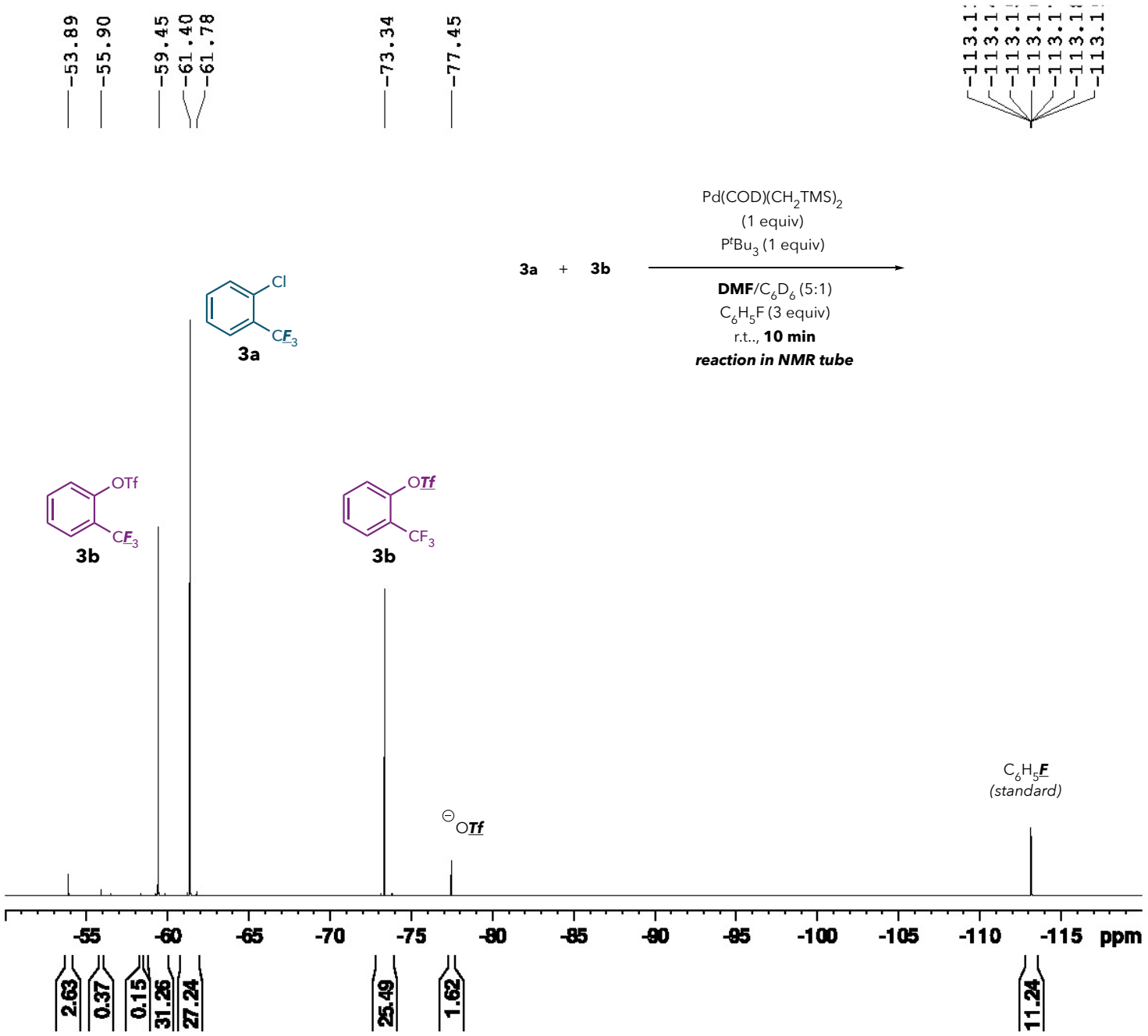



```
Current Data Parameters
NAME          6-SMR-42-8
EXPNO                 10
PROCNO                 1

F2 - Acquisition Parameter
Date_          20211117
Time             15.37 h
INSTRUM            spect
PROBHD   Z125869_0055 (
PULPROG           zgpg30
TD                65536
SOLVENT             C6D6
NS                    16
DS                     4
SWH           81521.742 Hz
FIDRES          2.487846 Hz
AQ            0.4019541 sec
RG                190.44
DW                6.133 usec
DE                18.00 usec
TE                273.0 K
D1           2.00000000 sec
D11          0.03000000 sec
TD0                    1
SFO1         202.4866909 MHz
NUC1                 31P
P0                4.00 usec
P1                12.00 usec
PLW1         40.26200104 W
SFO2         500.2320009 MHz
NUC2                 1H
CPDPRG[2          waltz16
PCPD2             80.00 usec
PLW2         11.44699955 W
PLW12         0.25756001 W
PLW13         0.12955000 W

F2 - Processing parameters
SI                 32768
SF           202.4968157 MHz
WDW                   EM
SSB       0
LB                1.00 Hz
GB        0
PC                1.40
```

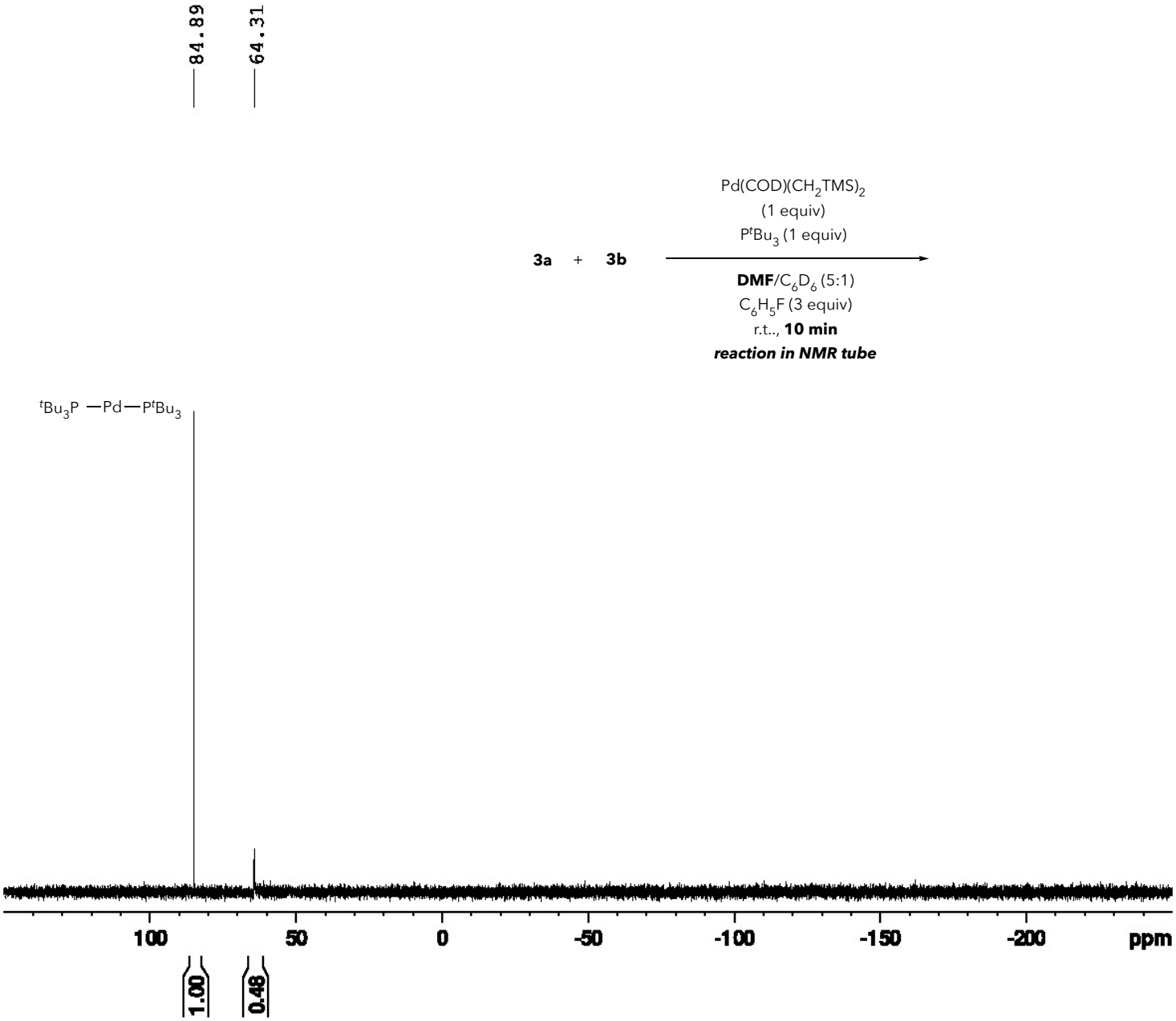
3. Monitoring the Reaction in DMF over Time [261]




```
Current Data Parameters
NAME      6-SMR-43-5min
EXPNO               10
PROCNO               2

F2 - Acquisition Parameter
Date_          20211117
Time               9.05 h
INSTRUM           spect
PROBHD   Z125869_0055 (
PULPROG           zgflqn
TD              131072
SOLVENT           C6D6
NS                  16
DS                   4
SWH          113636.367 Hz
FIDRES         1.733953 Hz
AQ           0.5767168 sec
RG                15.61
DW             4.400 usec
DE             18.00 usec
TE             298.0 K
D1          1.00000000 sec
TD0                  1
SFO1         470.6394024 MHz
NUC1               19F
P1             15.00 usec
PLW1        11.70800018 W

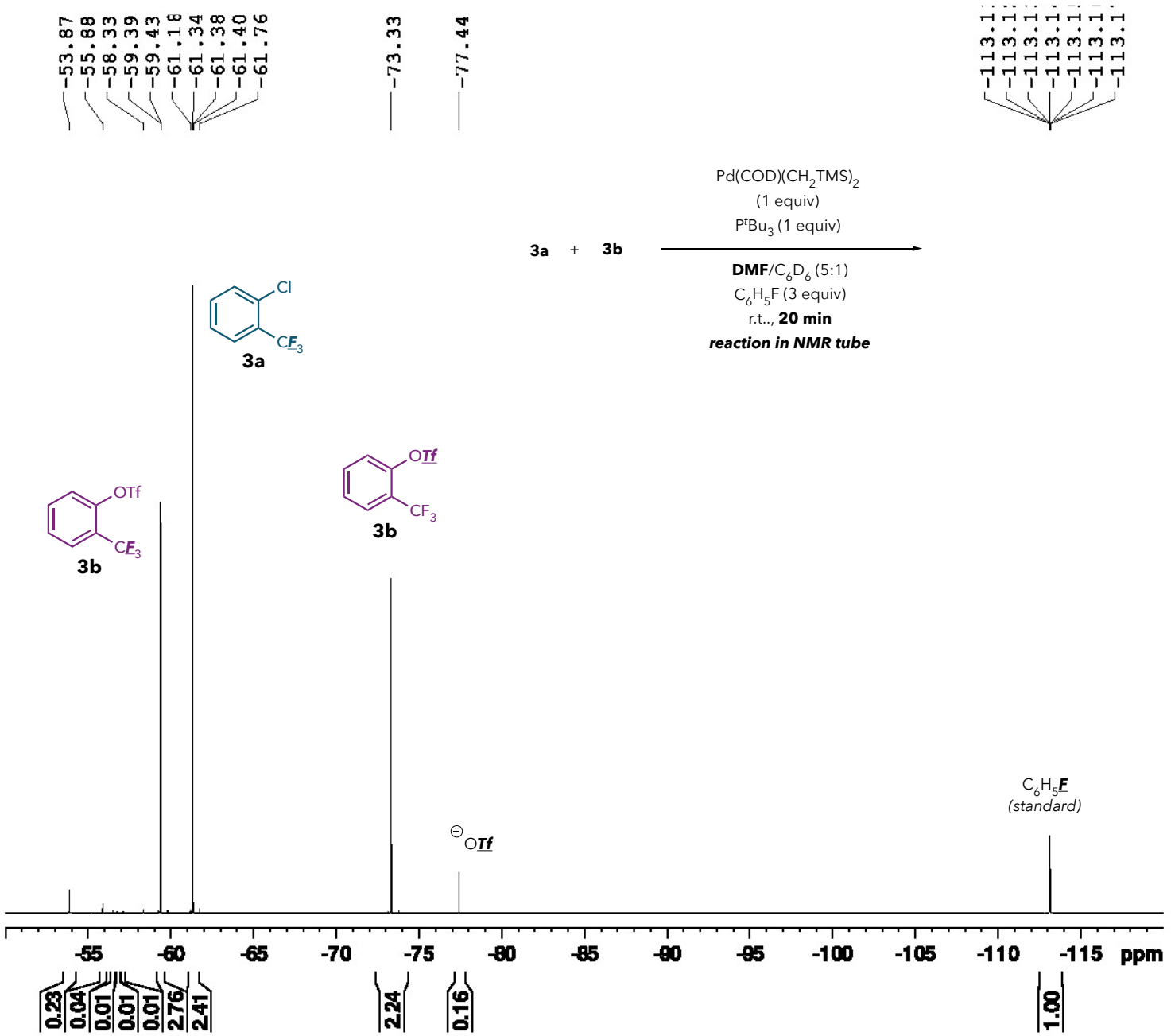
F2 - Processing parameters
SI                65536
SF          470.6858694 MHz
WDW                EM
SSB       0
LB             0.30 Hz
GB        0
PC             1.00
```




```
Current Data Parameters
NAME      6-SMR-43-5min
EXPNO                11
PROCNO                1

F2 - Acquisition Parameter
Date_          20211117
Time               9.09 h
INSTRUM           spect
PROBHD   Z125869_0055 (
PULPROG          zgpg30
TD                65536
SOLVENT            C6D6
NS                   16
DS                    4
SWH          81521.742 Hz
FIDRES         2.487846 Hz
AQ           0.4019541 sec
RG                190.44
DW              6.133 usec
DE             18.00 usec
TE              298.0 K
D1          2.00000000 sec
D11         0.03000000 sec
TD0                   1
SFO1        202.4866909 MHz
NUC1               31P
P0              4.00 usec
P1             12.00 usec
PLW1        40.26200104 W
SFO2        500.2320009 MHz
NUC2               1H
CPDPRG[2        waltz16
PCPD2           80.00 usec
PLW2        11.44699955 W
PLW12        0.25756001 W
PLW13        0.12955000 W

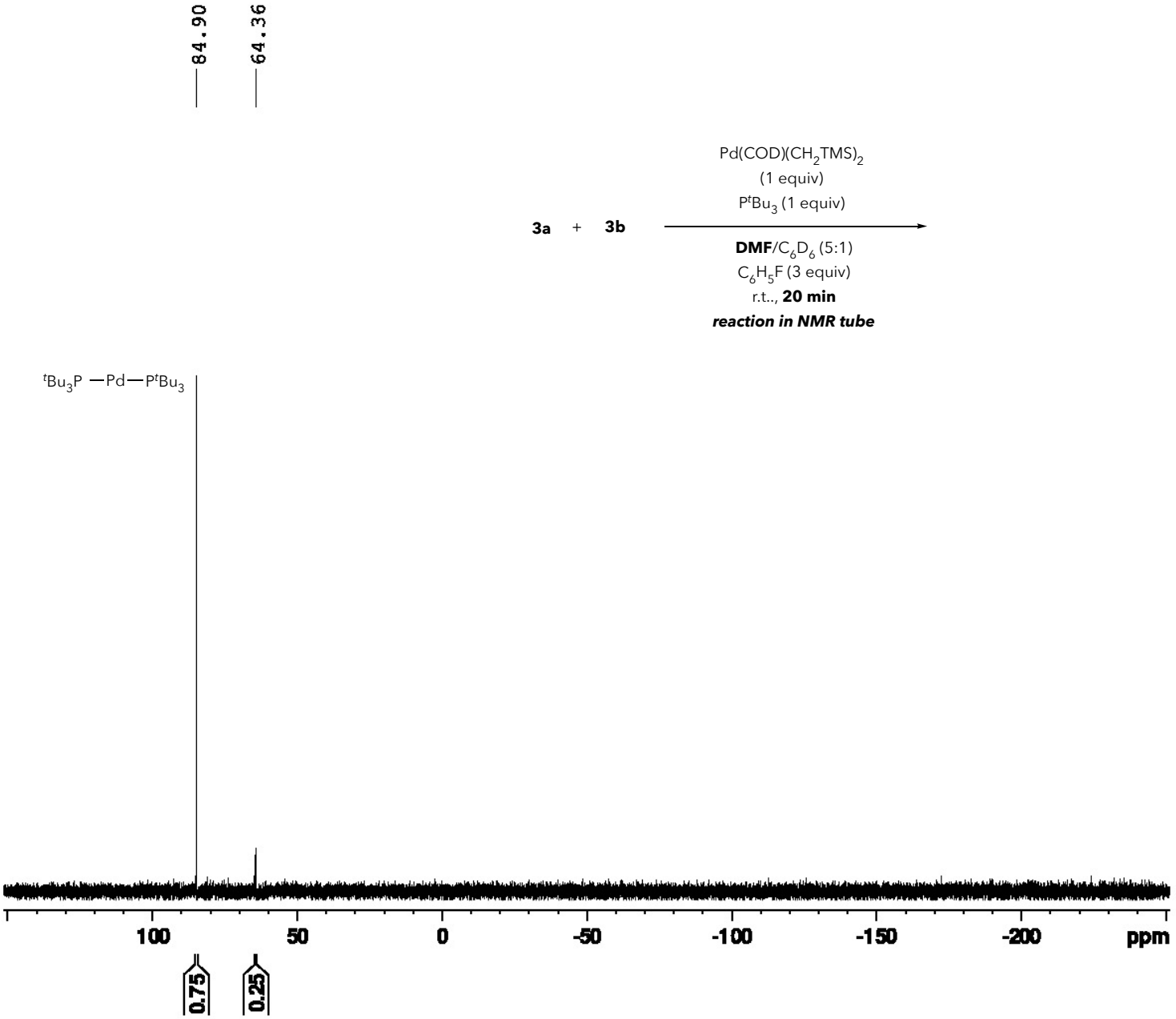
F2 - Processing parameters
SI                32768
SF          202.4968157 MHz
WDW                  EM
SSB       0
LB              1.00 Hz
GB        0
PC              1.40
```




```
Current Data Parameters
NAME      6-SMR-43-10min
EXPNO                 10
PROCNO                 2

F2 - Acquisition Parameter
Date_          20211117
Time               9.12 h
INSTRUM            spect
PROBHD   Z125869_0055 (
PULPROG            zgflqn
TD                131072
SOLVENT             C6D6
NS                    16
DS                     4
SWH           113636.367 Hz
FIDRES          1.733953 Hz
AQ             0.5767168 sec
RG                 15.61
DW                 4.400 usec
DE                18.00 usec
TE                298.0 K
D1            1.00000000 sec
TD0                    1
SFO1          470.6394024 MHz
NUC1                  19F
P1                15.00 usec
PLW1          11.70800018 W

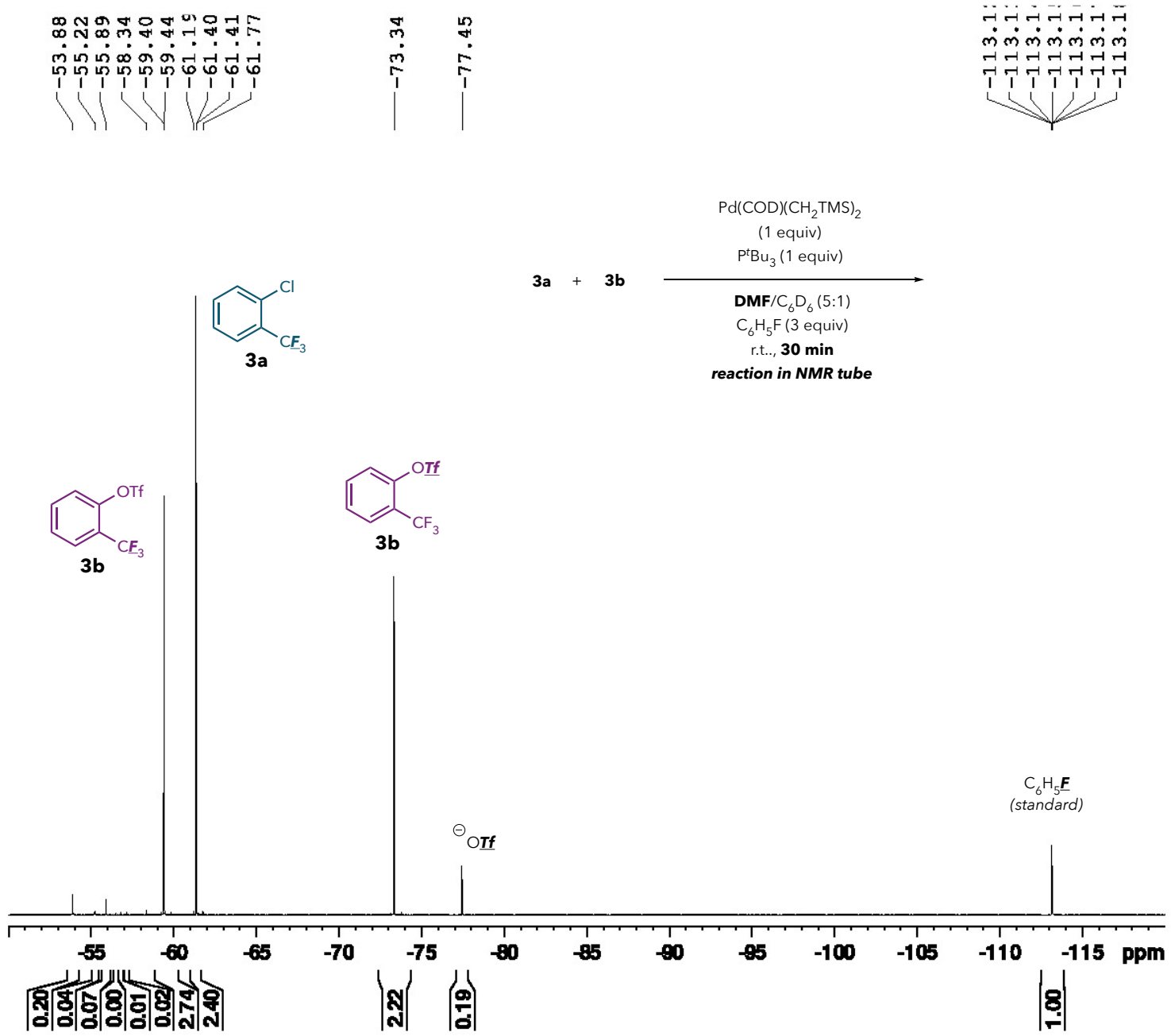
F2 - Processing parameters
SI                 65536
SF          470.6858608 MHz
WDW                   EM
SSB       0
LB                 0.30 Hz
GB        0
PC                 1.00
```




```
Current Data Parameters
NAME      6-SMR-43-10min
EXPNO                 11
PROCNO                 1

F2 - Acquisition Parameter
Date_          20211117
Time               9.17 h
INSTRUM            spect
PROBHD   Z125869_0055 (
PULPROG          zgpg30
TD                65536
SOLVENT            C6D6
NS                   16
DS                    4
SWH           81521.742 Hz
FIDRES         2.487846 Hz
AQ            0.4019541 sec
RG                190.44
DW                6.133 usec
DE                18.00 usec
TE                298.0 K
D1           2.00000000 sec
D11          0.03000000 sec
TD0                   1
SFO1        202.4866909 MHz
NUC1               31P
P0                4.00 usec
P1                12.00 usec
PLW1        40.26200104 W
SFO2        500.2320009 MHz
NUC2               1H
CPDPRG[2        waltz16
PCPD2            80.00 usec
PLW2        11.44699955 W
PLW12        0.25756001 W
PLW13        0.12955000 W

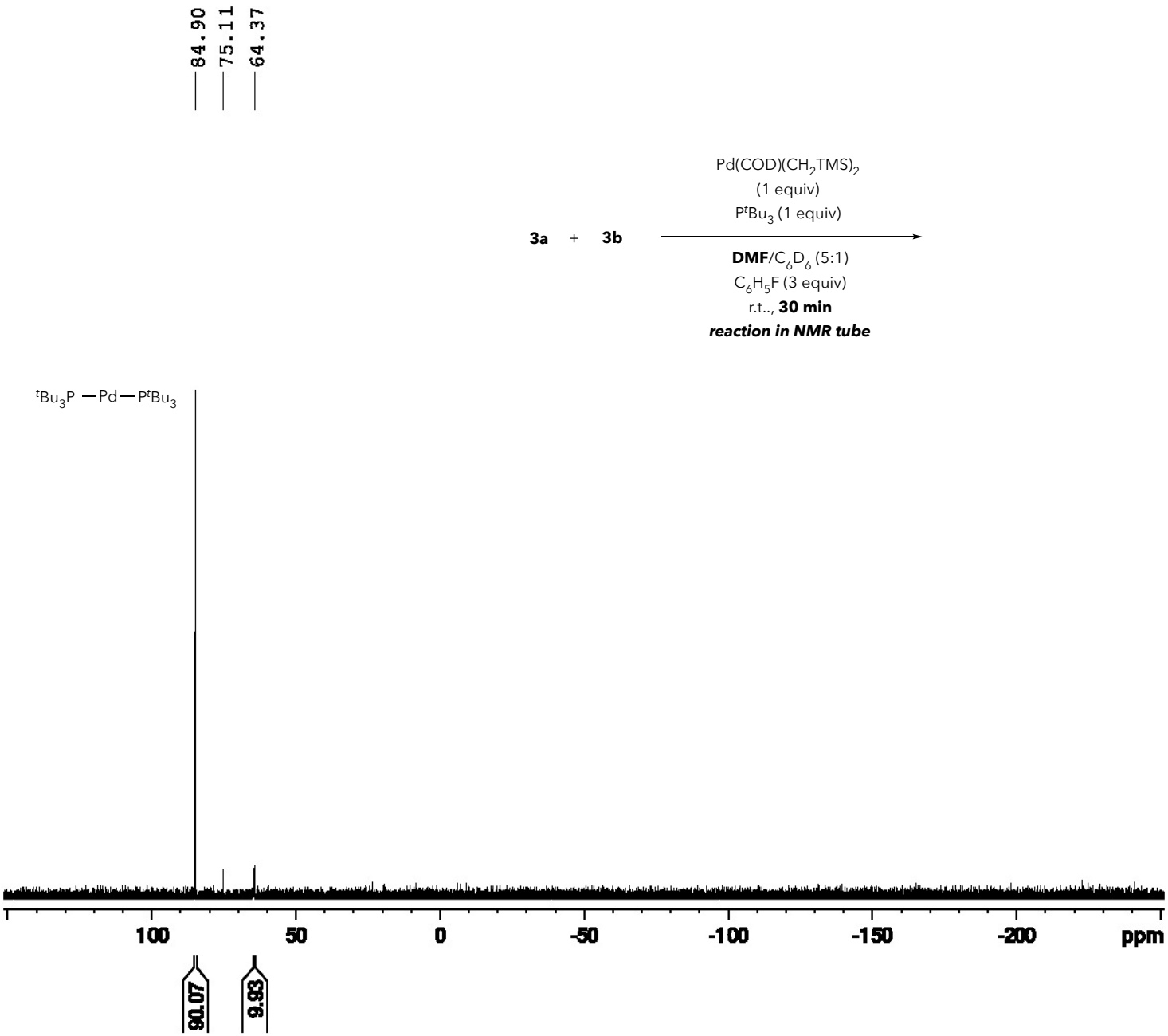
F2 - Processing parameters
SI                32768
SF          202.4968157 MHz
WDW                EM
SSB       0
LB                1.00 Hz
GB        0
PC                1.40
```




```
Current Data Parameters
NAME      6-SMR-43-30min
EXPNO                 10
PROCNO                 2

F2 - Acquisition Parameter
Date_           20211117
Time               9.26 h
INSTRUM            spect
PROBHD   Z125869_0055 (
PULPROG           zgflqn
TD                131072
SOLVENT             C6D6
NS                    16
DS                     4
SWH          113636.367 Hz
FIDRES         1.733953 Hz
AQ            0.5767168 sec
RG                 15.61
DW                4.400 usec
DE                18.00 usec
TE                298.0 K
D1           1.00000000 sec
TD0                    1
SFO1         470.6394024 MHz
NUC1                 19F
P1                15.00 usec
PLW1         11.70800018 W

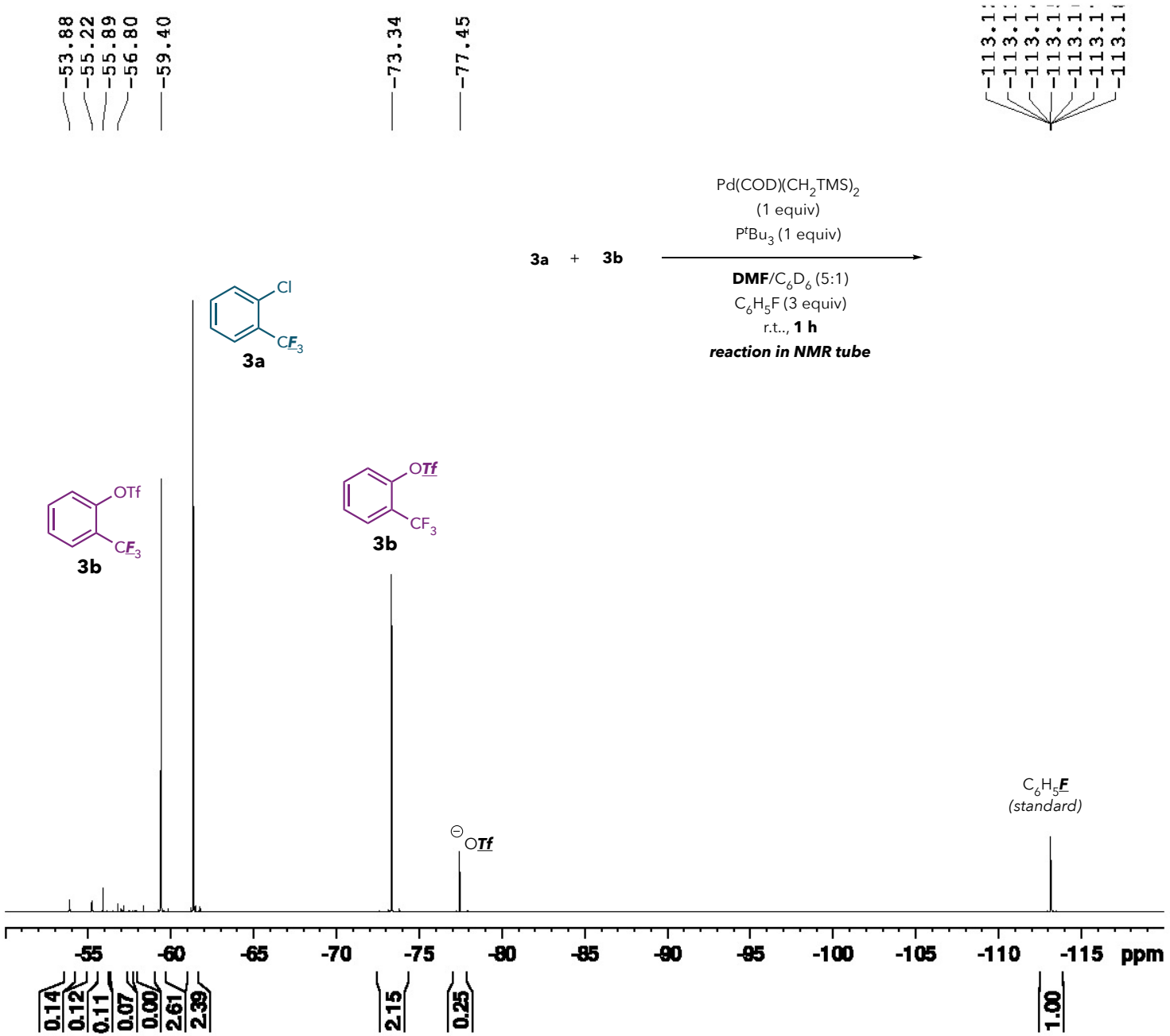
F2 - Processing parameters
SI                 65536
SF           470.6858658 MHz
WDW                  EM
SSB       0
LB                0.30 Hz
GB        0
PC                1.00
```




```
Current Data Parameters
NAME      6-SMR-43-30min
EXPNO                 11
PROCNO                 1

F2 - Acquisition Parameter
Date_          20211117
Time               9.29 h
INSTRUM            spect
PROBHD   Z125869_0055 (
PULPROG           zgpg30
TD                65536
SOLVENT             C6D6
NS                    16
DS                     4
SWH           81521.742 Hz
FIDRES         2.487846 Hz
AQ            0.4019541 sec
RG                190.44
DW                6.133 usec
DE                18.00 usec
TE                298.0 K
D1           2.00000000 sec
D11          0.03000000 sec
TD0                    1
SFO1         202.4866909 MHz
NUC1                 31P
P0                4.00 usec
P1                12.00 usec
PLW1         40.26200104 W
SFO2         500.2320009 MHz
NUC2                 1H
CPDPRG[2         waltz16
PCPD2             80.00 usec
PLW2         11.44699955 W
PLW12         0.25756001 W
PLW13         0.12955000 W

F2 - Processing parameters
SI                 32768
SF           202.4968157 MHz
WDW                   EM
SSB       0
LB                1.00 Hz
GB        0
PC                1.40
```

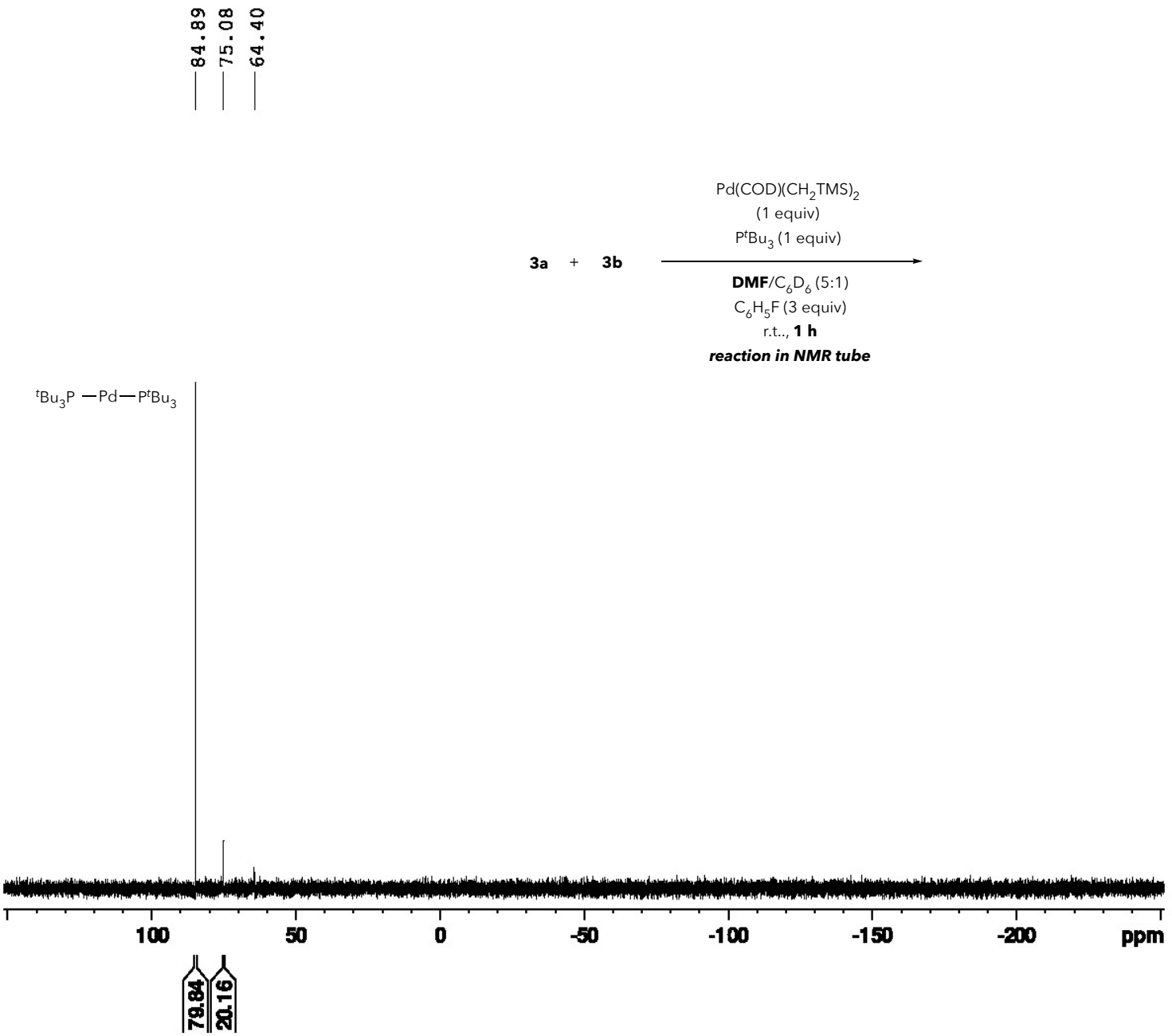


BRUKER

```
Current Data Parameters
NAME          6-SMR-43-1h
EXPNO                  10
PROCNO                  2

F2 - Acquisition Parameter
Date_           20211117
Time               9.56 h
INSTRUM            spect
PROBHD    Z125869_0055 (
PULPROG           zgflqn
TD                131072
SOLVENT             C6D6
NS                    16
DS                     4
SWH           113636.367 Hz
FIDRES          1.733953 Hz
AQ             0.5767168 sec
RG                 15.61
DW                4.400 usec
DE                18.00 usec
TE                298.0 K
D1             1.00000000 sec
TD0                    1
SFO1          470.6394024 MHz
NUC1                  19F
P1                15.00 usec
PLW1          11.70800018 W

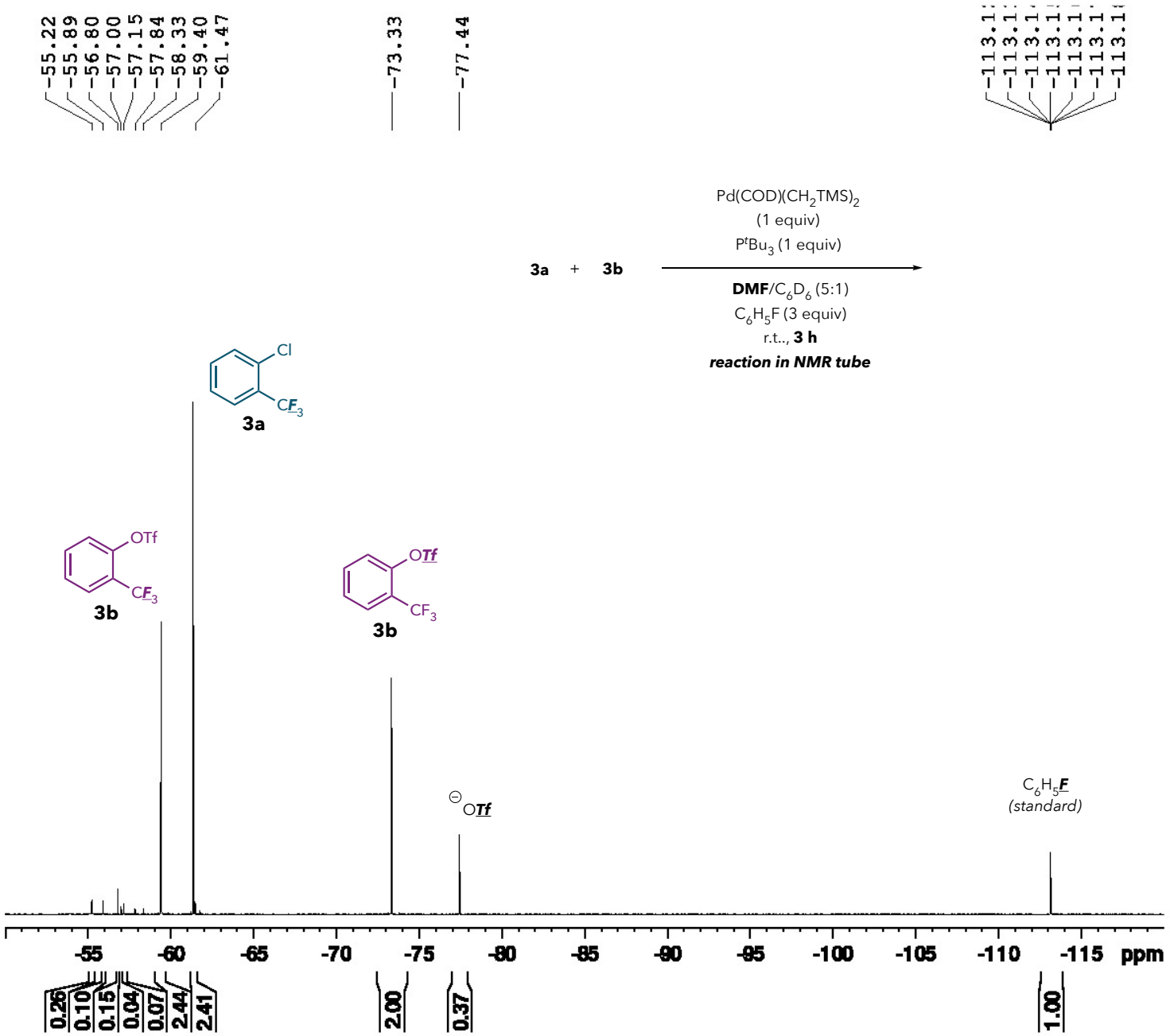
F2 - Processing parameters
SI                 65536
SF            470.6858656 MHz
WDW                   EM
SSB       0
LB                 0.30 Hz
GB        0
PC                 1.00
```




```
Current Data Parameters
NAME         6-SMR-43-1h
EXPNO                 11
PROCNO                 1

F2 - Acquisition Parameter
Date_          20211117
Time               9.59 h
INSTRUM           spect
PROBHD   Z125869_0055 (
PULPROG          zgpg30
TD                65536
SOLVENT            C6D6
NS                   16
DS                    4
SWH           81521.742 Hz
FIDRES          2.487846 Hz
AQ            0.4019541 sec
RG                190.44
DW               6.133 usec
DE               18.00 usec
TE               298.0 K
D1           2.00000000 sec
D11          0.03000000 sec
TD0                   1
SFO1         202.4866909 MHz
NUC1                 31P
P0               4.00 usec
P1               12.00 usec
PLW1         40.26200104 W
SFO2         500.2320009 MHz
NUC2                 1H
CPDPRG[2         waltz16
PCPD2             80.00 usec
PLW2         11.44699955 W
PLW12         0.25756001 W
PLW13         0.12955000 W

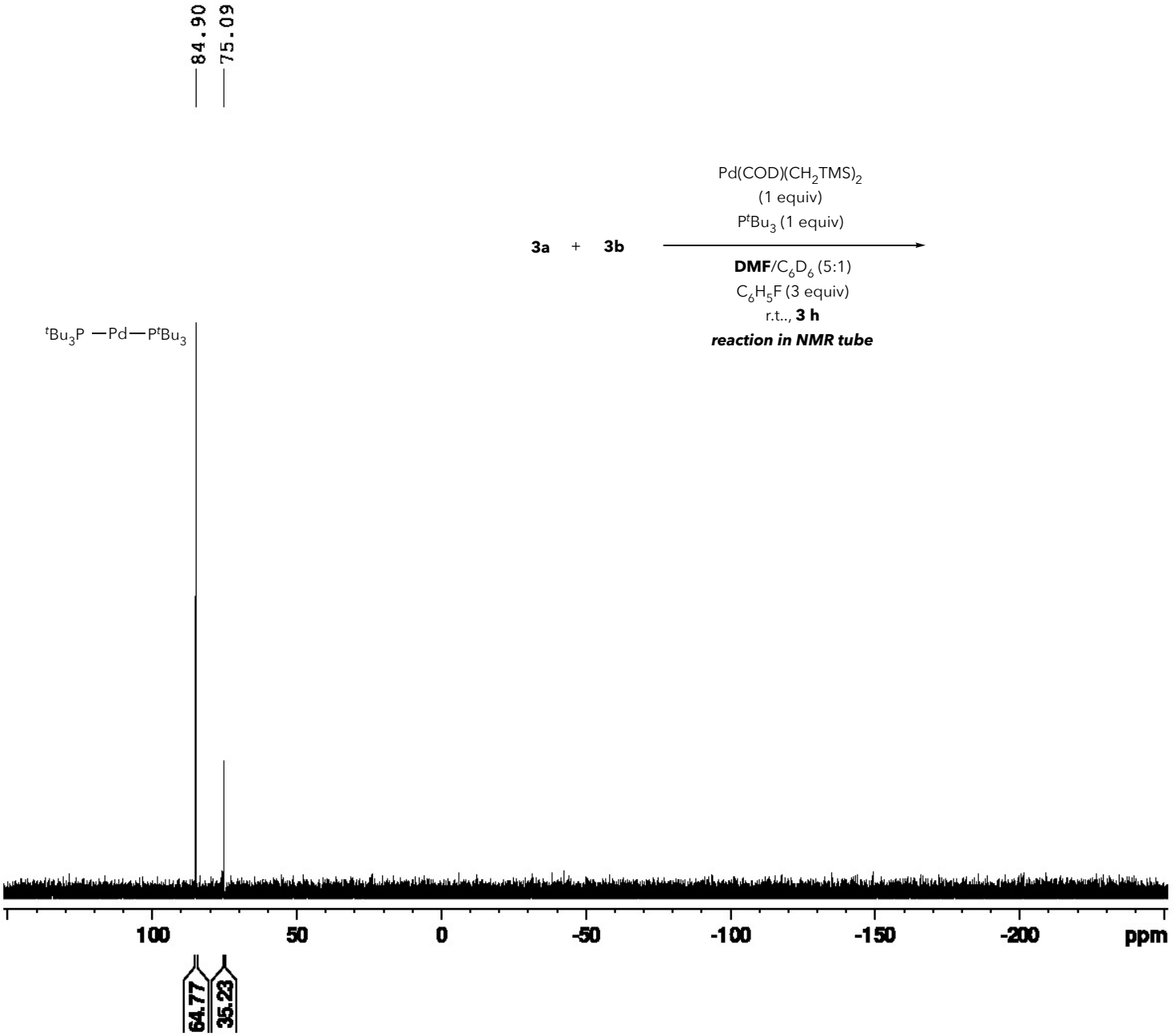
F2 - Processing parameters
SI                32768
SF          202.4968157 MHz
WDW                  EM
SSB       0
LB               1.00 Hz
GB        0
PC               1.40
```




```
Current Data Parameters
NAME          6-SMR-43-3h
EXPNO                  10
PROCNO                  2

F2 - Acquisition Parameter
Date_           20211117
Time              11.59 h
INSTRUM             spect
PROBHD    Z125869_0055 (
PULPROG             zgflqn
TD                131072
SOLVENT             C6D6
NS                    16
DS                     4
SWH           113636.367 Hz
FIDRES          1.733953 Hz
AQ             0.5767168 sec
RG                 15.61
DW                 4.400 usec
DE                18.00 usec
TE                298.0 K
D1             1.00000000 sec
TD0                    1
SFO1          470.6394024 MHz
NUC1                 19F
P1                15.00 usec
PLW1          11.70800018 W

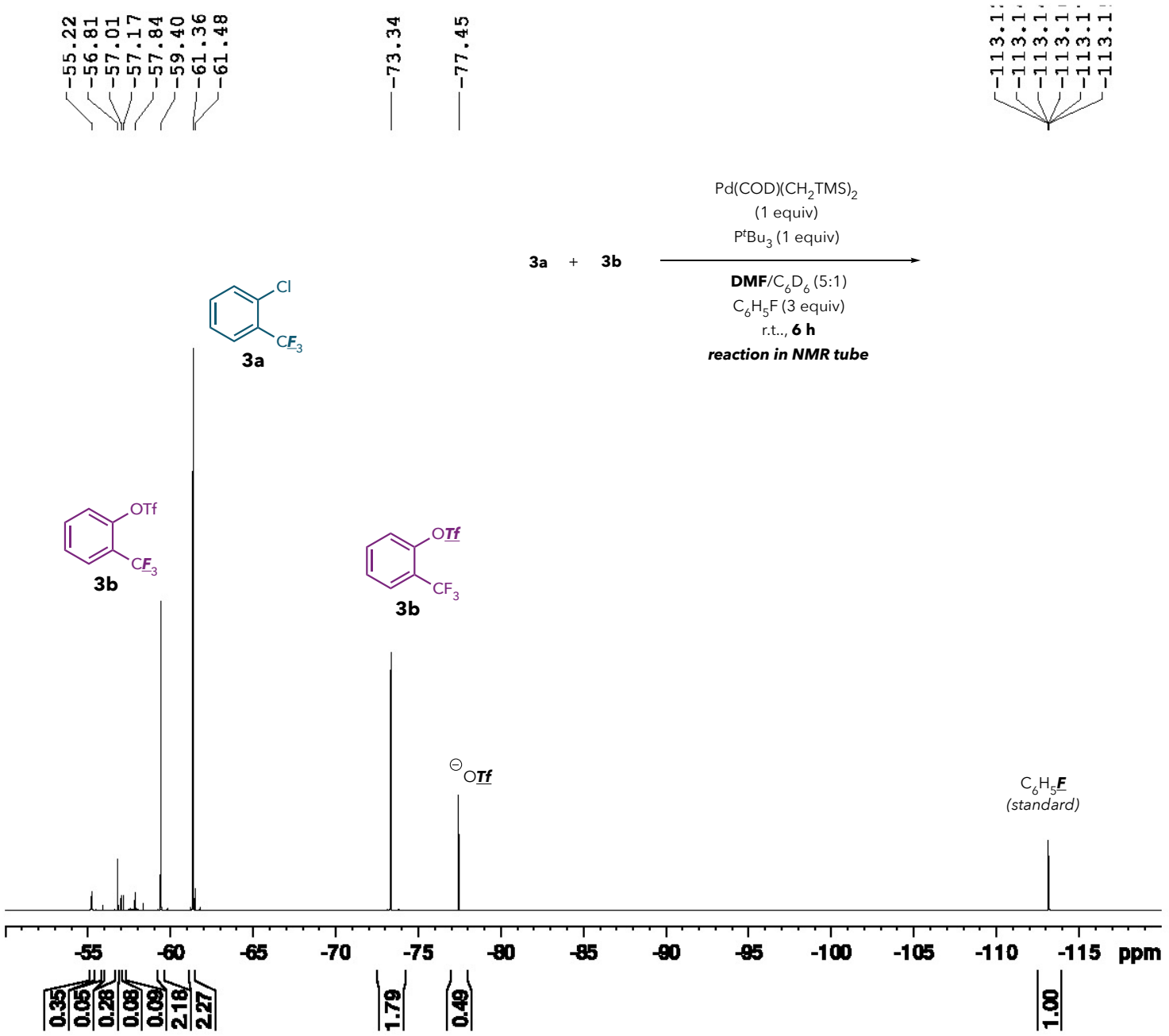
F2 - Processing parameters
SI                 65536
SF            470.6858650 MHz
WDW                  EM
SSB       0
LB                0.30 Hz
GB        0
PC                1.00
```




```
Current Data Parameters
NAME         6-SMR-43-3h
EXPNO                 11
PROCNO                 1

F2 - Acquisition Parameter
Date_          20211117
Time             12.03 h
INSTRUM            spect
PROBHD   Z125869_0055 (
PULPROG           zgpg30
TD                65536
SOLVENT             C6D6
NS                    16
DS                     4
SWH           81521.742 Hz
FIDRES          2.487846 Hz
AQ            0.4019541 sec
RG                190.44
DW                6.133 usec
DE                18.00 usec
TE                298.0 K
D1           2.00000000 sec
D11          0.03000000 sec
TD0                    1
SFO1         202.4866909 MHz
NUC1                 31P
P0                4.00 usec
P1               12.00 usec
PLW1         40.26200104 W
SFO2         500.2320009 MHz
NUC2                 1H
CPDPRG[2         waltz16
PCPD2             80.00 usec
PLW2         11.44699955 W
PLW12         0.25756001 W
PLW13         0.12955000 W

F2 - Processing parameters
SI                 32768
SF           202.4968157 MHz
WDW                   EM
SSB       0
LB                1.00 Hz
GB        0
PC                1.40
```

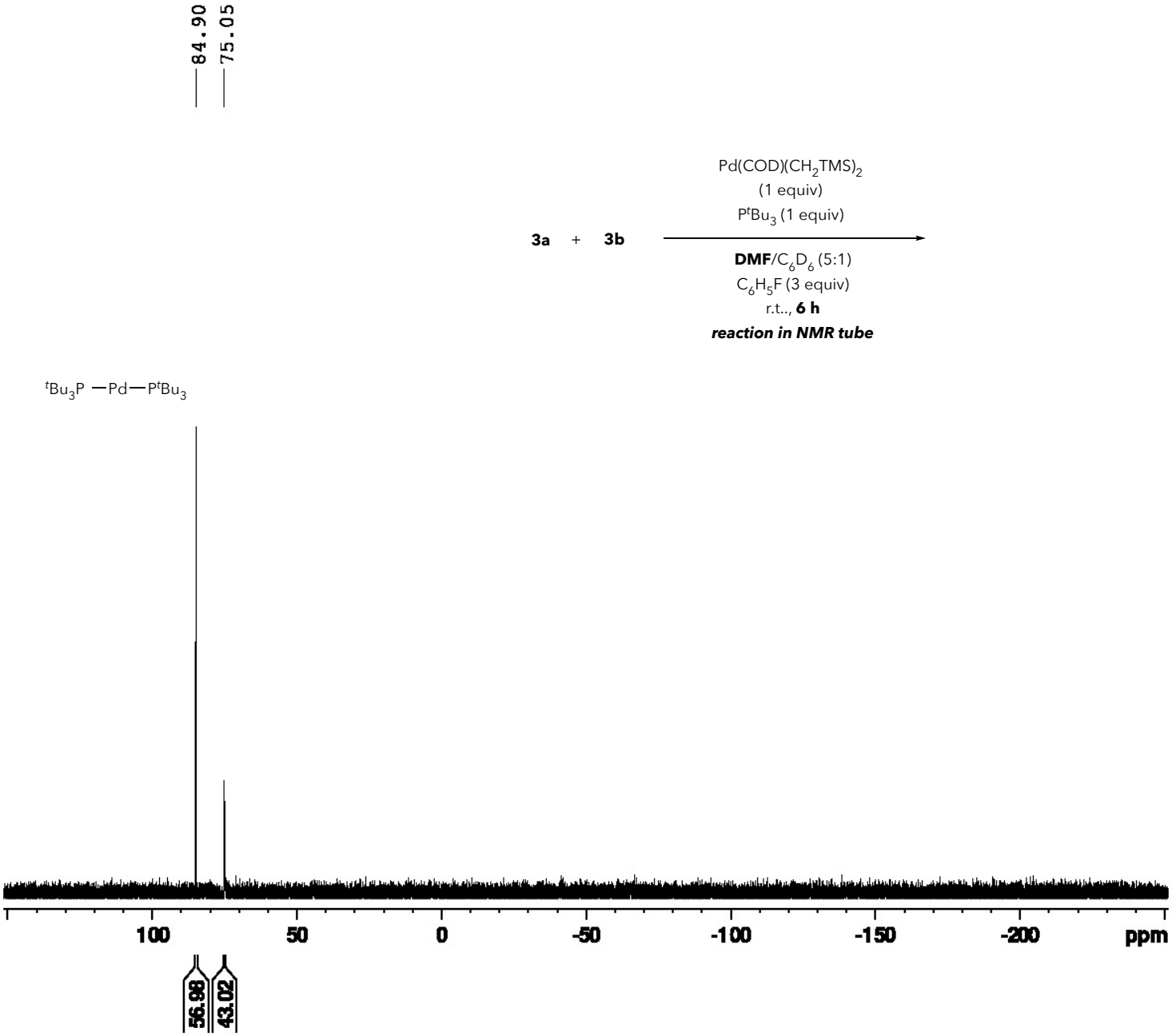


BRUKER

```
Current Data Parameters
NAME          6-SMR-43-65
EXPNO                  10
PROCNO                  2

F2 - Acquisition Parameter
Date_           20211117
Time              15.03 h
INSTRUM             spect
PROBHD   Z125869_0055 (
PULPROG             zgflqn
TD                131072
SOLVENT             C6D6
NS                    16
DS                     4
SWH           113636.367 Hz
FIDRES          1.733953 Hz
AQ             0.5767168 sec
RG                 15.61
DW                4.400 usec
DE                18.00 usec
TE                298.0 K
D1             1.00000000 sec
TD0                    1
SFO1          470.6394024 MHz
NUC1                  19F
P1                15.00 usec
PLW1          11.70800018 W

F2 - Processing parameters
SI                 65536
SF            470.6858683 MHz
WDW                   EM
SSB       0
LB                0.30 Hz
GB        0
PC                1.00
```

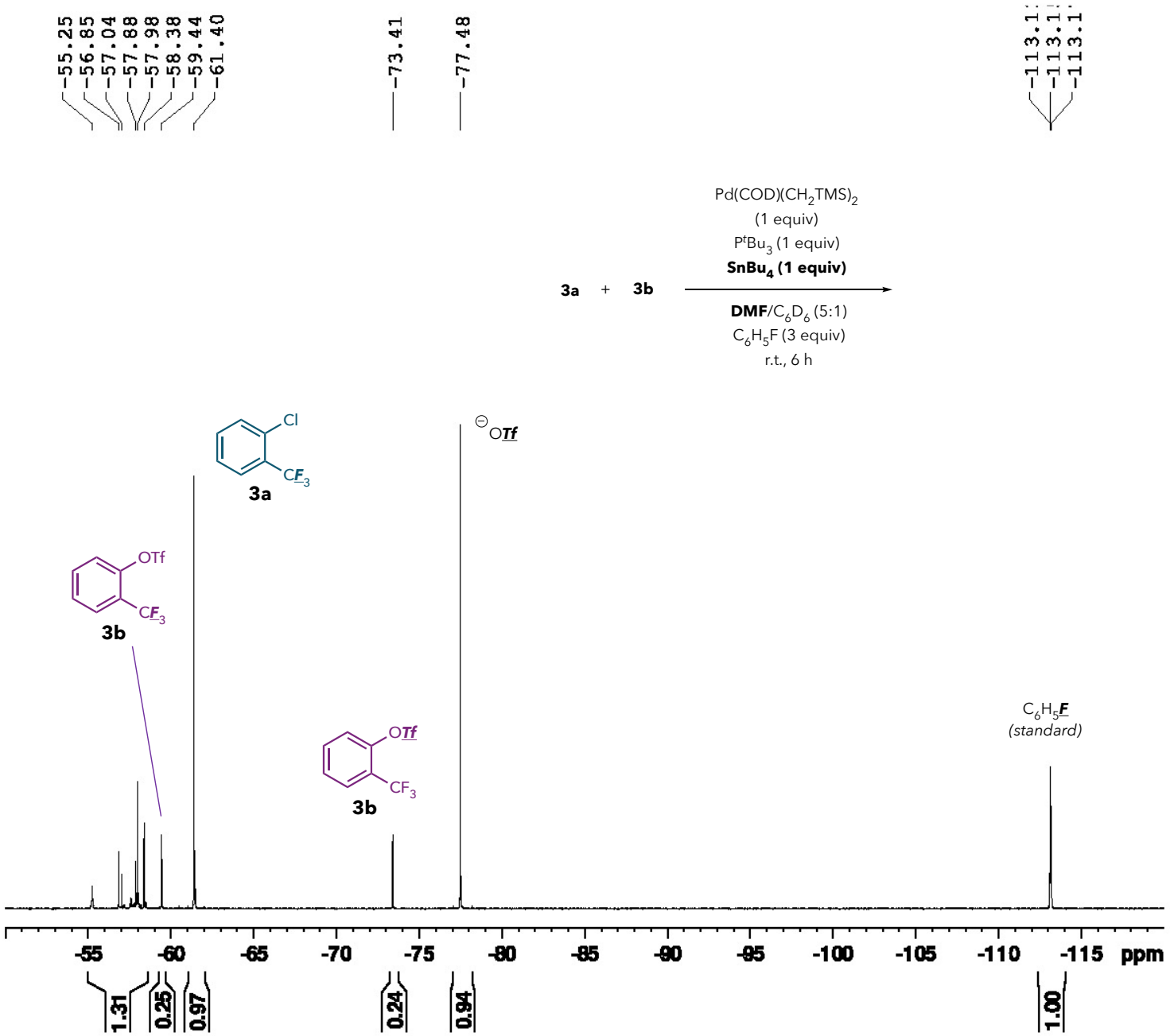


BRUKER

```
Current Data Parameters
NAME          6-SMR-43-65
EXPNO                  11
PROCNO                  1

F2 - Acquisition Parameter
Date_           20211117
Time              15.06 h
INSTRUM             spect
PROBHD    Z125869_0055 (
PULPROG           zgpg30
TD                65536
SOLVENT             C6D6
NS                    16
DS                     4
SWH           81521.742 Hz
FIDRES          2.487846 Hz
AQ             0.4019541 sec
RG                190.44
DW                 6.133 usec
DE                18.00 usec
TE                298.0 K
D1             2.00000000 sec
D11            0.03000000 sec
TD0                    1
SFO1          202.4866909 MHz
NUC1                 31P
P0                 4.00 usec
P1                12.00 usec
PLW1          40.26200104 W
SFO2          500.2320009 MHz
NUC2                 1H
CPDPRG[2          waltz16
PCPD2              80.00 usec
PLW2          11.44699955 W
PLW12          0.25756001 W
PLW13          0.12955000 W

F2 - Processing parameters
SI                 32768
SF            202.4968157 MHz
WDW                   EM
SSB       0
LB                 1.00 Hz
GB        0
PC                 1.40
```

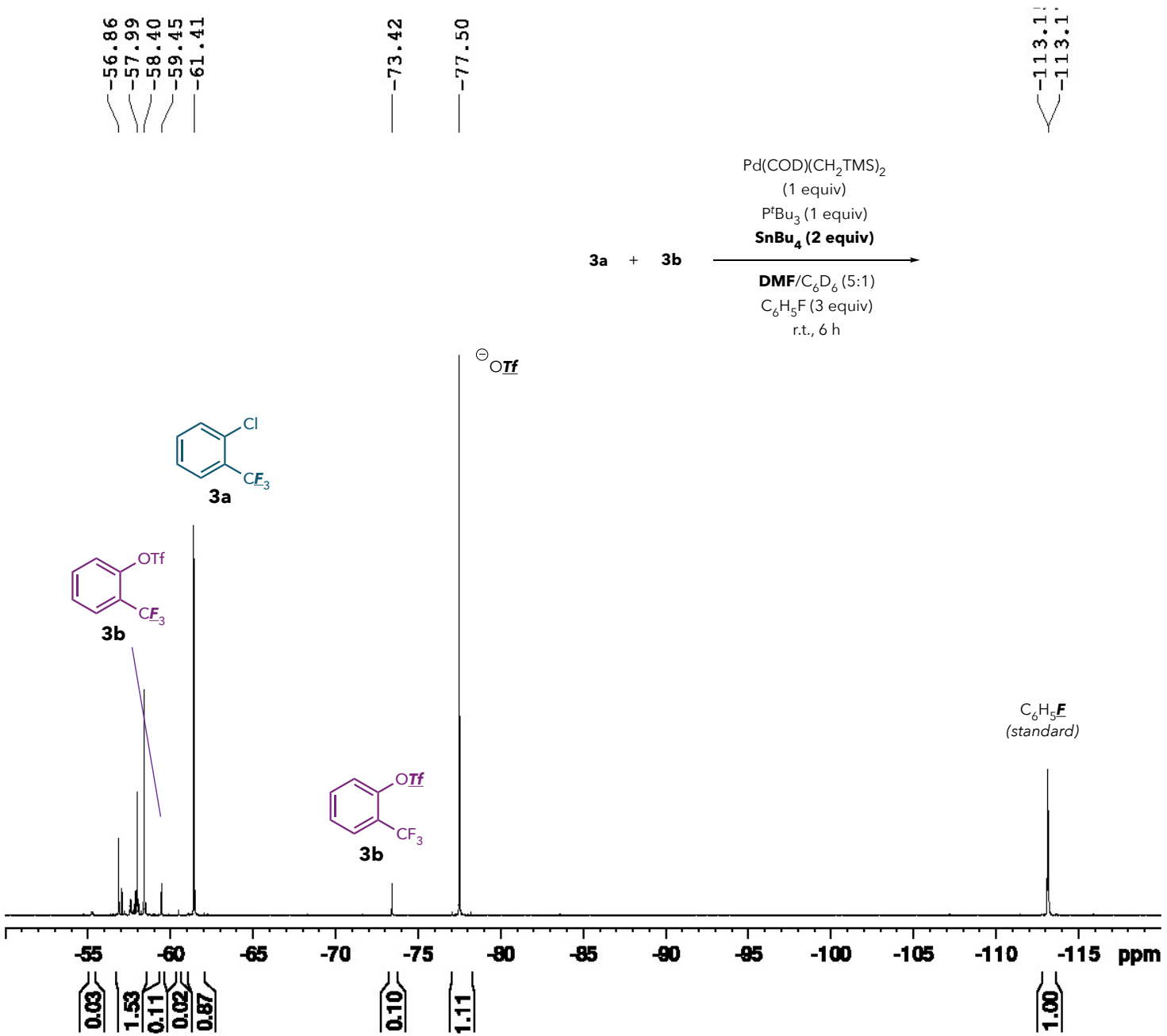



```
Current Data Parameters
NAME      ER-6-70-1_1SnBu4
EXPNO                    1
PROCNO                   1

F2 - Acquisition Parameter
Date_             20200831
Time                  7.31
INSTRUM              spect
PROBHD    5 mm QNP 1H/13
PULPROG             zgflqn
TD                   32768
SOLVENT               C6D6
NS                      64
DS                       0
SWH              50125.312 Hz
FIDRES             1.529703 Hz
AQ               0.3268608 sec
RG                  3649.1
DW                   9.975 usec
DE                   6.00 usec
TE                   683.2 K
D1              1.50000000 sec
TD0                      1

====== CHANNEL f1 ======
NUC1                   19F
P1                   9.00 usec
PL1        0 dB
SFO1          282.4250465 MHz

F2 - Processing parameters
SI                   65536
SF              282.4416810 MHz
WDW                    EM
SSB        0
LB                   0.30 Hz
GB         0
PC                   1.00
```

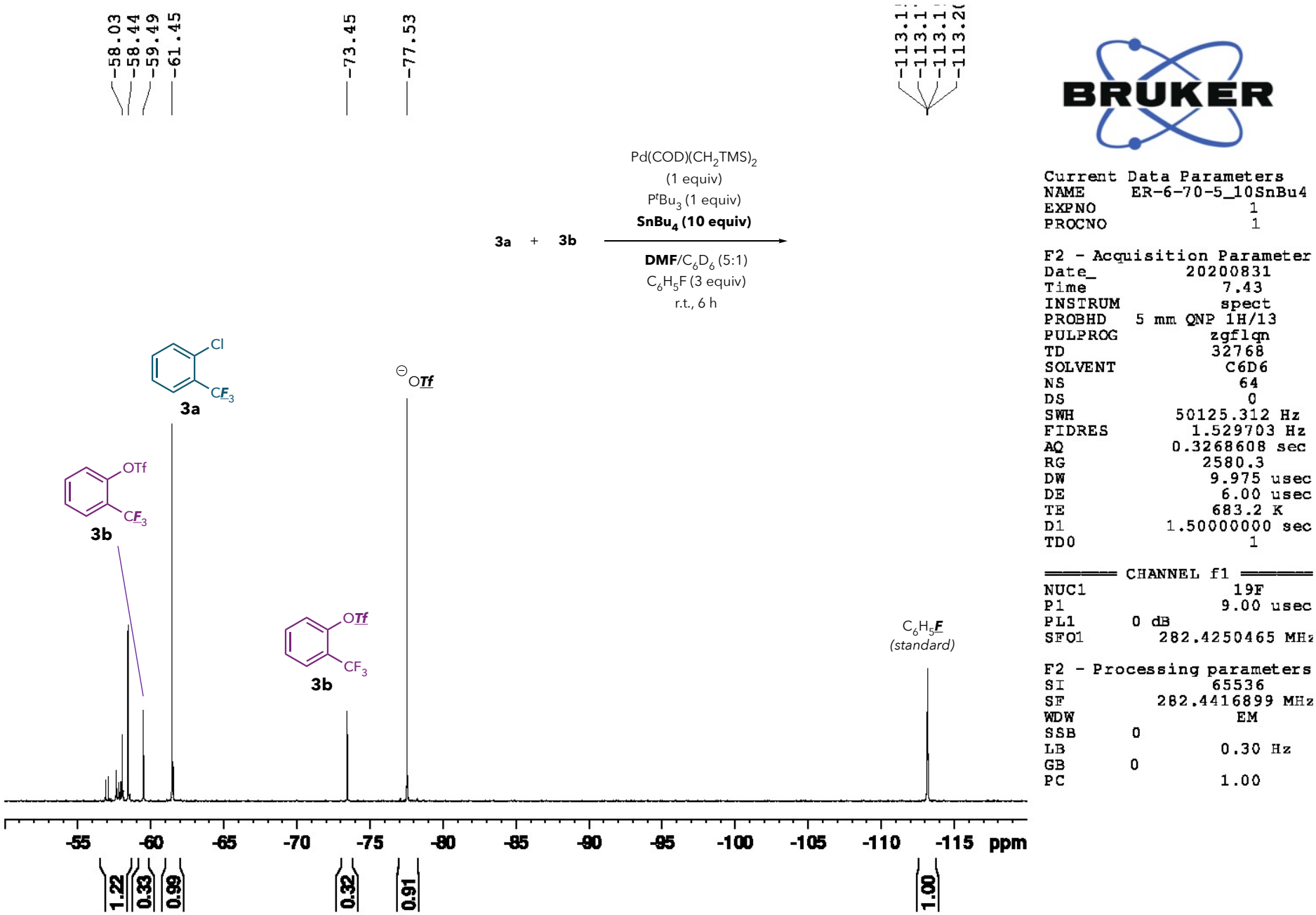



```
Current Data Parameters
NAME      ER-6-70-3_2SnBu4
EXPNO                    1
PROCNO                   1

F2 - Acquisition Parameter
Date_             20200831
Time                  7.37
INSTRUM              spect
PROBHD   5 mm QNP 1H/13
PULPROG              zgflqn
TD                    32768
SOLVENT                C6D6
NS                       64
DS                        0
SWH               50125.312 Hz
FIDRES             1.529703 Hz
AQ                0.3268608 sec
RG                   3649.1
DW                  9.975 usec
DE                  6.00 usec
TE                  683.2 K
D1               1.50000000 sec
TD0                      1

====== CHANNEL f1 ======
NUC1                   19F
P1                  9.00 usec
PL1        0 dB
SFO1          282.4250465 MHz

F2 - Processing parameters
SI                    65536
SF               282.4416834 MHz
WDW                      EM
SSB        0
LB                  0.30 Hz
GB         0
PC                    1.00
```

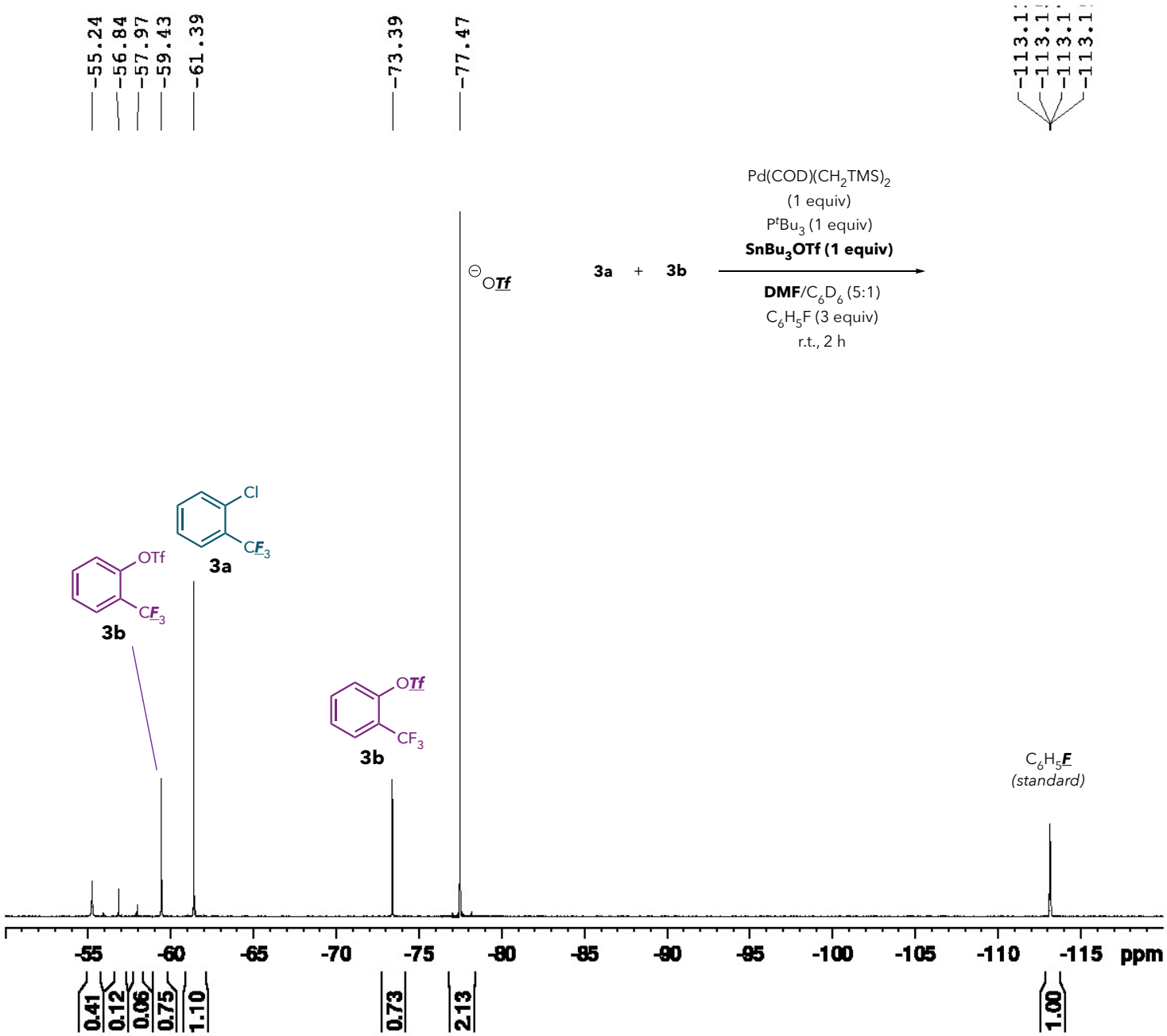



```
Current Data Parameters
NAME      ER-6-70-5_10SnBu4
EXPNO                    1
PROCNO                   1

F2 - Acquisition Parameter
Date_             20200831
Time                  7.43
INSTRUM              spect
PROBHD    5 mm QNP 1H/13
PULPROG              zgflqn
TD                    32768
SOLVENT                C6D6
NS                       64
DS                        0
SWH               50125.312 Hz
FIDRES             1.529703 Hz
AQ                0.3268608 sec
RG                   2580.3
DW                    9.975 usec
DE                    6.00 usec
TE                    683.2 K
D1               1.50000000 sec
TD0                      1

====== CHANNEL f1 ======
NUC1                   19F
P1                    9.00 usec
PL1          0 dB
SFO1           282.4250465 MHz

F2 - Processing parameters
SI                    65536
SF               282.4416899 MHz
WDW                      EM
SSB          0
LB                    0.30 Hz
GB           0
PC                    1.00
```

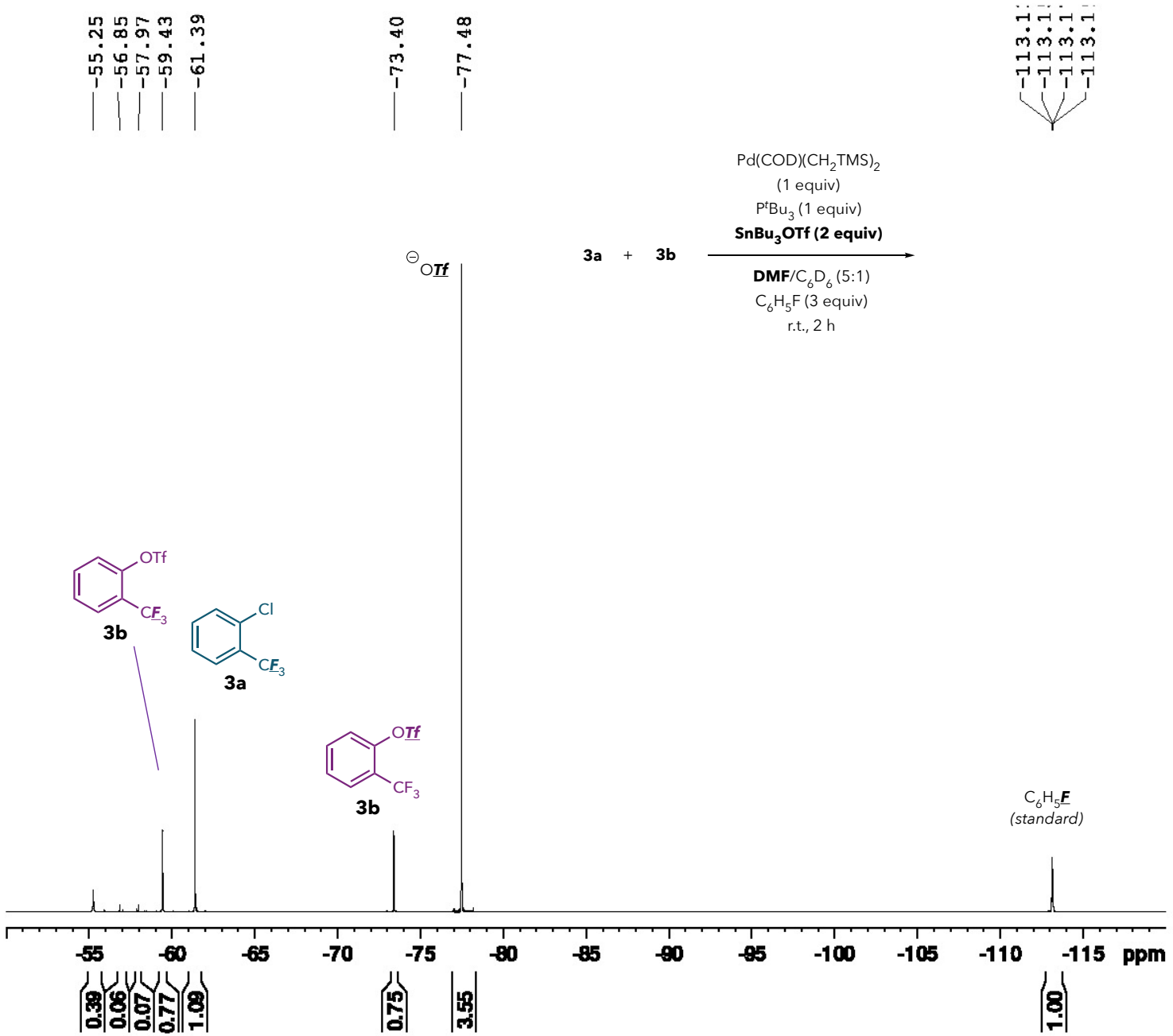



```
Current Data Parameters
NAME      ER-6-81_CA_1SnBu3OTf
EXPNO                        1
PROCNO                       1

F2 - Acquisition Parameters
Date_              20201026
Time                   7.51
INSTRUM               spect
PROBHD    5 mm QNP 1H/13
PULPROG             zgflqn
TD                    32768
SOLVENT                C6D6
NS                       64
DS                        0
SWH               50125.312 Hz
FIDRES             1.529703 Hz
AQ                0.3268608 sec
RG                   2580.3
DW                    9.975 usec
DE                     6.00 usec
TE                    683.2 K
D1              1.50000000 sec
TD0                          1

======== CHANNEL f1 ========
NUC1                       19F
P1                        9.00 usec
PL1         0 dB
SFO1           282.4250465 MHz

F2 - Processing parameters
SI                       65536
SF              282.4416787 MHz
WDW                         EM
SSB         0
LB                        0.30 Hz
GB          0
PC                        1.00
```

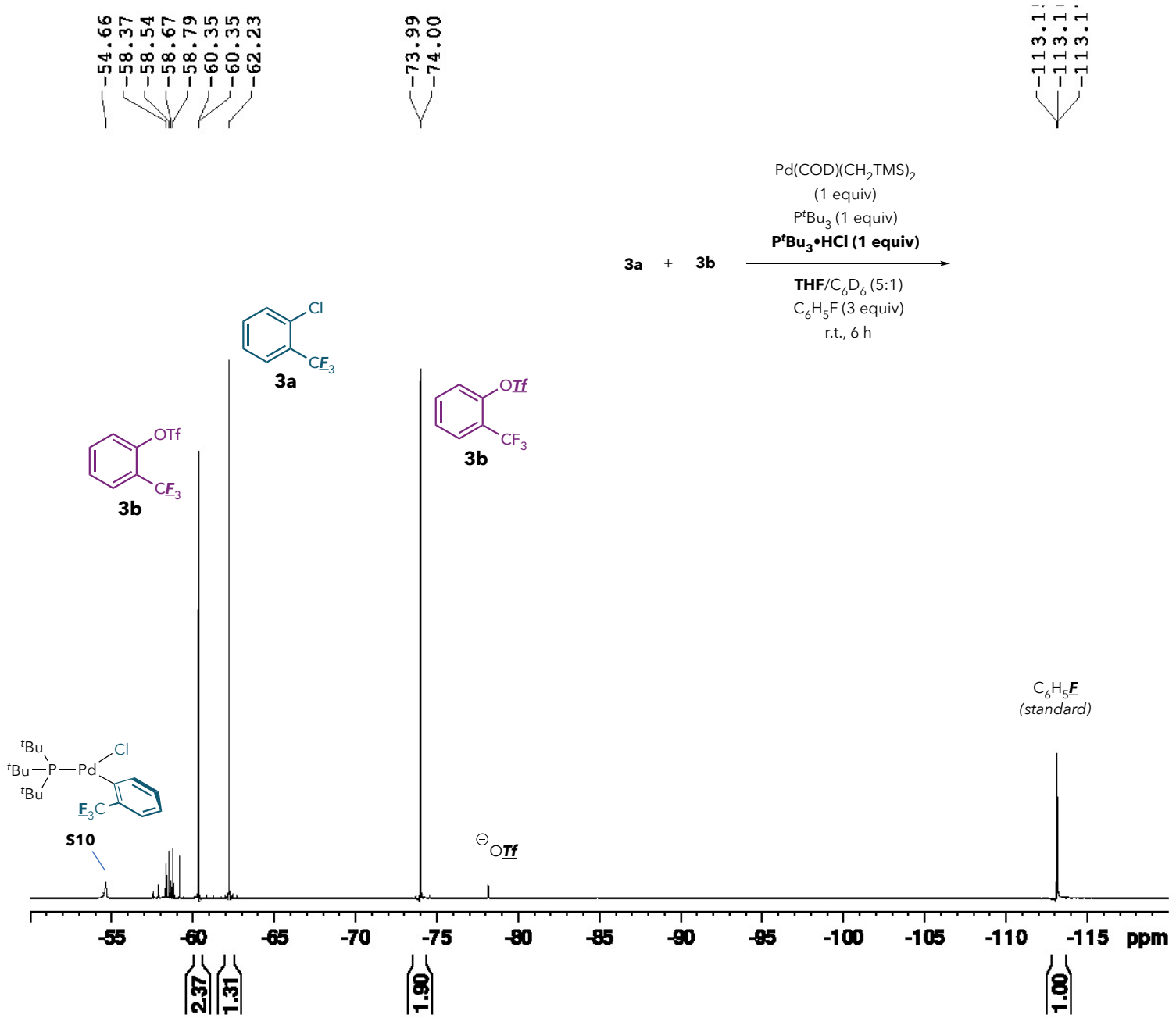



```
Current Data Parameters
NAME      ER-6-81_CA_2SnBu3OTf
EXPNO                        3
PROCNO                       1

F2 - Acquisition Parameters
Date_              20201026
Time                   7.55
INSTRUM               spect
PROBHD    5 mm QNP 1H/13
PULPROG             zgflqn
TD                   32768
SOLVENT               C6D6
NS                      64
DS                       0
SWH              50125.312 Hz
FIDRES            1.529703 Hz
AQ               0.3268608 sec
RG                  2580.3
DW                   9.975 usec
DE                    6.00 usec
TE                   683.2 K
D1              1.50000000 sec
TD0                      1

======== CHANNEL f1 ========
NUC1                   19F
P1                    9.00 usec
PL1        0 dB
SFO1          282.4250465 MHz

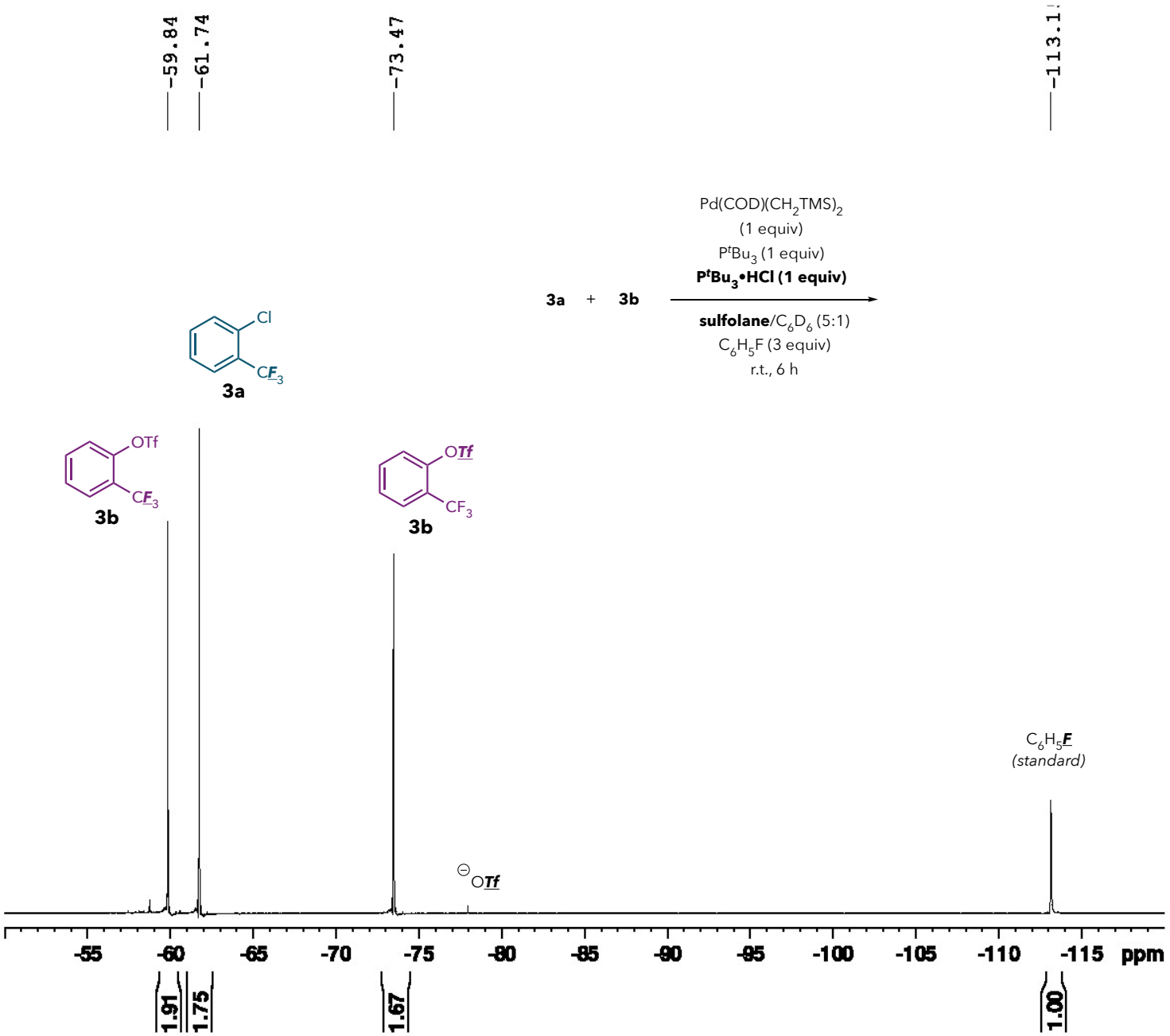
F2 - Processing parameters
SI                    65536
SF             282.4416809 MHz
WDW                     EM
SSB        0
LB                    0.30 Hz
GB         0
PC                    1.00
```




```
Current Data Parameters
NAME          6-SMR-6-3
EXPNO                10
PROCNO                2

F2 - Acquisition Parameter
Date_          20210912
Time             17.49 h
INSTRUM       Avance Neo
PROBHD   Z152088_0031 (
PULPROG              zg
TD               130892
SOLVENT            C6D6
NS                   16
DS                    4
SWH           90909.094 Hz
FIDRES         1.389070 Hz
AQ            0.7199060 sec
RG                  101
DW                5.500 usec
DE                6.50 usec
TE                298.0 K
D1           1.00000000 sec
TD0                   1
SFO1         376.4607164 MHz
NUC1                 19F
P1                12.00 usec
PLW1         31.08900070 W

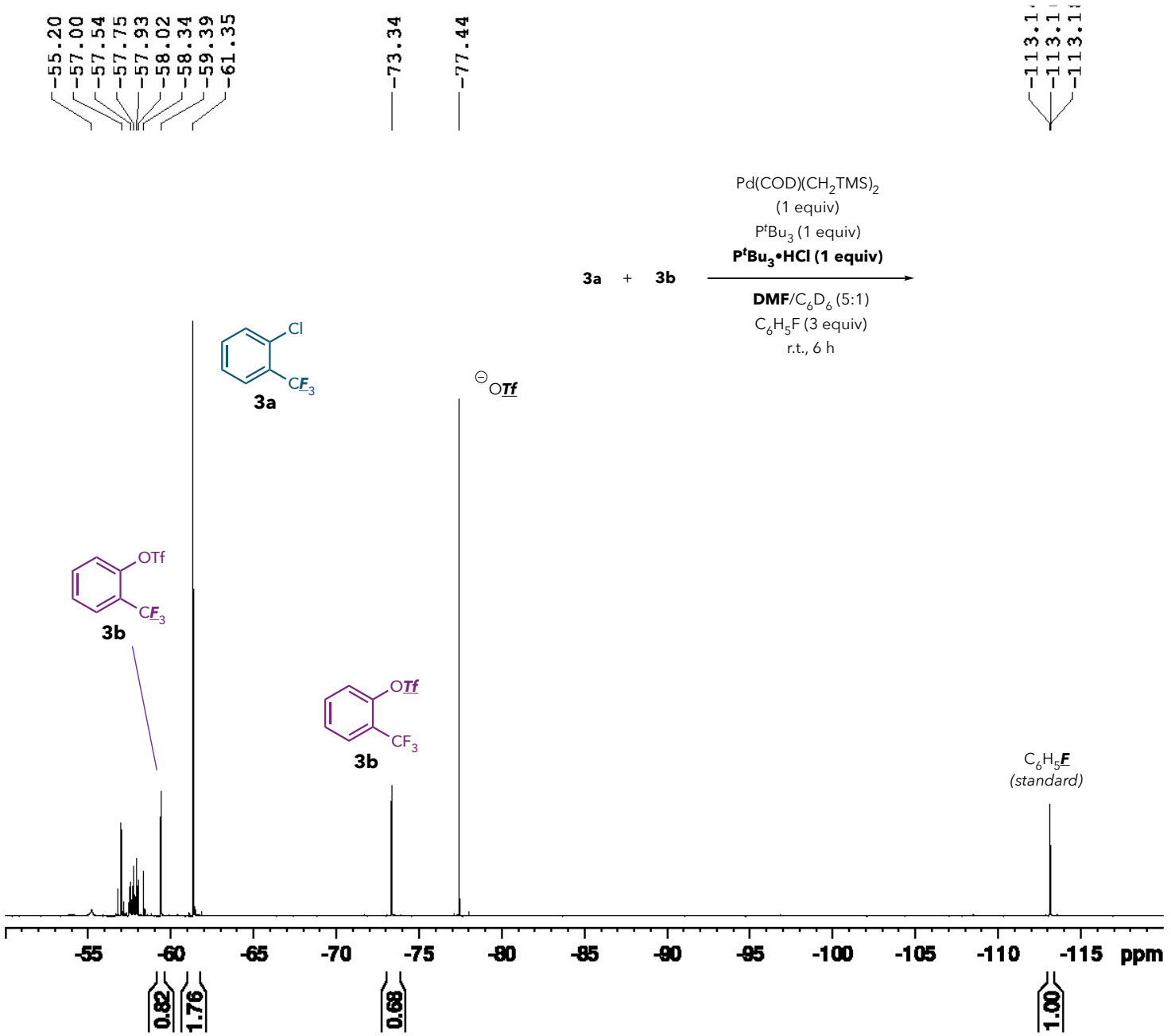
F2 - Processing parameters
SI                65536
SF           376.4979689 MHz
WDW                  EM
SSB       0
LB                0.30 Hz
GB        0
PC                1.00
```




```
Current Data Parameters
NAME          6-SMR-6-7
EXPNO                10
PROCNO                2

F2 - Acquisition Parameter
Date_          20210912
Time             18.08 h
INSTRUM       Avance Neo
PROBHD   Z152088_0031 (
PULPROG              zg
TD               130892
SOLVENT            C6D6
NS                   16
DS                    4
SWH           90909.094 Hz
FIDRES         1.389070 Hz
AQ            0.7199060 sec
RG                  101
DW                5.500 usec
DE                6.50 usec
TE                298.0 K
D1           1.00000000 sec
TD0                   1
SFO1         376.4607164 MHz
NUC1                 19F
P1                12.00 usec
PLW1         31.08900070 W

F2 - Processing parameters
SI                65536
SF           376.4982233 MHz
WDW                  EM
SSB       0
LB                0.30 Hz
GB        0
PC                1.00
```

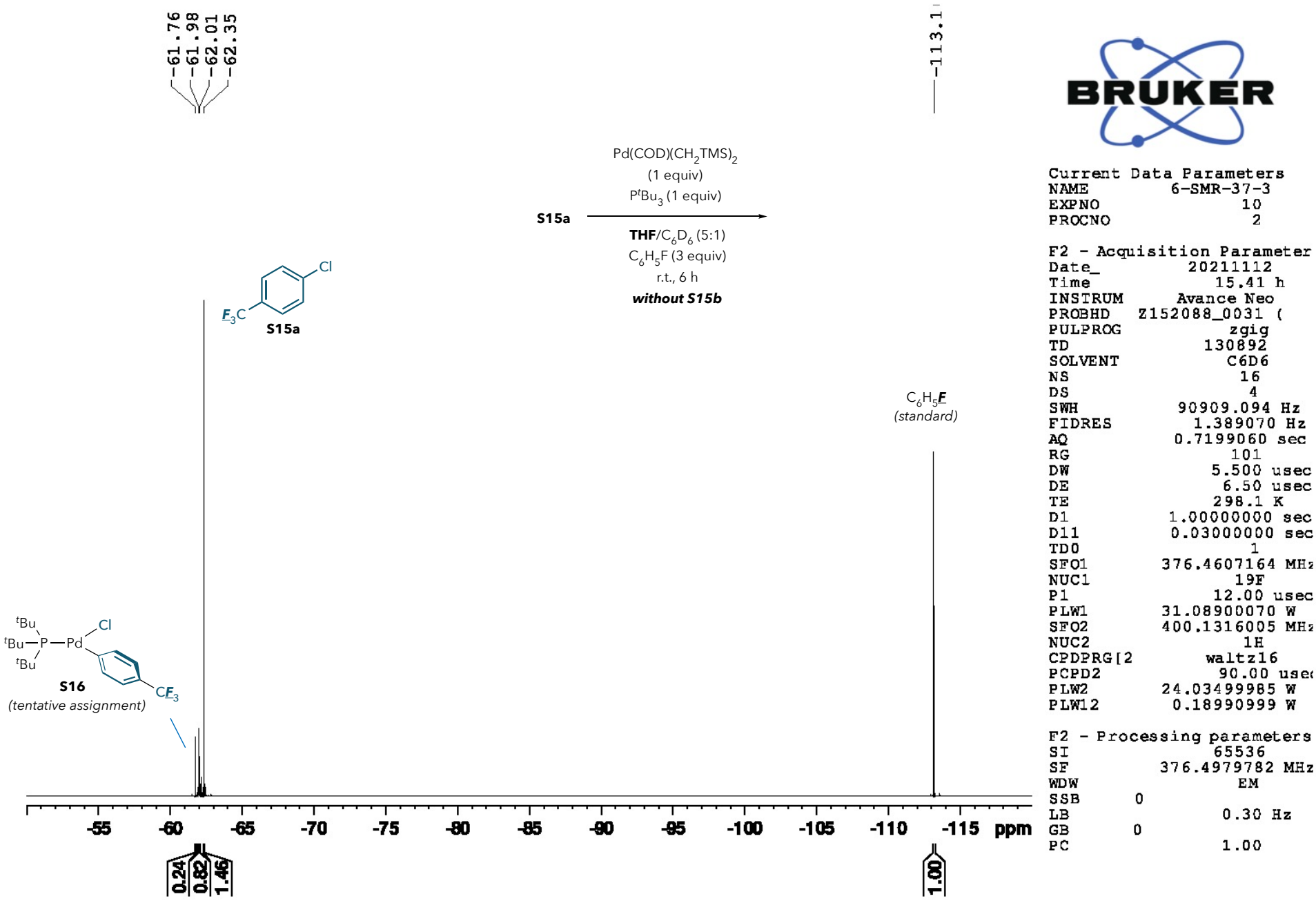



```
Current Data Parameters
NAME          6-SMR-6-11
EXPNO                 10
PROCNO                 2

F2 - Acquisition Parameter
Date_          20210912
Time             18.27 h
INSTRUM       Avance Neo
PROBHD   Z152088_0031 (
PULPROG               zg
TD                130892
SOLVENT             C6D6
NS                    16
DS                     4
SWH           90909.094 Hz
FIDRES          1.389070 Hz
AQ            0.7199060 sec
RG                   101
DW               5.500 usec
DE                6.50 usec
TE                298.0 K
D1           1.00000000 sec
TD0                    1
SFO1         376.4607164 MHz
NUC1                 19F
P1               12.00 usec
PLW1         31.08900070 W

F2 - Processing parameters
SI                 65536
SF           376.4978866 MHz
WDW                  EM
SSB       0
LB               0.30 Hz
GB        0
PC               1.00
```

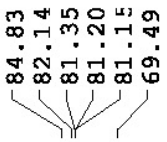
C. Stoichiometric Oxidative Addition Studies with S15a and S15b

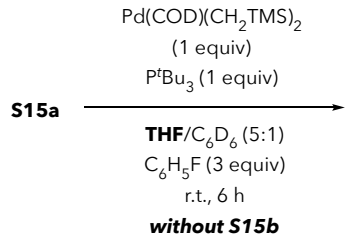


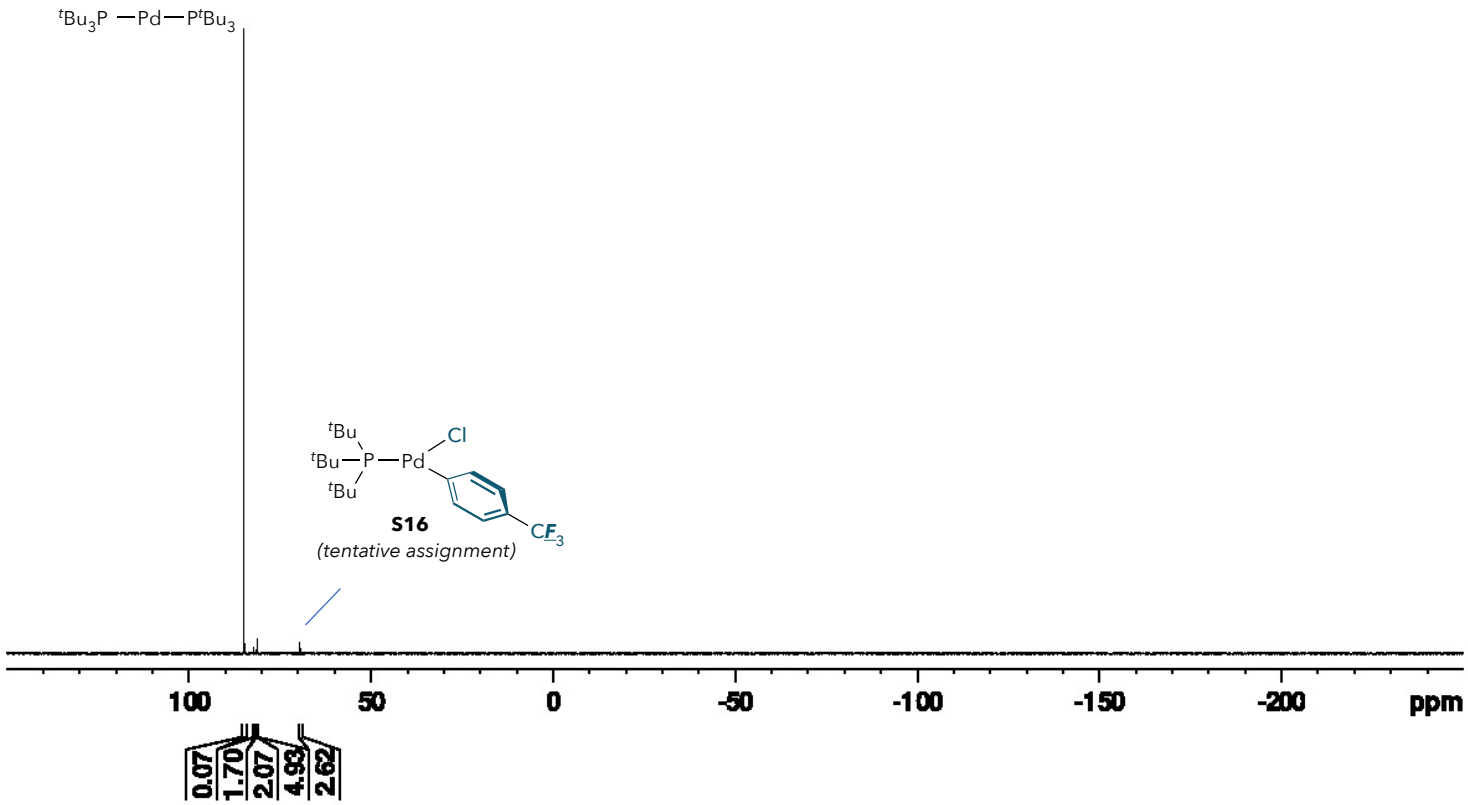

```
Current Data Parameters
NAME          6-SMR-37-3
EXPNO                 10
PROCNO                 2

F2 - Acquisition Parameter
Date_          20211112
Time             15.41 h
INSTRUM       Avance Neo
PROBHD    Z152088_0031 (
PULPROG            zgig
TD               130892
SOLVENT            C6D6
NS                   16
DS                    4
SWH           90909.094 Hz
FIDRES         1.389070 Hz
AQ            0.7199060 sec
RG                  101
DW              5.500 usec
DE              6.50 usec
TE              298.1 K
D1           1.00000000 sec
D11          0.03000000 sec
TD0                   1
SFO1         376.4607164 MHz
NUC1                19F
P1               12.00 usec
PLW1         31.08900070 W
SFO2         400.1316005 MHz
NUC2                1H
CPDPRG[2         waltz16
PCPD2             90.00 usec
PLW2         24.03499985 W
PLW12         0.18990999 W

F2 - Processing parameters
SI                 65536
SF           376.4979782 MHz
WDW                  EM
SSB       0
LB               0.30 Hz
GB        0
PC                 1.00
```



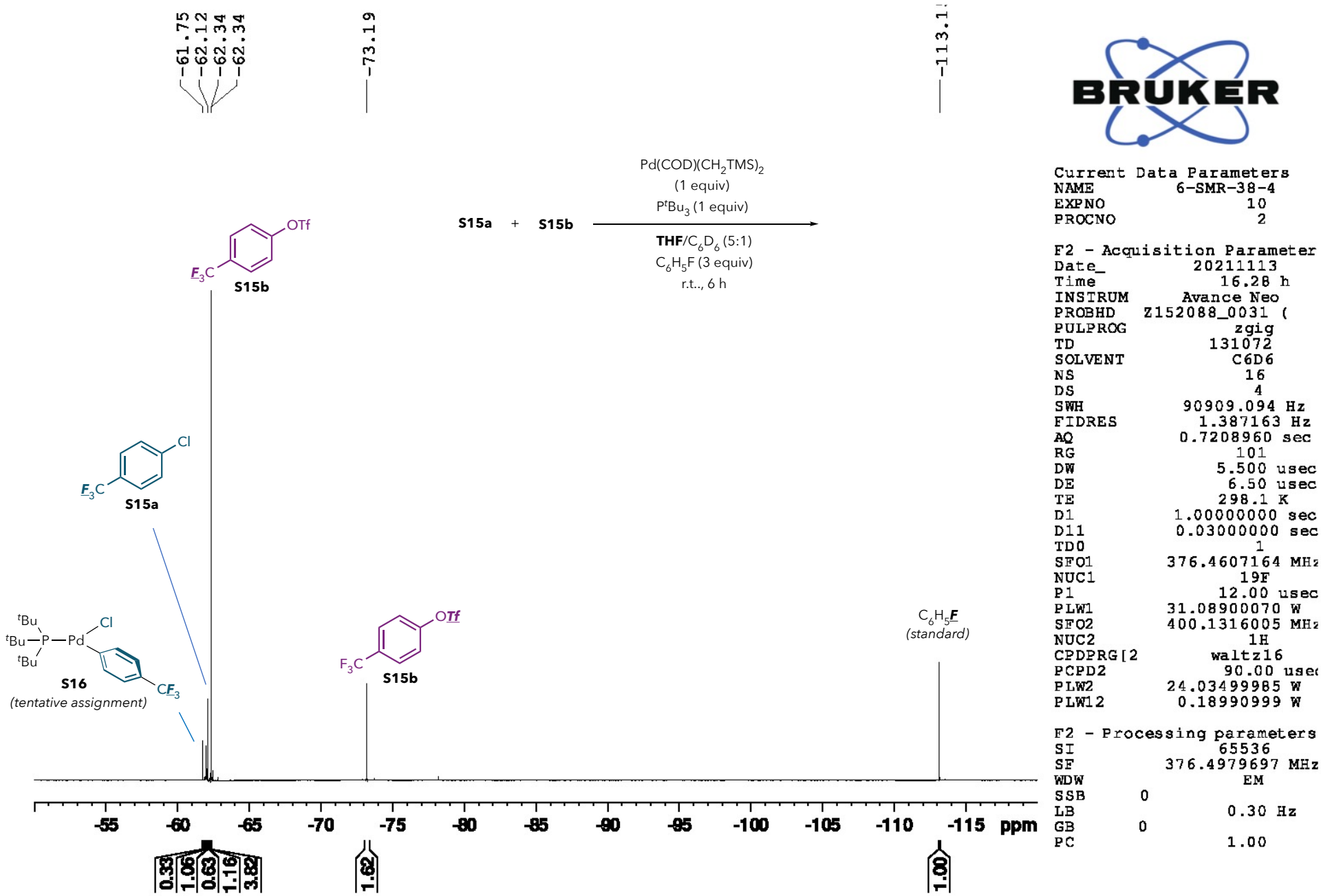





```
Current Data Parameters
NAME          6-SMR-37-4
EXPNO                 11
PROCNO                 1

F2 - Acquisition Parameter
Date_          20211112
Time             15.56 h
INSTRUM       Avance Neo
PROBHD   Z152088_0031 (
PULPROG          zgpg30
TD               65536
SOLVENT           C6D6
NS                  32
DS                   4
SWH           65789.477 Hz
FIDRES         2.007735 Hz
AQ            0.4980736 sec
RG                 101
DW               7.600 usec
DE               6.50 usec
TE               298.0 K
D1           2.00000000 sec
D11          0.03000000 sec
TD0                  1
SFO1        161.9674942 MHz
NUC1              31P
P0               2.67 usec
P1               8.00 usec
PLW1         45.86100006 W
SFO2        400.1316005 MHz
NUC2              1H
CPDPRG[2        waltz16
PCPD2            90.00 usec
PLW2         24.03499985 W
PLW12         0.18990999 W
PLW13         0.09552100 W

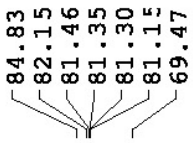
F2 - Processing parameters
SI                32768
SF          161.9755930 MHz
WDW                EM
SSB       0
LB               1.00 Hz
GB        0
PC               1.40
```



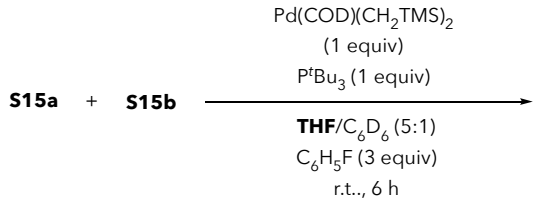

```
Current Data Parameters
NAME          6-SMR-38-4
EXPNO                 10
PROCNO                 2

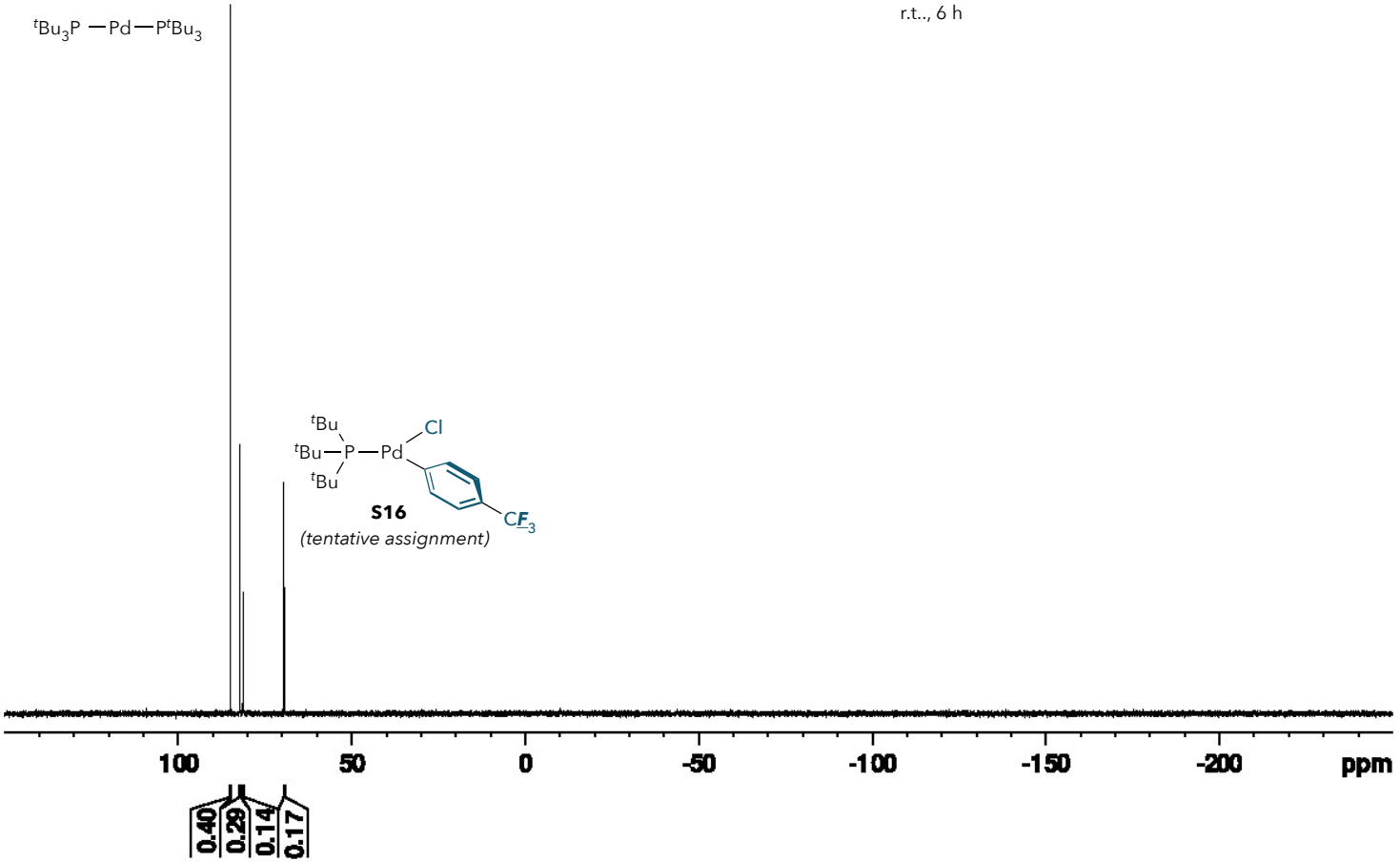
F2 - Acquisition Parameter
Date_          20211113
Time             16.28 h
INSTRUM       Avance Neo
PROBHD   Z152088_0031 (
PULPROG             zgig
TD                131072
SOLVENT             C6D6
NS                    16
DS                     4
SWH           90909.094 Hz
FIDRES         1.387163 Hz
AQ            0.7208960 sec
RG                   101
DW                5.500 usec
DE                6.50 usec
TE                298.1 K
D1           1.00000000 sec
D11          0.03000000 sec
TD0                    1
SFO1         376.4607164 MHz
NUC1                 19F
P1                12.00 usec
PLW1         31.08900070 W
SFO2         400.1316005 MHz
NUC2                 1H
CPDPRG[2         waltz16
PCPD2             90.00 usec
PLW2         24.03499985 W
PLW12         0.18990999 W

F2 - Processing parameters
SI                 65536
SF           376.4979697 MHz
WDW                   EM
SSB       0
LB                0.30 Hz
GB        0
PC                1.00
```





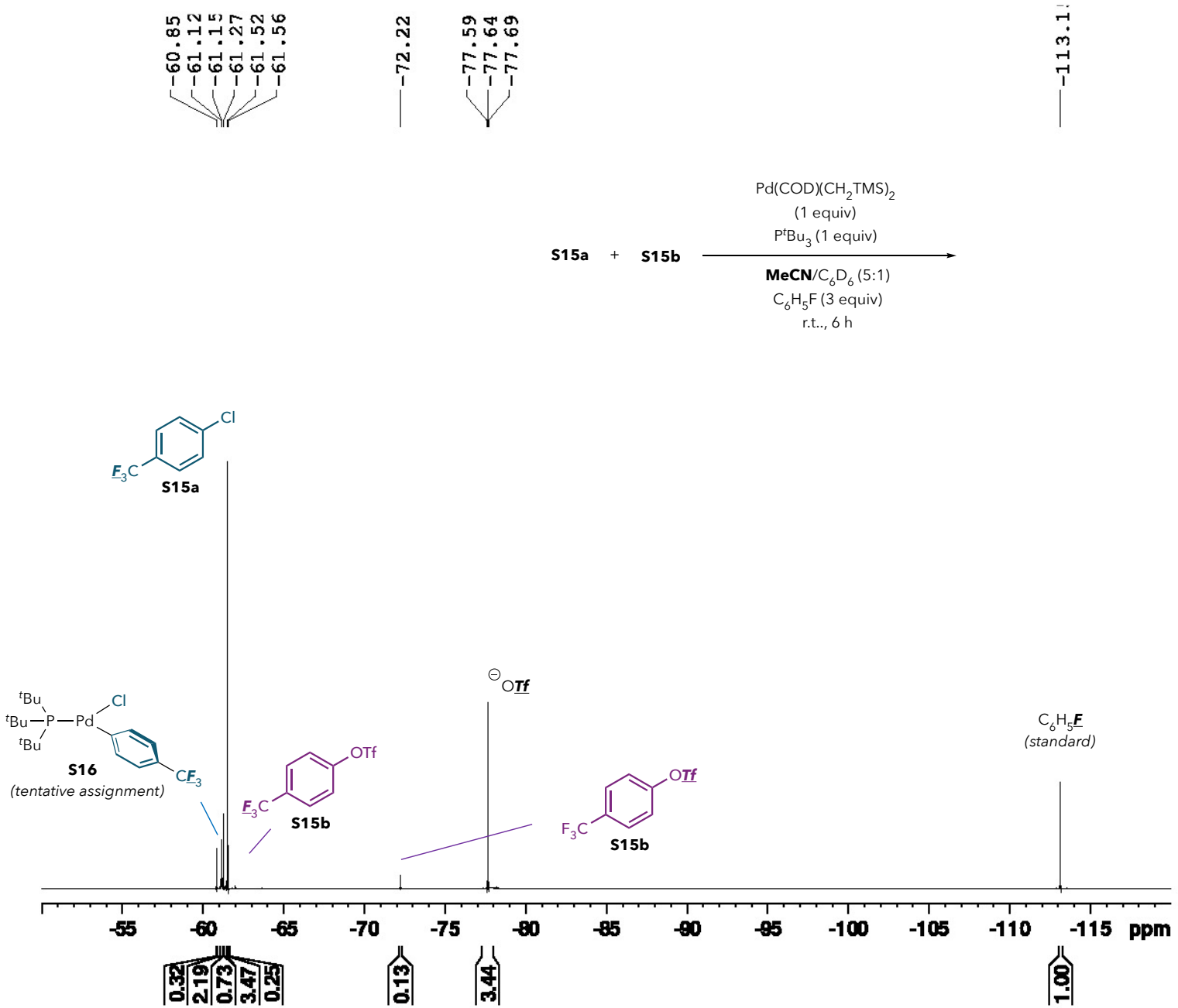





```
Current Data Parameters
NAME          6-SMR-38-4
EXPNO                 11
PROCNO                 1

F2 - Acquisition Parameter
Date_          20211113
Time             16.32 h
INSTRUM       Avance Neo
PROBHD   Z152088_0031 (
PULPROG          zgpg30
TD                65536
SOLVENT            C6D6
NS                   32
DS                    4
SWH           65789.477 Hz
FIDRES          2.007735 Hz
AQ            0.4980736 sec
RG                  101
DW                7.600 usec
DE                6.50 usec
TE                298.0 K
D1           2.00000000 sec
D11          0.03000000 sec
TD0                   1
SFO1        161.9674942 MHz
NUC1               31P
P0                2.67 usec
P1                8.00 usec
PLW1         45.86100006 W
SFO2        400.1316005 MHz
NUC2               1H
CPDPRG[2        waltz16
PCPD2            90.00 usec
PLW2         24.03499985 W
PLW12         0.18990999 W
PLW13         0.09552100 W

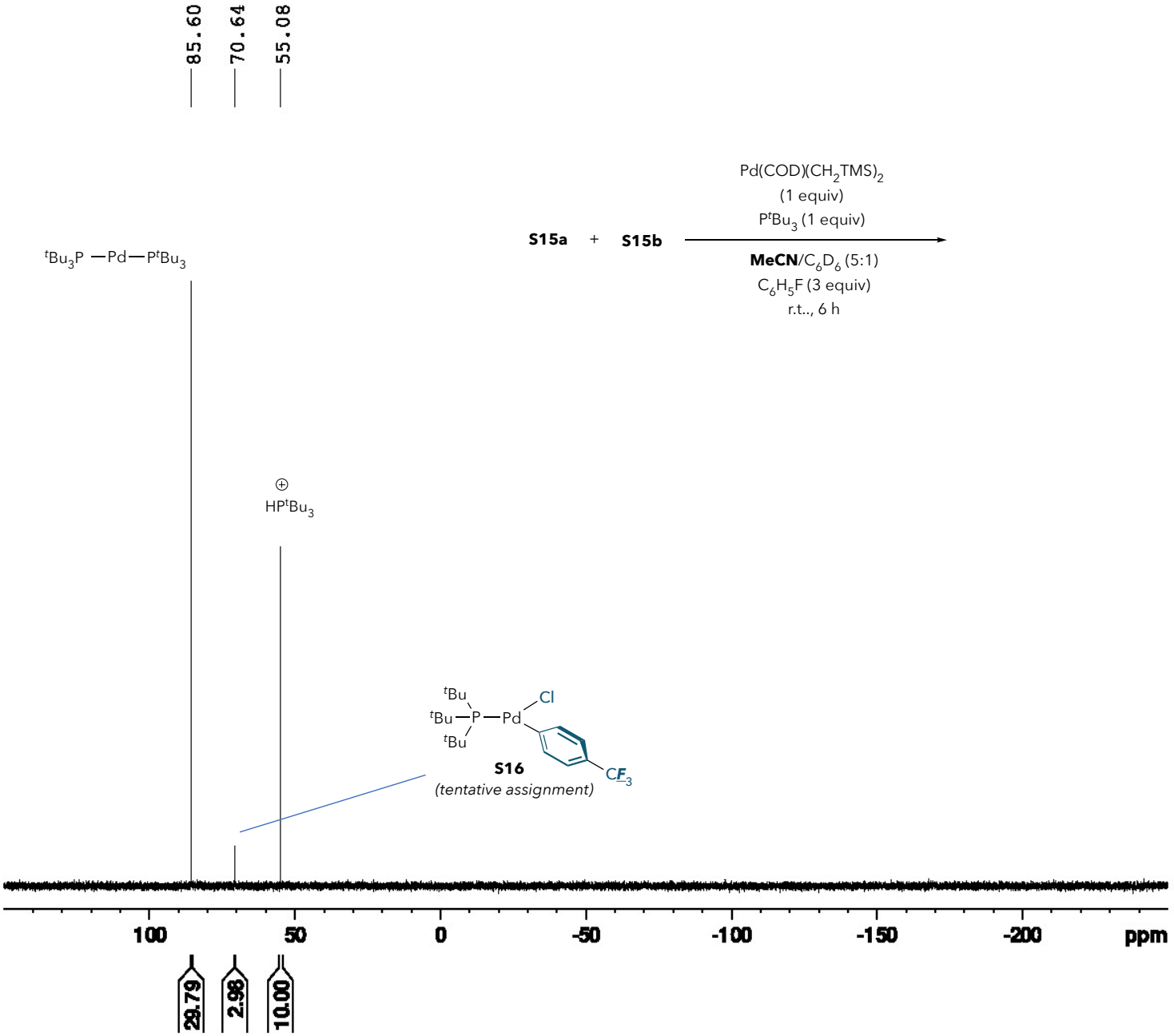
F2 - Processing parameters
SI                 32768
SF          161.9755930 MHz
WDW                  EM
SSB       0
LB                1.00 Hz
GB        0
PC                1.40
```




```
Current Data Parameters
NAME          6-SMR-38-7
EXPNO                 10
PROCNO                 2

F2 - Acquisition Parameter
Date_          20211113
Time             16.49 h
INSTRUM       Avance Neo
PROBHD   Z152088_0031 (
PULPROG             zgig
TD                131072
SOLVENT             C6D6
NS                    16
DS                     4
SWH           90909.094 Hz
FIDRES         1.387163 Hz
AQ            0.7208960 sec
RG                   101
DW               5.500 usec
DE               6.50 usec
TE               298.1 K
D1           1.00000000 sec
D11          0.03000000 sec
TD0                    1
SFO1         376.4607164 MHz
NUC1                 19F
P1               12.00 usec
PLW1         31.08900070 W
SFO2         400.1316005 MHz
NUC2                 1H
CPDPRG[2          waltz16
PCPD2             90.00 usec
PLW2         24.03499985 W
PLW12         0.18990999 W

F2 - Processing parameters
SI                 65536
SF           376.4977288 MHz
WDW                   EM
SSB       0
LB                0.30 Hz
GB        0
PC                1.00
```



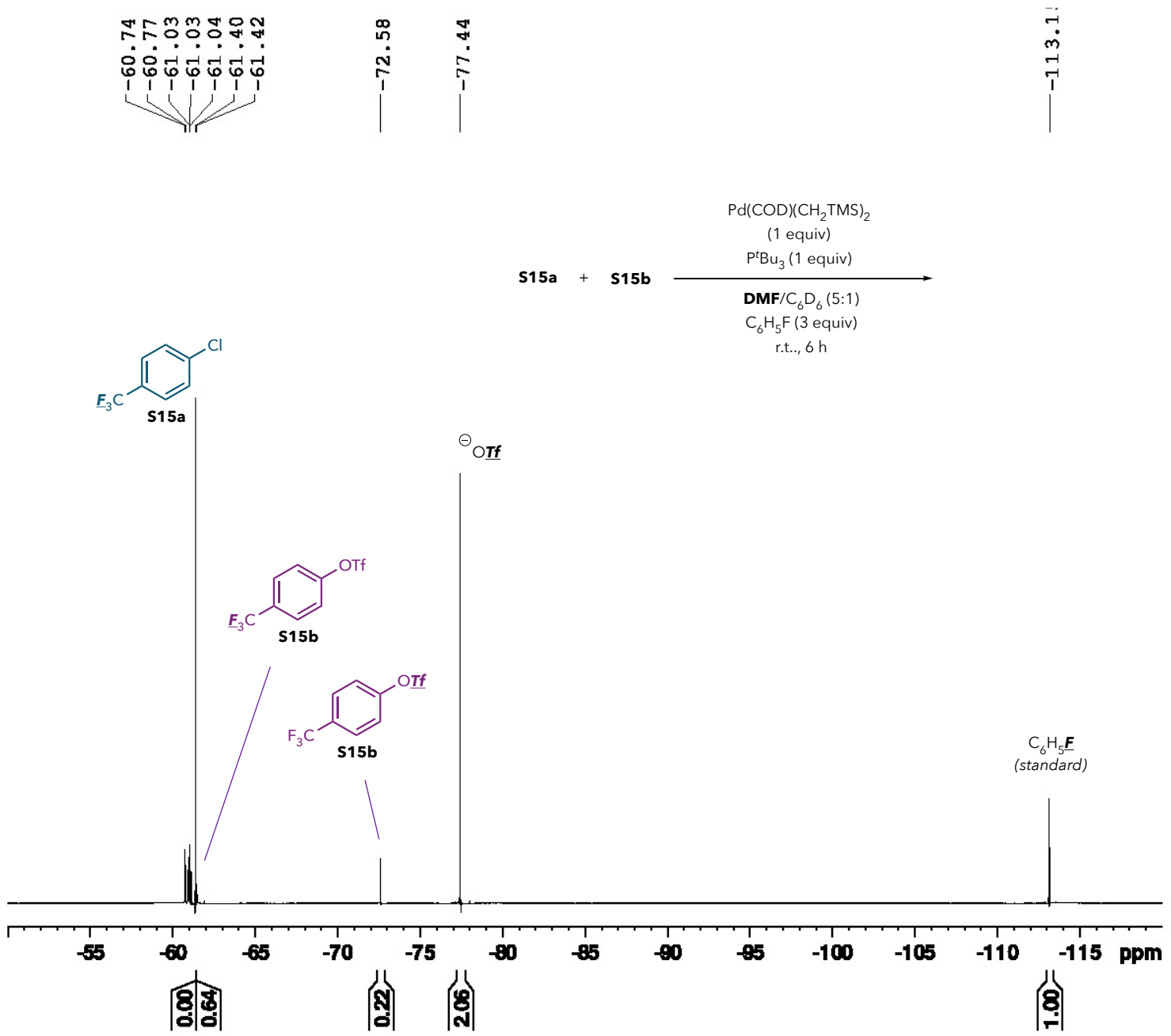
S16
(tentative assignment)




```
Current Data Parameters
NAME          6-SMR-38-7
EXPNO                 11
PROCNO                 1

F2 - Acquisition Parameter
Date_          20211113
Time             16.52 h
INSTRUM       Avance Neo
PROBHD   Z152088_0031 (
PULPROG          zgpg30
TD                65536
SOLVENT            C6D6
NS                   32
DS                    4
SWH           65789.477 Hz
FIDRES          2.007735 Hz
AQ            0.4980736 sec
RG                  101
DW                7.600 usec
DE                6.50 usec
TE                298.0 K
D1           2.00000000 sec
D11          0.03000000 sec
TD0                   1
SFO1        161.9674942 MHz
NUC1               31P
P0                2.67 usec
P1                8.00 usec
PLW1         45.86100006 W
SFO2        400.1316005 MHz
NUC2               1H
CPDPRG[2        waltz16
PCPD2            90.00 usec
PLW2         24.03499985 W
PLW12         0.18990999 W
PLW13         0.09552100 W

F2 - Processing parameters
SI                 32768
SF          161.9755930 MHz
WDW                  EM
SSB       0
LB                1.00 Hz
GB        0
PC                1.40
```

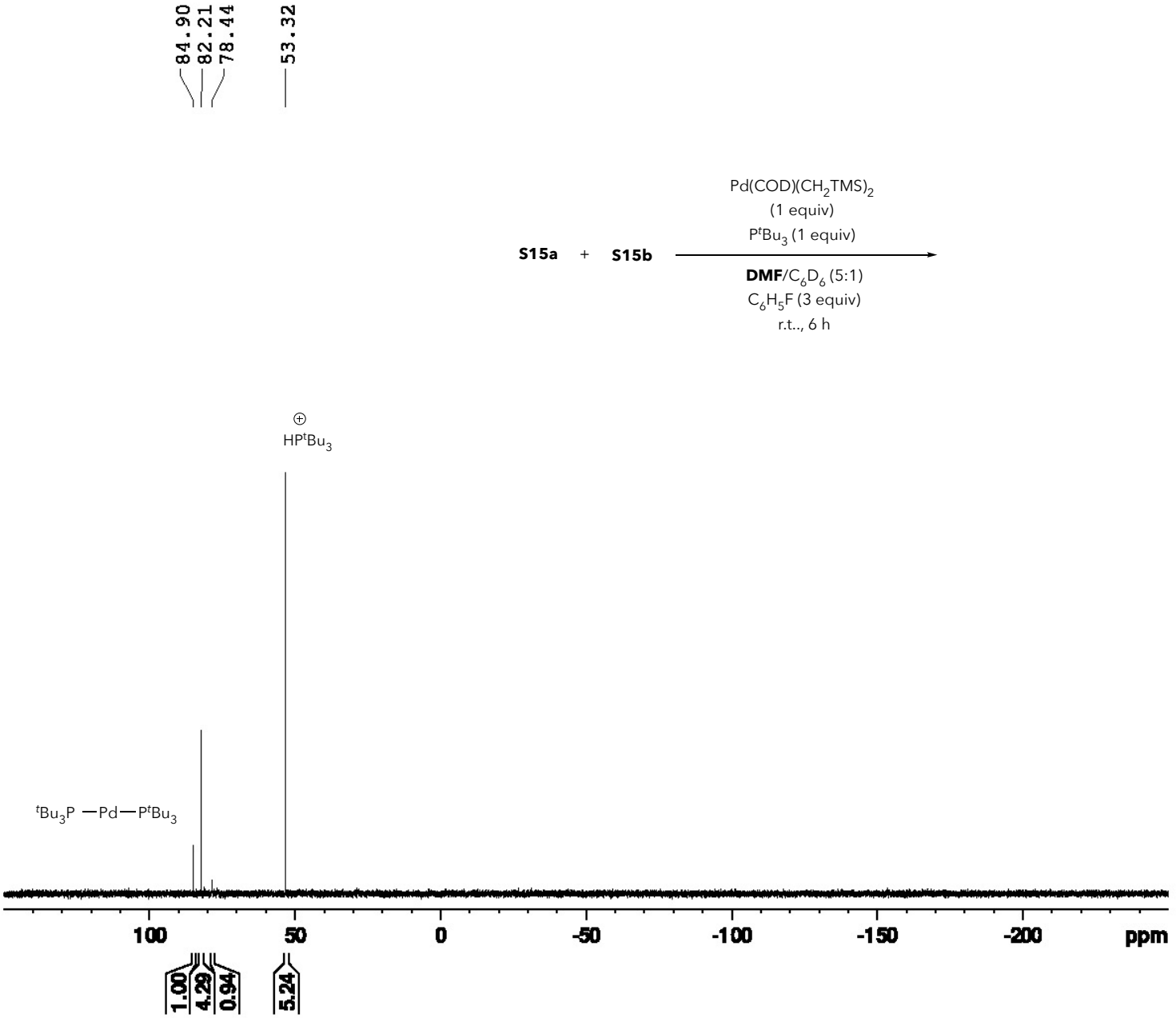


BRUKER

```
Current Data Parameters
NAME         6-SMR-38-11
EXPNO                 10
PROCNO                 2

F2 - Acquisition Parameter
Date_          20211113
Time             17.21 h
INSTRUM       Avance Neo
PROBHD   Z152088_0031 (
PULPROG            zgig
TD               131072
SOLVENT            C6D6
NS                   16
DS                    4
SWH           90909.094 Hz
FIDRES         1.387163 Hz
AQ            0.7208960 sec
RG                  101
DW                5.500 usec
DE                6.50 usec
TE                298.1 K
D1           1.00000000 sec
D11          0.03000000 sec
TD0                   1
SFO1         376.4607164 MHz
NUC1                 19F
P1                12.00 usec
PLW1         31.08900070 W
SFO2         400.1316005 MHz
NUC2                 1H
CPDPRG[2         waltz16
PCPD2             90.00 usec
PLW2         24.03499985 W
PLW12         0.18990999 W

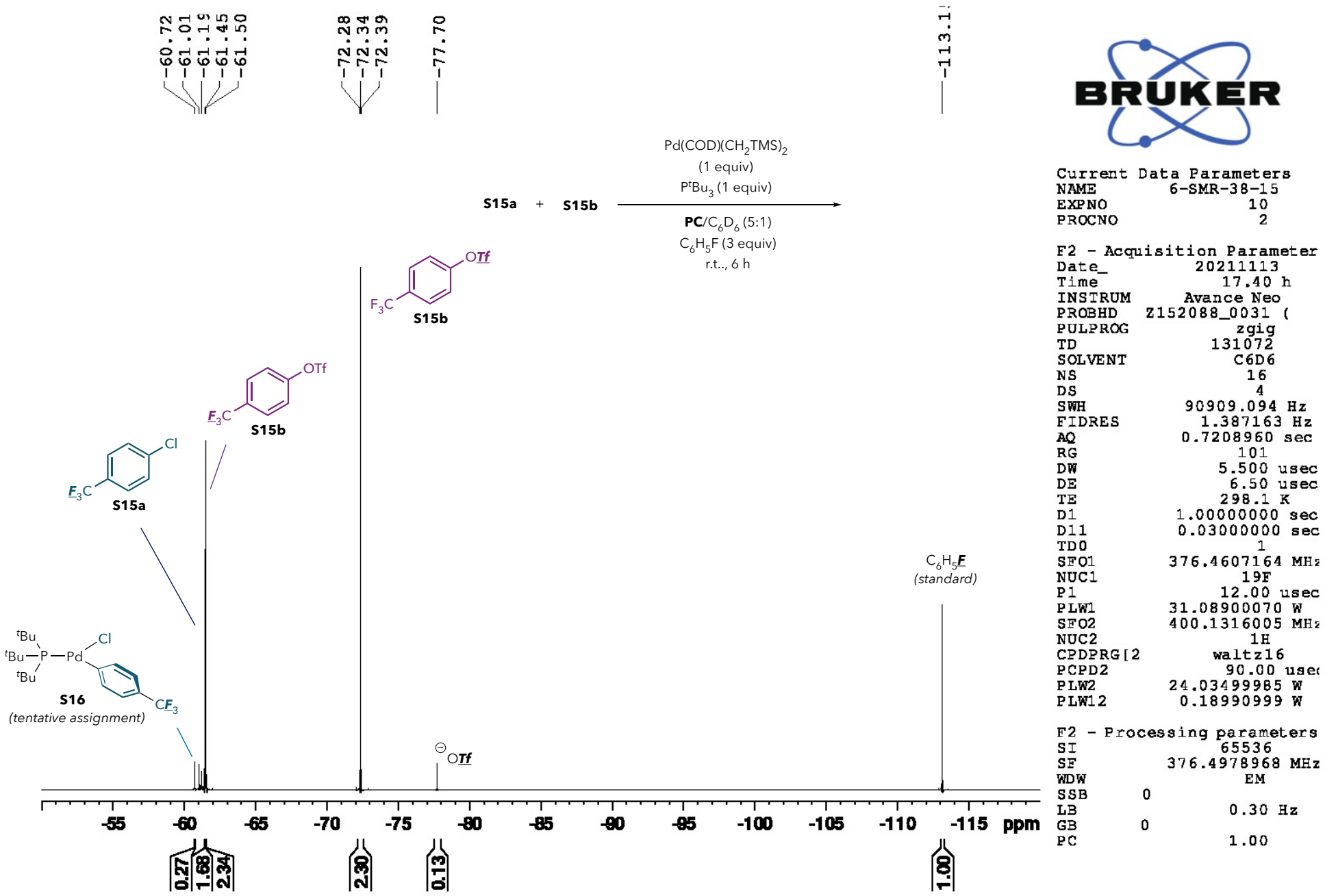
F2 - Processing parameters
SI                 65536
SF           376.4978876 MHz
WDW                  EM
SSB       0
LB                0.30 Hz
GB        0
PC                1.00
```




```
Current Data Parameters
NAME         6-SMR-38-11
EXPNO                 11
PROCNO                 1

F2 - Acquisition Parameter
Date_          20211113
Time             17.24 h
INSTRUM       Avance Neo
PROBHD   Z152088_0031 (
PULPROG          zgpg30
TD                65536
SOLVENT           C6D6
NS                   32
DS                    4
SWH           65789.477 Hz
FIDRES          2.007735 Hz
AQ            0.4980736 sec
RG                  101
DW                7.600 usec
DE                6.50 usec
TE                298.0 K
D1           2.00000000 sec
D11          0.03000000 sec
TD0                   1
SFO1         161.9674942 MHz
NUC1                31P
P0                2.67 usec
P1                8.00 usec
PLW1         45.86100006 W
SFO2         400.1316005 MHz
NUC2                1H
CPDPRG[2         waltz16
PCPD2             90.00 usec
PLW2         24.03499985 W
PLW12         0.18990999 W
PLW13         0.09552100 W

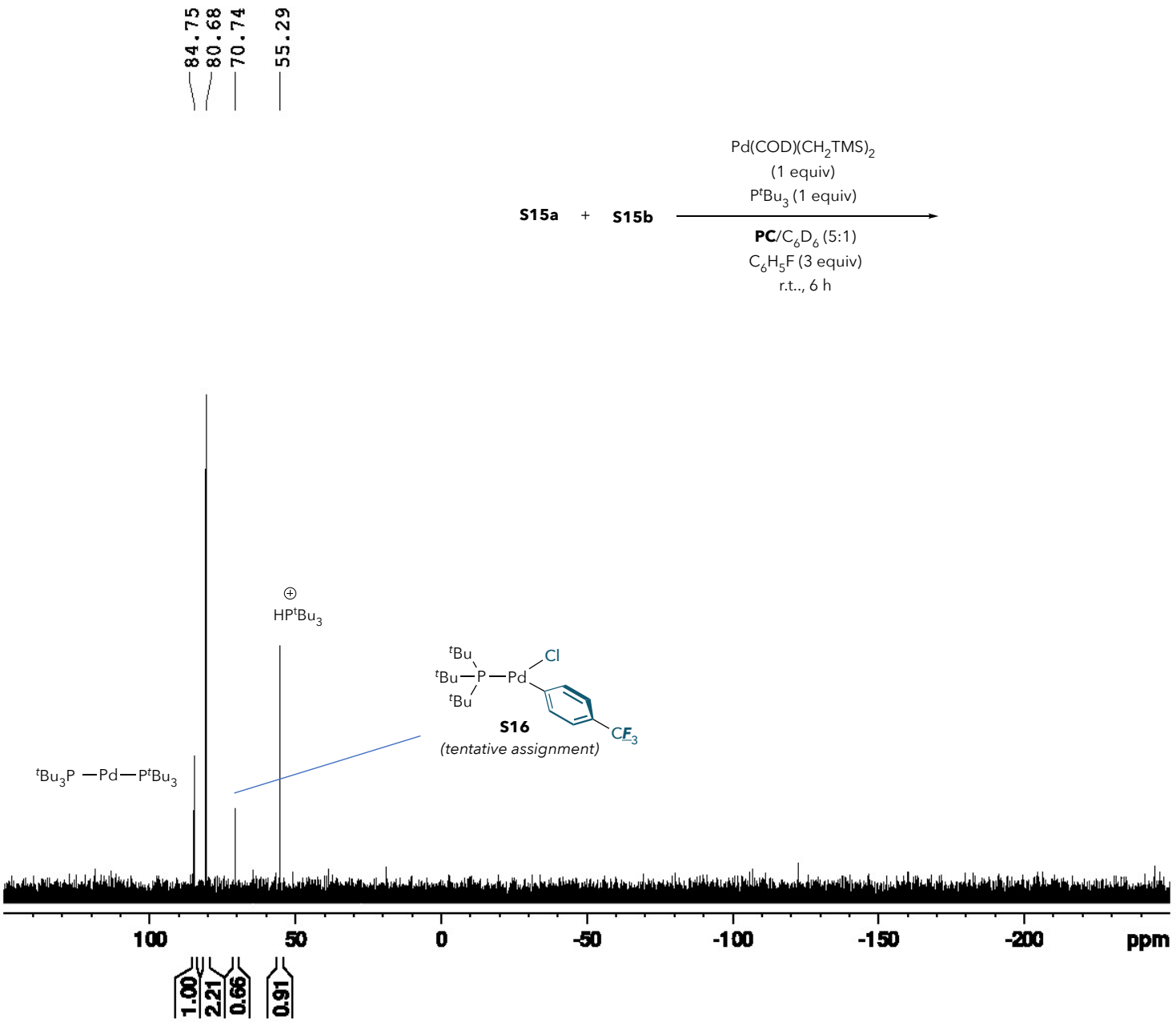
F2 - Processing parameters
SI                 32768
SF           161.9755930 MHz
WDW                  EM
SSB       0
LB                1.00 Hz
GB        0
PC                1.40
```




```
Current Data Parameters
NAME          6-SMR-38-15
EXPNO                  10
PROCNO                  2

F2 - Acquisition Parameter
Date_           20211113
Time              17.40 h
INSTRUM       Avance Neo
PROBHD    Z152088_0031 (
PULPROG            zgig
TD               131072
SOLVENT            C6D6
NS                   16
DS                    4
SWH           90909.094 Hz
FIDRES         1.387163 Hz
AQ            0.7208960 sec
RG                  101
DW              5.500 usec
DE              6.50 usec
TE              298.1 K
D1           1.00000000 sec
D11          0.03000000 sec
TD0                   1
SFO1         376.4607164 MHz
NUC1                19F
P1               12.00 usec
PLW1         31.08900070 W
SFO2         400.1316005 MHz
NUC2                1H
CPDPRG[2        waltz16
PCPD2            90.00 usec
PLW2         24.03499985 W
PLW12         0.18990999 W

F2 - Processing parameters
SI                 65536
SF           376.4978968 MHz
WDW                  EM
SSB       0
LB                0.30 Hz
GB        0
PC                1.00
```

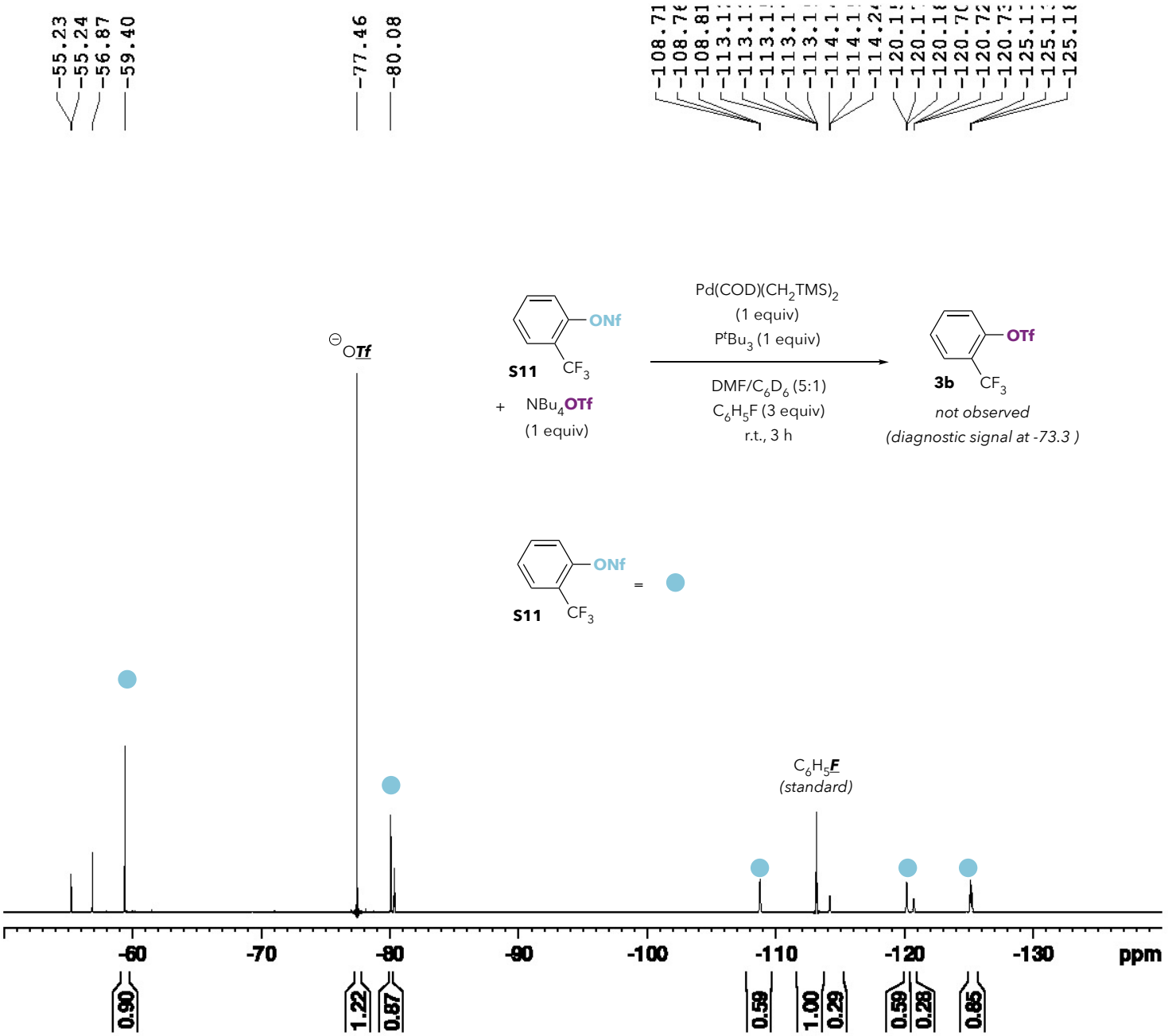



```
Current Data Parameters
NAME         6-SMR-38-15
EXPNO                 11
PROCNO                 1

F2 - Acquisition Parameter
Date_          20211113
Time             17.44 h
INSTRUM       Avance Neo
PROBHD   Z152088_0031 (
PULPROG          zgpg30
TD                65536
SOLVENT           C6D6
NS                   32
DS                    4
SWH           65789.477 Hz
FIDRES          2.007735 Hz
AQ            0.4980736 sec
RG                  101
DW                7.600 usec
DE                6.50 usec
TE                298.0 K
D1           2.00000000 sec
D11          0.03000000 sec
TD0                   1
SFO1         161.9674942 MHz
NUC1                31P
P0                2.67 usec
P1                8.00 usec
PLW1         45.86100006 W
SFO2         400.1316005 MHz
NUC2                1H
CPDPRG[2         waltz16
PCPD2             90.00 usec
PLW2         24.03499985 W
PLW12         0.18990999 W
PLW13         0.09552100 W

F2 - Processing parameters
SI                 32768
SF           161.9755930 MHz
WDW                  EM
SSB       0
LB                1.00 Hz
GB        0
PC                1.40
```

D. Reaction with S11 and NBu_4OTf



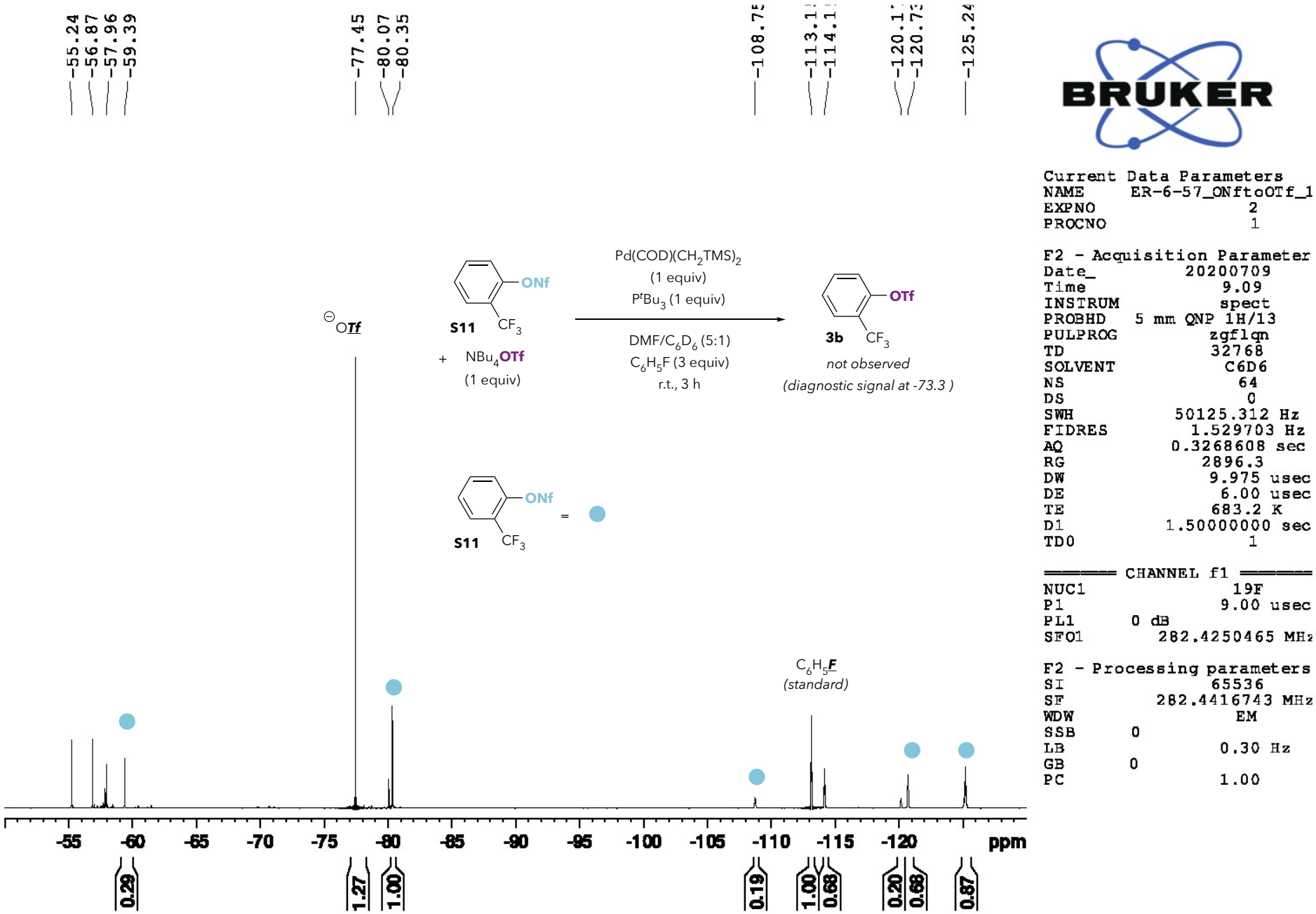
BRUKER

```
Current Data Parameters
NAME      ER-6-57_ONftoOTf_1
EXPNO                    1
PROCNO                   1

F2 - Acquisition Parameter
Date_          20200707
Time              10.36
INSTRUM           spect
PROBHD   5 mm QNP 1H/13
PULPROG          zgflqn
TD               32768
SOLVENT            C6D6
NS                   64
DS                    0
SWH           50125.312 Hz
FIDRES         1.529703 Hz
AQ            0.3268608 sec
RG               2896.3
DW                9.975 usec
DE                6.00 usec
TE               683.2 K
D1           1.50000000 sec
TD0                  1

====== CHANNEL f1 ======
NUC1                19F
P1                9.00 usec
PL1       0 dB
SFO1         282.4250465 MHz

F2 - Processing parameters
SI                65536
SF          282.4416726 MHz
WDW                 EM
SSB       0
LB                0.30 Hz
GB        0
PC                1.00
```




```
Current Data Parameters
NAME      ER-6-57_ONftoOTf_1
EXPNO                      2
PROCNO                     1

F2 - Acquisition Parameter
Date_              20200709
Time                   9.09
INSTRUM               spect
PROBHD   5 mm QNP 1H/13
PULPROG             zgflqn
TD                   32768
SOLVENT               C6D6
NS                      64
DS                       0
SWH              50125.312 Hz
FIDRES             1.529703 Hz
AQ               0.3268608 sec
RG                  2896.3
DW                   9.975 usec
DE                   6.00 usec
TE                  683.2 K
D1               1.50000000 sec
TD0                        1

====== CHANNEL f1 ======
NUC1                     19F
P1                    9.00 usec
PL1       0 dB
SFO1          282.4250465 MHz

F2 - Processing parameters
SI                       65536
SF              282.4416743 MHz
WDW                         EM
SSB       0
LB                    0.30 Hz
GB        0
PC                    1.00
```

REFERENCES

Almond-Thynne, J.; Blakemore, D. C.; Pryde, D. C.; Spivey, A. C. Site-selective Suzuki–Miyaura coupling of heteroaryl halides – understanding the trends for pharmaceutically important classes. *Chem. Sci.* **2017**, *8i, 40-62.*

Alvarez, S. Coordinating Ability of Anions, Solvents, Amino Acids, and Gases towards Alkaline and Alkaline-Earth Elements, Transition Metals, and Lanthanides. *Chem. Eur. J.* **2020**, *26*, 4350–4377.

Amatore, C.; Jutand, A. Anionic Pd(0) and Pd(II) Intermediates in Palladium-Catalyzed Heck and Cross-Coupling Reactions. *Acc. Chem. Res.* **2000**, *33*, 314-321.

Amatore, C.; Jutand, A. Mechanistic and kinetic studies of palladium catalytic systems. *J. Organomet. Chem.* **1999**, *576*, 254-278.

Andersen, T. L.; Friis, S. D.; Audrain, H.; Nordeman, P.; Antoni, G.; Skrydstrup, T. Efficient ^{11}C-Carbonylation of Isolated Aryl Palladium Complexes for PET: Application to Challenging Radiopharmaceutical Synthesis. *J. Am. Chem. Soc.* **2015**, *137*, 1548−1555.

Antonelli, D. M.; Schaefer, W. P.; Parkin, G.; Bercaw, J.E. Synthesis and characterization of (η^5-$C_5Me_5)_2TaCl(THF)$, a useful synthetic precursor for the preparation of oxo, imido and methylidene derivatives of permethyltantalocene. *J. Organomet. Chem*. **1993**, *462*, 213-220.

Antiñolo, A.; Carrillo-Hermosilla, F.; Fajardo, M.; Fernándex-Baeza, J.; García-Yuste, S.; Otero, A. Advances in the chemistry of bis-cyclopentadienyl hydride derivatives of niobium and tantalum. *Coord. Chem. Rev.* **1999**, *193-195*, 43-72.

Arakaweau,, H.; Aresta, M.; Armor, J.N.; Barteau, M.A.; Beckman, E.J.; Bell, A.T.; Bercaw, J.E.; Creutz, C.; Dinjus, E.; Dixon, D.A.; Domen, K.; DuBois, D.L.; Eckert, J.; Fujita, E.; Gibson, D.H.; Goddard, W.A.; Goodman, D.W.; Keller, J.; Kubas, G.J.; Kung, H.H.; Lyons, J.E.; Manzer, L.E.; Marks, T.J.; Morokuma, K.; Nicholas, K.M.; Periana, R.; Que, L.; Rostrup-Nielson, J.; Sachtler, W.M.H.; Schmidt, L.D.; Sen, A.; Somorjai, G.A.; Stair, P.C.; Stults, B.R.; Tumas, W. Catalysis Research of Relevance to Carbon Management: Progress, Challenges, and Opportunities. *Chem. Rev.* **2011,** *101*, 953-996.

Bailey, B.C.; Fan, H.; Baum, E.W.; Huffman, J.C.; Baik, M.-H.; Mindiola, D.J. Intermolecular C-H Bond Activation Promoted by a Titanium Alkylidyne. *J. Am. Chem. Soc.* **2005**, *127*, 16016-16017.

Ballard, K.R.; Gardiner, I.M.; Wigley, D.W. Evidence for intramolecular carbon-hydrogen bond activation and the formation of a tucked-in complex of hexamethylbenzene at a tantalum(III) center. *J. Am. Chem. Soc*. **1989,** *111,* 2159-2162.

Barefield, E.K.; Parshall, G.W.; Tebbe, F.N. Catalysis of Aromatic Hydrogen-Deuterium Exchange by Metal Hydrides. *J. Am. Chem. Soc*. **1970**, *92*, 5234-5235.

Barrios-Landeros, F.; Carrow, B. P.; Hartwig, J. F. Autocatalytic Oxidative Addition of PhBr to $Pd(P^tBu_3)_2$ via $Pd(P^tBu_3)_2(H)(Br)$ *J. Am. Chem. Soc.* **2008**, *130*, 5842-5843.
Barrios-Landeros, F.; Carrow, B. P.; Hartwig, J. F. Effect of Ligand Steric Properties and Halide Identity on the Mechanism for Oxidative Addition of Haloarenes to Trialkylphosphine Pd(0) Complexes. *J. Am. Chem. Soc.* **2009**, *131*, 8141-8154.

Basset, J. M.; Copéret, C.; Lefort, L.; Maunders, B. M.; Maury, O.; Le Roux, E.; Saggio, G.; Soignier, S.; Soulivong, D.; Sunley, G. J.; Taoufik, M.; Thivolle-Cazat, J. Primary Products and Mechanistic Considerations in Alkane Metathesis. *J. Am. Chem. Soc*. **2005**, *127*, 8604-8605.

Baynham, R.F.G.; Chetwynd-Talbot, J.; Grebenik, P.; Perutz, R.N.; Powell, M.H.A. Photochemistry of $M(\eta^5\text{-}C_5H_5)_2(H)CO$ and $M(\eta^5\text{-}C_5H_5)_2H_3$ (M = Nb, Ta) in low temperature matrices. *J. Organomet. Chem.* **1985**, *284*, 229-242.

Beaumier, E.P.; Pearce, A.J.; See, X.Y.; Tonks, I.A. Modern applications of low-valent early transition metals in synthesis and catalysis. *Nat. Chem. Rev.* **2019**, *3*, 15-34.

Becke, A. D. A new mixing of Hartree–Fock and local density-functional theories. *J. Chem. Phys.* **1993**, *98*, 1372.

Becke, A. D. Density-functional exchange-energy approximation with correct asymptotic behavior. *Phys. Rev. A* **1998**, *38*, 3098.

Becke, A. D. Density-functional thermochemistry. III. The role of exact exchange. *J. Chem. Phys.* **1993**, *98*, 5648.

Beckhaus, R. Pentafulvene complexes of group four metals: Versatile organometallic building blocks. *Coord. Chem. Rev*. **2018**, *376*, 467-477.

Benitez, D.; Tkatchouk, E.; Goddard, III, W. A. Relevance of cis- and trans-dichloride Ru intermediates in Grubbs-II olefin metathesis catalysis ($H_2IMesCl_2Ru$=CHR). *Chem. Commun.* **2008**, 6194-6196.

Bercaw, J.E.; Brintzinger, H.H. Bis(pentamethylcyclopentadienyl)titanium(II). Isolation and Reactions with Hydrogen, Nitrogen, and Carbon Monoxide. *J. Am. Chem. Soc.* **1971**, *93*, 2045-2046.

Besora, M.; Maseras, F. The diverse mechanisms for the oxidative addition of C–Br bonds to $Pd(PR_3)$ and $Pd(PR_3)_2$ complexes. *Dalton Trans.* **2019**, *48*, 16242-16248.

Bonney, K. J.; Schoenebeck, F. Experiment and computation: a combined approach to study the reactivity of palladium complexes in oxidation states 0 to IV. *Chem. Soc. Rev.* **2014**, *43*, 6609-6638.

Bregel, D.C.; Oldham, S.M.; Eisenberg, R. Mechanistic Studies on the Addition of Dihydrogen to Tantalocene Complexes. *J. Am. Chem. Soc.* **2002**, *124*, 13827-13832.

Brookes, N. J.; Ariafard, A.; Stranger, R.; Yates, B. F., Scission of Carbon Monoxide Using TaR_3, R = (N(tBu)Ph) or $OSi(tBu)_3$): A DFT Investigation. *Chem. Eur. J.* **2010**, *16*, 8117-8132.
Buckner, S.W.; MacMahon, T.J.; Byrd, G.D.; Freiser, B.S. Gas-phase reactions of niobium(1+) and tantalum(1+) with alkanes and alkenes. Carbon-hydrogen bond activation and ligand-coupling mechanisms. *Inorg. Chem.* **1989**, *28*, 3511-3518.

Burford, R.J.; Yeo, A.; Fryzuk, M.D. Dinitrogen activation by group 4 and group 5 metal complexes supported by phosphine-amido containing ligand manifolds. *Coord. Chem. Rev.* **2017**, *334*, 84-89.

Cao, M.; Xie, H. Recent advances in theoretical studies on ligand-controlled selectivity of nickel- and palladium-catalyzed cross-coupling reactions. *Chinese. Chem. Lett.* **2021**, *32*, 319-327.
Carrow, B. P.; Hartwig, J. F. Ligandless, Anionic, Arylpalladium Halide Intermediates in the Heck Reaction *J. Am. Chem. Soc.* **2010**, *132*, 79−81.

Chirik, P.J. Group 4 Transition Metal Sandwich Complexes: Still Fresh after Almost 60 Years. *Organometallics* **2010**, *29*, 1500-1517.

Cho, H.M.; Weissman, H.; Wilson, S.R.; Moore, J.S. A Mo(VI) Alkylidyne Complex with Polyhedral Oligomeric Silsesquioxane Ligands: Homogeneous Analogue of a Silica-Supported Alkyne Metathesis Catalyst. *J. Am. Chem. Soc.* **2006**, *128*, 14742-14743.

Clementi, E.; Raimond, D. L.; Reinhardt, W. P. Atomic Screening Constants from SCF Functions. II. Atoms with 37 to 86 Electrons. *J. Chem. Phys*. **1967,** *47*, 1300–1307.

Collins, R.A.; Russell, A.F.; Mountford, P., Group 4 metal complexes for homogeneous olefin polymerisation: a short tutorial review. *Appl. Petrochem. Res.* **2015**, *5*, 153-171.
Coşkun, N. and Erden, I., An efficient catalytic method for fulvene synthesis. *Tetrahedron* **2011**, *67*, 8607-8614.

Cossi, M.; Rega, N.; Scalmani, G.; Barone, V. Energies, structures, and electronic properties of molecules in solution with the C-PCM solvation model. *J. Comput. Chem*. **2003**, *24*, 669−681.

Cotton, F.A., Cyclopentadienyl–metal chemistry in the Wilkinson Group, Harvard, 1952–1955. *J. Organomet. Chem.* **2001**, *637-639*, 18-26

Crabtree, R.H. Alkane C–H activation and functionalization with homogeneous transition metal catalysts: a century of progress—a new millennium in prospect. *J. Chem. Soc, Dalton Trans.* **2001**, 2437-2450.

Crabtree, R.H. The organometallic chemistry of alkanes. *Chem. Rev.* **1985**, *85*, 245-269.

Crabtree, R.H., The Organometallic Chemistry of the Transition Metals, Seventh Edition; John Wiley & Sons Inc: Hoboken, New Jersey, 2019.

Cramer, C. J.; Truhlar, D. G., Density functional theory for transition metals and transition metal chemistry. *Phys. Chem. Chem. Phys.* **2009,** *11*, 10757-10816.

Curtis, D.M.; Bell, L.G.; Butler, W.M. C—H Activation. Synthesis of Silyl Derivatives of Niobocene and Tantalocene Hydrides, Their H/D Exchange Reactions with C_6D_6, and the Structure of $Cp_2Ta(H)_2SiMe_2Ph$. *Organometallics* **1985**, *4*, 701-707.
D'Alterio, M. C.; Casals-Cruañas, É.; Tzouras, N. V.; Talarico, G.; Nolan, S. P.; Poater, A. Mechanistic Aspects of the Palladium-Catalyzed Suzuki-Miyaura Cross-Coupling Reaction. *Chem. Eur. J.* **2021**, *early view* DOI: 10.1002/chem.202101880.

De Vries, A. H. M.; Parlevliet, F. J.; Schmieder-van de Vondervoort, L.; Mommers, J. H. M.; Henderickx, H. J. W.; Walet, M. A. M.; De Vries, J. G. A Practical Recycle of a Ligand-Free Palladium Catalyst for Heck Reactions. *Adv. Synth. Catal.* **2002**, *344*, 996−1002.

Deutsch, P.P.; Maguarie, J.A.; Jones, W.D.; Eisenberg, R. Hydride abstraction. The reaction of IrX(CO)(dppe) with Cp_2TaH_3. *Inorg. Chem.* **1990**, *29*, 686-690.

Diao, T.; White, P.; Guzei, I.; Stahl, S. S. Characterization of DMSO Coordination to Palladium(II) in Solution and Insights into the Aerobic Oxidation Catalyst, Pd(DMSO)2(TFA)2. *Inorg. Chem.* **2012**, *51*, 11898-11909.

Dry, M.E., The Fischer-Tropsch process: 1950-2000. *Catal. Today.* **2002**, *71*, 277-241.
Eckhard, J.F.; Masubauchu, T.; Tschurl, M.; Barnett, R.N.; Landman, U.; Heix, U. Thermal Dehydrogenation of Methane Enhanced by μ^2-Oxo Ligands in Tantalum Cluster Cations [TaxO]+, x = 4, 5. *J. Phys. Chem. C* **2018**, *122*, 25628-25637.

Du, F.; Nojabaei, B. A Review of Gas Injection in Shale Reservoirs: Enhanced Oil/Gas Recovery Approaches and Greenhouse Gas Control. *Energies* **2019**, *12*, 2355-2387.

Elson, I.H.; Kochi, J.K.; Klabunde, U.; Manzer, L.E.; Parshall, G.W.; Tebbe, F.N. Paramagentic hydride and alkyl complexes of niobium(IV) and tantalum(IV). *J. Am. Chem. Soc.* **1974**, *96*, 7374-7376.

Findlay, A.E.; Leelasubcharoen, S.; Kuzmina, L.G.; Howard, J.A.K.; Nikonov, G.I. Phosphido-bridged Ta/Rh bimetallic complex: synthesis, structure, and catalytic hydrosilylation of acetophenone. *Dalton Trans.* **2010**, *39*, 9264-9269.

Fischer, E. O. and Pfab, W., Cyclopentadien-Metallkomplexe, ein neuer Typ metallorganischer Verbindungen. *Zeitschrift für Naturforschung B* **1952**, 7**,** 377-379.

Flores, J.A.; Cavaliere, V.N.; Buck, D.; Pinter, B.; Chen. G.; Crestani, M.G.; Baik, M.-H.; Mindiola, D.J. Methane activation and exchange by titanium-carbon multiple bonds. *Chem. Sci.* **2011,** *2*, 1457-1462.

Fors, B. P.; Watson, D. A.; Biscoe, M. R.; Buchwald, S. L. A Highly Active Catalyst for Pd-Catalyzed Amination Reactions: Cross-Coupling Reactions Using Aryl Mesylates and the Highly Selective Monoarylation of Primary Amines Using Aryl Chlorides *J. Am. Chem. Soc.* **2008**, *130*, 13552−13554.

Foust, D.F.; Rogers, R.D.; Rausch, M.D.; Atwood, J.L. Photoinduced Reactions of (η^5-$C_5H_5)_2M(CO)H$ (M = Nb, Ta) and the Molecular Structure of (η^5-$C_5H_5)_2Ta(CO)H$. *J. Am. Chem. Soc*. **1982**, *104*, 5646-5650.

Frisch, M. J.; Trucks, G. W.; Schlegel, H. B.; Scuseria, G. E.; Robb, M. A.; Cheeseman, J. R.; Scalmani G., Barone, V.; Petersson, G. A.; Nakatsuji, H.; Li, X.; Caricato, M.; Marenich, A. V.; Bloino, J.; Janesko, B. G.; Gomperts, R.; Mennucci, B.; Hratchian, H. P.; Ortiz, J. V.; Izmaylov, A. F.; Sonnenberg, J. L.; Williams-Young, D.; Ding, F.; Lipparini, F.; Egidi, F.; Goings, J.; Peng, B.; Petrone, A.; Henderson, T.; Ranasinghe, D.; Zakrzewski, V. G.; Gao, J.; Rega, N.; Zheng, G.; Liang, W.; Hada, M.; Ehara, M.; Toyota, K.; Fukuda, R.; Hasegawa, J.; Ishida, M.; Nakajima, T.; Honda, Y.; Kitao, O.; Nakai, H.; Vreven, T.; Throssell, K.; Montgomery, J. A. Jr.; Peralta, J. E.; Ogliaro, F.; Bearpark, M. J.; Heyd, J. J.; Brothers, E. N.; Kudin, K. N.; Staroverov, V. N.; Keith, T. A.; Kobayashi, R.; Normand, J.; Raghavachari, K.; Rendell, A. P.; Burant, J. C.; Iyengar, S. S.; Tomasi, J.; Cossi, M.; Millam, J. M.; Klene, M.; Adamo, C.; Cammi, R.; Ochterski, J. W.; Martin, R. L.; Morokuma, K.; Farkas, O.; Foresman, J. B.; and Fox, D. J. *Gaussian 16*; Gaussian, Inc., Wallingford CT, 2016.

Fryzuk, M.D.; Clentsmith, G.K.B.; Rettig, S.J. Coordination behavior of $LiBEt_4$ towards (η^5-$C_5H_5)_2ReH$, (η^5-$C_5H_5)_2WH_2$ and (η^5-$C_5H_5)_2TaH_3$. Solid state structure of $[(\eta^5\text{-}C_5H_5)_2TaH \cdot A1H_2(OCH_2CH_2CH_2CH_3)]_2$. *Inorg. Chim. Acta*. **1997**, *259*, 51-59.
Fryzuk, M.D.; Johnson, S.A. The continuing story of dinitrogen activation. *Coord. Chem. Rev.* **2000**, *200-202*, 379-409.

Fukui, K. The Path of Chemical Reactions - the IRC Approach. *Acc. Chem. Res*. **1981**, *14*, 363−368

Galardon, E.; Rhamdeehul, S.; Brown, J. M.; Cowley, A.; Hii, K. K.; Jutand, A. Profound Steric Control of Reactivity in Aryl Halide Addition to Bisphosphane Palladium(0) Complexes. *Angew. Chem. Int. Ed.* **2002**, *41*, 1760-1763.

García-Melchor, M.; Braga, A. A. C.; Lledós, A.; Ujaque, G.; Maseras, F. Computational Perspective on Pd-Catalyzed C–C Cross-Coupling Reaction Mechanisms. *Acc. Chem. Res.* **2013**, *46*, 2626-2634.

GaussView, Version 6, Dennington, Roy; Keith, Todd A.; Millam, John M. Semichem Inc., Shawnee Mission, KS, 2016.

Gianetti, T.L.; Bergman, R.G.; Arnold, J. Carbon–fluorine bond cleavage in fluoroarenes via a niobium(III) imido complex: from stoichiometric to catalytic hydrodefluorination. *Chem. Sci.* **2014**, *5*, 2517-2524.

Gibson, V. C.; Parkin, G.; Bercaw, J. E. Synthesis and Reactivity of Permethyltantalocene Derivatives Possessing η^3-Allyl, η^2-Butadiene, η^2-Methylallene,and η^1-Alkenylidene Ligands. Model Studies for the Role of Surface Vinylidenes in the Fischer−Tropsch Hydrocarbon-Chain-Lengthening Process. *Organometallics* **1991**, *10*, 220−231.

Gomez-Bengoa, E.; Echavarren, A. M. Synthesis of isoascididemin, a regioisomer of the marine alkaloid ascididemin. *J. Org. Chem.* **1991**, *56*, 3497-3501.

Gonzalez, C.; Schlegel, H. B. An Improved Algorithm for Reaction Path Following. *J. Chem. Phys*. **1989**, *90*, 2154−2161.
Gonzalez, C.; Schlegel, H. B. Reaction Path Following in Mass-Weighted Internal Coordinates. *J. Phys. Chem*. **1990**, *94*, 5523−5527.

Goossen, L. J.; Koley, D.; Hermann, H. L.; Thiel, W. The Palladium-Catalyzed Cross-Coupling Reaction of Carboxylic Anhydrides with Arylboronic Acids: A DFT Study *J. Am. Chem. Soc.* **2005**, *127*, 11102−11114.

Green, J.C. Bent metallocenes revisited. *Chem. Soc. Rev.* **1998**, *27*, 263-271.

Green, M.L.H. & Jousseaume, B. Bis(η-isopropylcyclopentadienyl)tantalum chemistry: some hydride, carbonyl, alkyl, al-kyne and tertiaryphosphine derivatives, and an improved synthesis of dichlorobiscyclopentadienylniobium. *J. Organomet. Chem*. **1980**, *193*, 339-344.

Grimme, S.; Antony, J.; Ehrlich, S.; Krieg, H. A consistent and accurate ab initio parametrization of density functional dispersion correction (DFT-D) for the 94 elements H-Pu. *J. Chem. Phys.* **2010**, 132, 154104-154119. (b) Grimme, S.; Ehrlich, S.; Goerigk, L. Effect of the damping function in dispersion corrected density functional theory. *J. Comput. Chem.* **2011**, *32*, 1456-1465.

Gulyás, H.; Hayano, S.; Madarász, Á.; Pápai, I.; Sxabó, M.; Bucsai, Á.; Martin, E.; Benet-Bucholz, J., Air-stable 18-electron adducts of Schrock catalysts with tuned stability constants for spontaneous release of the active species. *Commun. Chem.* **2021**, *4*, 71.

Gunsalas, N.J.; Koppaka, A.; Park, S.H.; Bischof, S.M.; Hashiguchi, B.G.; Periana, R.A. Homogeneous functionalization of methane. *Chem. Rev.* **2017**, *117*, 8521-8573.

Halpern, J. Activation of Carbon-Hydrogen Bonds by Metal Complexes: Mechanism, Kinetic, and Thermodynamic Considerations. *Inorg. Chim. Acta.* **1985**, *100*, 41-48.

Hartwig, J. J. *Organotransition Metal Chemistry: From Bonding to Catalysis*; University Science Books: Sausalito, CA, 2010.

Hodala, J.L; Moon, D.J.; Reddy, K.R.; Reddy, C.V.; Kumar, T.N.; Ahamed, M.I.; Raghu, A.V. Catalyst design for maximizing C5+ yields during Fischer-Tropsch synthesis. *Int. J. Hydrogen Energy* **2021**, *46*, 3289-3301.

Hooker, L. V.; Neufeldt, S. R. Ligation state of nickel during CeO bond activation with monodentate phosphines. *Tetrahedron* **2018**, *74*, 6717-6725.

Jia, C.; Kitamura, T.; Fujiwara, Y. Catalytic Functionalization of Arenes and Alkanes via C-H Bond Activation. *Acc. Chem. Res.* **2001**, *34*, 633-639.

Jiang, Q.; Pestana, D.C.; Carroll, P.J.; Berry, D.H. Thermochemical Aspects of Arene C-H Activation by Tantalum Silyl Complexes: Relative Ta-Si and Ta-C Bond Enthalpies. *Organometallics* **1994**, *13*, 3679-3691.

Jones, D. J.; Lautens, M.; McGlacken, G. P. The emergence of Pd-mediated reversible oxidative addition in cross coupling, carbohalogenation and carbonylation reactions. *Nature Cat.* **2019**, *2*, 843-851.

Joy, J.; Stuyver, T.; Shaik, S. Oriented External Electric Fields and Ionic Additives Elicit Catalysis and Mechanistic Crossover in Oxidative Addition Reactions. *J. Am. Chem. Soc.* **2020**, *142*, 3836-3850.

Kaplan, J; Wilzbach, K.E. Photolysis of benzene vapor. Benzvalene formation at wavelengths 2537-2370 Å. *J. Am. Chem. Soc.* **1968**, *90*, 3291-3292.

Keim, W., Oligomerization of Ethylene to α-Olefins: Discovery and Development of the Shell Higher Olefin Process (SHOP). *Angew. Chem. Int. Ed.* **2013**, *52,* 12492-12496.

Kepp, K.P. A quantitative scale of oxophilicity and thiophilicity. *Inorg. Chem.* **2016**, *55*, 9461-9470.

Klabunde, U. and Parshall, G.W. Activation of Aromatic Carbon-Hydrogen Bonds by Transition Metal Complexes. II. Substituted Benzenes. *J. Am. Chem. Soc*. **1972**, *94*, 9081-9087.

Korolev, A.V., Rheingold, A.L., and Williams, D.W. A General Route to Labile Niobium and Tantalum d^0 Monoimides. Discussion of Metal-Nitrogen Vibrational Modes. *Inorg. Chem*. **1997**, *36,* 2647-2655.

Kozuch, S.; Amatore, C.; Jutand, A.; Shaik, S. What Makes for a Good Catalytic Cycle? A Theoretical Study of the Role of an Anionic Palladium(0) Complex in the Cross-Coupling of an Aryl Halide with an Anionic Nucleophile. *Organometallics* **2005**, *24*, 2319-2330.

Kuhl, N.; Hopkins, M.H.; Wencel-Delord, J.; Glorius, F. Beyond Directing Groups: Transition-Metal-Catalyzed C—H Activation of Simple Arenes. *Angew. Chem. Int. Ed***. 2012**, *51*, 10236-10254.

Labinger, J. A. Tutorial on Oxidative Addition. *Organometallics* **2015**, *34*, 4784–4795.

Labinger, J.A. and Bercaw, J.E. Understanding and exploiting C–H bond activation. *Nature* **2002**, *417*, 507-514.

Labinger, J.A. and Wong, K.S. Mechanism of Formation of $(\eta^5\text{-}C_5H_5)_2NbH_3$ from the Reaction of $(\eta^5\text{-}C_5H_5)_2NbCl_2$ with Hydroaluminate Reducing Agents. *J. Organomet. Chem.* **1979**, *170*, 373-384.

Labinger, J.A.; Bercaw, J.E. Understanding and exploiting C—H bond activation. *Nature* **2002**, *407*, 507-514.

Lam, K. C.; Marder, T. B.; Lin, Z. DFT Studies on the Effect of the Nature of the Aryl Halide Y-C_6H_4-X on the Mechanism of Its Oxidative Addition to Pd^0L versus Pd^0L_2. *Organometallics* **2007**, *26*, 758-760.
Lapoutre, V. J. F.; Redlich, B.; van der Meer, A. F. G.; Oomens, J.; Bakker, J. M.; Sweeney, A.; Mookherjee, A.; Armentrout, P. B. Structures of the Dehydrogenation Products of Methane Activation by 5d Transition Metal Cations. *J. Phys. Chem. A* **2013**, *117*, 4115-4126.

Larini, P.; Kefalidis, C. E.; Jazzar, R.; Renaudat, A.; Clot, E.; Baudoin, O. On the Mechanism of the Palladium-Catalyzed β-Arylation of Ester Enolates. *Chem. - Eur. J.* **2012**, *18*, 1932−1944.

Le Roux, E.; Taoufik, M.; Copéret, C.; de Mallmann, A.; Thivolle-Cazat, J.; Basset, J.-M.; Maunders, B. M.; Sunley, G. Development of Tungsten-Based Heterogeneous Alkane Metathesis Catalysts Through a Structure–Activity Relationship. *Angew. Chem., Int. Ed*. **2005**, *44*, 6755-6758.

Leblanc, J.-C.; Reynoud, J.-F.; Moise, C. Complexes bis cyclopentadienyles substitues du tantale: synthese et reactivite de dichlorures, de tri- et de monohydrures. *C. R. Acad. Sc. Paris* **1982**, *295*, 755-757.

Legault, C. Y. *CYLview, 1.0b*; Universitéde Sherbrooke, 2009 http://www.cylview.org.

Lersch, M.; Tilset, M. Mechanistic Aspects of C−H Activation by Pt Complexes. *Chem. Rev*. **2005**, *105*, 2471−2526.

Li, C.; Dinoi, C.; Coppel, T.; Etienne, M., CH Bond Activation of Methane by a Transient η^2-Cyclopropene/Metallabicyclobutane Complex of Niobium. *J. Am. Chem. Soc.* **2015**, *137*, 12450-12453.

Lill, S. O. N.; Ryberg, P.; Rein, T.; Bennström, E.; Norrby, P-O. *t*Bu or not *t*Bu? *Chem. Eur. J.* **2012**, *18*, 1640-1649.

Lin, X.; Xi, Y.; Zhang, G.; Phillips, D.L.; Guo, W. A Reaction Mechanism of Methane Coupling on a Silica-Supported Single-Site Tantalum Catalyst. *Organometallics* **2014**, *33*, 2172-2181.

Littke, A. F.; Dai, C.; Fu, G. C. Versatile Catalysts for the Suzuki Cross-Coupling of Arylboronic Acids with Aryl and Vinyl Halides and Triflates under Mild Conditions. *J. Am. Chem. Soc*. **2000**, *122*, 4020−4028.

Littke, A. F.; Schwarz, L.; Fu, G. C. Pd/P(*t*-Bu)$_3$: A Mild and General Catalyst for Stille Reactions of Aryl Chlorides and Aryl Bromides. *J. Am. Chem. Soc.* **2002**, *124*, 6343-6348.

Lyngvi, E.; Sanhueza, I. A.; Schoenebeck, F. Dispersion Makes the Difference: Bisligated Transition States Found for the Oxidative Addition of $Pd(P^tBu_3)_2$ to Ar-OSO_2R and Dispersion-Controlled Chemoselectivity in Reactions with $Pd[P(^iPr)(^tBu2)]_2$. *Organometallics* **2015**, *34*, 805-812.

Macrae, C. F.; Bruno, I. J.; Chisholm, J. A.; Edgington, P. R.; McCabe, P.; Pidcock, E.; Rodriguez-Monge, L.; Taylor, R.; van de Streek, J.; Wood, P. A., Mercury CSD 2.0 - new features for the visualization and investigation of crystal structures. Journal of Applied Crystallography 2008, 41, 466-470.

Mahatthananchai, J.; Dumas, A. M.; Bode, J. W. Catalytic Selective Synthesis. *Angew. Chem. Int. Ed.* **2012**, *51*, 10954-10990.
Manabe, K.; Ohba, M.; Matsushima, Y., A Repetitive One-Step Method for Oligoarene Synthesis Using Catalyst Controlled Chemoselective Cross-Coupling. *Org. Lett.* **2011***, 13*, 2436-2439.

Margulieux, G.W.; Semproni, S.P.; Chirik, P.J. Photochemically Induced Reductive Elimination as a Route to a Zirconocene Complex with a Strongly Activated N_2 Ligand. *Angew. Chem. Int. Ed*. **2014**, *53*, 9189-9192.

Mashima, K. Diagonal Relationship among Organometallic Transition-Metal Complexes. *Organometallics.* **2021**, *40*, 3497-3505.

McGlade, C.E. A review of the uncertainties in estimates of global oil resources. *Energy* **2012**, *47*, 262-270; (b) McGlade, C. & Ekins, P. The geographical distribution of fossil fuels unused when limiting global warming to 2 °C. *Nature* **2015**, *517*, 187-190.

McLain, S.J.; Sancho, J.; Schrock, R.R. Metallacyclopentane to Metallacyclobutane Ring Contraction. *J. Am. Chem. Soc.* **1979**, *101*, 5451-5453.

McLain, S.J.; Sancho, J.; Schrock, R.R. Selective Dimerization of Monosubstituted a-Olefins by Tantalacyclopentane Catalysts. *J. Am. Chem. Soc.* **1980**, *102*, 5610-5618.

McLain, S.J.; Wood, C.D.; Schrock, R.R. Preparation and Characterization of Tantalum(III) Olefin Complexes and Tantalum(V) Metallacyclopentane Complexes Made from Acyclic a Olefins. *J. Am. Chem. Soc.* **1979**, *101*, 4558-4570.

McMullin, C.; Fey, N.; Harvey, J. N. Computed ligand effects on the oxidative addition of phenyl halides to phosphine supported palladium(0) catalysts. *Dalton Trans.* **2014**, *43*, 13545-13556.

McMullin, C. L.; Jover, J.; Harvey, J. N.; Fey, N. Accurate modelling of Pd(0) + PhX oxidative addition kinetics. *Dalton Trans.* **2010**, *39*, 10833-10836. (d) Ahlquist, M. S. G.; Norrby, P.-O. Dispersion and Back-Donation Gives Tetracoordinate $[Pd(PPh_3)_4]$. *Angew. Chem. Int. Ed.* **2011**, *50*, 11794-11797.

Millar, S.P.; Zubris, D.L.; Bercaw, J.E.; Eisenberg, R. On the Mechanism of Dihydrogen Addition to Tantalocene Complexes. *J. Am. Chem. Soc*. **1998**, *120*, 5329-5330.

Milner, P. J.; Yang, Y.; Buchwald, S. L. In-Depth Assessment of the Palladium-Catalyzed Fluorination of Five-Membered Heteroaryl Bromides. *Organometallics* **2015**, *34*, 4775−4775.

Mindiola, D.J. Oxidatively Induced Abstraction Reactions. A Synthetic Approach to Low-Coordinate and Reactive Early Transition Metal Complexes Containing Metal—Ligand Multiple Bonds. *Acc. Chem. Res.* **2006**, *39*, 813-821.

Moltved, K. A.; Kepp, K. P. Chemical Bond Energies of 3d Transition Metals Studied by Density Functional Theory. *J. Chem. Theory Comput.* **2018**, *14*, 3479–3492.

Montzka, S.A.; Blugokencky, E.J.; Butler, J.H. Non-CO2 greenhouse gases and climate change. *Nature* **2011***, 476*, 43-50.

Neese, F., A critical evaluation of DFT, including time-dependent DFT, applied to bioinorganic chemistry. *J. Biol. Inorg. Chem.* **2006,** *11*, 702-711.

Niemeyer, Z. L.; Milo, A.; Hickey, D. P.; Sigman, M. S. Parameterization of Phosphine Ligands Reveals Mechanistic Pathways and Predicts Reaction Outcomes. *Nat. Chem.* **2016**, *8*, 610−617.

Nomura, K.; Zhang, S. Design of Vanadium Complex Catalysts for Precise Olefin Polymerization. *Chem. Rev.* **2011, *111*,** 2342-2362.

Nunez-Zarur, F.; Solans-Monfort, X.; Restrepo, A., Mechanistic Insights into Alkane Metathesis Catalyzed by Silica-Supported Tantalum Hydrides: A DFT Study. *Inorg. Chem.* **2017**, *56*, 10458-10473.

Ohata, J.; Teremoto, A.; Fujita, H.; Takemoto, S.; Matsuzaka, H. Linear Hydrocarbon Chain Growth from a Molecular Diruthenium Carbide Platform. *J. Am. Chem. Soc.* **2021**, *143*, 16105-16112.

Ohki, Y.; Fryzuk, M.D. Dinitrogen Activation by Group 4 Metal Complexes. *Angew. Chem. Int. Ed.* **2007**, *46*, 3180-3183.

Okuda, J., Ferrocene – 65 Years After. *Eur. J. Inorg. Chem.* **2017**, *2*, 217-219.

Palani, V.; Perea, M. A.; Sarpong, R. Site-Selective Cross-Coupling of Polyhalogenated Arenes and Heteroarenes with Identical Halogen Groups. *Chem. Rev.* **2021**, *Article ASAP*. DOI: 10.1021/acs.chemrev.1c00513.

Parke, L.G.; Hinton, C.S.; Arementrout, P.B. Experimental and Theoretical Studies of the Activation of Methane by Ta+. *J. Phys. Chem. C* **2007**, *111*, 17773-17787.

Parkin, G.; Bunel, E.; Burger, B.J.; Trimmer, M.S.; Van Asselt, A.; Bercaw, J.E. Alpha- and beta-migratory insertion and elimination processes for alkyl complexes of permethyl-scandocene and permethyltantalocene. *J. Mol. Catal***. 1987**, *41*, 21-39.

Parkin, G. Classification of Organotransition Metal Compounds. In *Comprehensive Organometallic Chemistry*, Third Edition. Michael, D., Mingos, P., Crabtree, R.H.; Elsevier Science: 2007; pp 1-57.

Parshall, G.W. Intramolecular aromatic substitution in transition metal complexes. *Acc. Chem. Res***. 1970**, *3*, 139-144.

Pasha, F.A.; Cavallo, L.; Basset, J-M. Mechanism of n-Butane Hydrogenolysis Promoted by Ta-Hydrides Supported on Silica. *ACS Catal*. **2014,** *4*, 1868-1874.

Pfab, W.; Fisher, E.O., Zur Kristallstruktur der Di-cyclopentadienyl-verbindungen des zweiwertigen Eisens, Kobalts und Nickels. *Zeitschrift für anorganische und allgemeine Chemie* **1953**, *274*, 316-322.

Proutiere, F.; Schoenebeck, F. Orthogonal Selectivities under Pd(0) Catalysis with Solvent Polarity: An Interplay of Computational and Experimental Studies. *Synlett* **2012**, *23*, 645-648.
Proutiere, F.; Schoenebeck, F. Solvent Effect on Palladium-Catalyzed Cross-Coupling Reactions and Implications on the Active Catalytic Species. *Angew. Chem., Int. Ed.* **2011**, *50*, 8192−8195.

Rabe, G.; Roesky, H.W.; Stalke, D.; Pauer, F.; Sheldrick, G.M., The preparation and crystal structures of sodium and potassium pentamethylcyclopentadienyl pyridine solvates. *J. Organomet. Chem*. **1991**, *403*, 11-19.

Ramirez-Contreras, R.; Bhuvanesh, N.; Ozerov, O. V. Cycloaddition and C-H Activation Reactions of a Tantalum Alkylidyne*. Organometallics* **2015**, *34*, 1143-1146.

Reeves, E. K.; Bauman, O. R.; Mitchem, G. B.; Neufeldt, S. R. Solvent Effects on the Selectivity of Palladium-Catalyzed Suzuki- Miyaura Couplings. *Isr. J. Chem.* **2020**, *60*, 406−409

Reeves, E. K.; Entz, E. D.; Neufeldt, S. R. Chemodivergence between Electrophiles in Cross-Coupling Reactions. *Chem. Eur. J.* **2021**, *27*, 6161–6177.

Rehbein, S.M.; Kania, M.J.; Neufeldt, S.R., Experimental and Computational Evaluation of Tantalocene Hydrides for C–H Activation of Alkanes. *Manuscript in preparation*

Rehbein, S.R.; Kania, M.J.; Neufeldt, S.R. Experimental and Computational Evaluation of Tantalocene Hydrides for C–H Activation of Arenes. *Organometallics* **2021**, *40*, 2666-2677.

Rej, S.; Das, A.; Chatani, N. Strategic evolution in transition metal-catalyzed directed C–H bond activation and future directions. *Coord. Chem. Rev.* **2021**, *431*, 213683.

Riley, P.N.; Parker, J.R.; Fanwick, P.E.; Rothwell, I.P. Formation of Tantalum "Tuck-in" Complexes by Activation of Methyl C-H Bonds in Pentamethylcyclopentadiene Groups by Carbazole Ligation. *Organometallics* **1999**, *18,* 3579-3583.
Roy, A. H.; Hartwig, J. F. Oxidative Addition of Aryl Sulfonates to Palladium(0) Complexes of Mono- and Bidentate Phosphines. Mild Addition of Aryl Tosylates and the Effects of Anions on Rate and Mechanism. *Organometallics*, **2004**, *23*, 194-202.

Roy, A.; Hartwig, J. F. Reductive Elimination of Aryl Halides from Palladium(II). *J. Am. Chem. Soc.* **2001**, *123*, 1232-1233.

Ryabov, A.D. Mechanisms of intramolecular activation of carbon-hydrogen bonds in transition-metal complexes. *Chem. Rev*. **1990**, *90*, 403-424.

Sanner, R.D.; Carter, S.T.; Bruton, Jr., W.J. The preparation of mono(η^5-pentamethylcyclopentadienyl) compounds of tantalum(V). *J. Organomet. Chem.* **1982**, *240*, 157-162.

Schaller, C.P.; Wolczanski, P.T. Methane vs Benzene Activation via Transient $^tBu_3SiNHTa(=NSi^tBu_3)_2$: Structure of $(py)_2MeTa(=NSi^tBu_3)_2$. *Inorg. Chem.* **1993**, *32*, 131-144.
Schmidt, S.; Sundermeyer, J. Höhervalente derivate der d-metall-säuren X. Imidokomplexe des fünf- und vierwertigen niobs und tantals mit halbsandwich- und metallocen- struktur *J. Organomet. Chem*. **1994**, *472*, 127-138.

Schoenebeck, F.; Houk, K. N. Ligand-Controlled Regioselectivity in Palladium-Catalyzed Cross-coupling Reactions. *J. Am. Chem. Soc*. **2010**, *132*, 2496−2497.

Schroeter, F.; Soellner, J.; Strassner, T. Cross-Coupling Catalysis by an Anionic Palladium Complex. *ACS Catal.* **2017**, *7*, 3004-3009.

Scott, N. W. J.; Ford, M. J.; Jeddi, N.; Eyles, A.; Simon, L.; Whitwood, A. C.; Tanner, T.; Willans, C. E.; Fairlamb, I. J. S. A Dichotomy in Cross-Coupling Site Selectivity in a Dihalogenated Heteroarene: Influence of Mononuclear Pd, Pd Clusters, and Pd Nanoparticles—the Case for Exploiting Pd Catalyst Speciation. *J. Am. Chem. Soc.* **2021**, *143*, 9682-9693.

Senn, H. M.; Ziegler, T. Oxidative Addition of Aryl Halides to Palladium(0) Complexes: A Density-Functional Study Including Solvation. *Organometallics* **2004**, *23*, 2980-2988.

Sergeev, A. G.; Schultz, T.; Torborg, C.; Spannenberg, A.; Neumann, H.; Beller, M. Palladium-Catalyzed Hydroxylation of Aryl Halides under Ambient Conditions. *Angew. Chem., Int. Ed.* **2009**, *48*, 7595−7599.

Sherwood, J.; Clark, J. H.; Fairlamb, I. J. S.; Slattery, J. M. Solvent effects in palladium catalysed cross-coupling reactions. *Green Chem.* **2019**, *21*, 2164.

Shilov, A.E. *Activation of Saturated Hydrocarbons by Transition Metal Complexes*; Reidel: Boston, 1984.

Solans-Monfort, X.; Chow, C.; Gouré, E.; Kaya, Y.; Basset, J.M.; Taoufik, M.; Alessandra Quadrelli, E.A.; Eisenstein, O. Successive Heterolytic Cleavages of H_2 Achieve N_2 Splitting on Silica-Supported Tantalum Hydrides: A DFT Proposed Mechanism. *Inorg. Chem.* **2012**, *51*, 7237-7249.

Soltanieh, M.; Zohrabian, A.; Gholipour, M.J.; Kalnay, E. A review of global gas flaring and venting and impact on the environment: Case study of Iran. *Int. J. Greenhouse Gas Control* **2016**, *49*, 488-509.

Soulivong, D.; Norsic, S.; Taoufik, M.; Copéret, C.; Thivolle-Cazat, J., Chakka, S.; Basset, J-M. Non-Oxidative Coupling Reaction of Methane to Ethane and Hydrogen Catalyzed by the Silica-Supported Tantalum Hydride: $(SiO)_2Ta$-H. *J. Am. Chem. Soc*. **2008**, *130*, 5044-5045.

Stahl, S. S.; Labinger, J. A.; Bercaw, J. E. Homogeneous Oxidation of Alkanes by Electrophilic Late Transition Metals. *Angew. Chem., Int. Ed*. **1998**, *37*, 2180−2192.

Stambuli, J. P.; Incarvito, C. D.; Bühl, M.; Hartwig, J. F. Synthesis, Structure, Theoretical Studies, and Ligand Exchange Reactions of Monomeric, T-Shaped Arylpalladium(II) Halide Complexes with an Additional, Weak Agostic Interaction. *J. Am. Chem. Soc.* **2004**, *126*, 1184-1194.

Sunley, G.J.; Waton, D.J., High productivity methanol carbonylation catalysis using iridium: The Cativa™ process for the manufacture of acetic acid. *Catal. Today* **2000**, *58*, 293-307.

Suzuki, K.; Shin-ya, M.; Ono, Y.; Matsumoto, T.; Nanbu, N.; Takehara, M.; Ue, M.; Sasaki, Y. Physical and Electrochemical Properties of Fluoroacetonitrile and Its Application to Electric Double-Layer Capacitors. *Electrochemistry* **2007**, *75*, 611-614.

Tanaka, H.; Nishibayashi, Y.; Yoshizawa, K. Interplay between Theory and Experiment for Ammonia Synthesis Catalyzed by Transition Metal Complexes. *Acc. Chem. Res.* **2016**, *49*, 987-995.

Tay, B.Y.; Wang, C.; Stubbs, L.P.; Jacob, C.; van Meurs, M., Deuterated dimethyl sulfoxide as a good NMR solvent for the characterization of alkali metal cyclopentadienides, amides, alkoxides and phenoxides. *J. Organomet. Chem*. **2011**, *686*, 3431-3435.
Tebbe, F.N. and Parshall, G.W. Hydride Derivatives of Niobocene and Tantalocene. *J. Am. Chem. Soc*. **1971**, *93*, 3793-3795.

Thieuleux, C.; Copéret, C.; Dufaud, V.;Marangelli, C.; Kuntz, E.; Basset, J.-M. Heterogeneous well-defined catalysts for metathesis of inert and not so inert bonds. *J. Mol. Catal. A* **2004**, *213*, 47-57.

Thomson, R.K; Monreal, M.J.; Masuda, J.D.; Scott, B.L.; Kiplinger, J.L. Lutetium gets a crown: Synthesis, structure and reaction chemistry of the separated ion pair complex, $[Li(12\text{-crown-}4)_2][(C_5Me_5)_2LuMe_2]$. *J. Organomet. Chem.* **2011**, *696*, 3966-3973.

Tobisu, M.; Chatani, N. Cross-Couplings Using Aryl Ethers via C–O Bond Activation Enabled by Nickel Catalysts. *Acc. Chem. Res.* **2015**, *48*, 1717-1726.

Van Asselt, A.; Burger, B.A.; Gibson, V.C.; Bercaw, J.E. Hydrido methylidene, hydrido vinylidene, hydrido oxo, and hydrido formaldehyde derivatives of bis(pentamethylcyclopentadienyl)tantalum. *J. Am. Chem. Soc*. **1986**, *108*, 5347-5349.

Vidal, V.; Theolier, A.; Thivolle-Cazat, J.; Basset, J.-M. Metathesis of Alkanes Catalyzed by Silica-Supported Transition Metal Hydrides. *Science* **1997**, *276*, 99-102.

Vidal, V.; Theólier, A.; Thivolle-Cazet, J.; Basset, J-M. Activation and Functionalisation of the C-H Bonds of Methane and Higher Alkanes by a Silica-supported Tantalum Hydride Complex. *J. Chem. Soc. Commun. **1995**,* 991-992.

Vilardo, J.S.; Lockwood, M.A.; Hanson, L.G.; Clark, J.R.; Parkin, B.C.; Fanwick, P.E.; Rothwell, I.P. Intramolecular activation of aromatic C–H bonds at tantalum(V) metal centers: evaluating cyclometallation 'resistant' and 'immune' aryloxide ligation. *J. Chem. Soc., Dalton Trans*. **1997**, 3353-3362.

Walton, J.W.; Wilkinson, L.A. π-Coordinated arene metal complexes and catalysis. In *Organometallic Chemistry: Volume 42*, Paymore, N.J., Elliot, P.P.; Royal Society of Chemistry: Cambridge, U.K., 2019: pp 125-171.

Waterman, R. σ-Bond Metathesis: A 30-Year Restrospective. *Organometallics* **2013**, *32*, 7249-7263.

Watson, D. A.; Su, M.; Teverovskiy, G.; Zhang, Y.; Garcia-Fortanet, J.; Kinzel, T.; Buchwald, S. L. Formation of ArF from LPdAr(F): Catalytic Conversion of Aryl Triflates to Aryl Fluorides. *Science* **2009**, *325*, 1661−1664.

Watson, P.L., Methane Exchange Reactions of Lanthanide and Early-Transition-Metal Methyl Complexes. *J. Am. Chem. Soc.* **1983**, *105*, 6491-6493.

Wesendrup, R. and Schwarz, H. Tantalum-Mediated Coupling of Methane and Carbon Dioxide in the Gas Phase. *Angew. Chem. Int. Ed*. **1995**, *34*, 2033-2035.

Wilkinson, G.; Rosenblum, M.C.; Whiting, M.C.; Woodward, R.B., The structure of iron bis-cyclopentadienyl. *J. Am. Chem. Soc.* **1952**, *74*, 2125-2126.

Williams, L.J.; Bhonoah, Y.; Wilkinson, L.A.; Walton, J.W. As Nice as p: Aromatic Reactions Activated by p -Coordination to Transition Metals. *Chem. Eur. J.* **2021**, *27*, 3650-3660.

Wilzbach, K.E.; Ritscher, J.S.; Kaplan, L. Benzvalene, the tricyclic valance isomer of benzene. *J. Am. Chem. Soc.* **1967**, *89*, 1031-1032.

Wohlfarth, C. "Permittivity (Dielectric Constant) of Liquids" in *CRC Handbook of Chemistry and Physics,* Rumble, Jr., J. R.; Lide, D. R.; Bruno, T. J., eds. CRC Press, Boca Raton, FL, **2020**.

Wolfsbergers, W.; Schmidbaur, H. Eine befriendegende darstellungsmethode für trimethylphosphin. *Syn. React. Inorg. Metal-Org. Chem.* **1974**, *4*, 149-156.
Woo, T.K.; Blöchl, P.E.; Ziegler, T. Monomer Capture in Brookhart's Ni(II) Diimine Olefin Polymerization Catalyst: Static and Dynamic Quantum Mechanics/Molecular Mechanics Study. *J. Phys. Chem. A.* **2000**, *104*, 121-129.

Xie, M.; Lu, W. Attraction or repulsion? Theoretical assessment of bulky alkyl groups by employing dispersion-corrected DFT. *RSC Adv.* **2018**, *8*, 2240-2247.

Xue, L.; Lin, Z. Theoretical aspects of palladium-catalysed carbon–carbon cross-coupling reactions. *Chem. Soc. Rev.* **2010**, *39*, 1692-1705.

Xue, X.S.; Ji, P.J.; Zhou, B.Y.; Cheng, J.P. The Essential Role of Bond Energetics in C—H Activation/Functionalization. *Chem. Rev.* **2017**, *117*, 8622-8648.
Yin, C.; Edy, A.; Ali, H.; Bilel, H.; Lyndon, E.; Basset, J.M. Alkane Metathesis with the Tantalum Methylidene [(≡SiO)Ta(:CH_2)Me_2]/ [(≡SiO)$_2$Ta(:CH_2)Me] Generated from Well-Defined Surface Organometallic Complex [(≡SiO)$Ta^{V}Me_4$]. *J. Am. Chem. Soc*. **2015,** *137*, 588-591.

Yu, H. S.; He, X.; Truhlar, D. G. MN15-L: A New Local Exchange-Correlation Functional for Kohn–Sham Density Functional Theory with Broad Accuracy for Atoms, Molecules, and Solids. *J. Chem. Theory Comput.* **2016**, *12*, 1280.

Zalesskiy, S. S.; Ananikov, V. P. $Pd_2(dba)_3$ as a Precursor of Soluble Metal Complexes and Nanoparticles: Determination of Palladium Active Species for Catalysis and Synthesis. *Organometallics* **2012**, *31*, 2302–2309.

Zhao, Y.; Truhlar, D. G. A New Local Density Functional for Main-Group Thermochemistry, Transition Metal Bonding, Thermo-chemical Kinetics, and Noncovalent Interactions. *J. Chem. Phys*. **2006**, *125*, 194101.

Zhao, Y.; Truhlar, D. G. Attractive Noncovalent Interactions in the Mechanism of Grubbs Second-Generation Ru Catalysts for Olefin Metathesis. *Org. Lett.* **2007**, *9*, 1967-1970.

Zhao, Y.;Truhlar, D. G. The M06 suite of density functionals for main group thermochemistry, thermochemical kinetics, noncovalent interactions, excited states, and transition elements: two new functionals and systematic testing of four M06-class functionals and 12 other functionals. *Theor. Chem. Acc.,* **2008**, *120,* 215–241.

Zhou, Q.; Srinivas, H. D.; Zhang, S.; Watson, M. P. Accessing Both Retention and Inversion Pathways in Stereospecific, Nickel-Catalyzed Miyaura Borylations of Allylic Pivalates. *J. Am. Chem. Soc.* **2016**, *138*, 11989-11995.

Zhu, J.; Liang, Y.; Wang, L.; Zheng, Z.-B.; Houk, K. N.; Tang, Y. Remote Ester Groups Switch Selectivity: Diastereodivergent Synthesis of Tetracyclic Spiroindolines. *J. Am. Chem. Soc.* **2014**, *136*, 6900-6903.